**Title**
Catalytic Chemistry Relating to the Au(I)/Au(III) Redox Couple



**Author**
Levin, Mark Daniel

**Publication Date**
2017

Peer reviewed|Thesis/dissertation

# Catalytic Chemistry Relating to the Au(I)/Au(III) Redox Couple

By

Mark Daniel Levin

A dissertation submitted in partial satisfaction of the

requirements for the degree of

Doctor of Philosophy

in

Chemistry

in the

Graduate Division

of the

University of California, Berkeley

Committee in charge:

Professor F. Dean Toste, Chair
Professor Robert G. Bergman
Professor Joseph L. Napoli

Spring 2017

Abstract

**Catalytic Chemistry Relating to the Au(I)/Au(III) Redox Couple**

by

Mark Daniel Levin

Doctor of Philosophy in Chemistry

University of California, Berkeley

Professor F. Dean Toste, Chair

This thesis represents a progression of ideas surrounding chemistry of the two dominant oxidation states for homogeneous complexes of gold. As with all science, a steady combination of successful ideas, happy accidents, and illuminating failures led to the evolution of a perspective on the nature of the two electron transformation between Au(III) and Au(I) that is the focus of this dissertation (though the exact typology of this focus varies, depending on the chapter). Along the way, a foray into platinum chemistry served to highlight both the similarities between these sister elements and their often stark differences. The thread between gold-catalyzed reactivity in Chapter 2 and transformations in which this paradigm is flipped such that a catalyst acts upon a gold complex in Chapters 3 and 4 is a direct result of the intervening failures which pointed the way towards new chemistry. Accordingly, in each chapter, an honest account of the travails leading to the ultimate discovery is attempted.

**Chapter 1** discusses the historical perspective on the Au(I)/Au(III) redox couple both in the context of catalytic chemistry and in stoichiometric organometallic transformations. An attempt is made to showcase, by means of this survey, the unique features of gold that give rise to its unusual behavior among its transition metal cohort.

**Chapter 2** summarizes the development of an Au-catalyzed C($sp^3$)-C($sp^2$) bond-forming cross-coupling reaction between allylic bromides and arylboronic acids. The scope of the process was examined revealing an unusual tolerance for steric hindrance and novel chemoselectivity profile compared to competitive technologies. Mechanistic studies are presented which support oxidative addition of the C-Br bond as the central elementary transformation enabling catalysis, including a model system in which cyclometallation enables observation of each intervening elementary step. This discovery was among the first reports of a gold-catalyzed reaction proceeding through Au(I)/Au(III) redox without the use of a sacrificial oxidant; several reports by other groups taking advantage of this reactivity paradigm since this initial disclosure are discussed, alongside unsuccessful attempts at extension of this reactivity to other substrate classes which ultimately informed the remaining chapters.

**Chapter 3** focuses on the discovery that C($sp^3$)-C($sp^3$) reductive elimination from Au(III) can be effected by the use of a $[Ga_4L_6]^{12-}$ supramolecular catalyst which recognizes and selectively stabilizes the transition state for C-C reductive elimination. This behavior was observed to extend to Pt(IV) complexes, and a series of mechanistic and structural studies support the formation of a coordinatively unsaturated cationic species within the supramolecular cavity prior to rate-limiting reductive elimination for both metals. A dual catalytic cross-coupling was developed in which iodomethane and tetramethyltin are coupled to afford ethane, notably requiring the collaborative action of both platinum and supramolecular catalysts to achieve efficient turnover, and a complete mechanistic picture for the overall process is delineated on the basis of stoichiometric experiments.

**Chapter 4** describes a serendipitous discovery of C($sp^3$)-$CF_3$ reductive elimination from Au(III) complexes in the presence of catalytic $B(C_6F_5)_3$ and the subsequent application of this discovery to the synthesis of PET tracers. Mechanistic experiments revealed a novel "fluoride-rebound" mechanism for reductive elimination involving C-F abstraction, migratory insertion, and C-F reductive elimination. The parent complexes were found to tolerate a surprising breadth of synthetic protocols, enabling the synthesis of complex organometallic derivatives *via* standard organic synthesis methodologies without cleavage of the Au-C bond. Interception of the rebounding fluoride in synthetically advanced complexes enabled the development of a protocol for the synthesis of [$^{18}$F] radiolabeled $CF_3$-containing compounds with substantial structural complexity.

## ACKNOWLEDGEMENTS

"Ladies and Gentlemen, I stand before you now because I never stopped dawdling like an eight-year-old on a spring morning on his way to school. Anything can make me stop and look and wonder, and sometimes learn. I am a very happy man."
- Excerpt from *Cat's Cradle* by Kurt Vonnegut

My father has always insisted (for the entirety of my life at least) that he must be the recipient of a "luck gene" which has afforded him unusual fortune in his own life. Looking back over my five years at UC Berkeley, I am beginning to believe that I inherited the same genetic predisposition, because I have an immense amount to be thankful for. That I have had not only the opportunity to pursue my interests, but that anything amounted of them is astounding to me, looking back. And it is precisely because of the people who supported me along the way that any of this was possible. I am inevitably going to omit someone whose influence was critical – please do not mistake incompetence for malice in that process.

Over the course of my studies I have to come to appreciate that my advisor, F. Dean Toste, maintains an exceptionally intellectually fostering academic environment in his research group. The patience and trust that he sustains in allowing students to pursue their own interests and ideas without barriers, no matter their level of experience, has given me a richly fulfilling academic experience. Dean's guidance is minimalistic, targeted with precision, and manages to offer a piece of his deep understanding of chemistry without taking the reins away from you. It is only with the experience of five years of graduate school that I've learned that even Dean's seemingly tangential suggestions are goldmines. I am also immensely grateful that he cares so deeply about the aspirations of his students; watching Dean "go to bat" for the students above me as they secured their next positions kept me reassured even before I had to face the prospect myself that I was in good hands. Thank you for everything.

To my parents, Victor and Janet Levin: thank you for providing a source of unconditional love, raising me to think for myself, entertaining my penchant for playing devil's advocate (even though arguing with me is "like mud-wrestling a pig"), and for continuing to give me advice even when I almost never listen. Your sacrifice in starting a new life in an unfamiliar country has given me every opportunity I could ever ask for, and you two are still the standard by which I try to live my life. I love you.

To the many teachers I've had along the path to graduate school, please know that you all inspired me. In particular, I have to thank my high school biology teacher Mr. Ward, who taught me that every corner of science can be interesting and that hard work is important because "if it was easy someone would have done it already." I owe too much to my undergraduate research advisor, Alison Frontier, whose introductory organic chemistry class sparked a love for mechanism and organic synthesis that has not relented since. Many professors I had at Rochester had teaching styles that I still try to emulate every time I get up in front of a class: Joe Dinnocenzo, Jim Farrar, Al Clark, Steven Landsburg, and Nick Rogers, among others. Bob Bergman and his physical organic chemistry class were transformative influences on the way I think about chemistry, and Bob has been an amazing resource for chemistry and career advice along the way. I also have had the incredible opportunity, thanks to Steve Pedersen, to get up and teach review sessions (and even "real" lectures) for Chem 3A

– teaching is still the part of science I get the most excited about and I wouldn't have made it through graduate school without the chance to do it.

As a beginning graduate student, I was fortunate to have three senior researchers who relented to my incessant questioning and served as *de facto* mentors to me. Though the three of them had very different styles, I learned everything I know about running a project from them: Yiming Wang, Matt Winston, and David Nagib. Having three answers to every question meant I was never short on ideas and helped me grow to appreciate all facets of synthetic chemistry. The rest of the Toste group numbers too many to mention, but has an unfair advantage over other groups because everyone is excited and always willing to talk about chemistry. Talking to people about my work and theirs has been the best source of learning throughout my time at Berkeley. Andrew Neel, Willie Wolf, Drew Samant, Richard Thornbury, and Brett Williams (among many others) were always willing to listen to me blather and I'm forever grateful. I'm indebted to Julian Chan, who convinced me in the first place to join the group, and to everyone with whom I shared a lab room for making it a fun place to work. I think I'm going to miss nicknames, holiday party skits, sitting in the sun at 'brown town', group meeting problem sets, paper airplane balcony parties, chem keg, and TBAG shotguns more than I could have anticipated.

Dave Kaphan has had an incomparable role in my development as a scientist. From our first day as lab partners in our first chemistry class at Rochester, Dave has been an amazing friend: reliable, hilarious, and patient with my social failings. I honestly don't think my intellectual development would be anywhere near where it is today without the constant counterpart (and sometimes rival) to discuss chemistry with as we came up together. How lucky it is that we got to collaborate in graduate school at all, let alone that it worked. I will always look back fondly on those many late nights in the NMR room collecting kinetics runs, and I hope we can work together again someday.

Finally, and most importantly, Lucia. Your love, support, insight, and friendship have been the defining characteristics of my life here in Berkeley. Having you around to celebrate triumphs and encourage me through failure has kept me going, and you inspire me every day to be a better person. I am thankful constantly that you decided to come to Berkeley with me, because I can't imagine my life without you and I don't think I'd be writing this dissertation successfully without you. I know I haven't always been the easiest person to support, and honestly, I'm pretty sure anyone else would have left the first time I trailed off mid-sentence thinking about something else (usually chemistry). Whatever I did to deserve you, it couldn't have been enough. Luckily, our adventures are only beginning, and I'm excited to see what's next.

*To Lucia,*
*because if this isn't nice, I don't know what is.*

**Catalytic Chemistry Relating to the Au(I)/Au(III) Redox Couple**

TABLE OF CONTENTS

## LIST OF ABBREVIATIONS

Ac = acetyl
Ar = generic aromatic substituent
$Ar_F$ = 3,5-bis(trifluoromethylphenyl)
BBN = 9-borabicyclononane
BCF = tris(pentafluorophenyl)borane
Boc = tertbutylcarbamoyl
bpy = 2,2'-bipyridine
Bu = butyl, $C_4H_9$
CFL = Compact Fluorescent Lamp
COD = 1,4-cyclooctadiene
CSA = camphor sulfonic acid
Cy = cyclohexyl
dba = dibenzylideneacetone
DCM = dichloromethane
DCE = dichloroethane
DFT = Density Functional Theory
DIAD = Diisopropylazodicarboxylate
DMF = dimethylformamide
dppm = diphenylphosphinomethane
$Et_2O$ = diethyl ether
EtOAc = ethyl acetate
Grubbs II = Grubbs' Second-Generation Olefin Metathesis Catalyst
HOMO = Highest Occupied Molecular Orbital
IPr = 1,3-bis(2,6-diisopropylphenyl)imidazol-2-ylidene
iPr = *iso*-propyl
Johnphos = 2-dicyclohexylphosphinobiphenyl
LED = light emitting diode
LUMO = Lowest Unoccupied Molecular Orbital
Me = methyl, $-CH_3$
Mes = mesityl, 1,3,5-trimethylphenyl
MIDA = methyliminodiacetic acid
MS = Mass Spectrometry
NBS = N-bromosuccinimide
NCS = N-Chlorosuccinimide
Neop = neopentylglycol ester
NMO = N-methylmorpholine-N-oxide
Nu = nucleophile
Pd/C = Palladium on Carbon
Ph = phenyl, $-C_6H_5$
Phth = phthaloyl
Pin = pinacol ester
Pr = propyl, $C_3H_7$
R = generic organic substituent
Rh/C = Rhodium on Carbon
SALC = Symmetry Adapted Linear Combination (of atomic orbitals)
$S_N2$ = bimolecular nucleophilic substitution
solv = solvent
SPhos = 2-Dicyclohexylphosphino-2',6'-dimethoxybiphenyl
TBAF = tetrabutylammonium fluoride
tBu = *tert*-butyl
Tf = trifluoromethylsulfonyl
TFAA = trifluoroacetic anhydride
THF = tetrahydrofuran
tht = tetrahydrothiophene
TMP – 2,2,6,6-tetramethylpiperidine
TMS = trimethylsilyl
Tol = toluene
Ts = 4-toluenesulfonyl
TS = transition state

# Chapter 1

C-X Oxidative Addition, C-C Reductive Elimination, and Oxidative Catalysis Chemistry of the Au(I)/Au(III) Redox Couple

## 1.1 Preface

This chapter serves to illustrate the historical context and traditional thinking associated with the redox chemistry of gold which preceded or was contemporary to the work in Chapters 2-4, as well as to address several common misconceptions regarding Au(I)/Au(III) redox reactivity. Though not a comprehensive survey of catalytic nor stoichiometric chemistry of redox-active homogeneous gold, the selected examples provide a sketch of precedent as a means to orient the reader to the unique chemistry of this corner of the periodic table. In particular, an attempt is made to showcase and in part explain the often paradoxical nature associated with the various redox transformations that gold undergoes and the significant influence of relativistic effects on the reactivity of gold. The many questions which still remain are highlighted as suggestions for future research.

## 1.2 Introduction

The periodic locale of gold introduces a great number of unusual properties. The typical lanthanide contraction of 3rd row transition metals is further accentuated at gold by the influence of relativistic effects, which are at a local maximum of influence (Figure 1.1).[1–4] This serves to contract the 6s orbital by an additional 20%, and by the same token, shield the 5d orbitals to a greater extent and thus induce a corresponding increase in diffusivity. Counterintuitively, this serves to increase ionization potentials for both sets of orbitals: the 6s experiences a greater attraction due to the closer contact with the nucleus, while the anticipated opposite effect in the 5d is in fact outweighed by a corresponding decrease in electron-electron repulsion.

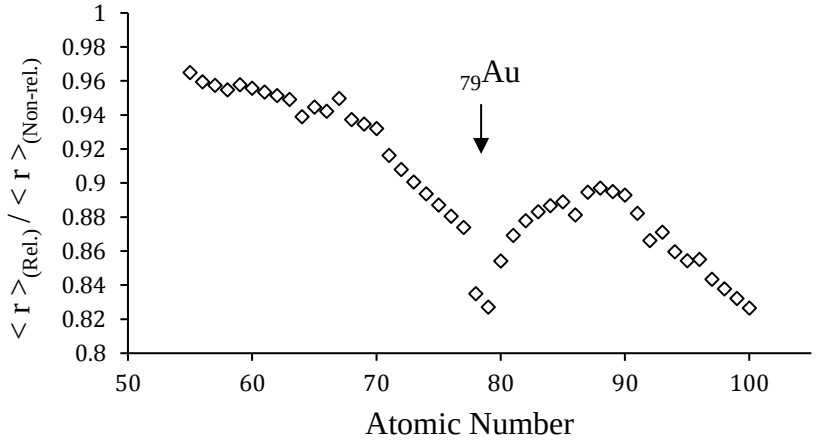


**Figure 1.1** Influence of Relativistic Effects on the Radius of the 6s Orbital. The quotient of the radial expectation values for relativistic Dirac-Fock and nonrelativistic Hartree-Fock calculations are shown.[5,6]

This relativistic electronic restructuring gives gold the highest electronegativity of the transition metals, nearly identical to that of carbon, such that the Au-C covalence is almost perfectly nonpolar.[7] The oxidation potentials tell the same story, requiring substantially higher energy to access the $d^8$ oxidation state via 2-electron oxidation than other members of the late transition metal block.[8] Finally, metal-ligand bond lengths decrease and (heterolytic) bond strengths increase for gold compared to silver, again due primarily to relativistic effects.[9]

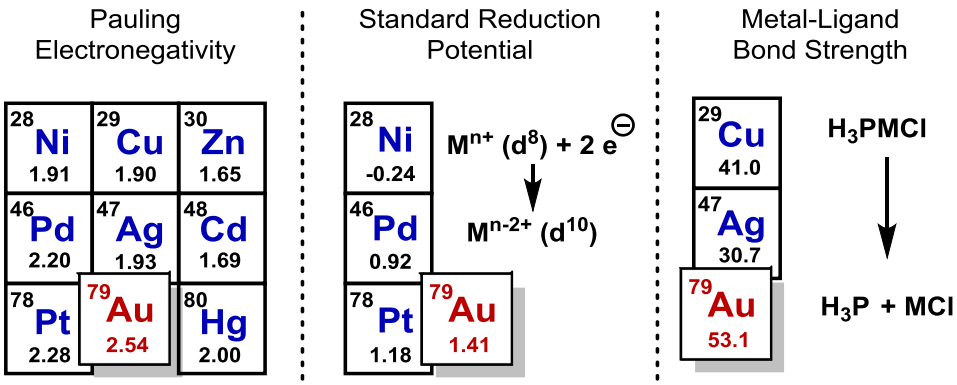


**Figure 1.2** Properties of Gold and its Neighboring Elements. Standard Reduction Potentials are in Volts, measured versus Standard Hydrogen Electrode at 298 K in water. Metal-Ligand Bond Strengths are heterolytic, measured in kcal/mol, computed at the MP2 level of theory.

This suite of properties enable what might by now be called "traditional" homogeneous gold catalysis, though by most standards the implementation of cationic, ligand-supported Au(I) catalysts in organic synthesis is a relatively new phenomenon (Figure 1.3). A compact yet polarizable (i.e. "soft") 6s orbital binds preferentially to π-systems, while diffuse, tightly-held 5d orbitals offer minimal Dewar-Chatt-Duncanson-type backbonding, affording substantial electrophilicity to the coordinated atoms and leading to efficient activation of C-C multiple bonds towards outer-sphere nucleophilic attack. Starting from the seminal work of Teles, and in an impressive array of work since, this reactivity paradigm has successfully enabled the synthesis of complex molecular architectures *via* the creative implementation of Au(I) catalysts.[10–18]

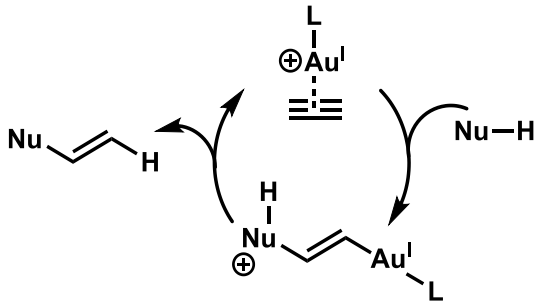


**Figure 1.3** Mechanism of "Traditional" Homogeneous Au Catalysis

While interception of the Au(I) intermediates by a variety of subsequent chemistries has further expanded the diversity of accessible products (and spurred a heated argument on the existence and bonding of carbenoid species at gold), a striking feature of all of these systems is the retention of the Au(I) oxidation state throughout the catalytic cycle.[19–26] Given the energetics involved in accessing the Au(III) oxidation state, this is hardly surprising. Indeed, conventional wisdom supported the notion that Au(III) intermediates were functionally irrelevant to catalytic chemistry, bolstered by evidence that much of putative Au(III) catalysis involves not an authentic Au(III) catalytic cycle but rather generation of acid, nanoparticulate complexes, or *in situ* reduction to an active Au(I) species.[27–30] Though the evidence behind this

consensus was strong, there existed orthogonal evidence that the Au(III) oxidation state offered an opportunity for unusual new reactivity when accessed.

The following sections serve to summarize such evidence in the form of the theoretical and historical underpinnings of three areas which pointed the way towards the work concerning redox chemistry of gold in Chapters 2-4: oxidative addition to Au(I), reductive elimination from Au(III), and gold catalysis involving sacrificial oxidants. No attempt at comprehensive survey is made, given that such reviews exist elsewhere.[31–33]

### 1.3 Oxidative Addition of Organic Electrophiles to Au(I)

This section seeks to provide a potential answer to the following question: "Why does gold undergo oxidative addition of carbon electrophiles *more slowly* than related $d^{10}$ transition metals?"[33,34]

Oxidative addition involves the formation of bonds between a metal and an electrophilic substrate concomitant with the formal two-electron oxidation of the metal center**.** For Au(I), this involves the transition from a linear, two-coordinate, $d^{10}$ metal center to a square-planar, four-coordinate, $d^8$ metal center. As such, this section begins with a treatment of the bonding preferences of Au(I).

Relativistic expansion of the 6s and contraction of the 5d corresponds to an energetic narrowing of these two orbitals, such that in the presence of an appropriate ligand field, productive mixing of the $d(z^2)$ and s orbitals can occur. This results in the formation of two orbitals which can be thought of as modified $d(z^2)$ orbitals, one with an accentuated "barbell" and one with an accentuated torus (Figure 1.4).

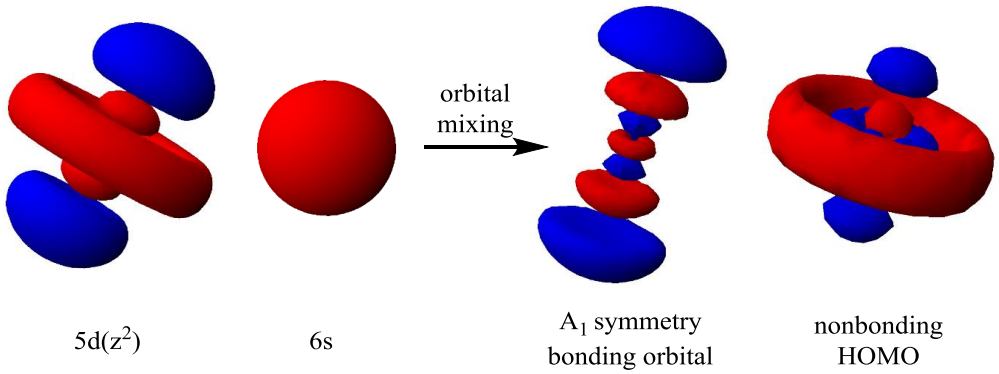


**Figure 1.4** Space-filling model of s-$dz^2$ hybrid orbitals, generated using Orbital Viewer.[35]

In linear complexes, this has a substantial impact on metal-ligand bonding, allowing more productive overlap with the $A_1$ symmetry-adapted linear combination of ligand orbitals (SALC) (Figure 1.5). Association of a third ligand breaks the symmetry of the ligand SALCs, such that overlap with the hybrids is weakened. When considered alongside the steric effects of additional ligands, the overall change from two- to three-coordinate is strongly disfavored

(though even for $H_3PAuCl$, association of an additional $PH_3$ unit has been calculated to be 6.3 kcal/mol uphill[36]). This leads to the well-known preference for linear two-coordination in Au(I).

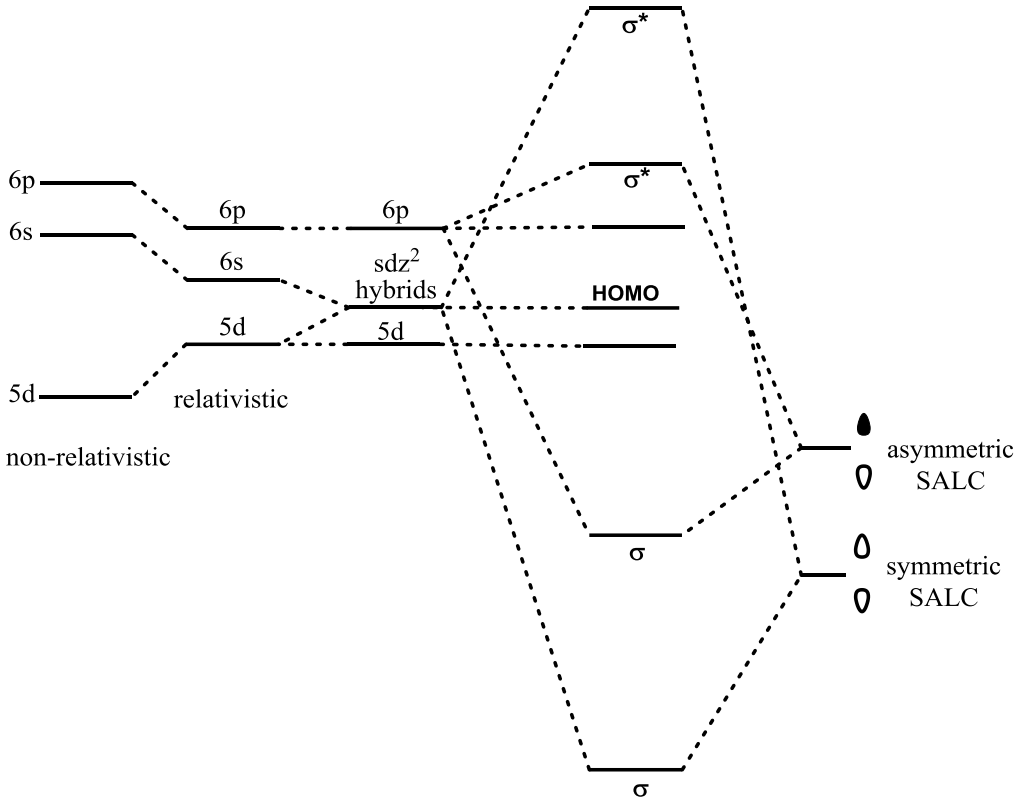


**Figure 1.5** Orbital Diagram for Relativistic s-d mixing in two coordinate gold complexes. Strong bonding to the symmetric SALC is due to the highly oriented s-$dz^2$ hybrids. Relativistic orbital splitting due to spin-orbit coupling is not shown.

Two salient consequences of this bonding model are key to the oxidative addition reaction at Au(I). First, bending of the coordination environment *en route* to the transition state affords a similar symmetry-related decrease in overlap to the hybrids, akin to association of a third ligand. Indeed, many oxidative additions have been demonstrated to proceed *via* pre-coordination of the electrophile to the metal center by σ-, π-, or n-coordination.[37,38] Second, the HOMO, being largely torus in character, is competent for $S_N2$-like oxidative addition reactions, whereas the orbitals bearing necessary symmetry for concerted oxidative additions are substantially lower in energy. This has important consequences for the *kinetic* chemoselectivity of oxidative addition to Au(I).

As such, the ensuing examples are selected from oxidative additions involving a carbon electrophile to argue that the situation for oxidative addition to Au(I) is more complex than a simple reticence due to intrinsic oxidation potentials. Kinetic factors stemming from the coordination preference play a large role in determining the rate of oxidative addition, and a simple thermodynamic argument does not suffice to explain the unusually slow kinetics for gold compared to other transition metal complexes. Rather, the oxidation potential serves only to limit classes of electrophiles which provide exergonic oxidative addition, though this category is in fact sufficiently broad to enable a survey. Indeed, several strategies have been

successful in overcoming this limitation, most of which do not induce a thermodynamic bias, but rather surmount the kinetic barrier to association of a third ligand by various means.

### 1.3.1 Oxidative Addition to "Typical" Two-Coordinate Au(I) Complexes

In the 1970s, the groups of Kochi, Schmidbaur, and Puddephatt studied the reaction of methylgold complexes bearing various phosphine ligands with iodomethane as neat solutions. The reaction is complicated by rapid, subsequent Au(I)-Au(III) transmetallation, affording trialkyl Au(III) products (**3**) rather than the expected direct oxidative addition products (**2**), with consequent mechanistic experiments supporting the pathway shown in Figure 1.6. For **1**, complete consumption of the starting methylgold(I) complex is complete after 1 hour at 33 °C.[39–43] However, reactions conducted in dilute benzene or ethereal solution required substantially longer reaction times, with a pseudo-first order rate constant $k_{obs} = 4.0 \times 10^{-5}\ s^{-1}$ in a 2M benzene solution of iodomethane at 33 °C, corresponding to a half-life of 4.8 hours.

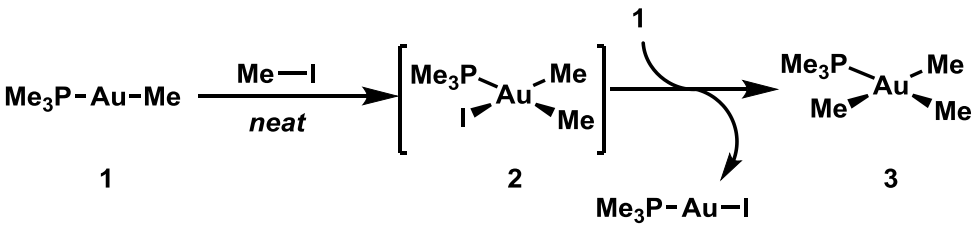


**Figure 1.6** Oxidative addition of iodomethane to phosphine supported methylgold complexes.

The corresponding reaction of *in situ* generated dimethylaurate is substantially faster, affording oxidative addition products in dilute ethereal solution "upon mixing" at 0°C, with a rough estimate of the rate of oxidative addition suggesting it is between 400 and 2,000 times faster than for **1** (Figure 1.7). This is a substantial rate increase, but pales in comparison to other transition metal/metallate pairs, which can show rate increases on the order of $10^5$ favoring the metallate. Nonetheless, this reaction allows direct comparison of the rates of oxidative addition to various alkyl halide electrophiles, showing classic hallmarks of $S_N2$-like oxidative addition with rate ordering following the trend of Me > Et > *n*Bu >> *i*Pr.[44–50]

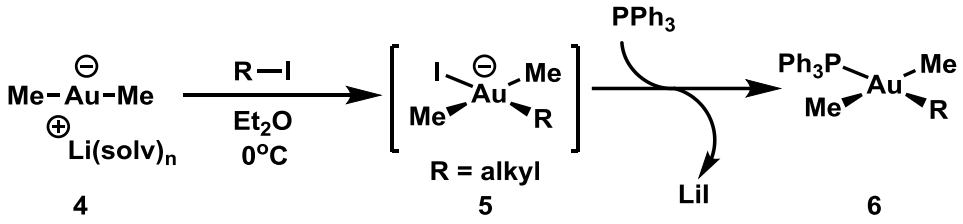


**Figure 1.7** Oxidative addition of alkyl halides to dimethyl aurate.

In contrast, no reaction is observed with aromatic electrophiles such as iodobenzene, and several calculations have shown exceptionally high barriers to this process (~33 kcal/mol for $(Me_3P)_2Au^+$), consistent with the electronic structure considerations discussed above.[51,52]

### 1.3.2 Oxidative Addition to Monocoordinated, Cationic Au(I) Complexes

A simple solution to the electronic cost of associating a third ligand to two-coordinate gold complexes is to begin with a monocoordinated Au(I) complex. However, the high metal-ligand bond strength of Au(I) complexes typically limits the accessibility of such pathways starting from classical L-Au-X compounds. And while isolable organogold complexes featuring a single Au-C linkage in the absence of a supporting ligand are known, they typically satisfy their coordination preferences by the formation of clusters featuring bridging ligands. Such interactions are suppressed electrostatically in cationic $[L\text{-}Au(I)]^+$ complexes, which can be easily generated *via* halide abstraction from the neutral parent L-Au-X species.[53]

For example, a gas-phase study showed that iodobenzene reacts with $Me_3PAu^+$ to afford $Me_3P^+$-Ph and AuI, with calculations supporting the intermediacy of oxidative addition product **8** and a calculated barrier for oxidative addition 8 kcal/mol lower than the corresponding bis-ligated species.[51]

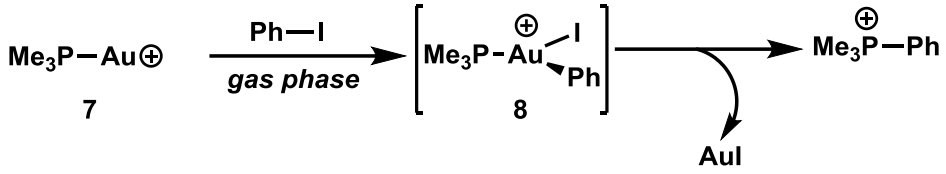


**Figure 1.8** Gas-phase reactivity of $Me_3PAu^+$ towards iodobenzene.

A corresponding solution-phase realization of this phenomenon was achieved in the oxidative addition of biphenylene to $[IPrAu]^+$. Faster rates of oxidative addition with more electron rich biphenylene analogues and more weakly coordinating anions suggest that pre-coordination of the biphenylene aromatic system to Au(I) is necessary prior to oxidative addition – a pre-equilibrium prohibitively costly for two-coordinate complexes.[54] The kinetic accessibility of this oxidative addition event is underscored by its reversibility. In the presence of added, exogenous, electron-rich aromatic ligands (e.g. trimethoxybenzene), biphenylene is released to afford the $IPrAu^+$–(arene) complex, whereas the Au(III) complex is favored in the presence of exogenous oxygen ligands such as water or DMF.[55]

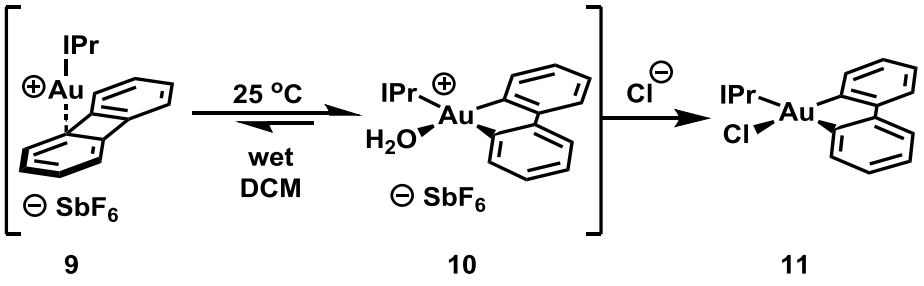


**Figure 1.9** Oxidative addition of biphenylene to cationic Au(I) complexes supported by carbene ligands.

### 1.3.3 Intramolecular Oxidative Addition to Au(I) complexes

Another strategy to induce oxidative addition is the pre-organization of the electrophile in the vicinity of the metal center by tethering to one of the coordinated ligands. This has met with mixed results, suggesting that substantial steric relief in the oxidative addition process is required beyond the simple entropic benefit of proximity. Two unsuccessful examples of this strategy are highlighted in Figure 1.10 below. Both complexes (**12** and **13**) lack reactivity between the Au center and the aromatic halide even upon prolonged heating.[56,57]

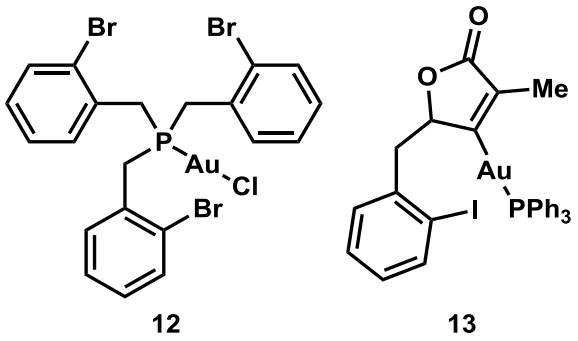


12 13

**Figure 1.10** Tethered electrophile Au(I) complexes inert towards oxidative addition.

Nonetheless, the same oxidative addition process occurs readily for the related systems **14** and **16** depicted in Figure 1.11. One potential explanation for the difference between these reactions and the inert analogues is the high strain and rigidity associated with the *peri* naphthalene positions of **14** and the cyclophane motif in **16**. Such an extreme extent of necessary pre-organization underscores the reticence for Au(I) to associate an additional ligand for oxidative addition.[58,59]

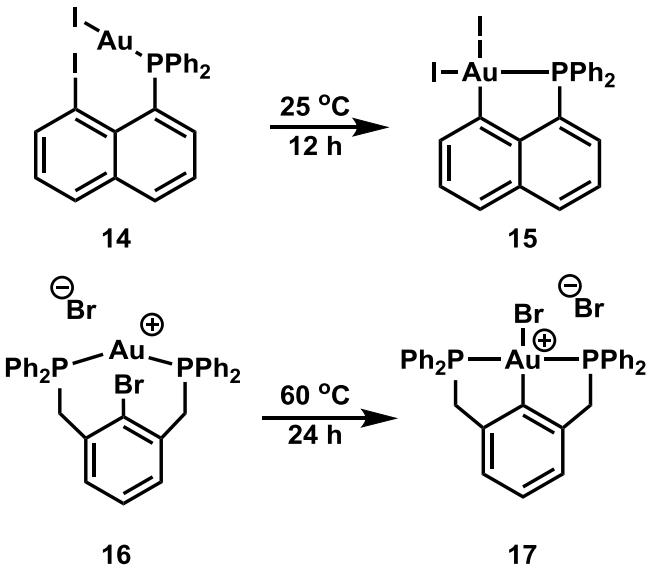


14 15

16 17

**Figure 1.11** Oxidative addition to *peri*-napthyl and metallacyclophane tethered Au(I) complexes

### 1.3.4 Oxidative Addition to Coordinatively Distorted Au(I) Complexes

An altogether distinct approach to enable oxidative addition at Au(I) is to systematically enforce a bent two-coordinate geometry at gold, effectively pre-paying the cost to deformation. This approach is complicated by the tendency for bidentate phosphine complexes of Au(I) to disproportionate into oligomeric chains of [-Au-L~L-Au-L~L-]$_n$ units with bridging phosphines, rather than maintain a bent geometry. Indeed many complexes for which solid state structures feature chelating geometries exhibit such disproportionation behavior upon dissolution.[60,61]

Nonetheless, headway has been made in identifying bidentate ligands which maintain their bent geometry. Didier Bourissou and coworkers reported the first such example based on a carborane bis(phosphine) ligand platform, which enables facile oxidative addition of iodobenzene even at low temperatures (Figure 1.12). Although no rationale for the maintenance of the bent geometry is immediately apparent, this example is a striking demonstration of the influence that the geometric preferences of gold have on the kinetics of the oxidative addition, given that C($sp^2$)-I oxidative addition to a cationic Au(I) complex occurs readily at -10 °C.[62]

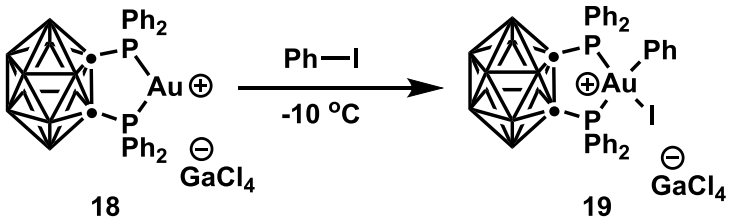


**Figure 1.12** Oxidative addition of iodobenzene to carborane bis(phosphine) complexes of Au(I) displaying bent geometry. The icosahedron represents a $B_{10}H_{10}C_2$ unit with carbons represented by solid black circles.

Several other oxidative addition reactions of complex **18** and related analogues have been demonstrated, including biphenylene and benzocyclobutanone.[63] The bending also offers a rationale for the chemoselectivity of this process – filled d orbitals bearing appropriate symmetry for concerted oxidative addition are destabilized by the ligand field, unlike in the linear analogues. In fact, alkyl electrophiles are substantially less reactive towards **18** compared to iodobenzene.

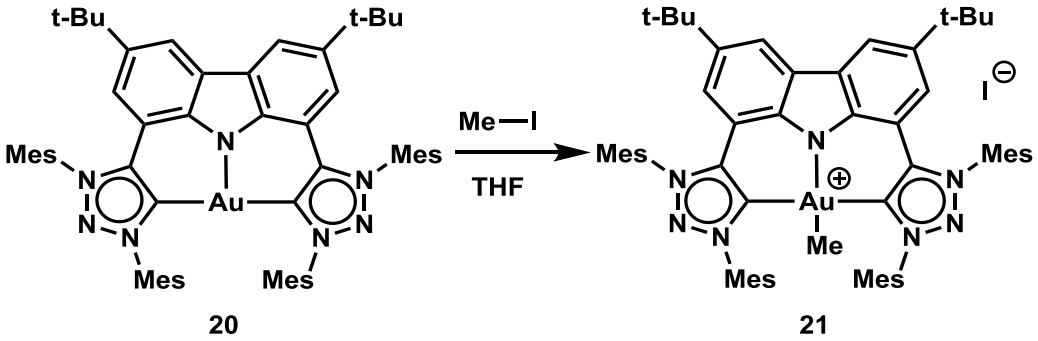


**Figure 1.13** Oxidative addition of iodomethane to a T-shaped Au(I) complex.

A related example of this strategy was reported employing a rigid carbazolide framework to enforce coordination of a third anionic ligand to the bis(carbene)Au(I) complex. Oxidative addition of iodomethane to the T-shaped complex **20** occurs readily, affording **21** in under 2 hours at room temperature.[64]

### 1.3.5 Oxidative Addition to Bimetallic Au(I) Complexes

Though the relativistic effects of gold are responsible for its reticence to associate a third ligand and thus for its sluggish oxidative addition chemistry, the torus-like HOMO afforded by these same relativistic effects induces a secondary effect which has been leveraged to accelerate oxidative addition. Au(I) complexes have a tendency to form close metal-metal contacts both inter- and intra-molecularly, with typical Au-Au distances of ~2.9 Å. This "aurophilic" interaction has been measured to be on the order of 10 kcal/mol, and is attributed to a 'hyper Van der Waals interaction' between the large polarizable HOMO orbitals on interacting gold atoms.[65,66]

In the extreme, these metal-metal contacts enable synchronized electron donation, such that Au(II)-Au(II) metal-metal bonded species are formed upon oxidative addition, rather than a discrete Au(III) complex. Closely associated Au(I) atoms tethered by a 3-atom linker appear to exploit this effect more readily than other complexes, with the most reactive examples featuring an A-frame bis(ylide) ligand (Figure 1.14).[67–73] These oxidative addition reactions are readily reversible, with **23** undergoing exchange with deuterated iodomethane at room temperature.

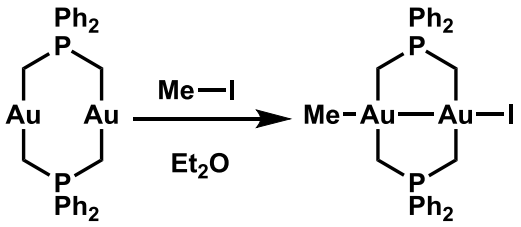


**22** **23**

**Figure 1.14** Oxidative addition of iodomethane to an A-frame bimetallic Au(I) bis(ylide) complex to afford an Au(II)-Au(II) species.

While it is tempting to ascribe a thermodynamic effect to the formation of these metal-metal bonded species, when less rigid ligands are employed, the kinetically formed Au(II)-Au(II) species readily rearrange into the mixed-valent Au(I)-Au(III) isomers, suggesting that the origin of the reactivity of these complexes is kinetic in nature (Figure 1.15).[74–77] Similar effects have been observed for Pd(II) to Pd(IV) oxidation *via* bimetallic Pd(III)-Pd(III) intermediates.[78] It is important to note, however, that no single bimetallic Au complex has been studied which both undergoes accelerated C-X oxidative addition and subsequently undergoes rearrangement – only $X_2$ oxidations have been studied in this regard.

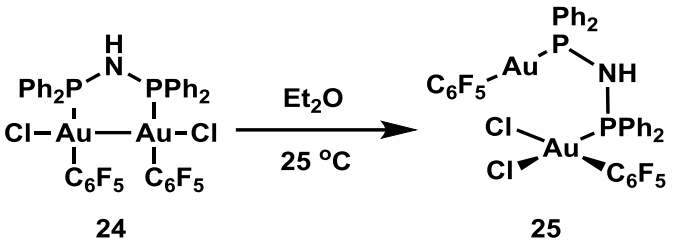


**Figure 1.15** Spontaneous isomerization of an Au(II)-Au(II) complex to the mixed valent Au(III)-Au(I) isomer.

### 1.3.6 Radical Chain Oxidative Addition to Au(I) Complexes

A final means by which oxidative addition has been accelerated at gold is to enter into a single electron reactivity manifold, such that a radical chain process affords the oxidative addition product sequentially *via* a metastable Au(II) intermediate. Our group reported that such a mechanism is operative in the oxidative addition of $CF_3I$ to arylgold(I) complexes. Initiation via photoexcitation generates a $CF_3$ radical, which adds to the Au(I) center. Subsequent iodide abstraction by the Au(II) species **26** from $CF_3I$ continues the chain reaction.[79] It remains unclear why this reactivity manifold so efficiently overcomes the kinetic barriers to this process, though the rapidity of single electron processes at transition metals is a common phenomenon.[80]

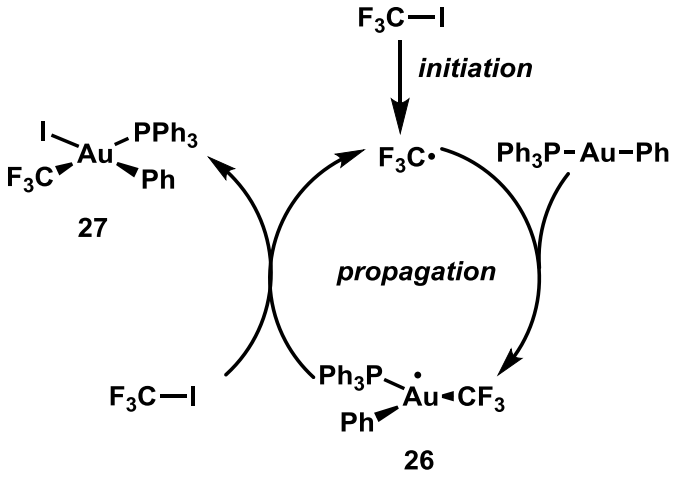


**Figure 1.16** Oxidative addition of $CF_3I$ to Au(I) complexes *via* a radical chain pathway.

A similar mechanism is operative in the numerous photoredox/Au(I) dual catalytic reactions, wherein a Ru(II) photocatalyst likely serves as an initiator, generating an aryl radical from aryldiazonium precursors.[81–89] Stoichiometric analogues of this process ultizing chelating ligands have validated the intervention of Au(III) species on the catalytic cycle, whereas the slow rate of oxidative addition in the absence of a photosensitizer supports the radical chain mechanism of oxidative addition.[90–92]

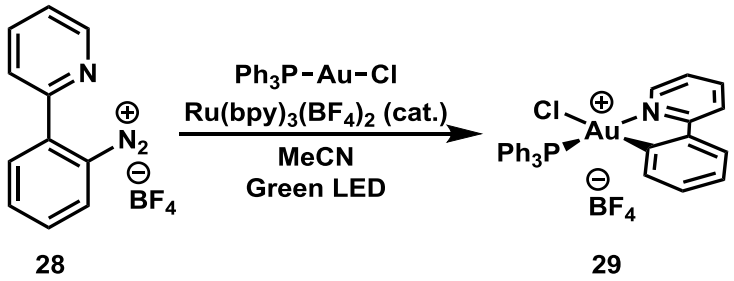


28 29

**Figure 1.17** Oxidative addition of aryldiazonium salts to Au(I) *via* a radical chain pathway

### 1.3.7 Conclusions

Relativistic effects are crucial to an understanding of the oxidative addition chemistry of Au(I). Though oxidation potential is a convenient scapegoat, such a thermodynamic treatment of the chemistry does not sufficiently explain the slow rate of many oxidative addition processes. Instead, the oxidation potential should be seen as a limitation on the classes of exergonic oxidative additions, with the kinetic barriers being dictated primarily by the intrinsic preference for linear two-coordinate gold, itself a relativistic consequence. Through that lens, the 'exceptions' to sluggish reactivity outlined above (coordinative unsaturation, intramolecular tethering, distorted coordination geometries, bimetallic oxidative addition, and radical chain mechanisms) can be seen as neatly consistent with the reactivity of more typical gold complexes.

## 1.4 Carbon-Carbon Reductive Elimination from Au(III)

This section aims to provide a survey of reductive elimination chemistry at Au(III). Until recently, this field was characterized by a small number of reports primarily from the 1970s which suggested that reductive elimination from Au(III) was intrinsically slow (paradoxically so, given the high oxidation potential of gold). As the topic has been revisited, it has become clear that this picture is incomplete, and understanding requires a similar holistic view to that offered for oxidative addition above.

Reductive elimination involves the formation of a new bond between ligands bound to a metal with concomitant 2-electron reduction of the metal center, and is thus the microscopic reverse of oxidative addition. For gold, this formally involves the formation of a linear, two-coordinate $d^{10}$ Au(I) complex from the corresponding square-planar, tetracoordinate $d^8$ Au(III) precursor. Four general classes of carbon ligands that can participate in this reaction are considered here: $sp^3$, $sp^2$, $sp$, and fluoroalkyl ($C_6F_5$ or $CF_3$). Each class of reductive elimination is treated below, with special attention to those for which rate data exists. Two key features common to all transition metal reductive eliminations are at play throughout and are thus summarized prior to the class-by-class treatment.

First, intrinsic rate differences between classes of carbon ligands exist. For example, reductive elimination to form C($sp^3$) bonds is typically slower than that for $sp^2$. Several reasons are typically offered: (1) decreased steric hindrance between planar $sp^2$ ligands in the transition state relative to three-dimensional $sp^3$ ligands, (2) the lesser directionality towards the metal of the C($sp^2$) hybrid allows for more productive overlap between the eliminating ligands in the transition state, and (3) because the immediate product of reductive elimination involves σ-coordination of the metal to the product, products which can more easily bind to the metal via

additional π-systems stabilize this interaction, which is likely present in the transition state, provided that the TS occurs sufficiently late on the reaction coordinate.[93–95] Meanwhile, fluoroalkyl complexes undergo slower reductive elimination than the parent organic analogues – an effect typically ascribed to the stronger (more ionic in character) carbon-metal bonds formed by these electron withdrawing ligands.[96] The often invoked secondary effect of metal → C-F σ* backbonding is almost certainly irrelevant for Au(III) given that its carbonyl complexes are non-classical.[97]

Second, reductive elimination from odd-coordinate complexes is generally faster than for even coordinate analogues. This difference is ascribed to a frontier molecular orbital effect wherein the product orbital which accepts the electrons on the metal is necessarily antibonding in character (with respect to ancillary ligands) for even-coordinate complexes and nonbonding for odd-coordinate complexes. For Au(III), this means that ligand dissociation (or more rarely association) generally precedes reductive elimination.[34,98,99]

For gold, product coordination is especially important given the noted preference for 2-coordinate gold (see 1.3 above). Namely, reductive elimination from a four coordinate complex affords the disfavored three-coordinate Au(I) whereas reductive elimination from a three-coordinate Au(III) complex affords the much more easily accessible two-coordinate Au(I) (Figure 1.18). Because ligand-metal bonding for gold is strengthened by relativistic influences, the formation of coordinatively unsaturated species is typically the major roadblock for reductive elimination.

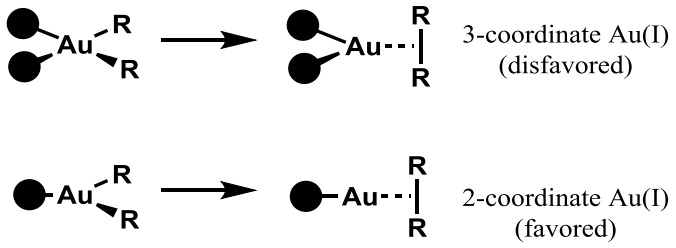


**Figure 1.18** Coordination number effects for reductive elimination from Au(III) based on the coordination preferences of Au(I)

For example, compound **11** in Figure 1.9 above is exceptionally thermally stable whereas **10** (which can be generated from **11** by halide abstraction with Ag(I) salts) undergoes rapid, reversible reductive elimination. (Given that the reaction mechanism depicted in Figure 1.9 represents the microscopic reverse of C-C reductive elimination, this new line of reasoning is simply a restatement of the remarks in section 1.3.2.)

Observable C($sp^3$)-$CF_3$ reductive eliminations are not represented in the literature to date for any metal, with the first example of formal C($sp^3$)-$CF_3$ reductive elimination delineated in Chapter 4.

### 1.4.1 C($sp^3$)-C($sp^3$) reductive elimination from Au(III)

The earliest examples of reductive elimination studies at Au(III) were carried out by the groups of Kochi, Komiya, and Tobias. Several classes of Au(III) dimethyl complexes were

studied, with the general conclusion that phosphine dissociation occurs before reductive elimination, as evidenced by phosphine inhibition in all cases (Figure 1.19).[40,42,100–104]

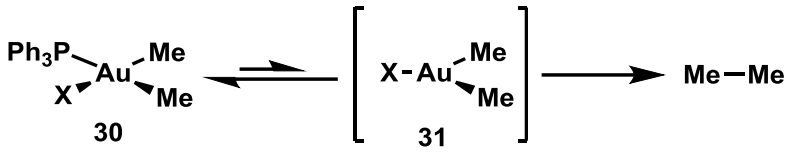


| Entry | X | Rate (Temp., Solvent) |
|---|---|---|
| a | Me | $3.5 \times 10^{-5}$ s$^{-1}$ (31°C, MeI) |
| b | Cl | $9.0 \times 10^{-7}$ s$^{-1}$ (45 °C, PhH) |
| c | I | $7.2 \times 10^{-6}$ s$^{-1}$ (31°C, MeI) |
| d | $NO_3$ | $9.7 \times 10^{-4}$ s$^{-1}$ (45 °C, PhH) |
| e | $PPh_3$, $BF_4$ | $1.9 \times 10^{-5}$ (50 °C, DCM) |

**Figure 1.19** Reductive elimination of ethane from various Au(III) complexes and their associated rates. For entry e, the bis(phosphine) complex and ensuing intermediate are cationic, with $BF_4$ serving as a weakly coordinating anion.

Several competition studies concerning the rate effects of higher alkyl substituents have been carried out, with the general finding that more substituted alkanes undergo faster reductive elimination ($2^o > 1^o >$ Me).[100,105] Three complications to this analysis were identified by Kochi and subsequently accounted for: (1) facile rearrangement of alkyl substituents (e.g. *n*-propyl to *i*-propyl, occurring *via* an unknown mechanism) occurs competitive to reductive elimination, and this isomerization prevents evaluation of the corresponding tertiary compounds due to rapid isomerization of *tert*-butylgold(III) to the *iso*-butyl isomer, (2) because the intermediate tricoordinate $d^8$ Au(III) species are Jahn-Teller unstable in the trigonal planar geometry, T- or Y- shaped geometries predominate, with isomerization of the intermediate sometimes competitive with reductive elimination, such that product ratios are a function of initial geometry and added triphenylphosphine, and (3) intermolecular alkyl scrambling between Au(III) complexes occurs in polar solvents but is slower than the corresponding reductive elimination in nonpolar solvent.

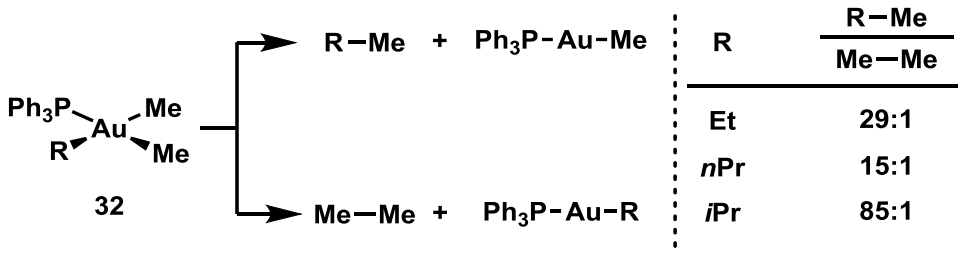


**Figure 1.20** Relative rates of various alkyl-alkyl reductive eliminations from Au(III).

An important observation in these systems is that despite the intervention of coordinatively unsaturated trialkylgold species possessing β-hydrogens in these processes, no alkene products resulting from β-hydride elimination are observed. This seems to be a general

feature of Au(III), with such eliminations only recently reported in systems for which competing reductive eliminations are suppressed.[106,107]

Though for **30b** and **30c** no inhibition by exogenous halide was observed, we found it prudent to re-examine this (based on consequences for chemistry which will be presented in Chapter 3). In methanolic solution (rather than a nonpolar solvent), it was found that indeed iodide dissociation from **33** is a competent mechanism for reductive elimination, with inverse first-order dependence on exogenous iodide observed (Figure 1.21).[108] It is likely that the ability for the protic solvent to stabilize the departing anion *via* hydrogen bonding is responsible for the change in mechanism, a phenomenon seen previously for Pt(IV).[34,109]

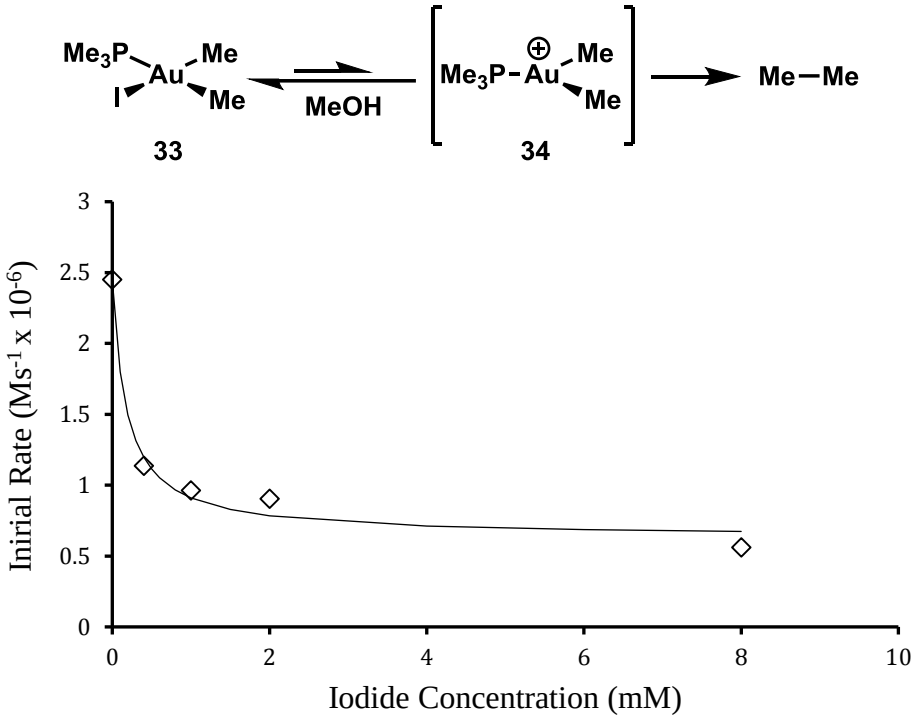


**Figure 1.21** Iodide dissociation as a mechanism for alkane reductive elimination from Au(III) and iodide dependence plot on initial rate for reductive elimination of ethane from **33** conducted at 58 $^{o}$C in MeOH-$d_4$ with varying concentrations of KI. Model line calculated for y = c + [a/(b+x)] shown, indicating nonzero rate at infinite iodide concentration.

### 1.4.2 C($sp^3$)-C($sp^2$) reductive elimination from Au(III)

Competition experiments similar to those depicted in Figure 1.20 have been conducted for aromatic and vinyllic substrates, indicating that C($sp^2$)-C($sp^3$) reductive elimination outcompetes ethane reductive elimination in all cases. Phosphine inhibition suggests that the same dissociative mechanism is operative as for the alkyl-alkyl reductive elimination, and electron rich aromatic ligands undergo faster reductive elimination than electron poor ones.[105,110]

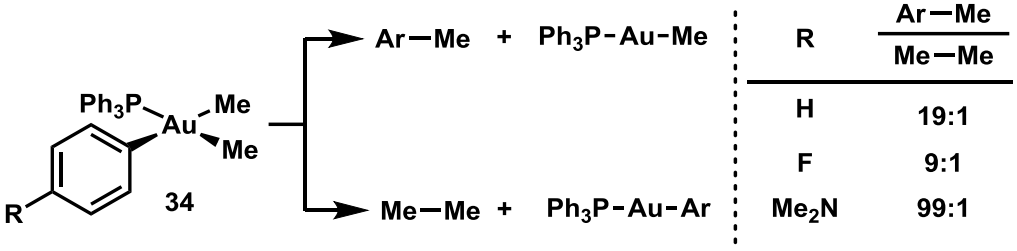


**Figure 1.22** Aryl-$CH_3$ reductive elimination from Au(III) complexes

Our group reported a reaction which likely precedes *via* C($sp^3$)-C($sp^2$) reductive elimination between difluorogold(III) complex **35** and arylboronic acids.[111] Though the initial report suggested an outer-sphere mechanism for reductive elimination, it seems likely based on reports since, that transmetallation occurs to afford an intermediate diorganoAu(III) complex and facile fluoride dissociation (potentially assisted by the boron-containing byproduct or by additional arylboronic acid) initiates reductive elimination.[112] Stereochemical experiments on related alkyl complexes indicated that this reductive elimination process occurs with retention of stereochemistry at the alkyl carbon.[113]

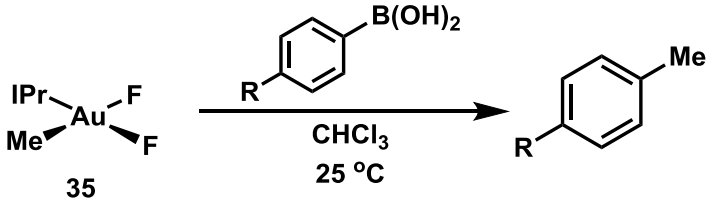


**Figure 1.23** Putative Aryl-$CH_3$ reductive elimination from an Au(III) difluoride.

### 1.4.3 C($sp^3$)-C($sp$) reductive elimination from Au(III)

No reports of clean C($sp^3$)-C($sp$) reductive elimination have been reported. Two reported Au(III) acetylide complexes undergo competitive ethane reductive elimination with minor amounts of $H_3C$-C≡C-R formed (4%), suggesting that the latter process is substantially slower.[105,114] For methyl as the coupling partner, this affords a relative rate comparison for organic substituents of $sp^2 > sp^3 > sp$, though this may be a feature unique to methyl groups rather than a general property for gold.

### 1.4.4 C($sp^2$)-C($sp^2$) reductive elimination from Au(III)

An early report by Vincente indicated that aryl-aryl reductive elimination from Au(III) was feasible, but no rate data for the reactivity of the cyclometallated complexes was provided.[115] A similar, more recent report by Nevado likewise featured cyclometallated complexes but offered no rate data.[112]

A subsequent study from our group revealed that observable diaryl Au(III) complexes are formed upon oxidation of the corresponding L-Au(I)-Ar complexes (*via* subsequent Au(I)/Au(III) transmetallation), ultimately affording biaryl. By conducting this reaction at low temperature, the rates for reductive elimination of these complexes could be measured, indicating a substantially faster process than for the corresponding ethane reductive elimination.

For complex **36**, reductive elimination was found to occur with a rate constant of 1.5 x $10^{-4}$ $s^{-1}$ at -55 °C (i.e. 150 times faster than for the analogous dimethyl complex, **30b**, at a temperature 100 °C lower!).[77]

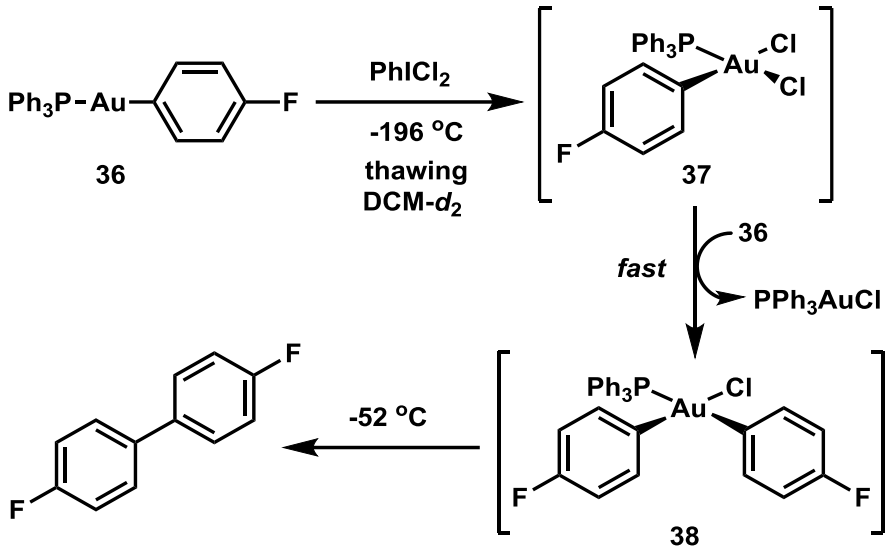


**Figure 1.24** Aryl-aryl reductive elimination from Au(III) from *in situ* generated complexes.

A further surprising result was that the process was not inhibited by exogenous phosphine nor halide, suggesting direct reductive elimination *directly from the four coordinate complex*.[116] Rather, phosphine was found to accelerate the reductive elimination, suggesting a secondary pathway *via* either a pentacoordinate or cationic four-coordinate bis(phosphine) complex.

This mechanism lies in stark contrast to the previous examples. An open question remains as to why ligand dissociation outcompetes both alkyl-alkyl and alkyl-aryl reductive elimination from the four-coordinate Au(III) complex but not aryl-aryl reductive elimination. Surely formation of a 3-coordinate species would result in an even faster reductive elimination, such as is the case for the more challenging elimination from cyclometallated biaryl complex **11** above. A full understanding of why this specific case is an exception remains elusive.

Another clue that this reaction is unusual compared even to other transition metals comes from a recent study of *in situ* generated cyclometallated diaryl gold complexes which undergo rate-limiting reductive elimination as part of a catalytic reaction. For platinum, the rate of biaryl reductive elimination increases for cases where the aromatic substituents are electronically most different (i.e. a nucleophilic and electrophilic partner).[117] In contrast to this, for gold, the rate of reductive elimination was observed to be fastest when both arenes are electron rich, such that the rate of reductive elimination can be predicted additively from the Hammett σ parameters of each arene.[118]

### 1.4.5 C($sp^2$)-C($sp$) reductive elimination from Au(III)

No isolable Au(III) complexes have been reported which subsequently undergo reductive elimination of C($sp^2$)-C($sp$) coupled products. However, treatment of complex **39**

with phenylacetylene at reflux in THF affords the corresponding C-C coupled product over 12 hours. No isolation of the Au(III) intermediates and no rate studies are reported.[119]

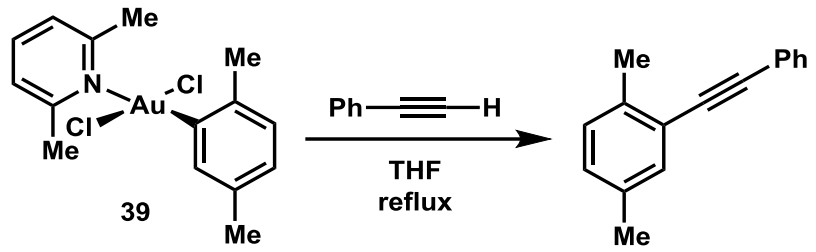


**Figure 1.25** Putative C($sp^2$)-C($sp$) reductive elimination from Au(III)

### 1.4.6 C($sp^2$)-fluoroalkyl reductive elimination from Au(III)

Nevado and Larossa have reported that $C_6F_5$-substituted Au(III) complex **40** reacts with electron rich arenes to afford the corresponding C-C coupled products in a stoichiometric fashion upon heating at 150 $^oC$ for 22 hours. The intermediate Au(III) complexes have not been isolated and no rate studies have been performed, and the mechanism may involve an $S_NAr$ mechanism rather than C-H auration/reductive elimination.[120,121]

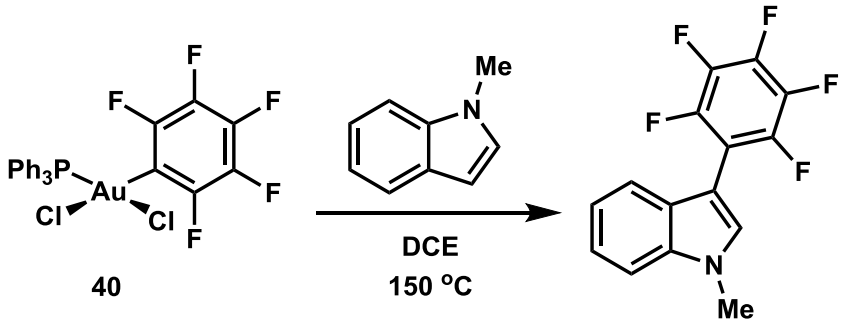


**Figure 1.26** Putative Aryl-$C_6F_5$ reductive elimination from Au(III)

In contrast to this sluggish reactivity, our group reported the facile formation of Ar-$CF_3$ compounds (<1 min for completion at room temp) upon halide abstraction from complex **41**.[79] The differences in reactivity between this and **40** are likely a result of the coordination number, wherein the putative bis(aryl) species formed from **40** must dissociate a phosphine or halide ligand prior to reductive elimination. This is supported by the observation that thermal reductive elimination from **41** precedes much more slowly *via* a phosphine dissociation mechanism, affording a mixture of Ar-X and Ar-$CF_3$ (composition of this mixture depends on the halide identity, $k_{obs}$ = 4.5 x $10^{-5}$ $Ms^{-1}$ for R = Me, X = I).[122]

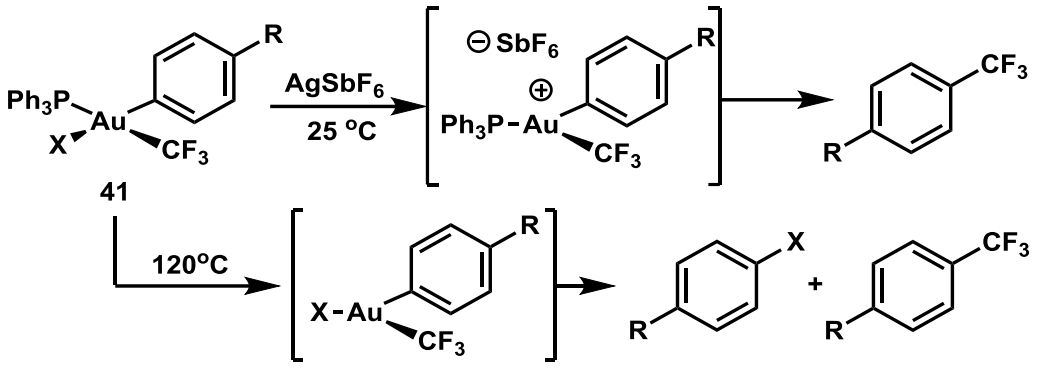


**Figure 1.27** Aryl-$CF_3$ reductive elimination *via* halide abstraction and thermolysis *via* three-coordinate intermediates.

### 1.4.7 C(*sp*)-C(*sp*) reductive elimination from Au(III)

Schmidbaur reported the isolable tris(alkynyl) complex **42**, which undergoes C-C reductive elimination upon heating or upon treatment with HCl. Related complexes featuring $PPh_3$ or P(*i*Pr)$_3$ ligands in place of $PMe_3$ were too unstable towards reductive elimination to isolate, supporting the idea that ligand dissociation precedes reductive elimination for **42**. However, no rate data (quantitative nor qualitative) were provided for this reaction.[123]

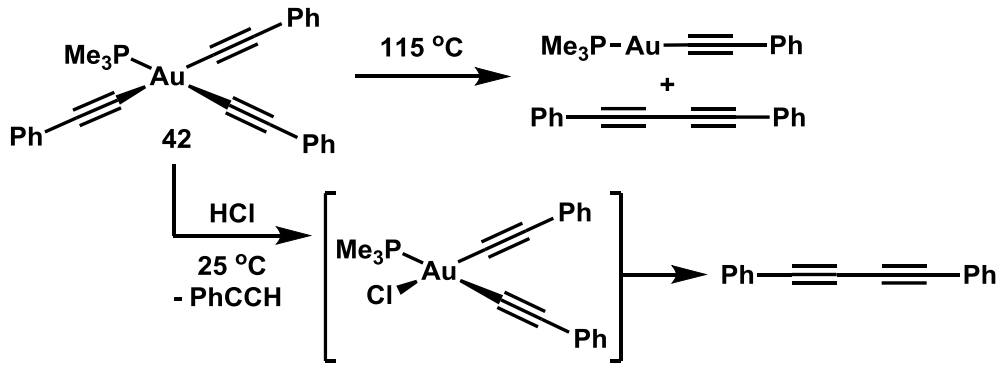


**Figure 1.28** C(*sp*)-C(*sp*) reductive elimination from tris(alkynyl) Au(III) complexes.

### 1.4.8 C(*sp*)-fluoroalkyl reductive elimination from Au(III)

Echavarren and Espinet have reported the reaction of Au(III) complex **43** with silver acetylide **44** to afford the corresponding C(*sp*)-$C_6F_5$ coupled product over 4 hours at room temperature, but no rate data were provided and the role of AgI in promoting the reductive elimination is unclear. Presumably an alkynyl-$C_6F_5$-Au(III) species is formed, and either phosphine dissociation or (more likely) AgI-promoted halide dissociation occurs prior to reductive elimination.[124]

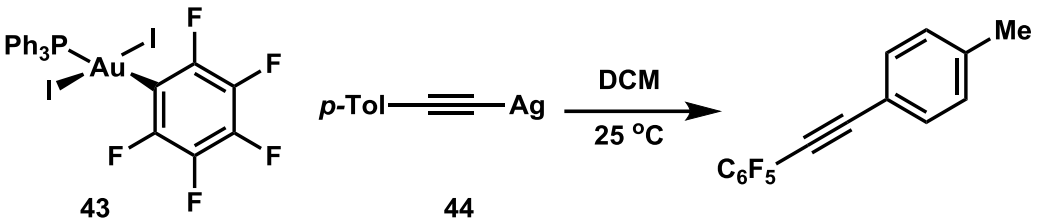


**Figure 1.29** Putative C(*sp*)-fluoroalkyl reductive elimination from Au(III)

No trifluoromethyl Au(III) complexes have been reported to undergo reductive elimination with C(*sp*) fragments to date.

### 1.4.9 Fluoroalkyl-fluoroalkyl reductive elimination from Au(III)

The tris(pentafluorophenyl)Au(III) complex is unusual because it represents a rare example of an isolable tricoordinate triorganogold complex, a testament to the stabilizing power of fluoroalkyl groups (though no characterization data have been provided). This species undergoes elimination of decafluorobiphenyl upon solution phase thermolysis or sublimation in the solid state, whereas its corresponding $PPh_3$ complex has not been reported to undergo the same reductive elimination reaction. No solution phase chemistry nor rate data have been reported, though the authors posit that **45** is likely isolated as the diethyl ether solvate and loses this stabilizing coordination upon sublimation.[125]

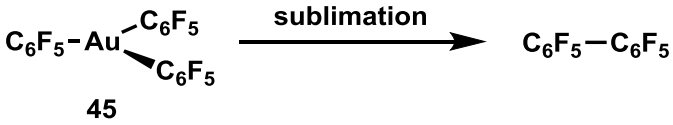


**Figure 1.30** Decafluorobiphenyl reductive elimination from $Au(C_6F_5)_3$

Nevado recently reported a similar reaction of bis($C_6F_5$) complex **46**, which undergoes decafluorobiphenyl reductive elimination over 20 hours at 150°C. Thermolysis of the monoaryl analogue **40** also affords decafluorobiphenyl, likely by disproportionation.[126]

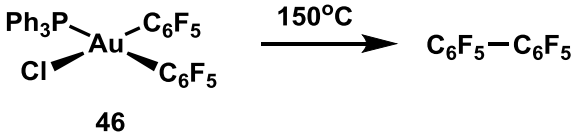


**Figure 1.31** Decafluorobiphenyl reductive elimination from phosphine supported Au(III)

No hexafluoroethane or octafluorotoluene reductive eliminations from Au(III) have been reported to date.

### 1.4.10 Conclusions

With the exception of aryl-aryl reductive elimination, all well-characterized C-C reductive eliminations from Au(III) proceed *via* the intermediacy of a coordinatively

unsaturated intermediate, by dissociation of either L or X type ligands. Qualitatively, it seems that the cationic intermediates formed by X-type ligand dissociation are more reactive, though a thorough comparison would require a phosphine scavenger effective at low temperature akin to silver for halogens. The nature of the uncharacteristic aryl-aryl reductive elimination remains mysterious. Computational studies have suggested that heavy-atom tunneling may in fact be at play, though little credence should be placed in that possibility in the absence of experimental evidence.[127]

Gold does seem to undergo fast reductive elimination when compared its neighboring metals, in line with the expectations provided by the high oxidation potential. Comparisons are complicated by the role of ligand dissociation, but offer a rough basis for understanding. For example, dialkyl platinum(II) complexes do not undergo reductive elimination upon thermolysis, instead engaging in a host of alternative (often redox-neutral) decomposition modes.[128–132] The palladium complex $(Ph_3P)_2PdMe_2$ eliminates ethane with an observed rate of $1.0 \times 10^{-3}$ $s^{-1}$ at 60 ºC *via* a mechanism involving pre-equilibrium phosphine dissociation.[133] This is faster than the rate for the most analogous Au(III) complex (*c.f.* **30e** above), though only by a factor of approximately 25, despite the well-known tendency for 3rd row metals to display much slower reactivity than their 2nd row congeners.[34,99] Octahedral trimethylPt(IV) complexes are known to undergo ethane reductive elimination *via* mechanisms involving ligand dissociation, with rates on the order of $10^{-4}$ between 60-80 ºC.[109,134,135] This is slower than the analogous Au system, despite accessing a higher oxidation state at the metal center.

The aryl-aryl reductive elimination from Au(III) similarly appears to be much faster than for Pd and Pt, though the best studied systems feature distinct (generally chelating) ligand systems whose influence is difficult to disentangle from the effects of the metal.[117,136] Indeed $(Ph_3P)_2PdPh_2$ is unknown, and only the *trans* isomers of (non-perfluorinated) derivatives are stable enough to enable isolation.[137]

No information about the direct reductive elimination from Au(II)-Au(II) species is available, with all studied examples proceeding by intitial isomerization to the mixed-valent Au(I)-Au(III) complexes.

In all, despite the unusual exception of aryl-aryl reductive elimination, an understanding of the reductive elimination chemistry of gold requires consideration of the relativistic effects which strengthen the noted preference for $d^8$ metals to undergo reductive elimination from three-coordinate intermediates *via* prior ligand dissociation.

### 1.5 Homogeneous oxidative gold catalysis utilizing sacrificial oxidants

The first examples of catalytic reactions leveraging the Au(I)/Au(III) redox couple involved oxidative coupling reactions, wherein two or more nucleophiles and a sacrificial oxidant were employed to generate coupled products (Figure 1.32). By utilizing strong $F^+$ or $I^{III}$ oxidants, the slow oxidative addition to Au(I) complexes was circumvented altogether. This section summarizes several key precedents in this area and the relevant mechanistic information which has been gleaned to date.

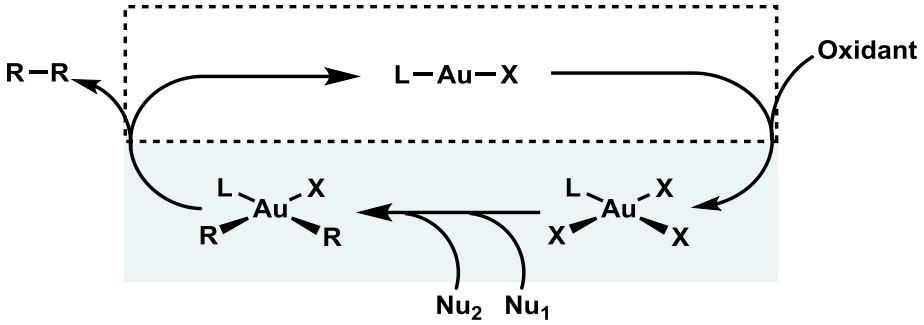


**Figure 1.32** General scheme for oxidative Au(I)/Au(III) catalysis

### 1.5.1 Key Examples

The seminal discovery in this area came from a series of reports by Liming Zhang concerning the rearrangement of propargyl esters.[138,139] Attempted fluorination of an intermediate vinylgold species afforded instead a dimer of the starting material, indicating that oxidation of the Au(I) intermediate by Selectfluor® had occurred.

Though isolated previous reports had pointed the way towards such chemistry, it was the subsequent discovery that the intermediate gold species could be intercepted for an oxidative cross-coupling reaction by arylboronic acids which kickstarted interest in this area (Figure 1.33).[140–142] Since this initial report, a range of transformations have been reported utilizing either fluoronium or hypervalent iodine oxidants to achieve an impressive variety of coupling reactions.

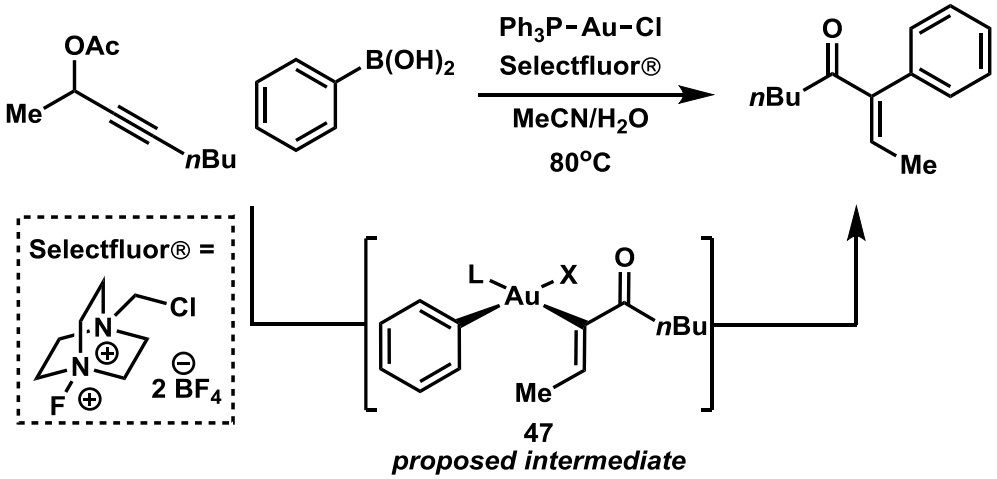


**Figure 1.33** Seminal report of C-C cross-coupling *via* oxidative gold catalysis

It is not particularly illuminating to include a laundry list of examples, though an attempt at a comprehensive list of references has been made.[31,32] Instead, two illustrative advances have been selected.

The first extensions of this methodology were to the difunctionalization of alkenes, a substrate for which "traditional" gold catalysis had met with limited success due to the slow protodeauration of C($sp^3$)-alkylgold species.[143,144] Amino- and oxy-arylation utilizing both $F^+$

and $I^{III}$ oxidants was reported by several groups including our own, with aryl boronic acids or aryl silanes (or arenes for intramolecular cases, *via* C-H auration) serving as the aromatic nucleophile.[145–153] An important development was the observation by our group that closely linked bimetallic catalysts allow reactivity at much lower temperatures (25 vs. 80 °C) than the corresponding monometallic catalysts, an effect ascribed to the lowered barrier to oxidation, akin to the corresponding oxidative addition chemistry described above (Section 1.3.5).[113,154]

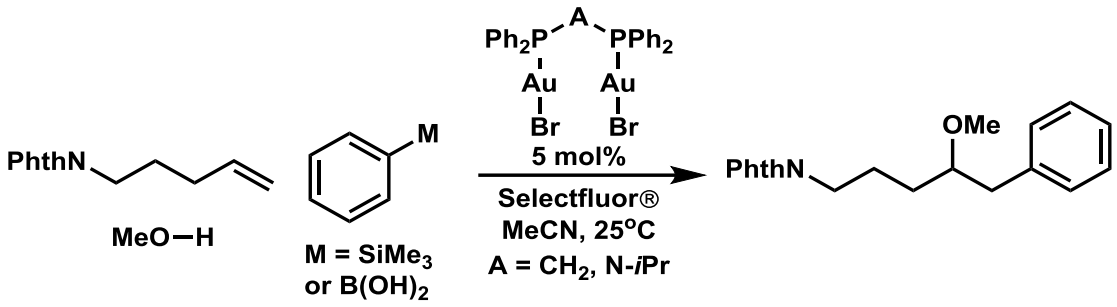


**Figure 1.34** Intermolecular oxyarylation of alkenes *via* oxidative bimetallic gold catalysis

The most impressive application of the oxidative Au(I)/Au(III) paradigm was the discovery that aryl trimethylsilanes and electron rich arenes can be directly coupled to afford C-H arylated products in high yields and with high selectivity utilizing a "ligand-free" gold precatalyst and a hypervalent iodine oxidant.[118,155–157] The orthogonality of this methodology to traditional cross-coupling technology is immediately apparent from the coupling partners (C-H and C-$SiMe_3$), the scope is broad, and the selectivity is surprisingly high for many arene coupling partners. Several other oxidative cross-coupling reactions involving C-H auration have been developed following this template.[121,158–166]

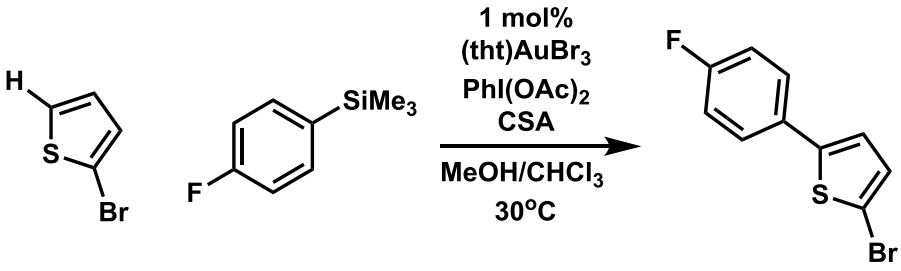


**Figure 1.35** Direct gold-catalyzed oxidative C-H arylation with aryltrimethylsilanes

### 1.5.2 Mechanistic aspects

The discovery of this reactivity paradigm ignited a fierce debate regarding the mechanism of these transformations, with several groups offering competing proposals. While the exact order of many steps and the extent to which conclusions regarding one reaction extend to other reports remains unclear, several insights seem to carry broad implications. Au(I) aryl complexes were found not to be relevant on-cycle species for both oxidant classes, given that their implementation as precatalysts does not result in incorporation of the aromatic substituent into the product, rather giving different decomposition products (Figure 1.35). Further kinetics studies by our group and by the Lloyd-Jones group have indicated that oxidation occurs prior to intervention of any nucleophile, as shown in Figure 1.32 above.[113,145,154,156]

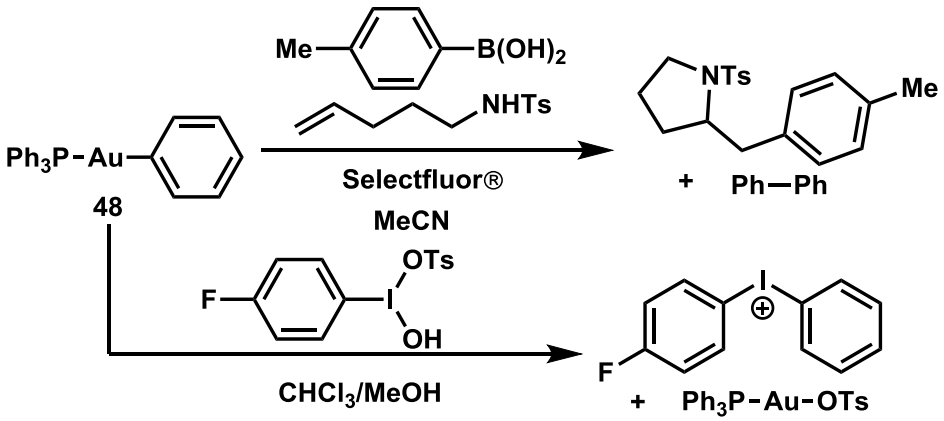


**Figure 1.36** Evidence against the intermediacy of arylgold(I) species in oxidative catalysis.

An interesting feature common to many of these systems is the superior performance of gold bromide precatalysts compared to typical chloride complexes. This has been rationalized by the observation of brominated aromatic species in the reaction mixtures, suggesting that halide oxidation is an initiation reaction required for the formation of the active catalyst which bears no halide ligands. The speciation of remaining X-type ligands likely depends on the exact reaction conditions (fluoride, sulfonate, alkoxide, etc.).[156]

The aromatic nucleophiles (silanes and boronic acids) are often homocoupled as a significant byproduct when the other reaction partner is slow to react. This is unsurprising given the chemistry outlined in Section 1.4.4 above, and likely represents the competitive double transmetallation to (or bimolecular disproportionation of) the intermediate Au(III) species as a side reaction.[77,118]

A final note concerns the role of the supporting ligands. The C-H auration reaction depicted in Figure 1.34 employs an Au(III) precatalyst that was developed after finding that $Ph_3PAuOTs$ exhibits an induction period before catalytic turnover during which $Ph_3P{=}O$ is generated, suggesting that a "ligand-free" (solvato) species is the active catalyst. This is in contrast to the observation that binuclear catalysts such as $dppm(AuBr)_2$ are superior catalysts for the oxy- and aminoarylation reactions. Similarly, phosphonium reductive elimination from Au(III) has been observed as a catalyst deactivation pathway in related reactions, with loss of ligand correlating with a slowdown in catalytic turnover.[81,167] The simplest explanation is that both "ligand-less" and ligand-supported Au(III) complexes are competent depending on the reaction involved, though the possibility that certain ligand frameworks lead to faster initiation by ligand oxidation remains, and a more thorough understanding will require additional experiments.

### 1.5.3 Conclusions

The implementation of redox cycling between the Au(I) and Au(III) oxidation states was demonstrated to be a powerful method for the development of new, often useful, catalytic reactions by the chemistry summarized here. By implementing a strong, sacrificial oxidant, the challenge of accessing the Au(III) oxidation state by means of oxidative addition is nullified, and the unique chemistry associated with rapid reductive elimination can be leveraged to provide a wealth of novel transformations.

The next chapter details the attempts to translate the lessons of this pioneering field of study into a gold-catalyzed reaction which does not require a sacrificial oxidant. The underlying hypothesis of the work was that the use of a bimetallic catalyst would allow more rapid oxidative addition to occur (*vide supra*). Many of the insights detailed throughout this chapter were ultimately important to understand the resulting chemistry.

## 1.6 Supporting Information

*Procedure for the kinetics experiment to determine iodide dependence on reductive elimination from **32***:

To an NMR tube, in an $N_2$ atmosphere wet glovebox was added 2-trimethylsilylethanol (0.01 mmol, 1 equiv, internal standard), **33** (0.01 mmol, 1 equiv), and potassium iodide (1 mol% to 40 mol%) each as solutions in $CD_3OD$, prepared as stock solutions, such that the total volume in the tube was equal to 500 μL. The NMR tube was then fitted with a septum top and removed from the glove box, followed immediately by the application of parafilm to seal the edges of the septum. The reaction mixture was then placed into the prewarmed (58 °C, calibrated vs. ethylene glycol), tuned and shimmed NMR spectrometer, and an automatic kinetics program was used to collect regular time points at 60 second intervals over a period of 2.5 hours.

*Representative Spectrum:*

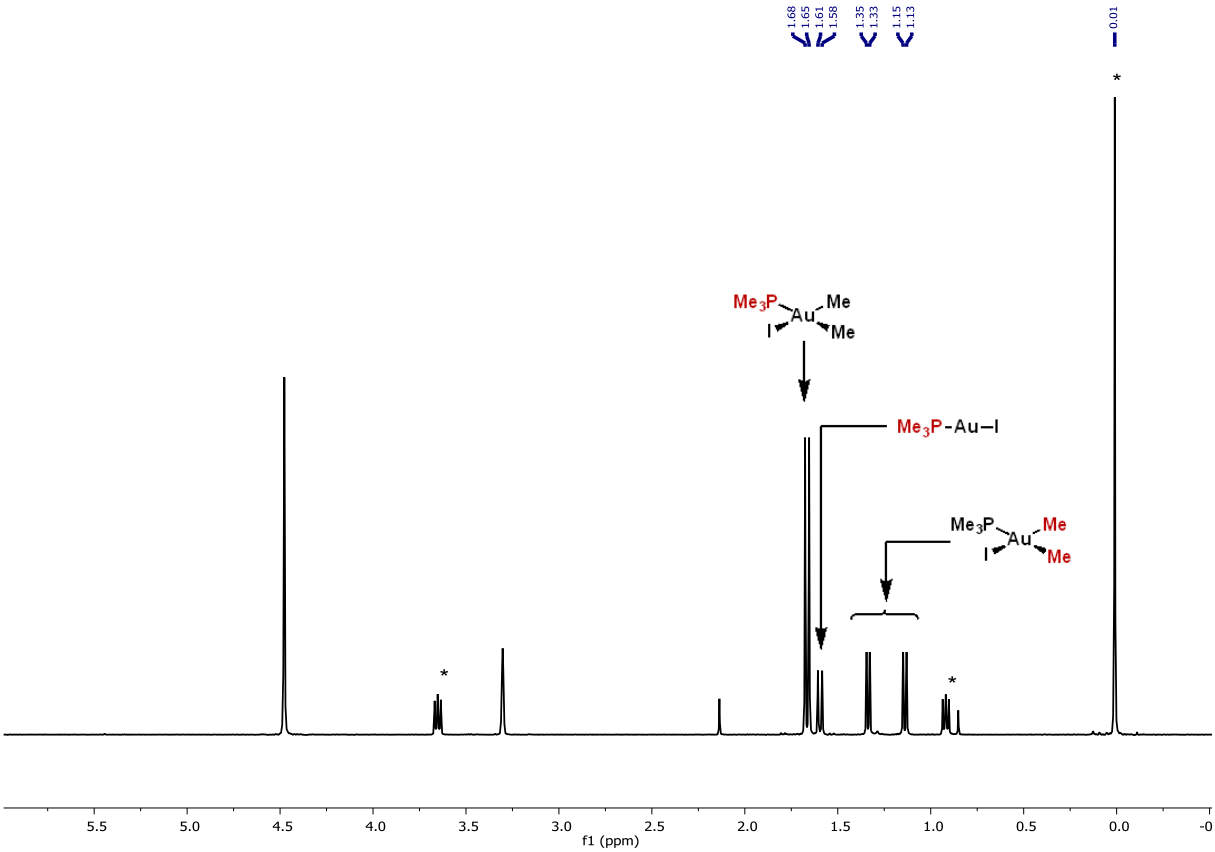


**Figure 1.37**

* = 2-trimethylsilyl ethanol (internal standard)

## 1.7 References


(1) Gorin, D. J.; Toste, F. D. *Nature* **2007**, *446* (7134), 395.
(2) Pyykkö, P. *Angew. Chem. Int. Ed.* **2002**, *41* (19), 3573.
(3) Pyykko, P.; Desclaux, J. P. *Acc. Chem. Res.* **1979**, *12* (8), 276.
(4) Schmidbaur, H.; Cronje, S.; Djordjevic, B.; Schuster, O. *Chem. Phys.* **2005**, *311* (1–2), 151.
(5) Desclaux, J. P. *At. Data Nucl. Data Tables* **1973**, *12* (4), 311.
(6) Considering that relativistic effects arise from the orbital speed of the electron and thus scale approximately with $Z^2$, the existence of a relative maximum at gold (rather than a monotonic increase as Z increases) for effects on the 6s orbital can be explained by considering the competing effects of interelectron repulsion. However, these are expected to change as a function of oxidation state. As such, the superlative of local maximum is less important than the fact that such effects are *among* the strongest for any transition metal and have important implications for the chemistry of gold.
(7) Haynes, W. M. (ed. *CRC Handbook of Chemistry and Physics*, 97th ed.; CRC Press/Taylor & Francis: Boca Raton, FL.
(8) *J. Phys. Chem. Ref. Data* **1989**, *18* (1), 1.
(9) Schwerdtfeger, P.; Hermann, H. L.; Schmidbaur, H. *Inorg. Chem.* **2003**, *42* (4), 1334.
(10) Teles, J. H.; Brode, S.; Chabanas, M. *Angew. Chem. Int. Ed.* **1998**, *37* (10), 1415.
(11) Shapiro, N.; Toste, F. *Synlett* **2010**, *2010* (5), 675.
(12) Fürstner, A. *Chem. Soc. Rev.* **2009**, *38* (11), 3208.
(13) Jiménez-Núñez, E.; Echavarren, A. M. *Chem. Rev.* **2008**, *108* (8), 3326.
(14) Gorin, D. J.; Sherry, B. D.; Toste, F. D. *Chem. Rev.* **2008**, *108* (8), 3351.
(15) Shen, H. C. *Tetrahedron* **2008**, *64* (18), 3885.
(16) Li, Z.; Brouwer, C.; He, C. *Chem. Rev.* **2008**, *108* (8), 3239.
(17) Hashmi, A. S. K. *Chem. Rev.* **2007**, *107* (7), 3180.
(18) Wang, Y.-M.; Lackner, A. D.; Toste, F. D. *Acc. Chem. Res.* **2014**, *47* (3), 889.
(19) Fürstner, A.; Morency, L. *Angew. Chem. Int. Ed.* **2008**, *47* (27), 5030.
(20) Hashmi, A. S. K. *Angew. Chem. Int. Ed.* **2008**, *47* (36), 6754.
(21) Benitez, D.; Shapiro, N. D.; Tkatchouk, E.; Wang, Y.; Goddard, W. A.; Toste, F. D. *Nat Chem* **2009**, *1* (6), 482.
(22) Hashmi, A. S. K. *Angew. Chem. Int. Ed.* **2010**, *49* (31), 5232.
(23) Harris, R. J.; Widenhoefer, R. A. *Angew. Chem. Int. Ed.* **2014**, *53* (35), 9369.
(24) Hussong, M. W.; Rominger, F.; Krämer, P.; Straub, B. F. *Angew. Chem. Int. Ed.* **2014**, *53* (35), 9372.
(25) Joost, M.; Estévez, L.; Mallet-Ladeira, S.; Miqueu, K.; Amgoune, A.; Bourissou, D. *Angew. Chem. Int. Ed.* **2014**, *53* (52), 14512.
(26) Sarria Toro, J. M.; García-Morales, C.; Raducan, M.; Smirnova, E. S.; Echavarren, A. M. *Angew. Chem.* **2017**, *129* (7), 1885.
(27) Bowring, M. A.; Bergman, R. G.; Tilley, T. D. *Organometallics* **2011**, *30* (6), 1295.
(28) Rosenfeld, D. C.; Shekhar, S.; Takemiya, A.; Utsunomiya, M.; Hartwig, J. F. *Org. Lett.* **2006**, *8* (19), 4179.
(29) Oliver-Meseguer, J.; Cabrero-Antonino, J. R.; Domínguez, I.; Leyva-Pérez, A.; Corma, A. *Science* **2012**, *338* (6113), 1452.
(30) Hashmi, A. S. K.; Blanco, M. C.; Fischer, D.; Bats, J. W. *Eur. J. Org. Chem.* **2006**, *2006* (6), 1387.

(31) Wegner, H. A.; Auzias, M. *Angew. Chem. Int. Ed.* **2011**, *50* (36), 8236.
(32) Hopkinson, M. N.; Gee, A. D.; Gouverneur, V. *Chem. – Eur. J.* **2011**, *17* (30), 8248.
(33) Joost, M.; Amgoune, A.; Bourissou, D. *Angew. Chem. Int. Ed.* **2015**, *54* (50), 15022.
(34) Hartwig, J. F. *Organotransition Metal Chemistry: From Bonding to Catalysis*; University Science Books, 2010.
(35) Manthey, D. *Orbital Viewer*; http://www.orbitals.com/orb/ov.htm.
(36) Carvajal, M. A.; Novoa, J. J.; Alvarez, S. *J. Am. Chem. Soc.* **2004**, *126* (5), 1465.
(37) Kulawiec, R. J.; Crabtree, R. H. *Coord. Chem. Rev.* **1990**, *99*, 89.
(38) Senn, H. M.; Ziegler, T. *Organometallics* **2004**, *23* (12), 2980.
(39) Shiotani, A.; Schmidbaur, H. *J. Organomet. Chem.* **1972**, *37* (1), C24.
(40) Tamaki, A.; Kochi, J. K. *J. Organomet. Chem.* **1972**, *40* (2), C81.
(41) Johnson, A.; Puddephatt, R. J. *Inorg. Nucl. Chem. Lett.* **1973**, *9* (11), 1175.
(42) Tamaki, A.; Kochi, J. K. *J. Organomet. Chem.* **1974**, *64* (3), 411.
(43) Johnson, A.; Puddephatt, R. J. *J. Organomet. Chem.* **1975**, *85* (1), 115.
(44) Tamaki, A.; Kochi, J. K. *J. Organomet. Chem.* **1973**, *51*, C39.
(45) Tamaki, A.; Kochi, J. K. *J Chem Soc Dalton Trans* **1973**, No. 23, 2620.
(46) Rice, G. W.; Tobias, R. S. *Inorg. Chem.* **1975**, *14* (10), 2402.
(47) Rice, G. W.; Tobias, R. S. *Inorg. Chem.* **1976**, *15* (2), 489.
(48) Komiya, S.; Albright, T. A.; Hoffmann, R.; Kochi, J. K. *J. Am. Chem. Soc.* **1977**, *99* (26), 8440.
(49) Kochi, J. K. *Organometallic Mechanisms and Catalysis*; Academic Press: New York, NY, 1978.
(50) Schuster, O.; Schmidbaur, H. *Inorganica Chim. Acta* **2006**, *359* (11), 3769.
(51) Robinson, P. S. D.; Khairallah, G. N.; da Silva, G.; Lioe, H.; O'Hair, R. A. J. *Angew. Chem. Int. Ed.* **2012**, *51* (16), 3812.
(52) Corma, A.; Juarez, R.; Boronat, M.; Sanchez, F.; Iglesias, M.; Garcia, H. *Chem Commun* **2011**, *47* (5), 1446.
(53) Gambarotta, S.; Floriani, C.; Chiesi-Villa, A.; Guastini, C. *J Chem Soc Chem Commun* **1983**, No. 22, 1304.
(54) Wu, C.-Y.; Horibe, T.; Jacobsen, C. B.; Toste, F. D. *Nature* **2015**, *517* (7535), 449.
(55) Wu, C.-Y., Toste, F.D. *Unpublished Results*.
(56) Livendahl, M.; Goehry, C.; Maseras, F.; Echavarren, A. M. *Chem Commun* **2014**, *50* (13), 1533.
(57) Hashmi, A. S. K.; Lothschütz, C.; Döpp, R.; Ackermann, M.; De Buck Becker, J.; Rudolph, M.; Scholz, C.; Rominger, F. *Adv. Synth. Catal.* **2012**, *354* (1), 133.
(58) Guenther, J.; Mallet-Ladeira, S.; Estevez, L.; Miqueu, K.; Amgoune, A.; Bourissou, D. *J. Am. Chem. Soc.* **2014**, *136* (5), 1778.
(59) Serra, J.; Parella, T.; Ribas, X. *Chem Sci* **2017**, *8* (2), 946.
(60) Partyka, D. V.; Updegraff III, J. B.; Zeller, M.; Hunter, A. D.; Gray, T. G. *Dalton Trans.* **2010**, *39* (22), 5388.
(61) Besenyei, G.; Bitter, I.; Párkányi, L.; Szalontai, G.; Baranyai, P.; Kunsági-Máté, É.; Faigl, F.; Grün, A.; Kubinyi, M. *Polyhedron* **2013**, *55*, 57.
(62) Joost, M.; Zeineddine, A.; Estévez, L.; Mallet−Ladeira, S.; Miqueu, K.; Amgoune, A.; Bourissou, D. *J. Am. Chem. Soc.* **2014**.
(63) Joost, M.; Estévez, L.; Miqueu, K.; Amgoune, A.; Bourissou, D. *Angew. Chem. Int. Ed.* **2015**, *54* (17), 5236.

(64) Kleinhans, G.; Hansmann, M. M.; Guisado-Barrios, G.; Liles, D. C.; Bertrand, G.; Bezuidenhout, D. I. *J. Am. Chem. Soc.* **2016**, *138* (49), 15873.
(65) Schmidbaur, H. *Gold Bull.* **2000**, *33* (1), 3.
(66) Schmidbaur, H.; Schier, A. *Chem Soc Rev* **2008**, *37* (9), 1931.
(67) Fackler, J. P. *Polyhedron* **1997**, *16* (1), 1.
(68) Murray, H. H.; Fackler, J. P. *Inorganica Chim. Acta* **1986**, *115* (2), 207.
(69) Laguna, A.; Laguna, M. *Coord. Chem. Rev.* **1999**, *193–195*, 837.
(70) Murray, H. H.; Fackler Jr., J. P.; Mazany, A. M.; Porter, L. C.; Shain, J.; Falvello, L. R. *Inorganica Chim. Acta* **1986**, *114* (2), 171.
(71) Fackler, J. P.; Basil, J. D. *Organometallics* **1982**, *1* (6), 871.
(72) Fackler, J. P.; Murray, H. H.; Basil, J. D. *Organometallics* **1984**, *3* (5), 821.
(73) Basil, J. D.; Murray, H. H.; Fackler, J. P.; Tocher, J.; Mazany, A. M.; Trzcinska-Bancroft, B.; Knachel, H.; Dudis, D.; Delord, T. J.; Marler, D. *J. Am. Chem. Soc.* **1985**, *107* (24), 6908.
(74) Uson, R.; Laguna, A.; Laguna, M.; Fraile, M. N.; Jones, P. G.; Sheldrick, G. M. *J Chem Soc Dalton Trans* **1986**, No. 2, 291.
(75) Laguna, A.; Laguna, M.; Jiménez, J.; Lahoz, F. J.; Olmos, E. *J. Organomet. Chem.* **1992**, *435* (1), 235.
(76) Bennett, M. A.; Hockless, D. C. R.; Rae, A. D.; Welling, L. L.; Willis, A. C. *Organometallics* **2001**, *20* (1), 79.
(77) Wolf, W. J.; Winston, M. S.; Toste, F. D. *Nat. Chem.* **2014**, *6* (2), 159.
(78) Powers, D. C.; Lee, E.; Ariafard, A.; Sanford, M. S.; Yates, B. F.; Canty, A. J.; Ritter, T. *J. Am. Chem. Soc.* **2012**, *134* (29), 12002.
(79) Winston, M. S.; Wolf, W. J.; Toste, F. D. *J. Am. Chem. Soc.* **2014**, *136* (21), 7777.
(80) Stiegman, A. E.; Tyler, D. R. *Comments Inorg. Chem.* **1986**, *5* (5), 215.
(81) Shu, X.; Zhang, M.; He, Y.; Frei, H.; Toste, F. D. *J. Am. Chem. Soc.* **2014**, *136* (16), 5844.
(82) Sahoo, B.; Hopkinson, M. N.; Glorius, F. *J. Am. Chem. Soc.* **2013**, *135* (15), 5505.
(83) Hopkinson, M. N.; Sahoo, B.; Glorius, F. *Adv. Synth. Catal.* **2014**, *356* (13), 2794.
(84) Tlahuext-Aca, A.; Hopkinson, M. N.; Garza-Sanchez, R. A.; Glorius, F. *Chem. – Eur. J.* **2016**, n/a.
(85) Tlahuext-Aca, A.; Hopkinson, M. N.; Sahoo, B.; Glorius, F. *Chem Sci* **2016**, *7* (1), 89.
(86) Um, J.; Yun, H.; Shin, S. *Org. Lett.* **2016**, *18* (3), 484.
(87) Kim, S.; Rojas-Martin, J.; Toste, F. D. *Chem Sci* **2016**, *7* (1), 85.
(88) Patil, D. V.; Yun, H.; Shin, S. *Adv. Synth. Catal.* **2015**, *357* (12), 2622.
(89) He, Y.; Wu, H.; Toste, F. D. *Chem Sci* **2015**, *6* (2), 1194.
(90) Huang, L.; Rominger, F.; Rudolph, M.; Hashmi, A. S. K. *Chem Commun* **2016**, *52* (38), 6435.
(91) Tlahuext-Aca, A.; Hopkinson, M. N.; Daniliuc, C. G.; Glorius, F. *Chem. – Eur. J.* **2016**, *22* (33), 11587.
(92) Asomoza-Solis, E. O.; Rojas-Ocampo, J.; Toscano, R. A.; Porcel, S. *Chem Commun* **2016**, *52* (45), 7295.
(93) Low, J. J.; Goddard, W. A. *J. Am. Chem. Soc.* **1984**, *106* (26), 8321.
(94) Low, J. J.; Goddard, W. A. *J. Am. Chem. Soc.* **1986**, *108* (20), 6115.
(95) Evitt, E. R.; Bergman, R. G. *J. Am. Chem. Soc.* **1980**, *102* (23), 7003.

(96) García-Monforte, M. A.; Martínez-Salvador, S.; Menjón, B. *Eur. J. Inorg. Chem.* **2012**, *2012* (31), 4945.
(97) Roşca, D.-A.; Fernandez-Cestau, J.; Morris, J.; Wright, J. A.; Bochmann, M. *Sci. Adv.* **2015**, *1* (9).
(98) Albright, T. A.; Burdett, J. K.; Whangbo, M. H. *Orbital Interactions in Chemistry*; Wiley and Sons, Inc.: New York, NY, 1985.
(99) Tatsumi, K.; Hoffmann, R.; Yamamoto, A.; Stille, J. K. *Bull. Chem. Soc. Jpn.* **1981**, *54* (6), 1857.
(100) Tamaki, A.; Magennis, S. A.; Kochi, J. K. *J. Am. Chem. Soc.* **1974**, *96* (19), 6140.
(101) Komiya, S.; Albright, T. A.; Hoffmann, R.; Kochi, J. K. *J. Am. Chem. Soc.* **1976**, *98* (23), 7255.
(102) Komiya, S.; Kochi, J. K. *J. Am. Chem. Soc.* **1976**, *98* (24), 7599.
(103) Lawrence Kuch, P.; Stuart Tobias, R. *J. Organomet. Chem.* **1976**, *122* (3), 429.
(104) Coates, G. E.; Parkin, C. *J Chem Soc* **1963**, No. 0, 421.
(105) Komiya, S.; Ozaki, S.; Shibue, A. *J. Chem. Soc. Chem. Commun.* **1986**, No. 20, 1555.
(106) Rekhroukh, F.; Estevez, L.; Mallet-Ladeira, S.; Miqueu, K.; Amgoune, A.; Bourissou, D. *J. Am. Chem. Soc.* **2016**, *138* (36), 11920.
(107) Rekhroukh, F.; Estévez, L.; Bijani, C.; Miqueu, K.; Amgoune, A.; Bourissou, D. *Angew. Chem. Int. Ed.* **2016**, *55* (10), 3414.
(108) Note that the nonzero rate at "infinite" iodide concentration suggests a second mechanism independent of iodide, which may involve phosphine dissociation or direct reductive elimination. Addition of $PMe_3$ to complex **33** results in the formation of bis(phosphine)dimethyl gold cation, complicating the analysis of this second mechanism.
(109) Goldberg, K. I.; Yan, J.; Breitung, E. M. *J. Am. Chem. Soc.* **1995**, *117* (26), 6889.
(110) Komiya, S.; Shibue, A. *Organometallics* **1985**, *4* (4), 684.
(111) Mankad, N. P.; Toste, F. D. *J. Am. Chem. Soc.* **2010**, *132* (37), 12859.
(112) Kumar, R.; Linden, A.; Nevado, C. *J. Am. Chem. Soc.* **2016**, *138* (42), 13790.
(113) Tkatchouk, E.; Mankad, N. P.; Benitez, D.; Goddard, W. A.; Toste, F. D. *J. Am. Chem. Soc.* **2011**, *133* (36), 14293.
(114) Schuster, O.; Liau, R.-Y.; Schier, A.; Schmidbaur, H. *Inorganica Chim. Acta* **2005**, *358* (5), 1429.
(115) Vicente, J.; Dolores Bermudez, M.; Escribano, J. *Organometallics* **1991**, *10* (9), 3380.
(116) It is possible for rate-limiting phosphine or halide dissociation to be operative but such a scenario is unlikely given the high barrier to phosphine dissociation seen in the trimethylgold system. It likewise seems unlikely that halide dissociation from Au(III) is substantially more facile from aryl vs. alkyl substituted complexes.
(117) Shekhar, S.; Hartwig, J. F. *J. Am. Chem. Soc.* **2004**, *126* (40), 13016.
(118) Corrie, T. J. A.; Ball, L. T.; Russell, C. A.; Lloyd-Jones, G. C. *J. Am. Chem. Soc.* **2017**, *139* (1), 245.
(119) Fuchita, Y.; Utsunomiya, Y.; Yasutake, M. *J Chem Soc Dalton Trans* **2001**, No. 16, 2330.
(120) Hofer, M.; Nevado, C. *Tetrahedron Young Investig. Award 2013 Dev. Appl. Transit. Met.-Catalyzed Bond-Form. React. Melanie Sanford* **2013**, *69* (27–28), 5751.
(121) Cambeiro, X. C.; Boorman, T. C.; Lu, P.; Larrosa, I. *Angew. Chem. Int. Ed.* **2013**, *52* (6), 1781.

(122) Winston, M. S.; Wolf, W. J.; Toste, F. D. *J. Am. Chem. Soc.* **2015**, *137* (24), 7921.
(123) Schuster, O.; Schmidbaur, H. *Organometallics* **2005**, *24* (10), 2289.
(124) Lauterbach, T.; Livendahl, M.; Rosellón, A.; Espinet, P.; Echavarren, A. M. *Org. Lett.* **2010**, *12* (13), 3006.
(125) Vaughan, L. G.; Sheppard, W. A. *J. Organomet. Chem.* **1970**, *22* (3), 739.
(126) Hofer, M.; Gomez-Bengoa, E.; Nevado, C. *Organometallics* **2014**, *33* (6), 1328.
(127) Nijamudheen, A.; Karmakar, S.; Datta, A. *Chem. – Eur. J.* **2014**, *20* (45), 14650.
(128) DiCosimo, R.; Moore, S. S.; Sowinski, A. F.; Whitesides, G. M. *J. Am. Chem. Soc.* **1982**, *104* (1), 124.
(129) Foley, P.; DiCosimo, R.; Whitesides, G. M. *J. Am. Chem. Soc.* **1980**, *102* (22), 6713.
(130) Hackett, M.; Whitesides, G. M. *Organometallics* **1987**, *6* (2), 403.
(131) McCarthy, T. J.; Nuzzo, R. G.; Whitesides, G. M. *J. Am. Chem. Soc.* **1981**, *103* (12), 3396.
(132) Nuzzo, R. G.; McCarthy, T. J.; Whitesides, G. M. *J. Am. Chem. Soc.* **1981**, *103* (12), 3404.
(133) Gillie, A.; Stille, J. K. *J. Am. Chem. Soc.* **1980**, *102* (15), 4933.
(134) Goldberg, K. I.; Yan, J. Y.; Winter, E. L. *J. Am. Chem. Soc.* **1994**, *116* (4), 1573.
(135) Brown, M. P.; Puddephatt, R. J.; Upton, C. E. E. *J Chem Soc Dalton Trans* **1974**, No. 22, 2457.
(136) Osakada, K.; Onodera, H.; Nishihara, Y. *Organometallics* **2005**, *24* (2), 190.
(137) Adamo, C.; Amatore, C.; Ciofini, I.; Jutand, A.; Lakmini, H. *J. Am. Chem. Soc.* **2006**, *128* (21), 6829.
(138) Cui, L.; Zhang, G.; Zhang, L. *Bioorg. Med. Chem. Lett.* **2009**, *19* (14), 3884.
(139) Peng, Y.; Cui, L.; Zhang, G.; Zhang, L. *J. Am. Chem. Soc.* **2009**, *131* (14), 5062.
(140) Kar, A.; Mangu, N.; Kaiser, H. M.; Beller, M.; Tse, M. K. *Chem Commun* **2008**, No. 3, 386.
(141) Jones, C.; Taube, D.; Ziatdinov, V. R.; Periana, R. A.; Nielsen, R. J.; Oxgaard, J.; Goddard, W. A. *Angew. Chem. Int. Ed.* **2004**, *43* (35), 4626.
(142) Zhang, G.; Peng, Y.; Cui, L.; Zhang, L. *Angew. Chem.* **2009**, *121* (17), 3158.
(143) Roth, K. E.; Blum, S. A. *Organometallics* **2010**, *29* (7), 1712.
(144) LaLonde, R. L.; Brenzovich, Jr., W. E.; Benitez, D.; Tkatchouk, E.; Kelley, K.; Goddard, III, W. A.; Toste, F. D. *Chem Sci* **2010**, *1* (2), 226.
(145) Brenzovich, W. E.; Benitez, D.; Lackner, A. D.; Shunatona, H. P.; Tkatchouk, E.; Goddard, W. A.; Toste, F. D. *Angew. Chem. Int. Ed.* **2010**, *49* (32), 5519.
(146) Melhado, A. D.; Brenzovich, W. E.; Lackner, A. D.; Toste, F. D. *J. Am. Chem. Soc.* **2010**, *132* (26), 8885.
(147) Zhang, G.; Cui, L.; Wang, Y.; Zhang, L. *J. Am. Chem. Soc.* **2010**, *132* (5), 1474.
(148) Ball, L. T.; Green, M.; Lloyd-Jones, G. C.; Russell, C. A. *Org. Lett.* **2010**, *12* (21), 4724.
(149) Brenzovich, W. E.; Brazeau, J.-F.; Toste, F. D. *Org. Lett.* **2010**, *12* (21), 4728.
(150) Ball, L. T.; Lloyd-Jones, G. C.; Russell, C. A. *Chem. – Eur. J.* **2012**, *18* (10), 2931.
(151) Hopkinson, M. N.; Tessier, A.; Salisbury, A.; Giuffredi, G. T.; Combettes, L. E.; Gee, A. D.; Gouverneur, V. *Chem. – Eur. J.* **2010**, *16* (16), 4739.
(152) Zhang, G.; Luo, Y.; Wang, Y.; Zhang, L. *Angew. Chem.* **2011**, *123* (19), 4542.
(153) Zhang, R.; Xu, Q.; Chen, K.; Gu, P.; Shi, M. *Eur. J. Org. Chem.* **2013**, *2013* (32), 7366.

(154) Wolf, W. J. Studies on the Organometallic Reactivity of Gold(III). Doctoral Dissertation, University of California, Berkeley: Berkeley, California, 2016.
(155) Ball, L. T.; Lloyd-Jones, G. C.; Russell, C. A. *Science* **2012**, *337* (6102), 1644.
(156) Ball, L. T.; Lloyd-Jones, G. C.; Russell, C. A. *J. Am. Chem. Soc.* **2014**, *136* (1), 254.
(157) Cresswell, A. J.; Lloyd-Jones, G. C. *Chem. – Eur. J.* **2016**, *22* (36), 12641.
(158) Marchetti, L.; Kantak, A.; Davis, R.; DeBoef, B. *Org. Lett.* **2015**, *17* (2), 358.
(159) Wu, Q.; Du, C.; Huang, Y.; Long, Z.; Liu, X.; Song, F.; You, J. *Chem. Sci.* **2014**.
(160) Leyva-Pérez, A.; Doménech, A.; Al-Resayes, S. I.; Corma, A. *ACS Catal.* **2012**, *2* (1), 121.
(161) Cambeiro, X. C.; Ahlsten, N.; Larrosa, I. *J. Am. Chem. Soc.* **2015**, *137* (50), 15636.
(162) Qian, D.; Zhang, J. *Beilstein J. Org. Chem.* **2011**, *7*, 808.
(163) Peng, H.; Xi, Y.; Ronaghi, N.; Dong, B.; Akhmedov, N. G.; Shi, X. *J. Am. Chem. Soc.* **2014**, *136* (38), 13174.
(164) Ma, Y.; Zhang, S.; Yang, S.; Song, F.; You, J. *Angew. Chem. Int. Ed.* **2014**, *53* (30), 7870.
(165) Hopkinson, M. N.; Ross, J. E.; Giuffredi, G. T.; Gee, A. D.; Gouverneur, V. *Org. Lett.* **2010**, *12* (21), 4904.
(166) Hofer, M.; Genoux, A.; Kumar, R.; Nevado, C. *Angew. Chem. Int. Ed.* **2017**, *56* (4), 1021.
(167) Kawai, H.; Wolf, W. J.; DiPasquale, A. G.; Winston, M. S.; Toste, F. D. *J. Am. Chem. Soc.* **2016**, *138* (2), 587.

# Chapter 2

Gold-Catalyzed Allylation of Aryl Boronic Acids

Portions of this chapter have been previously published in:

Levin, M. D.; Toste, F. D. *Angew. Chem. Int. Ed.* **2014**, *53*, 6211-6215.

## 2.1 Preface

Chapter 1 introduced key concepts associated with the redox chemistry of gold, highlighting the challenges associated with and strategies for enabling redox chemistry in both directions (oxidative addition and reductive elimination). The prior development of oxidative gold catalysis utilizing stoichiometric oxidants led us to consider the possibility for cross-coupling reactivity in the absence of such sacrificial additives by a direct oxidative addition of one coupling partner akin to other late-metal catalytic motifs. Our motivating hypothesis was that a bimetallic catalyst would overcome the kinetic barriers to oxidative addition. In examining this hypothesis, we developed among the first successful implementations of a redox cycle in gold catalysis without the use of a sacrificial oxidant.[1] Though the catalytic activity of the discovered reaction was indeed improved by the implementation of a digold complex, the lessons gleaned regarding Au(I)/Au(III) redox catalysis were ultimately more valuable than this demonstration of bimetallic reactivity. In particular, the competitive formation of biphenyl, initially a problematic side reaction, was used as the crux of the mechanistic argument outlined below. This chapter traces the story of that development and the attempts to extend the resulting reaction beyond the initial allylation chemistry, which ultimately pointed towards an underlying weakness that led to the development of work in Chapter 3.

## 2.2 Introduction

The air- and water-stability of gold catalysts, coupled with their ability to promote complex transformations under mild conditions has attracted considerable interest from the academic community.[2] Despite the rapid pace of recent developments, the majority of gold-catalyzed processes rely on a select few reaction manifolds: (i) Lewis acid catalysis, (ii) π-activation, and (iii) the generation of carbenoid intermediates (Figure 2.1).[3–9] While these modes of reactivity have yielded important catalytic methodologies of broad scope and synthetic utility, they are typified by catalytic cycles wherein gold maintains a +1 oxidation state, in stark contrast to the 2-electron redox cycles characteristic of late transition metal catalysis.[10] Indeed, access to $Au^{III}$ intermediates under catalytic conditions typically requires strong $F^+$ or $I^{3+}$ oxidants (See Chapter 1.5).[11–13]

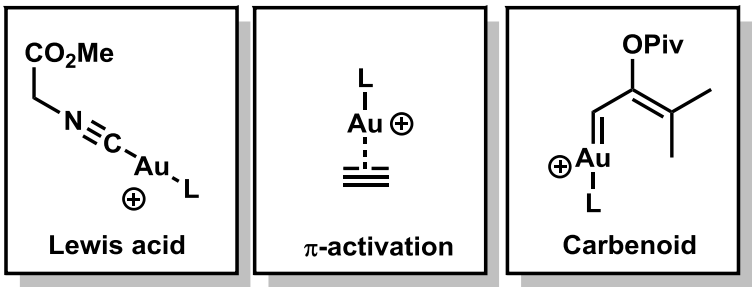


**Figure 2.1** Traditional reactivity manifolds for Au(I) catalysis.

Despite this limitation, seminal work by Kochi, Puddephatt, and Schmidbaur has shown that $Au^I$ complexes oxidatively add alkyl halides, and are further competent to undergo C-C reductive elimination, furnishing formally cross-coupled products (See Chapter 1.3).[14–17] However, despite a wealth of C-C bond-forming gold catalysis, such reactivity has not previously been realized in a catalytic fashion.[18]

A possible barrier to the implementation of such a redox cycle is the slow rate at which alkyl-alkyl reductive elimination occurs.[19–24] Nevertheless, we were encouraged by observations that in contrast, aryl-aryl reductive elimination from $Au^{III}$ is remarkably fast.[25] As such, we hypothesized that a process involving oxidative addition to a gold aryl species followed by C($sp^2$)-C($sp^3$) reductive elimination might prove achievable under the influence of a gold catalyst (Figure 2.2).

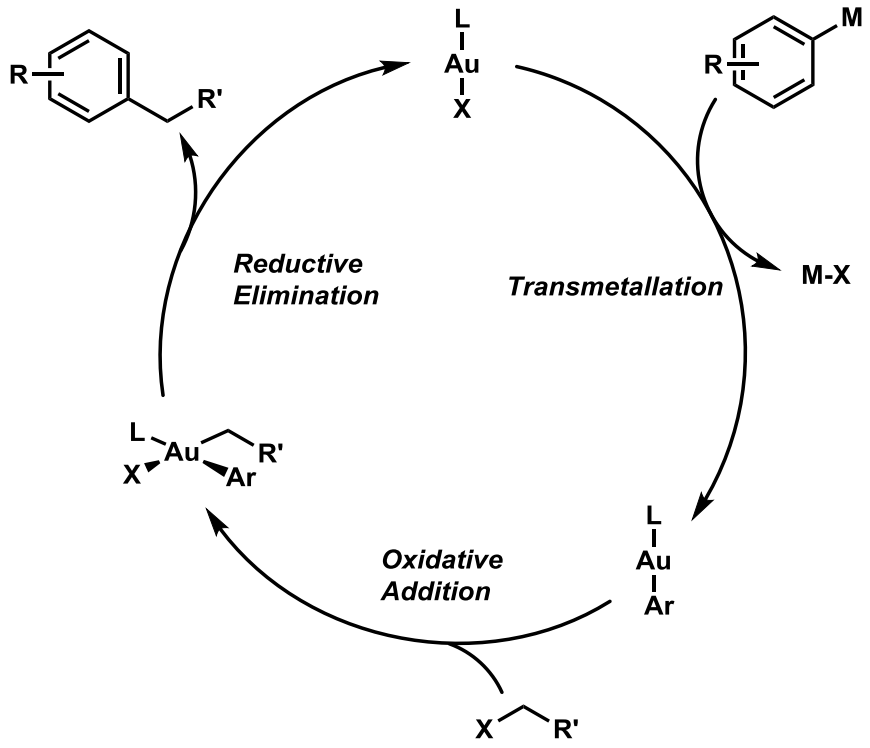


**Figure 2.2** Proposed catalytic cycle for gold-catalyzed cross-coupling

## 2.3 Results

### 2.3.1 Initial Investigation

Based on the above precedent, we suspected that examination of stoichiometric reactivity between isolable arylgold complexes and various alkyl electrophiles might offer a starting point for the development of a catalytic protocol. $Ph_3PAuPh$ (**1**) was prepared and subsequently examined against a survey of coupling partners, revealing that allyl iodide afforded $Ph_3PAuI$ (**2**), allylbenzene (**3a**) and biphenyl (**4a**) over a period of 24 hours at 50°C in acetonitrile solution (Figure 2.3).[26,27]

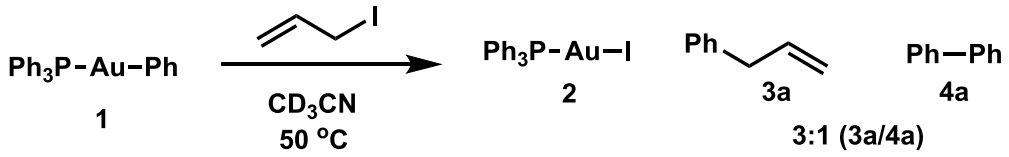


**Figure 2.3** Discovery of stoichiometric C-C coupling between arylgold and allyl iodide. Ratio measured at 60% conversion after 24 hours.

### 2.3.2 Development of a Catalytic Reaction

After examining several classes of aryl nucleophiles, we found that phenylboronic acid (along with cesium carbonate) produced allylbenzene and biphenyl as products when $Ph_3PAuCl$ was used as a catalyst in combination with allyl iodide at 80°C. Subsequent examination of the allylic electrophile revealed that allyl bromide offered superior performance, and that the reaction was more reproducible when conducted at 65°C, presumably due to the volatility of allyl bromide. Under these conditions, $Ph_3PAuCl$ afforded a 36% yield of **3a** accompanied by 10% of **4a** (Table 2.1, entry 1).

Examination of other typical gold catalysts revealed that sterically hindered gold complexes substantially diminished the reactivity (entries 2-4), whereas phosphite ligands were unstable toward hydrolysis under the reaction conditions, preventing their implementation (entry 5). Electronic modification of the phosphine ligand had little effect (entry 6), and increasing the catalyst loading resulted in incommensurate gains in the turnover (entry 11).

In seeking to improve the reaction, we were drawn to the observation that closely linked bimetallic gold complexes undergo accelerated oxidative addition, due to the formation of $Au^{II}$-$Au^{II}$ species (rather than discrete $Au^{III}$) upon oxidation (See Chapter 1.3).[28] While $dppm(AuCl)_2$ showed considerable instability under the reaction conditions, it nonetheless provided some catalytic turnover. However, the related bimetallic complex **5** produced the desired product in an improved 66% yield.[29] Intriguingly, the analogous monometallic aminophosphine complex **6** afforded substantially lower yield (even at 10% loading), suggesting that the bimetallic catalyst architecture is responsible for the activity of **5**, rather than the electronic character of the aminophosphine ligand.[12] However, because monometallic complexes are capable of catalyzing this transformation (albeit with lower efficiency), the influence of the bimetallic catalyst remains to be fully elucidated.

In the absence of allyl bromide (entry 14), neither product was observed, signifying that allyl bromide serves as the oxidant in the homo-coupling process (*vide infra*). Notably, the reaction proceeded with identical efficiency in the presence of air and water.

Several other features of the reaction were examined. They are summarized in Table 2.2 and will be the subject of a more detailed discussion below. The equivalency of allyl bromide was found to be critical for determining the overall conversion and the ratio of **3a** to **4a**, with increasing amounts leading to higher reactivity and selectivity (entries 2-4). With respect to the aromatic nucleophile, Boronic esters were found to be slightly less reactive than the free acids, allowing their implementation for substrates where the free acid is unavailable (entries 5-6). Aryltin nucleophiles were also reactive, but the reactions were substantially less clean, affording aryl halide byproducts alongside other unidentified species (entires 7-8).[30] Tetraarylborates (entry 9) were likewise reactive, but were deemed impractical based on low atom-economy and the high proportion of biaryl formed.[31–33] Various other nucleophiles including arylsilanes, trifluoroborates, and BMIDA esters were found to be unreactive (entries 10-12).[34–36]

**Table 2.1.** Catalyst Optimization

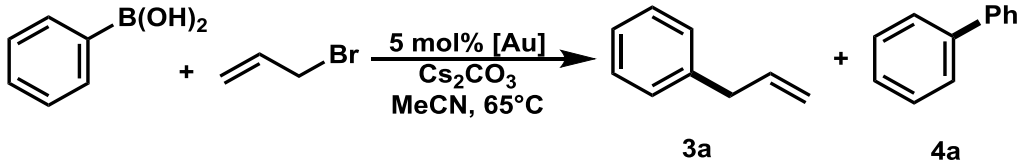


| Entry | Catalyst | Yield **3a** | Yield **4a** | Entry | Catalyst | Yield **3a** | Yield **4a** |
|---|---|---|---|---|---|---|---|
| 1 | $Ph_3PAuCl$ | 36% | 10% | 8 | **5** | 66% | 9% |
| 2 | IPrAuCl | 1% | 0% | 9 | **6** | 16% | 7% |
| 3 | $tBu_3PAuCl$ | 5% | 6% | 10[a] | **6** | 17% | 9% |
| 4 | (Johnphos)AuCl | 11% | 3% | 11[a] | $Ph_3PAuCl$ | 41% | 15% |
| 5 | $(PhO)_3PAuCl$ | 1% | 0% | 12 | IPrAuOH | 5% | 0% |
| 6 | $(pOMePh)_3PAuCl$ | 31% | 6% | 13 | None | 0% | 0% |
| 7 | $dppm(AuCl)_2$ | 24% | 14% | 14[b] | **5** | 0% | 0% |

Conditions: 4 equiv halide, 3 equiv base, 0.2 M, 18 hrs, Calibrated GC Yields vs. $PhCO_2Et$ as an internal standard. [a] 10 mol% catalyst [b] No allyl bromide added;

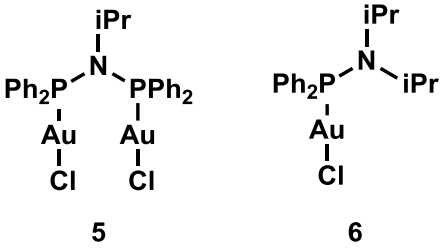


For the allylic electrophile, allyl iodide, bromide, and chloride were each found to be reactive, with the bromide offering the best results (entries 13-15). The reactivity of the allylic chlorides could be improved somewhat by increasing the reaction temperature. Many other classes of electrophile were found not to be reactive, including allyl phosphonates, sulfonates, and esters, as well as typical radical nucleofuges such as allyl xanthates (entries 16-19).[37] The reaction did not proceed at a substantial rate at room temperature, though this is complicated by the low solubility of most gold complexes in acetonitrile at this temperature (entry 20).

Acetonitrile was found to be a uniquely suitable solvent for the reaction, with other typical solvents affording little to no reactivity (entries 21, 23). Methanol and other alcohols were found to give good conversion but with much lower selectivity for the desired cross product (entries 22, 24). Addition of tetrabutylammonium bromide to the reaction substantially inhibited reactivity (entry 25). In a related finding, homogeneous bases (trialkylamines) were found to provide substantially lower conversion than heterogeneous ones, though in some cases

this could be restored by the addition of soluble sodium salts, with concomitant precipitation of sodium bromide as the reaction proceeded (entries 26-30).

**Table 2.2** Effect of selected changes to reaction conditions on the reaction outcome

| Entry | Deviation from Standard Conditions | Yield **3a** | Yield **4a** | Entry | Deviation from Standard Conditions | Yield **3a** | Yield **4a** |
|---|---|---|---|---|---|---|---|
| 1 | None | 66% | 9% | 16[b] | Allyl diethyl phosphonate | 0% | 0% |
| 2 | 1 equiv allyl bromide | 16% | 18% | 17[b] | Allyl mesylate | 0% | 0% |
| 3 | 2 equiv allyl bromide | 37% | 11% | 18[b] | Allyl Acetate | 0% | 0% |
| 4 | 10 equiv allyl bromide | 71% | 7% | 19[b] | Allyl Ethyl Xanthate | 0% | 0% |
| 5[a] | PhBPin | 47% | 10% | 20[d] | 25 $^{o}$C | 10% | 5% |
| 6[a] | PhBNeop | 62% | 9% | 21[e] | THF solvent | 5% | 1% |
| 7[a,c] | $PhSnMe_3$ | 33% | 12% | 22[e] | MeOH solvent | 34% | 25% |
| 8[a,c] | $PhSnBu_3$ | 35% | 15% | 23[e] | $CHCl_3$ solvent | 8% | 5% |
| 9[a] | Na $Ph_4B$ | 29% | 30% | 24[e] | 5:1 MeCN/ MeOH solvent | 42% | 21% |
| 10[a] | $PhSiMe_3$ | 0% | 0% | 25 | + 1 equiv $Bu_4N$ Br | 10% | 3% |
| 11[a] | $PhBF_3K$ | 0% | 0% | 26[f] | $K_2CO_3$ | 44% | 5% |
| 12[a] | PhBMIDA | 0% | 0% | 27[f] | $Et_3N$ | 3% | 1% |
| 13[b] | Allyl iodide | 23% | 6% | 28[f] | DIPEA | 12% | 3% |
| 14[b] | Allyl chloride | 5% | 1% | 29[f] | N-MeTMP | 29% | 5% |
| 15[b,g] | Allyl chloride at 80 $^{o}$C | 21% | 5% | 30[f] | N-MeTMP + 1 equiv $NaBF_4$ | 65% | 10% |

See Table 1 for Standard Conditions. Calbrated GC yields vs $PhCO_2Et$ as an internal standard. [a] instead of $PhB(OH)_2$, [b] instead of allyl bromide, [c] No $Cs_2CO_3$ added, [d] instead of at 65 $^{o}$C, [e] instead of MeCN [f] instead of $Cs_2CO_3$ [g] irreproducible due to volatility

### 2.3.3 Scope, Chemoselectivity, and Orthogonality

Figure 2.4 illustrates the scope of the boronic acid component. While highly basic or nucleophilic functionality was not tolerated, many heteroaromatic boronic acids were coupled smoothly (**3j**, **3k**). Of note, substrates bearing *aryl* halide moieties reacted with complete chemoselectivity for the external allylic halide (**3m**), showcasing the discrimination inherent in the $S_N2$-type oxidative addition typically observed with $Au^I$ (See Chapter 1.3). Interestingly, sterically encumbering substituents were found to *facilitate* the reaction (compare **3f**, **3g**, **3h**). This effect ostensibly arises because the ortho substituents block the formation of homo-coupling side-products. Electron-rich boronic acids are better tolerated than electron poor analogues, a trend that mirrors the efficiency of transmetallation previously observed.[26,27,38–40]

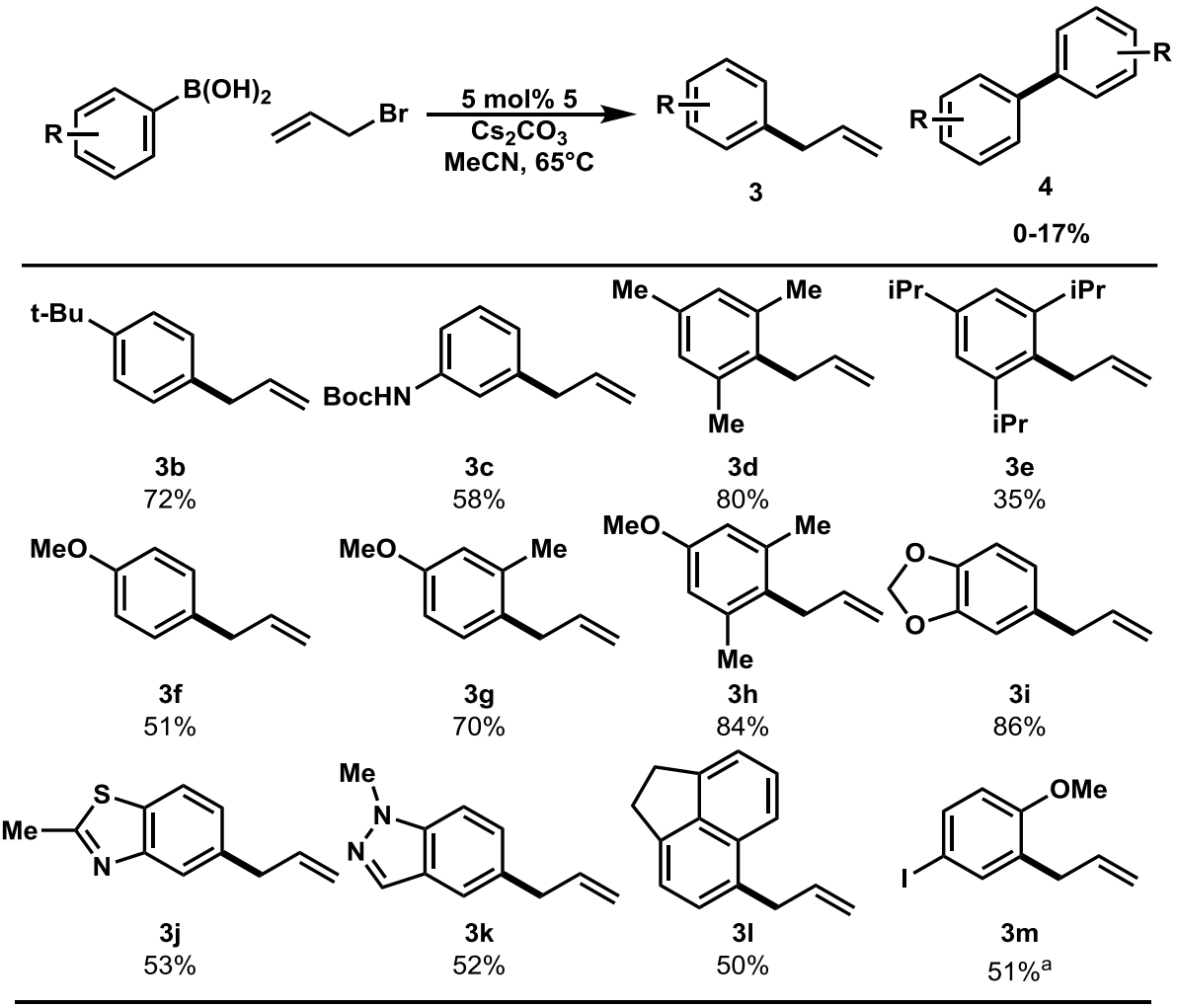


**Figure 2.4.** Arylboronic acid scope. Conditions: 4 equiv. halide, 3 equiv base, 0.2 M, 18 hrs. Isolated yields. Bolded lines represent the newly formed bonds. [a] 10 mol% catalyst.

The beneficial effect of sterics led us to examine the scope of the allylic electrophile with mesityl boronic acid, an otherwise challenging cross-coupling substrate (Figure 2.5). This effect is further exhibited in products **7f-7i**. In all cases, starting from the linear allylic bromides, only linear products were observed. The origin of this regioselectivity is not known.[10] Palladium

catalyzed allylic substitution typically affords linear products, whereas molybdenum, tungsten, and iridium afford branched products selectively.[41–43] Copper, on the other hand, affords products of formal $S_N2'$ substitution, with regiochemistry dictated by the starting material.[44] In each of these cases, though explanations have been offered, a complete understanding of the preferences of each metal remains lacking. The stereochemical erosion of crotyl bromide is an unusual feature; crotyl bromide is known to undergo thermal isomerization *via* the branched isomer, as are allylgold(III) complexes, so whether this occurs before or after oxidative addition is unknown.[45–49]

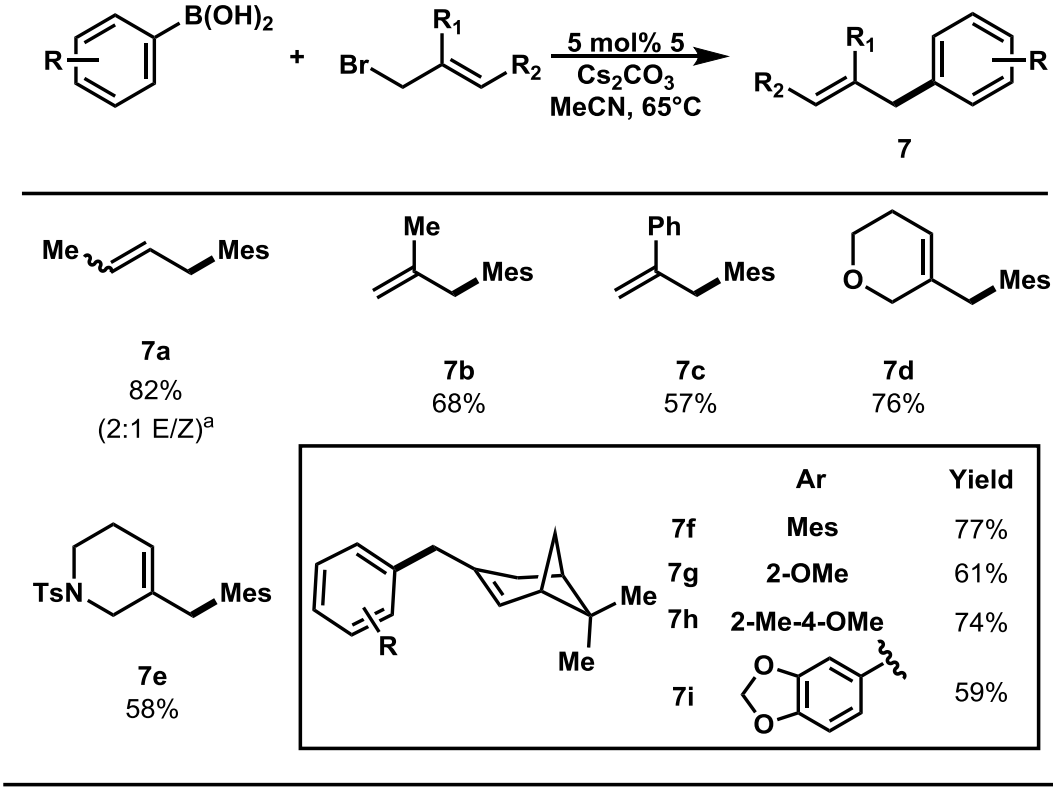


**Figure 2.5.** Allylic Bromide Scope. Conditions: 4 equiv. halide, 3 equiv. base, 0.2M, 18 hrs, isolated yields, starting from linear allylic bromide. No biaryl detected for any entry except **7i**. Bolded lines represent the newly formed bonds. [a] Starting from 5:1 E/Z crotyl bromide..

The orthogonality of this method to traditional cross-coupling reactions allows the chemoselective preparation of polyfunctionalized products (Figure 2.6). While gold and palladium catalysts are both capable of producing **7j**, our gold-catalyzed protocol provided higher efficiency and chemoselectivity, allowing access to bifunctionalized products such as **8**. Palladium catalysts, including one bearing the same ligand as in **5**, afforded lower yields under the same conditions while additionally forming the over-coupled product **9** in varying yields. No **9** was detected when **5** was employed as a catalyst.

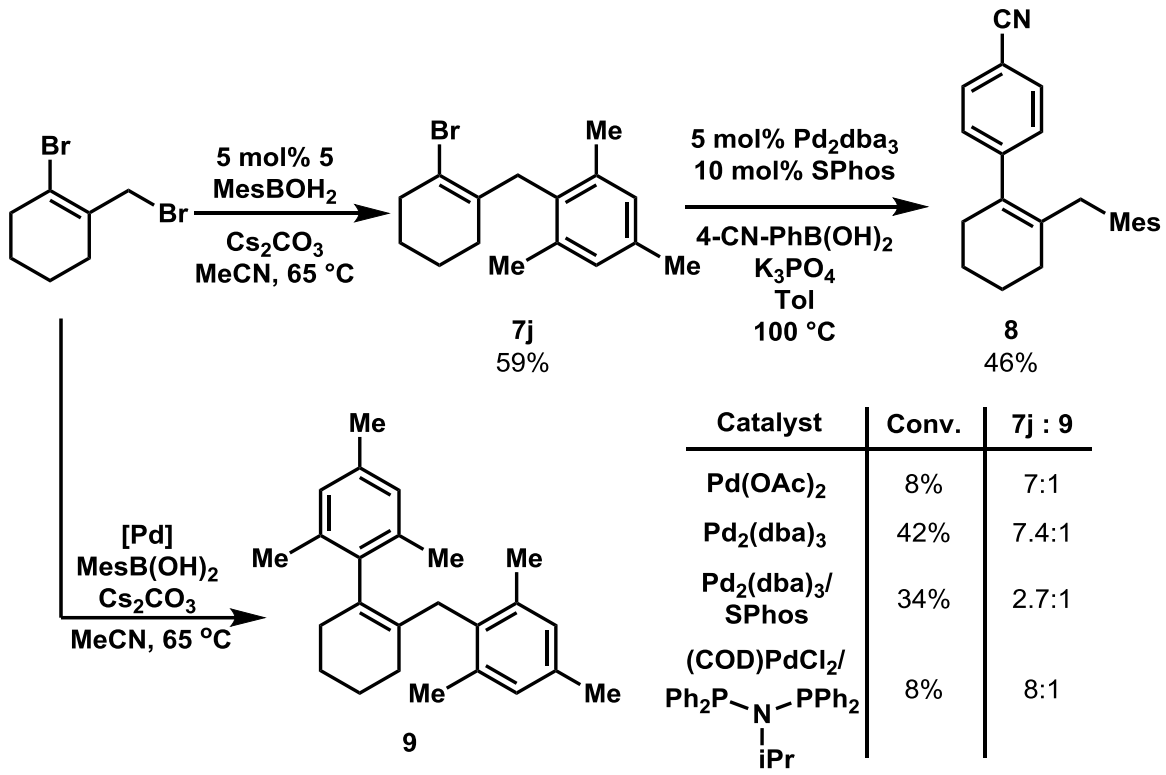


**Figure 2.6** Chemoselective iterative cross-coupling of allylic and vinylic bromides by gold and palladium, with comparisons to palladium catalysts

Furthermore, **3n**, which bears an aryl iodide moiety, can be prepared without competitive cyclization or oligomerization from boronic acid **10**. Palladium acetate, by comparison, afforded a lower yield, even in the presence of phosphine ligands.[50]

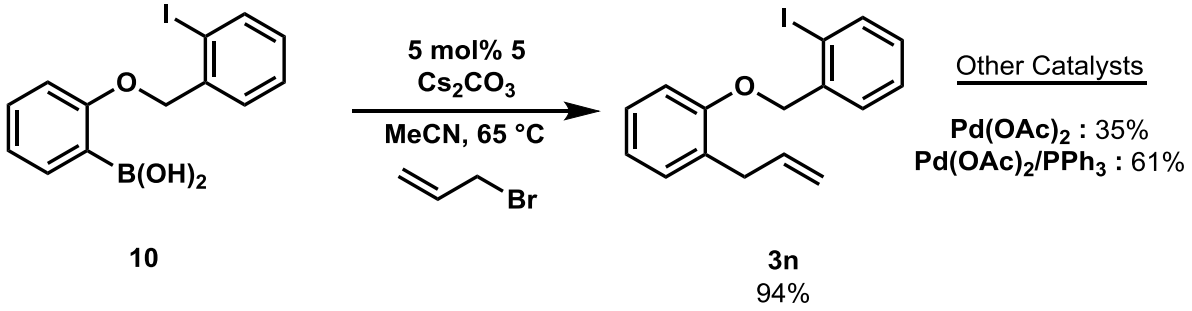


**Figure 2.7** Chemoselective cross-coupling in the presence of an aryl iodide. 5 mol% of $Pd(OAc)_2$ and 10 mol% of $PPh_3$ were employed for the indicated reactions.

### 2.3.4 Mechanistic Experiments

Having developed this method, we sought to better understand the mechanism of the overall transformation. In initial stoichiometric experiments (Figure 2.8), we found that while **5** underwent halide metathesis upon reaction with allyl bromide, no oxidized species were detected. Such halogen-exchange reactions have previously been observed with binuclear Au(I) complexes, *via* reversible oxidative addition.[51,52] Nonetheless, the gold aryl complex **11** was

formed cleanly *via* transmetallation from the boronic acid under the reaction conditions. Futhermore, **11** underwent facile conversion in reaction with allyl bromide to give the dibromide **12**, affording allylbenzene and biphenyl. These experiments suggest a mechanism for the catalytic process in which transmetallation to gold precedes oxidative addition (*vide infra).*

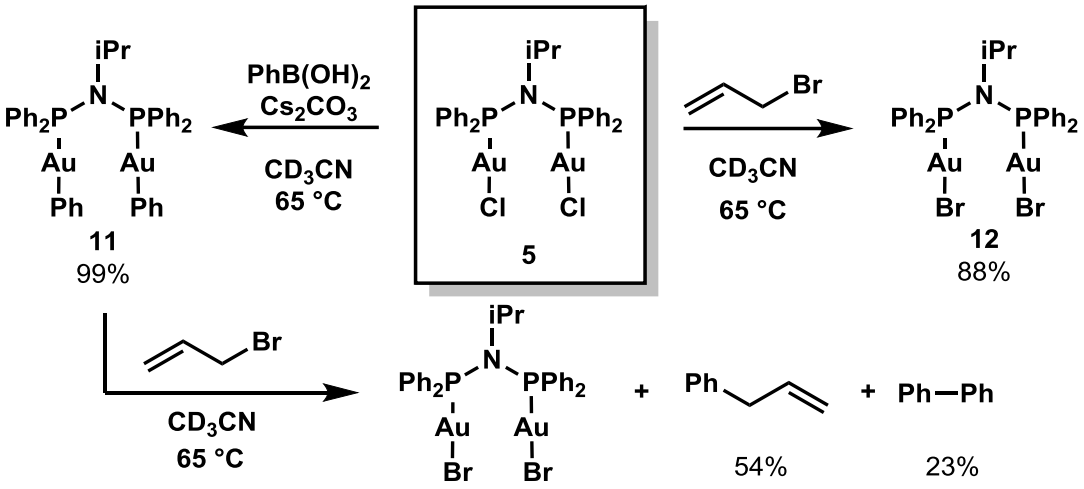


**Figure 2.8** Stoichiometric reactivity of **5** under catalytically relevant conditions

While a number of mechanisms can be proposed for the formation of the desired allylbenzene product from the gold aryl **11**, fewer mechanisms can account for the formation of biaryl. Because alternatives to the oxidative addition/reductive elimination process almost invariably necessitate distinct pathways to cross- and homo-coupled products, examination of potential homo-coupling processes can be used to discern between possible mechanistic scenarios (Figure 2.9).

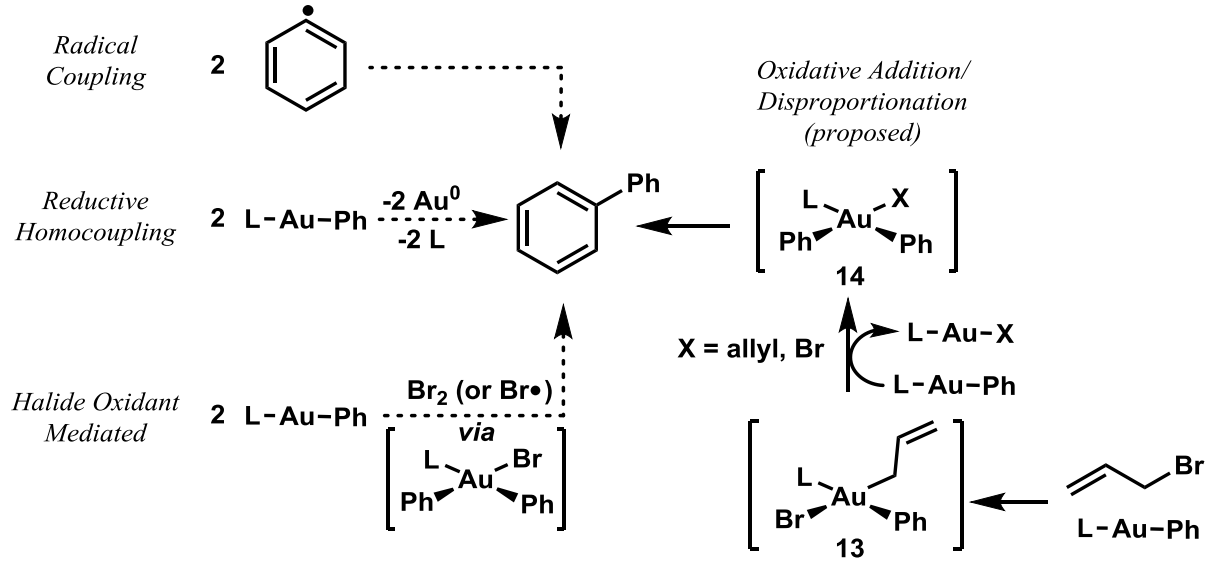


**Figure 2.9** Potential Mechanisms for biaryl formation.

Namely, homocoupling of $PhB(OH)_2$ is a net oxidative process, requiring an oxidant. Three likely mechanisms for biaryl formation *via* a process not involving oxidative addition to allyl bromide were considered. First, radical generation by any number of pathways (oxidant agnostic) could lead to the formation of phenyl radical, which could subsequently undergo radical homocoupling. A radical clock experiment was conducted to ascertain the viability of this pathway (Figure 2.10), and the lack of any observable cyclized products argues against the implication of aryl radicals.[53] Addition of 9,10-dihydroanthracene likewise does not affect the observed product distribution.

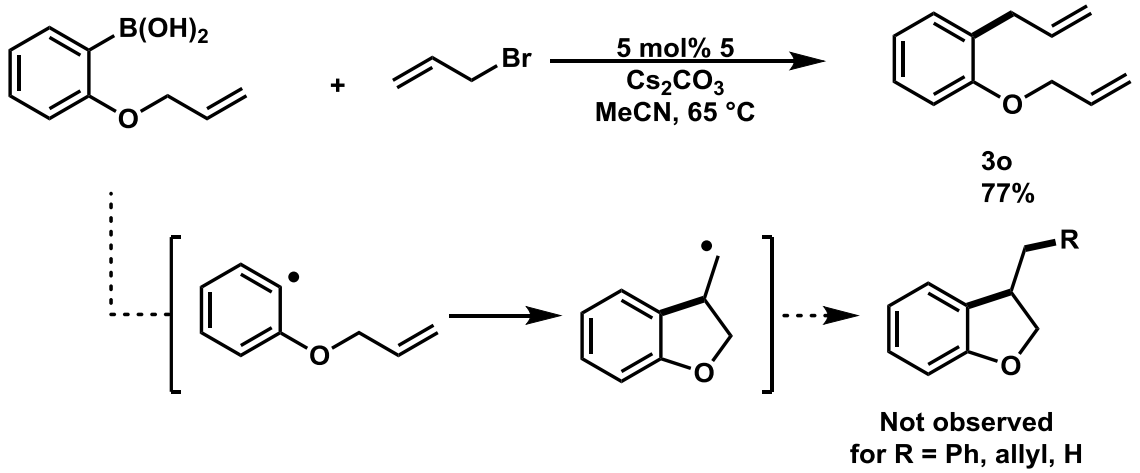


**Figure 2.10** Radical clock experiment for the intermediacy of aryl radicals

Gold(I) alkyl complexes are known to undergo spontaneous homocoupling to afford dimerized alkane and Au(0) by a process which involves phosphine ligand dissociation.[54] However, **11** is stable to heating at 80°C in acetonitrile for 24 hours, with no observed biaryl formation (Figure 2.11). Likewise, under catalytic conditions, omission of allyl bromide affords no biaryl (Table 2.1, entry 14). These experiments argue against the intermediacy of Au(I) homocoupling in the formation of biaryl.

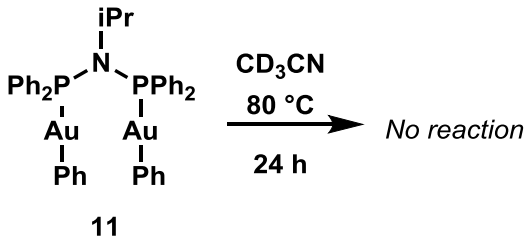


**Figure 2.11** Thermal stability of **11**

Finally, the generation of bromine or bromine radical under catalytic conditions could serve as an oxidant rather than allyl bromide. However, the addition of tetramethylethylene as a halide scavenger to a reaction which produces substantial quantities of homo-coupled product does not significantly decrease the observed yield of biaryl, arguing against halide oxidants as agents for the production of biaryl (Figure 2.12).

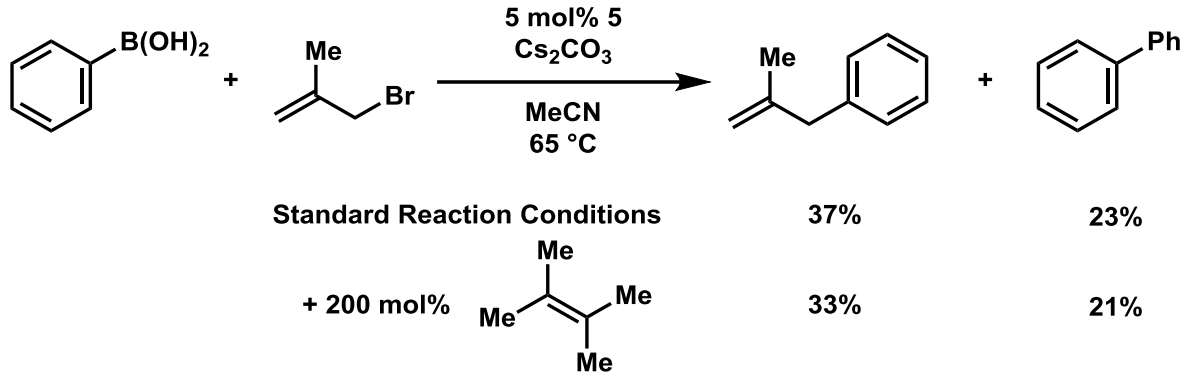


**Figure 2.12** Halide scavenger experiments

Combined, these experiments ultimately lead us to implicate an oxidative addition/disproportionation pathway *via* an intermediate such as **14** as the most likely source of biaryl. Reductive elimination from **13** or **14** can presumably also lead to alkyl-aryl bond formation, immediately suggesting a parsimonious mechanism for the overall transformation. Despite this evidence, attempts to isolate or detect oxidized Au(III) intermediates directly have so far proven fruitless, likely due to the rapid rate of reductive elimination.

In light of these difficulties, we turned to the tethered substrate **15** as a mechanistic probe, expecting that the resulting aurocyclic product (e.g. **18**) would exhibit hampered reductive elimination, allowing direct observation of reaction intermediates.[55]

Synthesis of **15** required the implementation of a modified strategy for introduction of the boronic ester and allylic bromide moieties, whose preparations are typically mutually incompatible (e.g. lithiation or cross-coupling of an aromatic bromide in the presence of an allylic bromide). Further complicating the synthesis was the observation that a pendant, free allylic alcohol formed boronic ester **16** (with loss of pinacol) which could not be elaborated to **15**. As a work-around, it was found that direct bromination of the silyl ether afforded the desired compound without competitive cyclization (Figure 2.13).

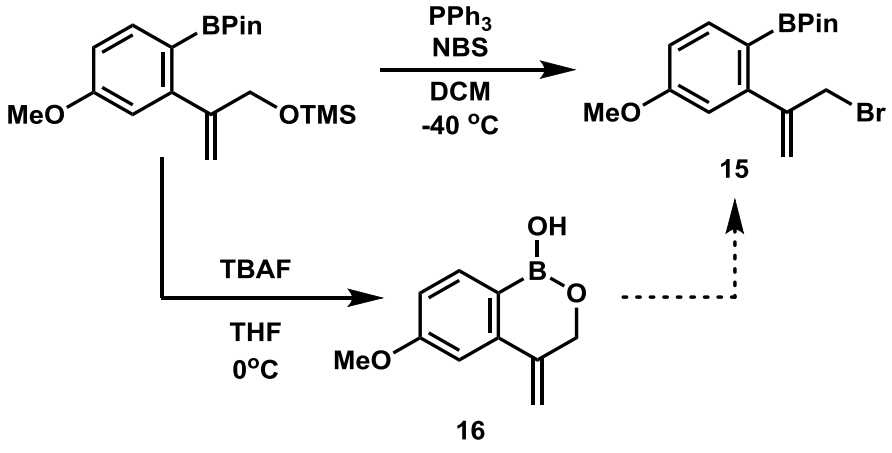


**Figure 2.13** Synthesis of mechanistic probe **15**

Although base-assisted transmetallation of **15** to phosphine supported gold complexes such as **1** was accompanied by hydrolysis of the allylic bromide moiety (presumably by an intramolecular displacement involving formation of a borate intermediate, given that allylic bromides are not typically hydrolyzed under the reaction conditions), it was found that clean transmetallation could be accomplished by employing IPrAuOH.[56] Although **17** does not react further in benzene, oxidative addition could be initiated upon gentle heating in acetonitrile to yield the isolable $Au^{III}$ species **18** (Figure 2.14). Finally, halide abstraction results in reductive elimination to give the exomethylene benzocyclobutene **19**.

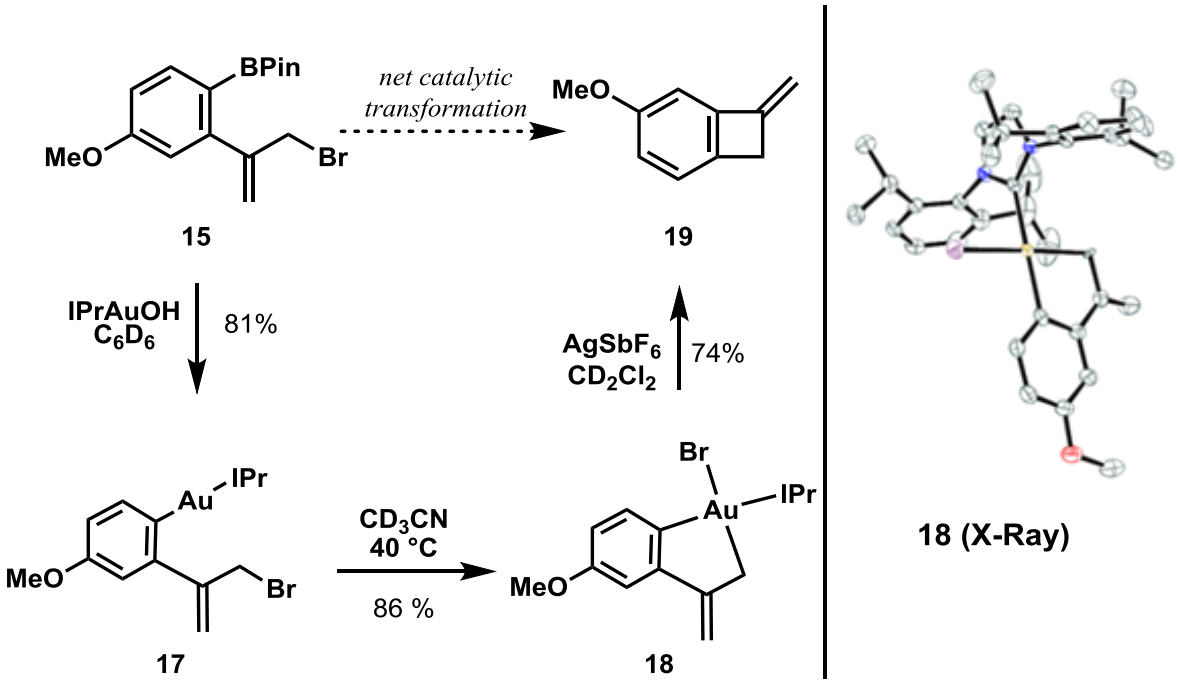


**Figure 2.14** Model catalytic cycle and isolable product of oxidative addition; asymmetric unit contains two molecules of **18**, only one shown; hydrogens omitted for clarity

With the viability of allylic halide oxidative addition to gold aryl complexes demonstrated, we propose the following overall mechanism for this process, following the general outline of Figure 2.2: (i) base-assisted transmetallation of the arylboronic acid to a gold bromide complex, (ii) bimetallic oxidative addition of an allylic halide to the gold aryl species, and either (iii) C-C reductive elimination to give allylbenzene or (iv) Au(III)/Au(I) disproportionation followed by reductive elimination to afford biaryl as product.

## 2.4 Discussion

From the above results, a number of intriguing features of this system merit further comment. Most are readily contextualized among related precedent discussed in Chapter 1, though several aspects remain unclear, namely the nature of the oxidative addition and reductive elimination. Where appropriate, the discussion is agnostic about the specific ligand, given that some monophosphine gold complexes catalyze this transformation.

### 2.4.1 Features of Transmetallation and Arylgold(I) Concentration

The transmetallation of boronic acids to phosphine-supported Au(I) assisted by heterogeneous basic additives was first reported by Gray, and is enhanced by the presence of alcoholic solvents.[26] Nolan subsequently reported the use of carbene supported hydroxides, which do not require additional basic additives.[56] This suggests the possible intermediacy of gold hydroxides in the former case, though no isolable terminal phosphine-supported hydroxides are known.[57–59]

In this system, the necessity for a heterogenerous base, inhibition by soluble bromide, and restoration of reactivity for heterogeneous bases by precipitation of sodium bromide all point towards the necessity for and difficulty associated with halide abstraction (Table 2.2). Formation of insoluble alkali bromides thus presumably drives the reaction forward. The effect of alcoholic (co)solvents observed by Gray can thus be rationalized by assistance by hydrogen bonding in the initial dissociation of the halide.

This is further consistent with observations regarding the ratio of allylbenzene and biphenyl under various conditions, by considering the competition between reductive elimination and disproportionation as a function of arylgold(I) concentration (Figure 2.15). For example, **11** forms a substantially higher proportion of biphenyl when treated with allylbromide than is observed under catalytic conditions (Figure 2.8). Here the concentration of arylgold(I) is in fact the highest possible for a given overall gold concentration. Alcoholic solvents are also expected to increase the concentration of arylgold(I) by increasing the rate of transmetallation, and correspondingly afford higher proportions of biaryl (Table 2.2). Higher equivalencies of allyl bromide improve the **3a**/**4a** ratio, again consistent with buildup of arylgold as the key variable. Finally, less reactive allylic bromides such as methallyl bromide provide similar increases in biaryl, here presumably due to the slower rate of oxidative addition (for steric reasons) compared to transmetallation (Figure 2.12).

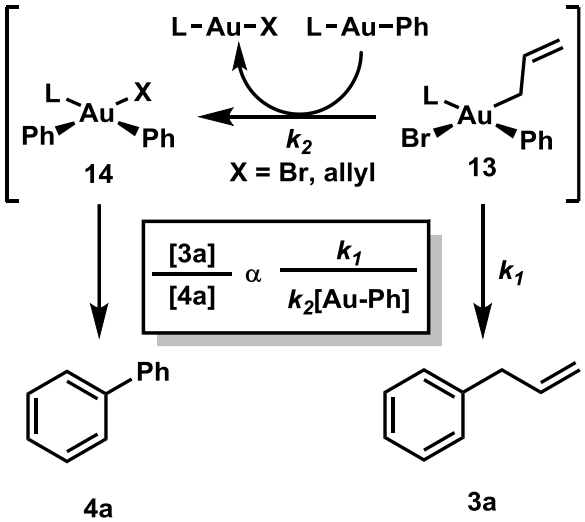


**Figure 2.15** Proposed origin of selectivity based on competition between reductive elimination and transmetallation from intermediate **13**. L is agnostic to mono or bimetallic catalysts, though intramolecular transmetallation may be faster than intermolecular.

This analysis relies on several features of Au(III) chemistry which are well-precedented. Au(I)/Au(III) transmetallation is well known for both alkyl and aryl substituents, and has been shown to be rapid on the timescale of reductive elimination for both classes of substituents by cross-over experiments.[19,25] Furthermore, reductive elimination of biaryl is expected to be substantially faster than reductive elimination of allylbenzene, given that the latter likely requires ligand dissociation (*vide infra*). However, a requirement for this analysis to be valid is that transmetallation is rate-limiting or similar in its rate to oxidative addition, a fact that has not been established given that the reaction is heterogeneous and as such accurate *in situ* monitoring of gold species has not been possible.

Finally, either by C-C transmetallation or by reductive elimination from a triorganogold complex, Au(I) allyl species are expected to form as a consequence of biaryl formation. Unlike other alkyl complexes, ligand supported allylgold(I) has resisted isolation, with only one report to date utilizing an IPr ligand.[34] The corresponding Au(III) allyl complexes are nucleophilic, engaging in allylation of aldehydes and protonolysis by alcohols.[48,49] Though no allylgold species have been detected under the reaction conditions, 1,5-hexadiene is observed, suggesting that such an Au(I) species may re-enter the catalytic cycle by reaction with allyl bromide (potentially *via* oxidative addition/reductive elimination) to afford L-Au-Br.

### 2.4.2 Oxidative Addition of Allyl Bromide

The chemistry presented here suggests indirectly that the rate of oxidative addition of allylbromide to arylgold(I) complexes is substantially faster than that for reaction of other alkyl halides to organogold(I). As noted in Chapter 1, oxidative addition of iodomethane to $Me_3PAuMe$ with a 2M iodomethane solution in benzene has a half-life of 4.8 hours, wildly incommensurate with the qualitative turnover frequency observed here for monophosphine complexes, even considering the enhanced rate of allylic $S_N2$.[17,60]

One potential explanation is a solvent effect. While typical solvent effects for $S_N2$-like oxidative addition to transition metals are smaller than $S_N2$ reactions of organic nucleophiles (e.g. 10-fold for benzene vs. DMF in the reaction of Vaska's complex with iodomethane), the difference seems to be more dramatic for gold, given that **17** does not undergo observable oxidative addition to the pendant allyl bromide in benzene solution over 48 hours, whereas the reaction proceeds smoothly in acetonitrile.[61] It seems reasonable that for a stepwise $S_N2$-like mechanism, coordination of acetonitrile to the intermediate cationic alkylgold(III) complex could serve to stabilize it prior to halide association. Indeed, reaction of $Ph_3PAuPh$ in THF with cinnamyl bromide had been previously reported to proceed in <15% yield, mirroring solvent effects in our hands (Table 2.2).[62] This likely accounts for some of the discrepancy, though other factors may be at play.

For one, though 9,10-dihydroanthracene does not influence the observed product distributions, in-cage radical oxidative addition cannot be ruled out, given that allylic stabilization may enable such a pathway. Attempts to synthesize a radical clock substrate amenable to the reaction conditions were unsuccessful.[63] However, the observation that allylic halides are reactive whereas the mesylate and phosphonate are completely unreactive is suggestive that such a pathway may be operative.

We had of course entered into the reaction development with the hypothesis that the known acceleration of oxidative addition to bimetallic complexes would translate to the catalytic protocol. However, the observed reactivity of monometallic catalysts (e.g. $Ph_3PAuCl$) suggests that such a bimetallic oxidative addition is not strictly necessary. One possibility is that association *via* aurophilic bonding of Au(I) aryl complexes allows bimetallic oxidative addition to occur to pre-organized species. Such a pathway has previously been examined computationally in the context of oxidatative gold catalysis, and is supported by the lack of reactivity for sterically demanding phosphine complexes (Table 1).[64]

A fascinating alternative proposal was recently put forward in a combined MS/DFT study of related *gem*-diaurated complex **20** (Figure 2.16).[65] The reaction between **20** and allyl bromide to afford allylbenzene was computed to occur *via* halide coordination to Au(I) followed by intramolecular oxidative addition at the γ-carbon, with the bimolecular scaffold serving to pre-organize the oxidative addition. Though the observed regioselectivity for our catalytic process is not consistent with attack at the olefin terminus, this proposal suggests an interesting alternative for activation of the allylic halide at gold, which in solution could potentially be amenable to both mono- and bi-metallic complexes.

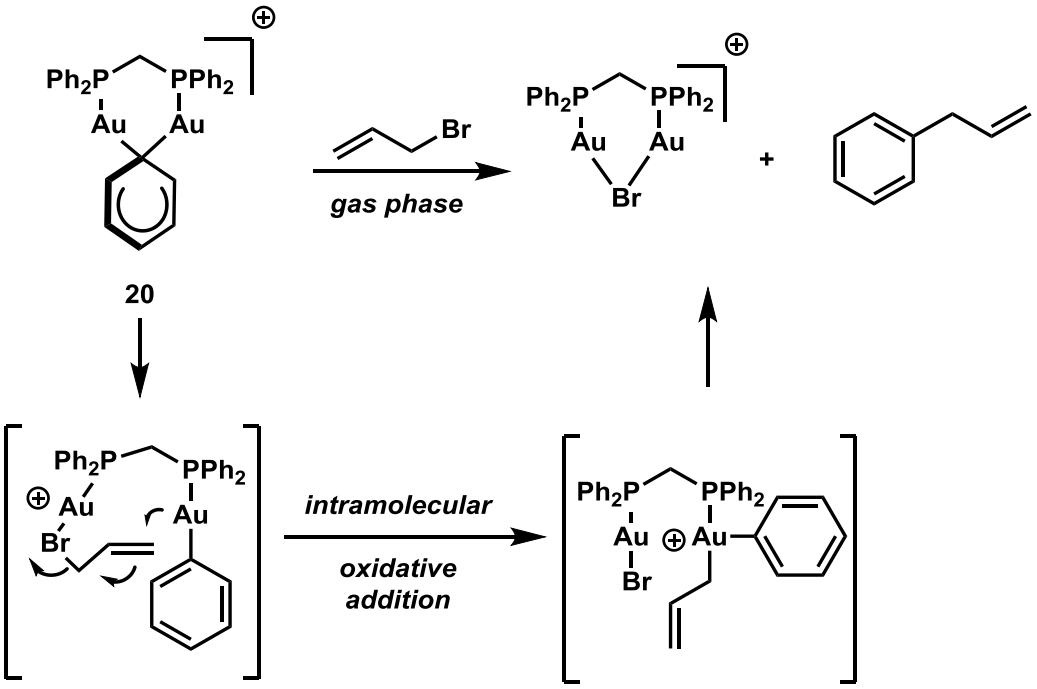


**Figure 2.16** Mass Spectrometry study and DFT-supported mechanistic proposal by O'Hair and coworkers for bimetallic oxidative addition of allylic halides to cationic bridged arylgold complexes.

### 2.4.3 Other Potential Mechanisms for Allylbenzene Formation

The mechanistic argument presented above takes the evidence for allyl bromide as the oxidant in biaryl formation and subsequently relies on an appeal to parsimony for the subsequent conclusion that allylbenzene formation likewise occurs from an Au(III)

intermediate. For the sake of completeness, two alternative mechanisms which do not account for the formation of biphenyl are presented here.

A simple alternative is attack of the allylic halide directly at the aromatic system, with gold serving to activate the arene for electrophilic substitution (Figure 2.17). This is in analogy to the proposed mechanism of protodeauration.[66] It should be noted that in addition to its failure to account for biaryl formation, such a mechanism was considered in the above computational study and found to have a substantially higher barrier than the corresponding oxidative addition process.[65]

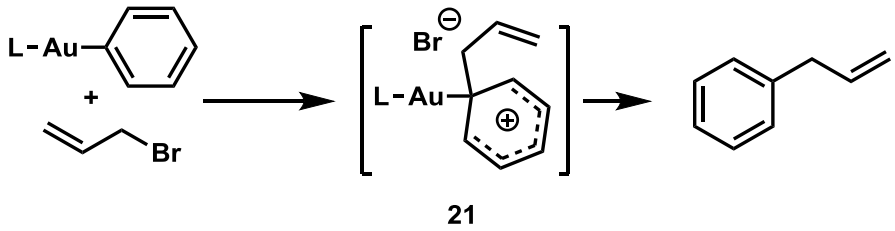


**Figure 2.17** Alternative (disfavored) mechanism for allylbenzene formation *via* electrophilic aromatic substitution

A second possibility is analogous to the proposed mechanism for copper catalyzed allylic substitution, as well as to the proposed mechanism of related "dehydrative" allylic substitutions catalyzed by gold.[44,67] Initial carboauration of the olefin followed by elimination of the gold halide could afford the observed product. It should be noted that the observed regioselectivity does not agree with this mechanism. Furthermore, migratory insertion to organogold(I) has rarely been observed (typically occurring via radical intermediates), as expected based on the reticence for two-coordinate Au(I) to associate an additional ligand.[68]

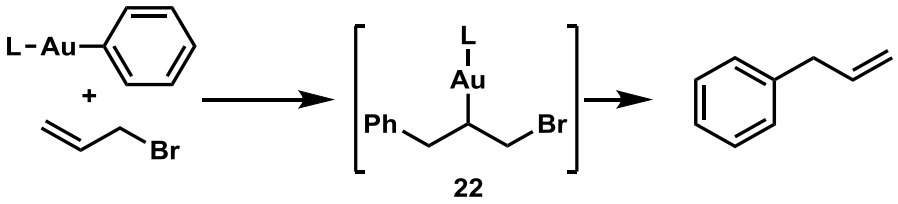


**Figure 2.18** Alternative (disfavored) mechanism for allylbenzene formation *via* carboauration/elimination, inconsistent with observed regioselectivity

A mechanism involving preequilibrium oxidative addition of allyl bromide followed by transmetallation of the arylboronic acid is also possible, and is fully consistent with our experimental observations. However, we favor the depicted mechanism based on the observed stepwise stoichiometric reactivity (Figure 2.8) whose rate is qualitatively consistent with the observed turnover frequency.

### 2.4.4 Other Examples of Redox Catalysis with Gold

Since the publication of this report, several examples of net-redox neutral Au(I)/Au(III) catalysis with gold have been reported. Three are highlighted below.

The Shi group reported the coupling of terminal alkynes with aryldiazonium salts in the presence of gold, with mass spectrometry studies supporting the intermediacy of Au(III) species.[69]

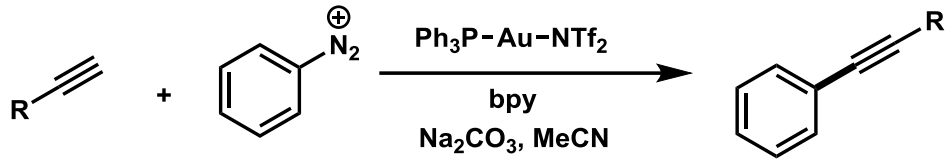


**Figure 2.19** Gold catalyzed C(*sp*)-C($sp^2$) catalyzed cross-coupling reported by Shi and coworkers

The Ribas group subsequently reported the cross-coupling of phenolates with aryl halides bearing appropriate directing groups, with stoichiometric experiments allowing isolation of the intermediate Au(III) aryl complex.[70,71]

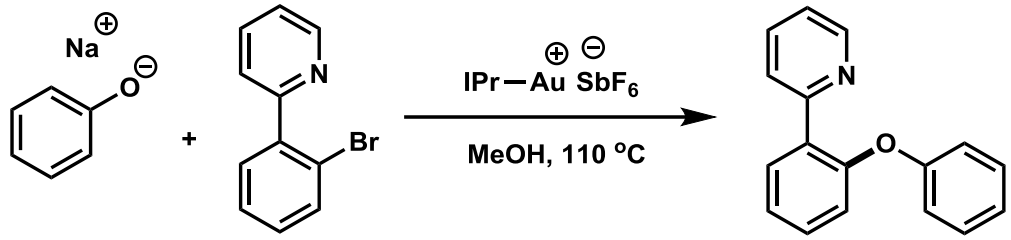


**Figure 2.20** Gold catalyzed C($sp^2$)-O cross-coupling reported by Ribas and coworkers

A prominent field of study for achieving redox chemistry with gold has been the implementation of photoredox catalysts to enable radical-chain oxidative addition of aryldiazonium salts to Au(I). This chemistry was first reported shortly before our own report, and is the first catalytic example of the reactivity manifold represented here.[72,73]

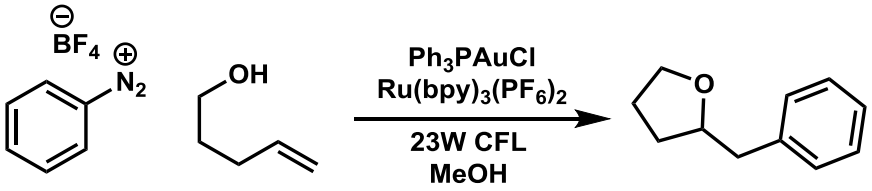


**Figure 2.21** Dual gold/photoredox oxyarylation reported by Glorius and coworkers

It should be noted that prior to the report of this method, several examples of putative gold-catalyzed cross-coupling reactions were reported, all of which were subsequently shown to be the result of Au(0) nanoparticles formed upon thermolysis of the gold complex.[74–77] Common to these methods was the use of high temperatures (>100 °C) and the presence of induction periods. In contrast, GC aliquot time course studies of our allylation chemistry reveals immediate onset of product formation with no observed induction period, suggesting that such adventitious nanoparticle catalysis is not operative here.

### 2.4.5 Attempts at Extension and Hypotheses Regarding Reductive Elimination

Attempts to extend the chemistry presented here to substrate classes beyond allylic halides were met with the same failure: the exclusive production of biaryl, typically with turnover numbers ≤ 1, and often with rapid decomposition of the precatalyst to afford metallic gold. Aliphatic, benzylic, and propargylic halides and psuedohalides as well as those with α-electron withdrawing groups, in reaction with a wide variety of aromatic nucleophiles, afforded either biaryl or no reaction, with no cross-products detected (Figure 2.22).

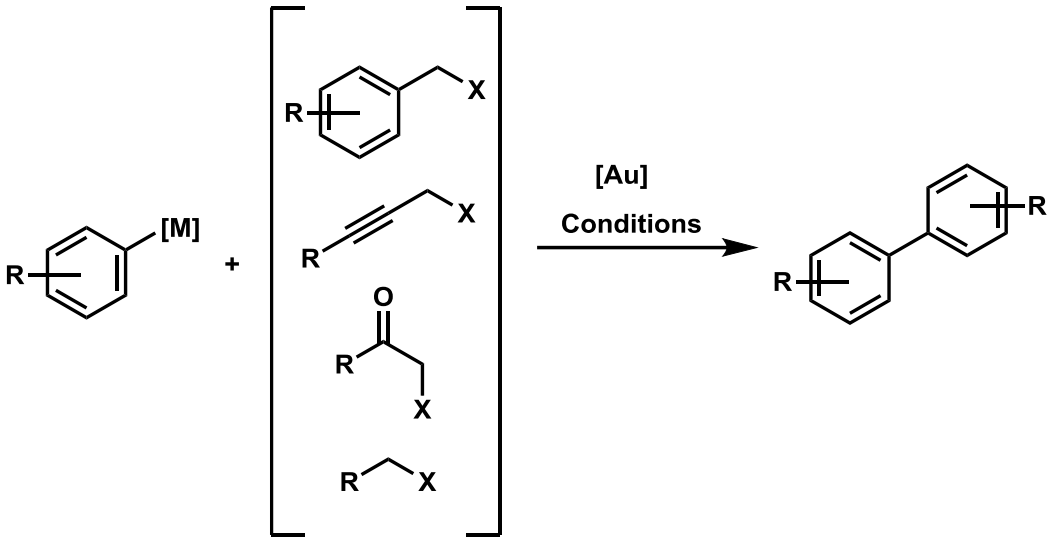


**Figure 2.22** Attempts to extend the allylation chemistry to other classes of electrophile

Based on the above argument for biaryl as a symptom of Au(III) intermediates and the rationale for product selectivity, it seems reasonable that slower reductive elimination from an intermediate analogous to **13** (relative to formation of **14**) would result in the selective formation of biaryl. This in turn suggests that allylic reductive elimination should be intrinsically more rapid than other C($sp^3$) reductive eliminations. A potential hypothesis for why this might be the case is the formation of $\eta^3$-allyl intermediates (e.g. **23**), assisting in ligand dissociation (either halide or phosphine) prior to reductive elimination (Figure 2.23). This is further consistent with the need to abstract the halide from complex **18** prior to reductive elimination of **19**; the cyclometallation prevents η3 coordination, stabilizing the resulting species against reductive elimination.

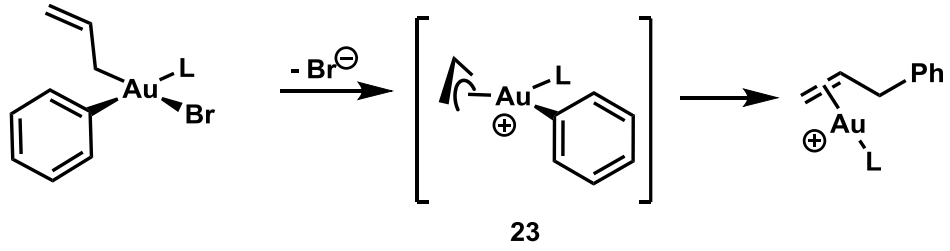


**Figure 2.23** Hypothesis for accelerated reductive elimination of allylgold(III) relative to other C($sp^3$) substituents

Though two $\eta^1$-allyldimethylgold(III) complexes have previously been reported, their thermolysis was not commented on in the reports.[48,49] No $\eta^3$-allylgold(III) complexes are known to date. However, Chapter 4 will deal with the chemistry of bis(trifluoromethyl) gold complexes, and in that context a related discovery was made which supports this proposal. Namely, oxidative addition of iodomethane to bis(trifluoromethyl)aurate(I) **24** affords a stable, isolable Au(III) complex **25**, whereas the analogous reaction with allyl bromide gives allyl $CF_3$ directly (Figure 2.24). $\eta^3$-assisted halide departure as a mechanism for reductive elimination neatly covers this divergent behavior as well.

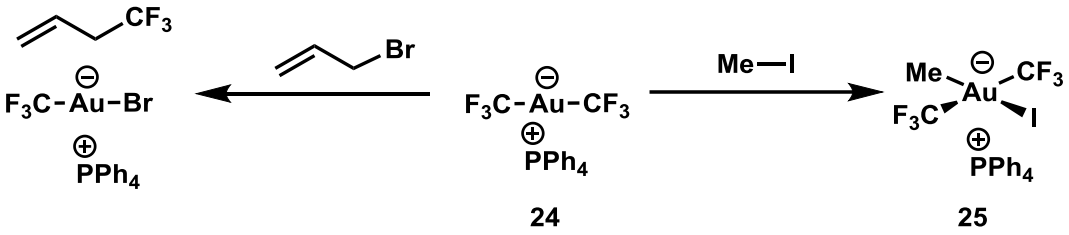


**Figure 2.24** Divergent reactivity of $(CF_3)$Au anion with methyl and allyl halides. (See Chapter 4 for details)

## 2.5 Conclusions

In conclusion, we have developed a leading example of net redox-neutral cross-coupling catalyzed by gold. The method provides access to C($sp^2$) – C($sp^3$) coupled products under mild conditions with complete tolerance for air and water. The reaction exhibits unique scope and chemoselectivity, allowing entry to a variety of allylbenzene products. Furthermore, initial experiments suggest a mechanism involving oxidative addition to a gold aryl species as a key step. Subsequent work by other groups has already demonstrated the potential of this reactivity manifold for the development of novel gold-catalyzed reactions, and will likely continue to serve as a fruitful area for exploration. Many questions regarding the nature of oxidative addition and reductive elimination to gold remain, and will hopefully be resolved in future studies.

The limitations outlined in section 2.4.5 suggested an important direction for development; circumventing the slow reductive elimination of alkyl substituents by employing a second catalyst is thus the focus of Chapter 3.

## 2.6 Supporting Information

### 2.6.1 General Methods

Unless otherwise noted, all glassware was oven- or flame-dried, and cooled under vacuum prior to use. All non-disposable glassware and magnetic stir bars were washed with freshly prepared aqua regia prior to use to minimize the potential for trace metal contamination. Unless otherwise noted, all commercial reagents were used without further purification, with the exception of commercially available allylic halides which were purified by filtration through a short plug of basic alumina or silica (depending on base sensitivity) and distilled prior to use and thermally stable boronic acids which were recrystallized from water, toluene, ethanol or hexanes depending on solubility prior to use and stored under $N_2$ or argon in the freezer.

The gold catalyzed allylation reactions were run in 1 dram (15 mm x 45 mm) vials (not dried) fitted with a screw cap and stirring was carried out using an 8 mm magnetic stir bar. All reactions were carried out under air unless otherwise noted. Dichloromethane, toluene, diethyl ether, tetrahydrofuran, dimethyl formamide, and triethylamine were purified by passage through an activated alumina column under argon. Thin-layer chromatography (TLC) analysis of reaction mixtures was performed using Merck silica gel 60 F254 TLC plates, and visualized under UV or by staining with ceric ammonium molybdate or $KMnO_4$. Flash column chromatography was carried out on Merck Silica Gel 60 Å, 230 x 400 mesh. Nuclear magnetic resonance (NMR) spectra were recorded using Bruker AV-600, DRX-500, AV-500, AVB-400, AVQ-400, and AV-300 spectrometers. $^{1}H$ and $^{13}C$ chemical shifts are reported in ppm downfield of tetramethylsilane and referenced to residual solvent peak ($CHCl_3$; $\delta H = 7.26$ and $\delta C = 77.0$, $CH_2Cl_2$; $\delta H = 5.30$ and $\delta C = 53.5$, $CH_3CN$; $\delta H = 1.94$ and $\delta C = 1.3$, 118.3). Multiplicities are reported using the following abbreviations: s = singlet, d = doublet, t = triplet, q = quartet, p = pentet, m = multiplet, bs = broad singlet. Gas Chromatography was conducted on an HP 6850A Series GC System on a Chiraldex 225 β-dex column with a flame ionization detector. Ethyl benzoate was used as an internal standard. Mass spectral data were obtained from the Thermo Scientific LTQ FT Ultra mass spectrometer (ESI) or the Autospec Premier magnetic sector mass spectrometer (EI) at the Micro-Mass/Analytical Facility operated by the College of Chemistry, University of California, Berkeley. Elemental Analyses were obtained from the Microanalytical Laboratory Perkin Elmer 2400 Series II combustion analyzer operated by the College of Chemistry, University of California, Berkeley.

Chloro(dimethylsulfide)gold(I) was prepared from $AuCl_3$ (purchased from Strem Chemical) according to a previously reported procedure.[78] $Ph_3PAuCl$ and $tBu_3PAuCl$ were purchased from Strem Chemical and used without further purification.

Bis(diphenylphosphino)isopropylamine,[79] (diphenylphosphino)diisopropylamine,[80] IPrAuCl,[81] JohnphosAuCl,[82] $PhO_3PAuCl$,[83] $pOMePh_3PAuCl$,[84] IPrAuOH,[56] 2-phenylprop-2-en-1-ol,[85] (5,6-dihydro-2H-pyran-3-yl)methanol,[86]and (2-bromocyclohex-1-en-1-yl)methanol[87]were prepared according to previously reported literature procedures.

### 2.6.2 General procedure for gold catalyzed allylation with allyl bromide.

**5** (5.4 mg, 0.006 mmol, carefully recrystallized and finely ground), boronic acid (0.123 mmol), and $Cs_2CO_3$ (120 mg, .379 mmol) were weighed into a vial equipped with a stirbar. MeCN (0.6 mL) was added followed by the allyl bromide (42 μL 0.492 mmol). The vial was equipped with a stirbar, capped tightly, and the reaction mixture was stirred vigorously for 18 hrs at 65°C in a heating block. Upon cooling, the reaction mixture was concentrated *in vacuo*, the residue was suspended in diethyl ether or dichloromethane and filtered through a pad of celite.

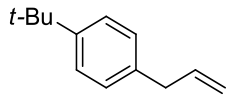


1-allyl-4-(tert-butyl)benzene, **3b**

Preparative TLC (3x elution with pentane) afforded the desired product as as colorless semisolid (15.4 mg, 72%). $^1$H NMR (600 MHz, $CDCl_3$) δ 7.33 (d, *J* = 7.8 Hz, 2H), 7.14 (d, *J* = 7.9 Hz, 2H), 5.98 (ddt, *J* = 16.8, 9.7, 6.8 Hz, 1H), 5.13 – 5.02 (m, 2H), 3.37 (d, *J* = 6.9 Hz, 2H), 1.32 (s, 9H). In accordance with previously reported spectra[88]

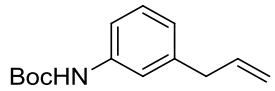


tert-butyl (3-allylphenyl)carbamate, **3c**

Column chromatography ($SiO_2$, eluting with 95:5 pentane/diethyl ether) afforded the desired product as a colorless film (16.4 mg, 58%). $^1$H NMR (400 MHz, $CDCl_3$) δ 7.25 – 7.15 (m, 3H), 6.88 (d, *J* = 7.2 Hz, 1H), 6.44 (s, 1H), 5.96 (ddt, *J* = 16.9, 10.1, 6.7 Hz, 1H), 5.17 – 4.97 (m, 2H), 3.37 (d, *J* = 6.7 Hz, 2H), 1.52 (s, 9H).$^{13}$C NMR (151 MHz, $CDCl_3$) δ 152.67, 141.06, 138.38, 137.17, 128.93, 123.26, 118.61, 116.23, 115.89, 80.40, 40.18, 28.31, 28.28. HRMS (EI) m/z: calculated for $[C_{14}H_{19}N_1O_2]^+$ 233.1416, found 233.1415.

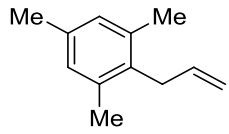


2-allyl-1,3,5-trimethylbenzene, **3d**

Column chromatography ($SiO_2$, eluting with pentane) afforded the desired product as a colorless oil (15.4 mg, 80%).$^1$H NMR (600 MHz, $CDCl_3$) δ 6.86 (s, 2H), 5.89 (td, *J* = 10.5, 5.0 Hz, 1H), 4.99 (dd, *J* = 9.9, 2.4 Hz, 1H), 4.92 – 4.77 (m, 2H), 3.36 (d, *J* = 5.7 Hz, 2H), 2.27 (s, 9H).In accordance with previously reported spectra[89]

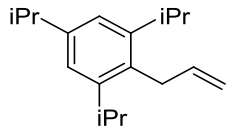


2-allyl-1,3,5-triisopropylbenzene, **3e**

Column chromatography ($SiO_2$, eluting with pentane) afforded the desired product as a colorless oil (10.4 mg, 35%). $^1$H NMR (600 MHz, $CDCl_3$) δ 7.00 (s, 2H), 5.98 (ddt, *J* = 16.1, 10.5, 5.4 Hz, 1H), 5.06 – 4.95 (m, 1H), 4.89 – 4.78 (m, 1H), 3.46 (d, *J* = 5.2 Hz, 2H), 3.13 (p, *J* = 6.9 Hz, 2H), 2.88 (p, *J* = 7.0 Hz, 1H), 1.26 (d, *J* = 6.9 Hz, 6H), 1.22 (d, *J* = 6.9 Hz, 12H). $^{13}$C NMR (151 MHz, $CDCl_3$) δ 147.14, 146.75, 138.06, 130.52, 121.00, 115.04, 34.28, 31.67, 29.44, 24.43, 24.23. HRMS (EI) m/z: calculated for $[C_{18}H_{28}]^+$ 244.2191, found 244.2192.

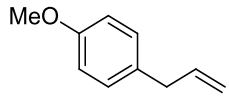


1-allyl-4-methoxybenzene, **3f**

Column chromatography ($SiO_2$, eluting with pentane) afforded the desired product as a colorless oil (9.3 mg, 51%). $^1$H NMR (600 MHz, $CDCl_3$) δ 7.11 (d, *J* = 8.4 Hz, 2H), 6.84 (d, *J* = 8.5 Hz, 2H), 5.95 (ddt, *J* = 16.8, 10.1, 6.7 Hz, 1H), 5.14 – 4.96 (m, 2H), 3.79 (s, 3H), 3.33 (d, *J* = 6.6 Hz, 2H). In accordance with previously reported spectra[90]

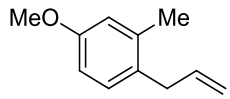


1-allyl-4-methoxy-2-methylbenzene, **3g**

Column chromatography ($SiO_2$, eluting with pentane) afforded the desired product as a colorless oil (14 mg, 70%).$^1$H NMR (600 MHz, $CDCl_3$) δ 7.04 (d, *J* = 8.2 Hz, 1H), 6.72 (d, *J* = 2.6 Hz, 1H), 6.70 (d, *J* = 8.3 Hz, 1H), 5.93 (ddt, *J* = 16.6, 9.9, 6.4 Hz, 1H), 5.03 (d, *J* = 10.1 Hz, 1H), 5.01 – 4.86 (m, 1H), 3.78 (s, 3H), 3.31 (d, *J* = 6.2 Hz, 2H), 2.27 (s, 3H). In accordance with previously reported spectra[91]

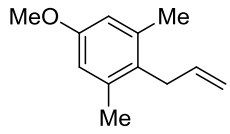


2-allyl-5-methoxy-1,3-dimethylbenzene, **3h**

Column chromatography ($SiO_2$, eluting with pentane) afforded the desired product as a colorless semisolid (18.2 mg, 84%). $^1$H NMR (600 MHz, $CDCl_3$) δ 6.60 (s, 2H), 5.89 (ddt, *J* = 16.3, 10.7, 5.7 Hz, 1H), 4.98 (dd, *J* = 10.0, 2.5 Hz, 1H), 4.85 (dd, *J* = 17.1, 2.7 Hz, 1H), 3.78 (s, 3H), 3.40 – 3.27 (m, 2H), 2.28 (s, 6H). In accordance with previously reported spectra[92]

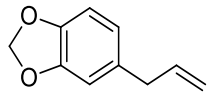

5-allylbenzo[d][1,3]dioxole, **3i**

Column chromatography ($SiO_2$, eluting on a gradient from pentane to 9:1 pentane/diethyl ether) afforded the desired product as a pale yellow oil (17.4 mg, 86%). $^1$H NMR (500 MHz, $CDCl_3$) δ 6.75 (d, *J* = 7.9 Hz, 1H), 6.69 (d, *J* = 1.8 Hz, 1H), 6.64 (dd, *J* = 7.8, 1.8 Hz, 1H), 5.96-5.86 (m, 3H), 5.10 – 5.02 (m, 2H), 3.37 – 3.24 (m, 2H).In accordance with previously reported spectra[93]

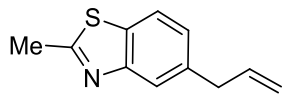

5-allyl-2-methylbenzo[d]thiazole, **3j**

Column chromatography ($SiO_2$, eluting with 95:5 pentane/diethyl ether) afforded the desired product as a colorless semisolid (12.2 mg, 53%). $^1$H NMR (600 MHz, $CDCl_3$) δ 7.84 (d, *J* = 8.3 Hz, 1H), 7.61 (s, 1H), 7.25 (d, *J* = 2.2 Hz, 1H), 6.11 – 5.76 (m, 1H), 5.10 (d, *J* = 5.6 Hz, 1H), 5.08 (s, 1H), 3.48 (d, *J* = 6.6 Hz, 2H), 2.80 (d, *J* = 1.9 Hz, 3H). $^{13}$C NMR (151 MHz, $CDCl_3$) δ 166.40, 152.10, 137.31, 137.03, 136.07, 127.10, 122.22, 121.03, 116.32, 40.22, 20.23. HRMS (EI) m/z: calculated for $[C_{11}H_{11}N_1S_1]^+$ 189.0612, found 189.0614.

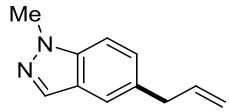

5-allyl-1-methyl-1H-indazole, **3k**

Column chromatography ($SiO_2$, eluting with 9:1 pentane/diethyl ether) afforded the desired product as a pale yellow solid (10.9 mg, 52%).

$^1$H NMR (600 MHz, $CDCl_3$) δ 7.91 (s, 1H), 7.51 (s, 1H), 7.33 (d, *J* = 8.6 Hz, 1H), 7.28 – 7.18 (m, 1H), 6.02 (ddt, *J* = 16.8, 10.1, 6.6 Hz, 1H), 5.15 – 5.00 (m, 2H), 4.06 (s, 3H), 3.50 (d, *J* = 6.7 Hz, 2H). $^{13}$C NMR (151 MHz, $CDCl_3$) δ 139.08, 138.02, 132.42, 132.28, 127.91, 124.50, 120.08, 115.79, 108.94, 40.17, 35.69. HRMS (ESI) m/z: calculated for $[C_{11}H_{12}N_2 + H]^+$ 173.1073, found 173.1073.

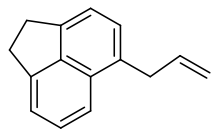

5-allyl-1,2-dihydroacenaphthylene, **3l**

Column chromatography ($SiO_2$, eluting with pentane) afforded the desired product as a pale yellow solid (11.8 mg, 50%). $^1$H NMR (600 MHz, $CDCl_3$) δ 7.69 (d, *J* = 8.3 Hz, 1H), 7.46 (dd,

*J* = 8.3, 6.9 Hz, 1H), 7.30 – 7.26 (m, 2H), 7.22 (d, *J* = 7.0 Hz, 1H), 6.09 (ddt, *J* = 16.7, 10.1, 6.4 Hz, 1H), 5.19 – 4.92 (m, 2H), 3.77 (d, *J* = 6.4 Hz, 2H), 3.46 – 3.25 (m, 5H). $^{13}$C NMR (151 MHz, $CDCl_3$) δ 146.56, 144.64, 139.71, 137.48, 131.99, 130.62, 127.79, 127.70, 119.58, 119.23, 119.21, 115.85, 36.54, 30.73, 30.02. HRMS (EI) m/z: calculated for $[C_{15}H_{14}]^+$ 194.1096, found 194.1097.

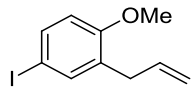


2-allyl-4-iodo-1-methoxybenzene, **3m**

Preparative TLC ($SiO_2$, 3x elution with pentane) afforded the desired product as a colorless solid (17.2 mg, 51%). $^1$H NMR (500 MHz, $CDCl_3$) δ 7.47 (dd, *J* = 8.6, 2.3 Hz, 1H), 7.41 (d, *J* = 2.4 Hz, 1H), 6.61 (d, *J* = 8.6 Hz, 1H), 5.93 (ddt, *J* = 15.8, 10.5, 6.8 Hz, 1H), 5.07 (t, *J* = 1.5 Hz, 1H), 5.04 (dt, *J* = 6.0, 1.7 Hz, 1H), 3.80 (d, *J* = 1.4 Hz, 3H), 3.31 (d, *J* = 6.7 Hz, 2H). In accordance with previously reported spectra[94]

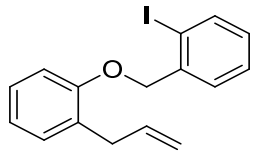


1-allyl-2-((2-iodobenzyl)oxy)benzene, **3n**

Column chromatography ($SiO_2$, eluting with pentane) afforded the desired product as a colorless oil (33.1 mg, 94%). The crude reaction mixture was also analyzed by GC-MS for the presence of de-iodinated or cyclized products, with no traces found. $^1$H NMR (600 MHz, $CDCl_3$) δ 7.88 (d, *J* = 7.8 Hz, 1H), 7.55 (d, *J* = 7.7 Hz, 1H), 7.39 (t, *J* = 7.5 Hz, 1H), 7.21 (d, *J* = 7.5 Hz, 2H), 7.04 (t, *J* = 7.6 Hz, 1H), 6.96 (t, *J* = 7.4 Hz, 1H), 6.91 (d, *J* = 8.1 Hz, 1H), 6.06 (ddt, *J* = 16.6, 9.5, 6.7 Hz, 1H), 5.15 – 5.00 (m, 4H), 3.51 (d, *J* = 6.6 Hz, 2H). $^{13}$C NMR (151 MHz, $CDCl_3$) δ 156.04, 139.55, 139.26, 137.05, 130.10, 129.44, 129.09, 128.49, 128.43, 127.53, 121.22, 115.72, 111.91, 96.95, 74.04, 34.67. HRMS (EI) m/z: calculated for $[C_{16}H_{15}O_1I_1]^+$ 350.0168, found 350.0169.

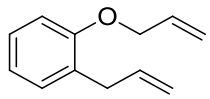


1-allyl-2-(allyloxy)benzene, **3o**

Column chromatography ($SiO_2$, eluting with pentane) afforded the desired product as a colorless oil (16.4 mg, 77%). The crude reaction mixture was also analyzed by GC-MS for the presence of cyclized dihydrobenzofuran derivatives, with no traces found. $^1$H NMR (500 MHz, $CDCl_3$) δ 7.21 – 7.14 (m, 2 H), 6.92 – 6.89 (m, 2H), 6.11-6.00 (m, 2H), 5.44 (d, *J* = 17.5 Hz, 1H), 5.26 (d, *J* = 10.5 Hz, 1H), 5.08-4.99 (m, 2H), 4.55 (d, *J* = 5 Hz, 2H), 3.39 (d, *J* = 6 Hz, 2H). In accordance with previously reported spectra[95]

### 2.6.3 General procedure for gold catalyzed allylation with substituted allylic bromides.

**5** (5.4 mg, 0.006 mmol, carefully recrystallized and finely ground), mesitylboronic acid (20.2 mg, 0.123 mmol), and $Cs_2CO_3$ (120 mg, .379 mmol) were weighed into a vial equipped with a stirbar. A solution of the allylic bromide (0.492 mmol) in MeCN (0.6 mL) was then added. The vial was equipped with a stirbar, capped tightly, and the reaction mixture was stirred for 18 hrs at 65ºC in a heating block. Upon cooling, 100 mg of diazabicylo[2.2.2]octane (DABCO) and an additional 1 mL of MeCN was added and the mixture was stirred at room temperature for 1.5 hours. The reaction mixture was then concentrated *in vacuo*, the residue was suspended in diethyl ether and filtered through a pad of celite.

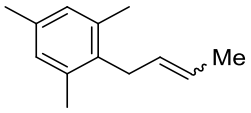


2-(but-2-en-1-yl)-1,3,5-trimethylbenzene, **7a**

Column chromatography ($SiO_2$, eluting with pentane) afforded the desired product as a colorless oil (17.9 mg, 82%, 2:1 *E/Z* mixture) *E* isomer: $^1$H NMR (600 MHz, $CDCl_3$) δ 6.86 (s, 2H), 5.49 (dddt, *J* = 13.5, 5.9, 4.3, 1.7 Hz, 1H), 5.40 – 5.30 (m, 1H), 3.30 (dd, *J* = 4.2, 1.8 Hz, 2H), 2.29 (s, 6H), 2.27 (s, 3H), 1.64 (dd, *J* = 6.4, 1.7 Hz, 3H). *Z* isomer: $^1$H NMR (600 MHz, $CDCl_3$) δ 6.86 (s, 2H), 5.49 (dddt, *J* = 13.5, 5.9, 4.3, 1.7 Hz, 1H), 5.27 (dtd, *J* = 10.6, 6.7, 1.9 Hz, 1H), 3.37 (d, *J* = 6.7 Hz, 2H), 2.29 (s, 3H), 2.29 (s, 6H), 1.81 – 1.76 (m, 3H). In accordance with previously reported spectra[96]

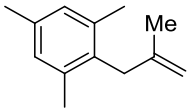


1,3,5-trimethyl-2-(2-methylallyl)benzene, **7b**

Column chromatography ($SiO_2$, eluting with pentane) afforded the desired product as a colorless oil (14.4 mg, 68%).$^1$H NMR (600 MHz, $CDCl_3$) δ 6.85 (s, 2H), 4.79 – 4.61 (m, 1H), 4.24 (d, *J* = 2.4 Hz, 1H), 3.25 (s, 2H), 2.27 (s, 3H), 2.22 (s, 6H), 1.83 (s, 3H).$^{13}$C NMR (151 MHz, $CDCl_3$) δ 143.31, 137.03, 135.38, 133.62, 128.73, 109.84, 37.18, 23.53, 21.01, 19.87. HRMS (EI) m/z: calculated for $[C_{13}H_{18}]^+$ 174.1409, found 174.1409.

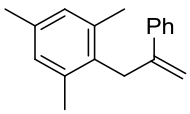


1,3,5-trimethyl-2-(2-phenylallyl)benzene, **7c**

Column chromatography ($SiO_2$, eluting with pentane) afforded the desired product as a colorless oil (16.6 mg, 57%). $^1$H NMR (600 MHz, $CDCl_3$) δ 7.57 (d, *J* = 7.6 Hz, 2H), 7.40 (t, *J* = 7.6 Hz, 2H), 7.33 (t, *J* = 7.4 Hz, 1H), 6.91 (s, 2H), 5.29 (s, 1H), 4.46 (d, *J* = 2.9 Hz, 1H), 3.72 (d, *J* = 3.0 Hz, 2H), 2.31 (s, 3H), 2.26 (s, 6H). $^{13}$C NMR (151 MHz, $CDCl_3$) δ 145.36, 142.30, 137.20, 135.72, 133.31, 128.84, 128.47, 127.65, 125.92, 111.90, 34.54, 21.07, 19.86, 19.84. HRMS (EI) m/z: calculated for $[C_{18}H_{20}]^+$ 236.1565, found 236.1568.

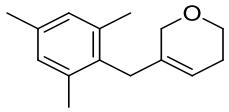


5-(2,4,6-trimethylbenzyl)-3,6-dihydro-2H-pyran, **7d**

Column chromatography ($SiO_2$, eluting with 9:1 pentane/diethyl ether) afforded the desired product as a colorless oil (20.2 mg, 76%). $^1$H NMR (600 MHz, $CDCl_3$) δ 6.85 (s, 2H), 5.06 (dt, *J* = 3.9, 2.0 Hz, 1H), 4.10 (q, *J* = 1.3 Hz, 2H), 3.74 (t, *J* = 5.5 Hz, 2H), 3.22 – 3.04 (m, 2H), 2.27 (s, 3H), 2.21 (s, 7H), 2.03 (dt, *J* = 4.0, 2.6 Hz, 2H). $^{13}$C NMR (151 MHz, $CDCl_3$) δ 136.92, 135.42, 134.46, 131.95, 128.62, 117.62, 68.38, 64.41, 32.01, 25.07, 20.84, 19.77. HRMS (EI) m/z: calculated for $[C_{15}H_{20}O]^+$ 216.1514, found 216.1514

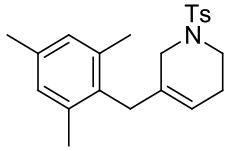


1-tosyl-5-(2,4,6-trimethylbenzyl)-1,2,3,6-tetrahydropyridine, 7**e**

Column chromatography ($SiO_2$, eluting with 9:1 pentane/diethyl ether) afforded the desired product as a colorless solid (26.4 mg, 58%). $^1$H NMR (600 MHz, $CDCl_3$) δ 7.69 (d, *J* = 8.0 Hz, 2H), 7.34 (d, *J* = 7.9 Hz, 2H), 6.83 (s, 2H), 4.91 (dt, *J* = 3.9, 2.0 Hz, 1H), 3.64 – 3.53 (m, 2H), 3.14 (s, 4H), 2.45 (s, 3H), 2.25 (s, 3H), 2.07 (dd, *J* = 5.9, 3.0 Hz, 2H). $^{13}$C NMR (151 MHz, $CDCl_3$) δ 143.58, 137.01, 135.81, 133.83, 131.72, 131.69, 129.79, 128.84, 127.78, 118.51, 48.04, 42.93, 33.74, 25.03, 21.67, 20.97, 19.88. HRMS (ESI) m/z: calculated for $[C_{22}H_{27}O_2N_1S_1 + H]^+$ 370.1835, found 370.1839.

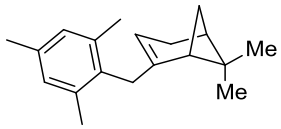


(1R,5S)-6,6-dimethyl-2-(2,4,6-trimethylbenzyl)bicyclo[3.1.1]hept-2-ene, 7**f**

Column chromatography ($SiO_2$, eluting with pentane) afforded the desired product as colorless film (24.5 mg, 77%). $^1$H NMR (600 MHz, $CDCl_3$) δ 6.86 (s, 2H), 4.70 – 4.49 (m, 1H), 3.28 – 3.10 (m, 2H), 2.40 (dt, *J* = 8.3, 5.5 Hz, 1H), 2.28 (s, 3H), 2.23 (s, 6H), 2.18 (dt, *J* = 17.8, 3.1 Hz, 1H), 2.11 (ddd, *J* = 14.6, 5.5, 2.8 Hz, 2H), 2.06 (td, *J* = 5.6, 1.4 Hz, 1H), 1.31 (s, 3H). $^{13}$C NMR (151 MHz, $CDCl_3$) δ 145.82, 136.93, 135.17, 133.26, 128.61, 115.41, 46.89, 41.25, 38.30, 36.45, 31.86, 31.30, 26.55, 21.18, 21.03, 19.86. HRMS (EI) m/z: calculated for $[C_{19}H_{26}]^+$ 254.2035, found 254.2035.

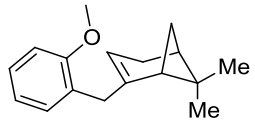


(1R,5S)-6,6-dimethyl-2-(2-methoxybenzyl)bicyclo[3.1.1]hept-2-ene, 7**g**

Column chromatography ($SiO_2$, eluting with pentane) afforded the desired product as colorless film (18.1 mg, 61%). $^1$H NMR (500 MHz, $CDCl_3$) δ 7.18 (td, *J* = 7.8, 1.8 Hz, 1H), 7.10 (dd, *J* = 7.5, 1.7 Hz, 1H), 6.92 – 6.81 (m, 2H), 5.14 (dt, *J* = 3.1, 1.5 Hz, 1H), 3.80 (s, 3H), 3.29 (dddd, *J* = 17.3, 15.5, 13.6, 1.8 Hz, 2H), 2.43 – 1.94 (m, 5H), 1.22 (s, 3H), 0.76 (s, 3H) . $^{13}$C NMR (126 MHz, $CDCl_3$) δ 157.61, 146.83, 130.53, 128.12, 127.01, 120.18, 117.28, 110.28, 55.32, 45.83, 40.78, 37.97, 36.82, 31.80, 31.42, 26.32, 20.87. HRMS (EI) m/z: calculated for $[C_{17}H_{22}O_1]^+$ 242.1671, found 242.1665.

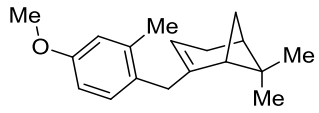


(1R,5S)-6,6-dimethyl-2-(2-methyl-4-methoxybenzyl)bicyclo[3.1.1]hept-2-ene, **7h**

Column chromatography ($SiO_2$, eluting with pentane) afforded the desired product as colorless film (24.3 mg, 74%). $^1$H NMR (500 MHz, $CDCl_3$) δ 7.02 (d, *J* = 8.2 Hz, 1H), 6.76 – 6.60 (m, 2H), 4.97 (dt, *J* = 3.1, 1.5 Hz, 1H), 3.81 (s, 3H), 3.21 (t, *J* = 2.1 Hz, 2H), 2.43 – 1.90 (m, 5H), 1.26 (s, 3H), 1.19 (d, *J* = 8.5 Hz, 1H), 0.81 (s, 3H). $^{13}$C NMR (126 MHz, $CDCl_3$) δ 157.80, 146.91, 138.06, 130.91, 129.81, 117.01, 115.64, 110.63, 55.17, 45.88, 40.83, 40.04, 38.02, 31.72, 31.33, 26.33, 20.94, 19.70. HRMS (EI) m/z: calculated for $[C_{18}H_{24}O_1]^+$ 256.1827, found 256.1821.

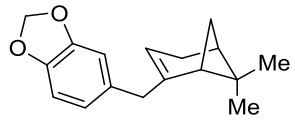


(1R,5S)-6,6-dimethyl-2-(3,4-methylenedioxybenzyl)bicyclo[3.1.1]hept-2-ene, **7i**

Column chromatography ($SiO_2$, eluting with pentane) afforded the desired product as colorless film (18.6 mg, 59%). $^1$H NMR (500 MHz, $CDCl_3$) δ 6.71 (d, *J* = 7.9 Hz, 1H), 6.65 (d, *J* = 1.7 Hz, 1H), 6.60 (dd, *J* = 7.9, 1.7 Hz, 1H), 5.92 (s, 2H), 5.23 (dt, *J* = 3.0, 1.5 Hz, 1H), 3.26 – 3.08 (m, 2H), 2.36 – 2.15 (m, 4H), 2.06 (dtd, *J* = 5.9, 3.0, 1.3 Hz, 1H), 1.96 (td, *J* = 5.6, 1.5 Hz, 1H), 1.20 (s, 3H), 1.13 (d, *J* = 8.5 Hz, 1H), 0.76 (s, 3H). $^{13}$C NMR (126 MHz, $CDCl_3$) δ 147.42, 147.36, 145.62, 133.41, 121.92, 117.65, 109.59, 107.86, 100.71, 45.33, 43.18, 40.66, 37.90, 31.85, 31.36, 26.23, 21.04. HRMS (EI) m/z: calculated for $[C_{17}H_{20}O_2]^+$ 256.1463, found 256.1467.

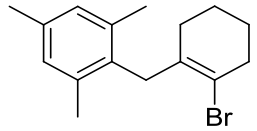


2-((2-bromocyclohex-1-en-1-yl)methyl)-1,3,5-trimethylbenzene, **7j**

Column chromatography ($SiO_2$, eluting with pentane) afforded the desired product as a colorless oil (21.2 mg, 59%). $^1$H NMR (600 MHz, $CDCl_3$) δ 6.83 (s, 2H), 3.63 (s, 2H), 2.56 (tt, *J* = 4.1, 2.1 Hz, 2H), 2.26 (s, 3H), 2.25 (s, 6H), 1.74 – 1.59 (m, 4H), 1.57 – 1.44 (m, 2H).$^{13}$C NMR (151 MHz, $CDCl_3$) δ 137.33, 135.57, 133.70, 132.94, 128.91, 120.02, 37.09, 36.68, 29.27, 24.99, 22.73, 20.98, 20.55. HRMS (EI) m/z: calculated for $[C_{16}H_{21}Br]^+$ 292.0827; 294.0806, found 292.0826; 294.0804.

### 2.6.4 Preparation of gold catalysts.

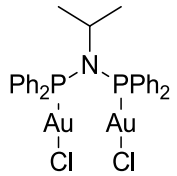

Dichloro(N-(diphenylphosphino)-N-isopropyl-1,1-diphenylphosphinamine) digold(I) (**5**)

To freshly prepared chloro(dimethylsulfide) gold(I) (310 mg, 1.45 mmol) and bis(diphenylphosphino)isopropylamine (309 mg, 0.725 mmol) under an atmosphere of $N_2$ was added dichloromethane (24 mL) with vigorous stirring. The reaction mixture was stirred for 20 minutes, filtered through a fine fritted funnel, and concentrated *in vacuo*. The residue was washed sequentially with pentane and ether to yield a colorless solid which was dried *in vacuo*. Recrystallization from (DCM + pentane) / $Et_2O$ by the layering method yields colorless crystals (473 mg, 73% yield). X-ray quality crystals grown from THF / $Et_2O$ by vapor diffusion.

$^1$H NMR (400 MHz, $CD_2Cl_2$) δ 7.81-7.87 (m, 8H), 7.63-7.67 (m, 4H), 7.54-7.58 (m, 8H), 3.96-4.08 (m, 1H), 1.10 (d, $J$ = 5.6, 6H) $^{13}$C NMR (101 MHz, $CD_2Cl_2$) δ 133.8-134.0 (m) 132.9, 129.9, 129.2-129.3 (m), 54.8, 24.2 $^{31}$P NMR (162 MHz, $CD_2Cl_2$) δ 75.3 (bs) $^{31}$P NMR (162 MHz, $CD_3CN$) δ 79.2 (s) HRMS (ESI) m/z: calculated for $[C_{27}H_{27}Au_2Cl_2NP_2 + Na]^+$ 914.0219, found 914.0224 EA: Calculated : C, 36.34; H, 3.05; N, 1.57; Found: C, 36.20; H, 3.08; N, 1.54 IR: 2957, 1572, 1432, 1113, 1099, 978, 948, 881, 850, 760, 747, 738, 713, 694, 684, 601, 544, 535, 502, 483, 472, 438 In accordance with previously reported spectra.[29]

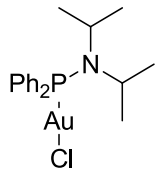

Chloro(N,N-diisopropyl-1,1-diphenylphosphinamine) gold(I) (**6**)

To chloro(dimethylsulfide) gold(I) (60 mg, 0.20 mmol) and (diphenylphosphino)diisopropylamine (60 mg, 0.21 mmol) under an atmosphere of $N_2$ was added dichloromethane (4.5 mL) with vigorous stirring. The reaction mixture was stirred for 20 minutes and concentrated *in vacuo*. The residue was washed sequentially with pentane, ether, and methanol to yield a colorless solid which was dried *in vacuo*. Recrystallized from DCM/Pentane by the layering method (81 mg, 80%).

$^1$H NMR (400 MHz, $CDCl_3$) δ 7.67-7.73 (m, 4H) 7.45-7.52 (m, 6H), 3.56-3.63 (m, 2H), 1.33 (d, 12H, $J$ = 6.4 Hz) $^{13}$C NMR (100.6 MHz, $CD_2Cl_2$) δ 132.7 (d, $J$ = 14.4 Hz), 132.3 (d, $J$ = 69.4Hz), 131.4, 128.7 (d, $J$ = 11.9 Hz), 48.0 (d, $J$ = 3.0 Hz), 23.2 (d, $J$ = 3.0 Hz) $^{31}$P NMR (162 MHz, $CDCl_3$) δ 51.07 (s) HRMS: (EI+) m/z: calculated for $[C_{18}H_{24}AuClNP]^+$: 517.1000, found 517.1006 EA: Calculated : C, 41.75; H, 4.67; N, 2.17; Found: C, 41.43; H, 4.35; N, 2.51 IR: 2959, 1433, 1369, 1172, 1149, 1112, 1100, 1006, 980, 749, 695, 637, 561, 543, 524, 493, 462, 455

### 2.6.5 Preparation of substrates

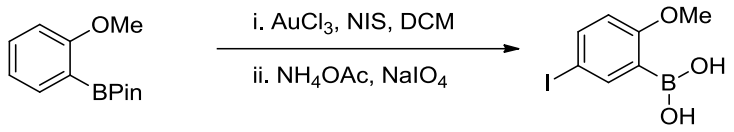


(5-iodo-2-methoxyphenyl)boronic acid, **S1**

Prepared according to a modification of a reported literature procedure:[97]

2-methoxyphenyboronic acid pinacol ester (585 mg, 2.5 mmol), $AuCl_3$ (7.6 mg, 0.025 mmol), and N-iodosuccinimide (563 mg, 2.5 mmol) were dissolved in DCE (5 mL) and the mixture was stirred overnight at room temperature. The mixture was concentrated, suspended in 2:1 Hexanes/diethyl ether, and filtered through a short $SiO_2$ plug. This crude material was dissolved in acetone (60 mL) and a solution of ammonium acetate (50 mL of 0.01 M aqueous solution) followed by sodium periodate (1.5 g, 7 mmol) was added. The reaction mixture was monitored by TLC for complete conversion of the boronic ester to the acid, and upon completion was quenched with 1M HCl. The aqueous layer was extracted 2x with ethyl acetate, and the combined organic layer was dried over $MgSO_4$, filtered, and concentrated. Recrystallization from ethyl acetate afforded the desired product as a pale tan solid (two crops totaling 152 mg, 20%).

$^1$H NMR (600 MHz, $CD_3CN$) δ 7.94 (s, 1H), 7.70 (dd, *J* = 8.9, 2.3 Hz, 2H), 6.81 (d, *J* = 8.7 Hz, 2H), 3.82 (s, 5H).$^{13}$C NMR (151 MHz, $CD_3CN$) δ 164.81, 144.99, 141.48, 113.80, 83.71, 56.01. (Ipso C-B carbon not detected due to quadrupole broadening) HRMS (ESI) m/z: calculated for $[C_7H_7O_3{}^{11}B_1{}^{127}I_1]^-$ 276.9538, found 276.9537

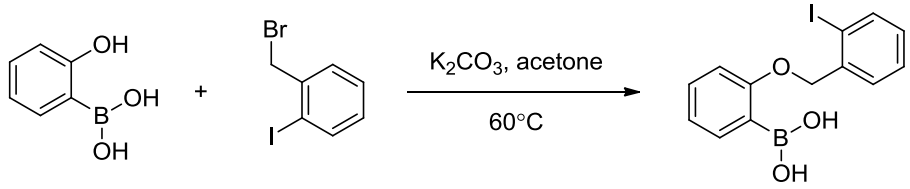


(2-((2-iodobenzyl)oxy)phenyl)boronic acid, **10**

2-hydroxyphenylboronic acid (690 mg, 5 mmol), 2-iodobenzyl bromide (1.78 g, 6 mmol), potassium carbonate (2.0 g, 15 mmol) and acetone (50 mL) were combined in a roundbottom flask equipped with a stirbar and reflux condenser. The solution was heated to reflux overnight. Upon cooling, water was added, and the mixture was extracted 3x with ethyl acetate. The combined organic layers were dried over $MgSO_4$, filtered, and concentrated. The solid was washed with hexanes, and recrystallized by slow evaporation from wet MeCN to afford the desired product as a colorless solid (two crops totaling 246 mg, 14%).

$^1$H NMR (600 MHz, $CD_3CN$) δ 7.95 (dd, *J* = 8.1, 1.4 Hz, 1H), 7.75 (dd, *J* = 7.2, 2.0 Hz, 1H), 7.50 (dd, *J* = 7.7, 1.8 Hz, 1H), 7.43 (tdd, *J* = 7.7, 4.4, 1.6 Hz, 2H), 7.11 (td, *J* = 7.7, 1.7 Hz, 1H), 7.02 (t, *J* = 7.9 Hz, 2H), 5.17 (s, 2H).$^{13}$C NMR (151 MHz, $CD_3CN$) δ 163.96, 140.40, 139.44, 137.12, 133.24, 131.04, 130.60, 129.47, 121.97, 112.21, 98.64, 74.63. HRMS (EI) m/z: calculated for $[C_{13}H_{12}B_1O_3I_1]^+$ 353.9924, found 353.9916

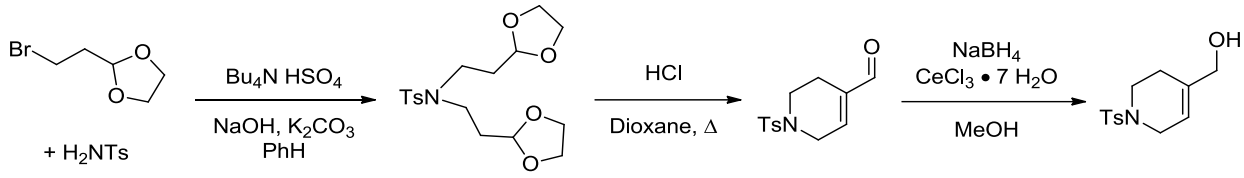


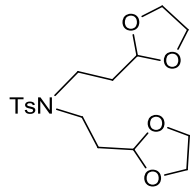


N,N-bis(2-(1,3-dioxolan-2-yl)ethyl)-4-methylbenzenesulfonamide, **S2**

Tosylamine (4.3 g, 25 mmol), 2-(bromoethyl)-1,3-dioxolane (12 mL, 100 mmol), tetrabutylammonium bisulfate (850 mg, 2.5 mmol), potassium carbonate (3.5 g, 25 mmol), and sodium hydroxide (3.5g, 88 mmol) were combined in benzene (25 mL). The mixture was stirred vigorously overnight at which time TLC showed consumption of the starting material. The mixture was diluted with ethyl acetate and washed with $H_2O$ three times. The organic layer was dried over $MgSO_4$, filtered, and concentrated. Column chromatography ($SiO_2$, eluting on a gradient from 9:1 Hexanes/ethyl acetate to 1:1 hexanes/ethyl acetate) afforded the desired product as a pale yellow oil (7.1 g, 76%).

$^1$H NMR (600 MHz, $CDCl_3$) δ 7.67 (d, *J* = 8.0 Hz, 2H), 7.26 (d, *J* = 8.0 Hz, 2H), 4.83 (t, *J* = 4.6 Hz, 2H), 3.89 (d, *J* = 7.0 Hz, 4H), 3.79 (d, *J* = 3.1 Hz, 4H), 3.28 – 3.08 (m, 4H), 2.38 (s, 3H), 1.95 – 1.79 (m, 4H). $^{13}$C NMR (151 MHz, $CDCl_3$) δ 143.21, 136.55, 129.70, 127.21, 102.22, 64.95, 53.55, 43.53, 32.87, 21.53. HRMS (ESI) m/z: calculated for $[C_{17}H_{25}O_6N_1S_1 + H]^+$ 372.1475, found 372.1480.

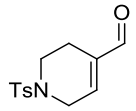


1-tosyl-1,2,3,6-tetrahydropyridine-4-carbaldehyde, **S3**

**S2** (5 g, 13.4 mmol) was dissolved in 4 mL of dioxane. 4 mL of 5 M HCl was added, and the solution was heated to reflux for 20 minutes. TLC showed consumption of product, and upon cooling the mixture was neutralized with 1M aqueous NaOH and extracted with ethyl acetate. The organic layer was washed with brine, fried over $MgSO_4$, filt. and concentrated to give a white solid (3.6 g, quantitative). Carried on without further purification.

$^1$H NMR (600 MHz, $CDCl_3$) δ 9.38 (d, *J* = 2.1 Hz, 1H), 7.67 (dd, *J* = 8.3, 2.2 Hz, 2H), 7.32 (d, *J* = 7.8 Hz, 2H), 6.84 (dd, *J* = 3.7, 2.0 Hz, 1H), 3.80 – 3.64 (m, 2H), 3.27 – 3.14 (m, 2H), 2.57 – 2.47 (m, 2H), 2.41 (d, *J* = 1.9 Hz, 3H). $^{13}$C NMR (151 MHz, $CDCl_3$) δ 191.23, 147.15, 144.03, 137.83, 132.94, 129.91, 129.90, 127.79, 42.53, 42.38, 26.61, 21.62. HRMS (ESI) m/z: calculated for $[C_{13}H_{15}O_3N_1S_1 + Na]^+$ 288.0665, found 288.0667.

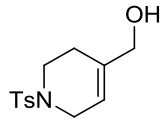


(1-tosyl-1,2,3,6-tetrahydropyridin-4-yl)methanol, **S4**

To **S3** (1.5 g, 5.6 mmol) in methanol (112 mL) was added $CeCl_3 \bullet 7\ H_2O$ (6.3 g, 17 mmol). After stirring for 10 min, $NaBH_4$ (3.2 g, 85 mmol) was added carefully in 5 portions. After stirring 1.5 hours, the reaction mixture was concentrated, and the residue was partitioned between DCM and $H_2O$. The layers were separated and the aqueous layer was extracted 2x with DCM. The combined organic layers were dried over $MgSO_4$, filtered, and concentrated. Column Chromatography ($SiO_2$, eluting with 1:1 Hexanes/Ethyl Acetate) afforded the desired product as a colorless solid (1.04 g, 70%).

$^1$H NMR (600 MHz, $CDCl_3$) δ 7.68 (d, *J* = 8.2 Hz, 2H), 7.32 (d, *J* = 8.0 Hz, 2H), 5.74 (dt, *J* = 3.6, 2.0 Hz, 1H), 4.12 – 3.96 (m, 2H), 3.59 (d, *J* = 2.3 Hz, 2H), 3.14 (t, *J* = 5.7 Hz, 3H), 2.43 (s, 4H), 2.30 – 2.19 (m, 2H). In accordance with previously reported spectra[98]

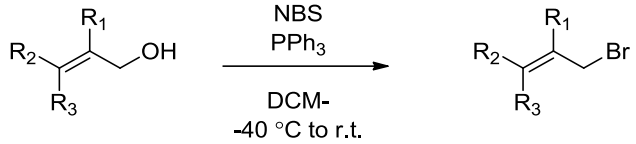


N-bromosuccinimide (1.1 equivalents) was dissolved in of DCM (0.15 M) under an atmosphere of $N_2$ and cooled to -40 $^o$C in a dry ice/acetonitrile bath. Triphenyl phosphine (1.1 equivalents) was added in one portion and the mixture was stirred for 40 min at -40$^o$C. A solution of allylic alcohol (1 equivalent) in DCM (0.3 M) was added, and the solution was allowed to warm to room temperature overnight. The solution was poured over pentane, filtered, and concentrated *in vacuo*. The crude residue was purified by chromatography on a short plug of silica, eluting rapidly to minimize product decomposition.

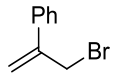


(3-bromoprop-1-en-2-yl)benzene, **S5**

3 mmol scale. Eluted with pentane to afford the desired product as a pale yellow oil (260 mg, 44%). $^1$H NMR (400 MHz, $CDCl_3$) δ 7.58 – 7.46 (m, 2H), 7.43 – 7.31 (m, 3H), 5.54 (dd, *J* = 27.1, 1.8 Hz, 2H), 4.40 (d, *J* = 1.8 Hz, 2H).In accordance with previously reported spectra[99]

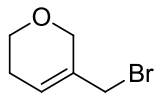


5-(bromomethyl)-3,6-dihydro-2H-pyran, **S6**

8.7 mmol scale. Eluted with pentane to afford the desired product as a pale yellow oil (954 mg, 61%). $^1$H NMR (400 MHz, $CDCl_3$) δ 6.21 – 5.82 (m, 1H), 4.27 (d, *J* = 2.3 Hz, 2H), 3.93 (d, *J*

= 1.2 Hz, 3H), 3.80 (t, *J* = 5.5 Hz, 3H), 2.22 (ddt, *J* = 5.5, 2.8, 1.4 Hz, 2H). In accordance with previously reported spectra[100]

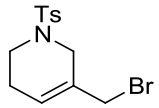


5-(bromomethyl)-1-tosyl-1,2,3,6-tetrahydropyridine, **S7**

2.62 mmol scale. Eluted with 1:1 Hexanes/Ethyl Acetate to afford the desired product as a pale yellow solid (706 mg, 82%). $^{1}$H NMR (600 MHz, $CDCl_3$) δ 7.68 (d, *J* = 7.9 Hz, 2H), 7.32 (d, *J* = 8.0 Hz, 2H), 5.90 (d, *J* = 2.1 Hz, 1H), 3.89 (s, 2H), 3.69 (d, *J* = 2.3 Hz, 2H), 3.14 (t, *J* = 5.8 Hz, 2H), 2.42 (s, 3H), 2.27 – 2.11 (m, 2H). $^{13}$C NMR (151 MHz, $CDCl_3$) δ 143.81, 133.37, 131.12, 129.83, 127.73, 127.72, 125.93, 45.88, 42.23, 34.60, 25.29, 21.63. HRMS (ESI) m/z: calculated for $[C_{13}H_{16}O_2N_1S_1Br_1 + Na]^+$ 351.9977, found 351.9982.

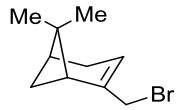


(1R,5S)-2-(bromomethyl)-6,6-dimethylbicyclo[3.1.1]hept-2-ene, **S8**

8.5 mmol scale. Eluted with pentane to afford the desired product as a colorless oil (1.14 g, 62% ). $^{1}$H NMR (400 MHz, $CDCl_3$) δ 5.68 (dd, *J* = 3.2, 1.7 Hz, 1H), 3.96 (dq, *J* = 2.3, 1.1 Hz, 2H), 2.45 (dt, *J* = 8.8, 5.6 Hz, 1H), 2.37 – 2.19 (m, 4H), 2.17 – 2.05 (m, 1H), 1.58 (s, 2H), 1.32 (s, 3H), 1.18 (d, *J* = 8.7 Hz, 1H), 0.83 (s, 3H). In accordance with previously reported spectra[101]

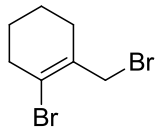


1-bromo-2-(bromomethyl)cyclohex-1-ene, **S9**

12.5 mmol scale. Eluted on a gradient from hexanes to 9:1 hexanes/diethyl ether to afford the desired product as a colorless oil (2.13 g, 67%). $^{1}$H NMR (400 MHz, $CDCl_3$) δ 4.11 (s, 2H), 2.52 (s, 2H), 2.29 (s, 2H), 1.71 (s, 4H). In accordance with previously reported spectra[102]

### 2.6.6 Palladium catalyzed elaboration and comparison experiments

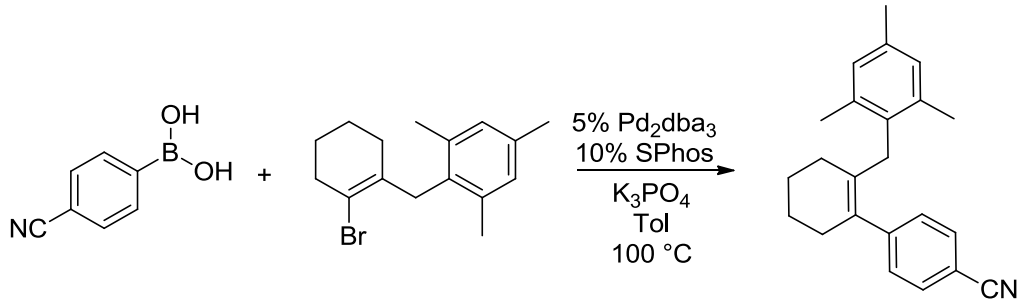


6'-(2,4,6-trimethylbenzyl)-2',3',4',5'-tetrahydro-[1,1'-biphenyl]-4-carbonitrile, **8**

Prepared by a slight modification of a previously reported procedure:[103]

Tris(dibenzylideneacetone)dipalladium(0) (2.7 mg, 0.003 mmol), Sphos (2.5 mg, 0.006 mmol), tribasic potassium phosphate (37.1 mg, 0.175 mmol), and 4-cyanophenylboronic acid (17.2 mg, 0.117 mmol) were combined in a vial equipped with a stirbar. A solution of **7j** (17.1 mg, 0.058 mmol), in 0.4 mL of dry toluene was added, and the solution was blanketed with argon and sealed tightly with a screw cap. The solution was heated to 100 °C overnight. Upon cooling, the mixture was dry loaded onto silica, and purified by column chromatography (eluting on a gradient from pentane to 10% diethyl ether in pentane) to afford the desired product as a pale yellow solid. (8.3 mg, 46% yield).

$^1$H NMR (600 MHz, $CDCl_3$) δ 7.64 (d, *J* = 8.2 Hz, 2H), 7.33 (d, *J* = 8.2 Hz, 2H), 6.76 (s, 2H), 3.28 (s, 2H), 2.25 (dt, *J* = 6.4, 3.2 Hz, 2H), 2.22 (s, 3H), 2.10 (s, 6H), 1.73 (dd, *J* = 7.6, 4.9 Hz, 2H), 1.70 – 1.64 (m, 2H), 1.58 (dd, *J* = 5.7, 2.6 Hz, 2H). $^{13}$C NMR (151 MHz, $CDCl_3$) δ 149.53, 136.93, 135.34, 133.45, 132.98, 132.15, 132.14, 129.42, 128.91, 119.29, 110.04, 34.03, 32.27, 27.47, 23.20, 22.95, 20.92, 20.62. HRMS (EI) m/z: calculated for $[C_{23}H_{25}N]^+$ 315.1987, found 315.1995.

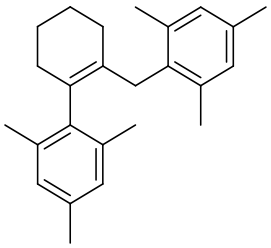

2',4',6'-trimethyl-6-(2,4,6-trimethylbenzyl)-2,3,4,5-tetrahydro-1,1'-biphenyl, **9**

Isolated from the palladium catalyzed synthesis of **7j**.

$^1$H NMR (600 MHz, $CDCl_3$) δ 6.91 (s, 2H), 6.77 (s, 2H), 3.05 (t, *J* = 2.3 Hz, 2H), 2.28 (s, 3H), 2.25 (s, 6H), 2.23 (s, 3H), 2.16 (s, 6H), 2.07 (q, *J* = 4.1 Hz, 2H), 1.71 – 1.63 (m, 2H), 1.58 (t, *J* = 2.3 Hz, 4H).$^{13}$C NMR (151 MHz, $CDCl_3$) δ 139.36, 136.87, 135.46, 134.91, 134.80, 133.66, 132.17, 130.25, 128.35, 128.31, 32.72, 30.82, 27.29, 23.36, 23.07, 20.98, 20.82, 20.51, 19.17. HRMS (EI) m/z: calculated for $[C_{25}H_{32}]^+$ 332.2504, found 332.2512

### 2.6.7 Stoichiometric Reactivity and Control Experiments

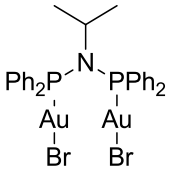


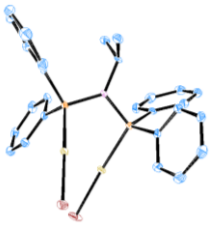

Dibromo(N-(diphenylphosphino)-N-isopropyl-1,1-diphenylphosphinamine) digold(I) (**12**)

Allyl Bromide (100 µL) was added to a solution of **1** (27.8 mg, 0.03 mmol) in MeCN (1.5 mL). The resulting mixture was stirred at 65°C overnight. The reaction mixture was concentrated and washed sequentially with pentane and ether to yield a colorless solid. Recrystallized from a saturated DCM/Pentane solution layered with diethyl ether (26 mg, 88%). X-ray quality crystals grown by slow evaporation of saturated DCM/pentane solution.

$^{1}$H NMR (400 MHz, $CD_2Cl_2$) δ 7.85 (q, *J* = 7.2 Hz, 8H), 7.66 (t, *J* = 7.4 Hz, 4H), 7.61 – 7.50 (m, 8H), 4.01 (dddd, *J* = 22.5, 16.0, 13.6, 6.9 Hz, 1H), 1.09 (d, *J* = 6.8 Hz, 6H). $^{13}$C NMR (101 MHz, $CD_2Cl_2$) δ 133.97, 133.82, 132.91, 129.35, 129.29, 129.23, 55.01, 24.15. $^{31}$P NMR (162 MHz, $CD_2Cl_2$) δ 77.3 (bs) $^{31}$P NMR (162 MHz, $CD_3CN$) δ 80.3 (s) EA: Calculated: C, 33.05; H, 2.77; N, 1.43; Found: C, 33.24; H, 3.09; N: 1.39

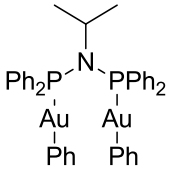


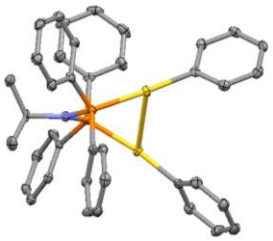

Diphenyl(N-(diphenylphosphino)-N-isopropyl-1,1-diphenylphosphinamine) digold(I) (**11**)

Phenylboronic acid (11 mg, 0.086 mmol), cesium carbonate (30 mg, 0.083 mmol), and **1** (22 mg, 0.024 mmol) were combined in a vial equipped with a stirbar. MeCN (0.6 mL) was added and the solution was heated to 65°C for 2 hours. The mixture was concentrated, and the residue was taken up in benzene and filtered through a celite plug. Upon concentration, the solid was washed with pentane and minimal methanol and dried *in vacuo* to give the desired product as a pale tan solid. (23.7 mg, 99%).

X-ray quality crystals were grown by vapor diffusion of hexanes into toluene.

$^{1}$H NMR (400 MHz, $CD_2Cl_2$) δ 7.93-7.97 (m, 8H), 7.52-7.61 (m, 12H), 7.11 (bs, 4H), 7.02 (t, *J* = 7.6 Hz, 4H), 6.88 (t, *J* = 7.2 Hz, 2H), 3.95-4.06 (m, 1H), 1.17 (d, *J* = 6.8 Hz, 6H) $^{13}$C NMR (101 MHz, $CD_2Cl_2$) δ 139.8, 133.8 (d, *J* = 15.6 Hz), 132.5 (d, *J* = 51 Hz) 131.7, 128.8 (d, *J* = 10.7 Hz), 127.4, 126.8 (d, *J* = 6.4 Hz), 125.0, 55.2, 24.4 [Gold aryl ipso carbon not found.] $^{31}$P NMR (162 MHz, $CD_2Cl_2$) δ 93.3 (bs) EA: Calculated: C, 48.01; H, 3.82; N, 1.44; Found: C, 48.36; H, 3.54; N, 1.56

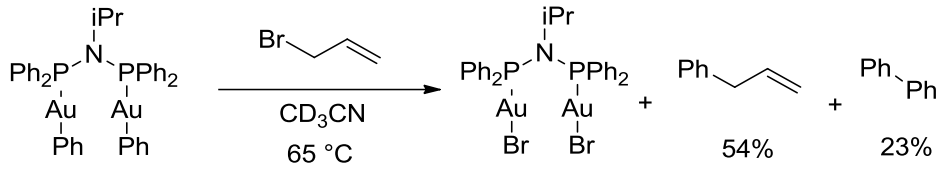


To a solution of **11** (6 mg, 0.006 mmol) in $CD_3CN$ was added allyl bromide (42 μL, 0.492 mmol) and the reaction mixture was heated to 65°C for 1.5 hours. Upon cooling, $PhCO_2Et$ (2 uL, 0.015 mmol) was added and the reaction mixture was analyzed by GC (to determine yields of allylbenzene and biphenyl) and $^{31}$PNMR (showing complete consumtion of **11** and the presence of **12**).

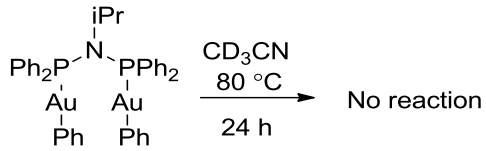


A solution of **11** (5 mg, 0.005 mmol) in $CD_3CN$ (0.2 mL) was heated in a vial at 80°C for 24 hrs. Upon cooling, $PhCO_2Et$ (5 uL, 0.035 mmol) was added and the reaction mixture was analyzed by GC, with no Ph-Ph detected. $^{31}$PNMR indicated the persistence of **11**.

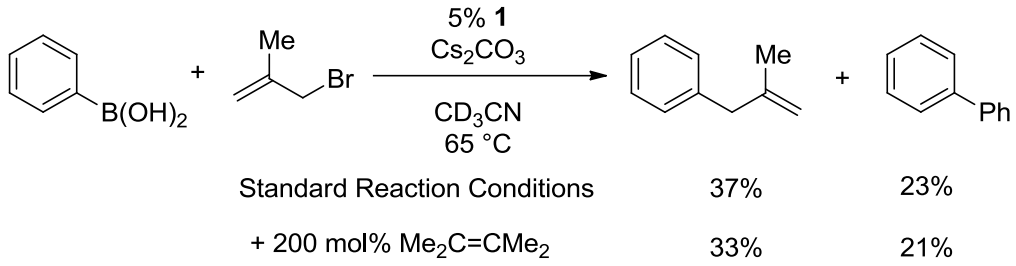


Following the general procedure for gold catalyzed allylation with substituted allylic bromides, substituting phenylboronic acid for mesityl boronic acid, the above results were obtained. In the latter case, 0.24 mmol (24 μL) of tetramethylethylene was added. The product ratios were determined by $^{1}$HNMR vs. trimethoxybenzene as an internal standard.

### 2.6.8 Preparation of Cyclometallated Gold (III)

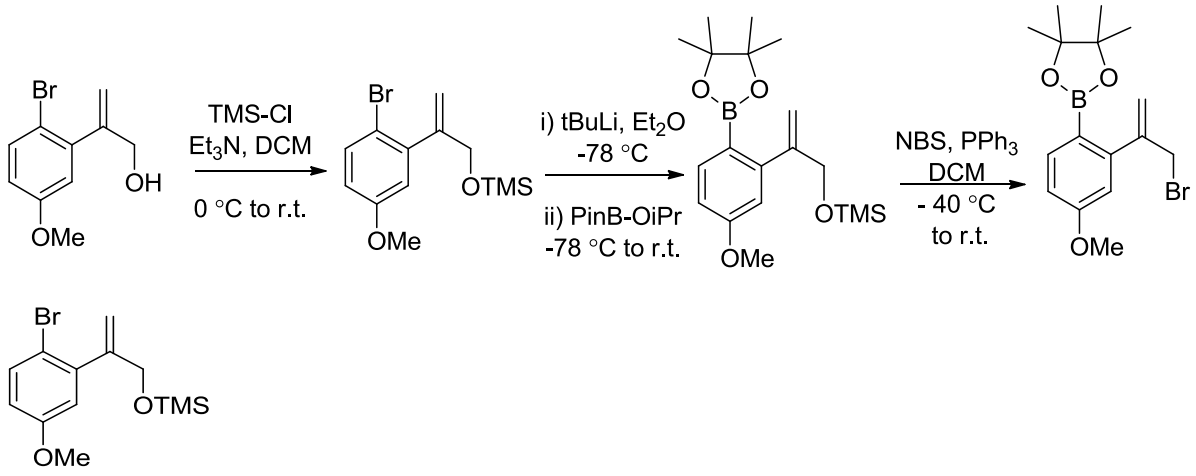


((2-(2-bromo-5-methoxyphenyl)allyl)oxy)trimethylsilane, **S10**

To a solution of 2-(2-bromo-5-methoxyphenyl)prop-2-en-1-ol[104] (681 mg, 2.8 mmol) in DCM under $N_2$ at 0 °C was added sequentially triethylamine (0.82 mL, 5.88 mmol) and chlorotrimethylsilane (0.39 mL, 3.08 mmol). The solution was stirred for 10 minutes at 0 °C, and then warmed to room temperature. After an additional 45 minutes, TLC showed complete consumption the starting material. The reaction mixture was concentrated directly, slurried in diethyl ether, and filtered through a fine fritted funnel. Concentration of this solution afforded the desired product as a pale yellow oil which was used without further purification. (716 mg, 81% yield)

$^1$H NMR (600 MHz, $CDCl_3$) δ 7.42 (d, *J* = 8.7 Hz, 1H), 6.75 (d, *J* = 3.1 Hz, 1H), 6.71 (dd, *J* = 8.8, 3.1 Hz, 1H), 5.52 (d, *J* = 1.8 Hz, 1H), 5.09 (d, *J* = 1.7 Hz, 1H), 4.33 (t, *J* = 1.7 Hz, 2H), 3.78 (s, 3H), 0.14 (s, 9H). $^{13}$C NMR (151 MHz, $CDCl_3$) δ 158.78, 148.77, 142.28, 133.33, 116.56, 114.85, 114.12, 112.88, 64.76, 55.60, -0.31. HRMS (EI) m/z: calculated for $[C_{13}H_{19}O_2Si_1Br_1]^+$ 314.0338; 316.0317, found 314.0346; 316.0323.

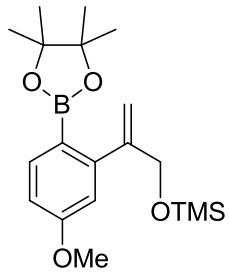


((2-(5-methoxy-2-(4,4,5,5-tetramethyl-1,3,2-dioxaborolan-2-yl)phenyl)allyl)oxy)trimethylsilane, **S11**

**S10** (716 mg, 2.27 mmol) was dissolved in $Et_2O$ under an atmosphere of nitrogen, and cooled to -78 °C. tBuLi (2.95 mL of a 1.7 M solution in pentane, 5 mmol) was added dropwise, and the solution was stirred at -78 °C for 1 hour. Freshly distilled 2-isopropoxy-4,4,5,5-tetramethyl-1,3,2-dioxaborolane (1.15 mL, 5.68 mmol) was added, and the solution was allowed to warm

to room temperature overnight. The reaction mixture was quenched with saturated aqueous ammonium chloride, and the layers were separated. The aqueous layer was extracted with ethyl acetate, and the combined organic layers were dried over $MgSO_4$, filtered, and concentrated. Column Chromatography on silica gel (eluting on a gradient from pentane to 97:3 pentane/diethyl ether) afforded the desired product as a colorless oil. (492 mg, 55% yield).

$^1$H NMR (400 MHz, $CDCl_3$) δ 7.72 (d, *J* = 8.3 Hz, 1H), 6.85 (dd, *J* = 8.3, 2.5 Hz, 1H), 6.79 (d, *J* = 2.5 Hz, 1H), 5.38 (d, *J* = 2.0 Hz, 1H), 5.03 (d, *J* = 1.9 Hz, 1H), 4.44 (t, *J* = 1.7 Hz, 2H), 3.85 (s, 3H), 1.34 (s, 12H), 0.19 (s, 9H). $^{13}$C NMR (101 MHz, $CDCl_3$) δ 161.21, 150.64, 148.87, 137.01, 114.57, 112.18, 111.93, 83.49, 66.12, 55.21, 24.81, -0.21. [Boronic ester ipso carbon not seen due to quadrupole broadening.] HRMS (ESI) m/z: calculated for $[C_{19}H_{31}O_4B_1Si_1 + Na]^+$ 385.1977, found 385.1981.

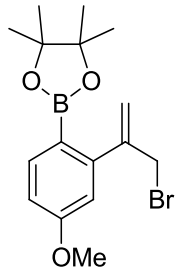


2-(2-(3-bromoprop-1-en-2-yl)-4-methoxyphenyl)-4,4,5,5-tetramethyl-1,3,2-dioxaborolane, **15**

N-bromosuccinimide (266 mg, 1.5 mmol) was dissolved in 14 mL of DCM under an atmosphere of $N_2$ and cooled to -40 $^o$C in a dry ice/acetonitrile bath. Triphenylphosphine (391 mg, 1.5 mmol) was added in one portion and the mixture was stirred for 40 min at -40$^o$C. A solution of **S11** (492 mg, 1.35 mmol) in 14 mL DCM was added, and the solution was allowed to warm to room temperature overnight. The solution was poured over pentane, filtered, and concentrated *in vacuo*. The crude residue was purified by chromatography, eluting with 8:2 pentane/diethyl ether on a short plug of silica, eluting rapidly to minimize product decomposition. The desired product was isolated as a pale yellow oil which solidified upon standing. (235 mg, 67% yield).

$^1$H NMR (600 MHz, $CDCl_3$) δ 7.75 (d, *J* = 8.3 Hz, 1H), 6.85 (dd, *J* = 8.3, 2.5 Hz, 1H), 6.80 (d, *J* = 2.5 Hz, 1H), 5.48 (q, *J* = 1.1 Hz, 1H), 5.12 (d, *J* = 1.3 Hz, 1H), 4.36 (d, *J* = 1.0 Hz, 2H), 3.84 (s, 3H), 1.29 (s, 13H). $^{13}$C NMR (151 MHz, $CDCl_3$) δ 161.49, 148.34, 148.23, 137.60, 118.35, 115.85, 112.42, 83.63, 55.31, 38.10, 24.90. [Ipso C-BPin not seen due to quadrupole broadening] HRMS (EI) m/z: calculated for $[C_{16}H_{22}B_1O_3Br_1]^+$ 352.0845; 354.0825, found 352.0850; 354.0842.

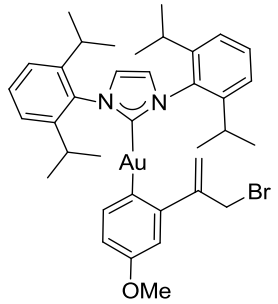


(1,3-bis(2,6-diisopropylphenyl)-1H-imidazol-2(3H)-ylidene)(2-(3-bromoprop-1-en-2-yl)-4-methoxyphenyl)gold(I), **17**

**15** (8.7 mg, 0.024 mmol) and 1,3-bis(2,6-diisopropylphenyl)-1H-imidazol-2(3H)-ylidene gold(I) hydroxide (7.4 mg, 0.012 mmol) were dissolved in $C_6D_6$ (0.6 mL) and stirred at room temperature for 2 hours at which time $^1$HNMR indicated the consumption of the gold hydroxide. The mixture was concentrated, and washed sequentially with pentane and ether to give the desired product as a colorless solid. (7.9 mg, 81%).

$^1$H NMR (600 MHz, $C_6D_6$) δ 7.33 (d, *J* = 8.0 Hz, 1H), 7.29 (t, *J* = 7.8 Hz, 2H), 7.13 (d, *J* = 2.7 Hz, 1H), 7.11 (d, *J* = 7.8 Hz, 4H), 6.79 (dd, *J* = 8.1, 2.7 Hz, 1H), 6.29 (s, 2H), 5.17 – 4.95 (m, 2H), 4.18 (s, 2H), 3.34 (s, 3H), 2.60 (p, *J* = 6.9 Hz, 4H), 1.43 (d, *J* = 6.9 Hz, 12H), 1.08 (d, *J* = 6.9 Hz, 12H).$^{13}$C NMR (151 MHz, $C_6D_6$) δ 158.83, 157.94, 153.49, 150.59, 146.04, 140.93, 135.11, 130.65, 124.34, 122.47, 116.04, 114.49, 112.53, 54.56, 39.19, 29.09, 24.74, 24.01. EA: Calculated: C, 54.75; H, 5.71; N, 3.45; Found: C, 55.12; H, 5.91; N, 3.35

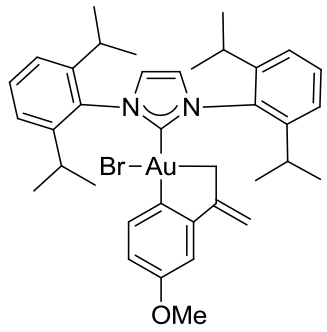


Bromo(1,3-bis(2,6-diisopropylphenyl)-1H-imidazol-2(3H)-ylidene) (1-methoxy-3-(prop-1-en-2-yl)benzene-4,3'-diyl)gold(III), **18**

**17** (69 mg, 0.084 mmol) was dissolved in $CD_3CN$ (1.5 mL) and the mixture was heated to 40 $^o$C. Reaction progress was monitored by $^1$HNMR for the consumption of **17**. Upon completion, the mixture was concentrated and washed with pentane and recrystallized by slow evaporation of an acetonitrile solution to yield the desired product. (80 mg, 86% yield)

X-ray quality crystals were grown by vapor diffusion of heptane into diisopropyl ether.

$^1$H NMR (600 MHz, $CD_3CN$) δ 7.97 (d, *J* = 8.6 Hz, 1H), 7.60 (s, 2H), 7.50 (t, *J* = 7.8 Hz, 2H), 7.35 (d, *J* = 7.8 Hz, 4H), 6.82 (d, *J* = 2.7 Hz, 1H), 6.55 (dd, *J* = 8.6, 2.8 Hz, 1H), 5.08 (d, *J* = 1.5 Hz, 1H), 4.72 (d, *J* = 1.6 Hz, 1H), 3.68 (s, 3H), 3.15 (s, 2H), 2.83 (t, *J* = 1.5 Hz, 2H), 2.70

(s, 2H), 1.37 (d, *J* = 6.5 Hz, 12H), 1.19 – 1.09 (m, 12H). $^{13}$C NMR (151 MHz, $CD_3CN$) δ 183.86, 159.39, 156.44, 151.74, 146.69, 137.18, 135.13, 131.54, 126.65, 114.64, 106.59, 104.08, 55.53, 45.12, 29.73, 26.46. [Hindered rotation causes significant broadening of several peaks, gold aryl ipso carbon not observed.] EA: Calculated: C, 54.75; H, 5.71; N, 3.45; Found: C, 54.90; H, 5.95; N, 3.37

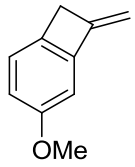


3-methoxy-8-methylenebicyclo[4.2.0]octa-1(6),2,4-triene, **18**

**17** (60 mg, 0.074 mmol) was dissolved in $CD_2Cl_2$ (3 mL) and the mixture was added to a vial containing $AgSbF_6$ (50 mg, 0.14 mmol). A precipitate formed immediately, and the suspension was sonicated for 3 minutes before filtering through a glass fiber filter. The mixture was concentrated and the residue was purified via column chromatography on silica, eluting with 95:5 Pentane/Ethyl Acetate to afford the title compound as a colorless oil. (8 mg, 74%).

$^1$H NMR (600 MHz, $CDCl_3$) δ 7.10 (d, *J* = 8.0 Hz, 1H), 6.79 (dd, *J* = 8.0, 2.2 Hz, 1H), 6.76 (d, *J* = 2.1 Hz, 1H), 5.27 (d, *J* = 1.7 Hz, 1H), 4.92 (s, 1H), 3.79 (s, 4H), 3.54 (s, 2H). $^{13}$C NMR (151 MHz, $CDCl_3$) δ 159.68, 145.69, 144.17, 137.12, 123.80, 116.29, 103.47, 102.90, 55.50, 37.69. HRMS (EI) m/z: calculated for $[C_{10}H_{10}O_1]^+$ 146.0732, found 146.0734.

## 2.6.9 NMR spectra of previously unreported compounds

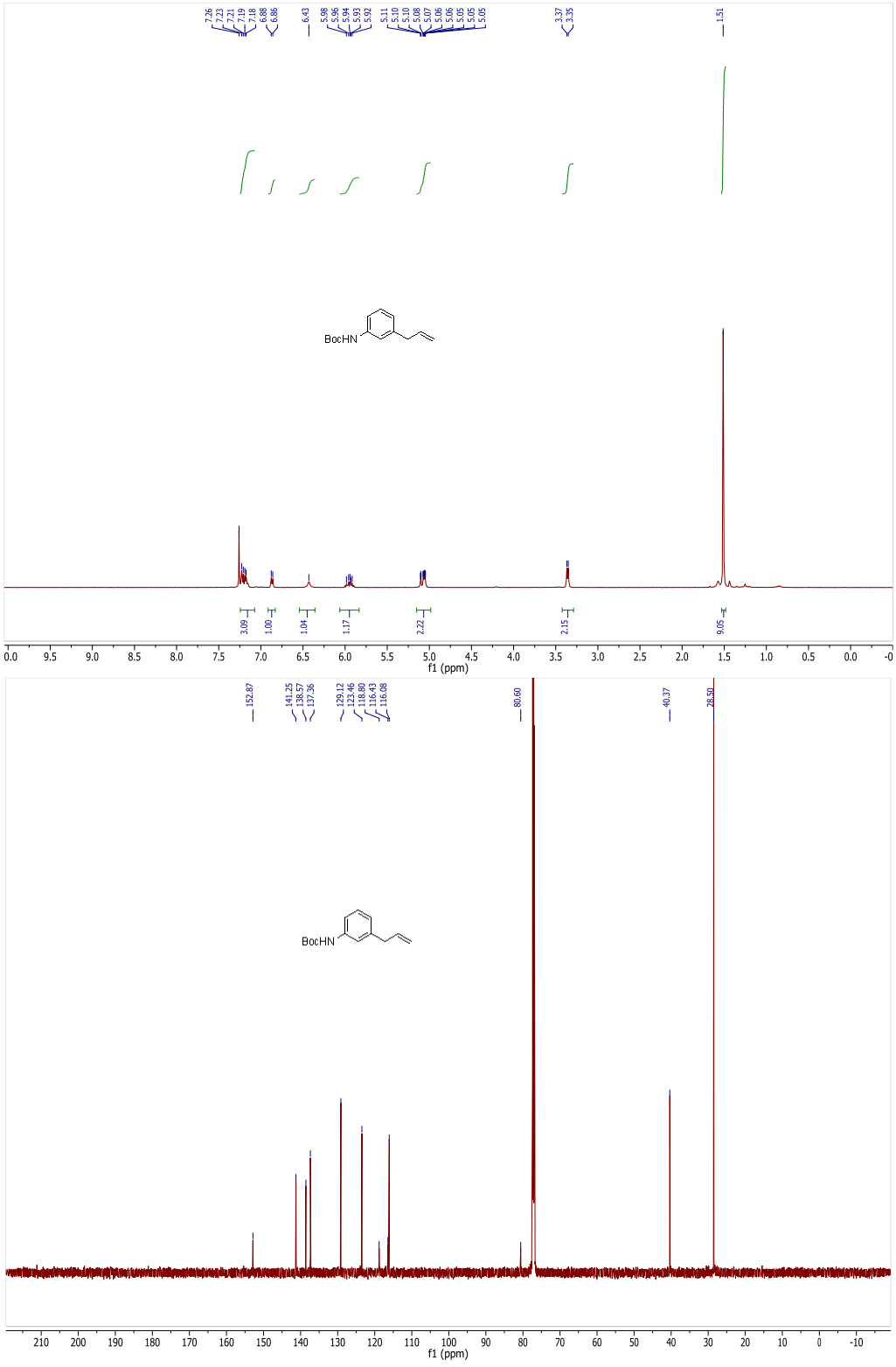

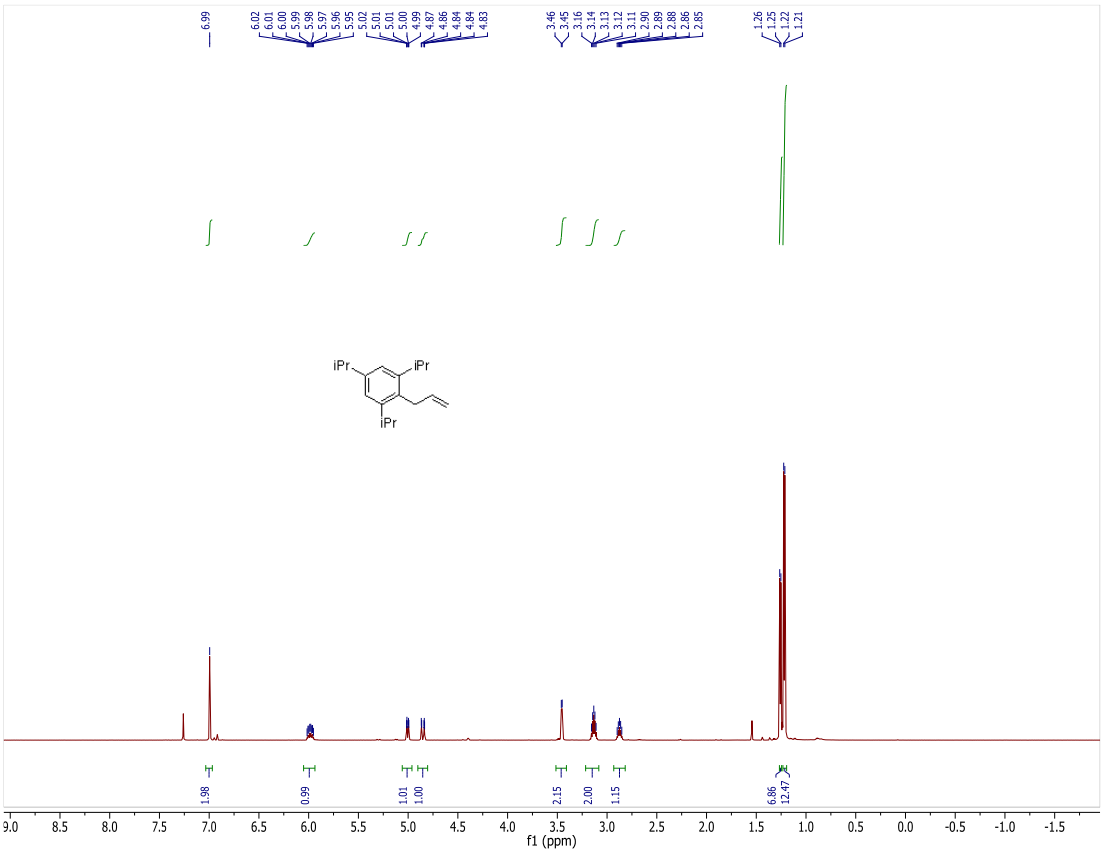
6.99
6.02
6.01
6.00
5.99
5.98
5.97
5.96
5.95
5.02
5.01
5.01
5.00
4.99
4.87
4.86
4.84
4.84
4.83
3.46
3.45
3.16
3.14
3.13
3.12
3.11
2.90
2.89
2.88
2.86
2.85
1.26
1.25
1.22
1.21
iPr
iPr
iPr
1.98
0.99
1.01
1.00
2.15
2.00
1.15
6.86
12.47
f1 (ppm)

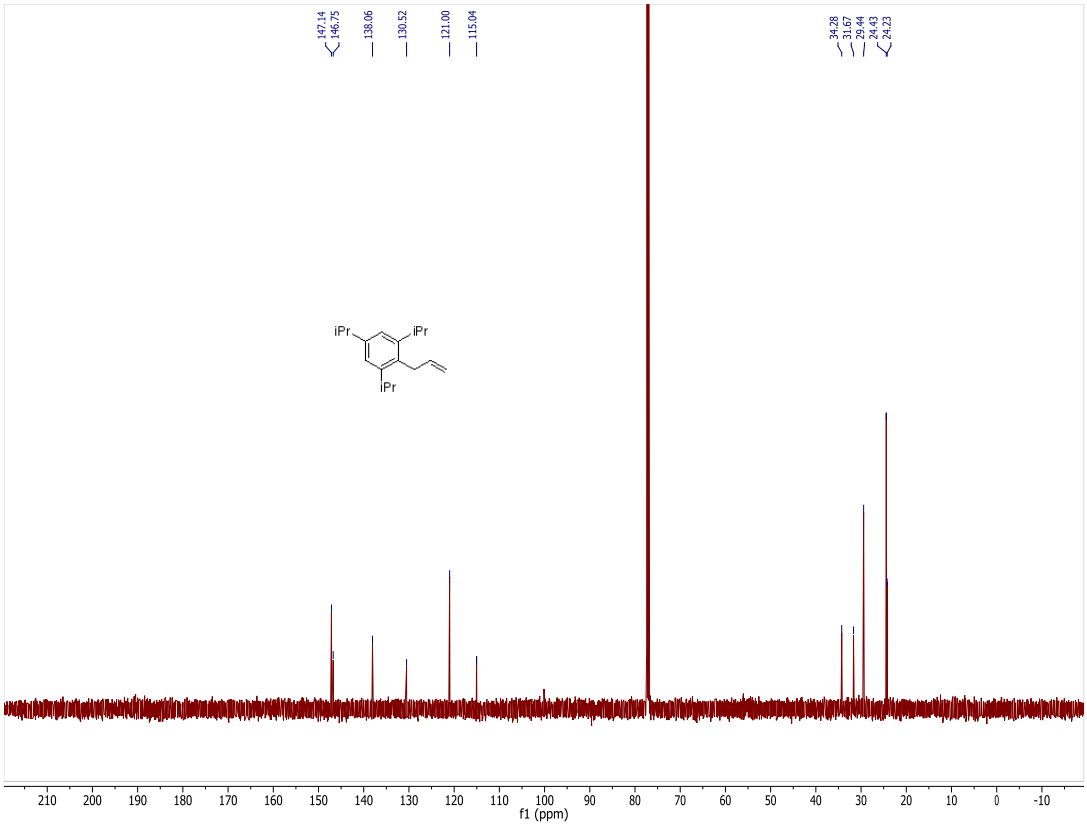
147.14
146.75
138.06
130.52
121.00
115.04
34.28
31.67
29.44
24.43
24.23
iPr
iPr
iPr
f1 (ppm)

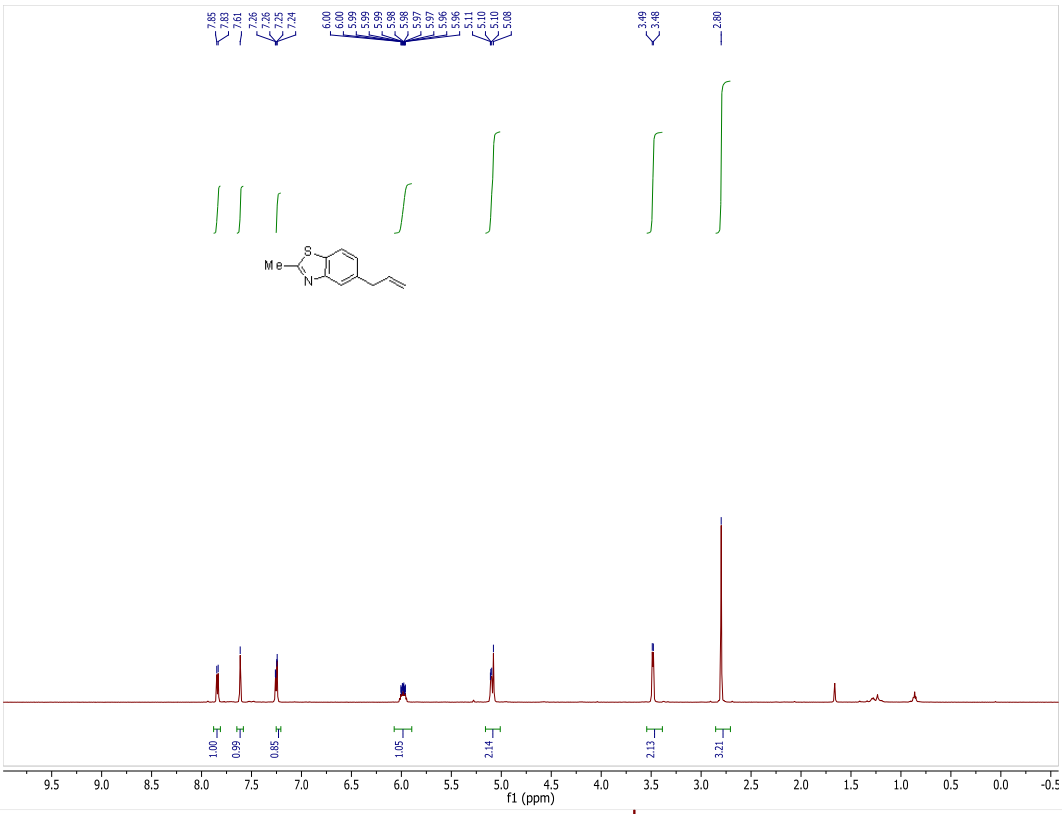
7.85
7.83
7.61
7.26
7.26
7.25
7.24
6.00
6.00
5.99
5.99
5.99
5.98
5.98
5.97
5.97
5.96
5.96
5.11
5.10
5.10
5.08
3.49
3.48
2.80
Me
S
N
1.00
0.99
0.85
1.05
2.14
2.13
3.21
f1 (ppm)

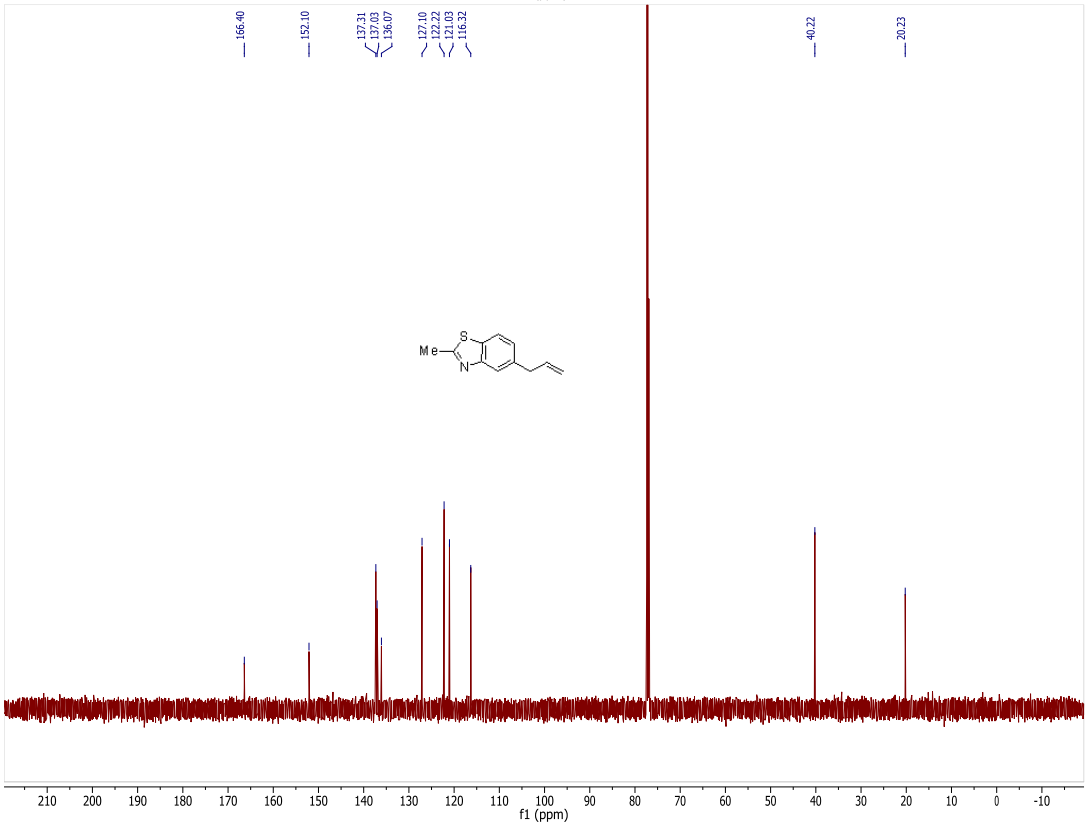
166.40
152.10
137.31
137.03
136.07
127.10
122.22
121.03
116.32
40.22
20.23
Me
S
N
f1 (ppm)

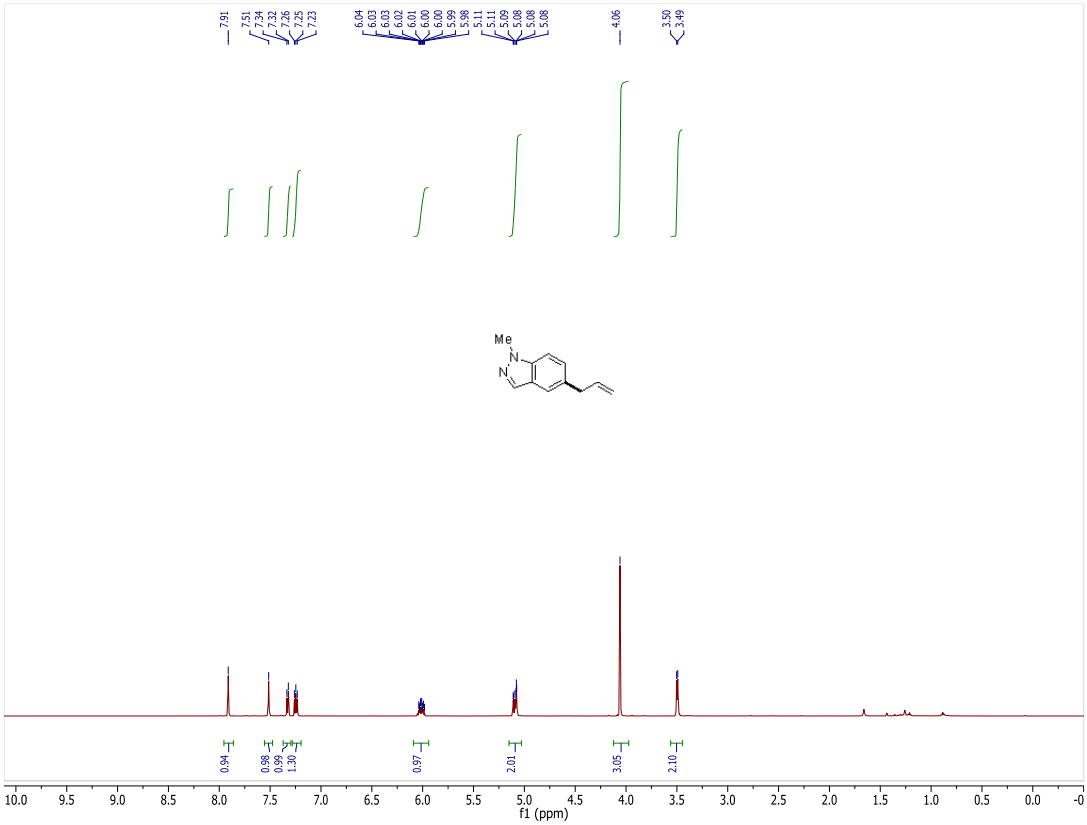
7.91
7.51
7.34
7.32
7.26
7.25
7.23
6.04
6.03
6.03
6.02
6.01
6.00
6.00
5.99
5.98
5.11
5.11
5.09
5.08
5.08
5.08
4.06
3.50
3.49
Me
0.94
0.98
0.99
1.30
0.97
2.01
3.05
2.10
f1 (ppm)

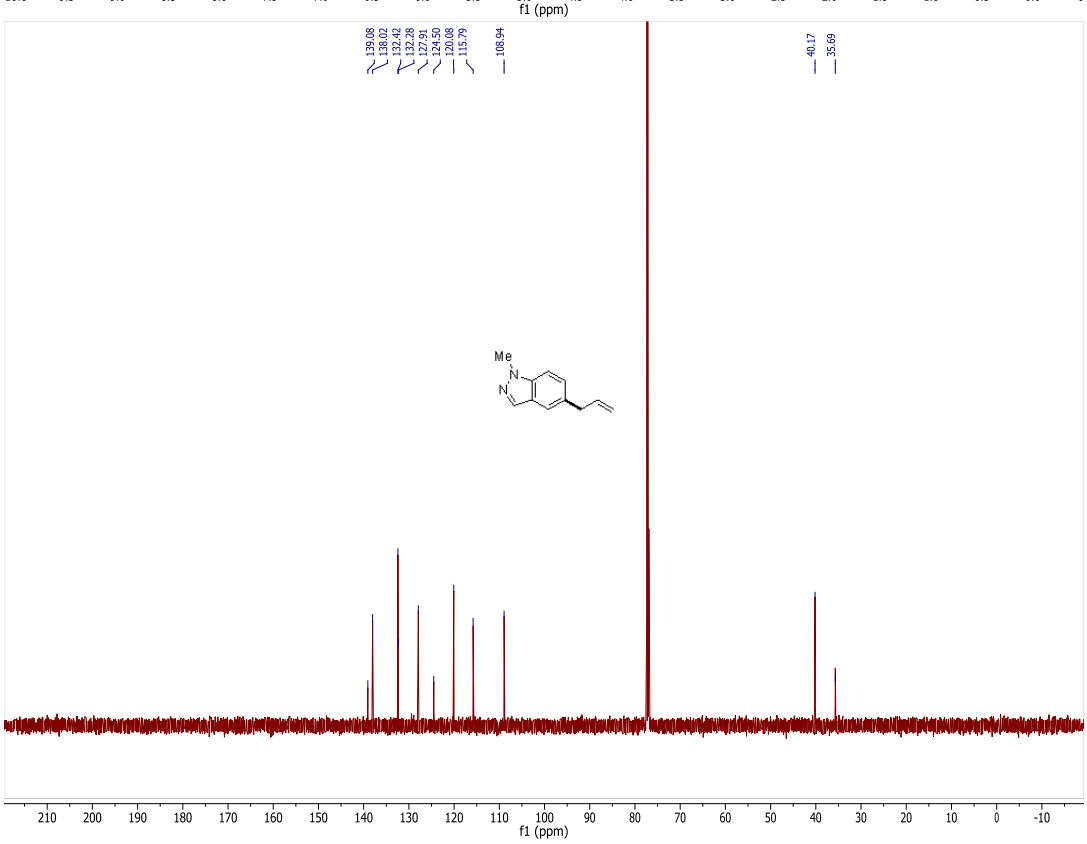
139.08
138.02
132.42
132.28
127.91
124.50
120.08
115.79
108.94
40.17
35.69
Me
f1 (ppm)

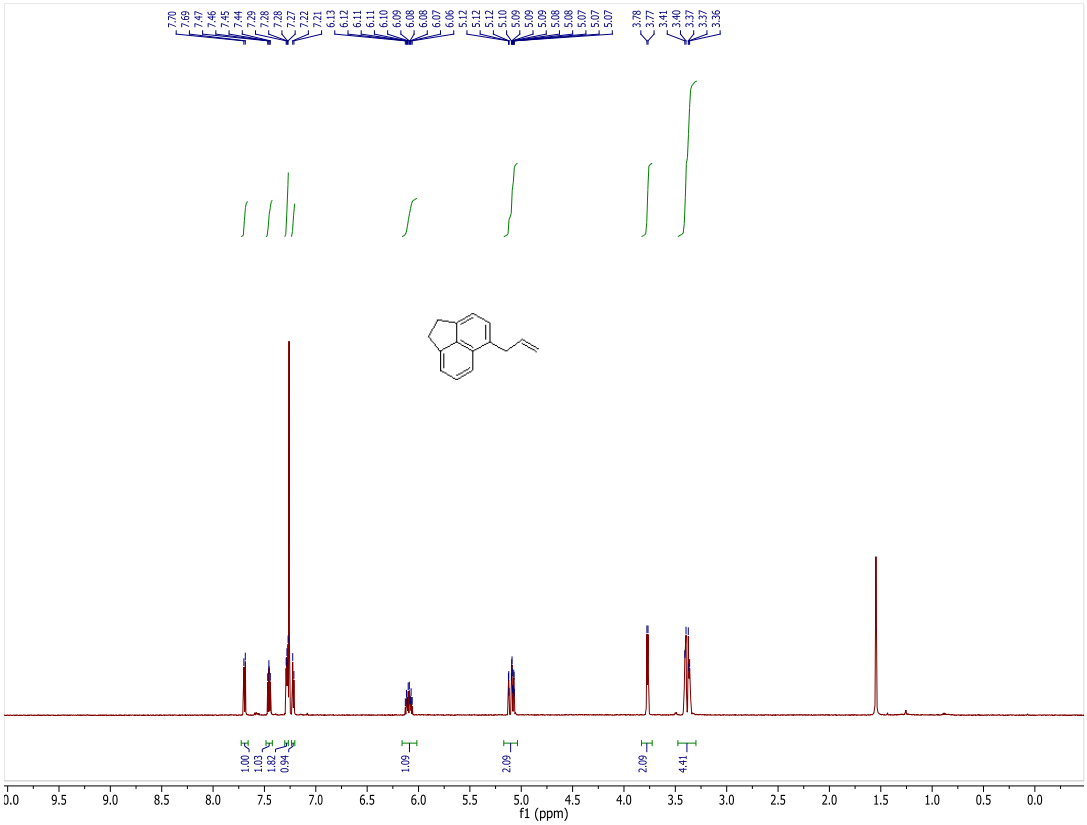
7.70
7.69
7.47
7.46
7.45
7.44
7.29
7.28
7.28
7.27
7.22
7.21
6.13
6.12
6.12
6.11
6.11
6.10
6.09
6.08
6.08
6.07
6.06
5.12
5.12
5.12
5.10
5.09
5.09
5.09
5.08
5.08
5.07
5.07
5.07
3.78
3.77
3.41
3.40
3.37
3.37
3.36
1.00
1.03
1.82
0.94
1.09
2.09
2.09
4.41
f1 (ppm)

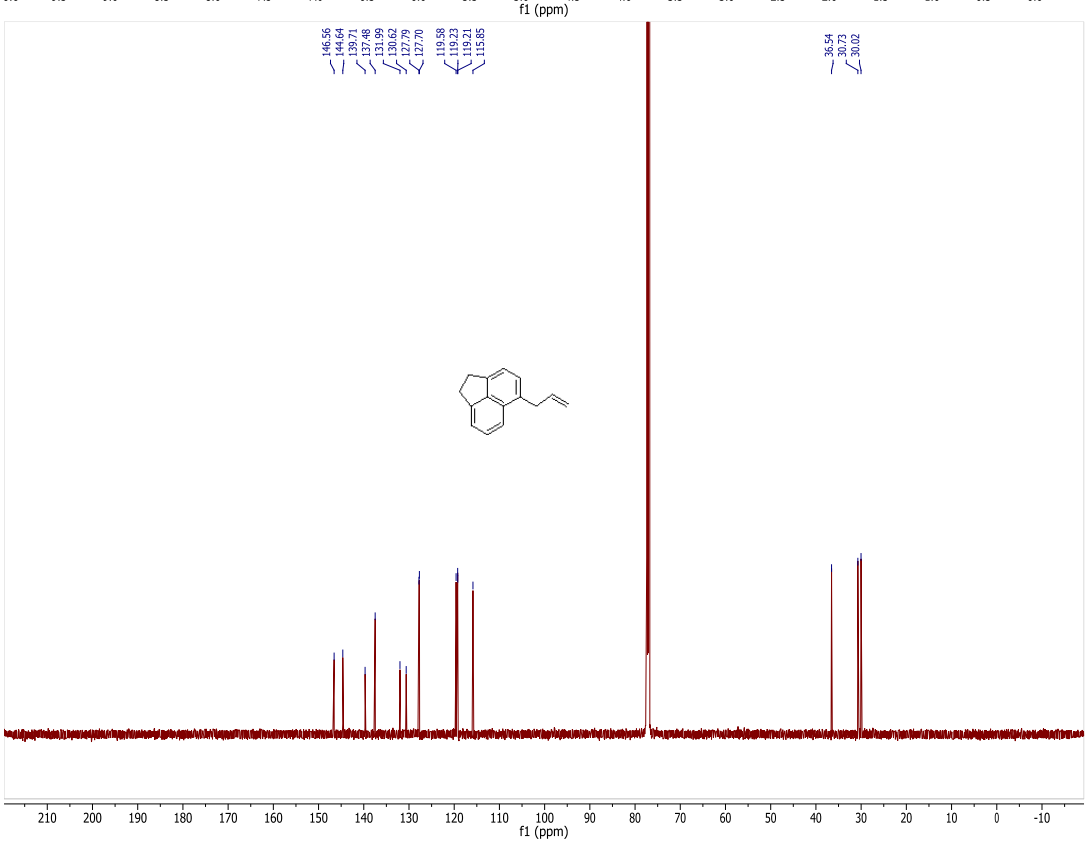
146.56
144.64
139.71
137.48
131.99
130.62
127.79
127.70
119.58
119.23
119.21
115.85
36.54
30.73
30.02
f1 (ppm)

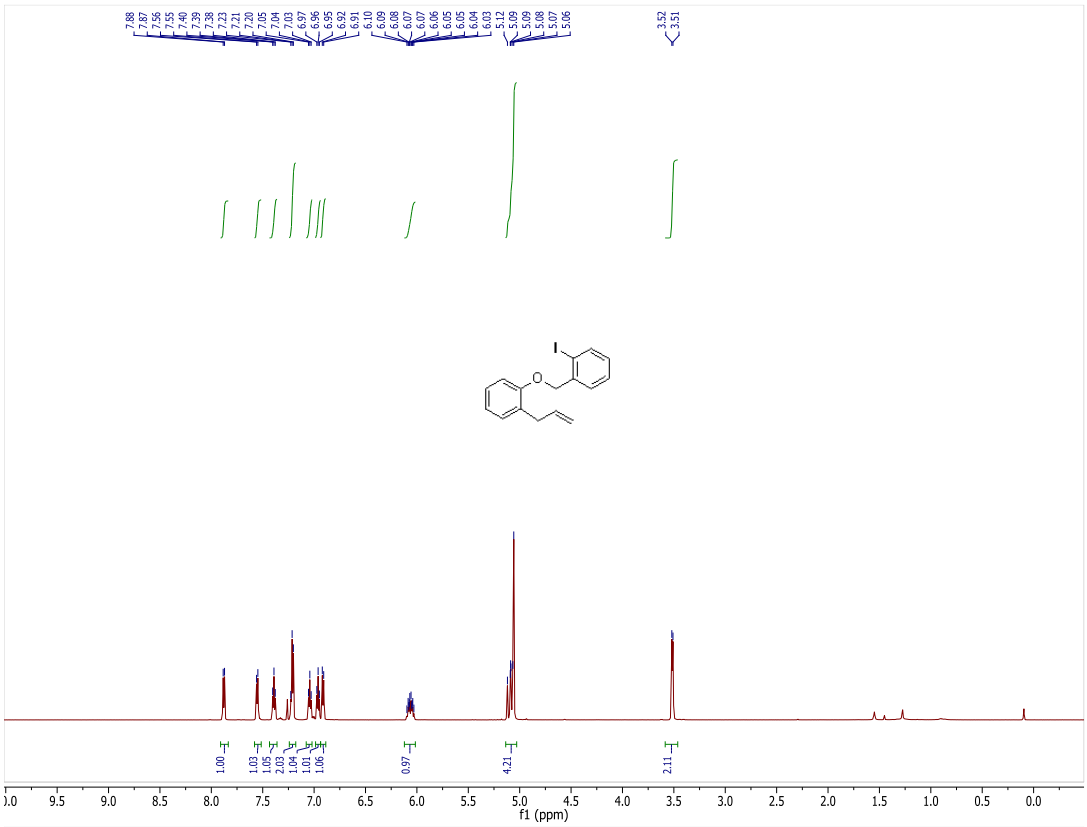
7.88
7.87
7.56
7.55
7.40
7.39
7.38
7.23
7.21
7.20
7.05
7.04
7.03
6.97
6.96
6.95
6.92
6.91
6.10
6.09
6.08
6.07
6.07
6.06
6.05
6.05
6.04
6.03
5.12
5.09
5.09
5.08
5.07
5.06
3.52
3.51
I
O
1.00
1.03
1.05
2.03
1.04
1.01
1.06
0.97
4.21
2.11
f1 (ppm)

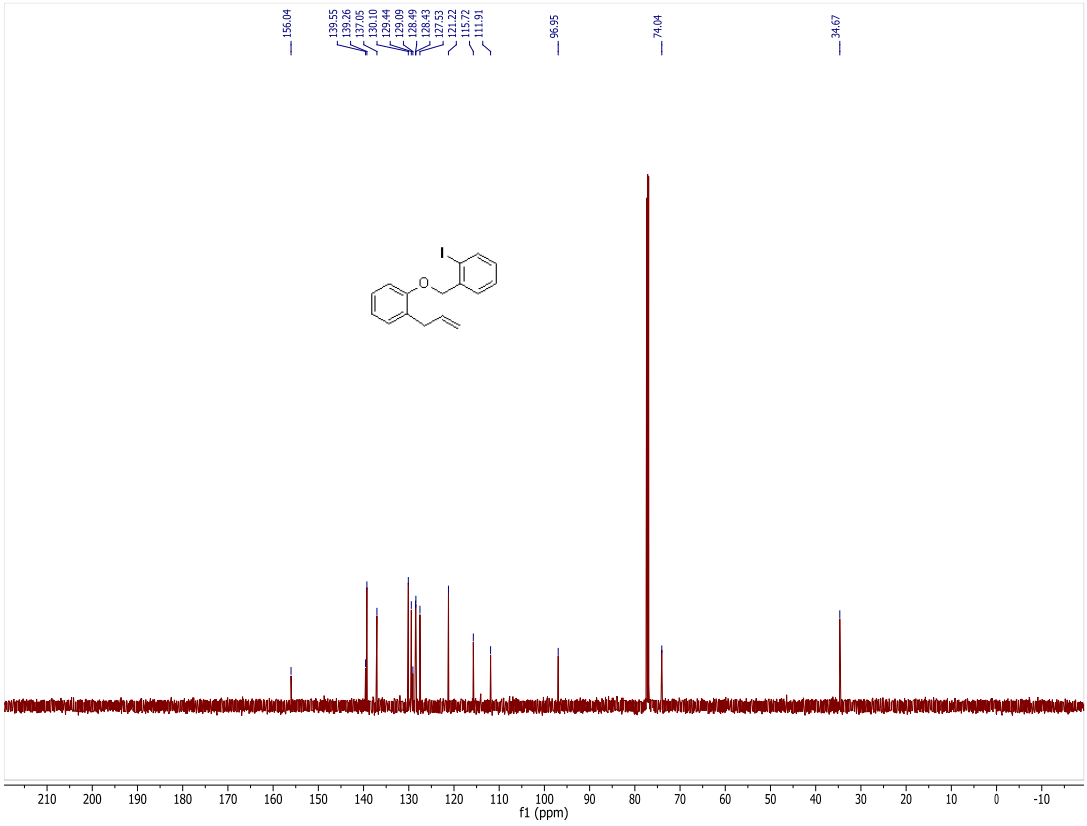
156.04
139.55
139.26
137.05
130.10
129.64
128.99
128.49
128.43
127.53
121.22
115.72
111.91
96.95
74.04
34.67
I
O
f1 (ppm)

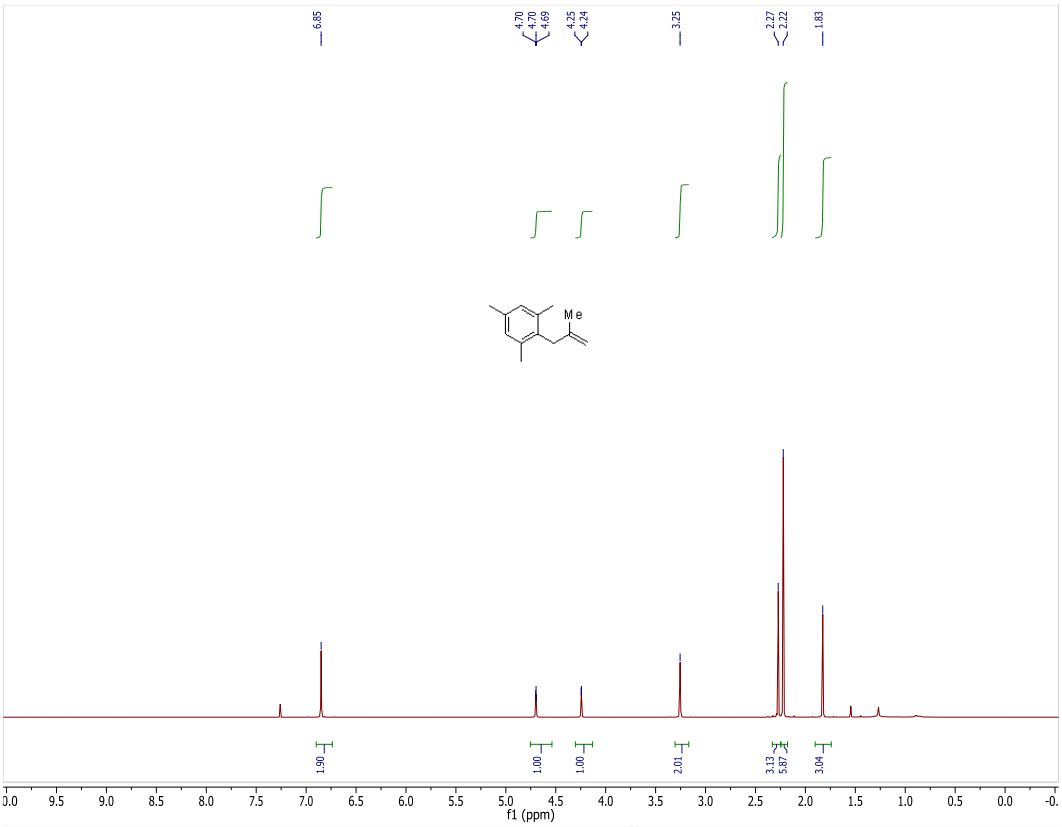
6.85
4.70
4.70
4.69
4.25
4.24
3.25
2.27
2.22
1.83
Me
1.90
1.00
1.00
2.01
3.13
5.87
3.04
f1 (ppm)

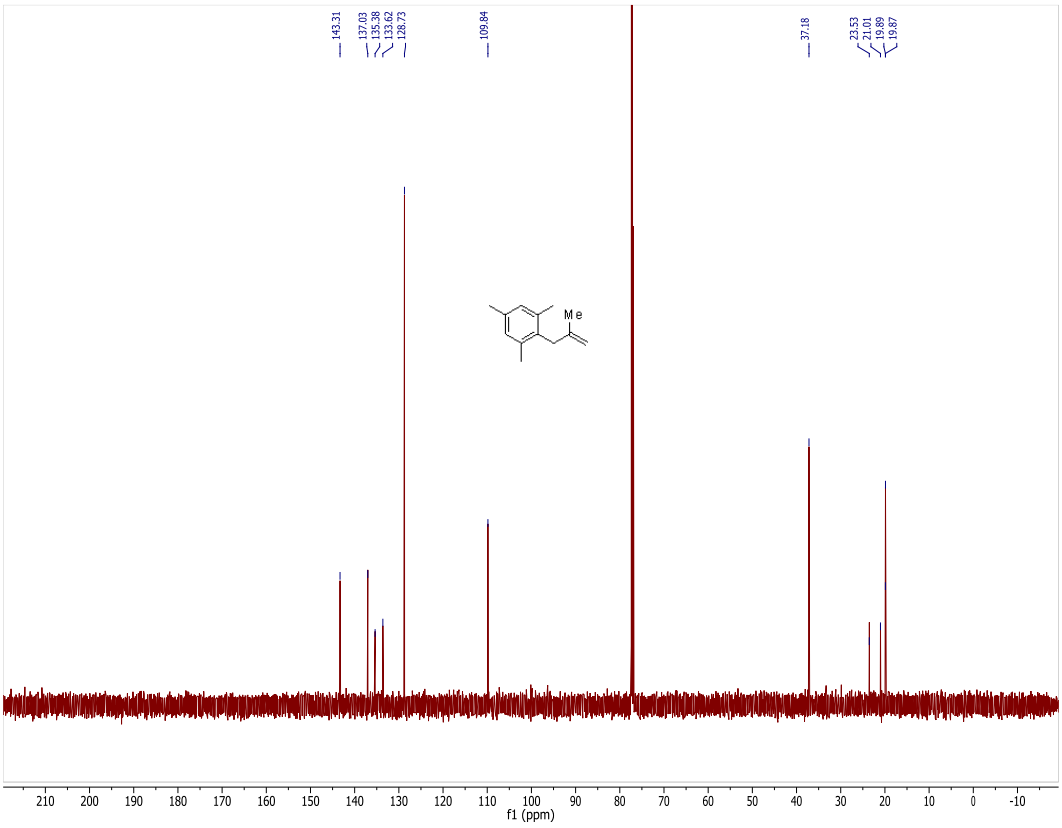
143.31
137.03
135.38
133.62
128.73
109.84
37.18
23.53
21.01
19.89
19.87
Me
f1 (ppm)

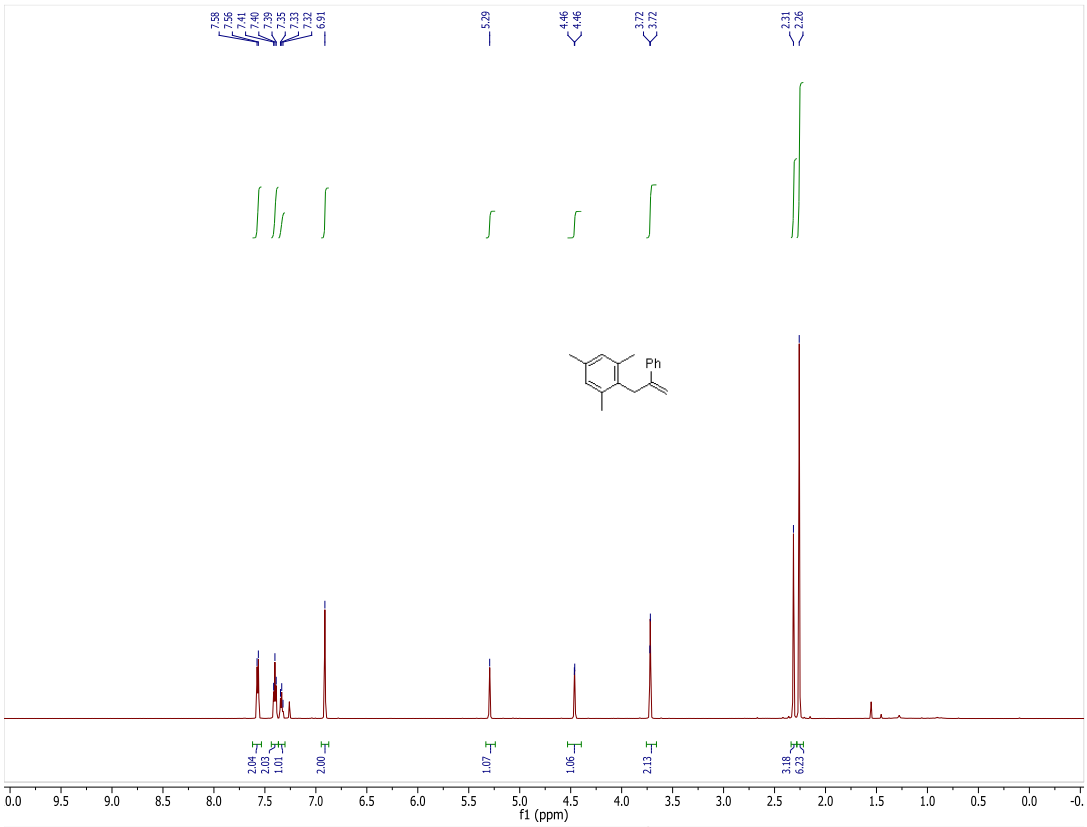
7.58
7.56
7.41
7.40
7.39
7.35
7.33
7.32
6.91
5.29
4.46
4.46
3.72
3.72
2.31
2.26
Ph
2.04
2.03
1.01
2.00
1.07
1.06
2.13
3.18
6.23
f1 (ppm)

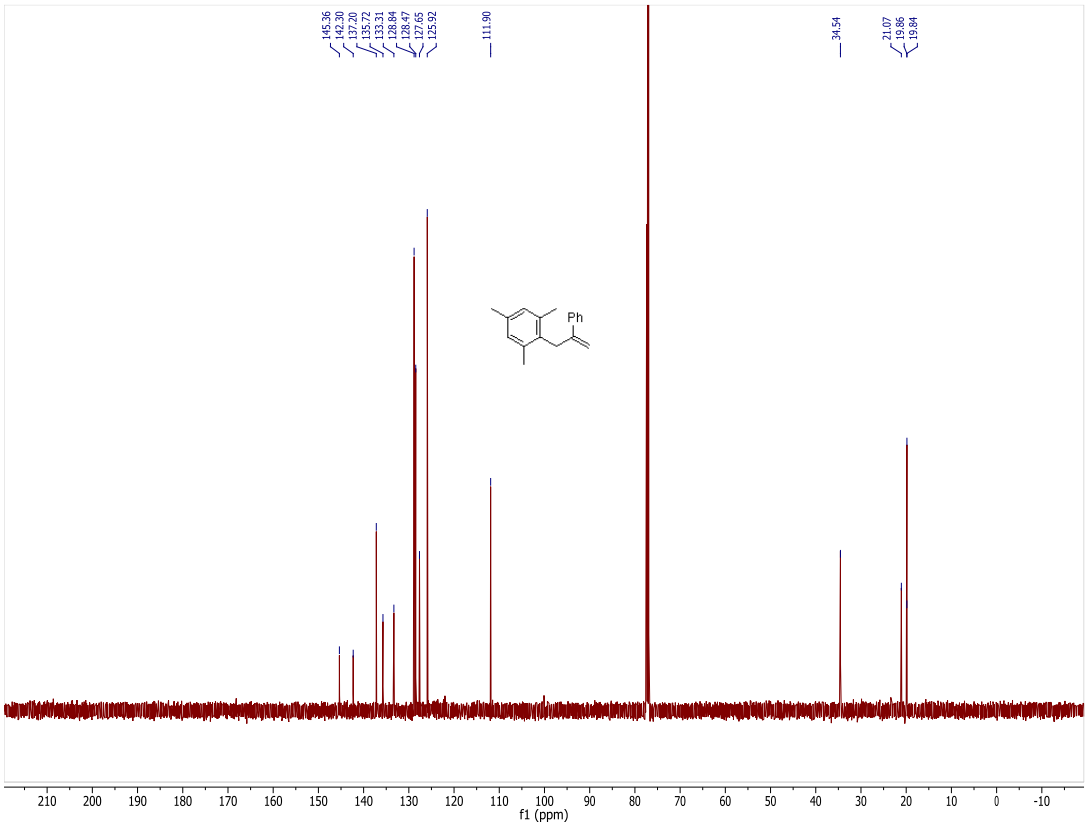
145.36
142.30
137.20
135.72
133.31
128.84
128.47
127.65
125.92
111.90
34.54
21.07
19.86
19.84
Ph
f1 (ppm)

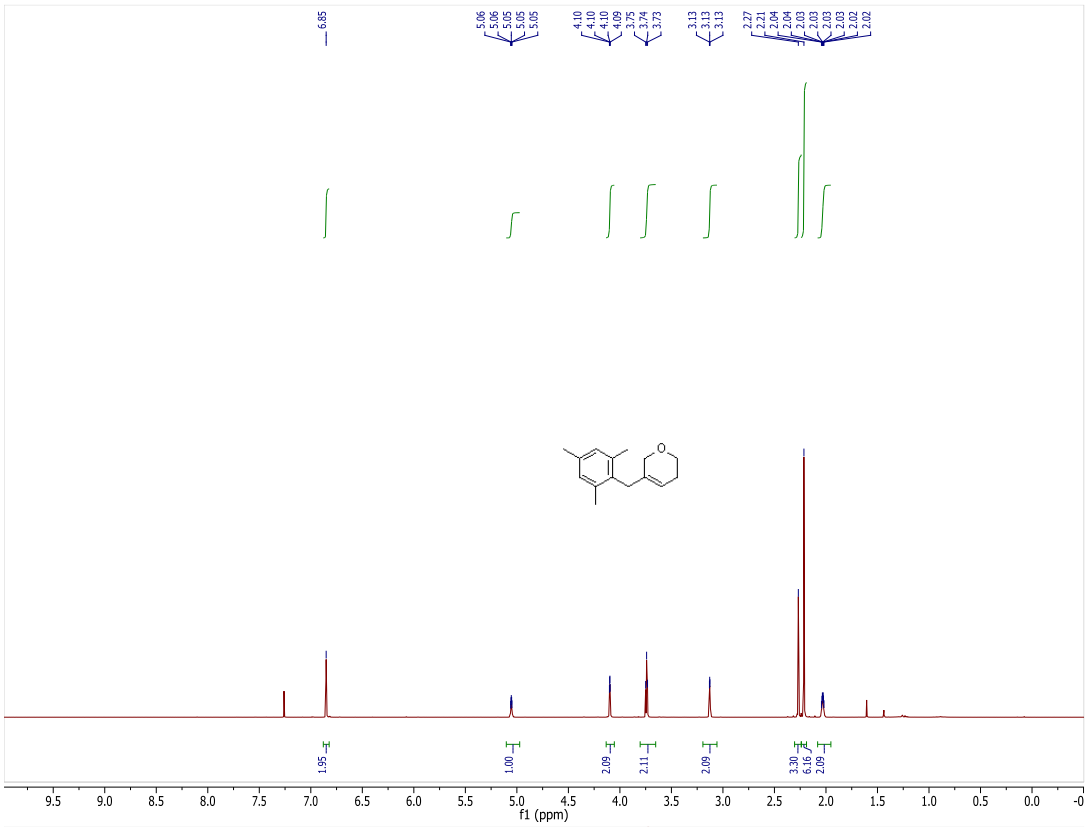
6.85
5.06
5.06
5.05
5.05
5.05
4.10
4.10
4.10
4.09
3.75
3.74
3.73
3.13
3.13
3.13
2.27
2.21
2.04
2.04
2.03
2.03
2.03
2.03
2.02
2.02
1.95
1.00
2.09
2.11
2.09
3.30
6.16
2.09
f1 (ppm)

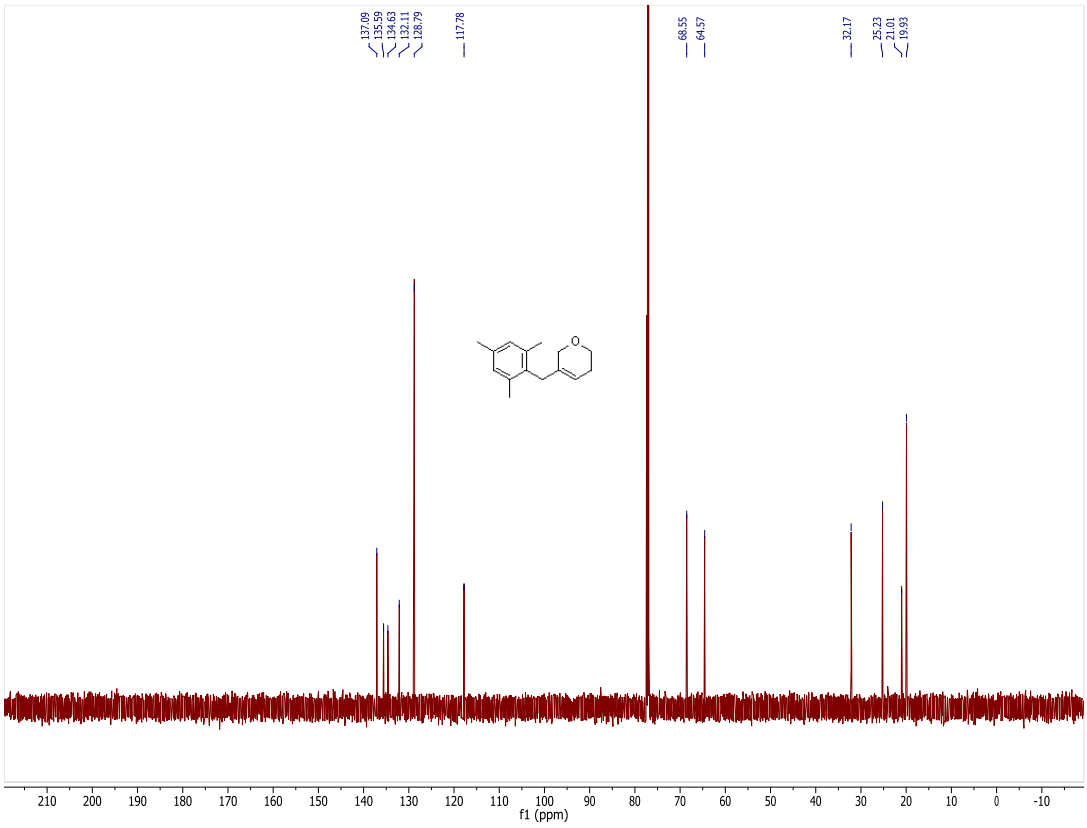
137.09
135.59
134.63
132.11
128.79
117.78
68.55
64.57
32.17
25.23
21.01
19.93
f1 (ppm)

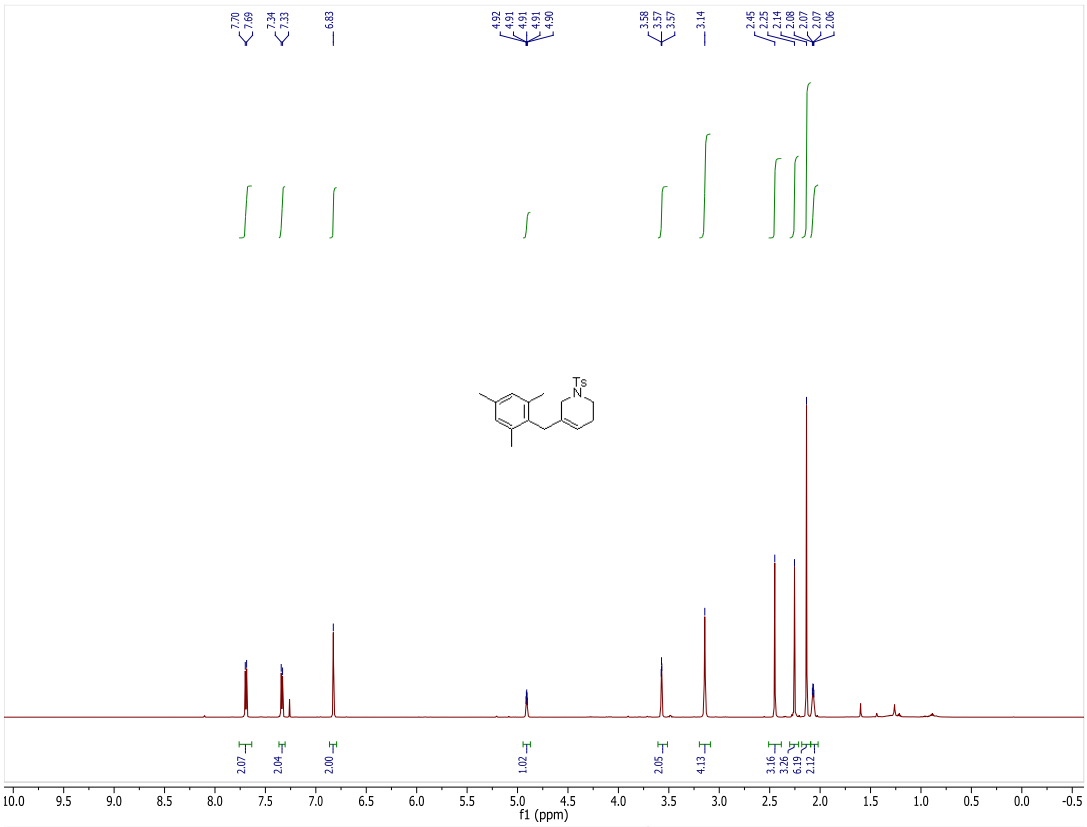
7.70
7.69
7.34
7.33
6.83
4.92
4.91
4.91
4.91
4.90
3.58
3.57
3.57
3.14
2.45
2.35
2.14
2.08
2.07
2.07
2.06
Ts
N
2.07
2.04
2.00
1.02
2.05
4.13
3.16
3.26
6.19
2.12
f1 (ppm)

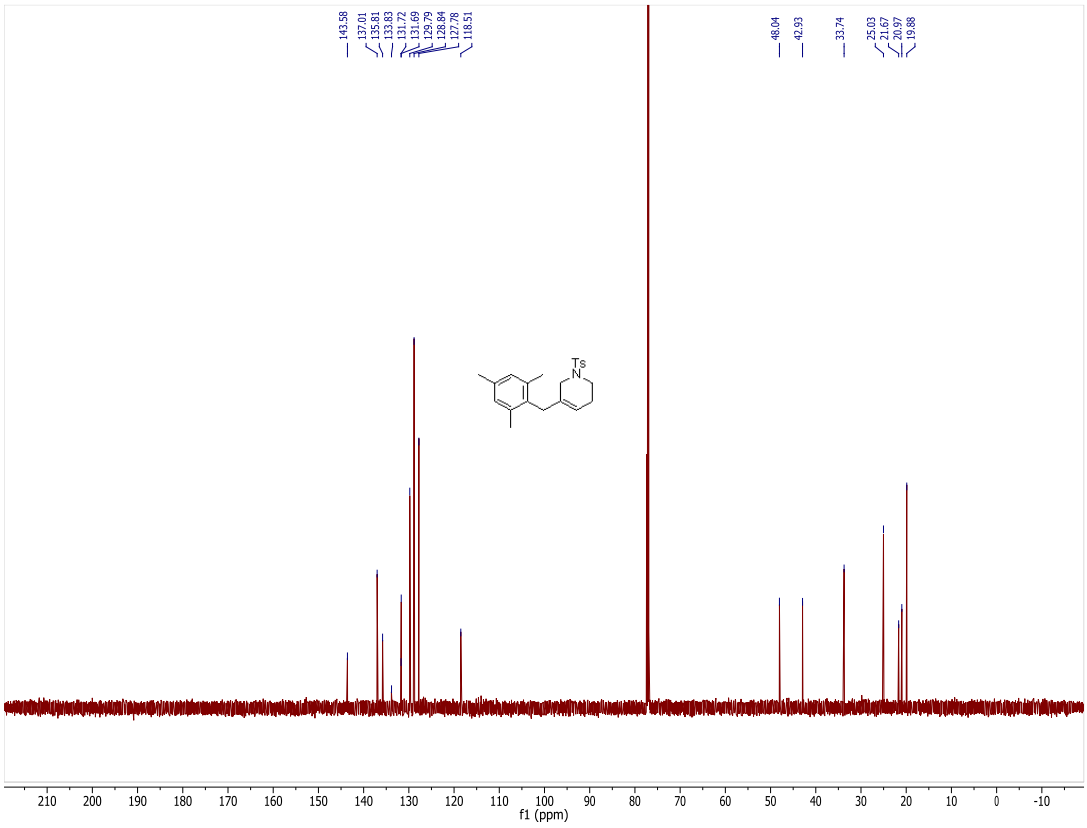
143.58
137.01
135.81
133.83
131.72
131.69
129.79
128.84
127.78
118.51
48.04
42.93
33.74
25.03
21.67
20.97
19.88
Ts
N
f1 (ppm)

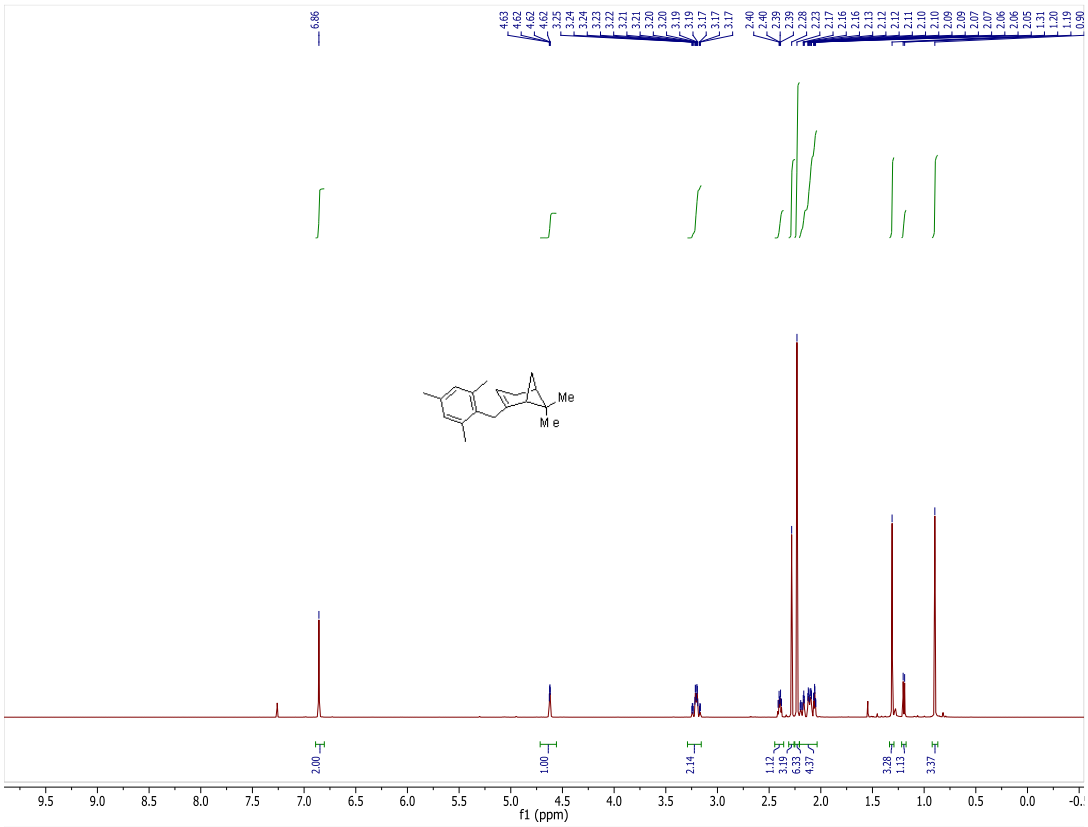
6.86
4.63
4.62
4.62
4.62
3.25
3.24
3.24
3.23
3.22
3.21
3.21
3.20
3.20
3.19
3.19
3.17
3.17
3.17
3.17
2.40
2.40
2.39
2.39
2.28
2.23
2.17
2.16
2.16
2.13
2.12
2.12
2.11
2.10
2.10
2.09
2.09
2.07
2.07
2.06
2.06
2.05
1.31
1.20
1.19
0.90
Me
Me
2.00
1.00
2.14
1.12
3.19
6.33
4.37
3.28
1.13
3.37
f1 (ppm)

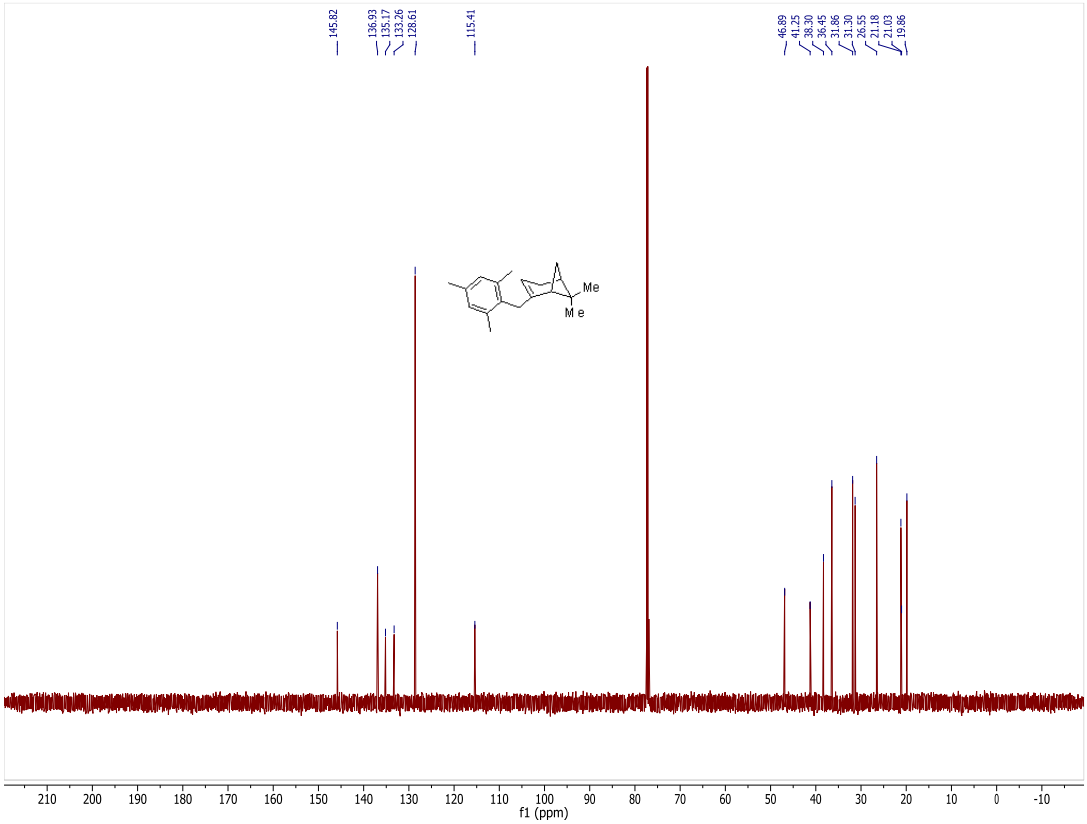
145.82
136.93
135.77
133.26
128.61
115.41
46.89
41.25
38.30
36.45
31.86
31.30
26.55
21.18
21.03
19.86
Me
Me
f1 (ppm)

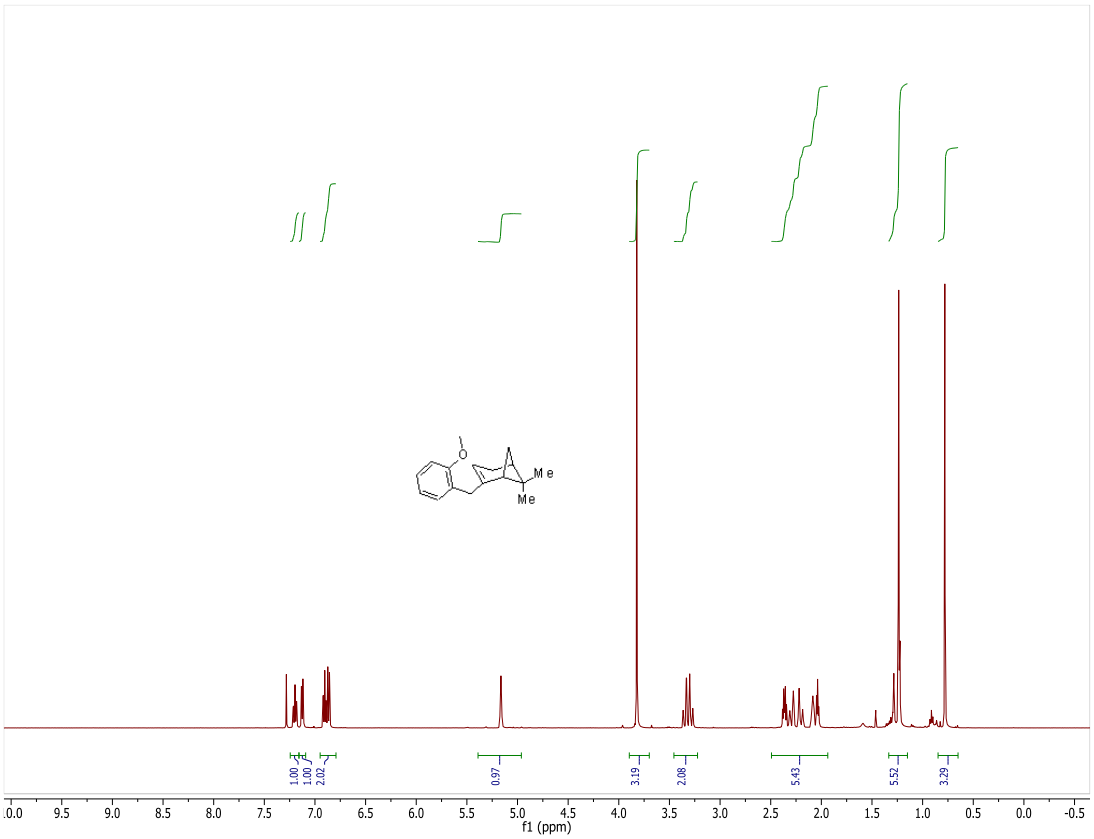
Me
Me
1.00
1.00
2.02
0.97
3.19
2.08
5.43
5.52
3.29
f1 (ppm)

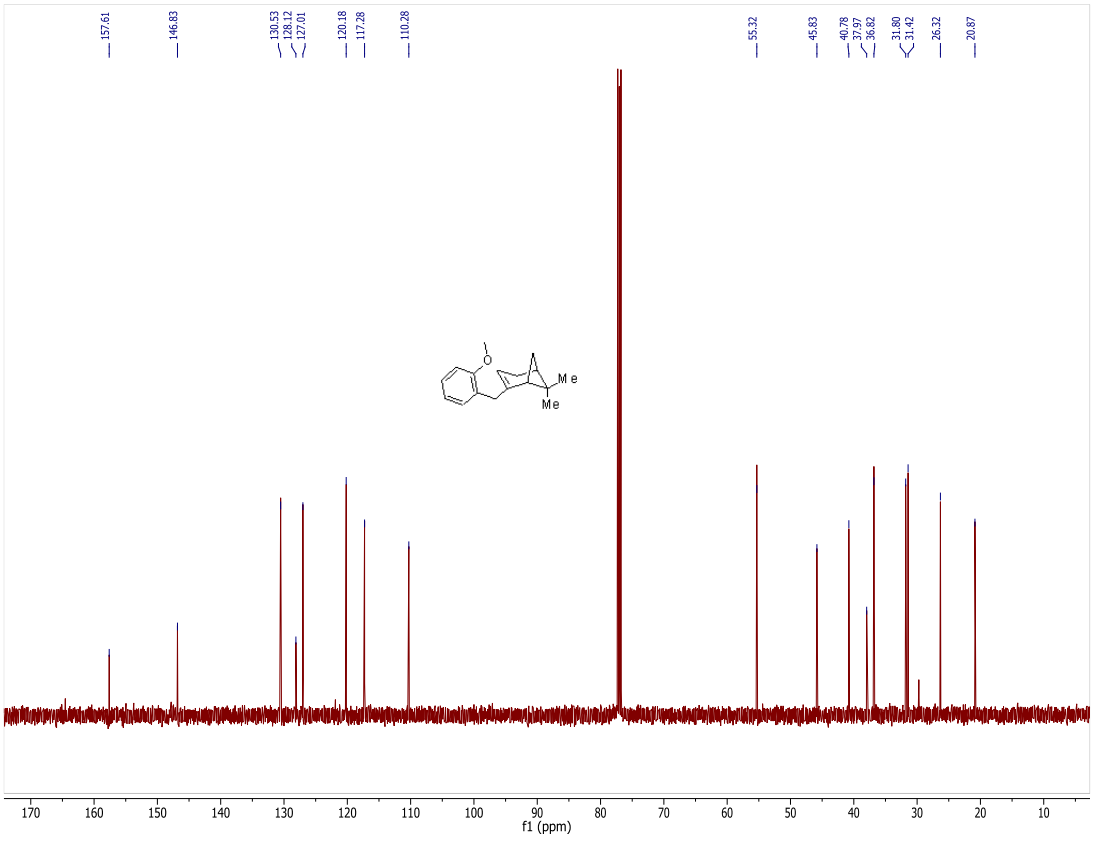
157.61
146.83
130.53
128.12
127.01
120.18
117.28
110.28
55.32
45.83
40.78
37.97
36.82
31.80
31.42
26.32
20.87
Me
Me
f1 (ppm)

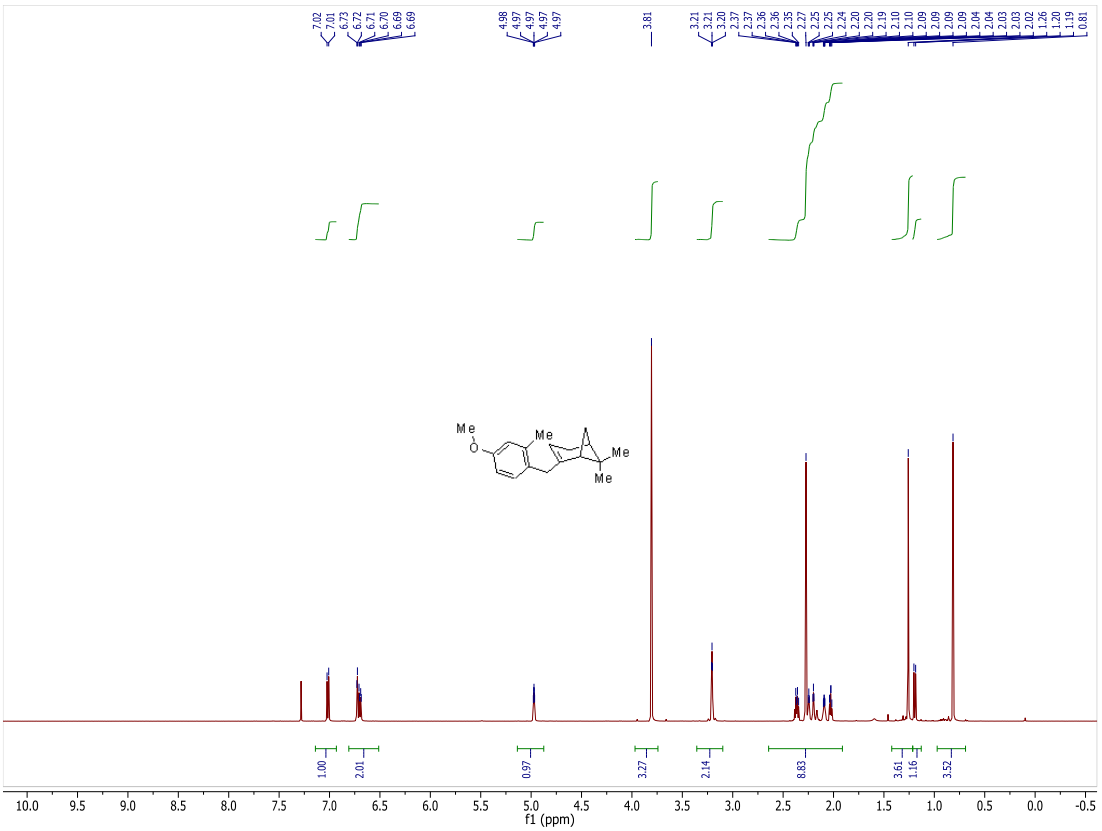
Me
Me
Me
Me
f1 (ppm)

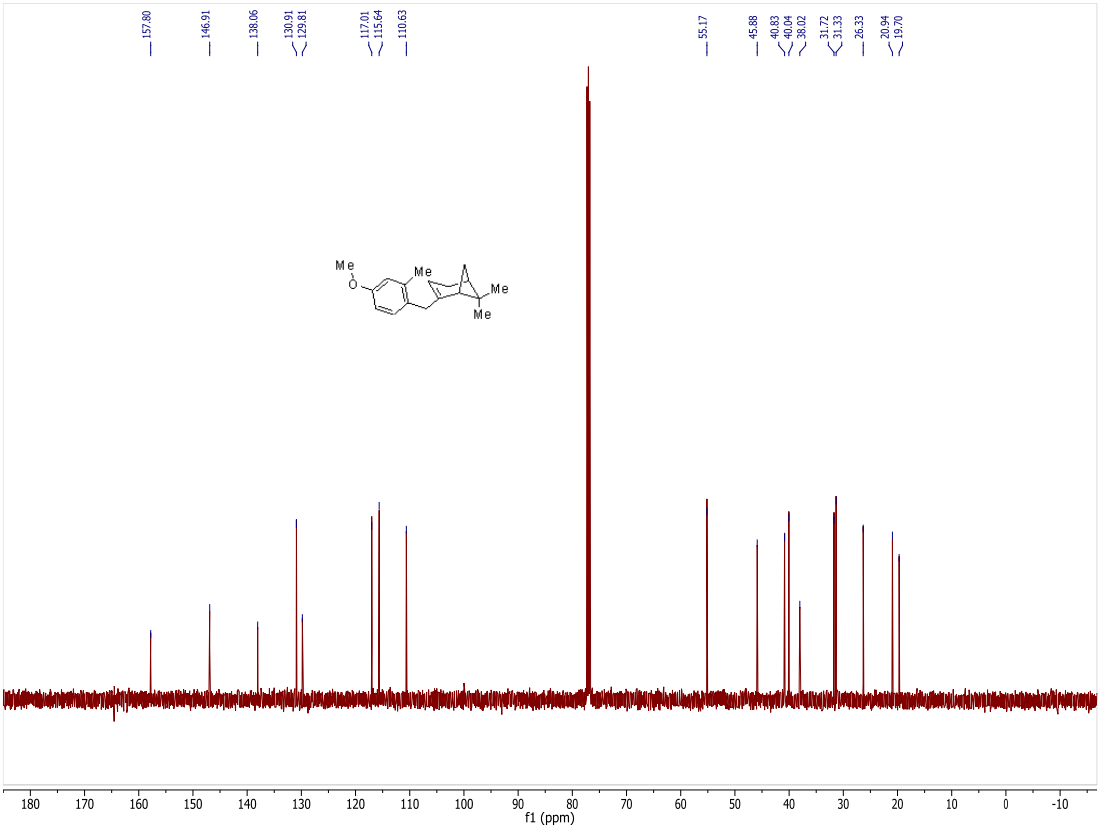
Me
Me
Me
Me
f1 (ppm)

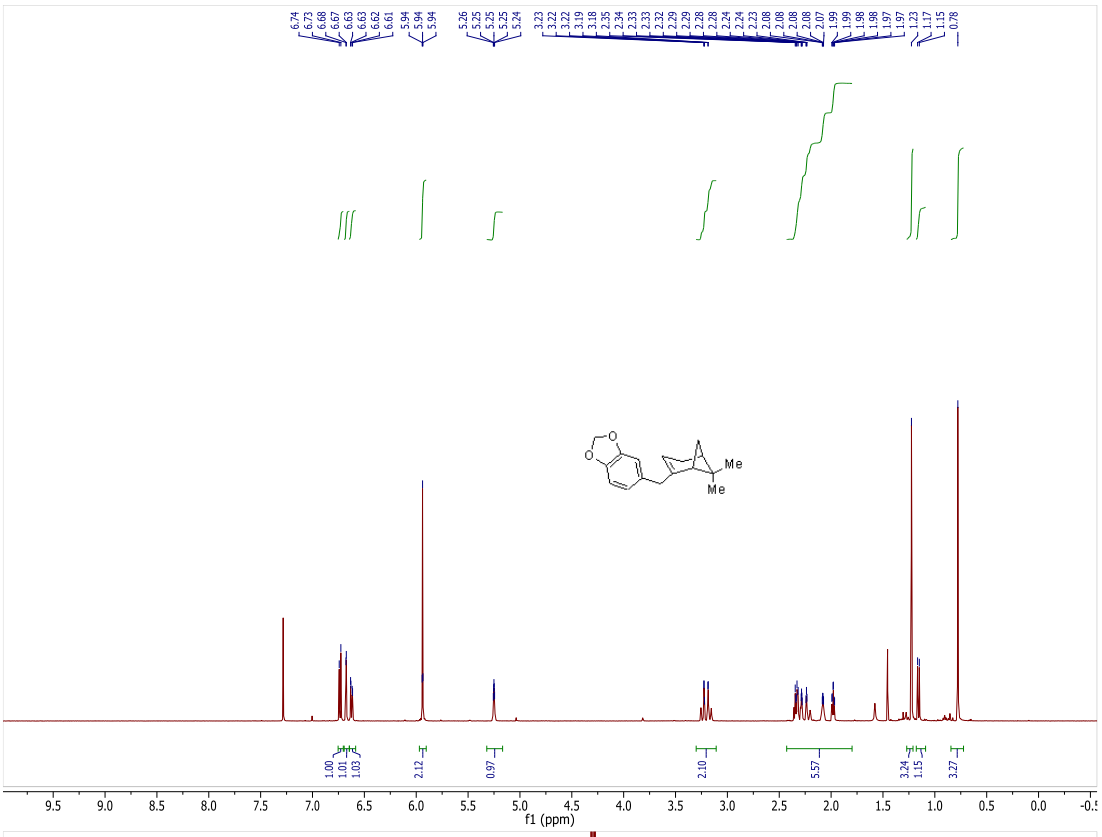
6.74
6.73
6.68
6.67
6.63
6.63
6.62
6.61
5.94
5.94
5.94
5.26
5.25
5.25
5.25
5.24
3.23
3.22
3.22
3.19
3.18
2.35
2.34
2.33
2.33
2.32
2.29
2.29
2.28
2.28
2.24
2.24
2.23
2.08
2.08
2.08
2.08
2.07
1.99
1.99
1.98
1.98
1.97
1.97
1.23
1.17
1.15
0.78
Me
Me
1.00
1.01
1.03
2.12
0.97
2.10
5.57
3.24
1.15
3.27
f1 (ppm)

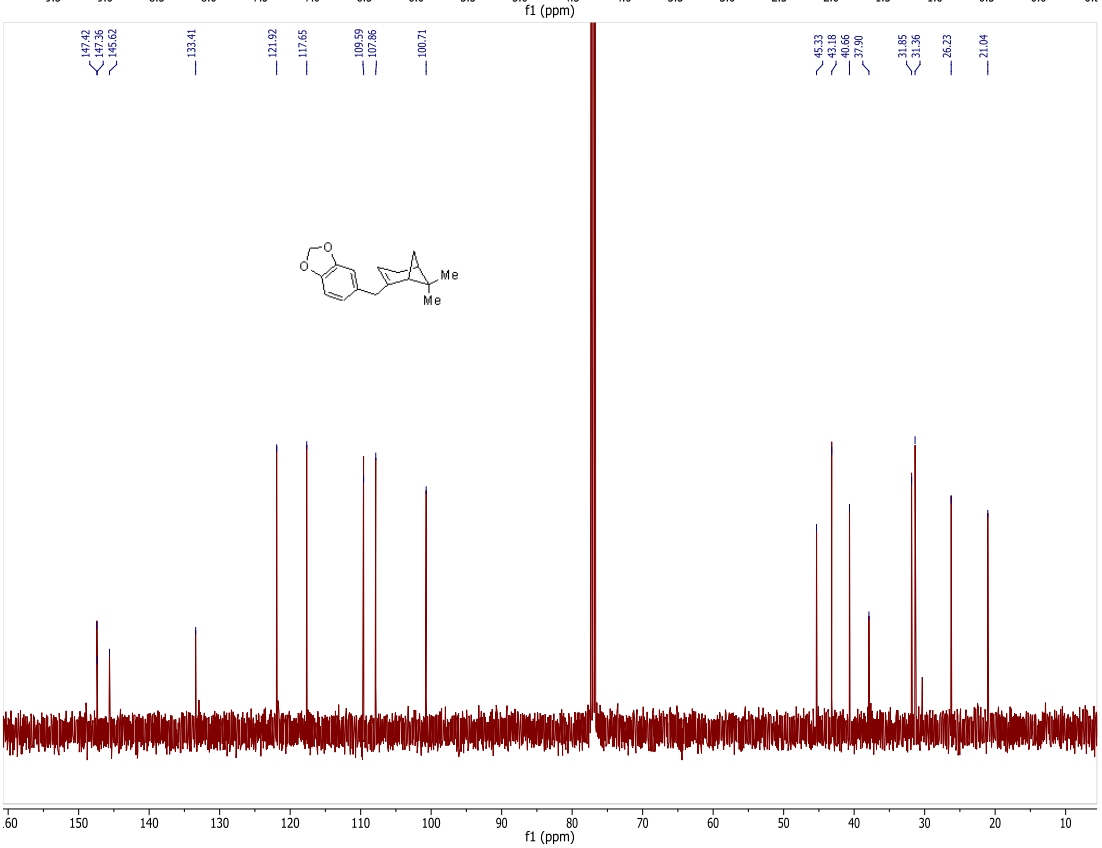
147.42
147.36
145.62
133.41
121.92
117.65
109.59
107.86
100.71
45.33
43.18
40.66
37.90
31.85
31.36
26.23
21.04
Me
Me
f1 (ppm)

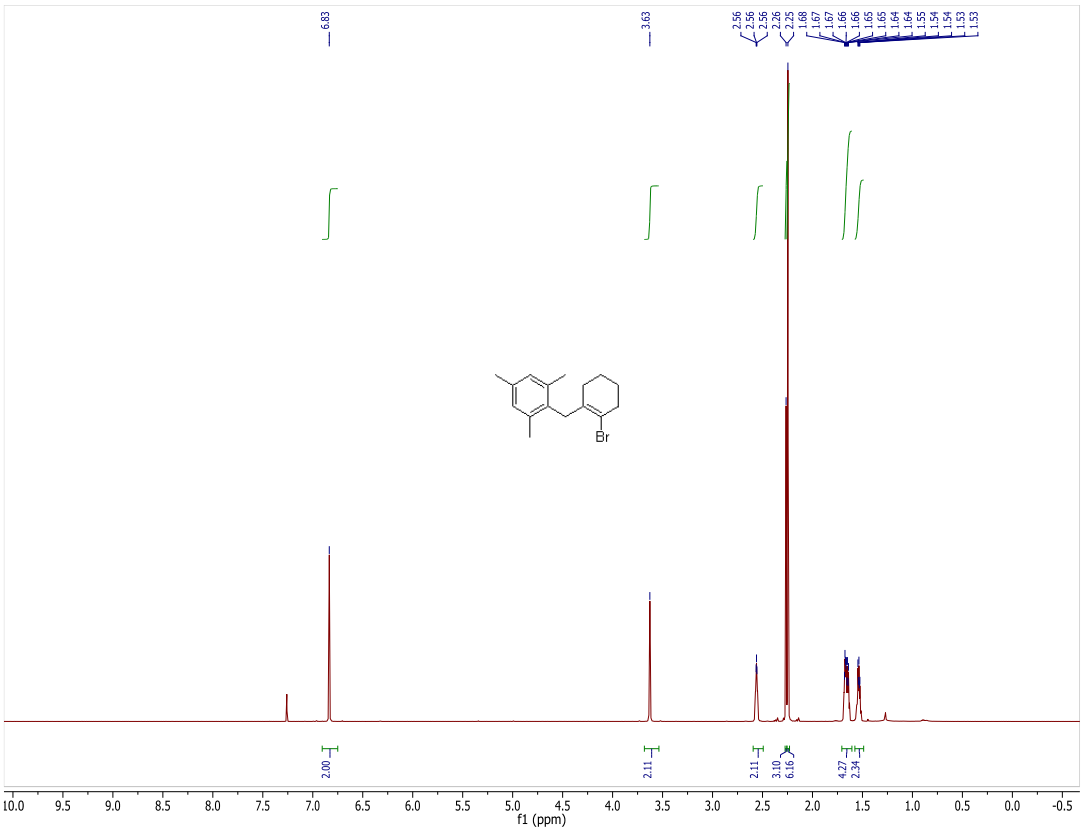
6.83
3.63
2.56
2.56
2.56
2.26
2.25
1.68
1.67
1.67
1.66
1.66
1.65
1.65
1.64
1.64
1.55
1.54
1.54
1.53
1.53
Br
2.00
2.11
2.11
3.10
6.18
4.27
2.34
f1 (ppm)

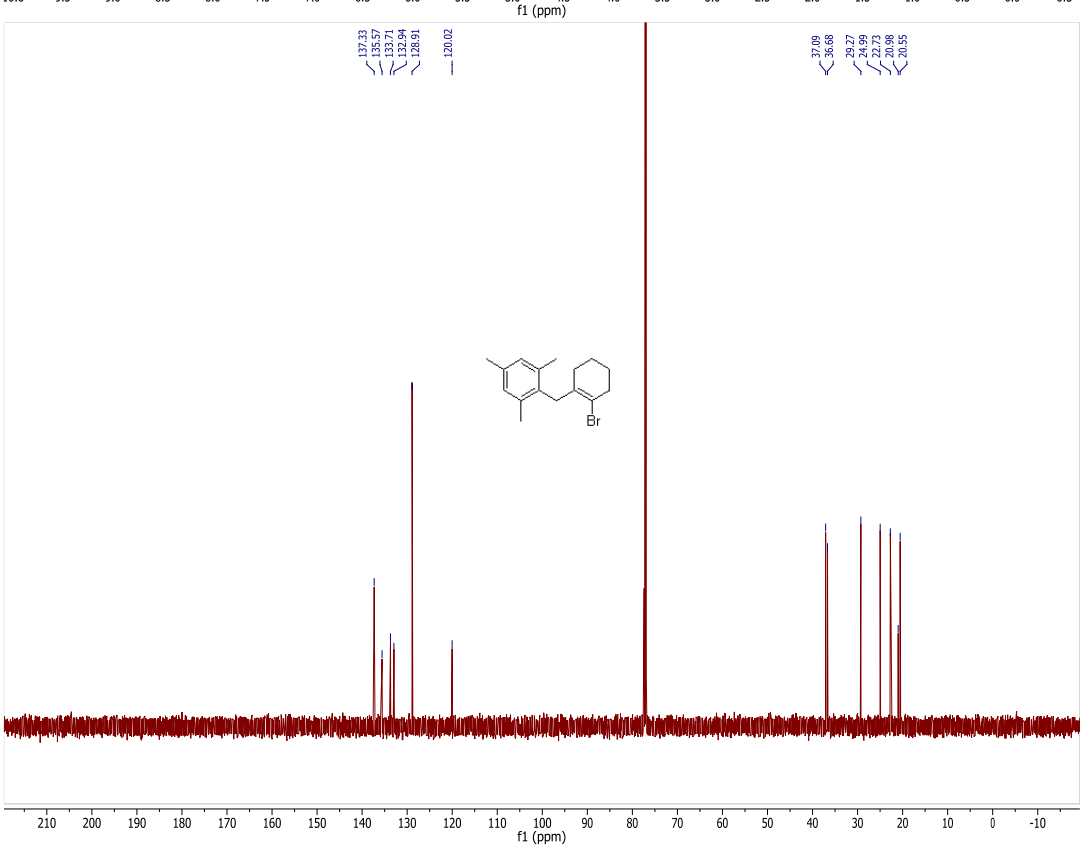
137.33
135.57
133.71
132.94
128.91
120.02
37.09
36.68
29.27
24.99
22.73
20.98
20.55
Br
f1 (ppm)

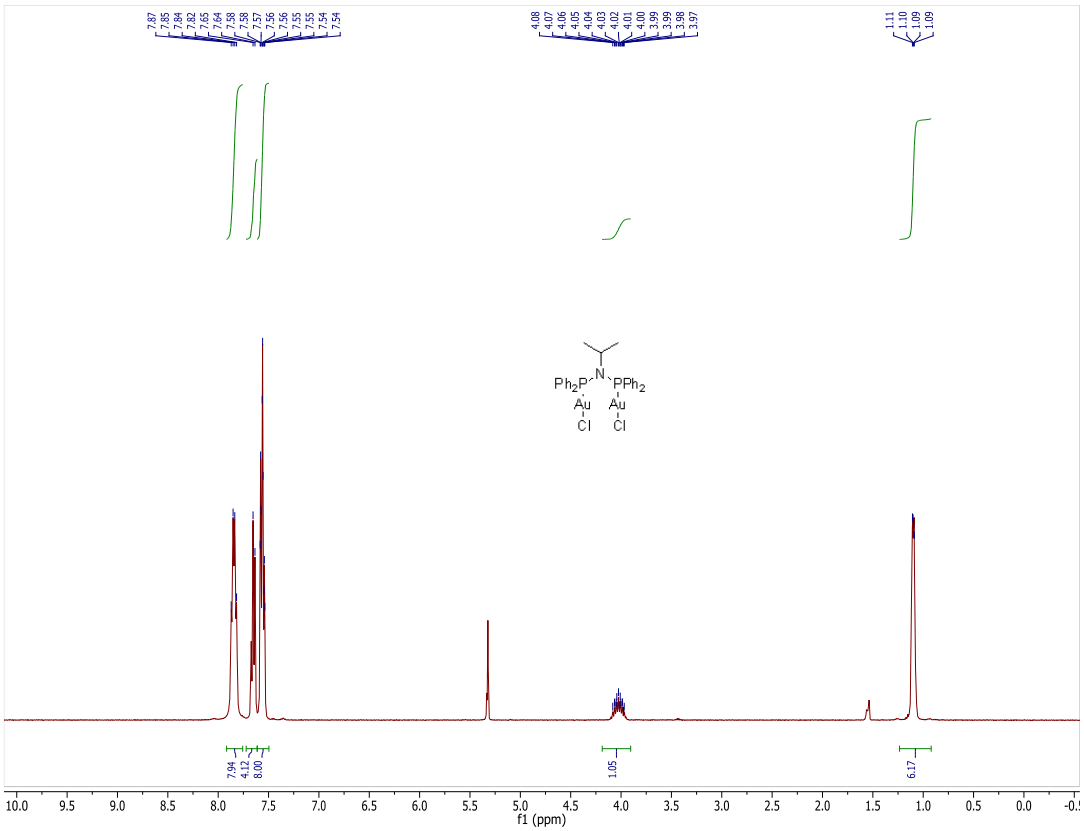
7.87
7.85
7.84
7.82
7.65
7.64
7.58
7.58
7.57
7.56
7.56
7.55
7.55
7.54
7.54
4.08
4.07
4.06
4.05
4.04
4.03
4.02
4.01
4.00
3.99
3.99
3.98
3.97
1.11
1.10
1.09
1.09
Ph2P
N
PPh2
Au
Au
Cl
Cl
7.94
4.12
8.00
1.05
6.17
f1 (ppm)

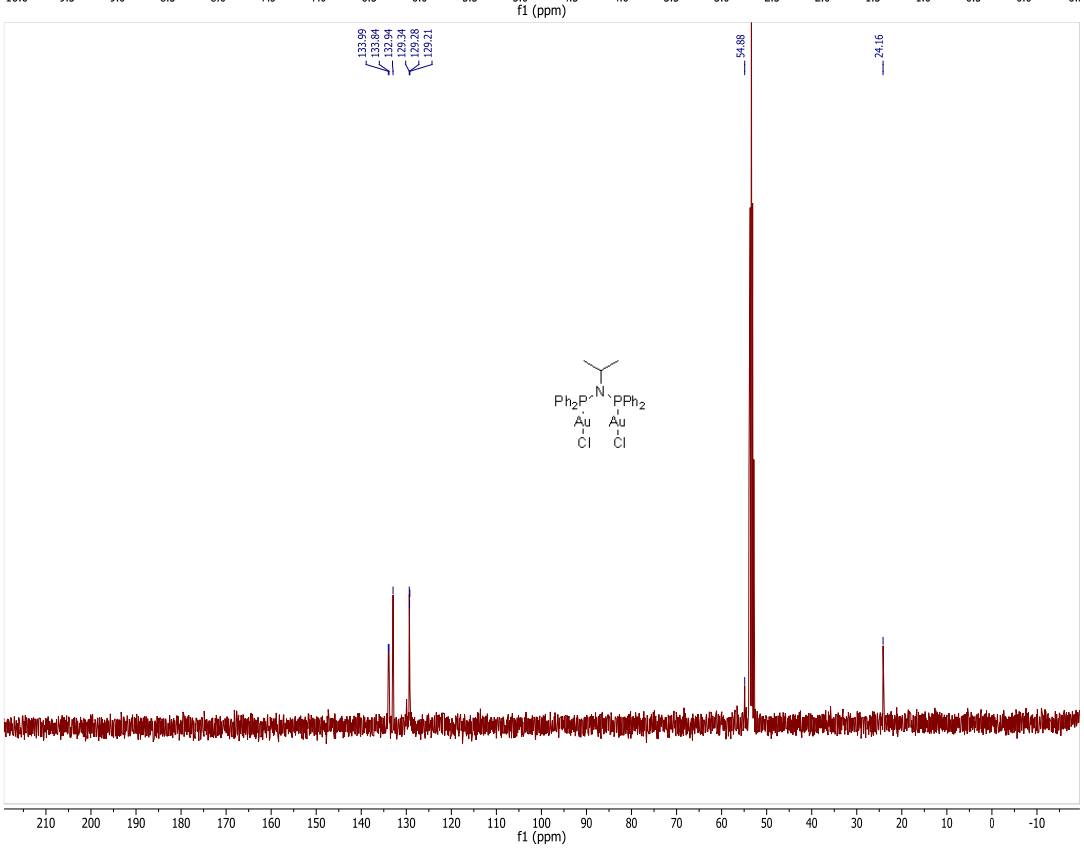
133.99
133.84
132.94
129.34
129.28
129.21
54.88
24.16
Ph2P
N
PPh2
Au
Au
Cl
Cl
f1 (ppm)

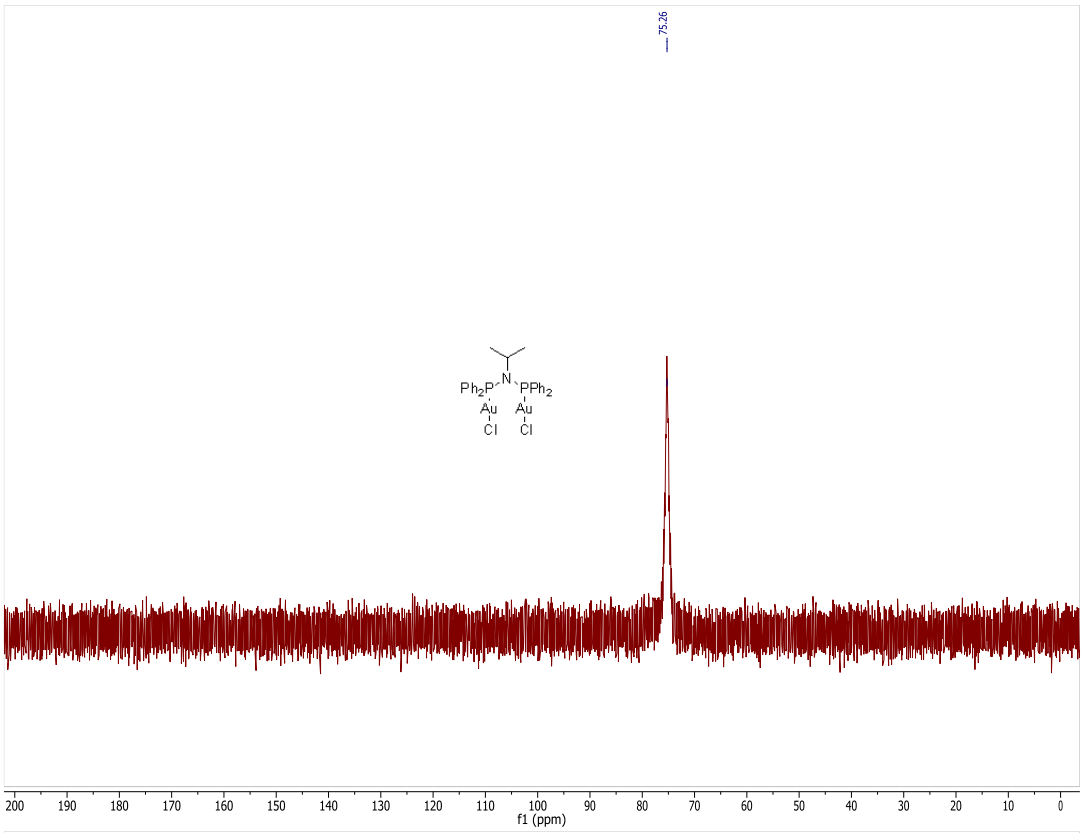
75.26
Ph2P
N
PPh2
Au
Au
Cl
Cl
200 190 180 170 160 150 140 130 120 110 100 90 80 70 60 50 40 30 20 10 0
f1 (ppm)

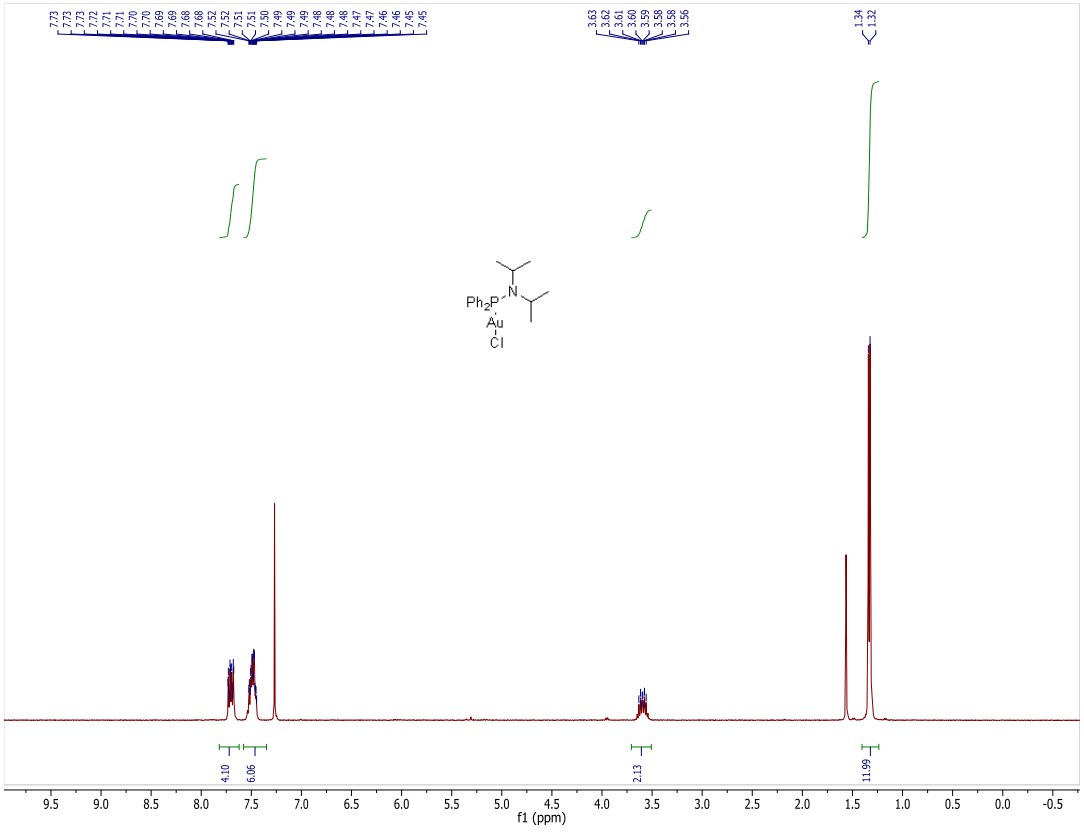
7.73 7.73 7.73 7.72 7.71 7.71 7.70 7.70 7.69 7.69 7.68 7.68 7.52 7.51 7.51 7.50 7.49 7.49 7.48 7.48 7.48 7.47 7.47 7.46 7.46 7.45 7.45
3.63 3.62 3.61 3.60 3.59 3.58 3.58 3.56
1.34 1.32
Ph2P
N
Au
Cl
4.10
6.06
2.13
11.99
9.5 9.0 8.5 8.0 7.5 7.0 6.5 6.0 5.5 5.0 4.5 4.0 3.5 3.0 2.5 2.0 1.5 1.0 0.5 0.0 -0.5
f1 (ppm)

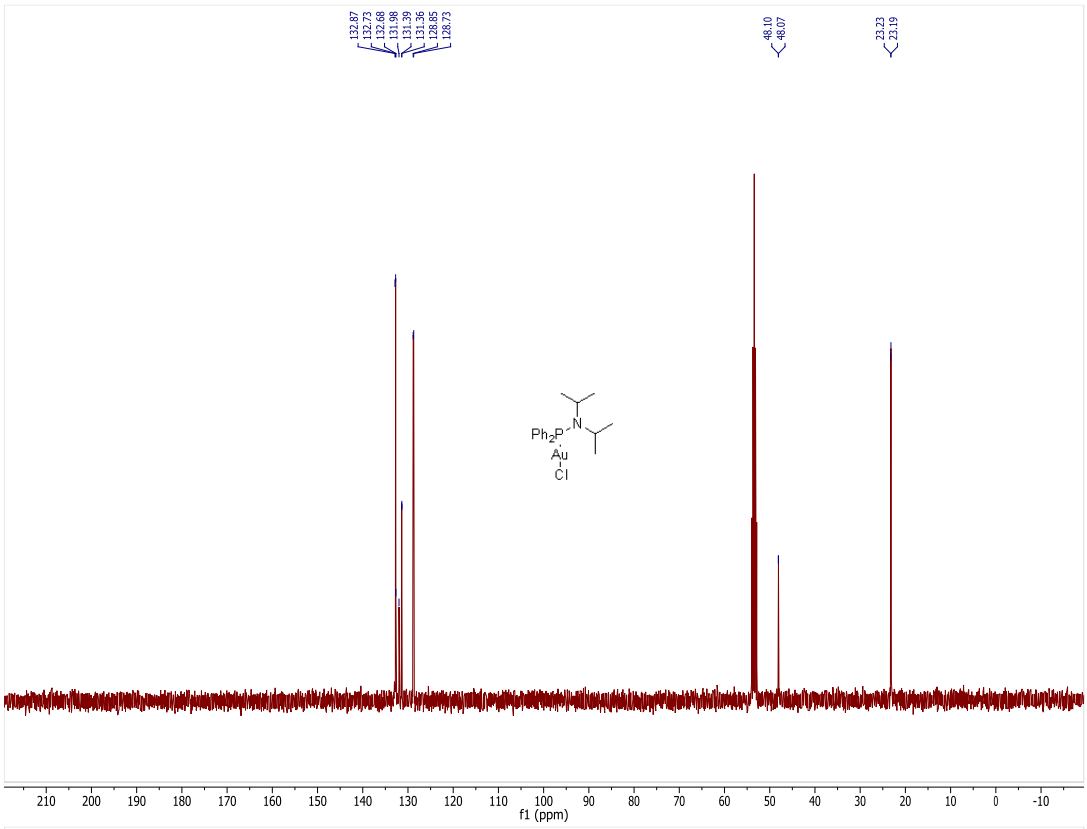
132.87
132.73
132.68
131.98
131.39
131.36
128.85
128.73
48.10
48.07
23.23
23.19
Ph2P
N
Au
Cl
210 200 190 180 170 160 150 140 130 120 110 100 90 80 70 60 50 40 30 20 10 0 -10
f1 (ppm)

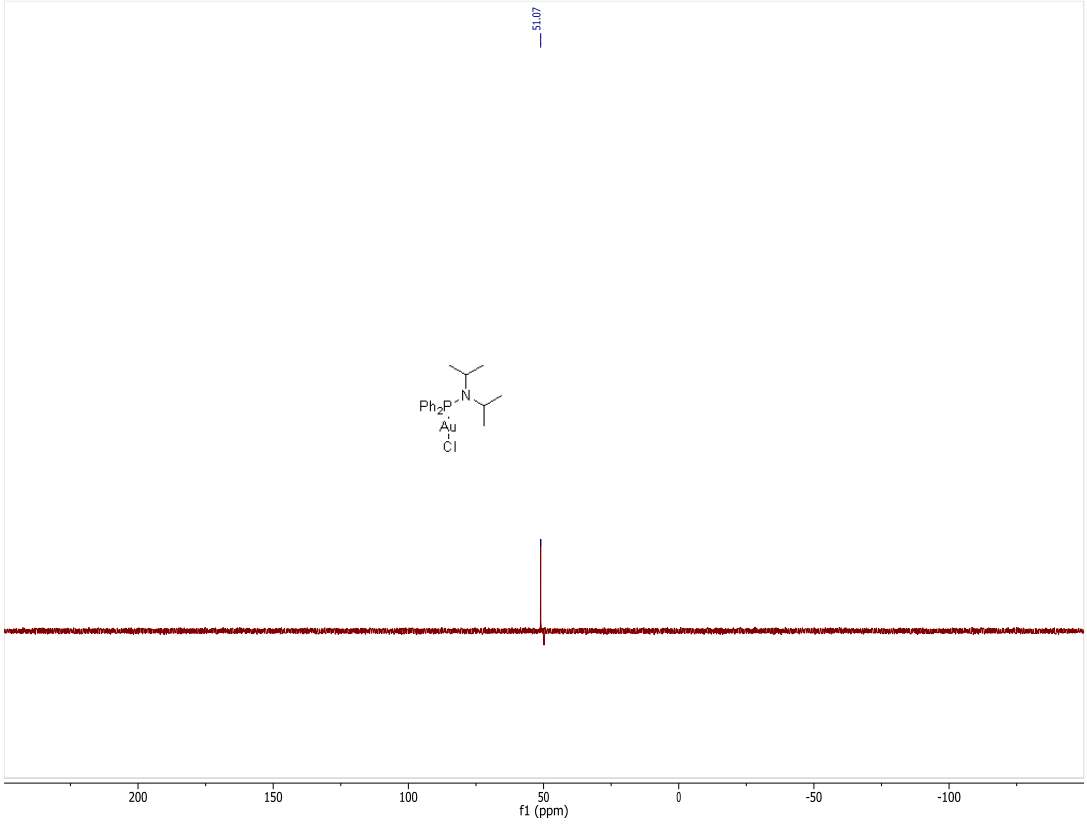
51.07
Ph2P
N
Au
Cl
200 150 100 50 0 -50 -100
f1 (ppm)

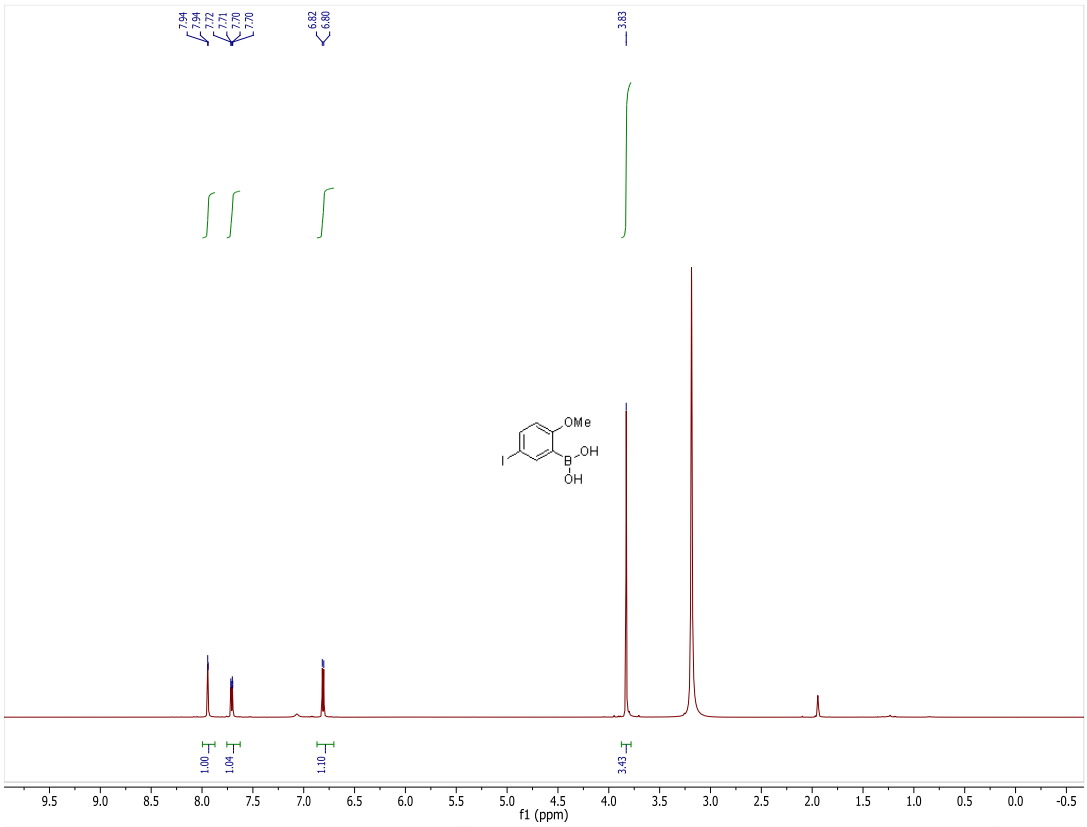
7.94
7.94
7.72
7.71
7.70
7.70
6.82
6.80
3.83
OMe
OH
B
OH
I
1.00
1.04
1.10
3.43
9.5 9.0 8.5 8.0 7.5 7.0 6.5 6.0 5.5 5.0 4.5 4.0 3.5 3.0 2.5 2.0 1.5 1.0 0.5 0.0 -0.5
f1 (ppm)

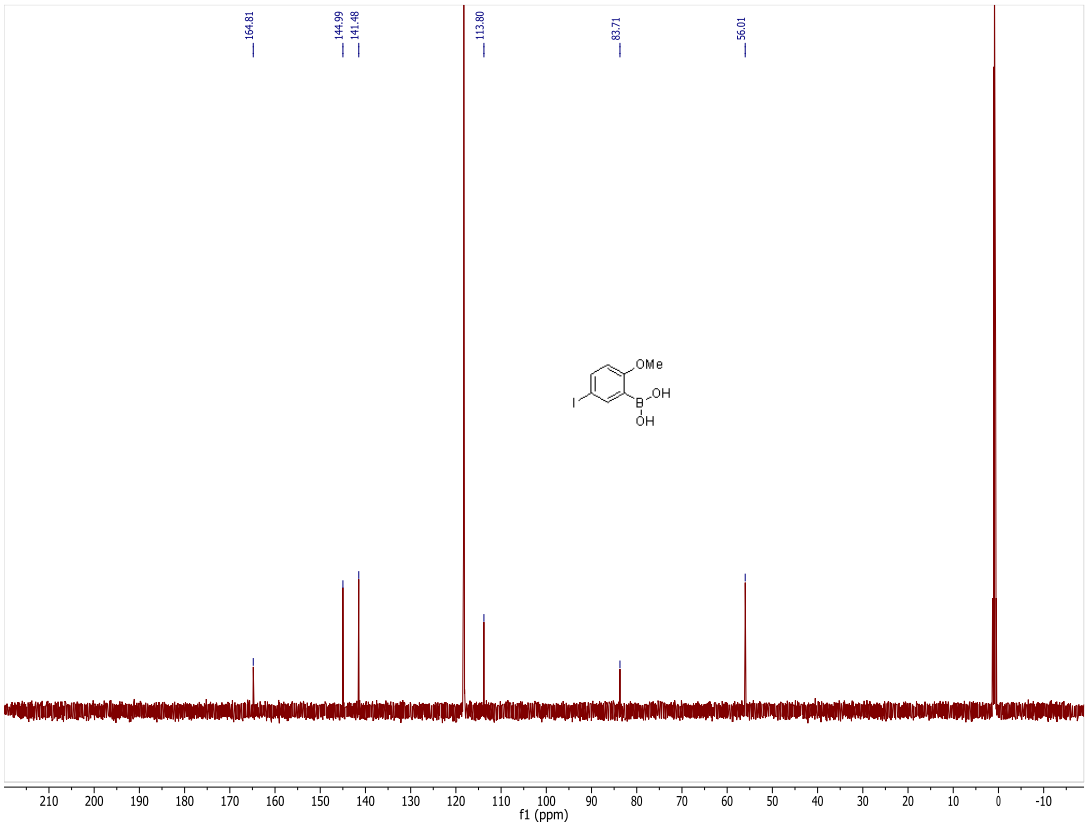
164.81
144.99
141.48
113.80
83.71
56.01
OMe
OH
B
OH
I
210 200 190 180 170 160 150 140 130 120 110 100 90 80 70 60 50 40 30 20 10 0 -10
f1 (ppm)

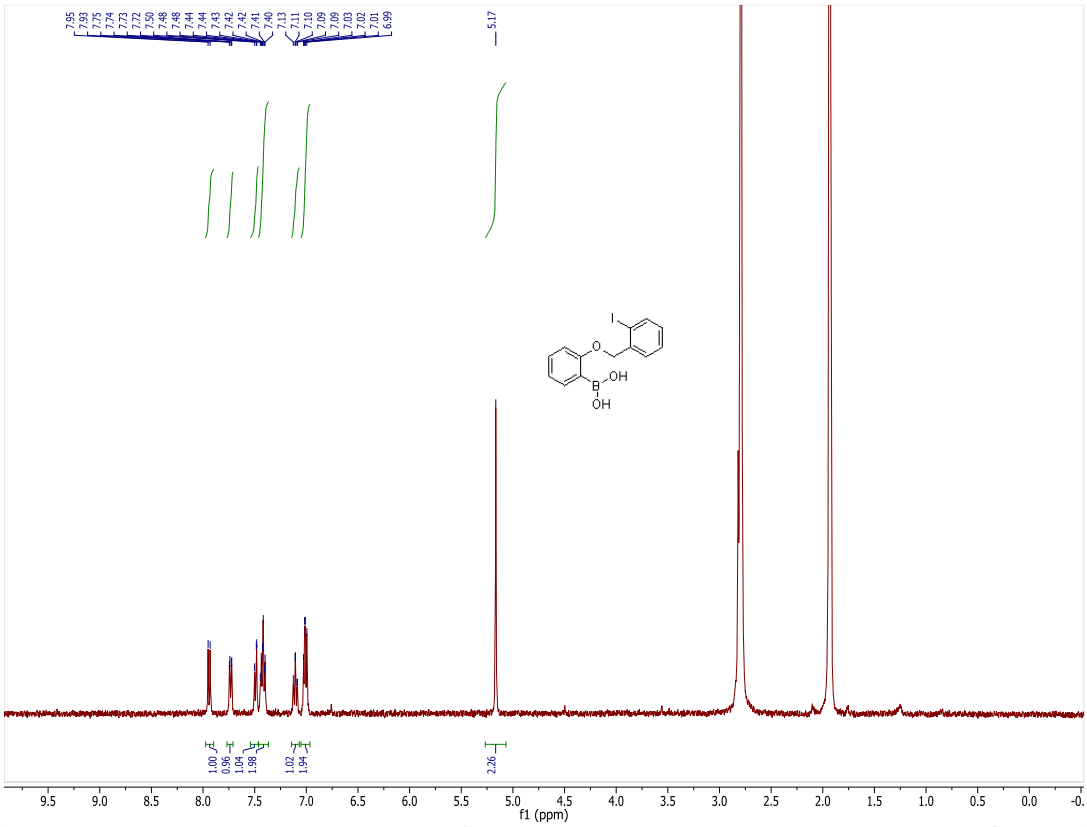
7.95
7.93
7.75
7.74
7.73
7.72
7.50
7.48
7.48
7.44
7.44
7.43
7.42
7.42
7.41
7.40
7.13
7.11
7.10
7.09
7.09
7.03
7.02
7.01
6.99
5.17
I
O
B
OH
OH
1.00
0.96
1.04
1.98
1.02
1.94
2.26
f1 (ppm)

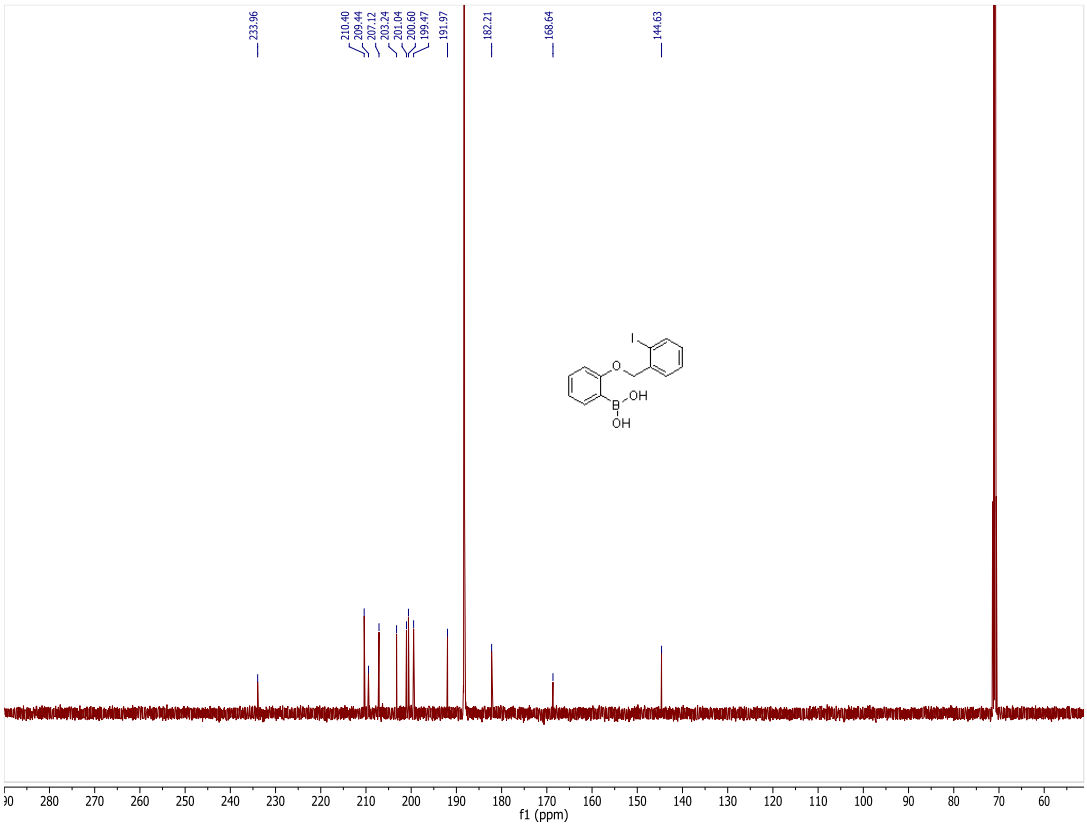
233.96
210.40
209.44
203.12
203.24
201.04
200.60
199.47
191.97
182.21
168.64
144.63
I
O
B
OH
OH
f1 (ppm)

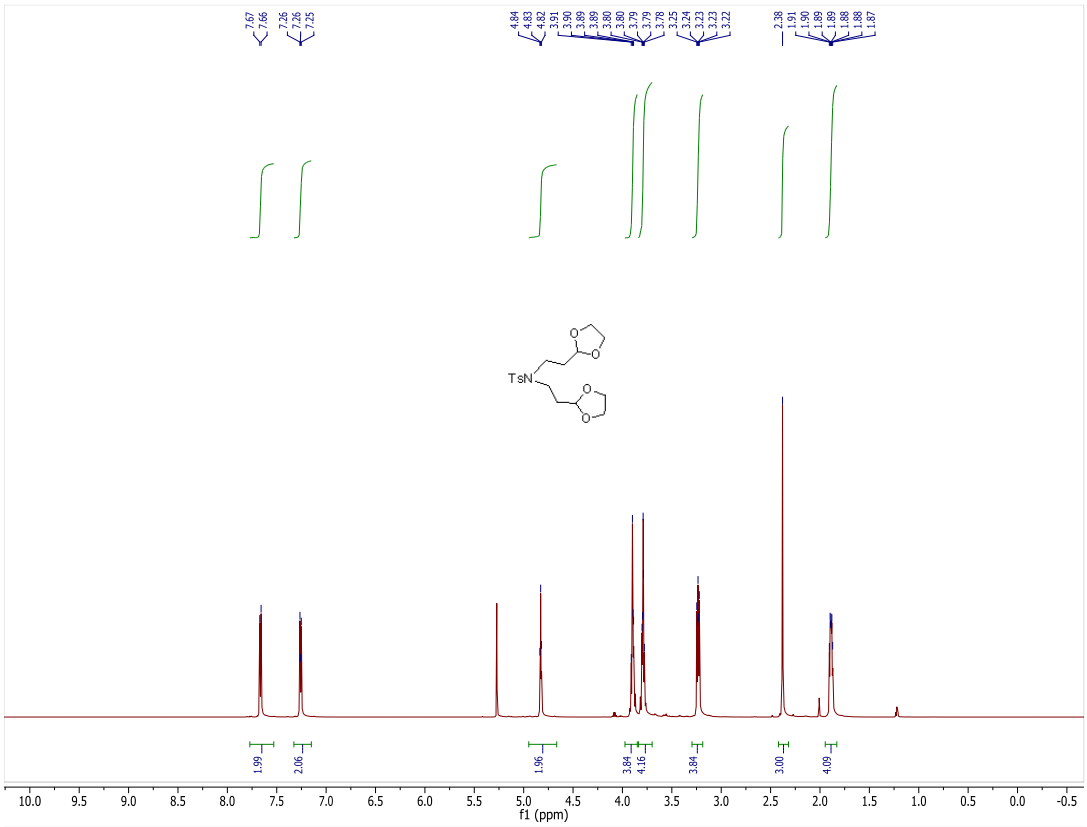
7.67
7.66
7.26
7.26
7.25
4.84
4.83
4.82
3.91
3.90
3.89
3.89
3.80
3.80
3.79
3.79
3.78
3.25
3.24
3.23
3.23
3.22
2.38
1.91
1.90
1.89
1.89
1.88
1.88
1.87
TsN
1.99
2.06
1.96
3.84
4.16
3.84
3.00
4.09
f1 (ppm)

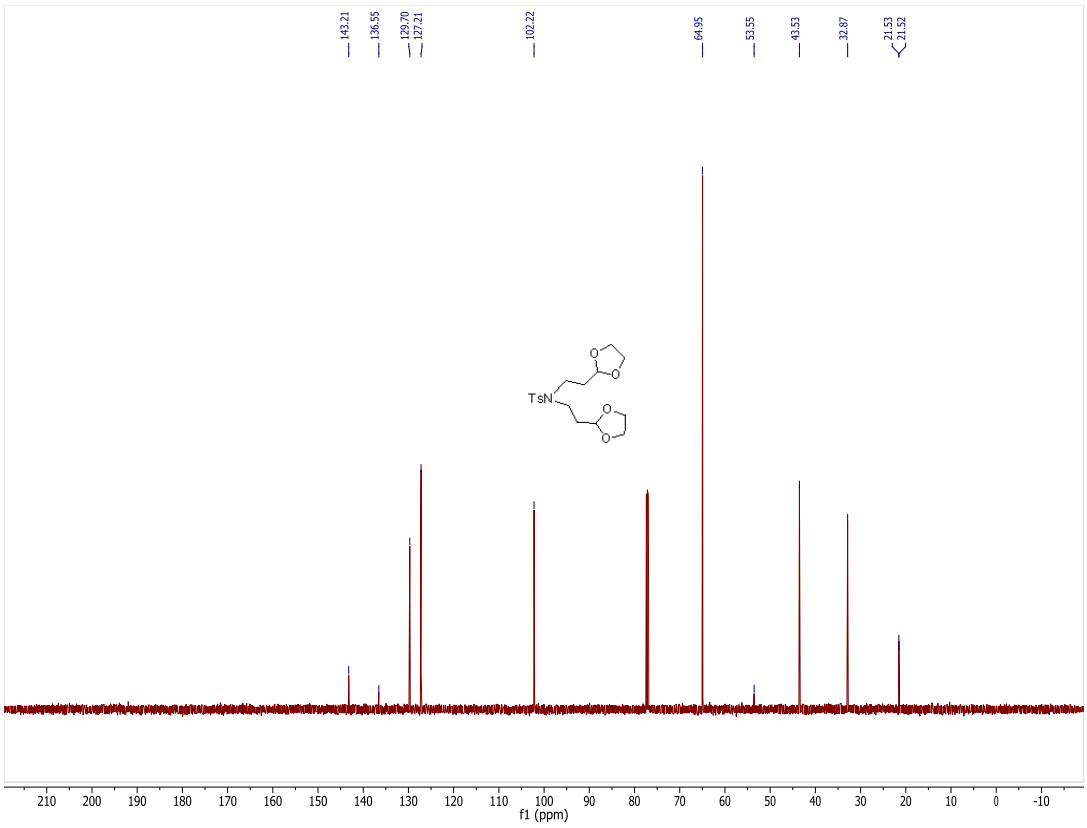
143.21
136.55
129.70
127.21
102.22
64.95
53.55
43.53
32.87
21.53
21.52
TsN
f1 (ppm)

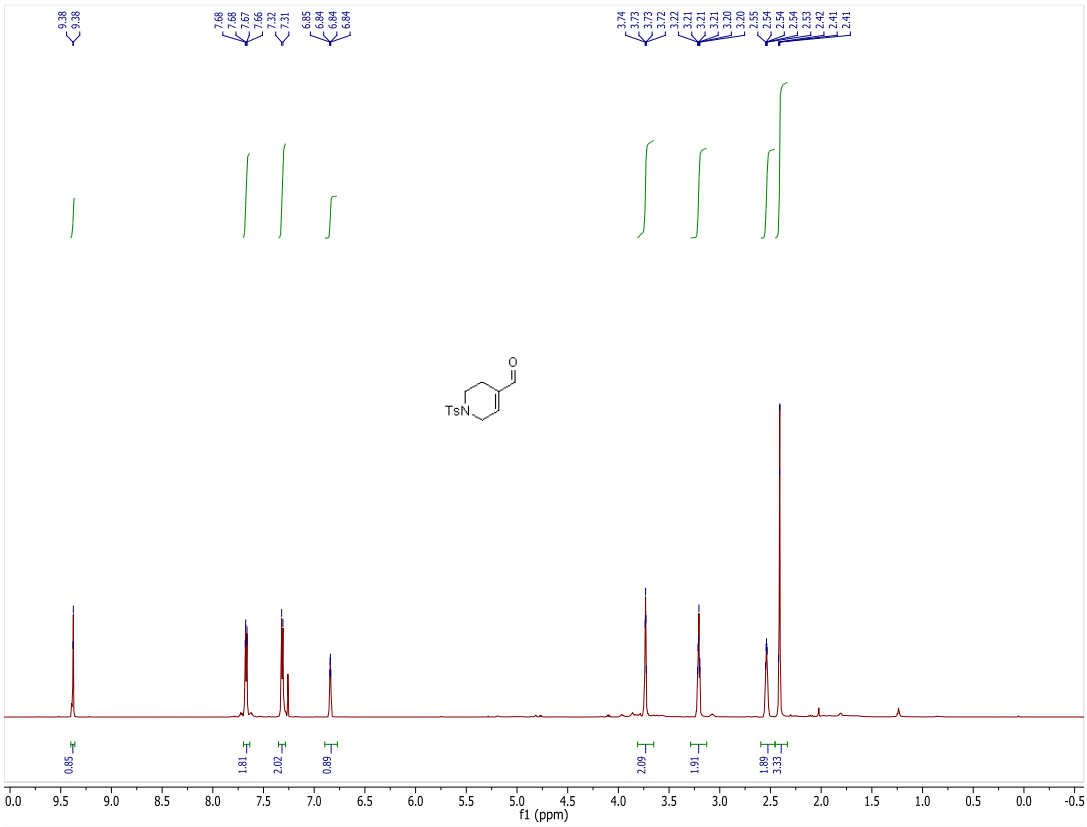
9.38
9.38
7.68
7.68
7.67
7.66
7.32
7.31
6.85
6.84
6.84
6.84
3.74
3.73
3.73
3.72
3.22
3.21
3.21
3.20
3.20
2.55
2.54
2.54
2.54
2.53
2.42
2.41
2.41
O
TsN
0.85
1.81
2.02
0.89
2.09
1.91
1.89
3.33
0.0
9.5
9.0
8.5
8.0
7.5
7.0
6.5
6.0
5.5
5.0
4.5
4.0
3.5
3.0
2.5
2.0
1.5
1.0
0.5
0.0
-0.5
f1 (ppm)

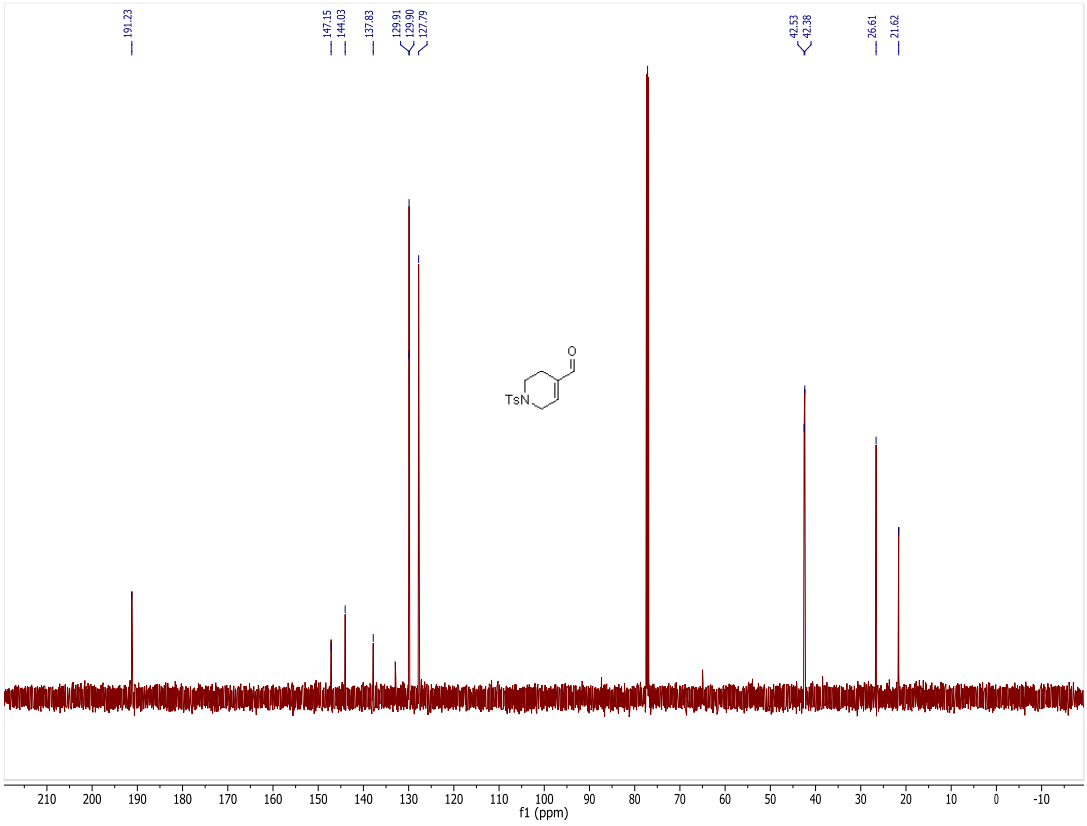
191.23
147.15
144.03
137.83
129.91
129.90
127.79
42.53
42.38
26.61
21.62
O
TsN
210
200
190
180
170
160
150
140
130
120
110
100
90
80
70
60
50
40
30
20
10
0
-10
f1 (ppm)

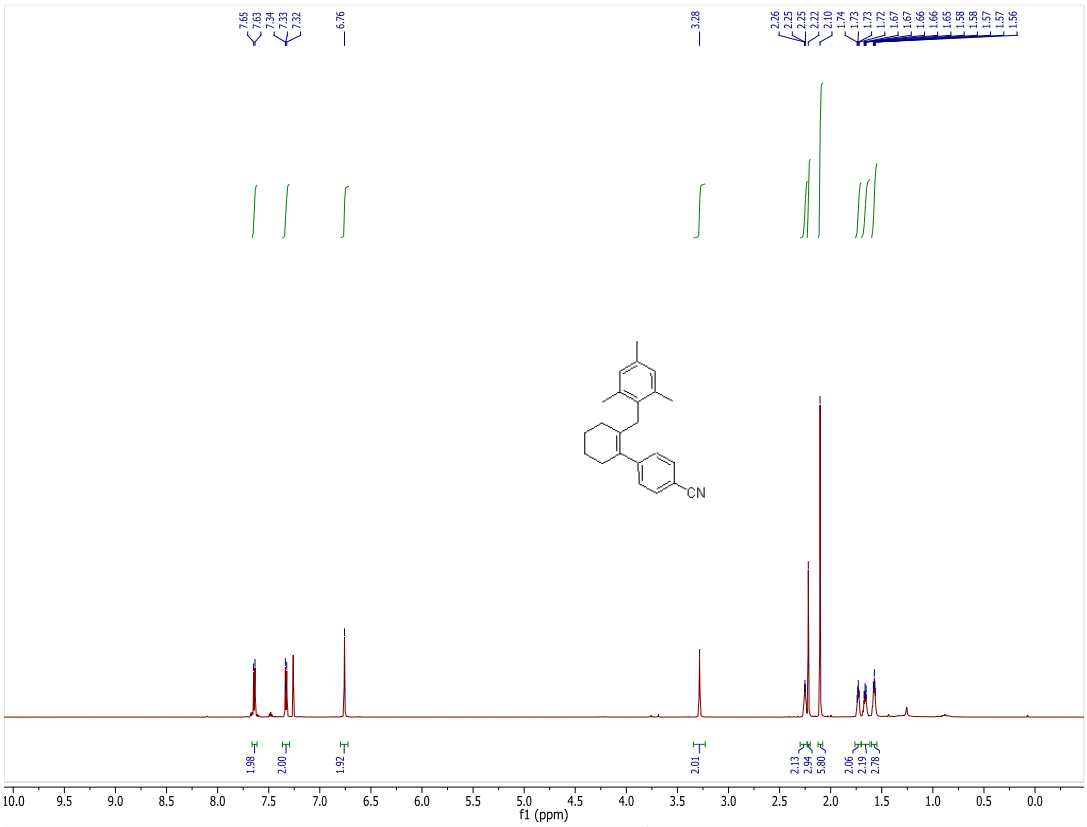
7.65
7.63
7.34
7.33
7.32
6.76
3.28
2.26
2.25
2.25
2.22
2.10
1.74
1.73
1.73
1.72
1.67
1.67
1.66
1.66
1.65
1.58
1.58
1.57
1.57
1.56
CN
1.98
2.00
1.92
2.01
2.13
2.94
5.80
2.06
2.19
2.78
f1 (ppm)

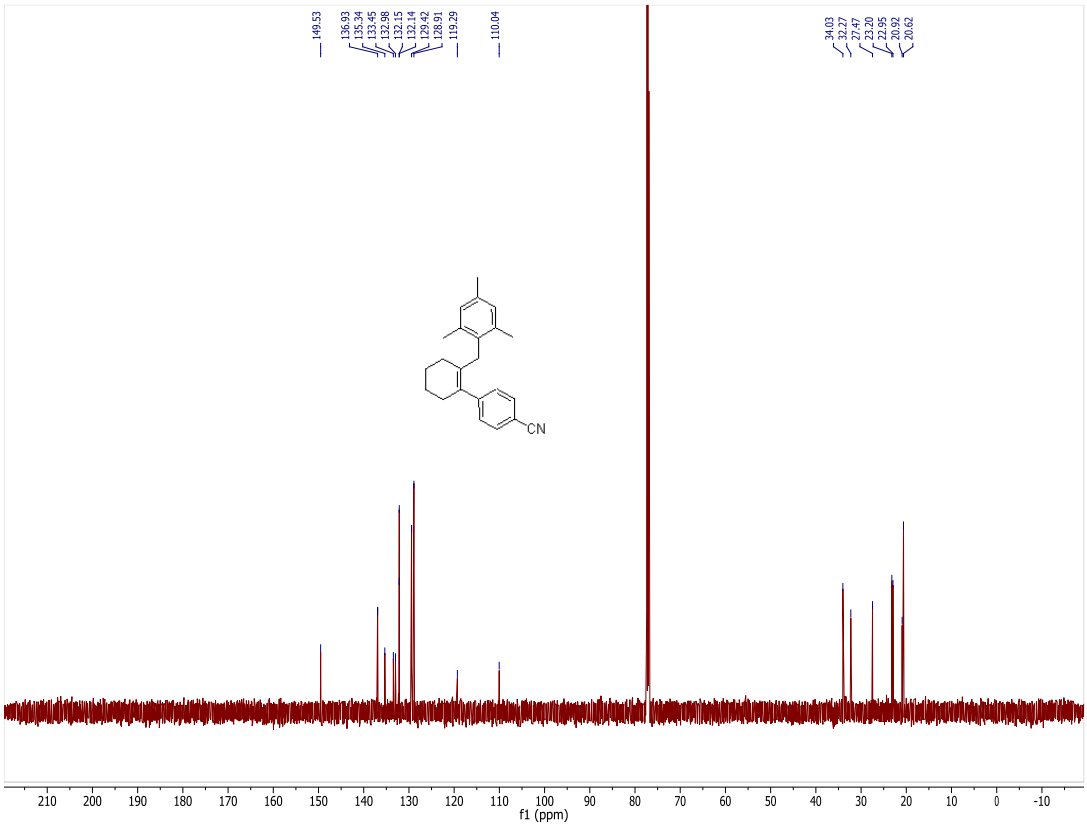
149.53
136.93
135.34
133.45
132.98
132.15
132.14
129.42
128.91
119.29
110.04
34.03
32.27
27.47
23.20
22.95
20.92
20.62
CN
f1 (ppm)

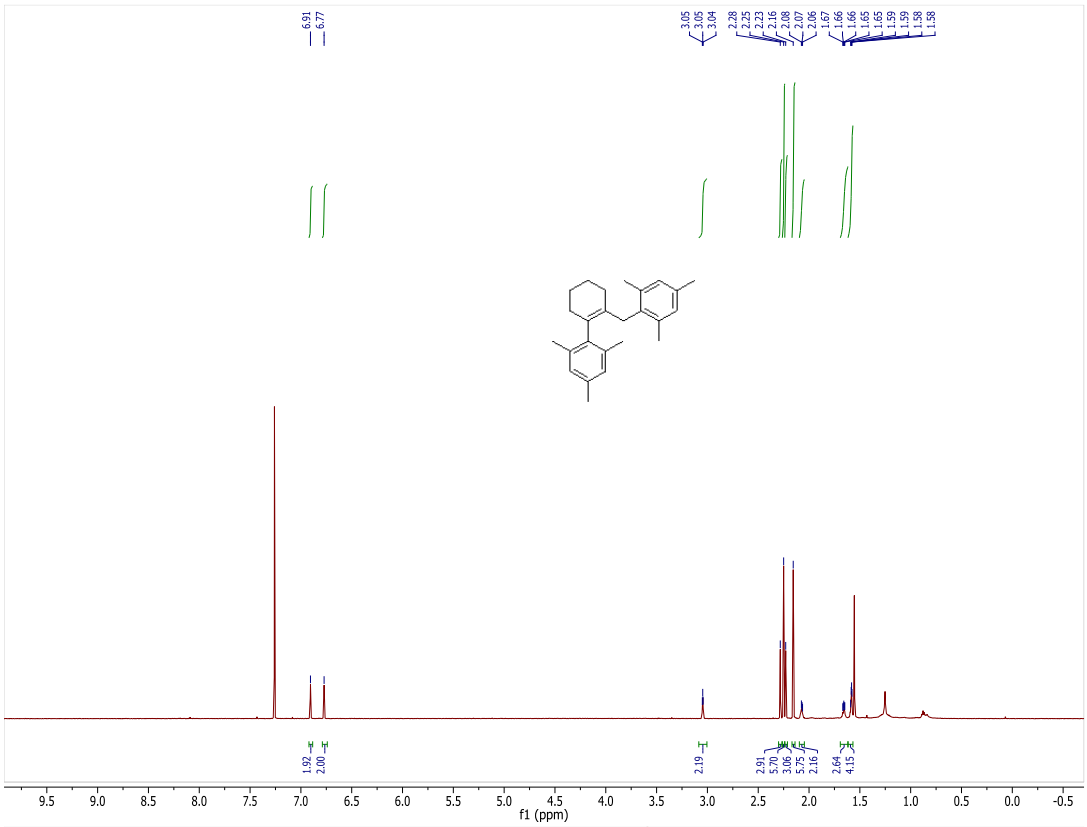
6.91
6.77
3.05
3.05
3.04
2.28
2.25
2.23
2.16
2.08
2.07
2.06
1.67
1.66
1.66
1.65
1.65
1.59
1.59
1.58
1.58
1.92
2.00
2.19
2.91
5.70
3.06
5.75
2.16
2.64
4.15
f1 (ppm)

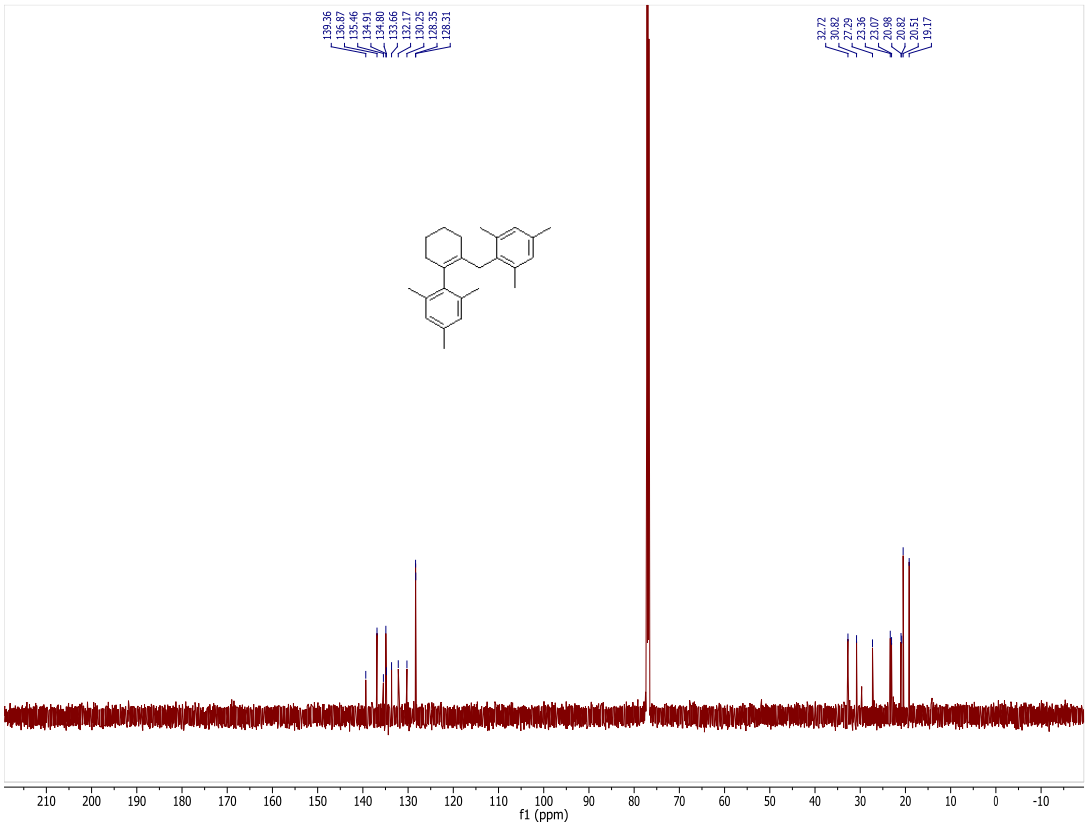
139.36
136.87
135.46
134.91
134.80
133.66
132.17
130.25
128.35
128.31
32.72
30.82
27.29
23.36
23.07
20.98
20.82
20.51
19.17
f1 (ppm)

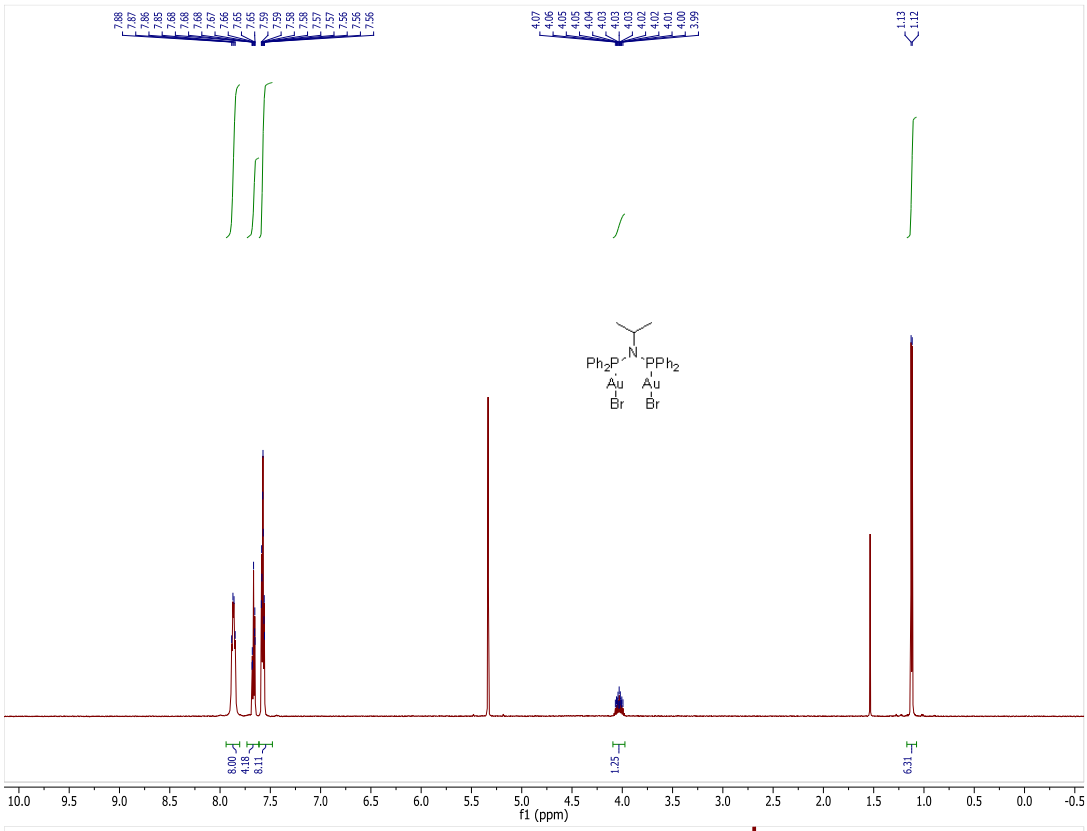
7.88
7.87
7.86
7.85
7.68
7.68
7.68
7.67
7.66
7.65
7.65
7.59
7.59
7.58
7.58
7.57
7.57
7.56
7.56
7.56
4.07
4.06
4.05
4.05
4.04
4.03
4.03
4.03
4.02
4.02
4.01
4.00
3.99
1.13
1.12
Ph2P
N
PPh2
Au
Au
Br
Br
8.00
4.18
8.11
1.25
6.31
10.0
9.5
9.0
8.5
8.0
7.5
7.0
6.5
6.0
5.5
5.0
4.5
4.0
3.5
3.0
2.5
2.0
1.5
1.0
0.5
0.0
-0.5
f1 (ppm)

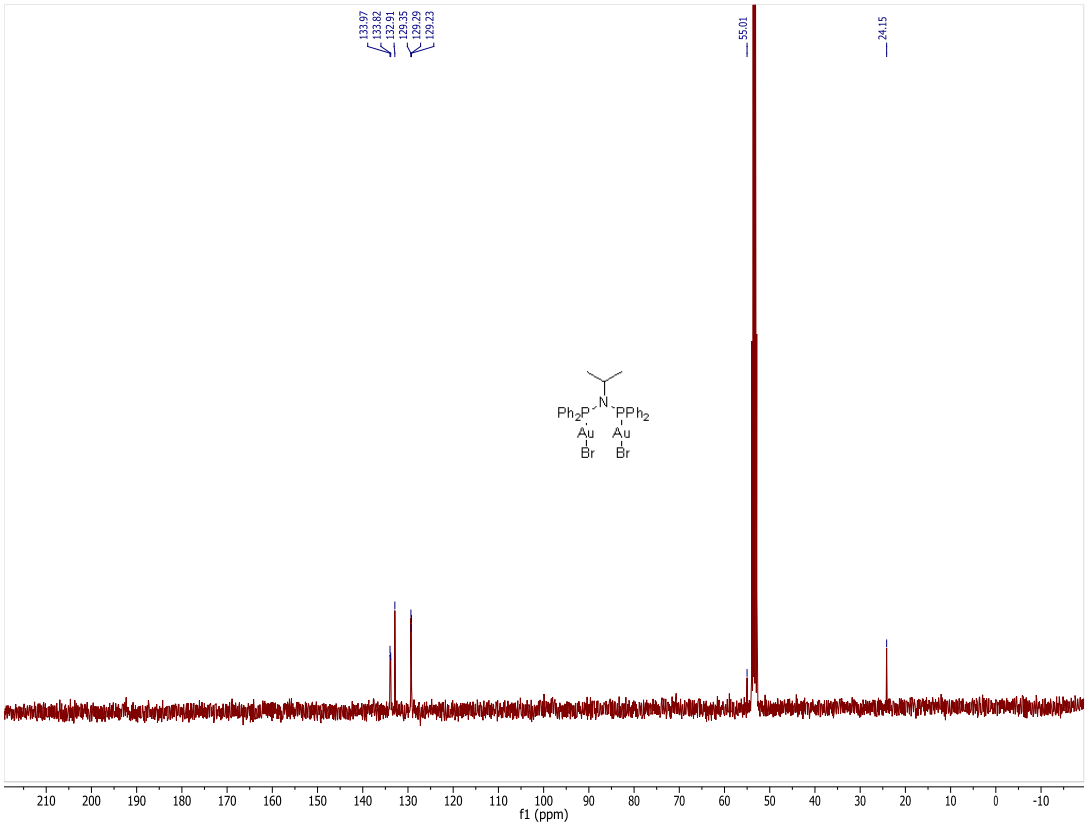
133.97
133.82
132.91
129.35
129.29
129.23
55.01
24.15
Ph2P
N
PPh2
Au
Au
Br
Br
210
200
190
180
170
160
150
140
130
120
110
100
90
80
70
60
50
40
30
20
10
0
-10
f1 (ppm)

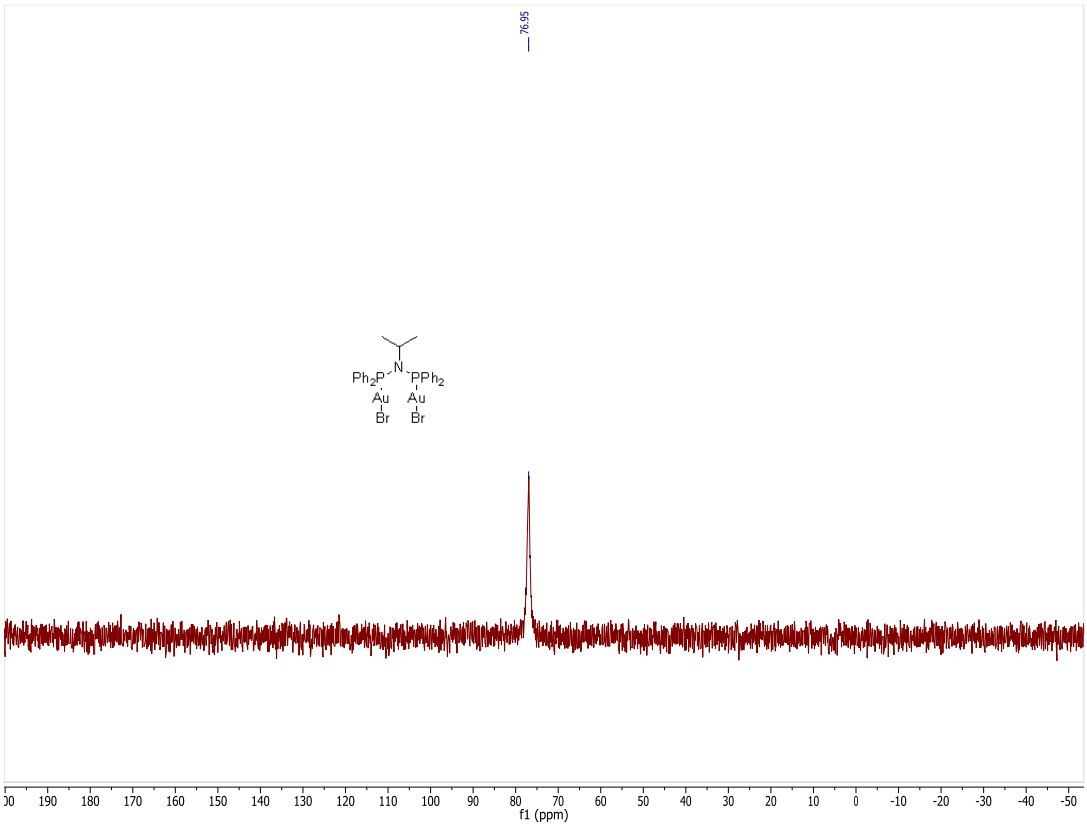
76.95
Ph2P
N
PPh2
Au
Au
Br
Br
f1 (ppm)

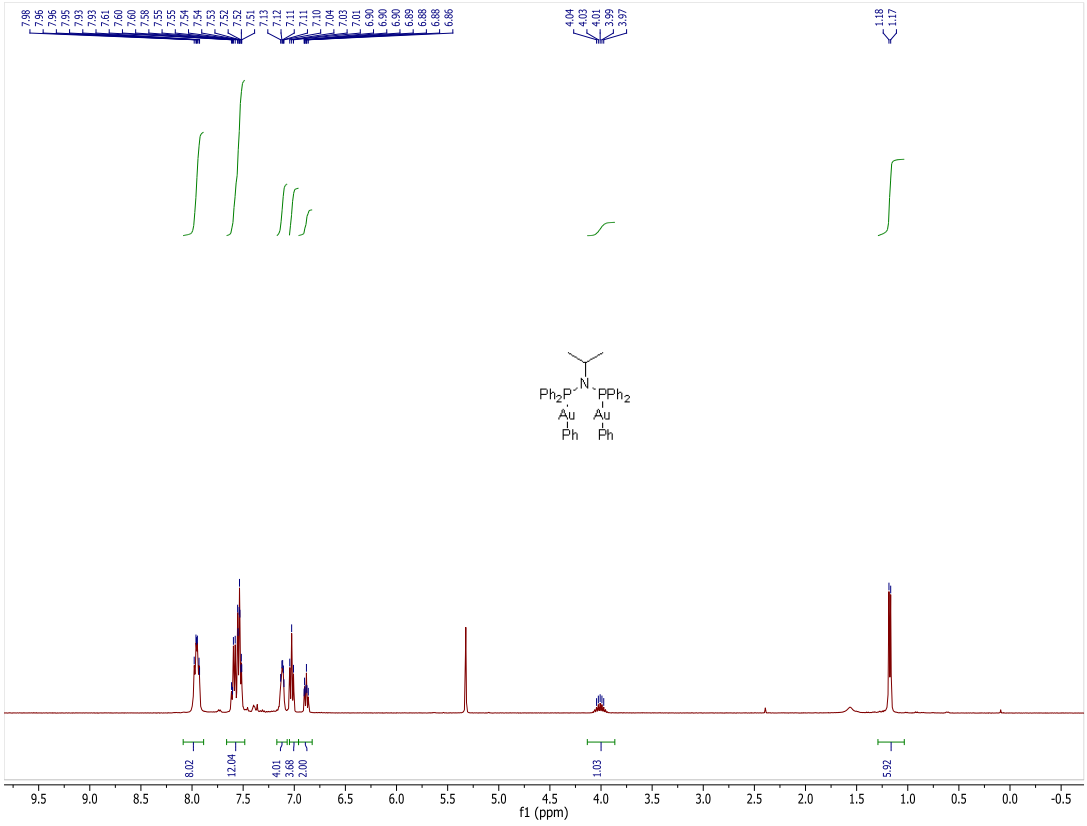
7.98
7.96
7.96
7.95
7.93
7.61
7.60
7.58
7.55
7.55
7.54
7.54
7.53
7.52
7.52
7.51
7.13
7.12
7.11
7.11
7.10
7.04
7.03
7.01
6.90
6.90
6.89
6.88
6.88
6.86
4.04
4.03
4.01
3.99
3.97
1.18
1.17
Ph2P
N
PPh2
Au
Au
Ph
Ph
8.02
12.04
4.01
3.88
2.00
1.03
5.92
f1 (ppm)

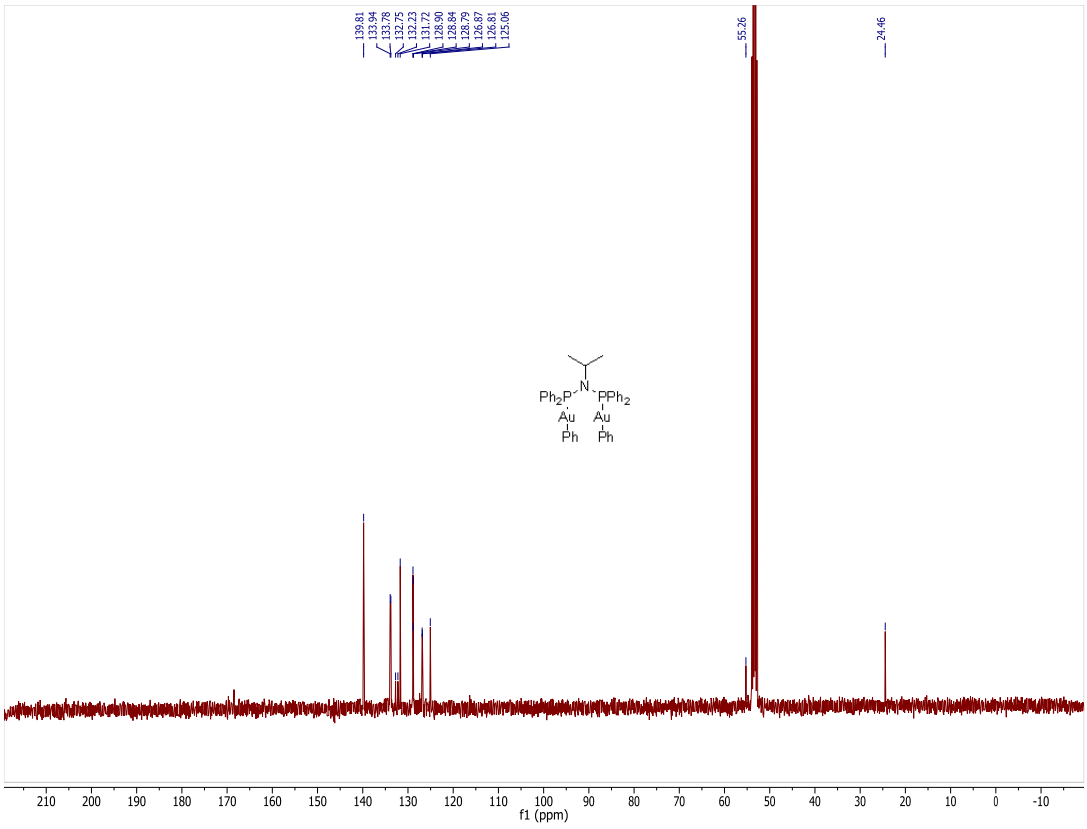
139.81
133.94
133.78
132.75
132.23
131.72
128.90
128.84
128.79
126.87
126.81
125.06
55.26
24.46
Ph2P
N
PPh2
Au
Au
Ph
Ph
210 200 190 180 170 160 150 140 130 120 110 100 90 80 70 60 50 40 30 20 10 0 -10
f1 (ppm)

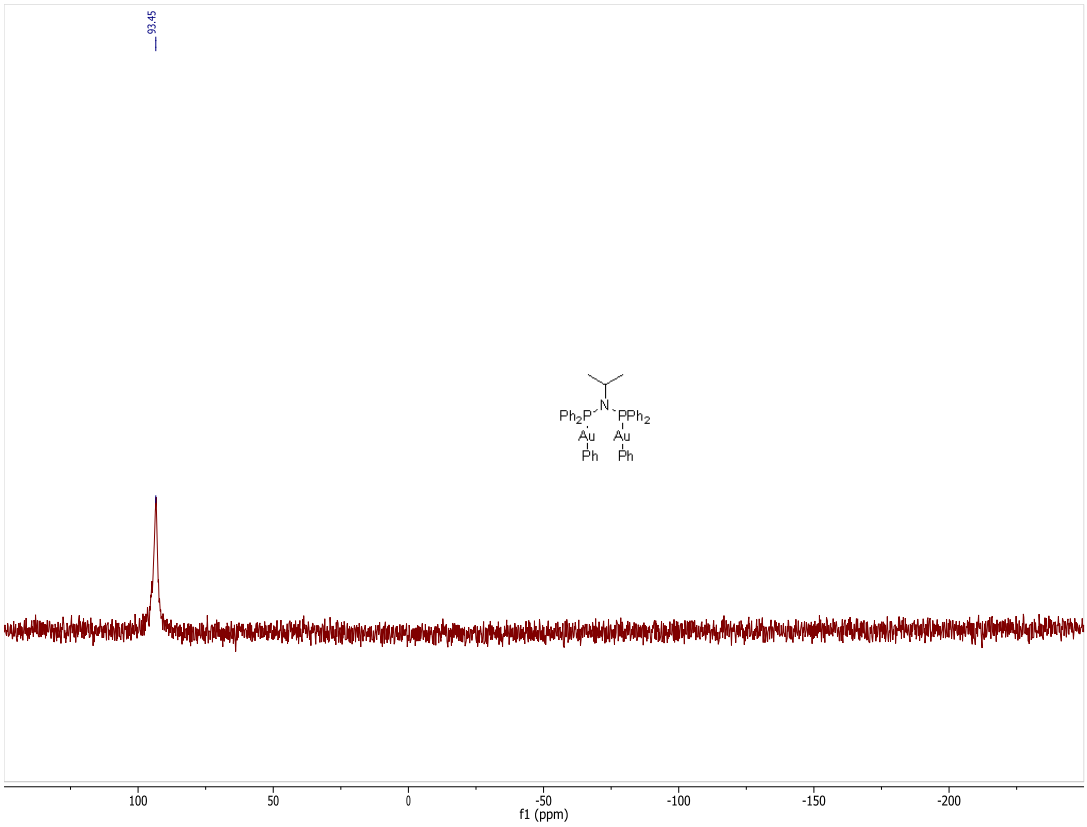
93.45
Ph2P
N
PPh2
Au
Au
Ph
Ph
100 50 0 -50 -100 -150 -200
f1 (ppm)

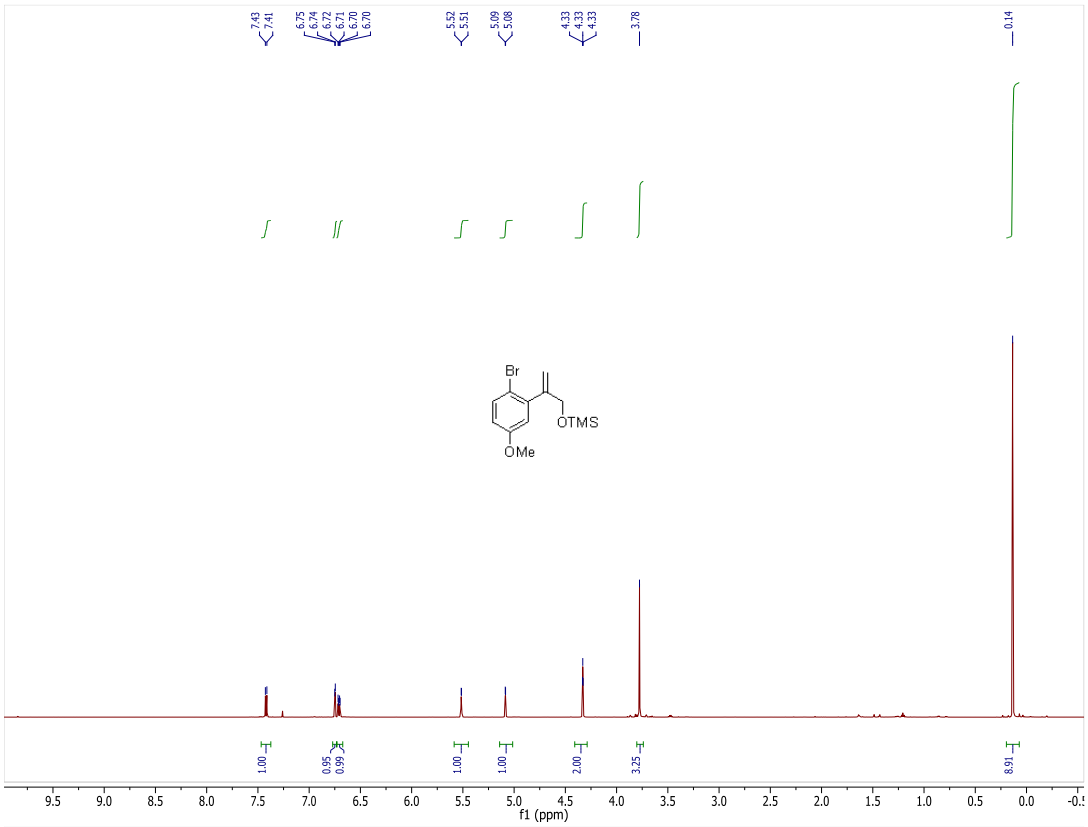
7.43
7.41
6.75
6.74
6.72
6.71
6.70
6.70
5.52
5.51
5.09
5.08
4.33
4.33
4.33
3.78
0.14
Br
OTMS
OMe
1.00
0.95
0.99
1.00
1.00
2.00
3.25
8.91
f1 (ppm)

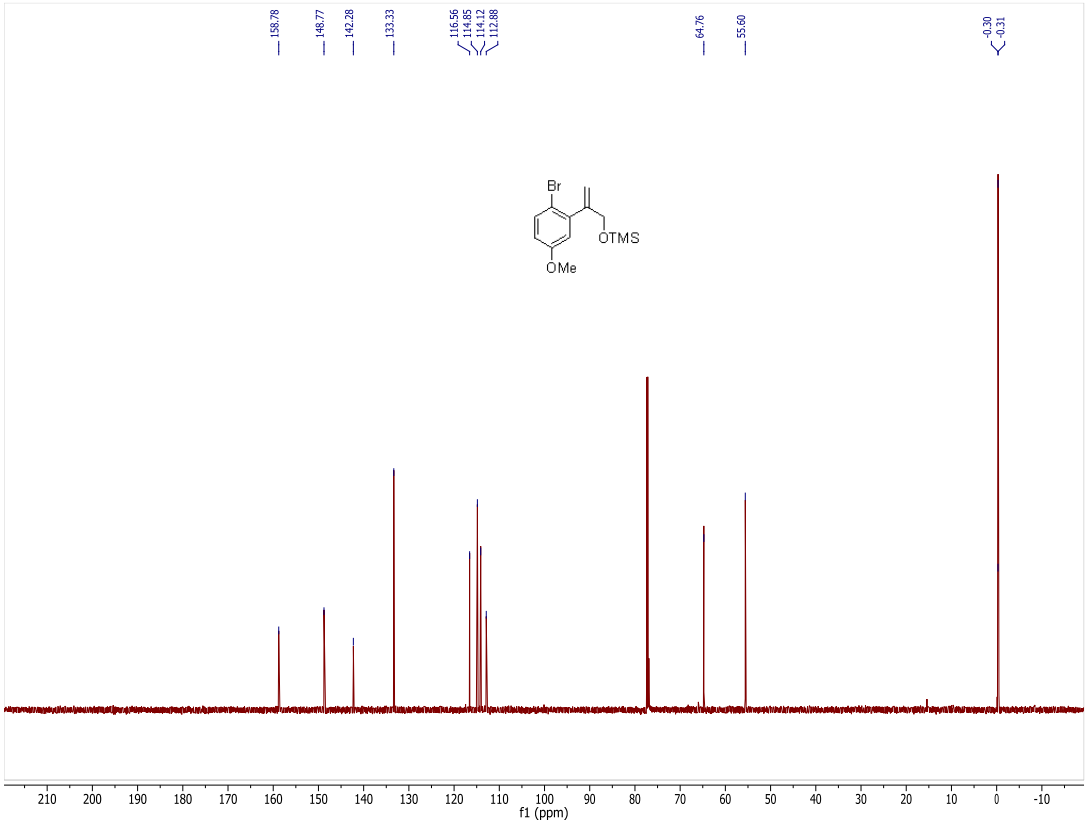
158.78
148.77
142.28
133.33
116.56
114.85
114.12
112.88
64.76
55.60
-0.30
-0.31
Br
OTMS
OMe
f1 (ppm)

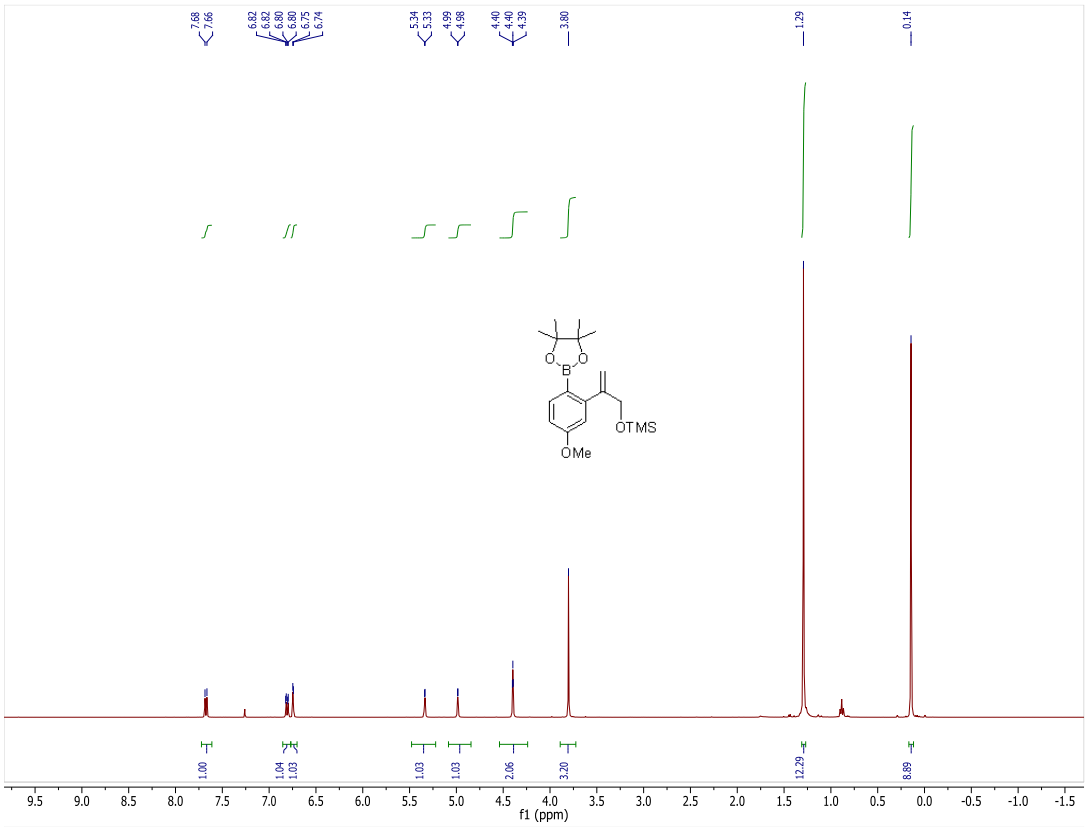
7.68
7.66
6.82
6.82
6.80
6.80
6.75
6.74
5.34
5.33
4.99
4.98
4.40
4.40
4.39
3.80
1.29
0.14
OTMS
OMe
1.00
1.04
1.03
1.03
1.03
2.06
3.20
12.29
8.89
f1 (ppm)

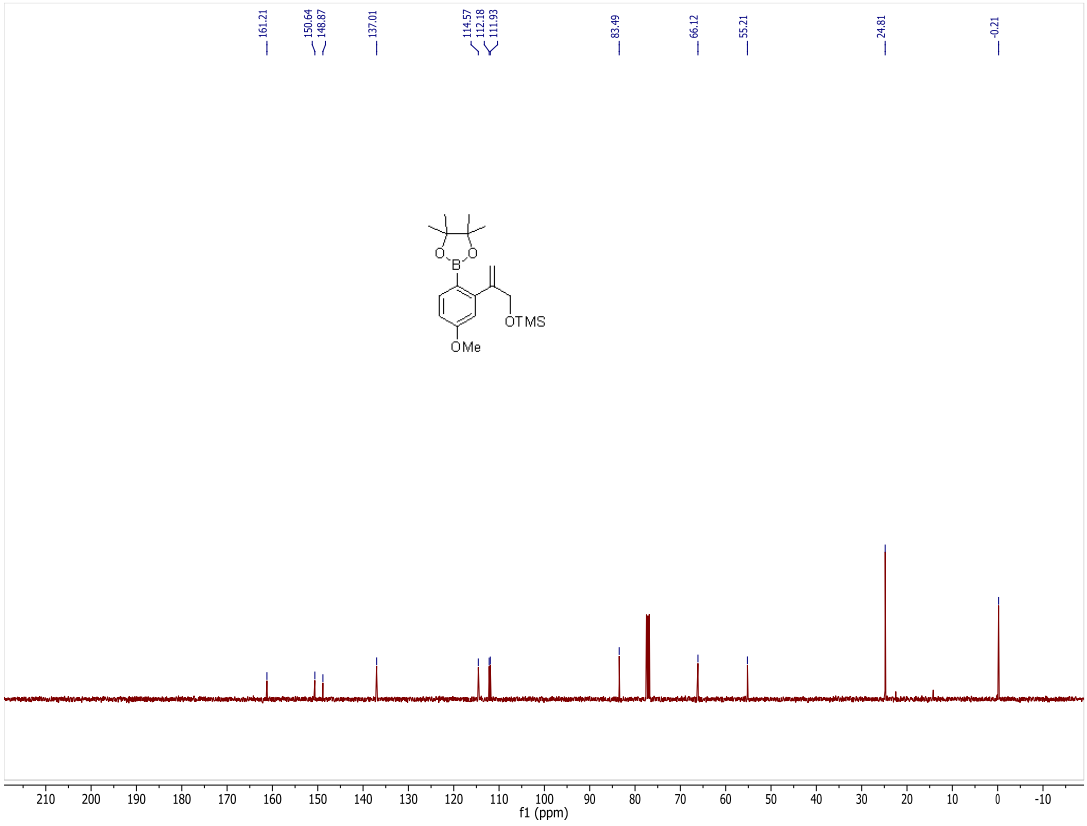
161.21
150.64
148.87
137.01
114.57
112.18
111.93
83.49
66.12
55.21
24.81
-0.21
OTMS
OMe
f1 (ppm)

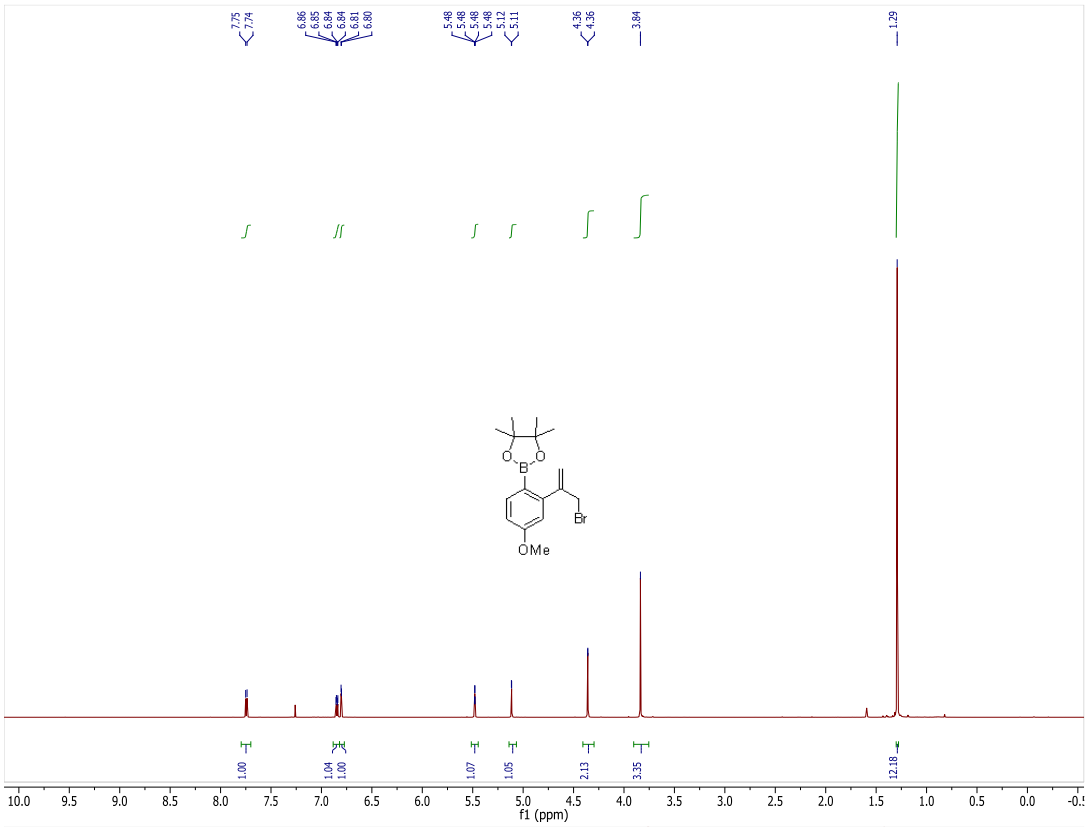
7.75
7.74
6.86
6.85
6.84
6.84
6.81
6.80
5.48
5.48
5.48
5.48
5.12
5.11
4.36
4.36
3.84
1.29
1.00
1.04
1.00
1.07
1.05
2.13
3.35
12.18
f1 (ppm)
B
O
O
Br
OMe

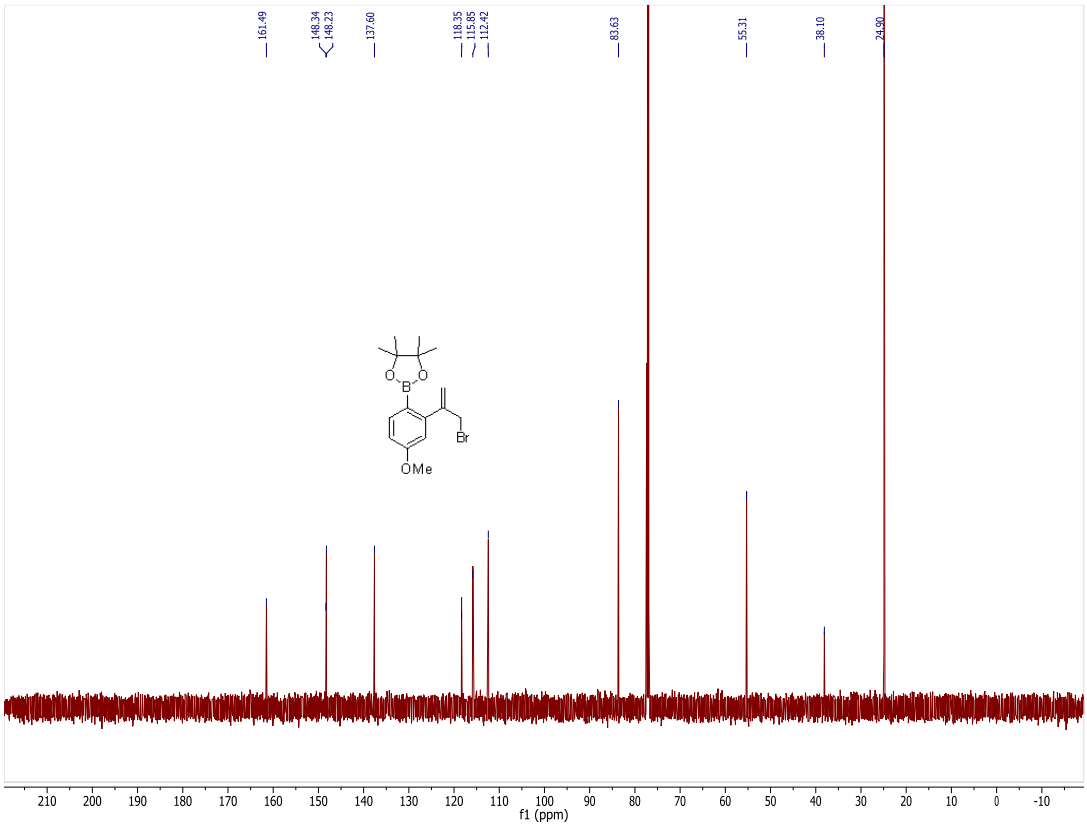
161.49
149.34
149.23
137.60
118.35
115.85
112.42
83.63
55.31
38.10
24.90
f1 (ppm)
B
O
O
Br
OMe

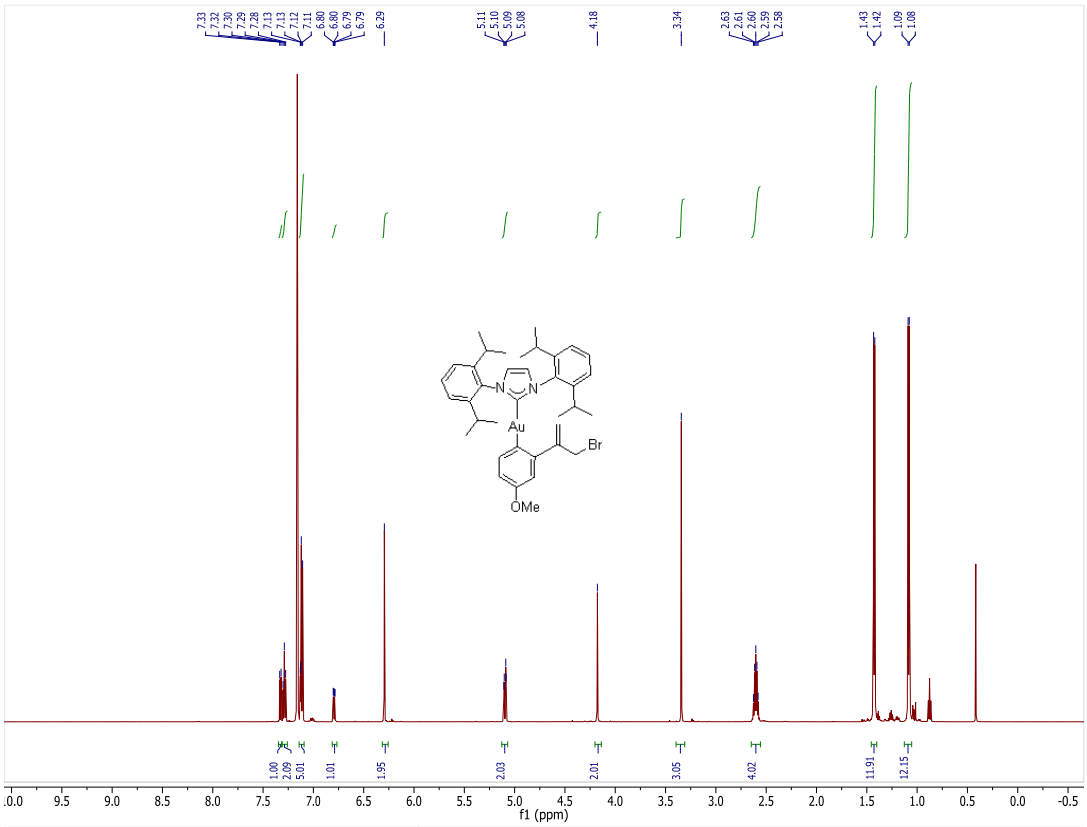
7.33
7.32
7.30
7.29
7.28
7.13
7.13
7.12
7.11
6.80
6.80
6.79
6.79
6.29
5.11
5.10
5.09
5.08
4.18
3.34
2.63
2.61
2.60
2.59
2.58
1.43
1.42
1.09
1.08
Au
Br
OMe
1.00
2.09
5.01
1.01
1.95
2.03
2.01
3.05
4.02
11.91
12.15
f1 (ppm)

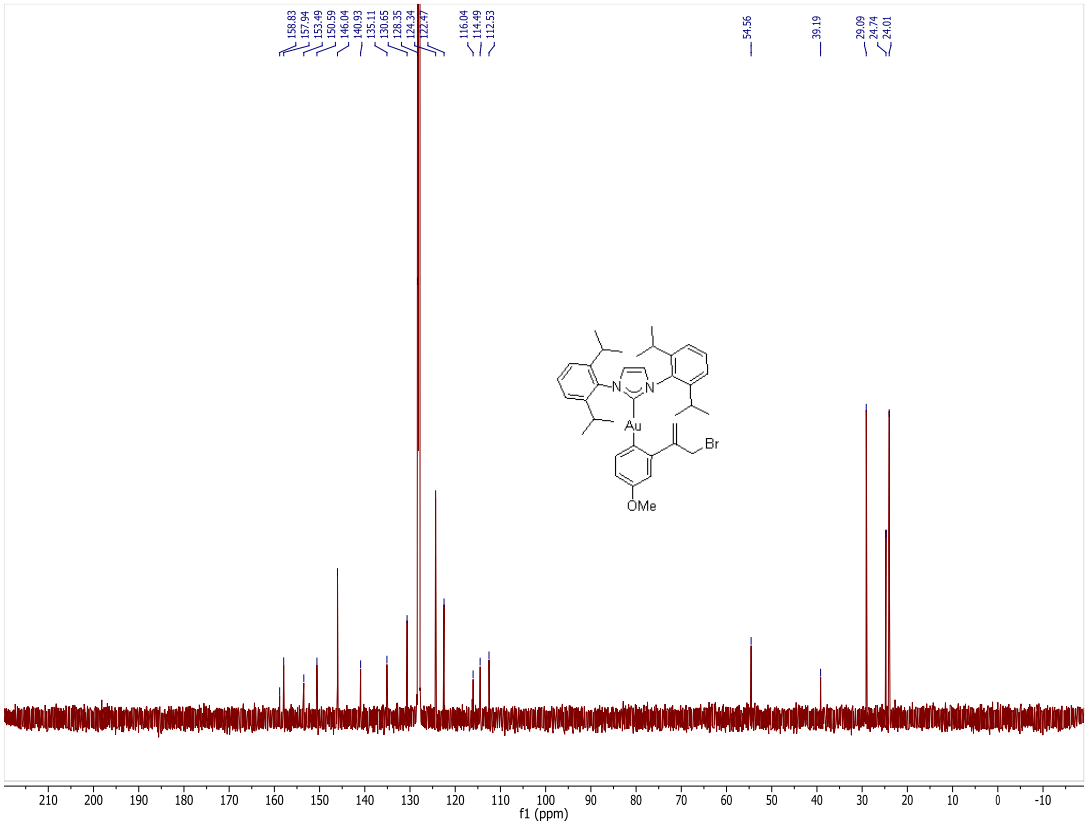
158.83
157.94
153.49
150.59
146.04
140.93
135.11
130.65
128.35
124.34
122.47
116.04
114.49
112.53
54.56
39.19
29.09
24.74
24.01
Au
Br
OMe
f1 (ppm)

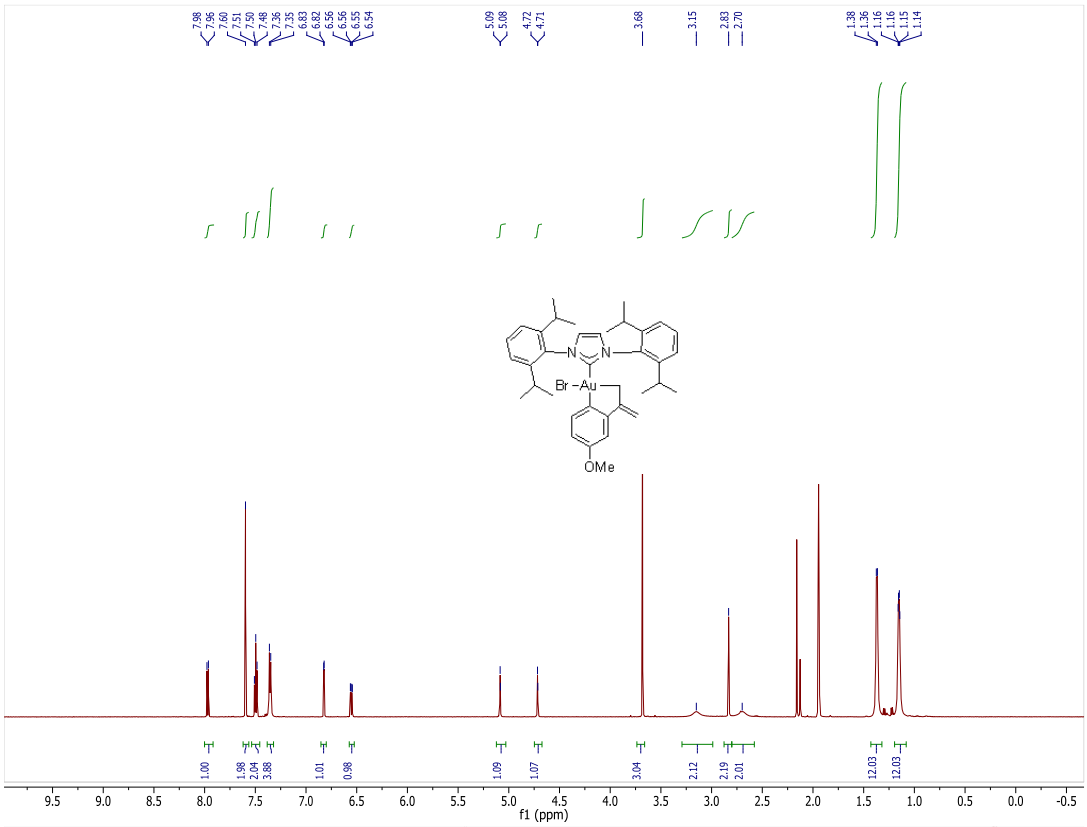
7.98
7.96
7.60
7.51
7.50
7.48
7.36
7.35
6.83
6.82
6.56
6.55
6.54
5.09
5.08
4.72
4.71
3.68
3.15
2.83
2.70
1.38
1.36
1.16
1.16
1.15
1.14
Br
Au
N
N
OMe
1.00
1.98
2.04
3.88
1.01
0.98
1.09
1.07
3.04
2.12
2.19
2.01
12.03
12.03
f1 (ppm)

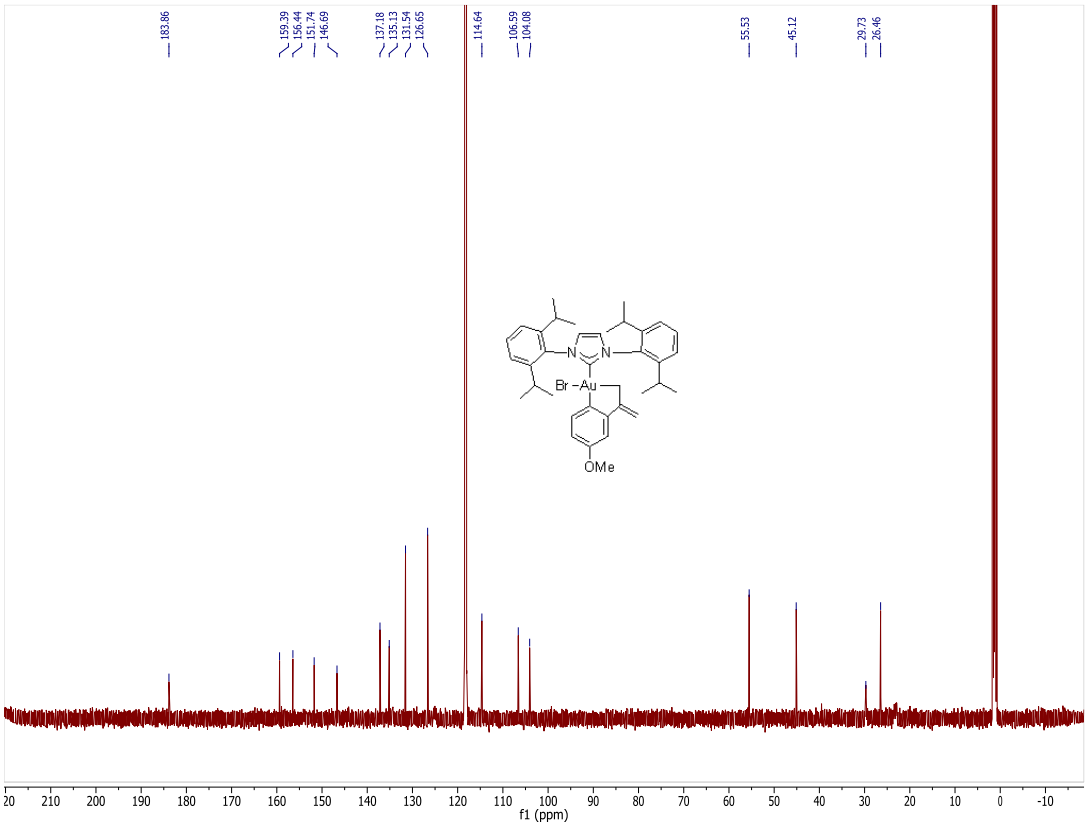
183.86
159.39
156.44
151.74
146.69
137.18
135.13
131.54
126.65
114.64
106.59
104.08
55.53
45.12
29.73
26.46
Br
Au
N
N
OMe
f1 (ppm)

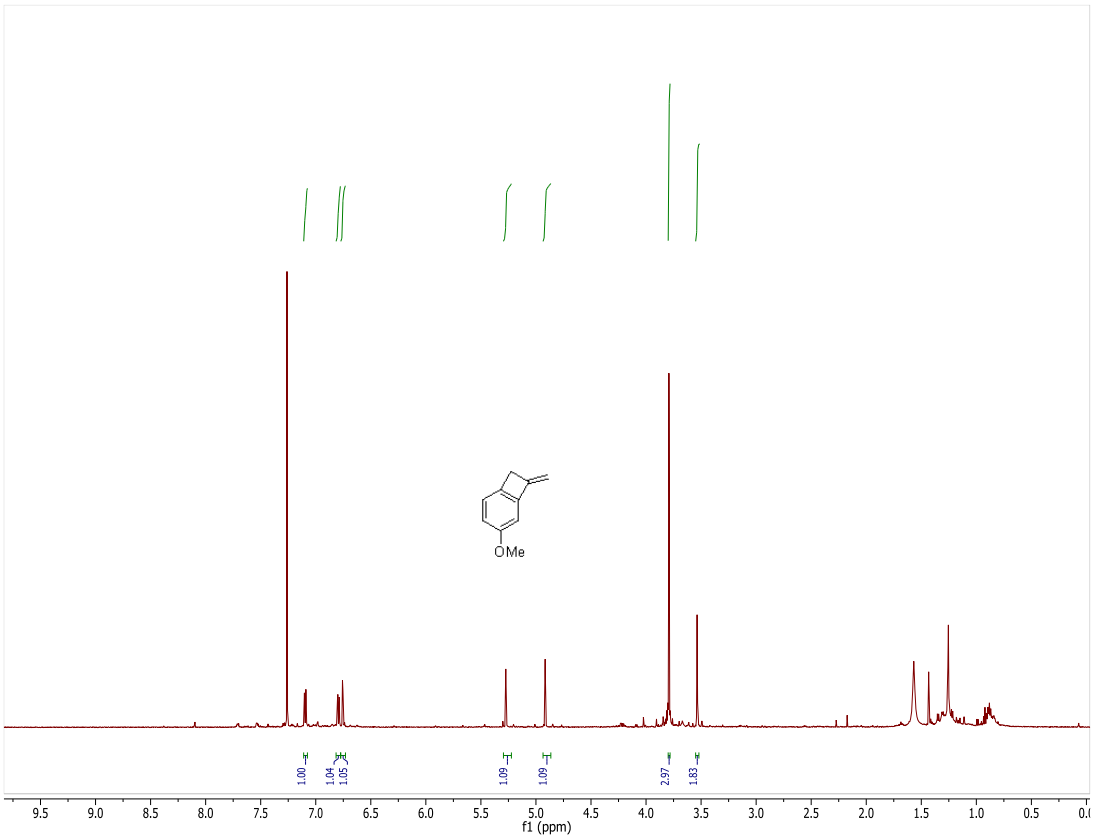
OMe
1.00
1.04
1.05
1.09
1.09
2.97
1.83
f1 (ppm)

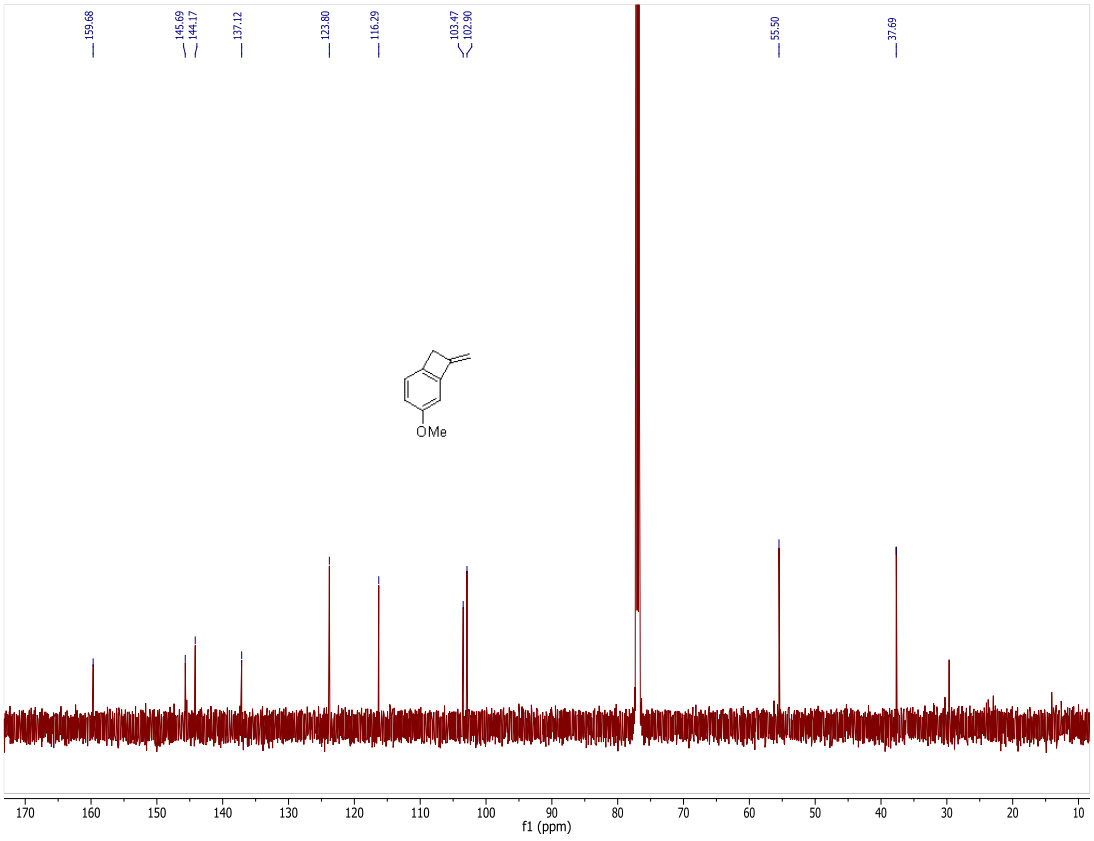
159.68
145.69
144.17
137.12
123.80
116.29
103.47
102.90
55.50
37.69
OMe
f1 (ppm)

## 2.7 References


(1) The initial report of this work claimed priority in this regard, but in light of recent mechanistic work, the development of photoredox/gold dual catalysis in fact deserves this title, such that a more accurate descriptor would be the first *non-photochemical* catalytic reaction utilizing Au(I)/Au(III) redox cycling in the absence of a stoichiometric oxidant.

(2) Nugent, W. A. *Angew. Chem. Int. Ed.* **2012**, *51* (36), 8936.

(3) Shapiro, N.; Toste, F. *Synlett* **2010**, *2010* (5), 675.

(4) Fürstner, A. *Chem. Soc. Rev.* **2009**, *38* (11), 3208.

(5) Jiménez-Núñez, E.; Echavarren, A. M. *Chem. Rev.* **2008**, *108* (8), 3326.

(6) Shen, H. C. *Tetrahedron* **2008**, *64* (18), 3885.

(7) Gorin, D. J.; Sherry, B. D.; Toste, F. D. *Chem. Rev.* **2008**, *108* (8), 3351.

(8) Li, Z.; Brouwer, C.; He, C. *Chem. Rev.* **2008**, *108* (8), 3239.

(9) Hashmi, A. S. K. *Chem. Rev.* **2007**, *107* (7), 3180.

(10) Hartwig, J. F. *Organotransition Metal Chemistry: From Bonding to Catalysis*; University Science Books, 2010.

(11) Gorin, D. J.; Toste, F. D. *Nature* **2007**, *446* (7134), 395.

(12) Melhado, A. D.; Brenzovich, W. E.; Lackner, A. D.; Toste, F. D. *J. Am. Chem. Soc.* **2010**, *132* (26), 8885.

(13) Ball, L. T.; Lloyd-Jones, G. C.; Russell, C. A. *Science* **2012**, *337* (6102), 1644.

(14) Tamaki, A.; Kochi, J. K. *J. Organomet. Chem.* **1974**, *64* (3), 411.

(15) Shiotani, A.; Schmidbaur, H. *J. Organomet. Chem.* **1972**, *37* (1), C24.

(16) Tamaki, A.; Magennis, S. A.; Kochi, J. K. *J. Am. Chem. Soc.* **1973**, *95* (19), 6487.

(17) Johnson, A.; Puddephatt, R. J. *J. Organomet. Chem.* **1975**, *85* (1), 115.

(18) Porcel, S.; López-Carrillo, V.; García-Yebra, C.; Echavarren, A. M. *Angew. Chem. Int. Ed.* **2008**, *47* (10), 1883.

(19) Tamaki, A.; Magennis, S. A.; Kochi, J. K. *J. Am. Chem. Soc.* **1974**, *96* (19), 6140.

(20) Komiya, S.; Albright, T. A.; Hoffmann, R.; Kochi, J. K. *J. Am. Chem. Soc.* **1976**, *98* (23), 7255.

(21) Komiya, S.; Kochi, J. K. *J. Am. Chem. Soc.* **1976**, *98* (24), 7599.

(22) Lawrence Kuch, P.; Stuart Tobias, R. *J. Organomet. Chem.* **1976**, *122* (3), 429.

(23) Komiya, S.; Ozaki, S.; Shibue, A. *J. Chem. Soc. Chem. Commun.* **1986**, No. 20, 1555.

(24) Vicente, J.; Dolores Bermudez, M.; Escribano, J. *Organometallics* **1991**, *10* (9), 3380.

(25) Wolf, W. J.; Winston, M. S.; Toste, F. D. *Nat. Chem.* **2014**, *6* (2), 159.

(26) Partyka, D. V.; Zeller, M.; Hunter, A. D.; Gray, T. G. *Angew. Chem. Int. Ed.* **2006**, *45* (48), 8188.

(27) Hashmi, A. S. K.; Ramamurthi, T. D.; Rominger, F. *J. Organomet. Chem.* **2009**, *694* (4), 592.

(28) Fackler, J. P. *Polyhedron* **1997**, *16* (1), 1.

(29) Yam, V. W.-W.; Chan, C.-L.; Cheung, K.-K. *J Chem Soc Dalton Trans* **1996**, No. 20, 4019.

(30) Chen, Y.; Chen, M.; Liu, Y. *Angew. Chem. Int. Ed.* **2012**, *51* (25), 6181.

(31) Sladek, A.; Hofreiter, S.; Paul, M.; Schmidbaur, H. *J. Organomet. Chem.* **1995**, *501* (1), 47.

(32) Forward, J. M.; Fackler, J. P.; Staples, R. J. *Organometallics* **1995**, *14* (9), 4194.

(33) Weber, S. G.; Zahner, D.; Rominger, F.; Straub, B. F. *Chem Commun* **2012**, *48* (92), 11325.
(34) Dupuy, S.; Slawin, A. M. Z.; Nolan, S. P. *Chem. – Eur. J.* **2012**, *18* (47), 14923.
(35) Gillis, E. P.; Burke, M. D. *J. Am. Chem. Soc.* **2008**, *130* (43), 14084.
(36) Lennox, A. J. J.; Lloyd-Jones, G. C. *Chem Soc Rev* **2014**, *43* (1), 412.
(37) Zard, S. Z. In *Encyclopedia of Radicals in Chemistry, Biology and Materials*; John Wiley & Sons, Ltd, 2012.
(38) Partyka, D. V.; Zeller, M.; Hunter, A. D.; Gray, T. G. *Inorg. Chem.* **2012**, *51* (15), 8394.
(39) Seidel, G.; Lehmann, C. W.; Fürstner, A. *Angew. Chem. Int. Ed.* **2010**, *49* (45), 8466.
(40) Heckler, J. E.; Zeller, M.; Hunter, A. D.; Gray, T. G. *Angew. Chem. Int. Ed.* **2012**, *51* (24), 5924.
(41) Trost, B. M.; Hung, M. H. *J. Am. Chem. Soc.* **1984**, *106* (22), 6837.
(42) Trost, B. M.; Toste, F. D. *J. Am. Chem. Soc.* **1999**, *121* (19), 4545.
(43) Madrahimov, S. T.; Li, Q.; Sharma, A.; Hartwig, J. F. *J. Am. Chem. Soc.* **2015**, *137* (47), 14968.
(44) Yoshikai, N.; Nakamura, E. *Chem. Rev.* **2012**, *112* (4), 2339.
(45) Winstein, S.; Young, W. G. *J. Am. Chem. Soc.* **1936**, *58* (1), 104.
(46) Young, W. G.; Lane, J. F. *J. Am. Chem. Soc.* **1937**, *59* (10), 2051.
(47) Young, W. G.; Lane, J. F. *J. Am. Chem. Soc.* **1938**, *60* (4), 847.
(48) Komiya, S.; Ozaki, S. *Chem. Lett.* **1988**, *17* (8), 1431.
(49) Sone, T.; Ozaki, S.; Kasuga, N. C.; Fukuoka, A.; Komiya, S. *Bull. Chem. Soc. Jpn.* **1995**, *68* (6), 1523.
(50) Hussain, M. M.; Walsh, P. J. *Angew. Chem. Int. Ed.* **2010**, *49* (10), 1834.
(51) Basil, J. D.; Murray, H. H.; Fackler, J. P.; Tocher, J.; Mazany, A. M.; Trzcinska-Bancroft, B.; Knachel, H.; Dudis, D.; Delord, T. J.; Marler, D. *J. Am. Chem. Soc.* **1985**, *107* (24), 6908.
(52) Fackler, J. P.; Murray, H. H.; Basil, J. D. *Organometallics* **1984**, *3* (5), 821.
(53) Anslyn, E. V.; Dougherty, D. A. *Modern Physical Organic Chemistry*; University Science Books: Sausalito, CA, 2006.
(54) Kochi, J. K. *Organometallic Mechanisms and Catalysis*; Academic Press: New York, NY, 1978.
(55) Albrecht, M. *Chem. Rev.* **2010**, *110* (2), 576.
(56) Gaillard, S.; Slawin, A. M. Z.; Nolan, S. P. *Chem. Commun.* **2010**, *46* (16), 2742.
(57) Komiya, S.; Iwata, M.; Sone, T.; Fukuoka, A. *J Chem Soc Chem Commun* **1992**, No. 16, 1109.
(58) Usui, Y.; Noma, J.; Hirano, M.; Komiya, S. *Inorganica Chim. Acta* **2000**, *309* (1–2), 151.
(59) Sutherland, B. R.; Folting, K.; Streib, W. E.; Ho, D. M.; Huffman, J. C.; Caulton, K. G. *J. Am. Chem. Soc.* **1987**, *109* (11), 3489.
(60) Johnson, A.; Puddephatt, R. J. *Inorg. Nucl. Chem. Lett.* **1973**, *9* (11), 1175.
(61) Chock, P. B.; Halpern, J. *J. Am. Chem. Soc.* **1966**, *88* (15), 3511.
(62) Pena-Lopez, M.; Ayan-Varela, M.; Sarandeses, L. A.; Sestelo, J. P. *Org Biomol Chem* **2012**, *10* (8), 1686.
(63) 3-Cyclopropyl allyl bromide decomposed thermally much faster than the corresponding coupling reaction, and the related allyl bromide shown below was

found not to cyclize under several conditions known to proceed via single electron pathways:

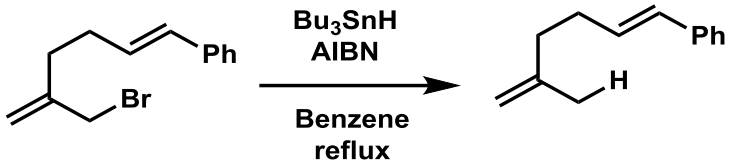



(64) Tkatchouk, E.; Mankad, N. P.; Benitez, D.; Goddard, W. A.; Toste, F. D. *J. Am. Chem. Soc.* **2011**, *133* (36), 14293.

(65) Vikse, K. L.; Zavras, A.; Thomas, T. H.; Ariafard, A.; Khairallah, G. N.; Canty, A. J.; Yates, B. F.; O'Hair, R. A. J. *Organometallics* **2015**, *34* (13), 3255.

(66) Roth, K. E.; Blum, S. A. *Organometallics* **2010**, *29* (7), 1712.

(67) Mukherjee, P.; Widenhoefer, R. A. *Angew. Chem. Int. Ed.* **2012**, *51* (6), 1405.

(68) Johnson, A.; Puddephatt, R. J. *J Chem Soc Dalton Trans* **1977**, No. 14, 1384.

(69) Cai, R.; Lu, M.; Aguilera, E. Y.; Xi, Y.; Akhmedov, N. G.; Petersen, J. L.; Chen, H.; Shi, X. *Angew. Chem. Int. Ed.* **2015**, *54* (30), 8772.

(70) Serra, J.; Whiteoak, C. J.; Acuña-Parés, F.; Font, M.; Luis, J. M.; Lloret-Fillol, J.; Ribas, X. *J. Am. Chem. Soc.* **2015**, *137* (41), 13389.

(71) Serra, J.; Parella, T.; Ribas, X. *Chem Sci* **2017**, *8* (2), 946.

(72) Sahoo, B.; Hopkinson, M. N.; Glorius, F. *J. Am. Chem. Soc.* **2013**, *135* (15), 5505.

(73) Shu, X.; Zhang, M.; He, Y.; Frei, H.; Toste, F. D. *J. Am. Chem. Soc.* **2014**, *136* (16), 5844.

(74) Li, P.; Wang, L.; Wang, M.; You, F. *Eur. J. Org. Chem.* **2008**, *2008* (35), 5946.

(75) González-Arellano, C.; Corma, A.; Iglesias, M.; Sánchez, F. *Eur. J. Inorg. Chem.* **2008**, *2008* (7), 1107.

(76) Oliver-Meseguer, J.; Cabrero-Antonino, J. R.; Domínguez, I.; Leyva-Pérez, A.; Corma, A. *Science* **2012**, *338* (6113), 1452.

(77) Lauterbach, T.; Livendahl, M.; Rosellón, A.; Espinet, P.; Echavarren, A. M. *Org. Lett.* **2010**, *12* (13), 3006.

(78) Brandys, M.-C.; Jennings, M. C.; Puddephatt, R. J. *J Chem Soc Dalton Trans* **2000**, No. 24, 4601.

(79) Elowe, P. R.; McCann, C.; Pringle, P. G.; Spitzmesser, S. K.; Bercaw, J. E. *Organometallics* **2006**, *25* (22), 5255.

(80) Cros, P.; Triantaphylides, C.; Buono, G. *J. Org. Chem.* **1988**, *53* (1), 185.

(81) Collado, A.; Gomez-Suarez, A.; Martin, A. R.; Slawin, A. M. Z.; Nolan, S. P. *Chem Commun* **2013**, *49* (49), 5541.

(82) Partyka, D. V.; Robilotto, T. J.; Zeller, M.; Hunter, A. D.; Gray, T. G. *Organometallics* **2008**, *27* (1), 28.

(83) Jones, P. G.; Williams, A. F. *J Chem Soc Dalton Trans* **1977**, No. 15, 1430.

(84) Molter, A.; Rust, J.; Lehmann, C. W.; Deepa, G.; Chiba, P.; Mohr, F. *Dalton Trans* **2011**, *40* (38), 9810.

(85) Hollingworth, C.; Hazari, A.; Hopkinson, M. N.; Tredwell, M.; Benedetto, E.; Huiban, M.; Gee, A. D.; Brown, J. M.; Gouverneur, V. *Angew. Chem. Int. Ed.* **2011**, *50* (11), 2613.

(86) Sato, K.; Miyamoto, O.; Inoue, S.; Honda, K. *Chem. Lett.* **1981**, *10* (8), 1183.

(87) Shunatona, H. P.; Früh, N.; Wang, Y.-M.; Rauniyar, V.; Toste, F. D. *Angew. Chem. Int. Ed.* **2013**, *52* (30), 7724.

(88) Qrareya, H.; Raviola, C.; Protti, S.; Fagnoni, M.; Albini, A. *J. Org. Chem.* **2013**, *78* (12), 6016.
(89) Denmark, S. E.; Werner, N. S. *J. Am. Chem. Soc.* **2008**, *130* (48), 16382.
(90) Li, Q. H.; Liu, Z. Q.; Liu, L. Z.; Du, S. S.; Deng, W. Z. *Molecules* **2013**, *18* (4).
(91) Su, W.; Urgaonkar, S.; McLaughlin, P. A.; Verkade, J. G. *J. Am. Chem. Soc.* **2004**, *126* (50), 16433.
(92) Murai, A.; Sato, S.; Masamune, T. *Bull. Chem. Soc. Jpn.* **1984**, *57* (8), 2276.
(93) Protti, S.; Fagnoni, M.; Albini, A. *Org Biomol Chem* **2005**, *3* (15), 2868.
(94) Furuyama, T.; Yonehara, M.; Arimoto, S.; Kobayashi, M.; Matsumoto, Y.; Uchiyama, M. *Chem. – Eur. J.* **2008**, *14* (33), 10348.
(95) Kadyrov, R. *Chem. – Eur. J.* **2013**, *19* (3), 1002.
(96) Wehrli, R.; Heimgartner, H.; Schmid, H.; Hansen, H.-J. *Helv. Chim. Acta* **1977**, *60* (6), 2034.
(97) Qiu, D.; Mo, F.; Zheng, Z.; Zhang, Y.; Wang, J. *Org. Lett.* **2010**, *12* (23), 5474.
(98) Verendel, J. J.; Zhou, T.; Li, J.-Q.; Paptchikhine, A.; Lebedev, O.; Andersson, P. G. *J. Am. Chem. Soc.* **2010**, *132* (26), 8880.
(99) Garzan, A.; Jaganathan, A.; Salehi Marzijarani, N.; Yousefi, R.; Whitehead, D. C.; Jackson, J. E.; Borhan, B. *Chem. – Eur. J.* **2013**, *19* (27), 9015.
(100) Hwu, J. R.; Leopold, E. J. *J Chem Soc Chem Commun* **1984**, No. 11, 721.
(101) Barrero, A. F.; Herrador, M. M.; Quílez del Moral, J. F.; Arteaga, P.; Arteaga, J. F.; Diéguez, H. R.; Sánchez, E. M. *J. Org. Chem.* **2007**, *72* (8), 2988.
(102) Chavan, S. P.; Chavan, S. P.; Sonawane, H. R.; Kalkote, U. R.; Sudrik, S. G.; Gonnade, R. G.; Bhadbhade, M. M. *Eur. J. Org. Chem.* **2007**, *2007* (20), 3277.
(103) Altman, R. A.; Buchwald, S. L. *Nat Protoc.* **2007**, *2* (12), 3115.
(104) Baran, P. S.; Burns, N. Z. *J. Am. Chem. Soc.* **2006**, *128* (12), 3908.

# Chapter 3

A Supramolecular Microenvironment Strategy for Organotransition Metal Catalysis

Portions of this chapter have been previously published in:

Kaphan, D. M.*; Levin, M. D.*; Bergman, R. G.; Raymond, K. N.; Toste, F. D. *Science,* **2015**, *350*, 1235-1238.

and

Levin, M. D.*; Kaphan, D. M.*; Hong, C. M.; Bergman, R. G.; Raymond, K. N.; Toste, F. D. *J. Am. Chem. Soc.* **2016**, *138*, 9682-9693.

*denotes equal contribution

## 3.1 Preface

Chapter 2 dealt with the development and mechanistic analysis of a gold-catalyzed cross-coupling reaction which was determined to proceed *via* an Au(I)/Au(III) redox cycle. Subsequent attempts to extend this chemistry beyond allylation revealed that other classes of C($sp^3$) reductive elimination were too slow to outcompete efficient biaryl reductive elimination. As such, we turned our attention to a conceptually distinct strategy for overcoming this problem from the routine catalyst structure and reaction condition optimization utilized in Chapter 2.

Namely, the implementation of a supramolecular catalyst was found to accelerate reductive elimination from Au(III) and Pt(IV), with enzyme-like rate accelerations of up to 1.9 x $10^7$ fold, which represents the largest rate acceleration by a synthetic microenvironment catalyst at the time of this report. Cluster-catalyzed reductive elimination was further incorporated into a dual-catalytic cross coupling transformation where both the cluster and an appropriate platinum precatalyst were necessary for efficient turnover to occur. Detailed studies concerning the mechanism of acceleration and of the dual catalysis, comparative studies, and a discussion on the nature of the encapsulated intermediate are presented below.

## 3.2 Introduction

Organotransition metal catalysis has flourished in recent years as the development of new catalyst systems has enabled methodologies of remarkable activity, selectivity and efficiency. In large part, the development of these methodologies can be attributed to the discovery and implementation of novel supporting ligand architectures, which modulate the metal center's local stereoelectronic microenvironment in order to influence the rates of individual elementary steps, control catalyst speciation, and disfavor catalyst deactivation pathways.[1–6] However, in this traditional approach, the ligand architecture necessarily defines an identical microenvironment at the metal center throughout the course of the catalytic cycle, and modifications necessary in order to facilitate one elementary step may result in deleterious effects on the remaining elementary steps in the catalytic cycle.

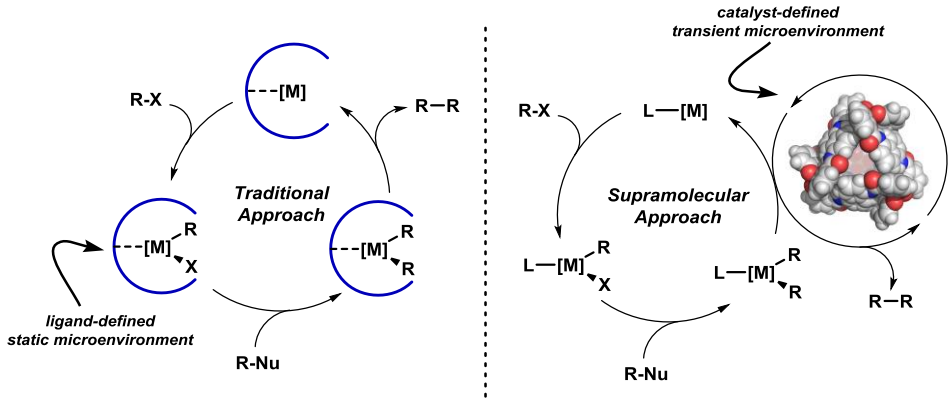


**Figure 3.1.** A supramolecular approach for transition metal catalyzed cross-coupling, comparing a traditional, exclusively ligand-defined microenvironment (left) and the proposed dual catalytic approach (right)

This necessity for stereoelectronic compromise might be circumvented by the application of a supramolecular microenvironment catalyst (such as tetrahedron **1**, below), which could engage one elementary step by transient encapsulation and stabilization of the appropriate catalytic intermediate and its subsequent transition state, while leaving the remainder of the catalytic cycle unperturbed (Figure 3.1).[7–11] In such an approach, the microenvironment of the transition metal can be defined for a problematic step by selective and specific molecular recognition, without complicating deleterious effects on the remainder of the cycle.[12–14] One might imagine that if this strategy is successful for the acceleration of one kinetically prohibitive elementary step, multiple orthogonal supramolecular microenvironment catalysts could be applied in concert in order to differentially define an optimized microenvironment for each elementary step of the reaction.[15–18]

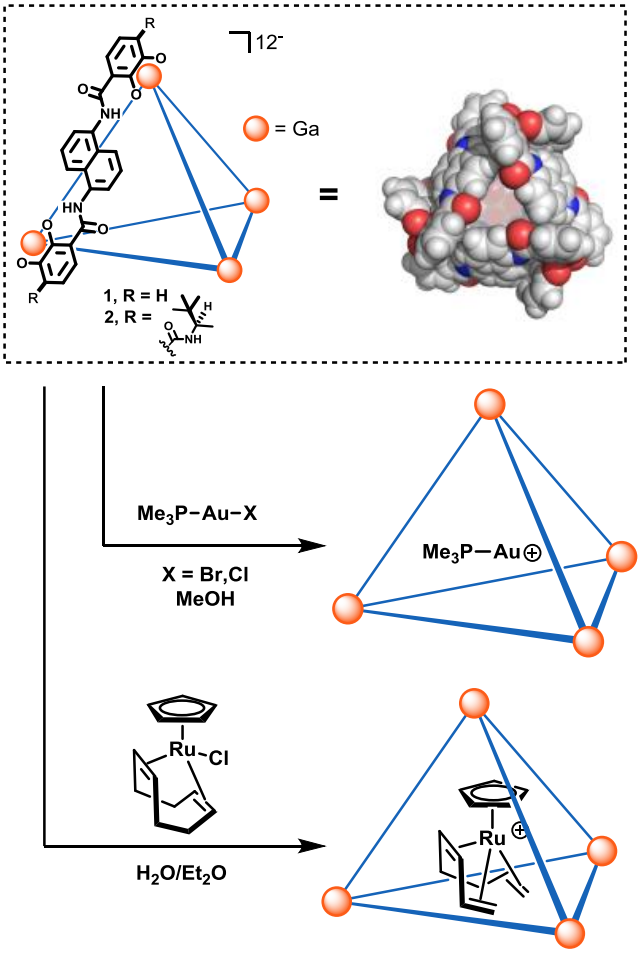


**Figure 3.2.** Molecular structure of $[Ga_4L_6]^{12-}$ assemblies **1** and **2**, and selected precedent for encapsulation of cationic metal complexes by cluster **1**. Blue lines = ligand, one ligand of the assembly shown for clarity.

Along these lines we determined that the implementation of cluster **1** as a "microenvironment catalyst" would achieve such a goal. Host **1** has been studied in depth and a number of general features have been ascertained which are important to an understanding of the chemistry presented here:

1. The host complex is dodecaanionic (typically balanced by potassium cations) but features a hydrophobic internal cavity, such that it is soluble in water, and encapsulates guest molecules by a mechanism involving aperture dilation (rather than ligand dissociation), at a rate typically rapid on the NMR time-scale at room temperature.[19–22]
2. Encapsulation is primarily driven by the hydrophobic effect (i.e. displacement of ordered solvent from within the cavity of the assembly), though electrostatic effects play a role such that cationic but otherwise "greasy" guests are more strongly encapsulated than neutral congeners.[23,24] This leads to solvent exclusion from the active-site for appropriately sized guests.[25,26]
3. Encapsulation is identifiable by $^{1}$H-NMR due to a convenient, dramatic upfield shift (1-3 ppm, often to $\delta < 0$ ppm) of encapsulated species' resonances by virtue of their close contact with the flanking naphthalene walls (i.e. ring current).[27]
4. The cavity of the host is capable of breathing to accommodate guests, with internal volumes ranging from 250-450 Å$^3$, though substantially large guests are excluded, leading to size-dependent selectivity.[28–31]
5. This limited size also leads to effects from "constrictive binding" such that the entropic cost to more spherical transition states is effectively paid upon encapsulation.[32,33]
6. Related host **2** bears electron withdrawing amide substituents which alter its binding properties and stability profile.[34,35]
7. The assembly induces a pKa shift of up to 4.5 units such that guests which are neutral in bulk solution can undergo protonation within the assembly.[31,36]

Host **1** has previously been shown to encapsulate various transition metal complexes, typically with concomitant loss of a halide or other X-type ligand, as demonstrated by two representative examples shown in Figure 3.2. For example, trimethylphosphine gold(I) bromides and chlorides are strongly encapsulated as their corresponding cation in water.[37,38] By promoting halide dissociation upon encapsulation, the metal center is rendered electron-poor and has its coordination number decreased by one. Cluster **1** has also been shown to effect stoichiometric organometallic reactivity upon encapsulation, as exemplified by the retro-cycloisomerization of cyclooctadiene ruthenium complexes upon encapsulation. (However, no catalytic turnover could be achieved in this system).[39–42]

One catalytically relevant, yet particularly sluggish, transformation is the carbon-carbon bond forming reductive elimination of C($sp^3$) fragments from transition metals. As a result, alkyl-alkyl cross-coupling processes are often plagued by slow turnover or undesired side-reactions.[43] This phenomenon was discussed in Chapter 2 as the origin of biaryl side-products in attempts at gold-catalyzed cross-coupling and is strikingly demonstrated by the difference in the rate of reductive elimination of methyl and aryl substituents from gold(III) complexes (Figure 3.3, see Chapter 1 for more details).[44,45] The rate of biaryl elimination from gold(III) at cryogenic temperatures (-55 ºC) was at least two orders of magnitude faster than ethane elimination at elevated temperatures (45 ºC), a range of nearly 100 ºC.

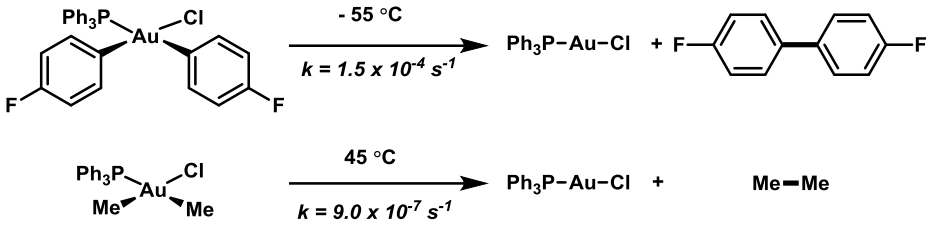


**Figure 3.3** Rates of reductive elimination of C($sp^2$) and C($sp^3$) fragments from Au(III).

The properties of cluster **1** make it particularly amenable to application as a microenvironment catalyst for reductive elimination. A number of factors affect the rate of reductive elimination from a metal center (see Chapter 1).[46] Briefly, electron poor metal centers undergo reductive elimination more rapidly than electron rich metal centers, due to the fact that reductive elimination intrinsically increases electron density at the metal center. Additionally, odd-coordinate metals undergo reductive elimination faster than even-coordinate complexes due to orbital symmetry considerations. Finally, more sterically congested metal centers undergo faster reductive elimination as a result of steric relief in the transition state, and destabilization of the ground state. Each of these considerations might contribute to an increased rate of reductive elimination upon inclusion within supramolecular cluster **1**, given that encapsulation generates a constricted, cationic species of decreased coordination number.

## 3.3 Results and Discussion

### 3.3.1 Cluster Catalysis of Reductive Elimination from Gold(III)

In order to evaluate this hypothesis, cluster **1** was explored as a catalyst for the elimination of ethane from dialkyl Au(III) iodide complex **3-I** with dramatic results. The observed half-life for reductive elimination under a 10 mol% loading of **1** decreased from 20 weeks to just 53 minutes, corresponding to a 4,000-fold acceleration in the observed initial rate (Figure 3.4). Blocking the cluster's interior cavity with the strongly encapsulated $Et_4P$ cation eliminated the accelerating effect of **1**, suggesting that access to the interior cavity of **1** is essential for efficient catalysis.

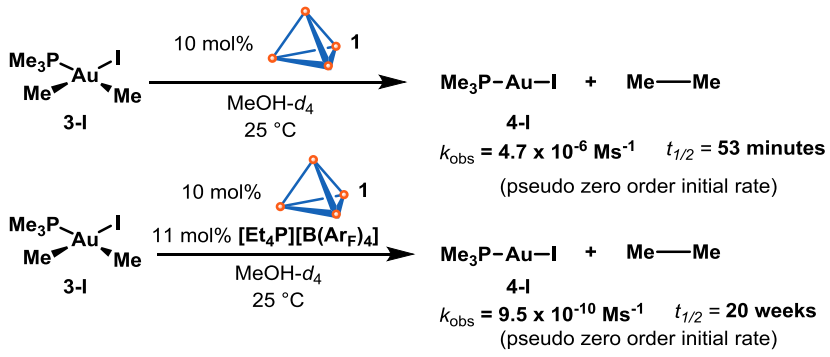


**Figure 3.4** Reductive elimination from **3-I** catalyzed by cluster **1**.

Additionally, substitution of the compact trimethylphosphine ligand by its more sterically demanding triphenyl congener in complex **5** resulted in no observable acceleration

for reductive elimination in the presence of **1**, which is indicative of size-exclusion from the internal cavity of the catalyst (Figure 3.5).

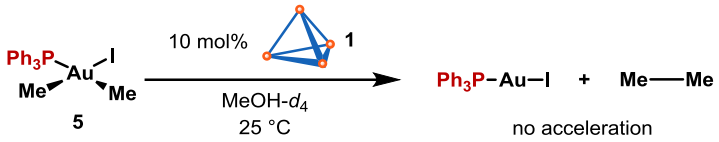


**Figure 3.5** Size selection exhibited by **1**.

Upon inspection of the kinetic profile for the catalyzed reductive elimination from **3-I**, it became clear that a catalyst deactivation pathway was operative at extended reaction times (Figure 3.6). While product inhibition is commonly observed in supramolecular catalysis, under catalytically relevant conditions, it was shown that product **4-I** did not engage cluster **1**.

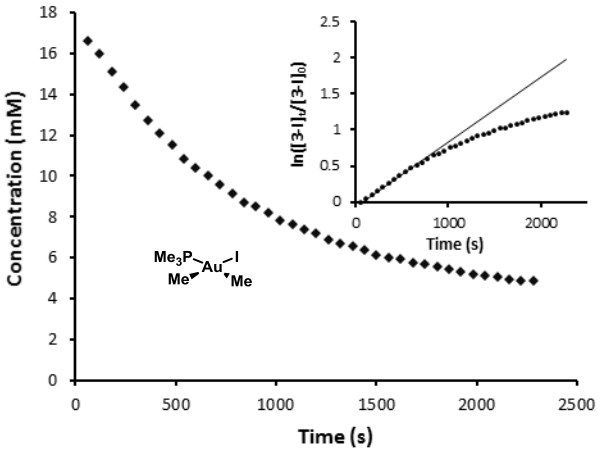


**Figure 3.6** Kinetic profile of reductive elimination from **3-I** catalyzed by **1**, with inset log-plot showing deviation from first order behavior.

Rather, examination of the reaction mixture by $^{1}$H-NMR spectroscopy revealed a strongly encapsulated species, which was identified as the cationic bis(phosphine) complex **6** (Figure 3.7).

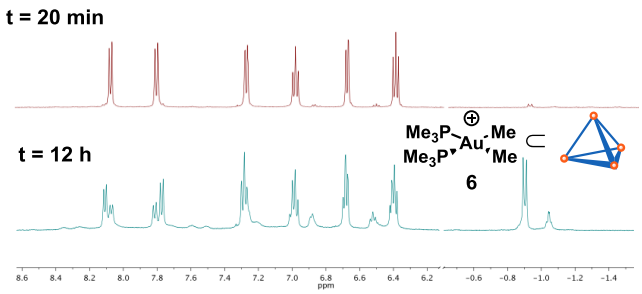


**Figure 3.7** $^{1}$H-NMR spectrum at early and late reaction times, showing encapsulated **6** ⊂ **1** in the upfield region.

The identity of inclusion complex **6** ⊂ **1** was verified by independent synthesis and could be characterized single-crystal X-ray diffractometry (Figure 3.8). Suitable crystals of complex **6** ⊂ **1** were obtained by vapor diffusion of acetone into a solution of the complex in 1:1 water and methanol over two weeks. Due to limited crystal size and a high degree of solvent disorder, synchrotron radiation was required to collect a sufficient data set at 0.88 Å resolution with 1.2276 Å radiation. Complex **6** ⊂ **1** crystallized in the monoclinic space group $P2_1/c$ with 4 formula units per unit cell, and the data are consistent with a molecule of **6** encapsulated within the cavity of **1**.[47,48] Further crystallographic information can be found in the supporting information below.

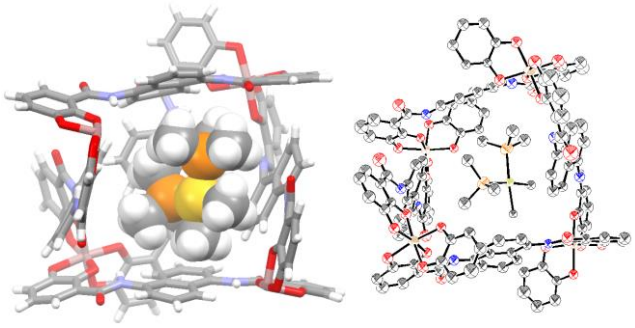

**Figure 3.8.** Crystal structure of **6** ⊂ **1**, space-filling model (left), and thermal ellipsoids (50% probability, right). Potassium ions, solvent, and one (left) or two (right) ligands of **1** have been removed for clarity.

### 3.3.2 Mechanistic Investigation

In order to better understand the catalyzed reductive elimination process, kinetic experiments were conducted to determine the order in each reactant using the method of initial rates. For the reductive elimination of ethane from complex **3-I**, the reaction displayed first order dependence on catalyst **1**, as measured by competitive inhibition with $Et_4P^+$ (a linear relationship was observed between the rate of reductive elimination and the concentration of unblocked cluster) (Figure 3.9, top). Conversely, the rate of reductive elimination was found to be dramatically attenuated in the presence of exogenous iodide, in the form of potassium iodide added to the reaction mixture (Figure 3.9, middle). The rate dependence on gold concentration showed saturation behavior, which could be linearized by plotting the double reciprocal of concentration and rate (Figure 3.9, bottom). Gold complex **3-Br** was employed rather than **3-I** because it was expected to show a higher affinity for the interior of **1** (*vide infra*), however, the calculated value for $k_{cat}$ is necessarily identical for **3-I** and **3-Br** due to the mechanistic convergence in the encapsulated intermediate.

These results are consistent with an overall Michaelis-Menten type mechanism involving pre-equilibrium halide dissociation followed by a transient and reversible encapsulation of the nascent cationic species, and, finally, an irreversible reductive elimination event within the cluster cavity (Figure 3.10). Accordingly, the aforementioned double reciprocal plot of substrate concentration and rate is directly analogous to a Lineweaver-Burk plot, and from these data the Michaelis-Menten parameter $k_{cat}$ could be assessed. The measured $k_{cat}$ for complex **3-I** was found to be $3.3 \times 10^{-2}$ $s^{-1}$, corresponding to an overall acceleration ($k_{cat}/k_{uncat}$) of $5.0 \times 10^5$. It should be noted that this mechanistic scenario is kinetically

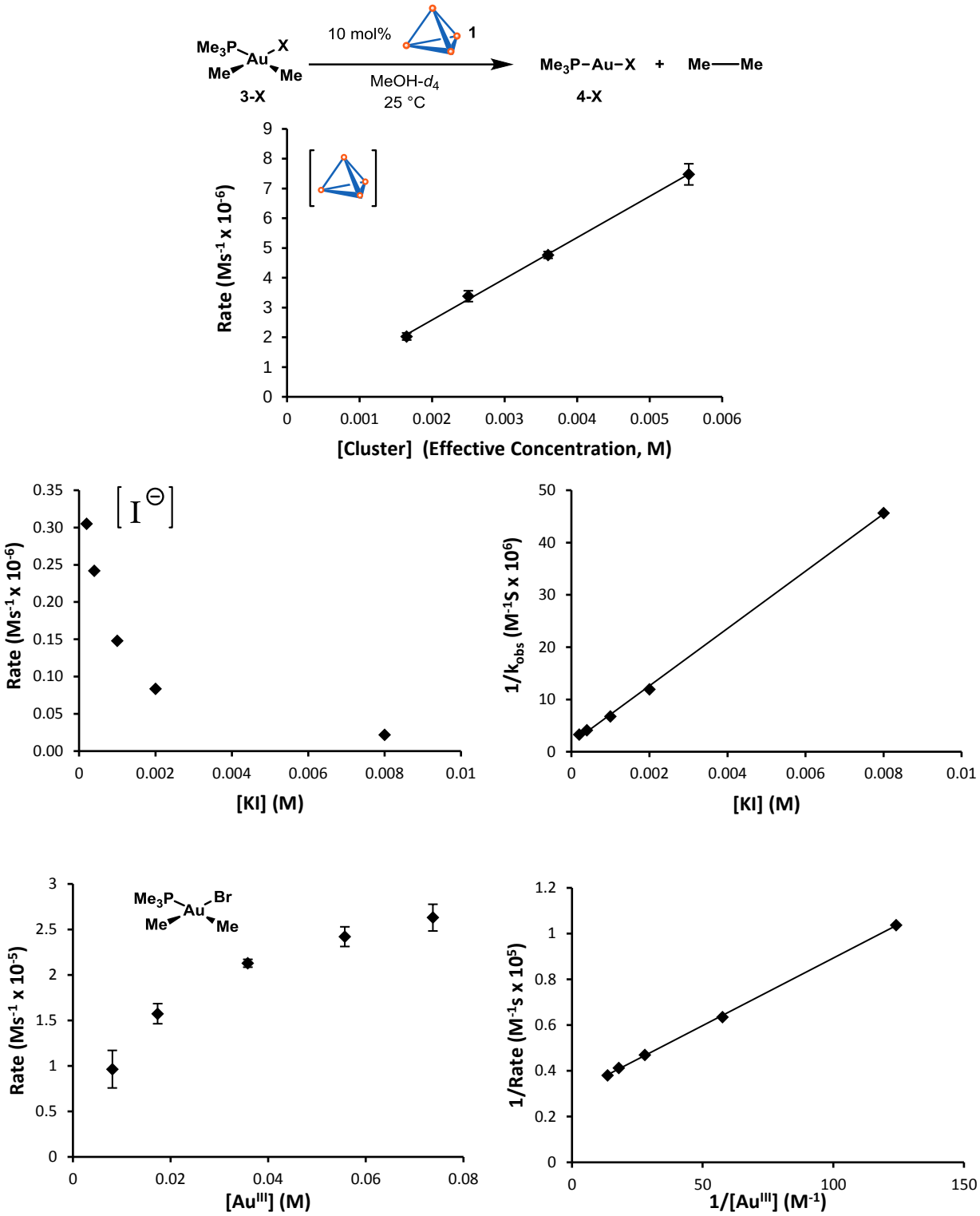


**Figure 3.9.** Rate dependencies for reductive elimination from **3-I**, catalyzed by cluster **1**. (Top) Cluster open active site dependence, X = I (Middle) Iodide dependence, measured by adding exogenous NaI, X = I (Bottom) Rate dependence on substrate concentration (**3-Br** used in order to accentuate saturation behavior, *vide infra*).

indistinguishable from a mechanism in which the neutral gold(III) complex is encapsulated, followed by halide dissociation inside of the cluster, however, we disfavor such a mechanism based on considerations of microscopic reversibility— in the forward direction the same pathway would require metal cation egress to occur by a mechanism wherein iodide must approach and enter the undecaanionic inclusion complex, which seems kinetically prohibitive.

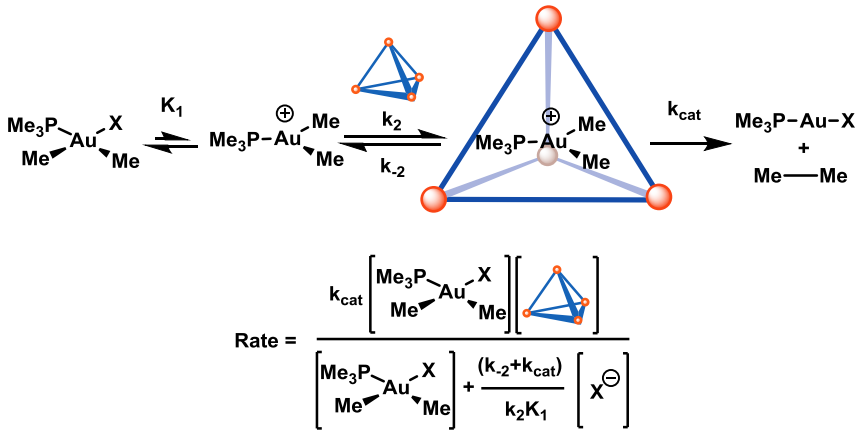


**Figure 3.10.** (Top) Michaelis-Menten-like mechanism consistent with kinetic observations. (Bottom) Rate law derived from steady state analysis of Michaelis Menten mechanism with pre-equilibrium halide dissociation.

### 3.3.3 Influence of Spectator Ligands

Having established a likely mechanism for the catalysis of reductive elimination from **3** by cluster **1**, the effect of substitution on reactivity was investigated. It was hypothesized that it might be possible to disfavor the bisphosphine gold(III) cation catalyst deactivation pathway by increasing the bulk of the supporting phosphine ligand, such that the bisphosphine cation would be sufficiently large to disfavor inclusion within the cavity of **1**. In accordance with this hypothesis, triethylphosphine ligated complex **7-I** exhibited rapid and complete reductive elimination in the presence of **1** (Figure 3.11). No catalyst deactivation was observed, with the decay of **7-I** following first order kinetics over multiple half-lives, and a turnover number (TON) in excess of 300. The catalyzed reaction of **7-I** exhibits a half-life of just 47 seconds compared to 45 days in the uncatalyzed reaction, corresponding to an observed rate acceleration of 80,000-fold.

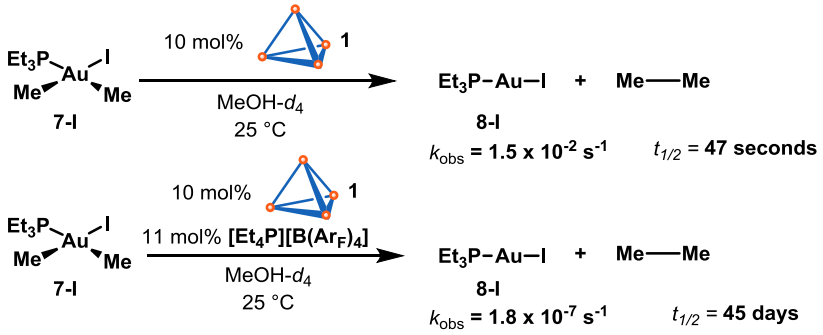


**Figure 3.11.** Reductive elimination from **7-I** catalyzed by cluster **1**.

The rate dependence on substrate, cluster, and iodide concentration for reductive elimination from **7-I**, catalyzed by **1**, was consistent with those of **3-I**, indicating that the Michaelis-Menten-like mechanism remains operative (for halide and cluster dependence plots, see supporting information below). However, the rapidity of this reaction introduced substantial error into the estimation of $k_{cat}$ by the method of initial rates (Figure 3.12, left, orange squares). Instead, since no catalyst deactivation was observed, the technique of Reaction Progress Kinetic Analysis (RPKA) could be applied in order to generate a larger data set (Figure 3.4, left, blue diamonds).[49]

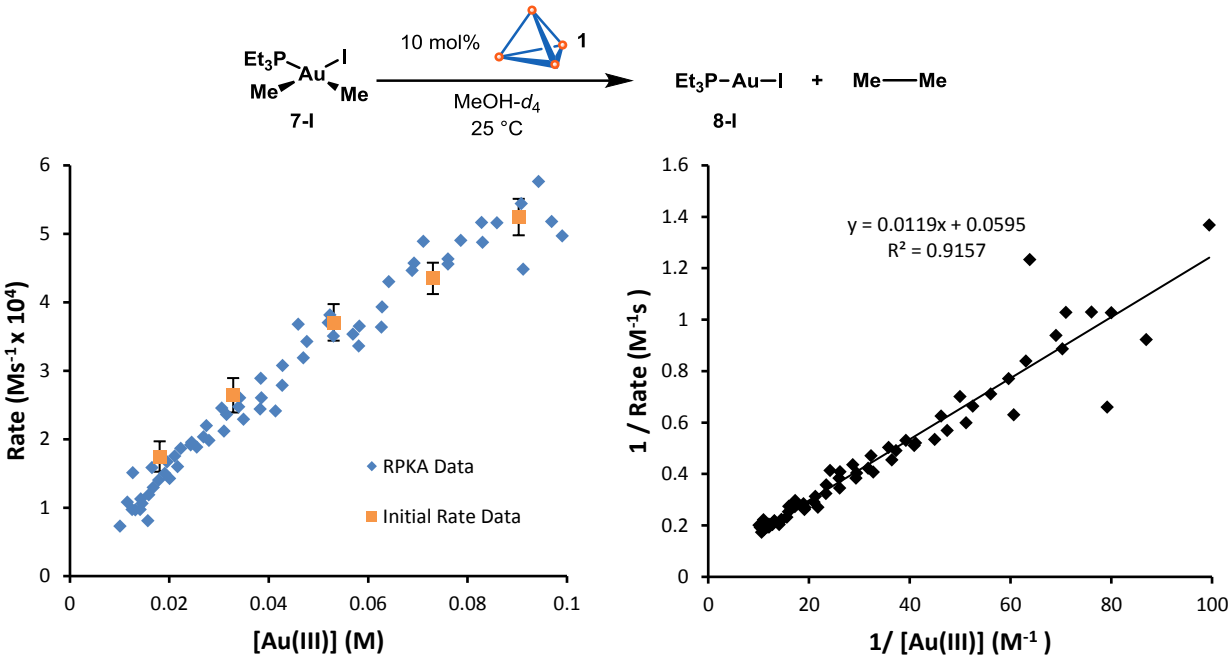


**Figure 3.12.** (Left) Rate dependence on concentration of **7-I** by initial rates (orange square) and RPKA (blue dots). (Right) Lineweaver-Burk plot from RPKA data used to calculate $k_{cat}$.

The corresponding Lineweaver-Burk plot (Figure 3.12, right) affords an estimate for $k_{cat}$ of 3.4 $s^{-1}$, corresponding to a rate acceleration ($k_{cat}/k_{uncat}$) of 1.9 x $10^7$. The data obtained by RPKA are consistent with the initial rate data, while providing a more robust measurement due to the expanded data set. This rate acceleration is on par with that of many enzymatic processes; for comparison, chymotrypsin has been shown to accelerate amide bond hydrolysis with rate accelerations of $10^7$-fold.[50]

A more detailed comparison of the rates for reductive elimination from trimethylphosphine complex **3-I** and triethylphosphine complex **7-I** catalyzed by cluster **1** provides some additional insights into the influence of the phosphine ligand; namely, **7-I** is bound more tightly than **3-I** by **1** and, after the binding event, the transition state for reductive elimination from **7-I** is more stabilized by **1** than the transition state of reductive elimination from **3-I** (for a graphical depiction of the following analysis, see Figure 3.13).

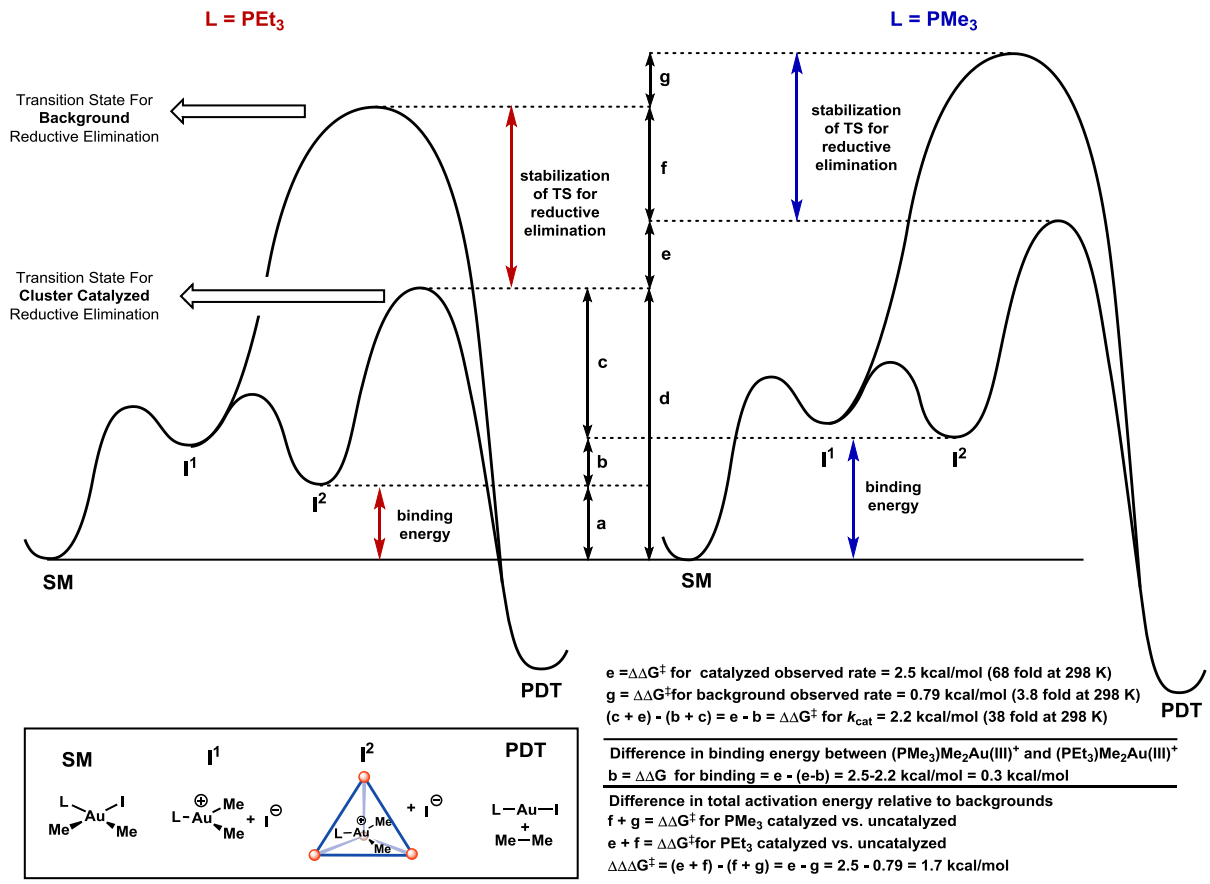


**Figure 3.13.** Reaction coordinate diagrams for reductive elimination from **7-I** and **3-I**.

In detail, **7-I** undergoes catalyzed reductive elimination with a half-life 68 times shorter than the catalyzed half-life for **3-I** (47 seconds vs. 53 minutes), while the half-lives for uncatalyzed reductive elimination differ by only a factor of four. Additionally, as determined by Michaelis-Menten analysis, the measured rate of reductive elimination within the supramolecular assembly ($k_{cat}$) is 38 times faster for **7** than for **3**. Comparison of the ratio of catalyzed observed rates (68-fold, corresponding to $\Delta\Delta G^{\ddagger}$ = 2.5 kcal/mol) to the ratio of $k_{cat}$ (38-fold, corresponding to $\Delta\Delta G^{\ddagger}$ = 2.2 kcal/mol) suggests that the triethylphosphine ligated complex shows higher binding affinity for the interior of **1** ($\Delta\Delta G$ = 0.3 kcal/mol). Furthermore, comparison of the ratio of background rates of reductive elimination from **3-I** and **7-I** (3.8-fold, corresponding to $\Delta\Delta G^{\ddagger}$ = 0.79 kcal/mol) to the ratio of the catalyzed rate of reductive elimination suggests that **1** more effectively stabilizes the transition state for reductive elimination from the triethylphosphine ligated complex ($\Delta\Delta\Delta G^{\ddagger}$ = 1.7 kcal/mmol).Several possible explanations for these phenomena are consistent with the experimental results: (i) increased steric compression of the larger complex within the supramolecular cavity (thus destabilizing the bound ground state relative to the transition state for reductive elimination),[46] (ii) increased hydrophobicity of $Et_3P$,[23] (iii) better shape complementarity resulting in better solvent exclusion and increased contact surface area,[51] or (iv) higher concentrations of the free cationic Au(III) complex as a result of the stronger electron donation from the triethylphosphine ligand.[1]

The identity of the halide substituent on **3** also has a dramatic effect on the rate of the reaction, as well as the catalyst deactivation pathways. Examination of the iodide, bromide and chloride congeners **3-I**, **3-Br**, and **3-Cl**, revealed a significant influence on the observed rate of reductive elimination, with the relative rates increasing in the order Cl ~ Br > I (Figure 3.15). Inhibition was also observed from encapsulation of the resulting Au(I) complexes **4-Cl** and **4-Br** but not for **4-I** (Figure 3.16).

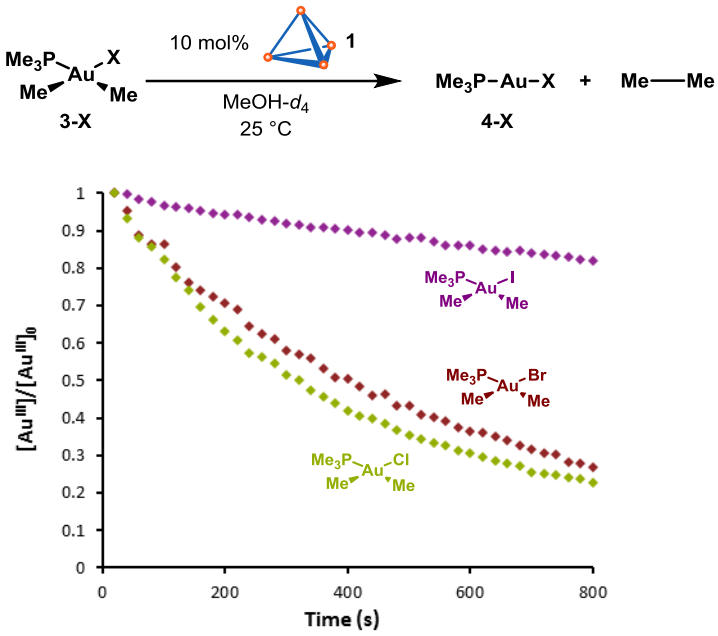


**Figure 3.15.** Kinetic traces for reductive elimination from **3-I**, **3-Br**, and **3-Cl** catalyzed by 10 mol% **1**

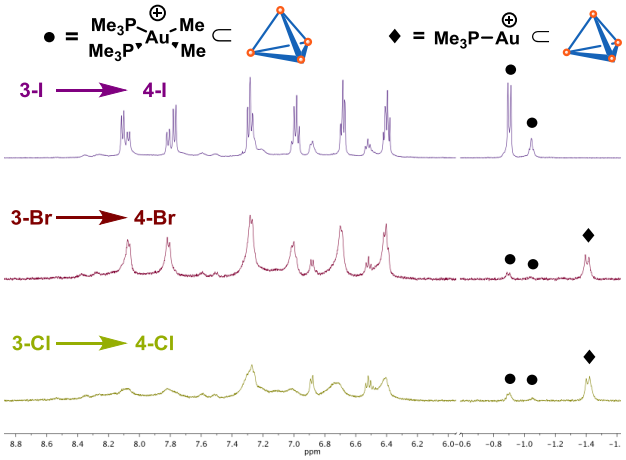


**Figure 3.16** $^1$H-NMR spectrum showing product inhibition at long reaction times by **4-Br** and **4-Cl**

In order to determine the generality of this behavior, the corresponding triethylphosphine ligated analogues **7-Cl** and **7-Br** were prepared and subjected to cluster catalyzed reductive elimination. In this experiment, significant product inhibition by **8-Cl** and **8-Br** was observed, with substantial deviation from first-order decay (Figure 3.17). In contrast,

**7-I** and its product **8-I** followed an uninhibited first order reaction profile past five half-lives. The rapid rate of the reaction and sheer extent of product inhibition in the case of **7-Cl** and **7-Br** precluded a quantitative comparison of the initial rate differences between this halide series, however, the qualitative trend for overall reaction rate of Cl ~ Br > I is consistent between the **3-X** and **7-X** series.

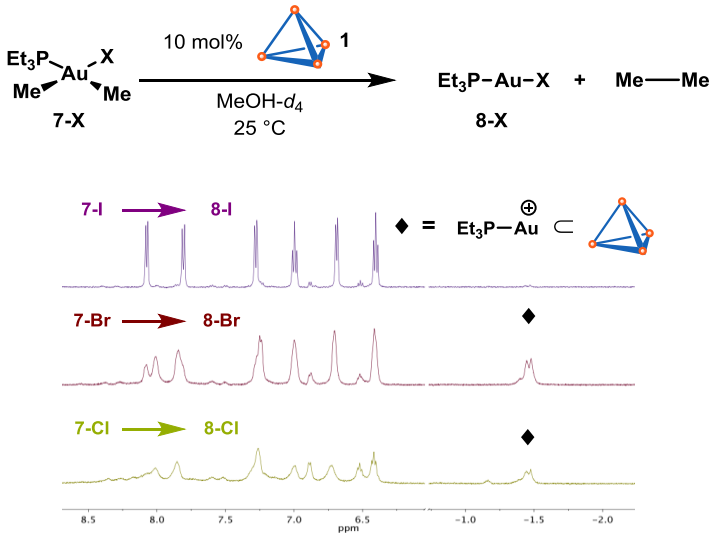


**Figure 3.17.** [1]H-NMR spectrum showing product inhibition by **8-Br** and **8-Cl**, with no encapsulation observed for **8-I**.

Based on the proposed mechanism for cluster catalyzed reductive elimination, one would expect pre-equilibrium halide dissociation to influence the overall rate. However, *a priori*, the direction of this influence with respect to halide identity is unclear. Examination of a generalized equilibrium for encapsulation reveals that the empty cluster and encapsulated cation are identical for all members of the series, and as such only the Au–X heterolytic bond dissociation energies and differences in solvation of the dissociated halide anion can influence the position of the equilibrium (Figure 3.18).

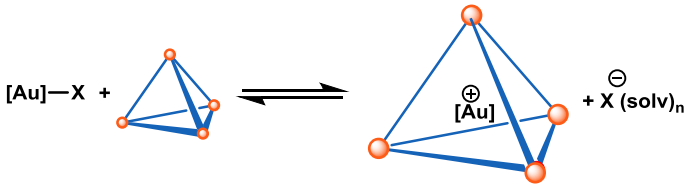


**Figure 3.18** Generalized equilibrium for encapsulation for gold halides.

For Au(III), the Au–X heterolytic bond strengths trend as Au–I < Au–Br < Au–Cl while solvation enthalpy of the dissociated halides trends as Cl > Br > I.[52,53] (To calculate the heterolytic bond strengths, the differences in homolytic bond strengths[54] were combined with the differences in electron affinity for the halides,[55–57] treating the dissociated neutral atoms as isoenergetic. The ionization potential of gold can be omitted from the calculation because the energies are relative. The results are that in a heterolytic sense, the Au–Cl bond is approximately 9 kcal/mol stronger than the Au–Br bond which is approximately 11 kcal/mol more stable than

the Au–I bond.) Clearly the observed rates for reductive elimination for **3** (Cl ~ Br > I) correlate more strongly with the halide solvation enthalpy than the relevant Au(III) halide bond strengths (one would expect the gold chloride complexes to undergo slower reductive elimination in that case).

For Au(I), the relative influence of solvation and bond strength is less clear. The heterolytic bond strengths trend as Au–Br < Au–Cl < Au–I (determined as for Au(III)[58]). Here, the observation of product inhibition in the case of the Au(I) bromide and chloride complexes is consistent with both solvation-dependent and bond strength-dependent equilibrium for encapsulation of **4-X** and **8-X**, but the observation of solvation-dominated behavior for Au(III) suggests that the influence of solvation is likely also the major factor in this trend.

### 3.3.4 Exploration of Generality

The phenomenon responsible for the catalytic acceleration of reductive elimination from gold(III) dialkyl halide complexes by cluster **1** should be generalizable to other high valent metal centers, so long they bare an appropriate heterolytically labile X-type ligand to facilitate encapsulation. To test this hypothesis, platinum(IV) complex **9** was prepared, and subjected to catalysis by cluster **1**.[59–61] The observed half-life for reductive elimination of ethane was just 6 minutes in the presence **1**, as compared to about 9 days when the internal cavity of cluster **1** was blocked with tetraethylphosphium, corresponding to a 2,300-fold acceleration of the observed rate (Figure 3.19).

The rate dependence on the catalyzed reductive elimination from **9** with respect to substrate, cluster and exogenous iodide concentration were also consistent with a Michaelis-Menten-like mechanism (see supporting information below). Analysis of the Lineweaver-Burk plot for **5** afforded a $k_{cat}$ of 2.3 x $10^{-2}$ $s^{-1}$, corresponding to a rate acceleration of 2.6 x $10^4$ fold (Figure 3.20).

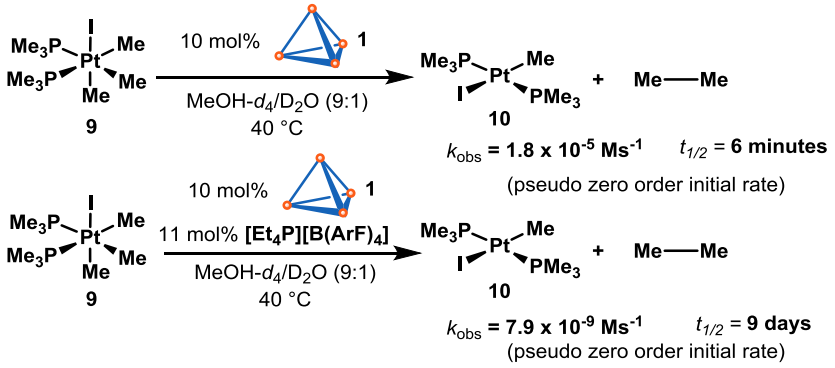


**Figure 3.19.** Reductive elimination from **9**, catalyzed by cluster **1**.

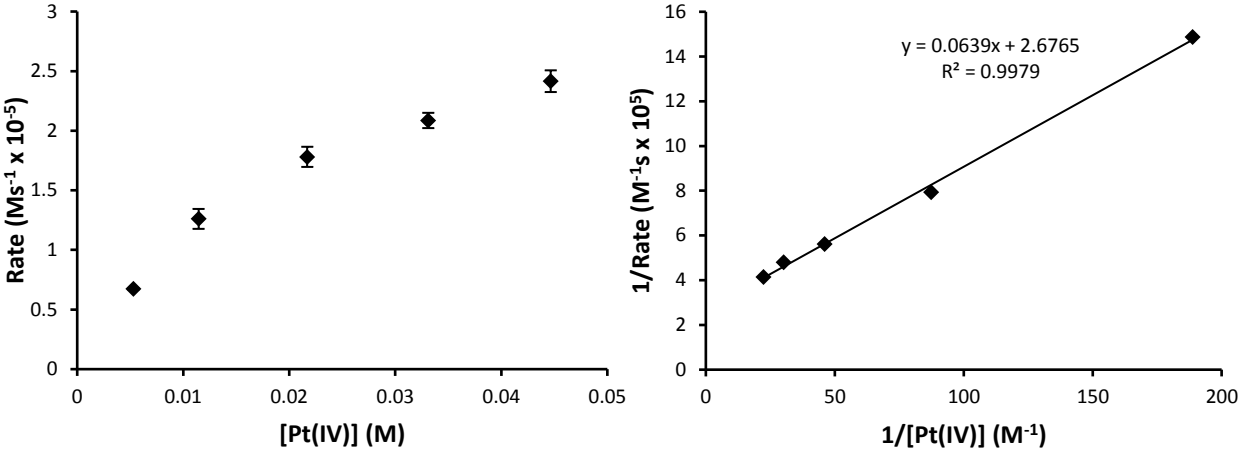


**Figure 3.20.** (left) Rate dependence on substrate concentration for reductive elimination from **9**, catalyzed by cluster **1**. (right) Lineweaver-Burk plot corresponding for reductive elimination from **9**, catalyzed by cluster **1**.

It should be noted that while cluster catalyzed reductive elimination from **9** did proceed under the standard conditions developed for gold complexes **3-I** and **7-I**, the reaction proved too sluggish under these conditions for efficient kinetic analysis. It was hypothesized that, given the role of solvation in the relative rates of reductive elimination for the **3-X** and **7-X** halide series, the addition of a small amount of $D_2O$ as co-solvent for the reaction would promote halide dissociation, and thus accelerate the overall catalytic process. In order to evaluate this hypothesis, the rate of reductive elimination from platinum complex **9**, catalyzed by cluster **1**, was evaluated with solvent mixtures ranging from pure methanol to an 85:15 mixture of methanol and water (Figure 3.21). Indeed, as the water content increased, a corresponding increase was observed in the rate of catalyzed reductive elimination.

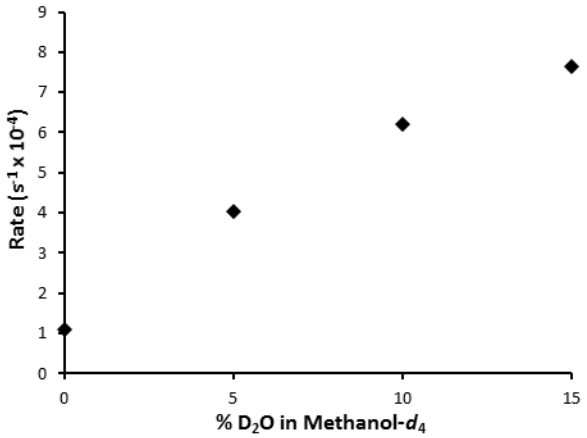


**Figure 3.21.** Influence of solvent composition on the rate of cluster catalyzed reductive elimination from **9.**

This increase correlates with the strength of solvation for the dissociated halide anions in each solvent, though the effect of the increased binding affinity driven by the greater

solventophobic effect for water cannot be disentangled. A water content of 10 percent v/v was selected as a compromise between reaction acceleration and maintaining homogeneity over the course of the reaction, and was employed in all reactions pertaining to the mechanistic analysis of cluster catalyzed reductive elimination from **9** (*vide supra*).

In order to glean further mechanistic insights as well as to determine the scope of cluster catalyzed reductive elimination, a survey of the groups undergoing coupling in the elimination was examined. Diethyl gold complex **11**, in the presence of 10 mol % of cluster **1**, underwent catalyzed reductive elimination to form butane with an observed rate constant of 7.6 x $10^{-3}$ $s^{-1}$, a relative rate of 29 when compared to catalyzed reductive elimination from dimethyl gold complex **3-I** ($k_{obs}$ = 2.6 x $10^{-4}$ $s^{-1}$) (Figure 3.22).

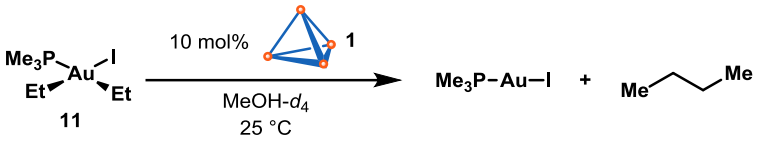


**Figure 3.22.** Butane forming reductive elimination from **11** catalyzed by cluster **1**.

The consumption of ethyldimethyl platinium complex **12** was also accelerated dramatically in the presence of cluster **1**, however, instead of observing carbon-carbon bond formation, the exclusive organic products of the reaction were methane and ethylene (Figure 3.23). These products arise from β-hydride elimination from the pentacoordinate cationic encapsulated species to release ethylene, and subsequent methyl-hydrogen reductive elimination to form methane.[59] The catalyzed process took place with a half-life around one hour, while, in the uncatalyzed reaction, only trace β-hydride elimination was observed after 16 hours. The acceleration of β-hydride elimination from **12** indicates that the intrinsic reactivity preferences of the metal are not overridden by the cluster; however, it highlights the fact that other elementary transformations are also subject to catalytic acceleration by **1**, so long as they also proceed through cationic transition states.

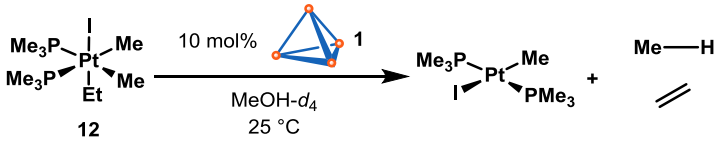


**Figure 3.23.** β-hydride elimination from platinum complex **12** catalyzed by cluster **1**.

Acyl dimethyl platinum complex **13** undergoes reductive elimination, catalyzed by cluster **1**, to form acetone. The observed 15-fold acceleration over background in this case is modest relative to the aforementioned C($sp^3$)–C($sp^3$) reductive eliminations, with an initial rate of 2.2 x $10^{-3}$ $s^{-1}$ in the presence of 10 mol % cluster, and 1.5 x $10^{-4}$ $s^{-1}$ in the background reaction (Figure 3.24).[21] This can be explained by the relatively low barrier to reductive elimination in the uncatalyzed reaction for the $sp^2$-hybridized and electron-deficient acyl group. In this case, the kinetic product is the *cis*-chloroplatinum complex which undergoes isomerization to the *trans*- isomer after reductive elimination.

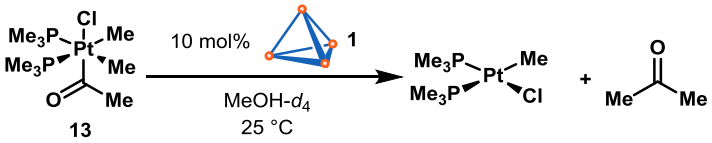


**Figure 3.24.** Acetone forming reductive elimination from platinum complex **13** catalyzed by cluster **1**.

### 3.3.5 The Nature of the Michaelis Complex

While kinetic investigations of the catalytic reductive elimination process reveal a Michaelis-Menten-like mechanism reminiscent of enzymatic catalysis, these data do not provide insight into the nature of the organometallic species undergoing reductive elimination; in the case of reductive elimination from platinum complex **9**, C–C bond formation might occur from a pentacoordinate intermediate, or alternatively from the hexacoordinate solvento complex. Reductive elimination has previously been observed from hexacoordinate $d^6$ and square planar $d^8$ metals both with and without prior ancillary ligand dissociation in different cases, suggesting that either pathway might be competent.[44,45,62–73] While direct observation of this transient intermediate is precluded, some insight into its nature may be gained from the observation of an inactivated inclusion complex upon the introduction of appropriate non-solvent neutral donors.

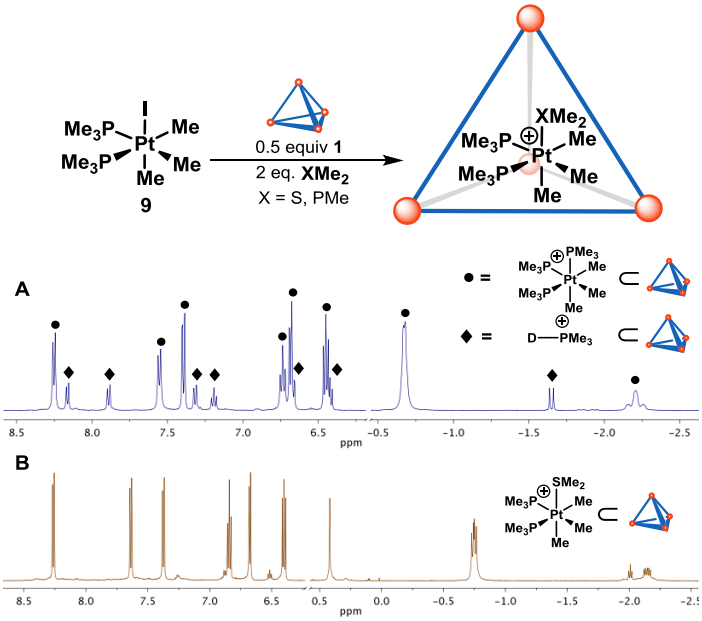


**Figure 3.25.** Donor-arrested complexes derived from trimethylphosphine and dimethylsulfide. A: MeOD/$D_2O$ 8:2, B: pure MeOD

Indeed, donor-arrested reductive elimination was first observed as a cluster deactivation pathway in the catalyzed reductive elimination from **3-I** (*vide supra*). In contrast to the transient substrate-host complexes that rapidly undergo reductive elimination, the deactivated inclusion complex **6** ⊂ **1** was persistent enough to allow characterization by single-crystal X-ray diffractometry. Furthermore, when **3-I** is subjected to **6** ⊂ **1** in lieu of empty cluster **1**, no

catalysis of reductive elimination was observed, supporting the idea that ligand dissociation is essential for efficient catalysis to occur.

Similarly, the addition of exogenous neutral ligands to a solution of **9** and cluster **1** inhibited the catalyzed reductive elimination, and afforded the corresponding high valent cationic inclusion complexes. A small excess of either trimethylphosphine or dimethylsulfide both effected the uptake of the cationic Pt(IV) after displacement of the iodide ligand to form a kinetically stable 1:1 host-guest complex (Figure 3.25). These inclusion complexes were persistent even upon heating over 48 hours, with no detectable reductive elimination observed. In the absence of cluster **1**, no iodide displacement could be detected by $^{1}$H-NMR in the presence of dimethylsulfide, and only slow, partial displacement was observed with trimethylphosphine alone. In contrast, added trimethylamine had no effect on **9** or the supramolecular cluster, and the catalyzed reductive elimination proceeded unabated, a phenomenon that likely reflects the low innate affinity of platinum for amine donors.

Surprisingly, carbon monoxide was capable of displacing iodide from **5** to form a hexacoordinate inclusion complex within cluster **2** (albeit with only partial occupancy of **2**, indicating a lower overall association constant). This observation was first made quite unexpectedly in the context of an attempted carbonylative coupling (*vide infra*), where no reactivity was observed, due to the encapsulation of the cationic Pt(IV) carbonyl **14** (Figure 3.26). While Pt(IV) carbonyl complexes have been previously observed, their rarity can be attributed to the paucity of electron density available for backdonation to carbonyl antibonding orbitals, underscoring the ability of **2** to perturb otherwise unfavorable equilibria.[74–77] Indeed, the IR spectrum of **14** ⊂ **2** showed a C=O stretch at ν = 2110 cm$^{-1}$, indicative of a relatively strong CO bond. Heating **14** ⊂ **2** at 40 °C effected reductive elimination of ethane with a half-life of about 4 hours to afford the corresponding cationic Pt(II) carbonyl **15** ($\nu_{CO}$ = 2078 cm$^{-1}$).

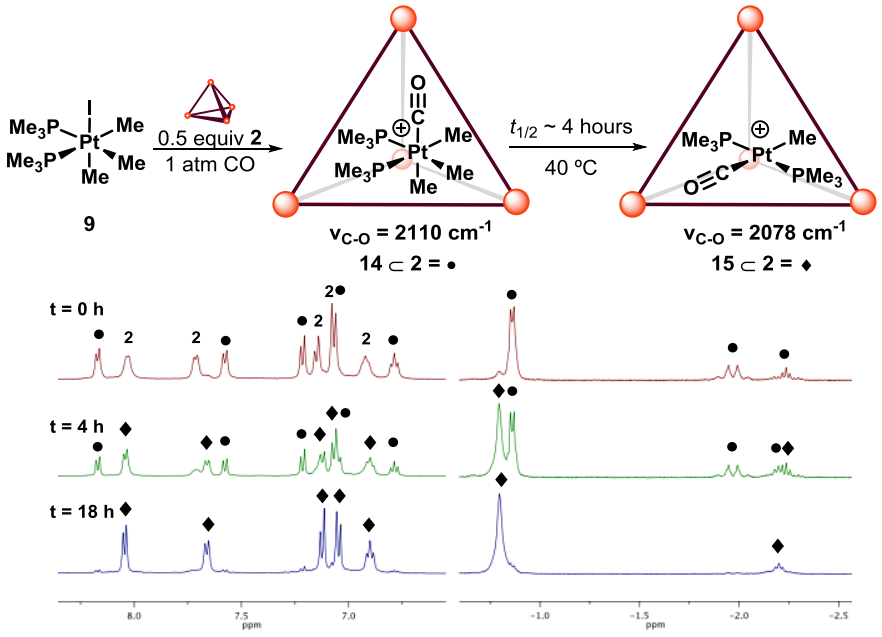


**Figure 3.26.** Carbon Monoxide trapping of the Michaelis complex and slow reductive elimination.

The phenomenon of donor-arrested reductive elimination was not limited to exogenous neutral donors. Allyl platinum **16** did not undergo catalyzed reductive elimination in the presence of cluster **1**; instead, a platinum species, consistent with the $\eta^3$-allyl platinum(IV) complex **17**, was observed as a strongly bound guest in the cluster cavity. The chiral *cis*-dimethyl $\eta^3$-allyl platinum cation is kinetically trapped as a diastereomeric mixture within the homochiral *T*-symmetric cluster. However, after 24 hours, the complex isomerizes to favor the achiral *trans*-dimethyl $\eta^3$-allyl platinum cation **18** as the thermodynamic product (Figure 3.12). It should be noted that we cannot distinguish conclusively between the depicted isomer for **18** and the alternative achiral complex bearing *trans* phosphine donors based on $^1$H-NMR, but have based our tentative assignment on the chemical shifts of methyl groups in **23**, **25**, and **26**, in which mutually *trans* methyl groups show a substantial upfield shift compared to methyl groups *trans* to phosphine or halide donors.

The equilibrium mixture of **17** ⊂ **1** and **18** ⊂ **1** was persistent, with no reductive elimination observed even after heating to 45 ºC for 48 hours. For encapsulated **17**, reductive elimination is decelerated relative to the background reaction, and can be viewed as a case of intramolecular donor-arrested reductive elimination, analogous to the above described behavior in the presence of exogenous neutral donors. For a similar allyldimethyl complex, Puddephatt and coworkers were unable to observe an $\eta^3$-allyl complex by treatment with $AgPF_6$. Instead, disproportionation products following reductive elimination were observed highlighting the divergent behavior enabled by the constrictive microenvironment of **1**.[59]

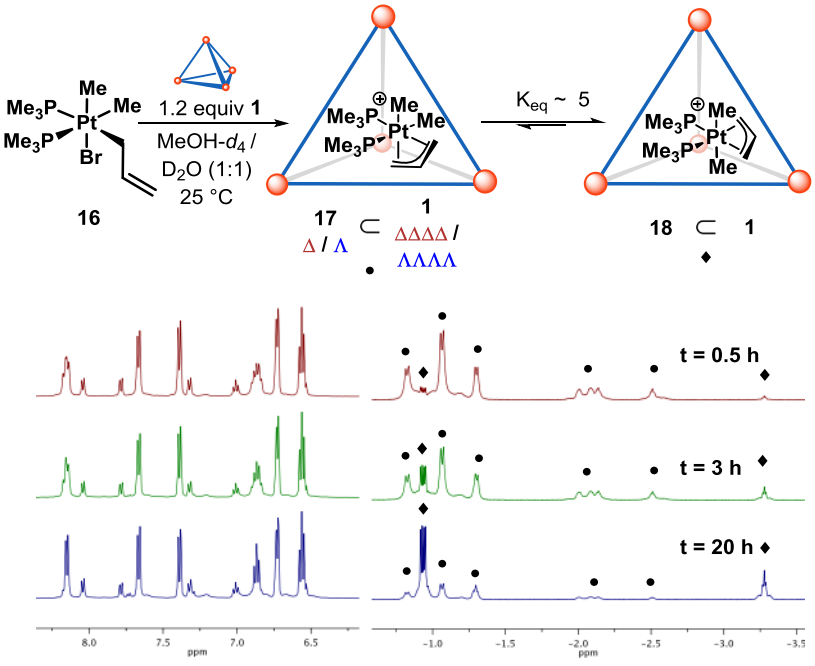


**Figure 3.27.** $\eta^3$-allyl platinum complexes formed upon encapsulation of **16**.

To probe the limits of the intramolecular donor-arrested reductive elimination, the homologated series of ω-butenyl, -pentenyl and -hexenyl platinum(IV) complexes **19**, **20** and **21** were investigated (Figure 3.28). Unfortunately, the high propensity of these complexes to undergo β-hydride elimination prevented their isolation and purification. To circumvent this, the platinum(IV) complexes were generated in situ, followed by treatment with cluster **1**. The

butenyl and pentenyl complexes were strongly encapsulated, and while both inclusion complexes were persistent on the timescale of days, the broadened $^{1}$H-NMR resonances in the encapsulation region for pentenyl complex **20** ⊂ **1** suggest that it is less strongly bound than the butenyl analogue. Conversely, only trace encapsulation of hexenyl analogue **21** is observed after 30 minutes at ambient temperature, and no species are encapsulated after 12 hours with background formation of products from β-hydride elimination observed. This trend can potentially be explained as the result of several phenomena, including (i) conformational strain of the expanded ring complexes, (ii) the entropic cost of folding the homologated chains to bring the donor olefin into contact with the Pt cation, and (iii) size exclusion of the less compact complexes. It is additionally relevant to note that platinum complex **9**, under an atmosphere of ethylene, did not form an inclusion complex with cluster **1**.

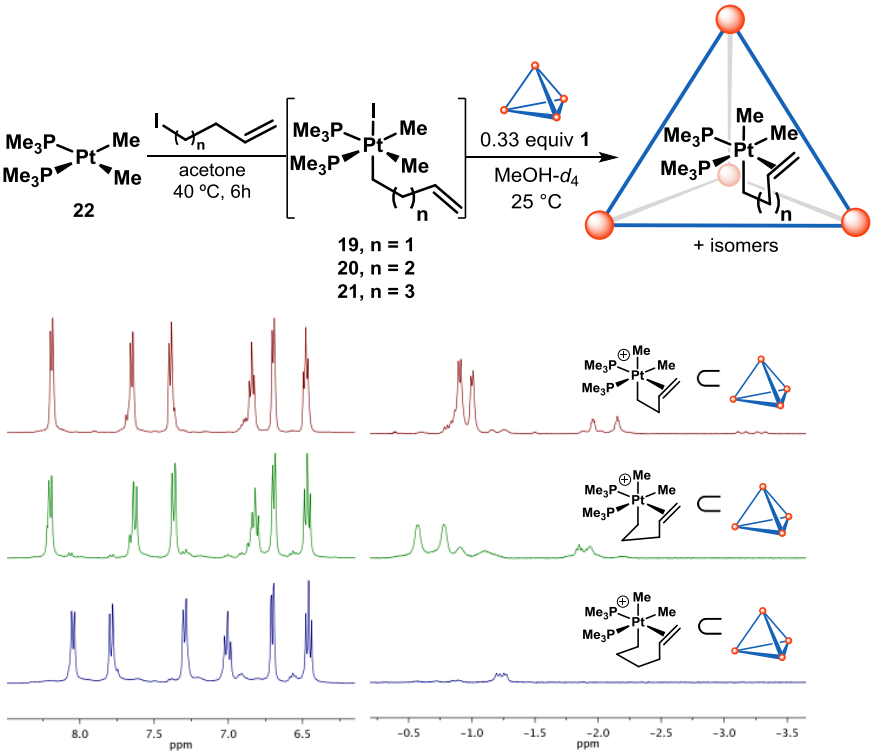


**Figure 3.28.** Homologous series of cyclic alkene-coordinated encapsulated platinum complexes.

Clearly, a variety of neutral donors are capable of trapping the high valent cationic platinum intermediate to form a persistent inclusion complex within the cavity of the supramolecular cluster. The fact that so many of these hexacoordinate cationic species, even with donors as weak as carbon monoxide, undergo substantially inhibited reductive elimination compared to the parent catalytic process, provides evidence by analogy that the putative oxygen-coordinated solvento complex is unlikely to be the relevant species undergoing carbon-carbon bond formation. A model is therefore favored in which a coordinatively unsaturated cationic metal complex — pentacoordinate for platinum(IV), tricoordinate for gold(III) — undergoes reductive elimination within the cavity of the supramolecular assembly. The stereochemistry of such an intermediate is unknown. For gold, both T- and Y-shaped three-coordinate complexes are possible, whereas for platinum, trigonal bipyramidal and square

pyramidal isomers (among other intermediate geometries) are possible. It is likely that whatever the global minimum, both species should be highly fluxional.

### 3.3.6 Dual Catalysis

The initial impetus for the investigation of cluster catalyzed reductive elimination was to demonstrate that the application of a microenvironment catalyst to one problematic organometallic elementary step could facilitate a kinetically prohibitive, but otherwise desirable cross-coupling process.[78] Based on the stoichiometric reactivity (*vide supra*), a co-catalytic cross coupling of a methyl electrophile with a complementary nucleophilic alkyl metal species was targeted as proof of principle. Achieving this goal was impeded by one immediate roadblock: supramolecular assembly **1** was found to decompose in the presence of electrophilic methyl sources, such as methyl iodide.

In order to overcome this difficulty, supramolecular cluster **2** (Figure 3.2), a previously reported analogue of cluster **1**, which bares less electron-rich and more sterically shielded catechol ligands was evaluated as an alternative catalyst for reductive elimination.[34] The rate of reductive elimination of both gold complex **3-I** and platinum complex **9** catalyzed by **2** was measured. In each case, **2** was found to give an observed rate of reductive elimination approximately 1.5 times faster than the rate measured with cluster **1**. Similar relative rates have previously been reported for transformations catalyzed by **1** and **2**.[35]

Interestingly, the reductive elimination of **3-I** catalyzed by **2** does not deviate from first order behavior, with no bis(phosphine)gold(III) inclusion complex (**6** ⊂ **2**) detected (Figure 3.29). One possible explanation for this phenomenon (as compared to the behavior observed with **1**) is that bis(phosphine)Au(III) complex **6** is formed from trimethylphosphine liberated upon oxidation of the supramolecular catalyst by Au(I) products **3-I** or **4-I**. The decreased electron density of the catecholate ligands on **2** (relative to **1**) reduces the driving force for this deleterious redox reaction, slowing formation of the inhibitory Au(III) side-product.

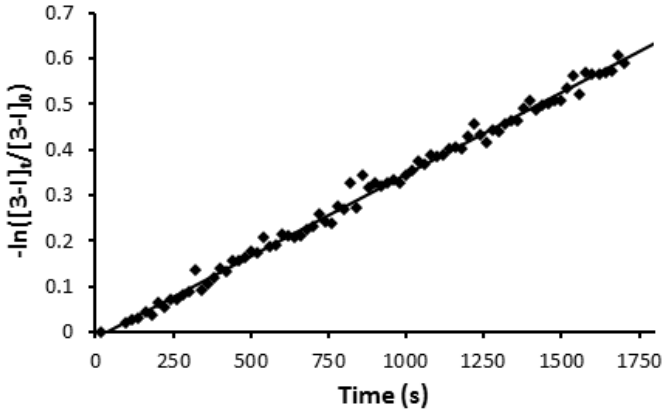


**Figure 3.29.** Clean exponential behavior for the reductive elimination from **3-I** catalyzed by cluster **2**.

Catalyst **2** was also found to serve as a more robust catalyst in the reductive elimination from **7-I**, with a turnover number (TON) of 947, compared to the measured TON of 312 for

complex **1**. Though the catalyst deactivation pathway in this case is unknown, it again seems plausible that **1** and **2** are oxidized by **8-I**, and that the less electron-rich catecholate ligands are less susceptible to oxidation. This is supported by the formation of $Au^0$ precipitate after a large number of turnovers with **1** but not with **2**.

The next major obstacle to overcome was the identification of a nucleophile capable of transmetallating to platinum(II), while remaining tolerant of protic solvent and of the supramolecular catalyst.[79] Stannanes were found to be suitable coupling partners under these criteria, however, the $R_3SnI$ byproduct formed upon transmetallation was a strong guest for **2**, deactivating the supramolecular catalyst after only one turnover (Figure 3.30).

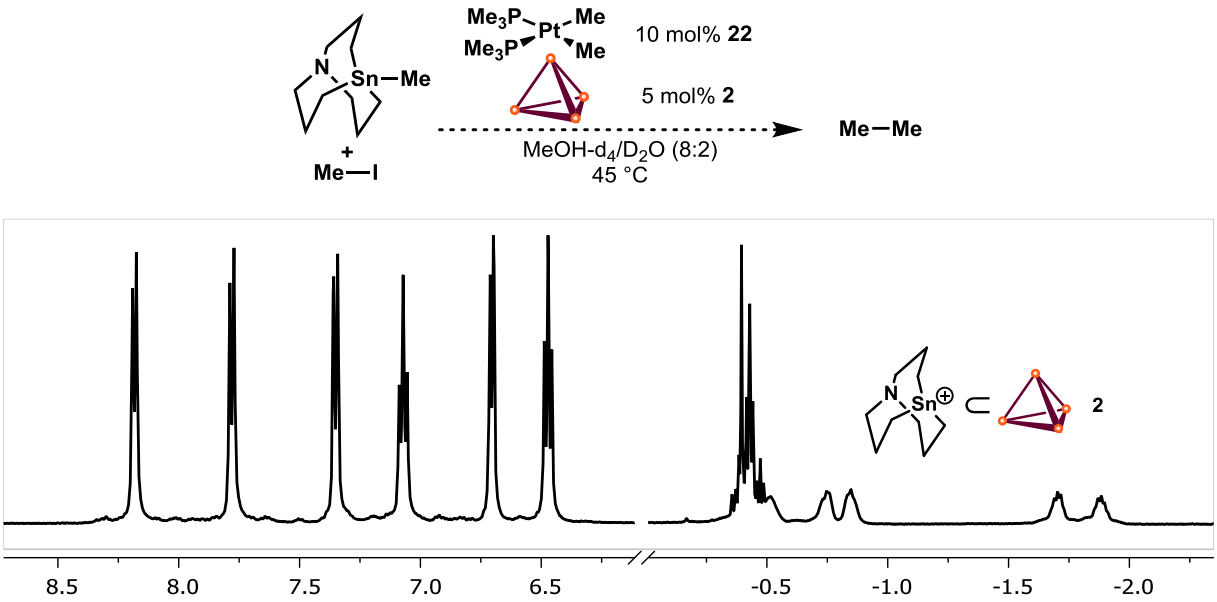


**Figure 3.30** $^1$H-NMR showing encapsulation of $R_3Sn^+$ during attempted dual catalysis

The addition of potassium fluoride, in order to generate the significantly less labile $R_3SnF$, effectively sequestered the trialkyltin cation and prevented catalyst deactivation. Under these conditions, efficient C–C coupling between tetramethyltin and iodomethane occurred, and the presence of both the platinum and supramolecular catalysts were necessary to achieve turnover (Figure 3.31).

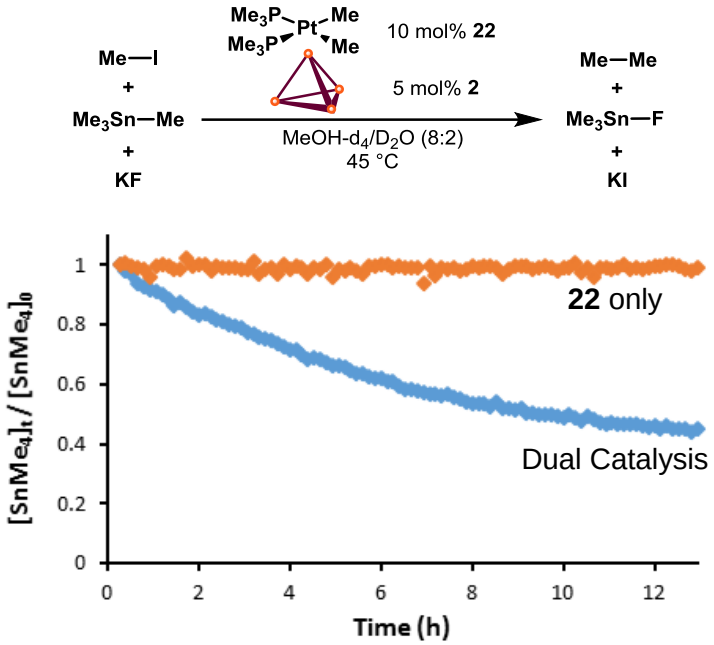


**Figure 3.31.** Dual Supramolecular and Transition Metal Catalysis in the C–C coupling of tetramethyltin and methyl iodide.

The observation of efficient alkyl-alkyl cross coupling dependent on both the transition metal catalyst and the supramolecular microenvironment catalyst represents a proof of principle for the initial motivating hypothesis for this work. However, further questions persisted about the overall mechanism by which dual catalysis occurred. Namely, despite the presumed involvement of the stoichiometrically validated supramolecular catalysis of the C–C reductive elimination, the remaining elements of the catalytic cycle remained unclear. For one, limited precedent for transmetallation of alkyl stannanes to phosphine-supported platinum existed, and any additional role of fluoride (originally added to scavenge trimethytin iodide) in this step was unclear.[80–84] Beyond this, oxidative addition of methyl iodide has been reported to both mono- and di-alkyl Pt(II) complexes, suggesting that either pathway might be relevant.[59]

In order to gain further insight into the mechanism of this dual-catalytic process, the platinum speciation over the course of the reaction was interrogated by examination of the reaction mixture by a combination of $^{1}$H- and $^{31}$P-NMR spectroscopy. Four unique platinum species could be identified and definitively confirmed by independent synthesis. These species were assigned as the platinum(II) complex **10**, and the three platinum(IV) complexes **9**, **23** and **24** (Figure 3.16). While the presence of platinum complexes **9** and **10** was not unexpected considering their role in the previously described stoichiometric reactivity, the involvement of **23** and **24** was less easily accommodated by our initial mechanistic hypothesis. The evolution of the speciation for these complexes over the course of the reaction is depicted in Figure 3.32. While **10** maintains roughly steady concentration, the initial burst and subsequent decay of **23** is accompanied by the growth in concentration of **9**, with **24** growing in gradually at late reaction times. In the absence of the supramolecular catalyst, only **9** and **23** are observed.

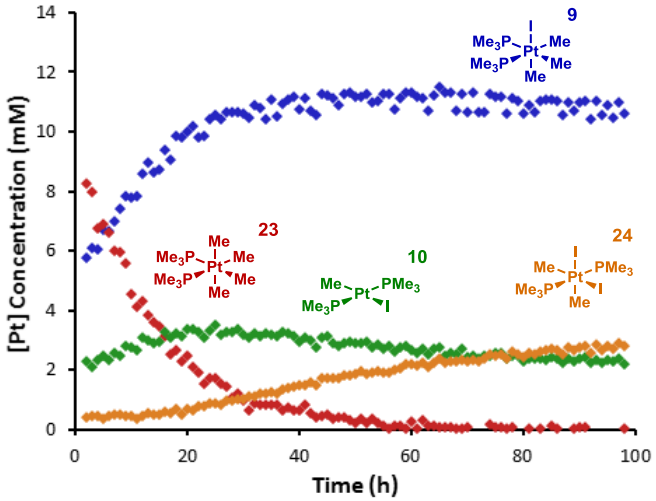


**Figure 3.32.** Concentration of major platinum species under dual catalytic conditions.

In order to understand the origin of the unexpected platinum complexes **23** and **24**, a series of stoichiometric experiments were performed, beginning with an investigation into the formation of tetramethylplatinum(IV) complex **23**.[85,86] Treatment of **9** with tetramethyltin under catalytically relevant conditions led to no reaction. However, addition of potassium fluoride to the same mixture resulted in rapid transmetallation to generate **23** and trimethyltin fluoride (Figure 3.33). Surprisingly, this process was found to be reversible, and in the presence of trimethyltin fluoride and potassium iodide, **23** was found to undergo conversion to tetramethyltin and **9**.[87–89] In the absence of KI, two trialkyl Pt(IV) complexes are formed which are not sufficiently stable to enable isolation. We speculate that these are fluoride and solvato complexes but cannot definitively assign them. Nonetheless, taken together, these results suggest a dynamic Pt(IV)/Sn transmetallation equilibrium mediated by fluoride and iodide, in which the relative concentrations of the six species dictate the overall distribution.

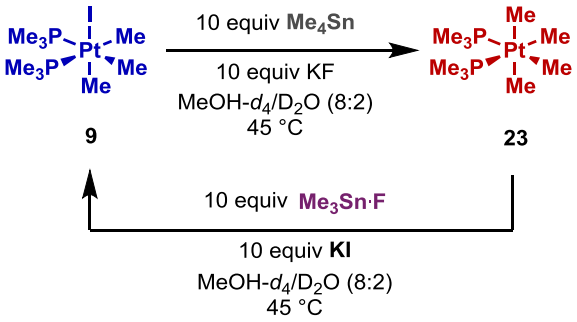


**Figure 3.33.** Fluoride-promoted transmetallation to **9** and demonstration of reversibility

With the likely origin of **23** elucidated, efforts were focused on identifying the pathway by which the putative substrate for cluster catalyzed reductive elimination, **9**, was regenerated from platinum(II) complex **10**. This process requires a transmetallation event, an oxidative addition event, and a ligand isomerization, however, their relative order was unclear. Suprisingly, transmetallation experiments similar to those which demonstrated the interconversion of platinum(IV) complexes **9** and **23** indicated that tetramethyltin was unreactive with **10** on catalytically relevant timescales, either in the presence or absence of potassium fluoride. However, it was observed that an equimolar mixture of **10** and **23**, allowed

to equilibrate under conditions similar to those used in the dual catalytic reaction, resulted in formation of **9** and **22** (Figure 3.34). The kinetic product of transmetallation is the *trans*-dimethylplatinum(II) complex **27** (*vide infra*), but it undergoes isomerization to the *cis*- isomer. The overall process was found to be reversible, suggesting a possible Pt(IV)/Pt(II) transmetallation equilibrium.

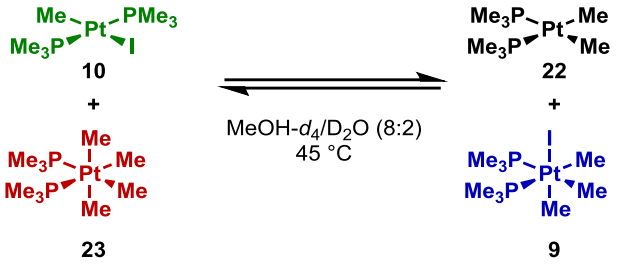


**Figure 3.34.** Reversible Pt(II)/Pt(IV) transmetallation between **10** and **23**

Furthermore, **22** was shown to undergo exceedingly rapid oxidative addition of methyl iodide under relevant conditions to generate **9**, demonstrating that a mechanism involving transmetallation followed by oxidative addition could potentially be achieved with platinum(IV) complex **23** effectively shuttling a methyl group from tetramethyl tin to complex **10**. However, in a separate experiment, **10** was shown to undergo oxidative addition of methyl iodide directly to afford **24** (Figure 3.35).

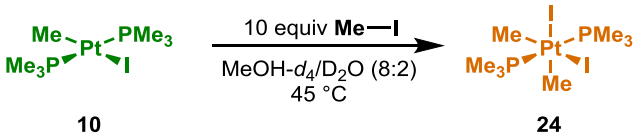


**Figure 3.35**. Oxidative addition of iodomethane to **10**

In order to determine the fate of platinum complex **10**, the rates of transmetallation and oxidative addition under catalytically relevant conditions were measured. Direct comparison of these rates showed that oxidative addition outcompetes transmetallation by a substantial factor (Figure 3.36). With oxidative addition established as the dominant pathway for consumption complex **10**, the behavior of **24** was examined in order to obtain a complete understanding of the closure of the catalytic cycle.

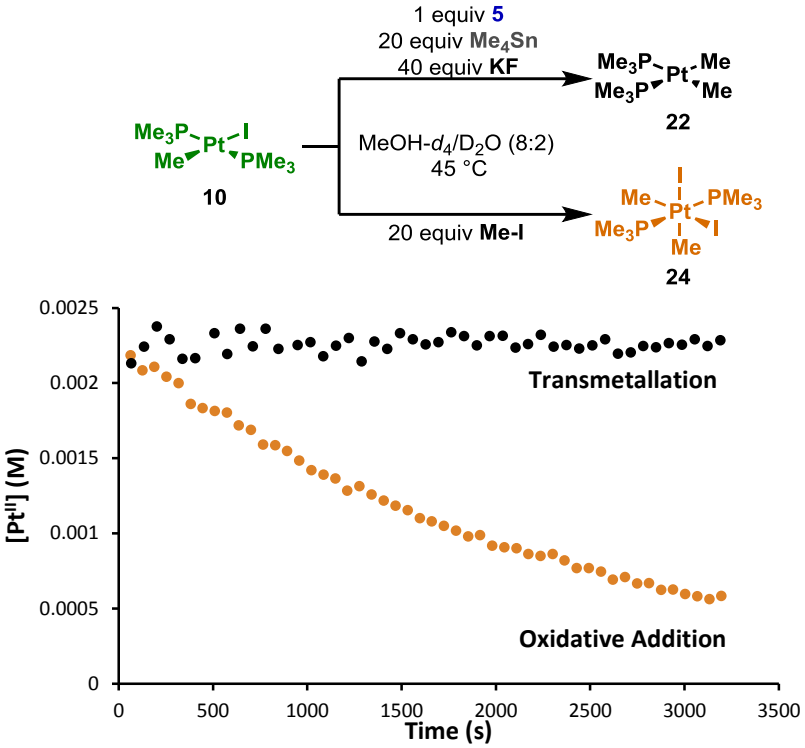


**Figure 3.36.** Direct rate comparison under catalytically relevant conditions for oxidative addition and transmetallation pathways for the consumption of platinum complex **10**.

No reductive elimination from **24** was observed in the presence or absence of a supramolecular catalyst. However, in a fashion similar to that previously observed with platinum complex **9**, fluoride-promoted transmetallation of tetramethyltin to **24** generated a mixture of platinum(IV) complexes **25** and **26**, which could be isolated and fully characterized (Figure 3.37). Complexes **25** and **26** are the *trans*-phosphine analogues of **9** and **23**, but do not undergo detectable thermal isomerization to the thermodynamically favored *cis*-isomers on catalytically relevant timescales. Moreover, **24** and **26** were observed to conproportionate to afford **25** in the absence of tin, and **25** was observed to disproportionate into **24** and **26** under similar conditions, suggesting that equilibration *via* platinum(IV)/platinum(IV) methyl transfer is possible under catalytic conditions.

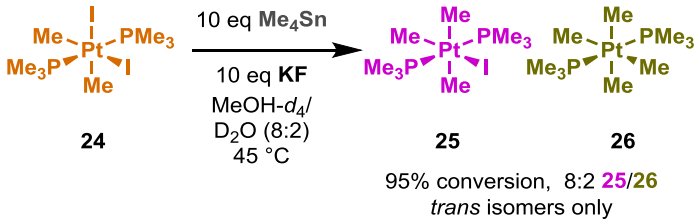


**Figure 3.37.** Observation of transmetallation to platinum(IV) complex **24**.

The failure to generate complex **9** from transmetallation to **24** was initially surprising, given that **25** and **26** are not detectable as intermediates in the dual catalytic reaction, and **9** is the dominant platinum species in solution for the majority of the reaction. However, treatment of **25** with the supramolecular catalyst **2** leads to rapid consumption of the *trans*- starting material, affording a mixture of *cis*- isomer **9** and reductive elimination product **10**, along with

ethane (Figure 3.38). The reaction at the catalytically relevant temperature of 45 ºC afforded an initial ratio of isomerized complex **9** to elimination product **10** of approximately 1:1.15 upon complete consumption of **25**, but was too rapid to determine a rate constant by $^{1}$H-NMR. Monitoring the reaction by $^{1}$H-NMR at 25 ºC afforded a rate constant of 2.0 x $10^{-2}$ $s^{-1}$ for the combined isomerization / reductive elimination process, which could not be accurately deconvoluted, due to overlapping resonances. For comparison, the pseudo-first order rate constant for oxidative addition of methyl iodide to **10** at 45 ºC was measured to be 4.38 x $10^{-4}$ $s^{-1}$. This disparity clearly suggests that the failure to detect **25** under catalytic conditions is due to its rapid consumption in the presence of the supramolecular catalyst.

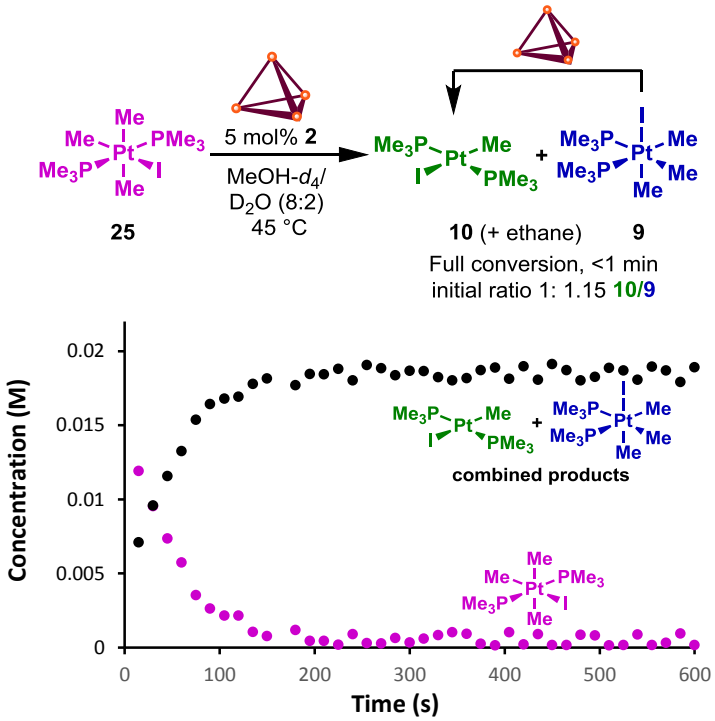


**Figure 3.38.** Rapid consumption of **25** in the presence of cluster **2** at 45ºC, with kinetic trace conducted at 25ºC.

The fact that reductive elimination from **25** catalyzed by cluster **2** is significantly more rapid than the catalyzed elimination from **9** (*vide supra*), can be rationalized as a ground state destabilization of **25** relative to **9**, where the enthalpic penalty of *trans*-methyl groups for **25** is alleviated as the transition state for reductive elimination is approached. (It is not clear if the Michaelis complexes for **9** and **25** immediately converge as depicted below, or if there is some significant barrier to isomerization maintained after ionization in the cluster.)

These observations collectively suggest an overall mechanism for the dual catalytic process in which the *trans*-isomers of the platinum(II) and platinum(IV) complexes lie on cycle, with **9** serving as a readily-engaged off-cycle resting state and reservoir (Figure 3.39). Oxidative addition precedes transmetallation, and **25** is rapidly engaged by the supramolecular catalyst. This mechanism is consistent with the observed platinum speciation, and suggests that as the concentration of tetramethyltin decreases, the reaction undergoes a shift in the turnover-limiting step (from oxidative addition to transmetallation) and concomitant change in the on-cycle resting state (from **10** to **24**).

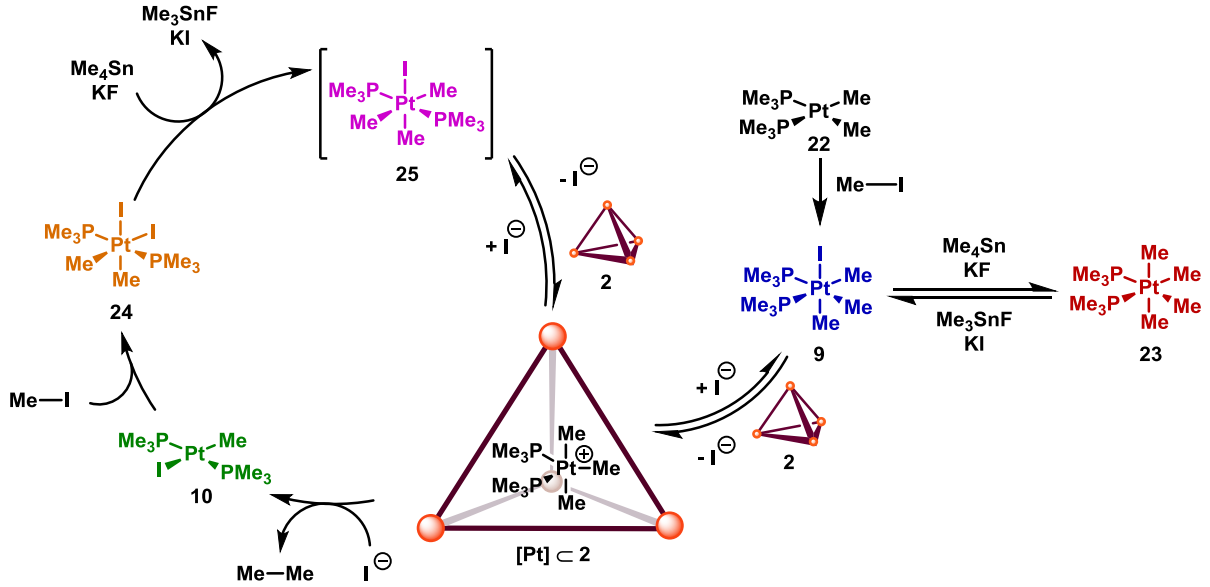


**Figure 3.39.** Mechanism for the dual catalytic cross-coupling consistent with experimental evidence.

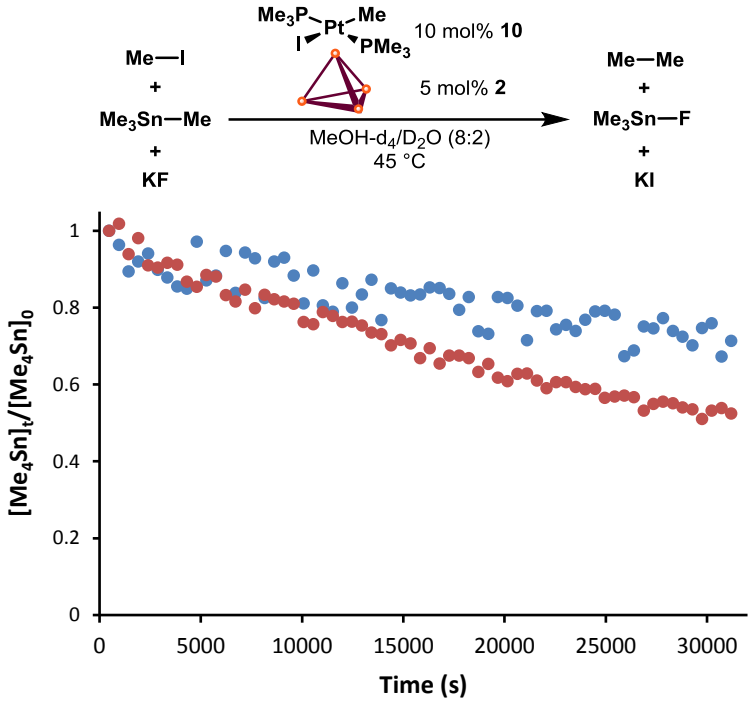


**Figure 3.40.** Consumption of $SnMe_4$ under dual catalytic conditions, cluster **2** with precatalyst **10** (blue circles) or with **22** (red circles).

Additionally consistent is the observation that monomethyl platinum(II) complex **10** is a competent precatalyst for this process, although slightly diminished rates are observed (Figure 3.40). This is explained by the fact that oxidative addition product **24** is only marginally soluble in the MeOD/$D_2O$ solvent mixture, and when it rapidly forms under these conditions, it reaches sufficient concentration to crystallize out, lowering the overall catalyst loading. Further support

is garnered from flooding experiments; when a 10-fold excess of methyl iodide is introduced, **6** is no longer detectable as a persistent intermediate, whereas introduction of a 10-fold excess of tetramethyltin allows **26** to build to detectable levels under catalytic conditions. Using the modeling program COPASI, this mechanism can be used to fit the observed concentrations of each platinum species, as well as the tin and alkyl halide species observed under the reaction conditions, generating a set of kinetic parameters that accurately reproduces the chemical dynamics of the reaction (see supporting information below for more detail).[90]

Several alternative mechanisms are also potentially consistent with our combined experimental observations and merit comment. If the kinetic product of reductive elimination is the *cis* isomer of **10** (akin to Figure 3.24 above), and transmetallation to this species (either from $Me_4Sn$ or **23**) is substantially faster than for the *trans* isomer (such that it outcompetes isomerization to **10**), **22** could be directly formed and close the cycle by oxidative addition of iodomethane to afford **9**. Alternatively, this same *cis* isomer of **10** could undergo oxidative addition of iodomethane to give an isomer of **24** followed by transmetallation to afford **9** (again requiring oxidative addition to outcompete isomerization). We disfavor both of these mechanisms due to the kinetic invisibility of such a *cis* isomer (both in the stoichiometric and dual catalytic reactions), suggesting that any potential isomerization is rapid, whereas we suspect a modest difference if any between the *trans* and putative *cis* isomers for both transmetallation and oxidative addition rates, thus making isomerization unlikely to be outcompeted by either reaction. Any alternative mechanism resting on the transmetallation between **23** and **10** is unlikely to be relevant beyond early reaction times. Beyond the slow kinetics measured above (Figure 3.36), the concentration of **23** drops sharply after the initial reaction period, further limiting its potential involvement in turnover.

A final note regarding Sn/Pt transmetallation is appropriate: an apparent contradiction is found in the simultaneous observation that no transmetallation to **9**, **10**, or **24** occurs in the absence of fluoride, yet trialkyltin cation is formed under catalytic conditions in the absence of fluoride (Figure 3.30 above). The contradiction is resolved if transmetallation between the iodoplatinum species and tetraalkyltin is uphill and reversible, with the equilibrium shifted either by fluoride or by encapsulation of the tin cation within the supramolecular assembly.

### 3.3.7 Identification of an Acidolysis Side Reaction

In addition to the desired cross-product, ethane, small amounts of methane-$d_1$ were detected by GC-MS of the reaction headspace. Upon examining several potential sources of this side-product, it was observed that treatment of **23** with supramolecular complex **1** results in the formation of ethane, methane-$d_1$, and **22** (Figure 3.41)

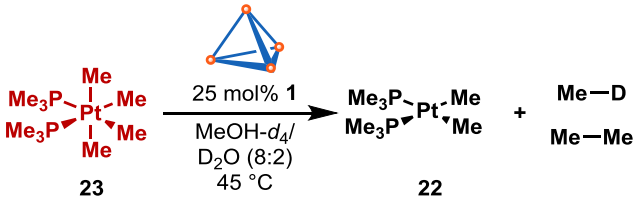


**Figure 3.41.** Identification cluster mediated decomposition of **23**, resulting in methane formation.

Interestingly, the addition of potassium iodide halts the formation of ethane, instead slowly affording a mixture of **9** and methane-$d_1$. In the absence of cluster **1**, no significant protonolysis of **23** was observed (Figure 3.42).

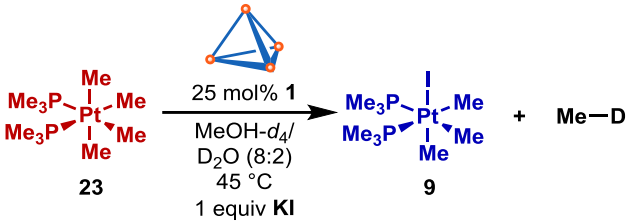


**Figure 3.42** Iodide trapping of the intermediate in the acidolysis of **23**, affording **9**.

Monitoring this process by $^1$H-NMR shows a sigmoidal decay profile for **23**, with formation of **27** as an intermediate *en route* to **22**. The observed reaction mass balance decreases over the course of the reaction, but can be restored upon the addition of potassium iodide to the completed reaction, affording a mixture of **9** and **10** (Figure 3.43). These data are consistent with a mechanism involving cluster-promoted acidolysis of **23**,[36] which generates the corresponding cationic trimethyl Pt(IV) complex. Upon cluster-promoted reductive elimination of ethane, the cationic monomethyl Pt(II) complex can abstract a methyl from **23**, continuing the chain reaction (Figure 3.44). The decrease in mass balance, then, corresponds to the formation of rapidly exchanging unsaturated cationic complexes, either bound within the cluster or free in solution.

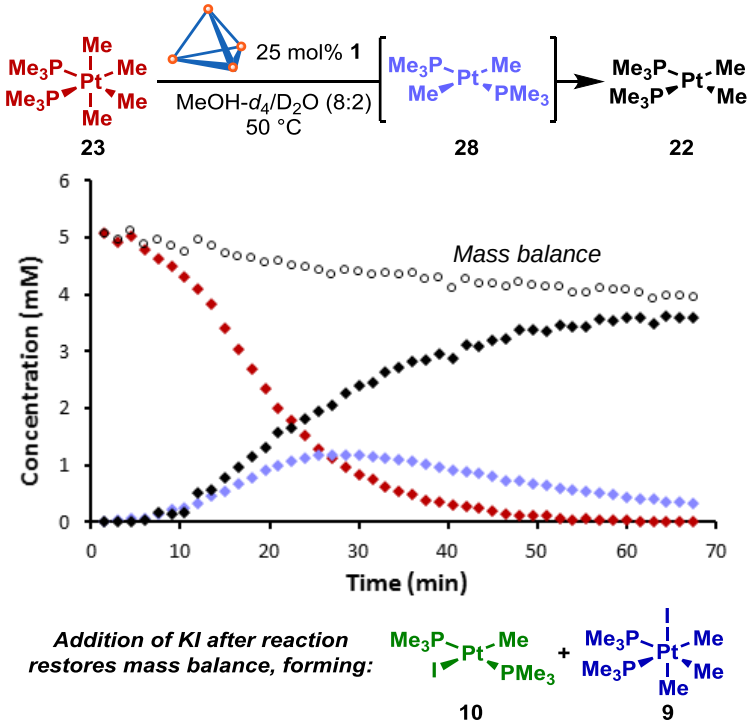


**Figure 3.43.** Kinetic profile for the cluster catalyzed acidolysis of **23**, displaying sigmoidal kinetics.

Similar behavior has previously been observed for Pt(IV) complexes by Puddephatt in the absence of a supramolecular host, wherein initiation occurs by the addition of an extrinsically-prepared coordinatively unsaturated cationic Pt(II) complex.[91,92] Because the propagation of this pathway is inhibited by iodide, it is unlikely to occur with significant chain-length under catalytic conditions. Furthermore, the substrate for acidolysis (**23**) is present in substantial concentrations only at early reaction times. Nonetheless, this reactivity likely explains some of the observed side-product formation.

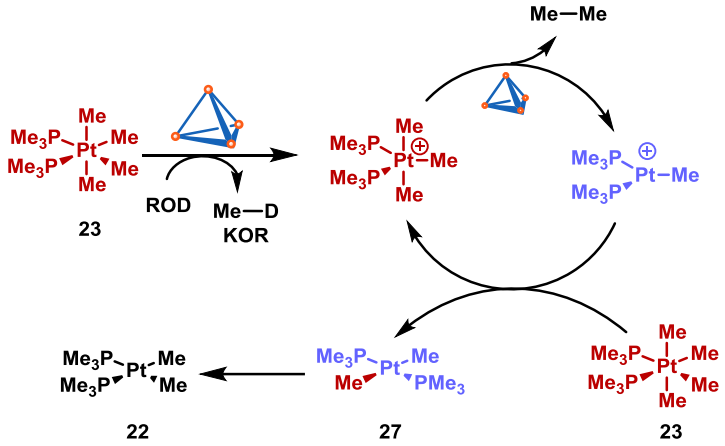


**Figure 3.44.** Proposed mechanism for protonolysis-initiated reductive elimination, involving cluster catalysis of both initiation and reductive elimination.

## 3.4 Conclusions

Microenvironment catalysis affords a unique opportunity to transiently modulate the stereoelectronic condition of a catalytic intermediate for one step of a cycle, while leaving the remainder of the cycle unperturbed. In this work, the cationic intermediates preceding, and transition states for carbon-carbon bond-forming, reductive elimination that are recognized by a co-catalytic supramolecular cluster were thoroughly examined. The substitutional effects of spectator ligand, halide, reactive group, solvent and catalyst were explored, and insight into the nature of the resultant Michaelis complex was garnered. A full mechanism for the dual catalytic coupling reaction of alkyl tin and alkyl halide was elucidated on the basis of stoichiometric experiments under catalytically relevant conditions, as well as the mechanism of an acidolysis side reaction.

The strategy outlined herein should be broadly applicable to other elementary steps of interest, and the implementation of other supramolecular catalysts with orthogonal properties and reactivity preferences should allow the extension to other manifolds of reactivity (e.g. transmetallation, oxidative addition, migratory insertion, etc.). As the instances of this strategy proliferate, catalytic cycles could be developed for which each elementary step is individually engaged by a uniquely tailored microenvironment catalyst. Furthermore, the evolution of more sophisticated supramolecular architectures which are capable of influencing a metal's innate reactivity preferences rather than amplifying them are also surely on the horizon.

Moreover, the insight that an elementary step at a transition metal could be catalyzed ultimately found itself applicable again in the work detailed in Chapter 4.

## 3.5 Supporting Information

### 3.5.1 General Methods

Unless stated otherwise, all reactions were performed in oven-dried glassware sealed with rubber septa under a nitrogen atmosphere and were stirred with Teflon-coated magnetic stir bars. Dry tetrahydrofuran (THF), toluene, dimethylfomamide (DMF), acetonitrile, triethylamine (TEA) and dichloromethane (DCM) were obtained by passing these previously degassed solvents through activated alumina columns. All other reagents were used as received. Reactions were monitored by thin layer chromatography (TLC) on Silicycle Siliaplate$^{TM}$ glass backed TLC plates (250 μm thickness, 60 Å porosity, F-254 indicator) and visualized by UV irradiation and *p*-Anisaldehyde stain. Volatile solvents were removed under reduced pressure with a rotary evaporator and dried on high vacuum on a Schlenk line. $^{1}$H-NMR, $^{13}$C-NMR, and $^{31}$P-NMR spectra were taken with Bruker spectrometers operating at 300, 400, 500, or 600 MHz for $^{1}$H (75, 100, 125, and 150 MHz for $^{13}$C). Chemical shifts are reported relative to the residual solvent signal. NMR data are reported as follows: chemical shift (multiplicity, coupling constants where applicable, number of hydrogens). Splitting is reported with the following symbols: s = singlet, bs = broad singlet, d = doublet, t = triplet, hept = heptet, dd = doublet of doublets, dt = doublet of triplets, m = multiplet, at = apparent triplet, dq = doublet of quartets. High-resolution mass spectra (HRMS) were performed on a Thermo LTQ-FT-ICR (7T, ESI) by the QB3 mass spectral facility at the University of California, Berkeley. Elemental Analyses were performed by the Microanalytical Facility at the University of California, Berkeley. Previously reported compounds were synthesized according to literature procedures.

### 3.5.2 Synthesis of Previously Unreported Compounds

*General Procedure for preparation of Au(III) complexes*
(adapted from the method of Schmidbaur[93])

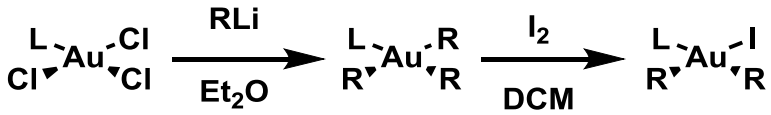


**Stage 1:** A suspension of the phosphine-supported Au(III) trichloride complex (1 equivalent) in diethyl ether (0.2 M) was placed in a room-temperature water bath, and a solution of R-Li was added dropwise to the suspension (3.0 equivalents). The resulting mixture was stirred at ambient temperature for 2 hours before being quenched with water. The resulting suspension was filtered through Celite into a separatory funnel. The layers were separated and the aqueous layer was extracted twice more with diethyl ether. The combined organic layers were dried over $Na_2SO_4$, filtered, and concentrated in vacuo to yield a black oil. The oil was dissolved in diethyl ether and filtered through neutral alumina. Upon concentration, a colorless oil was obtained, comprised primarily of the desired Au(III) trialkyl complex, typically contaminated with 5-10% of the corresponding Au(I) alkyl. The mixture discolors upon standing and was used immediately without further purification.

**Stage 2:** The crude product from the previous step was dissolved in dichloromethane (DCM; 0.1 M) and a saturated solution of iodine (1 equivalent) in DCM was added dropwise to the suspension causing an immediate color-change to bright yellow. As each drop was added, the

purple color fades to golden-yellow. *The addition was monitored colorimetrically and the addition was halted at the endpoint, which is marked by a sharp transition from yellow to orange-brown.* The mixture was stirred for 2 hours at room temperature and then concentrated. Purification was performed as described below for each complex.

**_cis_-iododimethyl(trimethylphosphine)gold(III), 3-I**

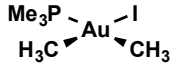

The crude residue was extracted with diethyl ether, filtered and concentrated. The solid product was recrystallized from DCM/n-pentane in the freezer at -20 °C, and collected in two crops.

Starting from 760 mg (2.0 mmol) of trichlorotrimethylphosphinegold(III), 302 mg (35% over two steps) of **3-I** were obtained as a colorless solid.

$^{1}$H NMR (600 MHz, Methanol-$d_4$) δ 1.62 (d, 9H), 1.30 (d, 3H), 1.09 (d, 3H).
$^{31}$P NMR (243 MHz, Methanol-$d_4$) δ -7.9.
In accordance with previously recorded spectra.[93]

*General Procedure for halogen exchange reactions from **3-I***

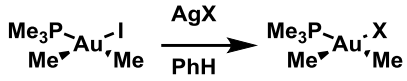


To a solution of **3-I** (100 mg, 0.23 mmol) in benzene (2.5 mL) was added 20 equivalents of AgX (X = Cl, Br). The heterogeneous mixture was stirred vigorously for 20 minutes, and then filtered. The filter cake was washed with additional benzene. An additional 20 equivalents of AgX was added, and the mixture was again stirred vigorously for 20 minutes. The mixture was filtered, the filter cake was washed with benzene and the combined filtrate was concentrated yielding the desired product as a colorless solid.

**_cis_-bromodimethyl(trimethylphosphine)gold(III), 3-Br**

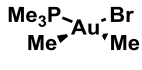

90 mg, 98% yield.

$^{1}$H NMR (500 MHz, Methanol-$d_4$) δ 1.62 (d, $J$ = 10.9 Hz, 9 H), 1.23 (d, $J$ = 8.7 Hz, 3H), 0.99 (d, $J$ = 9.6 Hz, 3H).
$^{13}$C NMR (126 MHz, Methanol-$d_4$) δ 13.5 (d, $J$ = 125.5 Hz), 10.5 (d, $J$ = 30.6 Hz), 8.1 (d, $J$ = 5.4 Hz).
$^{31}$P NMR (202 MHz, Methanol-$d_4$) δ -1.8.
EA: Calculated : C, 15.68; H, 3.95; Found: C, 16.06; H, 3.97;

**_cis_-chlorodimethyl(trimethylphosphine)gold(III), 3-Cl**

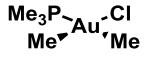

75 mg, 95% yield.

$^{1}$H NMR (500 MHz, Methanol-$d_4$) δ 1.58 (d, $J$ = 11.1 Hz, 9H), 1.15 (d, $J$ = 8.8 Hz, 3H), 0.91 (d, $J$ = 9.7 Hz, 3H).
$^{13}$C NMR (126 MHz, Chloroform-$d$) δ 15.0 (d, $J$ = 124.9 Hz), 9.9 (d, $J$ = 30.2 Hz), 4.3 (d, $J$ = 5.4 Hz).
$^{31}$P NMR (202 MHz, Chloroform-$d$) δ 1.9.
EA: Calculated : C, 17.74; H, 4.47; Found: C, 17.66; H, 4.39;

**_cis_-iododimethyl(triphenylphosphine)gold(III), 5**

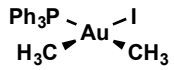

The crude residue was taken up in DCM and layered with hexanes. Upon crystallization of the $Ph_3PAuI$ impurity, the impurity was filtered off and the mother liquor was concentrated. This residue was further purified by dissolution in methanol, filtration, and concentration, yielding the desired product as a colorless solid.

Starting from 292 mg (0.5 mmol) of trichlorotriphenylphosphinegold(III), 140 mg (45% over two steps) of **5** were obtained as a colorless solid.

$^{1}$H NMR (600 MHz, Methanol-$d_4$) δ 7.35-7.71 (m, 15H), 1.56 (d, 3H), 1.16 (d, 3H).
$^{31}$P NMR (243 MHz, Methanol-$d_4$) δ 29.1.
In accordance with previously recorded spectra.[44]

**_cis_-iododimethyl(triethylphosphine)gold(III), 7-I**

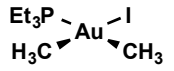

The crude residue was extracted with hexanes, filtered and concentrated. The resulting residue was dissolved in methanol (0.1 M) and KI (2 equivalents) was added. The solution was stirred for 1 hour, concentrated, and extracted with diethyl ether. The ether layer was washed five times with water, dried over $Na_2SO_4$, filtered, and concentrated. The resulting solid was recrystallized fractionally by cooling a saturated pentane solution to -20°C.

Starting from 1.34 g (3.1 mmol) of trichlorotriethylphosphinegold(III), 950 mg (65% over two steps) of **1b** were obtained as a colorless solid.

$^{1}$H NMR (600 MHz, Methanol-$d_4$) δ 2.17 (dt, $J$ = 9.2, 7.6 Hz, 6H), 1.33 (d, $J$ = 7.4 Hz, 3H), 1.23 – 0.95 (m, 12H).
$^{13}$C NMR (151 MHz, Methanol-$d_4$) δ 14.1 (d, $J$ = 27.8 Hz), 12.8, 12.3 (d, $J$ = 112.7 Hz), 6.5 (d, $J$ = 1.9 Hz).
$^{31}$P NMR (243 MHz, Methanol-$d_4$) δ 18.5.
EA: Calculated : C, 20.35; H, 4.48; Found: C, 20.70; H, 4.44;

*General Procedure for halogen exchange reactions from **7-I***

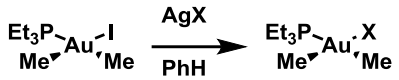


To a solution of **7-I** (80 mg, 0.17 mmol) in benzene (1.5 mL) was added 20 equivalents of AgX (X = Cl: 364 mg, X = Br 478 mg). The heterogeneous mixture was stirred vigorously for 20 minutes, and then filtered. The filter cake was washed with additional benzene. An additional 20 equivalents of AgX was added, and the mixture was again stirred vigorously for 20 minutes. The mixture was filtered, the filter cake was washed with benzene and the combined filtrate was concentrated yielding the desired product as a colorless solid.

**_cis_-bromodimethyl(triethylphosphine)gold(III), 7-Br**

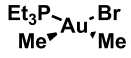

64 mg, 89%

$^{1}$H-NMR (300 MHz, Methanol-$d_4$) δ 2.08 (dq, $J$ = 10.1, 7.6 Hz, 6H), 1.21 – 1.05 (m, 12H), 0.98 (d, $J$ = 9.0 Hz, 3H).
$^{13}$C-NMR (126 MHz, Methanol-$d_4$) δ 15.90 (d, $J$ = 117.5 Hz), 13.08 (d, $J$ = 27.1 Hz), 7.58 (d, $J$ = 5.6 Hz), 6.57 (d, $J$ = 2.0 Hz).
$^{31}$P-NMR (202 MHz, Methanol-$d_4$) δ 24.63.
EA: Calculated: C, 22.60; H, 4.98; Found: C, 22.88; H, 5.14

**_cis_-chlorodimethyl(triethylphosphine)gold(III), 7-Cl**

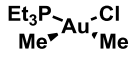

60 mg, 92%

$^{1}$H-NMR (500 MHz, Methanol-$d_4$) δ 2.06 (dq, $J$ = 9.9, 7.6 Hz, 1H), 1.29 – 1.07 (m, 2H), 0.93 (d, $J$ = 9.1 Hz, 3H).
$^{13}$C-NMR (126 MHz, Methanol-$d_4$) δ 17.47 (d, $J$ = 117.3 Hz), 12.62 (d, $J$ = 26.4 Hz), 6.55 (d, $J$ = 1.9 Hz), 3.98 (d, $J$ = 5.7 Hz).
$^{31}$P-NMR (202 MHz, Methanol-$d_4$) δ 27.73
EA: Calculated: C, 25.24; H, 5.56; Found: C, 25.24; H, 5.68

**_fac_-iodotrimethylbis(trimethylphosphino)platinum(IV), 9**

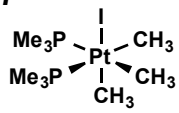

Bis(dimethylphosphino)dimethylplatinum(II) was dissolved in dry, degassed DCM, and 20 equivalents of methyl iodide were added. The solution was stirred at ambient temperature for 6 hours, and then concentrated. The crude product was recrystallized from DCM/pentane at -20°C. Starting from 566 mg (1.5 mmol) of the platinum (II) complex, 533 mg of **9** was obtained (68% yield).

$^{1}$H NMR (500 MHz, Methanol-$d_4$) δ 1.57 (dd, $J$ = 8.7, 5.6 Hz, 18H), 1.07 – 0.72 (m, 9H).
$^{13}$C NMR (126 MHz, Methanol-$d_4$) δ 13.5 – 12.1 (m), 3.1, 1.9 (dd, $J$ = 127.1, 7.6 Hz).
$^{31}$P NMR (202 MHz, Methanol-$d_4$) δ -54.4 (s + d, $J_{Pt-P}$ = 1246 Hz).
EA: Calculated : C, 20.82; H, 5.24; Found: C, 20.67; H, 5.11;

**Tetraethylphosphonium tetrakis(3,5-bistrifluoromethylphenyl)borate**

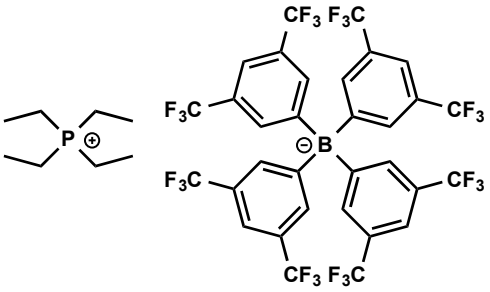

Tetraethylphosphonium bromide (115 mg, 0.5 mmol) was dissolved in minimal acetonitrile. In a separate flask, sodium tetrakis(3,5-bistrifluoromethylphenyl)borate (451 mg, 0.5 mmol) was also dissolved in minimal acetonitrile. The two solutions were combined, resulting in a thick white precipitate (NaBr). The mixture was stirred for 20 minutes, filtered through a glass fiber filter, and concentrated. The solid was extracted with diethyl ether, filtered, and layered with hexanes. The colorless blocks crystallized in this way were dried in vacuo yielding 452 mg of the desired product (86% yield).

$^{1}$H NMR (500 MHz, Methanol-*d*$_4$) δ 7.62 (s, 12H), 2.26 (dq, *J* = 12.9, 7.7 Hz, 8H), 1.27 (dt, *J* = 18.0, 7.7 Hz, 12H).
$^{13}$C NMR (126 MHz, Methanol-*d*$_4$) δ 161.5 (m), 134.4, 130.2 – 127.9 (m), 124.4 (q, *J* = 271.5 Hz), 117.1, 10.3 (d, *J* = 49.7 Hz), 4.1 (d, *J* = 5.3 Hz).
$^{19}$F NMR (470 MHz, Methanol-d$_4$) δ -64.3.
$^{31}$P NMR (202 MHz, Methanol-*d*$_4$) δ 40.5 .
EA: Calculated : C, 47.55; H, 3.19; Found: C, 47.52; H, 3.12;
HRMS (ESI) m/z calculated for $[C_{32}H_{12}B_1F_{24}]^-$ 863.0654, found 863.0663; m/z calculated for $[C_8H_{20}P_1]^+$ 147.1297, found 147.1295

***Cis*-iododiethyl(trimethylphosphine)gold(III), 11**

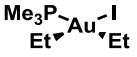

A suspension of the trichlorotrimethylphosphineAu(III) (190 mg, 0.5 mmol, 1 equiv.) in diethyl ether (2.5 mL, 0.2 M) was placed in a room-temperature water bath, and a solution of EtLi was added dropwise to the suspension (3 mL, 0.5M in benzene/cyclohexane, 1.5 mmol, 3 equiv). The resulting mixture was stirred at ambient temperature for 2 hours before being quenched with water. The resulting suspension was filtered through Celite into a separatory funnel. The layers were separated and the aqueous layer was extracted twice more with diethyl ether. The combined organic layers were dried over $Na_2SO_4$, filtered, and concentrated in vacuo to yield a black oil. The oil was dissolved in diethyl ether and filtered through neutral alumina. Upon concentration, a colorless oil was obtained (120 mg), comprised primarily of the desired Au(III) trialkyl complex, contaminated with a small amount of ethyl(trimethylphosphine)Au(I). The mixture discolors upon standing and was used immediately without further purification. The crude product from the previous step was dissolved in dichloromethane (3.3 mL DCM; ~0.1 M) and a saturated solution of iodine (85 mg, 0.33 mmol, ~1 equiv) in DCM was added dropwise to the suspension causing an immediate color-change to bright yellow. As each drop was added, the purple color fades to golden-yellow. *The addition was monitored colorimetrically and the addition was halted at the endpoint, which is marked by a sharp transition from yellow to orange-brown.* The mixture was stirred for 2 hours at room temperature and then concentrated. The resulting residue was extracted with hexanes, filtered through a glass fiber filter and then concentrated. The crude product was purified by recrystallization from a saturated pentane solution at -20 °C. Two crops of colorless

needles were collected, totaling 50 mg (22% yield over 2 steps). The compound was stored in the freezer, as it readily melts near room temperature and is far less stable in the liquid state.

$^{1}$H-NMR (500 MHz, Methanol-$d_4$) δ 2.18 (dq, $J$ = 10.6, 7.3 Hz, 2H), 2.04 (dq, $J$ = 7.8, 7.9 Hz, 2H), 1.69 (d, $J$ = 10.4 Hz, 9H), 1.35 (dt, $J$ = 15.0, 7.7 Hz, 3H), 1.22 (t, $J$ = 7.6 Hz, 3H).
$^{13}$C-NMR (126 MHz, Methanol-$d_4$) δ 31.52 (d, $J$ = 5.6 Hz), 28.50 (d, $J$ = 119.0 Hz), 14.60 (d, $J$ = 7.0 Hz), 14.46, 12.01 (d, $J$ = 29.1 Hz).
$^{31}$P-NMR (202 MHz, Methanol-$d_4$) δ -6.51.
EA: Calculated: C, 18.35; H, 4.18; Found: C, 19.61; H, 4.55 (sample instability prevented a satisfactory analysis)

*General Procedure for Synthesis of **12**, **13**, and **16** by oxidative addition to **22***

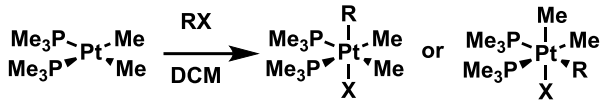


Bis(dimethylphosphino)dimethylplatinum(II) was dissolved in dry, degassed DCM, and 20 equivalents of the corresponding electrophile were added. The solution was stirred at ambient temperature for 30 minutes unless otherwise noted, and then concentrated. The crude residue was dissolved in a minimum volume of DCM, followed by layering with pentane. The layered solution was placed in a -20 ºC freezer overnight, and the resulting crystalline solids were isolated by filtration.

**Iodobis(trimethylphosphine)dimethyl-ethylplatinum(IV), 12**

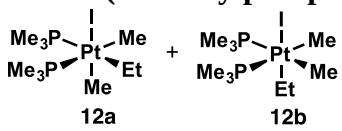


Starting from 188 mg (0.50 mmol) of platinum (II) complex **22**, 168 mg of **12** were obtained (63% yield). An extended reaction time of 6 hours was required in order to observe consumption of **22**. **12** was isolated as a mixture of two isomers.

$^{1}$H-NMR (500 MHz, Methylene Chloride-$d_2$) **12a** + **12b** δ 1.94 – 1.67 (m, C$H_2$ **a** or **b**), 1.61 – 1.47 (m, 18H, P(C$H_3$)$_3$ **a** and **b**), 1.40 – 1.16 (m, C$H_2$ **a** or **b**), 1.07 – 0.57 (m, Pt(C$H_3$)$_2$ **a** and **b**).
$^{13}$C-NMR (151 MHz, Methylene Chloride-$d_2$) **12a** δ 14.9 (dd with $^{195}$Pt satellites, $J_{PC}$ = 28.8 Hz, $J_{PtC}$ = 8.2 Hz, $J_{PtC}$ = 1.6 Hz), 14.4 (dd with $^{195}$Pt satellites, $J_{PC}$ = 28.2 Hz, $J_{PtC}$ = 9.6 Hz, $J_{PtC}$ = 1.9 Hz), 11.3 (dd with $^{195}$Pt satellites, $J_{PtC}$ = 450 Hz, $J_{PC}$ = 122 Hz, $J_{PC}$ = 7.9 Hz), 2.8 (at with $^{195}$Pt satellites, $J_{PtC}$ = 652 Hz, $J_{PC}$ = 2.8 Hz), 2.3 (dd with $^{195}$Pt satellites, $J_{PtC}$ = 512 Hz, $J_{PC}$ = 121 Hz, $J_{PC}$ = 5.6 Hz), one additional peak could not be located for isomer **a**. It is assumed that this peak overlaps with the phosphine-methyl resonances for **12b**; **12b** δ 18.4 – 18.1 (m), 14.7 – 14.3 (m), 11.9 (s with $^{195}$Pt satellites, $J_{PtC}$ = 619 Hz), 3.1 (dd with $^{195}$Pt satellites, $J_{PtC}$ = 406 Hz, $J_{PC}$ = 122 Hz, $J_{PC}$ = 7.9 Hz)
$^{31}$P-NMR (162 MHz, Methylene Chloride-$d_2$) **12a** δ -51.6 (d with $^{195}$Pt satellites, $J_{PtP}$ = 1078.7 Hz , $J_{pp}$ = 11.7 Hz), -52.4 (d with $^{195}$Pt satellites, $J_{PtP}$ = 1287.7 Hz , $J_{pp}$ = 13.8 Hz); **12b** δ -53.0 (s with $^{195}$Pt satellites, $J_{PtP}$ = 1258.8 Hz).
EA: Calculated: C, 22.52; H, 5.48; Found: C, 22.55; H, 5.48

**Chlorobis(trimethylphosphine)dimethylacetylplatinum(IV), 13**

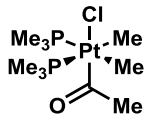

Starting from 76 mg (0.20 mmol) of platinum (II) complex **22**, 64 mg of **13** was obtained (70% yield).

$^{1}$H-NMR (600 MHz, Methylene Chloride-$d_2$) δ 2.08 (s with $^{195}$Pt satellites, $J_{PtH}$ = 13.0 Hz, 3H), 1.46 (d with $^{195}$Pt satellites, $J_{PH}$ = 9.8 Hz, $J_{PtH}$ = 11.6 Hz, 18H), 1.00 (dd with $^{195}$Pt satellites, $J_{PtH}$ = 57.4 Hz, $J_{PH}$ = 7.7 Hz, $J_{PH}$ = 6.2 Hz, 6H).
$^{13}$C-NMR (151 MHz, Methylene Chloride-$d_2$) δ 194.6 (s with $^{195}$Pt satellites, $J_{PtC}$ = 8.0 Hz), 36.6 (s with $^{195}$Pt satellites, $J_{PtC}$ = 220 Hz), 13.8 – 13.4 (m), 4.5 (dd with $^{195}$Pt satellites, $J_{PtC}$ = 454 Hz, $J_{PC}$ = 113 Hz, $J_{PC}$ = 9.0 Hz)
$^{31}$P-NMR (162 MHz, Methylene Chloride-$d_2$) δ -37.4 (s with $^{195}$Pt satellites, $J_{PtC}$ = 1413 Hz)
EA: Calculated: C, 26.35; H, 5.97; Found: C, 26.19; H, 5.75

**Bromobis(trimethylphosphine)dimethylallylplatinum(IV), 16**

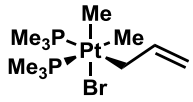

Starting from 200 mg (0.53 mmol) of platinum (II) complex **22**, 148 mg of **16** were obtained (56% yield). **17** was obtained predominantly as the depicted isomer with ~9% of the trans Br-allyl isomer. Spectroscopic characterization is provided only for the major isomer.

$^{1}$H-NMR (500 MHz, Methylene Chloride-$d_2$) δ 6.01 – 5.88 (m, 1H), 4.84 – 4.73 (m, 2H), 2.72 – 2.45 (m, 1H), 2.35 – 2.10 (m, 1H), 1.53 – 1.43 (m, 18H), 0.78 (at with $^{195}$Pt satellites, $J_{PtH}$ = 55.1 Hz, $J_{PH}$ = 7.8 Hz, 3H), 0.57 (t with $^{195}$Pt satellites, $J_{PtH}$ = 71.6 Hz, $J_{PH}$ = 7.3 Hz, 3H).
$^{13}$C-NMR (151 MHz, Methylene Chloride-$d_2$) δ 144.7, 109.2, 22.7 (dd, $J_{PC}$ = 116.9 Hz, $J_{PC}$ = 4.4 Hz), 13.5 (dd with $^{195}$Pt satellites, $J_{PC}$ = 28.5 Hz, $J_{PtC}$ = 10.1 Hz, $J_{PtC}$ = 1.6 Hz), 13.1 (dd with $^{195}$Pt satellites, $J_{PC}$ = 27.7 Hz, $J_{PtC}$ = 12.3 Hz, $J_{PtC}$ = 1.9 Hz), 6.8 (dd, $J_{PC}$ = 120 Hz, $J_{PC}$ = 6.3 Hz), -1.1 (at, $J_{PC}$ = 3.5 Hz).
$^{31}$P-NMR (162 MHz, Methylene Chloride-$d_2$) δ -43.2 (d with $^{195}$Pt satellites, $J_{PtP}$ = 1260 Hz , $J_{pp}$ = 13.6 Hz), -46.8 (d with $^{195}$Pt satellites, $J_{PtP}$ = 1270 Hz , $J_{pp}$ = 13.9 Hz).
EA: Calculated: C, 26.51; H, 5.87; Found: C, 26.59; H, 5.94

*Synthesis of cis-bis(trimethyl)phosphinetetramethylplatinum(IV), **23***

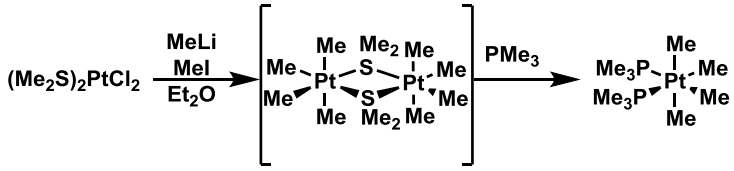

To a solution of bis(dimethylsulfide)dichloroplatinum(II) (390 mg, 1 mmol) in diethyl ether (0.1 M, 10 mL) was added iodomethane (0.4 mL, 6.5 mmol), and the solution was cooled to 0 °C. Methyllithium (1.9 mL of a 1.6M solution, 3 mmol) was added dropwise, and the mixture was stirred for 30 minutes at 0 °C, with formation of an orange precipitate. The mixture was quenched with saturated aqueous ammonium chloride, and the organic layer was separated. The aqueous layer was extracted three more times with diethyl ether and the combined organic

layers were dried over sodium sulfate, filtered and concentrated. The resulting product was immediately dissolved in diethyl ether and degassed. Trimethylphosphine (0.2 mL, 2.05 mmol) was added with immediate formation of a precipitate. The mixture was stirred for 30 min, and then filtered. The filtrate was concentrated, and the crude residue was further purified by chromatography on neutral alumina (80:20 benzene/pentane eluent) to afford the desired product as a colorless solid. (271 mg, 66% yield).

$^{1}$H-NMR (600 MHz, Methylene Chloride-$d_2$) δ 1.37 – 1.30 (d with $^{195}$Pt satellites, $J_{PH}$ = 8.4 Hz, $J_{PtH}$ = 11.6 Hz 18H), 0.35 – 0.18 (dd with $^{195}$Pt satellites $J_{PH}$ = 7.9 Hz, 6.8 Hz, $J_{PtH}$ = 56.7 Hz, 6H), -0.28 – -0.46 (t with $^{195}$Pt satellites, $J_{PH}$ = 6.6 Hz, $J_{PtH}$ = 44.3 Hz, 6H).
$^{13}$C-NMR (151 MHz, Methylene Chloride-$d_2$) δ 12.34 – 11.96 (m), 2.24 (dd with $^{195}$Pt satellites, $J_{PC}$ = 134.3, 8.3 Hz, $J_{PtC}$ = 523.0 Hz), -14.22 (t with $^{195}$Pt satellites, $J_{PC}$ = 5.0 Hz $J_{PtC}$ = 403.1 Hz).
$^{31}$P-NMR (243 MHz, Methylene Chloride-$d_2$) δ -54.61 (s with $^{195}$Pt satellites, $J_{PPt}$ = 1292.4 Hz)
EA: Calculated: C, 29.48; H, 7.42; Found: C, 29.83; H, 7.58

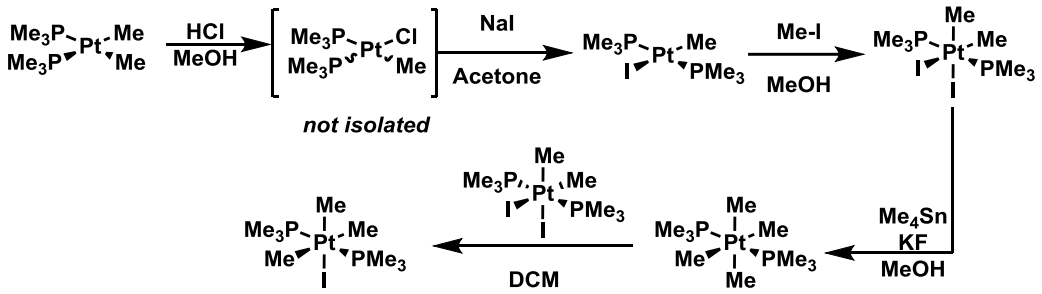


**Figure 3.45.** *Synthetic Scheme for **10, 24**, **25**, and **26***

### *Trans*-iodo(bistrimethylphosphine)methylplatinum(II), 10

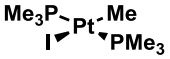

To a solution of bis(trimethylphosphine)dimethylplatinum(II) (2.44 g, 6.5 mmol) in methanol (0.1 M, 65 ml), was added a solution of HCl in methanol (13 mL, 6.5 mmol, 0.5 M, freshly prepared from acetyl chloride). The mixture was stirred for 20 minutes, and the precipitate was filtered off. The filtrate was concentrated, and carried on to the next step without further purification. The crude product (consisting of a mixture of cis- and trans- chloroplatinum complexes) was dissolved in acetone (60 mL) and a saturated solution of sodium iodide (1.84g, 13 mmol, 2 equiv) in acetone was added, with immediate formation of a precipitate. After 30 minutes, the mixture was filtered and the filtrate was concentrated. The mixture was extracted with diethyl ether, filtered through a plug of neutral alumina, and concentrated. This crude product was further purified by recrystallization from diethyl ether/hexanes by the layering method. Three crops of pale yellow crystals were collected, totaling 2.40g (76% yield).

$^{1}$H-NMR (600 MHz, Methanol-$d_4$) δ 1.58 (t with $^{195}$Pt satellites, $J_{PH}$ = 3.6 Hz $J_{PtH}$ = 28.1 Hz, 18H), 0.62 (t with $^{195}$Pt satellites, $J_{PH}$ = 7.1 Hz $J_{PtH}$ = 80.3 Hz, 3H).
$^{13}$C-NMR (151 MHz, Methanol-$d_4$) δ 13.57 (t with $^{195}$Pt satellites, $J_{CP}$ = 19.3 Hz $J_{CPt}$ = 79.1 Hz), -12.62 (t, $J$ = 6.1 Hz).

$^{31}$P-NMR (243 MHz, Methanol-$d_4$) δ -20.19 (s with $^{195}$Pt satellites, $J_{PPt}$ = 2660 Hz)
EA: Calculated: C, 17.19; H, 4.33; Found: C, 17.30; H, 4.20

**_cis,trans,cis_-diiodobis(trimethylphosphine)dimethylplatinum(IV), 24**

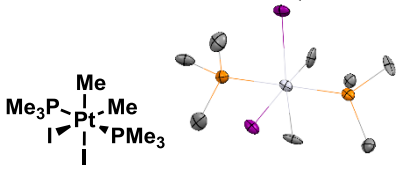


To a solution of **10** (1.22g, 2.5 mmol) in methanol (150 mL, 0.015 M) was added iodomethane (3.1 mL, 50 mmol). The mixture was stirred for 18 hours in the dark and then concentrated. The crude product was recrystallized from DCM/Methanol by the layering method yielding colorless needles (978 mg, 62% yield). X-ray quality crystals were obtained by vapor diffusion of diethyl ether into a saturated DCM solution.

$^{1}$H-NMR (600 MHz, Methylene Chloride-$d_2$) δ 1.93 (t with $^{195}$Pt satellites, $J_{PH}$ = 4.0 Hz $J_{PtH}$ = 18.9 Hz, 18H), 1.43 (t with $^{195}$Pt satellites, $J_{PH}$ = 5.7 Hz, $J_{PtH}$ = 65.9 Hz, 6H).
$^{13}$C-NMR (151 MHz, Methylene Chloride-$d_2$) δ 14.44 (t with $^{195}$Pt satellites, $J_{PC}$ = 10.1 Hz $J_{PtC}$ = 42.0 Hz) 6.51 (t, $J$ = 2.8 Hz $J_{PtC}$ = 539 Hz).
$^{31}$P-NMR (243 MHz, Methylene Chloride-$d_2$) δ -39.67 (s with $^{195}$Pt satellites. $J_{PtP}$ = 1950 Hz).
EA: Calculated: C, 15.22; H, 3.83; Found: C, 15.28; H, 3.80

**_trans_-bis(trimethylphosphine)tetramethylplatinum(IV), 26**

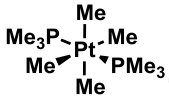


Tetramethyltin (1.67 mL, 12 mmol, 40 equiv.), potassium fluoride dihydrate (1.13 g, 12 mmol, 40 equiv) and **24** (189 mg, 0.3 mmol) were dissolved in methanol (30 mL, 0.01M). The solution was degassed and heated at 40 °C for 12 hours under $N_2$. The mixture was concentrated and the residue was extracted with dichloromethane, filtered, and concentrated. The resulting product was dissolved in hexanes and filtered through a short plug of neutral alumina, affording a light yellow solid which discolors upon extended exposure to air (82 mg, 67%).

$^{1}$H-NMR (500 MHz, Methylene Chloride-$d_2$) δ 1.33 (t with $^{195}$Pt satellites, $J_{PH}$ = 3.5 Hz $J_{PtH}$ = 18.8 Hz, 18H), -0.46 (t with $^{195}$Pt satellites, $J_{PH}$ = 5.7 Hz $J_{PtH}$ = 43.3 Hz, 12H).
$^{13}$C-NMR (126 MHz, Methylene Chloride-$d_2$) δ 8.98 (t with $^{195}$Pt satellites, $J_{PC}$ = 10.0 Hz $J_{PtC}$ = 39.1 Hz), -17.34 (t, $J_{PC}$ = 6.8 Hz).
$^{31}$P-NMR (202 MHz, Methylene Chloride-$d_2$) δ -36.68 (s with $^{195}$Pt satellites, $J_{PtP}$ = 2120 Hz).
EA: Calculated: C, 29.48; H, 7.42; Found: C, 29.48; H, 7.44

***trans,mer*-iodobis(trimethylphosphine)trimethylplatinum(IV), 25**

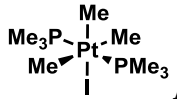


A mixture of **26** (82 mg, 0.2 mmol) and **24** (126 mg, 0.2 mmol) was dissolved in 4 mL of degassed dichloromethane (0.05 M) and heated at 40 °C for 12 hours, affording an equilibrated mixture of **24**, **25**, and **26** (~73% conversion). The mixture was dry loaded onto neutral alumina, and chromatographed, eluting on a gradient from pure hexanes to 20:80 diethyl ether/hexanes. The pure fractions were combined and concentrated, affording 78 mg of a pale yellow solid which discolors upon extended exposure to air (38% yield).

$^{1}$H-NMR (500 MHz, Methylene Chloride-$d_2$) δ 1.66 (t with $^{195}$Pt satellites, $J_{PH}$ = 3.7 Hz $J_{PtH}$ = 18.4 Hz, 18H), 0.80 (t with $^{195}$Pt satellites, $J_{PH}$ = 6.0 Hz $J_{PtH}$ = 68.2 Hz, 3H), 0.13 (t with $^{195}$Pt satellites, $J_{PH}$ = 5.6 Hz $J_{PtH}$ = 42.1 Hz, 6H).
$^{13}$C-NMR (126 MHz, Methylene Chloride-$d_2$) δ 11.95 (t with $^{195}$Pt satellites, $J_{PC}$ = 10.1 Hz $J_{PtC}$ = 41.0 Hz), 3.35 (t $J_{PC}$ = 3.7 Hz), -14.02 (t with $^{195}$Pt satellites, $J_{PC}$ = 6.2 Hz $J_{PtC}$ = 374 Hz).
$^{31}$P-NMR (202 MHz, Methylene Chloride-$d_2$) δ -38.70 (s with $^{195}$Pt satellites, $J_{PtP}$ = 2050 Hz).
EA: Calculated: C, 20.82; H, 5.24; Found: C, 20.93; H, 5.31

### 3.5.3 Procedures for Non-preparative Reactions

*General procedures for kinetics*

2-trimethylsilylethanol was used as an internal standard except for dual catalysis reactions, where dimethylacetamide was used in order to avoid overlapping with the tin-methyl resonances, and where otherwise noted. Platinum kinetics on **9** were performed with quantitatively decoupled $^{1}$H {$^{195}$Pt} NMR to eliminate satellites, which was tuned to optimally decouple the starting material resonances. Gold reactions were conducted at 25 °C, platinum reactions at 40 °C, and dual catalysis at 45 °C. Background reactions for **3-I**, **7-I**, and **9** were carried out in sealed NMR tubes and monitored by heating in an oil bath at the specified temperature, and taking time points on a daily basis. One scan was used per time point in order to minimize integration error. All solvents were sparged with nitrogen for 30 minutes prior to use.

*General procedure for kinetics analysis for halide dependence*

To an NMR tube, in an $N_2$ atmosphere wet glove box, was added cluster **1** (0.001 mmol, 0.1 eq.) and 2-trimethylsilylethanol (0.01 mmol, 1 eq.) as a solution in $CD_3OD$ (200 μL). The NMR tube was then fitted with a septum top and removed from the glove box, followed immediately by the application of parafilm to seal the edges of the septum. Immediately prior to the kinetics experiment, by microliter syringe the desired amount of potassium iodide was added as a solution in $CD_3OD$, in addition to excess $CD_3OD$ and finally **3-I**, **7-I**, or **9** (0.01 mmol, 1 eq.) as a solution in $CD_3OD$, such that the total volume in the tube was equal to 500 μL. The reaction mixture was then placed into the prewarmed, tuned and shimmed NMR spectrometer, and an automatic kinetics program was used to collect regular time points at 15 to 60 second intervals, depending on the rate of the reaction.

*General procedure for kinetics analysis for cluster dependence*

To an NMR tube, in an $N_2$ atmosphere wet glove box, was added cluster **1** (0.004 mmol, 0.1 eq.) and 2-trimethylsilylethanol (0.01 mmol, 1 eq.) as a solution in $CD_3OD$ (300 μL). The NMR tube was then fitted with a septum top and removed from the glove box, followed immediately by the application of parafilm to seal the edges of the septum. Immediately prior to the kinetics experiment, by microliter syringe, the desired amounts of $PEt_4BAr^f_4$ and $NaBAr^f_4$ were added as a solution in $CD_3OD$, and finally **3-I**, **7-I**, or **9** (0.01 mmol, 1 eq.) as a solution in $CD_3OD$, such that the total volume in the tube was equal to 500 μL. The reaction mixture was then placed into the prewarmed, tuned and shimmed NMR spectrometer, and an automatic kinetics program was used to collect regular time points at 15 to 60 second intervals, depending on the rate of the reaction.

*General procedure for kinetics analysis for Substrate dependence*

To an NMR tube, in an $N_2$ atmosphere wet glove box, was added cluster **1** (0.001 mmol, 0.1 eq.) and 2-trimethylsilylethanol (0.01 mmol, 1 eq.) as a solution in $CD_3OD$ (100 μL). The NMR tube was then fitted with a septum top and removed from the glove box, followed immediately by the application of parafilm to seal the edges of the septum. Immediately prior to the kinetics experiment, by microliter syringe, the desired amount of $CD_3OD$, followed by the desired amount of **3-Br**, **7-I**, or **9** as a solution in $CD_3OD$, such that the total volume in the tube was equal to 500 μL. The reaction was then placed into the prewarmed, tuned and shimmed NMR spectrometer, and an automatic kinetics program was used to collect regular time points at 15 to 60 second intervals, depending on the rate of the reaction.

*General procedure for dual catalysis:*

A J. Young tube was charged with bis(trimethylphosphine)dimethylplatinum(II) (**22**) (3.8 mg, 0.01 mmol, 0.1 equiv.) and cluster **2** (24 mg, 0.005 mmol, 0.05 equiv.). The tube was then transferred to an wet-atmosphere $N_2$ atmosphere glove box, and methyl iodide (28.3 mg, 0.2 mmol, 2 equiv.), tetramethyl tin (17.9 mg, 0.l mmol, 1 equiv.), potassium fluoride (11.6 mg, 0.2 mmol, 2 equiv.) and dimethylacetamide (1.74 mg, 0.02 mmol, 0.2 equiv.) (as an internal standard) were added as a stock solution in methanol-$d_4$ (0.80 mL) and D2O (0.20 mL). The tube was then sealed, removed from the glove box and placed into a preheated, tuned and shimmed NMR spectrometer at 45 ºC. Scans were collected at 480 second intervals. For the control reaction, cluster **2** was omitted.

<u>General procedure for encapsulation of "donor arrested reductive elimination" complexes:</u>

– *Trimethylphosphine and dimethylsulfide:*

To an NMR tube was added platinum complex **9** (5.2 mg, 0.01 mmol, 1.0 equiv). The NMR tube was brought into an $N_2$ atmosphere wet glove box, and cluster **1** (0.002 mmol, 0.2 equiv) was added as a solution in $CD_3OD$ (500 μL). Agitation was minimized to keep the dissolution of **5** to a minimum, and thus minimize background reductive elimination prior to the addition of the neutral donor. A septum topped NMR cap was added to the NMR tube, and the tube was removed from the glovebox, followed immediately by the application of parafilm to seal the edges of the septum. Trimethyl phosphine or dimethyl sulfide (0.02 mmol, 2.0 equiv) was

added by microliter syringe through the septum top of the NMR tube. The septum top was further sealed with electrical tape, and the tube was sonicated until homogeneous. Encapsulation was then assessed by $^1$H-NMR spectroscopy.

– *Platinum allyl:*

To an NMR tube was added platinum complex **16** (2.5 mg, 0.005 mmol, 1.0 equiv). The NMR tube was brought into an $N_2$ atmosphere wet glove box, and cluster **1** (0.00625 mmol, 1.25 equiv) was added as a solution in $CD_3OD$ (500 μL). The NMR tube was capped, and the tube was removed from the glovebox, followed immediately by the application of parafilm to seal the edges of the cap. Encapsulation was then assessed by $^1$H-NMR spectroscopy.

– *Platinum butenyl, pentenyl, and hexenyl complexes:*

To an NMR tube was added Pt(II) complex **22** (5.7 mg, 0.015 mmol, 1.0 equiv), followed by acetone-$d_6$ (0.5 mL) and then the appropriate alkyl iodide (butenyl-, pentenyl or hexenyliodide) (0.225 mmol, 15.0 equiv). The reaction was placed in a oil bath, which was preheated to 40 ºC. After 4 hours, the NMR tube was placed in a vacuum chamber, and volatiles were removed *in vacuo*. The NMR tube, with the crude Pt(IV) residue, was pumped into an $N_2$ atmosphere wet glove box, and cluster **1** (0.005 mmol, 0.33 equiv) was added as a solution in $CD_3OD$ (500 μL). The NMR tube was capped, and the tube was removed from the glovebox, followed immediately by the application of parafilm to seal the edges of the cap. Encapsulation was then assessed by $^1$H-NMR spectroscopy.

Kinetics for cluster promoted acidolysis of **23**:

To an NMR tube, in an $N_2$ atmosphere wet glove box, was added platinum tetramethyl complex **23** (0.005 mmol, 1.0 equiv) and dimethylacetamide (internal standard) (0.005 mmol, 1.0 equiv) as a stock solution in methanol-$d_4$ (400 μL). Cluster **1** (0.00125 mmol, 0.25 equiv) was added as a stock solution in $D_2O$ (100 μL). The NMR tube was capped and removed from the glove box, followed immediately by the application of parafilm to seal the edges of the cap. The reaction mixture was then placed into the prewarmed, tuned and shimmed NMR spectrometer, and an automatic kinetics program was used to collect regular time points at 60-second intervals. Time between the addition of **1** and first acquisition was minimized, and was generally about 120 seconds.

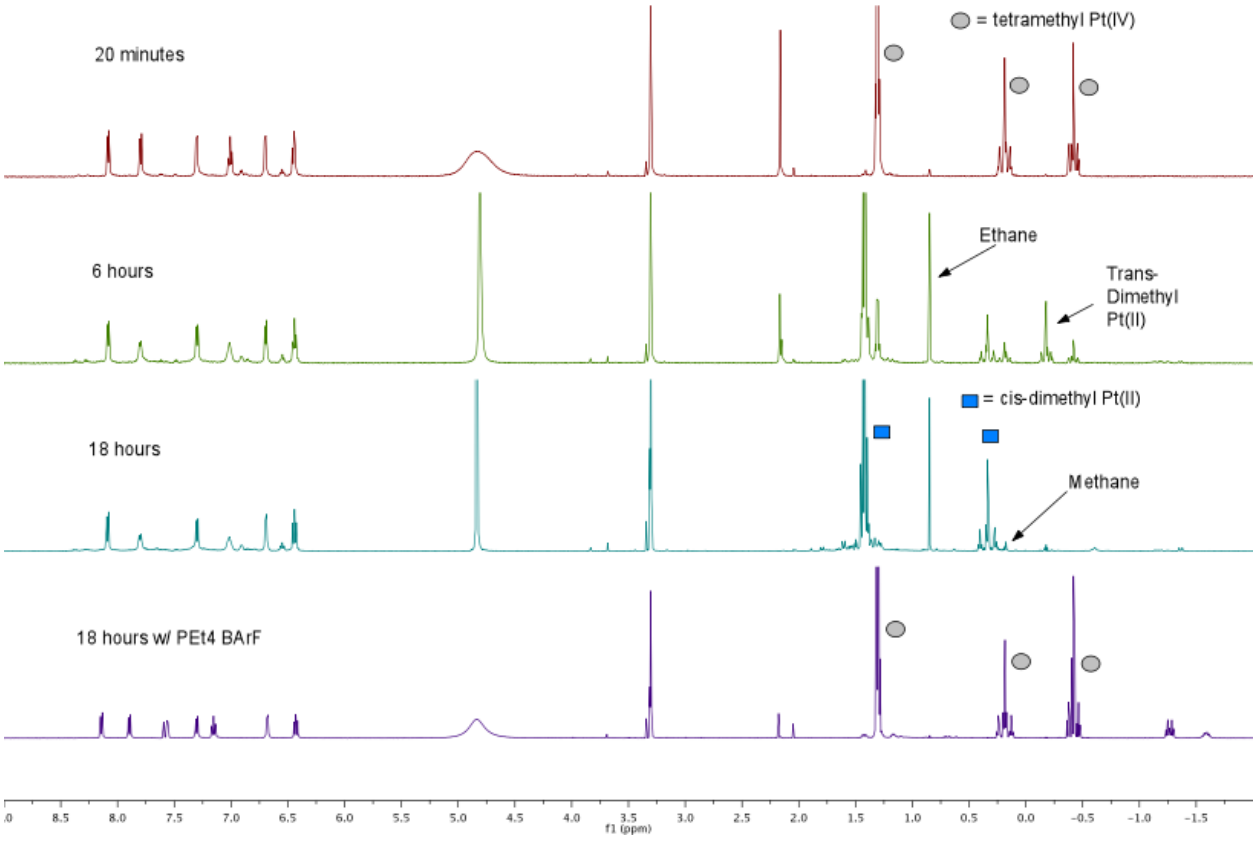


**Figure 3.46.** Representative $^1$H-NMR spectra from the cluster promoted acidolysis of **23**.

Competition between transmetallation and oxidative addition to **10**:

– *Transmetallation:*

To an NMR tube, in an $N_2$ atmosphere wet glove box, was added platinum(II) complex **10** (0.0025 mmol, 1.0 equiv) and platinum(IV) complex **9** (0.0025 mmol, 1.0 equiv) and dimethylacetamide (internal standard) (0.02 mmol, 8.0 equiv) as a stock solution in 8:2 methanol-$d_4$:$D_2O$ (300 μL). The NMR tube was then fitted with a septum top and removed from the glove box, followed immediately by the application of parafilm to seal the edges of the

septum. Immediately prior to the kinetics experiment, tetramethyl tin (0.05 mmol, 20 equiv) and potassium fluoride (0.1 mmol, 40 equiv) were added by microliter syringe as a solution in 8:2 methanol-$d_4$:$D_2O$ (200 μL). The reaction mixture was then placed into the prewarmed (45 ºC), tuned and shimmed NMR spectrometer, and an automatic kinetics program was used to collect regular time points at 60 second intervals.

– *Oxidative Addition:*

To an NMR tube, in an $N_2$ atmosphere wet glove box, was added platinum(II) complex **10** (0.0025 mmol, 1.0 equiv) and dimethylacetamide (internal standard) (0.02 mmol, 8.0 equiv) as a stock solution in 8:2 methanol-$d_4$:$D_2O$ (300 μL). The NMR tube was then fitted with a septum top and removed from the glove box, followed immediately by the application of parafilm to seal the edges of the septum. Immediately prior to the kinetics experiment, methyl iodide (0.05 mmol, 20 equiv) was added by microliter syringe as a solution in 8:2 methanol-$d_4$:$D_2O$ (200 μL). The reaction mixture was then placed into the prewarmed (45 ºC), tuned and shimmed NMR spectrometer, and an automatic kinetics program was used to collect regular time points at 60 second intervals.

Kinetic investigation of **25** under kinetically relevant conditions:

To an NMR tube, in an $N_2$ atmosphere wet glove box, was added cluster **2** (0.001 mmol, 0.1 eq.) and dimethylacetamide (0.01 mmol, 1 eq.) as a solution in $CD_3OD$ (225 μL) and $D_2O$ (75 μL). The NMR tube was then fitted with a septum top and removed from the glove box, followed immediately by the application of parafilm to seal the edges of the septum. Immediately prior to the kinetics experiment, **25** (0.01 mmol, 1 eq.) was added by microliter syringe as a solution in $CD_3OD$ (300μL). The reaction mixture was then placed into the prewarmed, tuned and shimmed NMR spectrometer, and an automatic kinetics program was used to collect regular time points at 15 to 60 second intervals, depending on the rate of the reaction. While the disappearance of **25** could be tracked, overlapping peaks of the isomerized Pt(IV) complex **9**, and the product of reductive elimination, **10**, prevented deconvolution of the two relative rates. However, since the disappearance of **25** is significantly faster than catalyzed reductive elimination from **9**, the ratio of **9** and **10** when **25** is consumed is similar to ratio of the rates for cluster catalyzed isomerization of **25** and reductive elimination from **25**. Note the difference in scale of the x-axes on the plots below for data collected at 25 and 45 degrees Celsius.

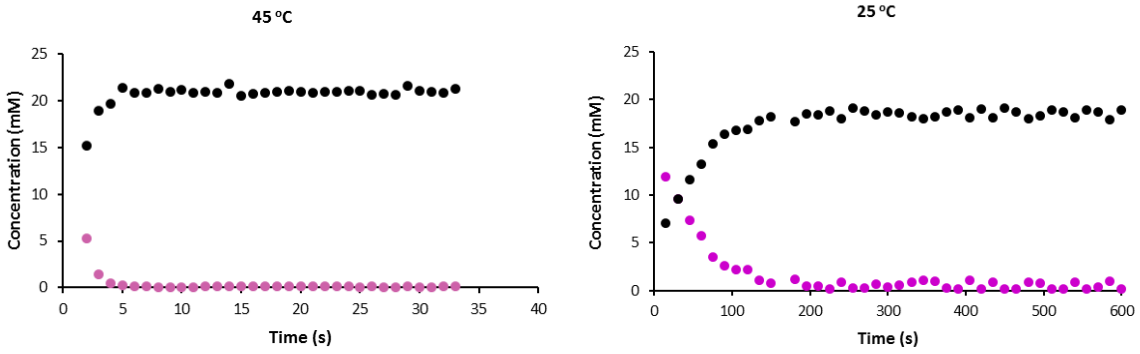


**Figure 3.47.** Kinetic traces showing rapid consumption of **25** in the presence of **2**. Pink = **25**, black = combined [Pt] products (**9** and **10**)

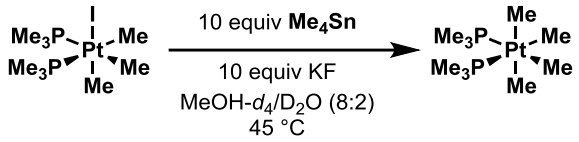


To a solution of **9** (2.6 mg, 0.005 mmol, prepared as a stock solution) in Methanol-$d_4$/$D_2O$ (4:1, 0.5 mL total) was added 7 μL (0.05 mmol, 10 equiv) of tetramethyl tin, and 5 mg of potassium fluoride dihydrate (0.05 mmol, 10 equiv). After 20 minutes at room temperature, a $^1$H-NMR spectrum was recorded, showing a 1.5:1 ratio of **9** to **23**, with concomitant formation of $Me_3SnF$. The mixture was heated at 45 °C for 3 hours, and a $^1$H-NMR spectrum was again recorded, showing a 1.2:1 ratio of **9** to **23**.

When this procedure was followed omitting potassium fluoride, the concentration of **23** was below the detection limit for $^1$H-NMR (>30:1), even after heating.

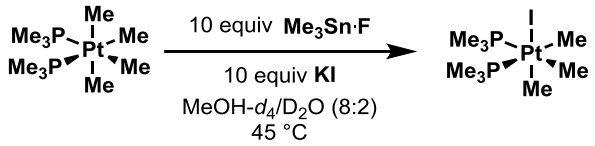


To a solution of **23** (2.0 mg, 0.005 mmol, prepared as a stock solution) in Methanol-$d_4$/$D_2O$ (4:1, 0.5 mL total) was added 9 mg of trimethyltin fluoride (0.05 mmol, 10 equiv) and 8 mg of potassium iodide (0.05 mmol, 10 equiv). After 15 minutes at room temperature, a $^1$H-NMR spectrum was recorded, showing complete conversion to **9**.

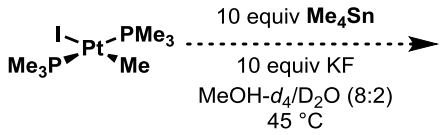


To a solution of **10** (2.5 mg, 0.005 mmol, prepared as a stock solution) in Methanol-$d_4$/$D_2O$ (4:1, 0.5 mL total) was added 7 μL (0.05 mmol, 10 equiv) of tetramethyl tin, and 5 mg of potassium fluoride dihydrate (0.05 mmol, 10 equiv). After 20 minutes at room temperature, a $^1$H-NMR spectrum was recorded, showing no reaction. The mixture was heated at 45 °C for 3 hours, and a $^1$H-NMR spectrum was again recorded, again showing no reaction.

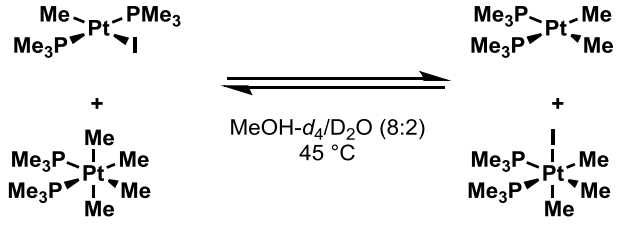


To a solution of **10** (2.5 mg, 0.005 mmol, prepared as a stock solution) in Methanol-$d_4$/$D_2O$ (4:1, 0.5 mL total) was added 6 mg of **23** (0.015 mmol, 3 equiv). The mixture was heated at 45 °C for 3 hours, and a $^1$H-NMR spectrum was recorded, showing the formation of **9** and **22** in approximately equimolar amounts.

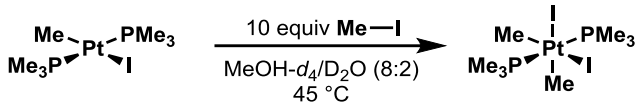


To a solution of **10** (2.5 mg, 0.005 mmol, prepared as a stock solution) in Methanol-$d_4$/$D_2O$ (4:1, 0.5 mL total) was added 3 μL of iodomethane (0.05 mmol, 10 equiv). The mixture was heated at at 45 °C for 30 minutes, and a $^1$H-NMR spectrum was recorded, showing the formation of **24** (approx. 30% conversion). Heating was continued for an additional four hours, and a $^1$H-NMR spectrum was again recorded, showing approximately 95% conversion to give **24**.

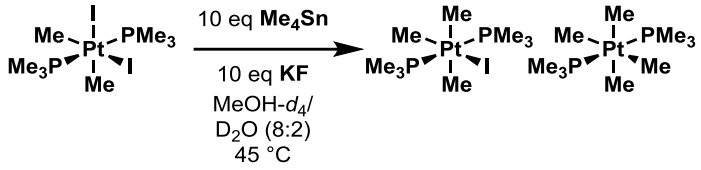


To a solution of **24** (6.3 mg, 0.01 mmol, prepared as a stock solution) in Methanol-$d_4$/$D_2O$ under $N_2$ (4:1, 0.5 mL total) was added 13.8 μL of tetramethyl tin (0.1 mmol, 10 equiv) and 9.4 mg of potassium fluoride dehydrate (0.1 mmol, 10 equiv). The mixture was heated at at 45 °C for 30 minutes, and a $^1$H-NMR spectrum was recorded, showing the formation of **25** and **26** (55:42:3 **24**/**25**/**26**). Heating was continued for an additional three hours, and a $^1$H-NMR spectrum was again recorded, showing complete consumption of **24**, and an 8:2 ratio of **25** to **26**.

*Control experiments for acid catalysis of reductive elimination:*

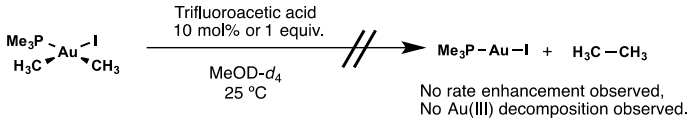


To a solution of **3-I** (0.01 mmol, 4.3 mg) in Methanol-$d_4$ (0.4 mL) was added a solution of trifluoroacetic acid (0.1 mL, either 0.01 mmol of TFA or 0.001 mmol of TFA, with solutions prepared by serial dilution in volumetric glassware). The reaction mixtures (in NMR tubes) were places in a bath maintained at 25 °C sealed with septa, and the mixture was monitored periodically for 4 days via $^1$H-NMR. No significant deviation from the observed background rate of reductive elimination was observed, and no Au(III) decomposition was observed.

## 3.5.4 Supporting Figures and Observations

*Derivation of the rate law*

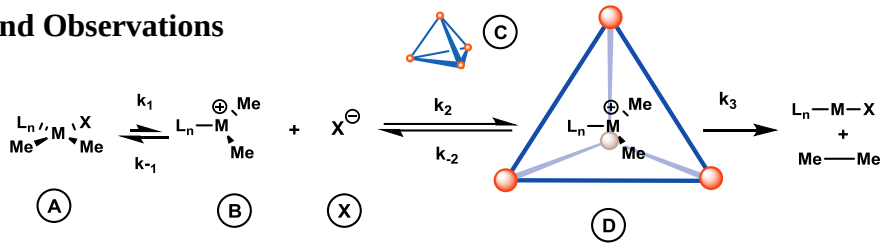


$$\frac{d[D]}{dt} = k_2[B][C] - k_{-2}[D] - k_3[D]$$

$$[C] = [C]_0 - [D]$$

$$\frac{d[D]}{dt} = k_2[B]\left([C]_0 - [D]\right) - k_{-2}[D] - k_3[D] = k_2[B][C]_0 - [D]\left(k_2[B] + k_{-2} + k_3\right)$$

Steady State Approximation: $\frac{d[D]}{dt} = 0$

$$0 = k_2[B][C]_0 - [D]\left(k_2[B] + k_{-2} + k_3\right)$$

$$[D] = \frac{k_2[B][C]_0}{k_2[B] + k_{-2} + k_3} = \frac{[B][C]_0}{[B] + \frac{k_{-2} + k_3}{k_2}}$$

Pre-equilibrium Approximation: $K_1 = \frac{k_1}{k_{-1}} = \frac{[B][X]}{[A]}$

$$[B] = \frac{K_1[A]}{[X]}$$

$$[D] = \frac{\frac{K_1[A]}{[X]}[C]_0}{\frac{K_1[A]}{[X]} + \frac{k_{-2} + k_3}{k_2}} = \frac{[A][C]_0}{[A] + \frac{k_{-2} + k_3}{K_1 k_2}[X]}$$

$$\frac{d[P]}{dt} = k_3[D] = \frac{k_3[A][C]_0}{[A] + \frac{k_{-2} + k_3}{K_1 k_2}[X]}$$

$k_3 = k_{cat}$

*So,*

$$Rate = \frac{k_{cat}[A][C]_0}{[A] + \frac{k_{-2} + k_{cat}}{K_1 k_2}[X]}$$

Alternatively, if you apply a pre-equilibrium approximation to [D] instead of a Steady-State approximation:

$$K_2 = \frac{k_2}{k_{-2}} = \frac{[D]}{[B][C]}$$

$$[D] = K_2[B][C] = K_2[B][C]_0 - K_2[B][D]$$

$$[D](1 + K_2[B]) = K_2[B][C]_0$$

$$[D] = \frac{K_2[B][C]_0}{1 + K_2[B]} = \frac{K_2\left(\frac{K_1[A]}{[X]}\right)[C]_0}{1 + K_2\left(\frac{K_1[A]}{[X]}\right)} = \frac{K_2 K_1[A][C]_0}{[X] + K_2 K_1[A]} = \frac{[A][C]_0}{[A] + \frac{1}{K_1 K_2}[X]}$$

*So,*

$$Rate = \frac{k_{cat}[A][C]_0}{[A] + \frac{1}{K_1 K_2}[X]}$$

Note, that these are indistinguishable experimentally and that in the limit that $k_{cat} << k_{-2}$

$$\frac{k_{-2} + k_{cat}}{K_1 k_2} \approx \frac{k_{-2}}{K_1 k_2} = \frac{1}{K_1 K_2}$$

We favor the steady state approximation as it is the more general solution.

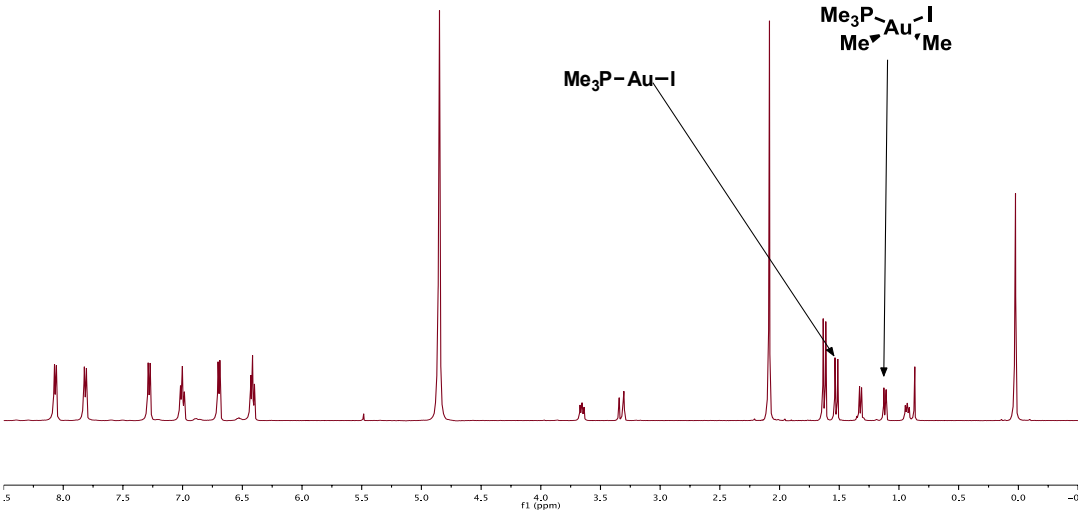


**Figure 3.48.** A representative spectrum from the kinetics analysis of the cluster catalyzed reductive elimination from **3-I**.

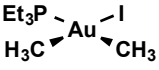


**(7-I)**

Representative trace:

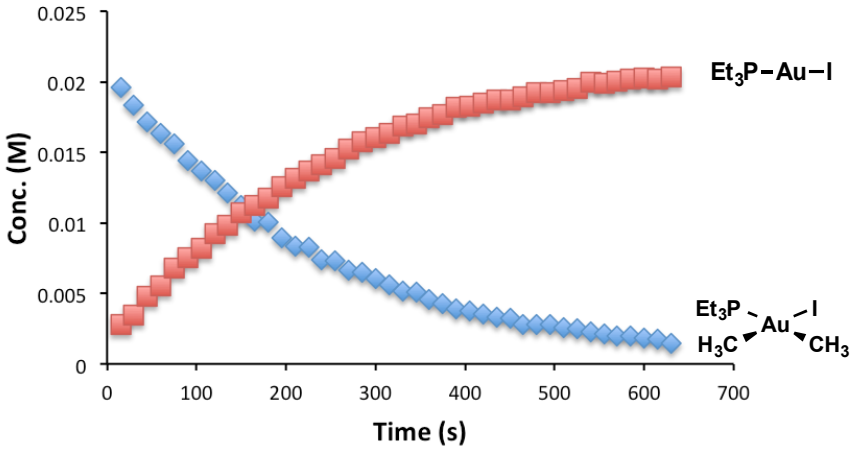


**Figure 3.49.** A representative kinetic trace of cluster catalyzed reductive elimination from **7-I**.

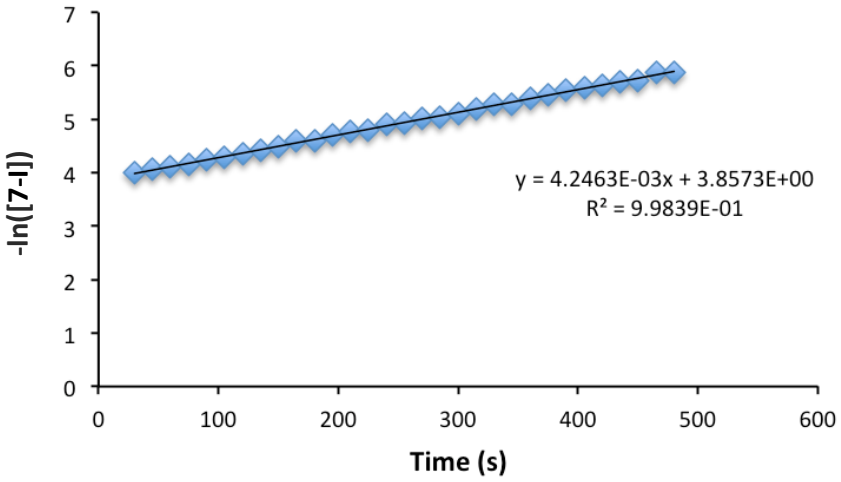


**Figure 3.50.** Natural log plot affording the first order rate constant for the catalyzed reductive elimination from **7-I**.

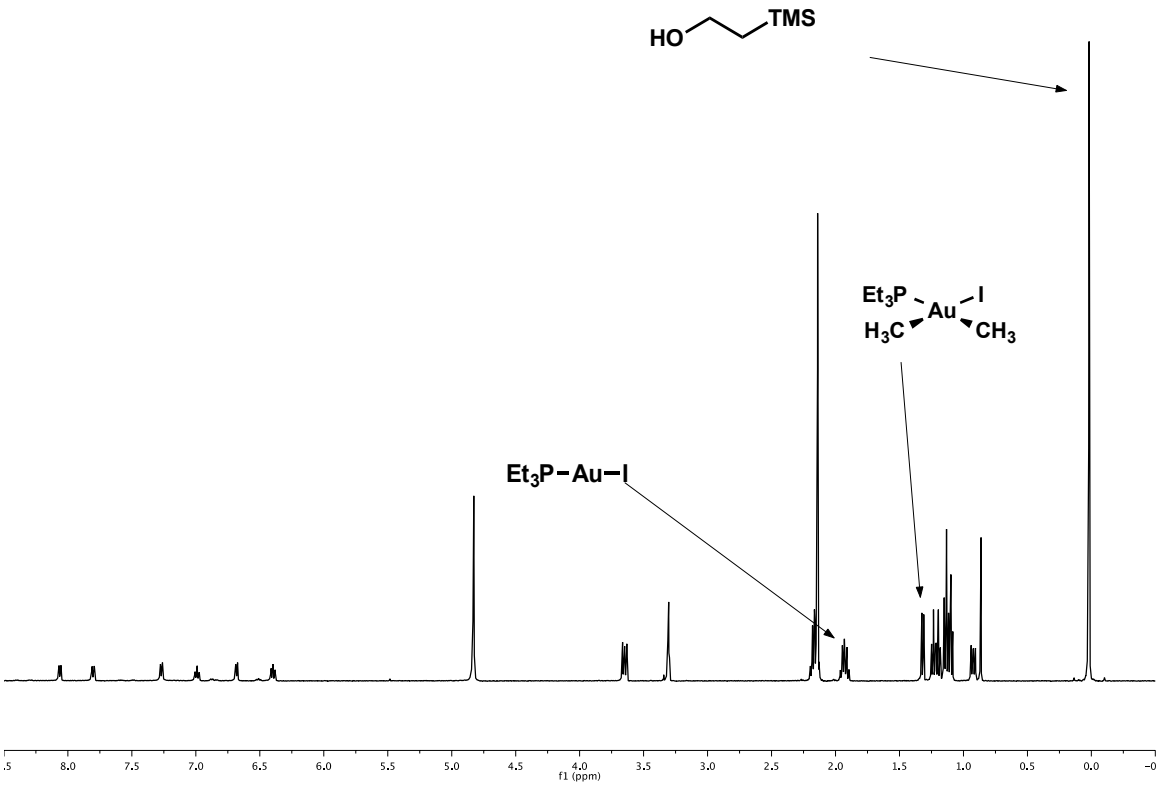


**Figure 3.51.** A representative spectrum from the kinetics analysis of the catalyzed reductive elimination from **7-I**.

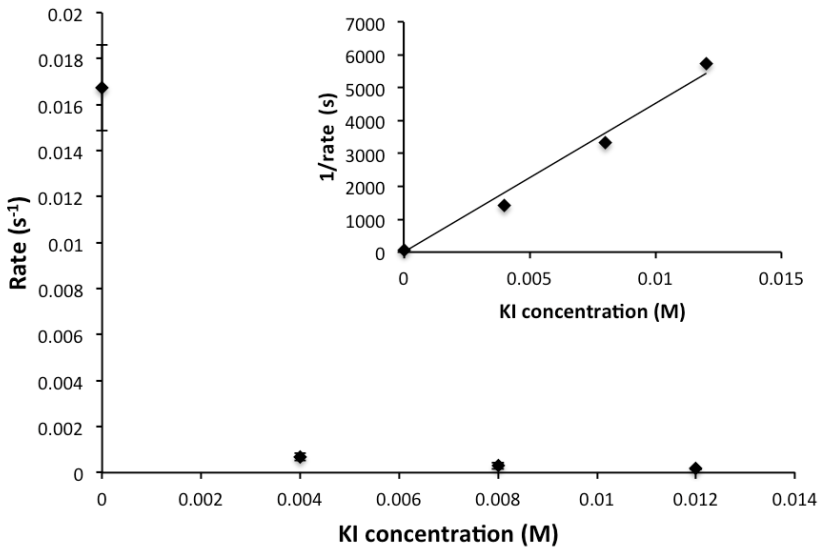


**Figure 3.52.** Rate dependence of catalyzed reductive elimination from **7-I** on iodide concentration. All error bars represent one standard deviation based on three replicates.

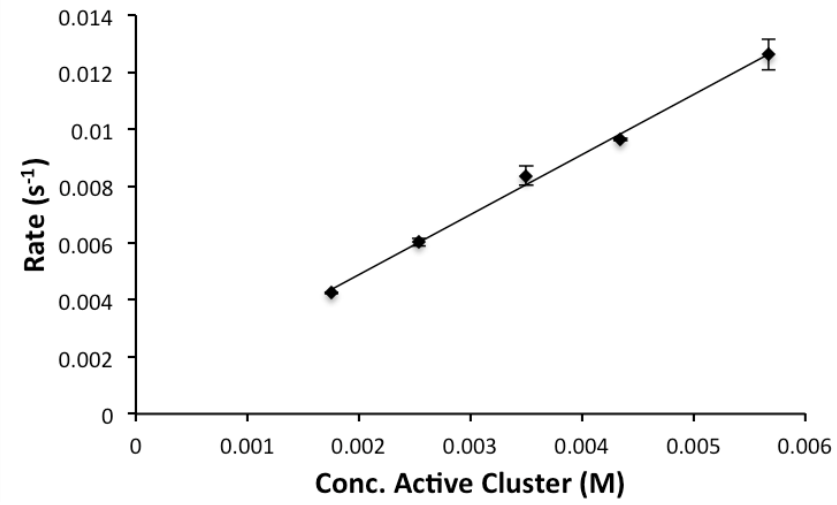


**Figure 3.53.** Rate dependence of catalyzed reductive elimination from **7-I** on active cluster concentration. All error bars represent one standard deviation based on three replicates.

*RPKA Data for Figure 3.4 were generated by application of the Five-Point Stencil method for numerical differentiation*

$$\left[ f'(t) \approx \frac{-f(t+2h)+8f(t+h)-8f(t-h)+f(t-2h)}{12h} \right],\ h=15\ s$$

*to three independent runs for the reductive elimination of ethane from **4** catalyzed by **1** with a starting concentration for **7-I** of 0.1M. The resulting three data sets for rate vs. concentration were aggregated to give the blue data points shown in Figure 3.4. Similar results were obtained using a polynomial fit method for numerical differentiation. The former method is preferred due to the introduction of artifacts at the high and low concentration ends of the data by the polynomial fit method.*

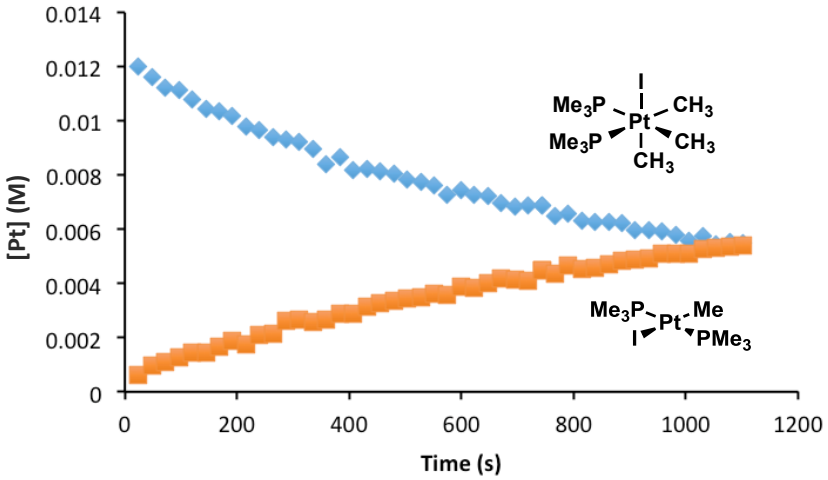


**Figure 3.54.** A representative kinetic trace of catalyzed reductive elimination from **9**.

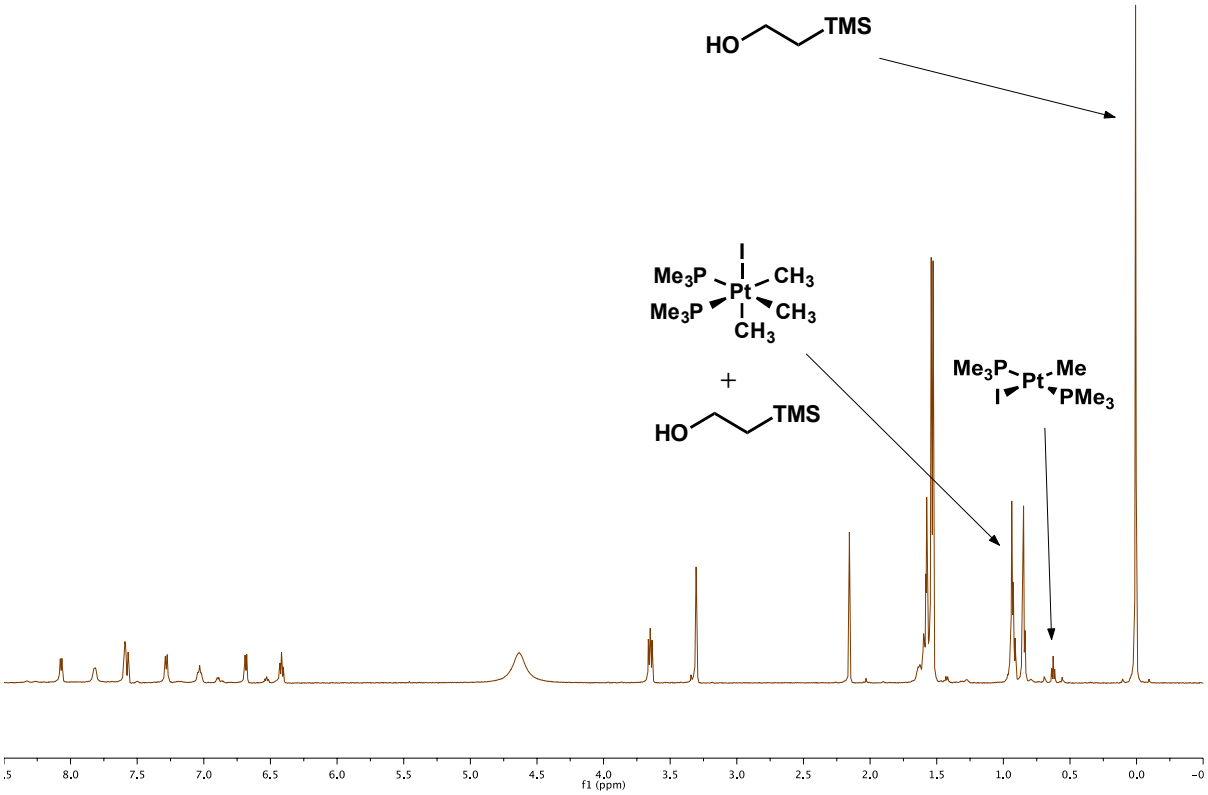


**Figure 3.55.** A representative spectrum from the kinetics analysis of the catalyzed reductive elimination from **9**.

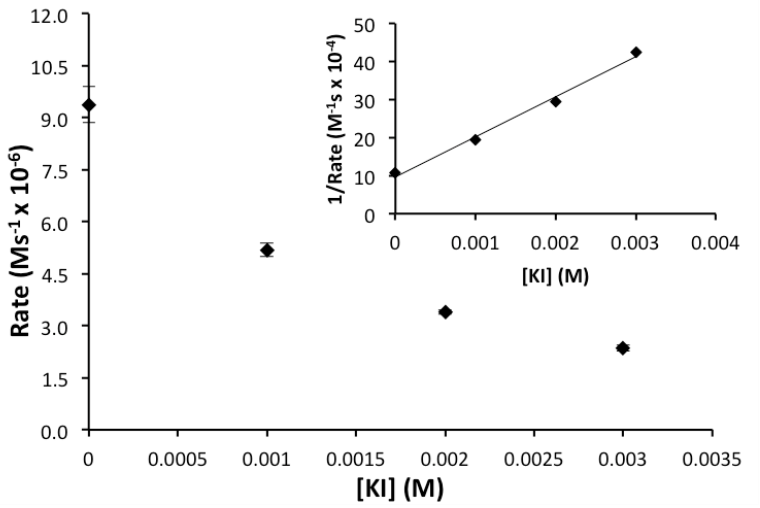


**Figure 3.56.** Rate dependence of catalyzed reductive elimination from **9** on iodide concentration. All error bars represent one standard deviation based on three replicates.

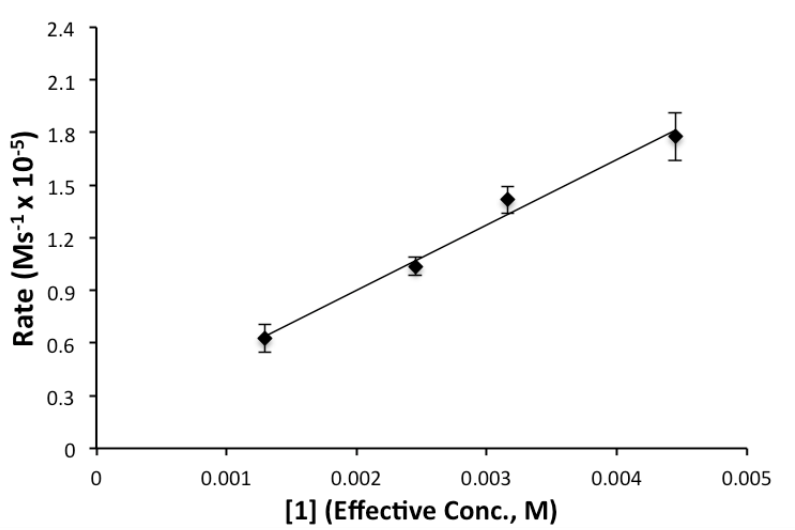


**Figure 3.57.** Rate dependence of catalyzed reductive elimination from **9** on active cluster concentration. All error bars represent one standard deviation based on three replicates.

*Representative Spectra of Platinum Speciation for Dual Catalysis*

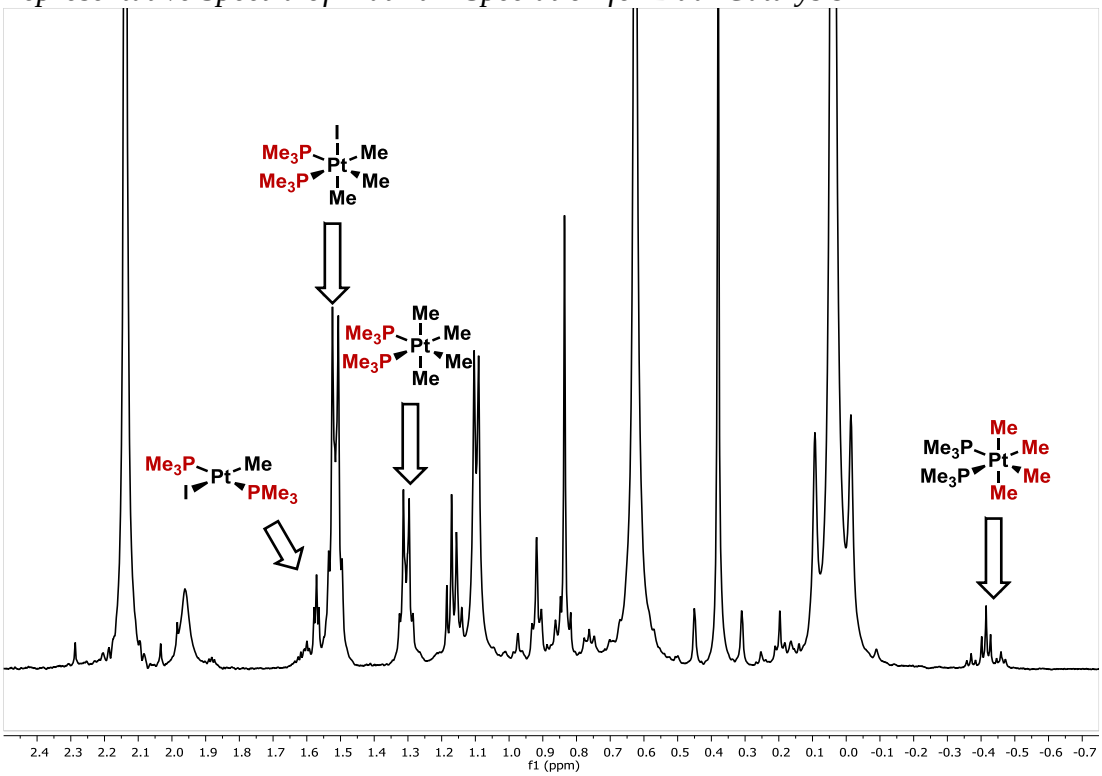


**Figure 3.58.** Representative spectrum for platinum speciation under dual catalytic conditions at early reaction times.

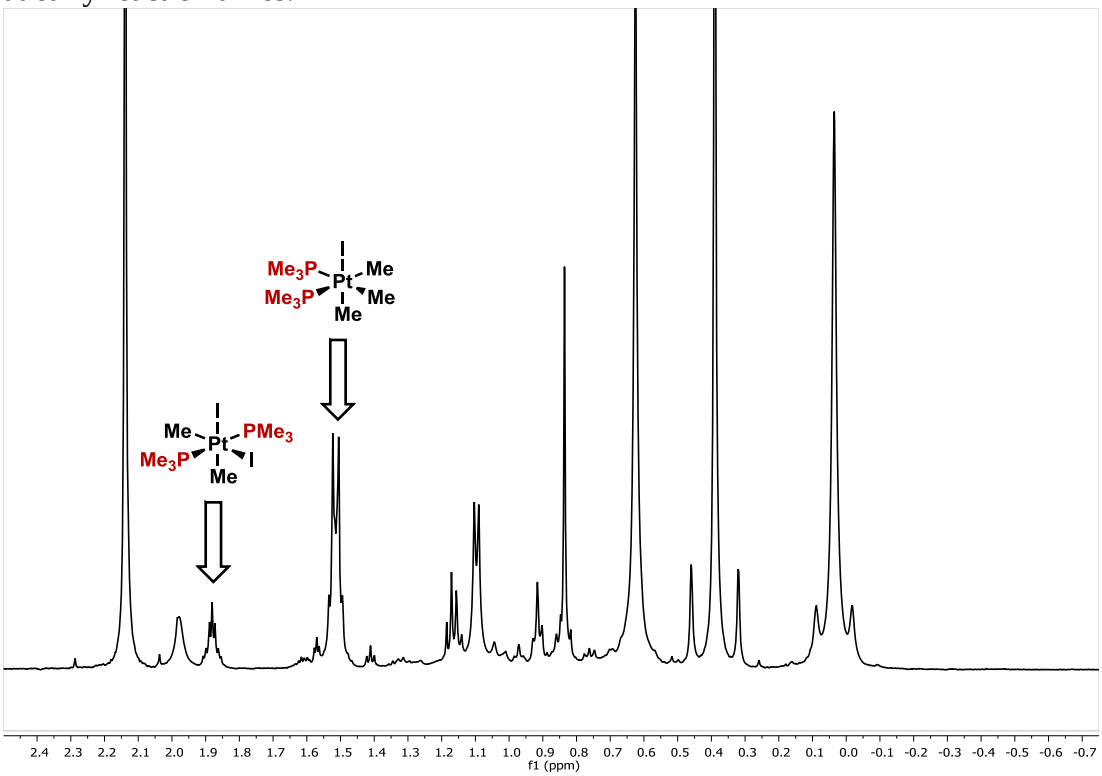


**Figure 3.59.** Representative spectrum for platinum speciation under dual catalytic conditions at late reaction times.

*Precatalyst examination*

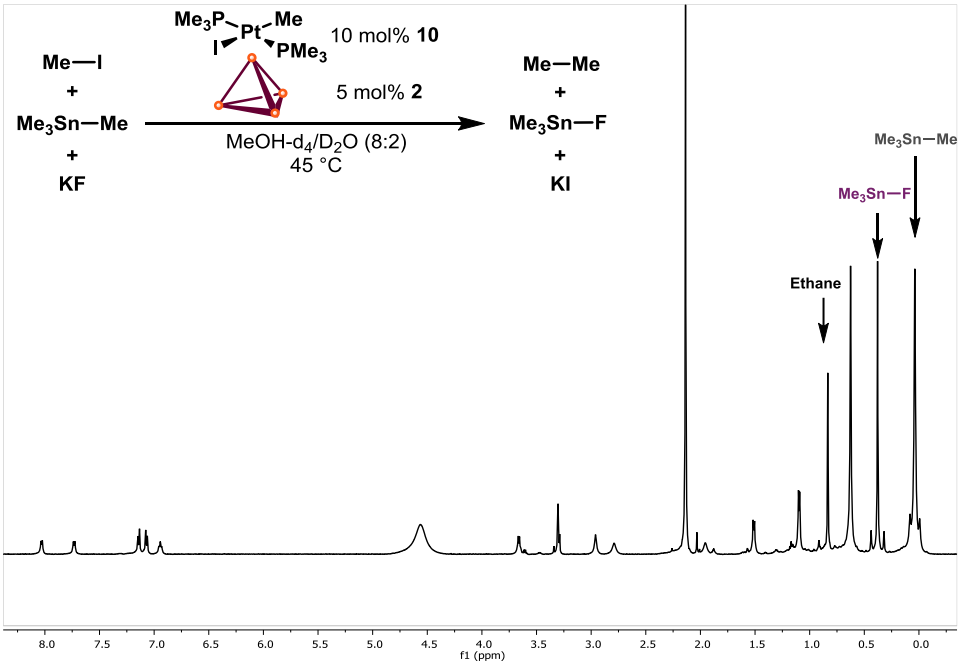


**Figure 3.60**. Representative NMR spectrum for dual catalysis with **10** and **2**.

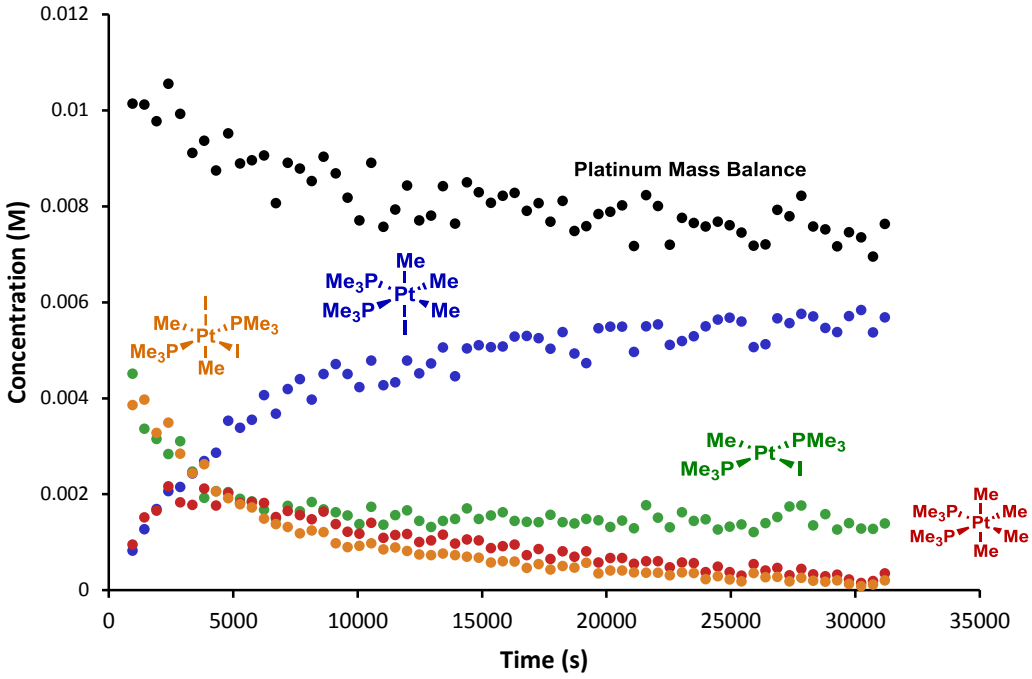


**Figure 3.61**. Platinum concentrations under dual catalysis with **10** and **2**, showing mass balance decrease due to precipitation of **24** (orange)

*In order to probe whether or not methyl groups were incorporated from both iodomethane and tetramethyl tin, a labeling experiment was performed using $d_3$-iodomethane. It was expected that $d_0$-, $d_3$-, and $d_6$-ethane would be observed due to both inter- and intra-molecular scrambling of alkyl groups on platinum complexes. It is unknown which two of three methyl groups on a given $[Pt^{IV}]Me_3$ complex reductively eliminate.*

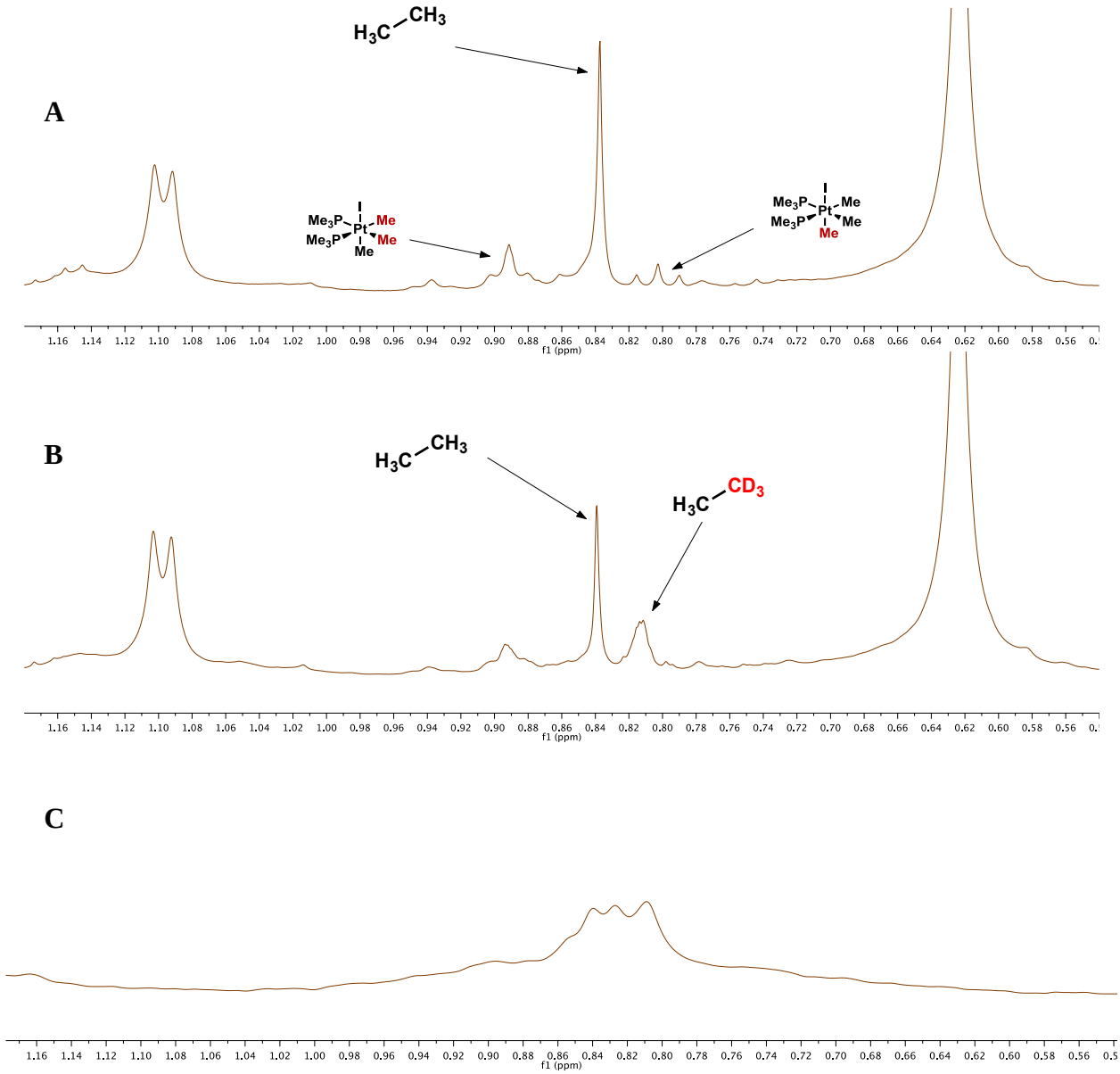


**Figure 3.62.** Iodomethane labeling experiment. (**A**) Proton NMR spectrum of dual catalytic cross coupling with proteomethyl iodide starting material. Only $H_6$-ethane is detectable. (**B**) Proton NMR spectrum of coupling with trideuteromethyl iodide starting material. Both $H_6$-ethane and $d_3$-ethane are detectable (**C**) Deuterium NMR spectrum of coupling with trideuteromethyl iodide starting material. Peaks at 0.82 ppm are consistent with a mixture of $d_3$-ethane and $d_6$-ethane.

*Copasi Model:*

Global kinetic modeling was performed using COPASI modeling software (http://www.copasi.org). These individual rate constants do not have have any intrinsic significance as the number of kinetic constants being fit results in this model being underdetermined (7 observables and 11 parameters). Rather, this is meant to demonstrate that it is *possible for the proposed mechanism to yield kinetics with the same overall characteristics as those experimentally observed.*

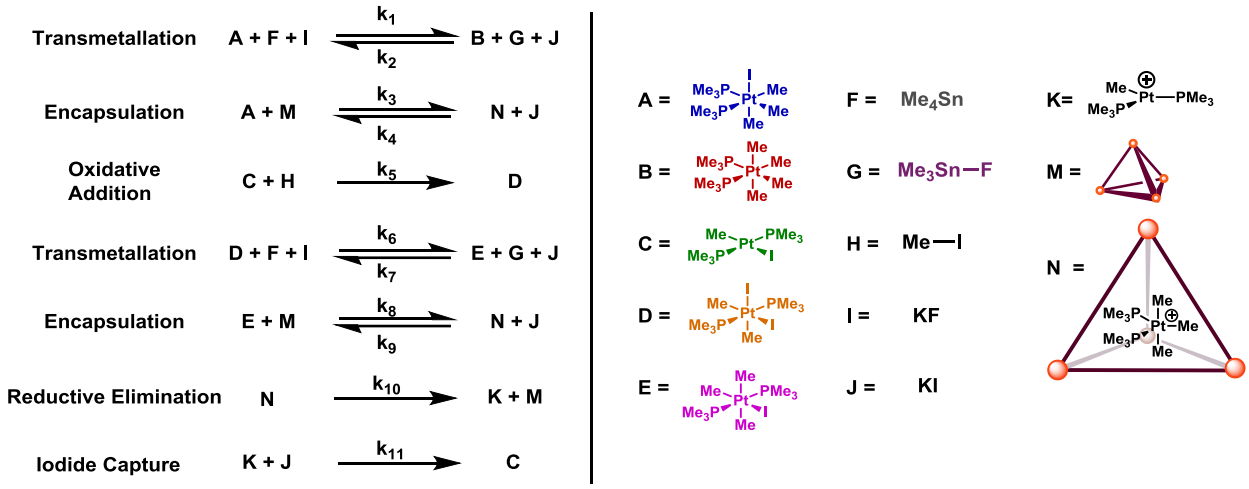


**Figure 3.63**. Copasi Model

Parameter estimation was performed on $k_1$- $k_{10}$ with the constraints of $0.001 < k_5 < 0.1$, based on the measured rate for oxidative addition under similar conditions of 0.010 $M^{-1}s^{-1}$ and $0.002 < k_{10} < 0.2$ based on the measured $k_{cat}$ at 40°C with supramolecular catalyst **1** of 0.024 $s^{-1}$. (In the former case, the supramolecular assembly **2** is expected to exert a salt effect slowing oxidative addition, and in the latter, the higher temperature and different supramolecular assembly were expected to increase $k_{10}$, though neither of the absolute numbers obtained for the fitted data should be interpreted with particular significance). The model was optimized using the Evolutionary Strategy (SRES) method to yield the kinetic constants in Table S1, and the starting values were randomized several times to counteract false minima. Most repetitions of the simulation converged to the given values after several iterations of optimization. The simulation results for **9**, **10**, **23**, **24**, iodomethane, tetramethyl tin, and trimethyltin fluoride are shown below.

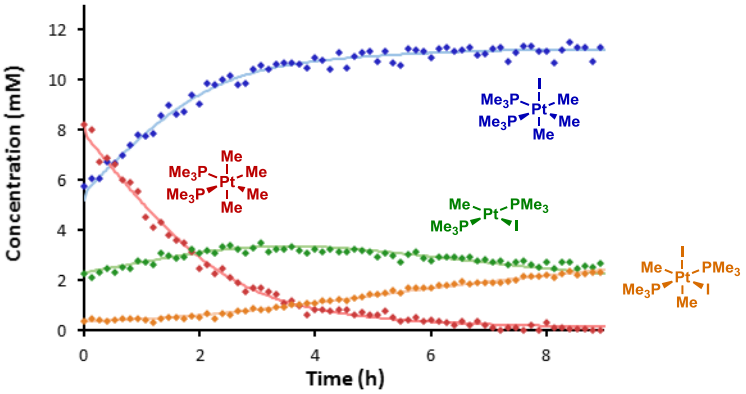


**Figure 3.64.** COPASI Model of Platinum Speciation. Points represent measured data, lines represent the fitted model.

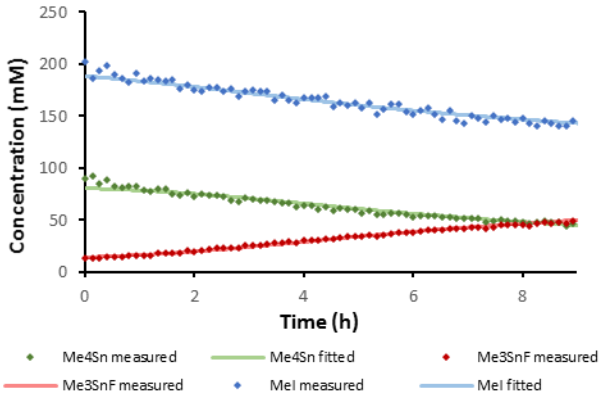


**Figure 3.65.** [Sn] and MeI concentrations modeled by COPASI compared to measured values

**Table 3.1.** Fitted parameters from COPASI model of the dual catalytic reaction.

| Rate Constant | Fitted Value |
|---|---|
| **9** + **2** → **[Pt]** ⊂ **2** + KI | 3.54 x $10^{-4}$ $M^{-1}s^{-1}$ |
| **[Pt]** ⊂ **2** + KI → **9** + **2** | 2.56 $M^{-1}s^{-1}$ |
| **9** + $Me_4Sn$ + KF → **23** + $Me_3SnF$ + KI | 13.3 $M^{-2}s^{-1}$ |
| **23** + $Me_3SnF$ + KI → **9** + $Me_4Sn$ + KF | 5.89 x $10^{3}$ $M^{-2}s^{-1}$ |
| **10** + MeI → **25** | 2.93 x $10^{-3}$ $M^{-1}s^{-1}$ |
| **[Pt]** ⊂ **2** → **[K]** + **2** ($k_{cat}$) | 0.296 $s^{-1}$ |
| **25** + **2** → **[Pt]** ⊂ **2** + KI | 6.16 x $10^{3}$ $M^{-1}s^{-1}$ |
| **[Pt]** ⊂ **2** + KI → **25** + **2** | 1.00 x $10^{-4}$ $M^{-1}s^{-1}$ |
| **24** + $Me_4Sn$ + KF → **25** + $Me_3SnF$ + KI | 0.154 $M^{-2}s^{-1}$ |
| **25** + $Me_3SnF$ + KI → **26** + $Me_4Sn$ + KF | 9.54 x $10^{5}$ $M^{-2}s^{-1}$ |
| **[K]** + **KI** → **10** | 118 $M^{-1}s^{-1}$ |

In order to account for iodide association to the Pt(II) cation formed upon reductive elimination without introducing a dependence on iodide concentration in $k_{cat}$, an additional irreversible iodide capture step was incorporated into the model following reductive elimination (not shown above).

*Single Crystal X-ray Crystallography of* **6** ⊂ **1**

A yellow block crystal with the dimensions of approximately 0.01 x 0.01 x 0.005 mm was grown by slow vapor diffusion of acetone into a solution of the complex in 1:1 water and methanol. The crystal was mounted and single-crystal X-ray data were collected at 100 K on a Bruker D8 with PHOTON 100 detector. Synchrotron radiation at 1.22760 Å was used for data collection and the diffraction measurement method was φ and ω shutterless scans. The structure was solved using direct methods and refined by full-matrix least squares on $F^2$. Non-hydrogen atoms were refined with anisotropic displacement parameters and hydrogen atoms were placed following a riding model of the attached atom. All refinements were carried out using the SHELXL-2014 software package.

Crystal growth of this complex proved to be challenging and the obtained crystals suffered from high degrees of disorder. Synchrotron radiation was necessary for data collection up to 0.88 Å with 93.8% completeness, however, the model contains irregularities such as large thermal parameters and prolate atoms. Attempts to include complete solvent molecules in the final model yielded unsatisfactory results. Instead, 16 placeholder oxygen atoms were modeled as chelating the 8 potassium ions to represent disordered water and methanol. The final chemical formula has been adjusted with 32 additional hydrogen atoms to represent the 16 placeholder oxygen atoms as water. In addition, the unit cell featured 6106.3 $Å^3$ of disordered solvent channels (25.7% of the total unit cell). This residual electron density could not be further modeled and was treated with the Squeeze algorithm of the PLATON package to correct 1777 unresolved electrons within the void. It should also be noted that the data suggest a small twinned domain from the C-orthorhombic pseudo cell, but accounting for this in the model gave little to no improvements. Therefore, the final model is presented without twinning considerations. Although the model suffers from deficiencies, it is sufficient for the purposes of demonstrating atom connectivity and the encapsulation of **6** in **1**.

Crystal data and structure refinement for **6⊂1**.

| | |
|---|---|
| Identification code | shelx |
| Empirical formula | $C_{152}$ $H_{140}$ Au $Ga_4$ $K_8$ $N_{12}$ $O_{52}$ $P_2$ |
| Formula weight | 3817.37 |
| Temperature | 100(2) K |
| Wavelength | 1.2276 Å |
| Crystal system, space group | Monoclinic, P 21/c |
| Unit cell dimensions | a = 19.9478(10) Å alpha = 90 deg.<br>b = 60.836(3) Å beta = 118.988(2) deg.<br>c = 19.5518(11) Å gamma = 90 deg. |
| Volume | 20754.5(19) $Å^3$ |
| Z, Calculated density | 4, 1.176 $Mg/m^3$ |
| Absorption coefficient | 1.935 $mm^{-1}$ |
| F(000) | 7405 |
| Crystal size | 0.010 x 0.010 x 0.005 mm |
| Theta range for data collection | 2.137 to 44.033 deg. |
| Limiting indices | -22<=h<=18, -68<=k<=68, -19<=l<=21 |
| Reflections collected / unique | 63064 / 29588 [R(int) = 0.0486] |
| Completeness to theta = 44.000 | 93.8 % |
| Refinement method | Full-matrix least-squares on $F^2$ |
| Data / restraints / parameters | 29588 / 0 / 2072 |
| Goodness-of-fit on $F^2$ | 1.112 |
| Final R indices [I>2sigma(I)] | R1 = 0.1570, wR2 = 0.3706 |
| R indices (all data) | R1 = 0.1739, wR2 = 0.3818 |
| Extinction coefficient | n/a |
| Largest diff. peak and hole | 5.676 and -1.644 e.A^-3 |

## 3.6 References


(1) Tolman, C. A. *Chem. Rev.* **1977**, *77* (3), 313.
(2) Berrisford, D. J.; Bolm, C.; Sharpless, K. B. *Angew. Chem. Int. Ed. Engl.* **1995**, *34* (10), 1059.
(3) van Leeuwen, P. W. N. M.; Kamer, P. C. J.; Reek, J. N. H.; Dierkes, P. *Chem. Rev.* **2000**, *100* (8), 2741.
(4) Surry, D. S.; Buchwald, S. L. *Angew. Chem. Int. Ed.* **2008**, *47* (34), 6338.
(5) Hartwig, J. F. *Acc. Chem. Res.* **2008**, *41* (11), 1534.
(6) Fu, G. C. *Acc. Chem. Res.* **2008**, *41* (11), 1555.
(7) Cram, D. J.; Cram, J. M. *Science* **1974**, *183* (4127), 803.
(8) Meeuwissen, J.; Reek, J. N. H. *Nat. Chem.* **2010**, *2* (8), 615.
(9) Brown, C. J.; Toste, F. D.; Bergman, R. G.; Raymond, K. N. *Chem. Rev.* **2015**, *115* (9), 3012.
(10) Yoshizawa, M.; Klosterman, J. K.; Fujita, M. *Angew. Chem. Int. Ed.* **2009**, *48* (19), 3418.
(11) Catti, L.; Zhang, Q.; Tiefenbacher, K. *Synthesis* **2016**, *48* (3), 313.
(12) Zhao, Y.; Cotelle, Y.; Sakai, N.; Matile, S. *J. Am. Chem. Soc.* **2016**, *138* (13), 4270.
(13) Knowles, R. R.; Jacobsen, E. N. *Proc. Natl. Acad. Sci.* **2010**, *107* (48), 20678.
(14) Wheeler, S. E. *Acc. Chem. Res.* **2013**, *46* (4), 1029.
(15) Salles, A. G.; Zarra, S.; Turner, R. M.; Nitschke, J. R. *J. Am. Chem. Soc.* **2013**, *135* (51), 19143.
(16) Yoshizawa, M.; Tamura, M.; Fujita, M. *Science* **2006**, *312* (5771), 251.
(17) Cullen, W.; Misuraca, M. C.; Hunter, C. A.; Williams, N. H.; Ward, M. D. *Nat Chem* **2016**, *8* (3), 231.
(18) Zhang, Q.; Tiefenbacher, K. *Nat. Chem.* **2015**, *7* (3), 197.
(19) Caulder, D. L.; Powers, R. E.; Parac, T. N.; Raymond, K. N. *Angew. Chem. Int. Ed.* **1998**, *37* (13–14), 1840.
(20) Davis, A. V.; Raymond, K. N. *J. Am. Chem. Soc.* **2005**, *127* (21), 7912.
(21) Caulder, D. L.; Brückner, C.; Powers, R. E.; König, S.; Parac, T. N.; Leary, J. A.; Raymond, K. N. *J. Am. Chem. Soc.* **2001**, *123* (37), 8923.
(22) Davis, A. V.; Fiedler, D.; Seeber, G.; Zahl, A.; van Eldik, R.; Raymond, K. N. *J. Am. Chem. Soc.* **2006**, *128* (4), 1324.
(23) Biros, S. M.; Bergman, R. G.; Raymond, K. N. *J. Am. Chem. Soc.* **2007**, *129* (40), 12094.
(24) Leung, D. H.; Bergman, R. G.; Raymond, K. N. *J. Am. Chem. Soc.* **2008**, *130* (9), 2798.
(25) Brumaghim, J. L.; Michels, M.; Pagliero, D.; Raymond, K. N. *Eur. J. Org. Chem.* **2004**, *2004* (24), 5115.
(26) Hart-Cooper, W. M.; Clary, K. N.; Toste, F. D.; Bergman, R. G.; Raymond, K. N. *J. Am. Chem. Soc.* **2012**, *134* (43), 17873.
(27) Mugridge, J. S.; Bergman, R. G.; Raymond, K. N. *J. Am. Chem. Soc.* **2011**, *133* (29), 11205.
(28) Mugridge, J. S.; Bergman, R. G.; Raymond, K. N. *Angew. Chem. Int. Ed.* **2010**, *49* (21), 3635.
(29) Mugridge, J. S.; Szigethy, G.; Bergman, R. G.; Raymond, K. N. *J. Am. Chem. Soc.* **2010**, *132* (45), 16256.
(30) Mugridge, J. S.; Zahl, A.; van Eldik, R.; Bergman, R. G.; Raymond, K. N. *J. Am. Chem. Soc.* **2013**, *135* (11), 4299.
(31) Pluth, M. D.; Bergman, R. G.; Raymond, K. N. *Science* **2007**, *316* (5821), 85.

(32) Kaphan, D. M.; Toste, F. D.; Bergman, R. G.; Raymond, K. N. *J. Am. Chem. Soc.* **2015**, *137* (29), 9202.
(33) Fiedler, D.; Bergman, R. G.; Raymond, K. N. *Angew. Chem. Int. Ed.* **2004**, *43* (48), 6748.
(34) Zhao, C.; Sun, Q.-F.; Hart-Cooper, W. M.; DiPasquale, A. G.; Toste, F. D.; Bergman, R. G.; Raymond, K. N. *J. Am. Chem. Soc.* **2013**, *135* (50), 18802.
(35) Hart-Cooper, W. M.; Zhao, C.; Triano, R. M.; Yaghoubi, P.; Ozores, H. L.; Burford, K. N.; Toste, F. D.; Bergman, R. G.; Raymond, K. N. *Chem. Sci.* **2015**, *6* (2), 1383.
(36) Pluth, M. D.; Bergman, R. G.; Raymond, K. N. *J. Am. Chem. Soc.* **2007**, *129* (37), 11459.
(37) Wang, Z. J.; Brown, C. J.; Bergman, R. G.; Raymond, K. N.; Toste, F. D. *J. Am. Chem. Soc.* **2011**, *133* (19), 7358.
(38) Wang, Z. J.; Clary, K. N.; Bergman, R. G.; Raymond, K. N.; Toste, F. D. *Nat. Chem.* **2013**, *5* (2), 100.
(39) Fiedler, D.; Bergman, R. G.; Raymond, K. N. *Angew. Chem. Int. Ed.* **2006**, *45* (5), 745.
(40) Fiedler, D.; Pagliero, D.; Brumaghim, J. L.; Bergman, R. G.; Raymond, K. N. *Inorg. Chem.* **2004**, *43* (3), 846.
(41) Fiedler, D.; Leung, D. H.; Bergman, R. G.; Raymond, K. N. *J. Am. Chem. Soc.* **2004**, *126* (12), 3674.
(42) Leung, D. H.; Fiedler, D.; Bergman, R. G.; Raymond, K. N. *Angew. Chem.* **2004**, *116* (8), 981.
(43) Jana, R.; Pathak, T. P.; Sigman, M. S. *Chem. Rev.* **2011**, *111* (3), 1417.
(44) Komiya, S.; Kochi, J. K. *J. Am. Chem. Soc.* **1976**, *98* (24), 7599.
(45) Wolf, W. J.; Winston, M. S.; Toste, F. D. *Nat. Chem.* **2014**, *6* (2), 159.
(46) Hartwig, J. F. *Organotransition Metal Chemistry: From Bonding to Catalysis*; University Science Books, 2010.
(47) Leung, D. H.; Fiedler, D.; Bergman, R. G.; Raymond, K. N. *Angew. Chem. Int. Ed.* **2004**, *43* (8), 963.
(48) Mecozzi, S.; Rebek, J., Jr. *Chem. – Eur. J.* **1998**, *4* (6), 1016.
(49) Blackmond, D. G. *Angew. Chem. Int. Ed.* **2005**, *44* (28), 4302.
(50) Silverman, R. B. *The Organic Chemistry of Enzyme-Catalyzed Reactions*; Academic Press, 2002.
(51) Sgarlata, C.; Mugridge, J. S.; Pluth, M. D.; Tiedemann, B. E. F.; Zito, V.; Arena, G.; Raymond, K. N. *J. Am. Chem. Soc.* **2010**, *132* (3), 1005.
(52) Slansky, C. M. *J. Am. Chem. Soc.* **1940**, *62* (9), 2430.
(53) Morris, D. F. C. In *Structure and Bonding*; Springer Berlin Heidelberg: Berlin, Heidelberg, 1968; pp 63–82.
(54) Winston, M. S.; Wolf, W. J.; Toste, F. D. *J. Am. Chem. Soc.* **2015**, *137* (24), 7921.
(55) Berzinsh, U.; Gustafsson, M.; Hanstorp, D.; Klinkmüller, A.; Ljungblad, U.; M\aartensson-Pendrill, A.-M. *Phys Rev A* **1995**, *51* (1), 231.
(56) Blondel, C.; Cacciani, P.; Delsart, C.; Trainham, R. *Phys Rev A* **1989**, *40* (7), 3698.
(57) Peláez, R. J.; Blondel, C.; Delsart, C.; Drag, C. *J. Phys. B At. Mol. Opt. Phys.* **2009**, *42* (12), 125001.
(58) Brown, J. R.; Schwerdtfeger, P.; Schröder, D.; Schwarz, H. *J. Am. Soc. Mass Spectrom.* **2002**, *13* (5), 485.
(59) Brown, M. P.; Puddephatt, R. J.; Upton, C. E. E.; Lavington, S. W. *J Chem Soc Dalton Trans* **1974**, No. 15, 1613.
(60) Goldberg, K. I.; Yan, J. Y.; Winter, E. L. *J. Am. Chem. Soc.* **1994**, *116* (4), 1573.

(61) Goldberg, K. I.; Yan, J.; Breitung, E. M. *J. Am. Chem. Soc.* **1995**, *117* (26), 6889.
(62) Komiya, S.; Albright, T. A.; Hoffmann, R.; Kochi, J. K. *J. Am. Chem. Soc.* **1976**, *98* (23), 7255.
(63) Tamaki, A.; Kochi, J. K. *J. Organomet. Chem.* **1974**, *64* (3), 411.
(64) Tamaki, A.; Kochi, J. K. *J. Organomet. Chem.* **1972**, *40* (2), C81.
(65) Gillie, A.; Stille, J. K. *J. Am. Chem. Soc.* **1980**, *102* (15), 4933.
(66) Tatsumi, K.; Hoffmann, R.; Yamamoto, A.; Stille, J. K. *Bull. Chem. Soc. Jpn.* **1981**, *54* (6), 1857.
(67) Levin, M. D.; Toste, F. D. *Angew. Chem. Int. Ed.* **2014**, *53* (24), 6211.
(68) Joost, M.; Amgoune, A.; Bourissou, D. *Angew. Chem. Int. Ed.* **2015**, *54* (50), 15022.
(69) Roy, S.; Puddephatt, R. J.; Scott, J. D. *J. Chem. Soc. Dalton Trans.* **1989**, No. 11, 2121.
(70) Crumpton-Bregel, D. M.; Goldberg, K. I. *J. Am. Chem. Soc.* **2003**, *125* (31), 9442.
(71) Deutsch, P. P.; Eisenberg, R. *J. Am. Chem. Soc.* **1990**, *112* (2), 714.
(72) Buchanan, J. M.; Stryker, J. M.; Bergman, R. G. *J. Am. Chem. Soc.* **1986**, *108* (7), 1537.
(73) Harper, T. G. P.; Desrosiers, P. J.; Flood, T. C. *Organometallics* **1990**, *9* (9), 2523.
(74) Forniés, J.; Gómez-Saso, M. A.; Martín, A.; Martínez, F.; Menjón, B.; Navarrete, J. *Organometallics* **1997**, *16* (26), 6024.
(75) Scott, J. D.; Puddephatt, R. J. *Organometallics* **1986**, *5* (6), 1253.
(76) Howard, W. A.; Bergman, R. G. *Polyhedron* **1998**, *17*, 803.
(77) Martínez-Salvador, S.; Forniés, J.; Martín, A.; Menjón, B. *Chem. – Eur. J.* **2011**, *17* (29), 8085.
(78) Allen, A. E.; MacMillan, D. W. C. *Chem. Sci.* **2012**, *3* (3), 633.
(79) Johansson Seechurn, C. C. C.; Kitching, M. O.; Colacot, T. J.; Snieckus, V. *Angew. Chem. Int. Ed.* **2012**, *51* (21), 5062.
(80) Romeo, R.; Scolaro, L. M.; Catalano, V.; Achar, S. In *Inorganic Syntheses*; John Wiley & Sons, Inc., 2007; pp 153–158.
(81) Clark, H. C.; Goel, A. B.; Jain, V. K.; Tyers, K. G.; Wong, C. S. *J. Organomet. Chem.* **1987**, *321* (1), 123.
(82) Rakowsky, M. H.; Woolcock, J. C.; Rettig, M. F.; Wing, R. M. *Organometallics* **1988**, *7* (10), 2149.
(83) Dekker, G. P. C. M.; Buijs, A.; Elsevier, C. J.; Vrieze, K.; Van Leeuwen, P. W. N. M.; Smeets, W. J. J.; Spek, A. L.; Wang, Y. F.; Stam, C. H. *Organometallics* **1992**, *11* (5), 1937.
(84) Nilsson, P.; Plamper, F.; Wendt, O. F. *Organometallics* **2003**, *22* (25), 5235.
(85) Hux, J. E.; Puddephatt, R. J. *Inorganica Chim. Acta* **1985**, *100* (1), 1.
(86) Lashanizadehgan, M.; Rashidi, M.; Hux, J. E.; Puddephatt, R. J.; Ling, S. S. M. *J. Organomet. Chem.* **1984**, *269* (3), 317.
(87) Herzog, A.; Liu, F.-Q.; Roesky, H. W.; Demsar, A.; Keller, K.; Noltemeyer, M.; Pauer, F. *Organometallics* **1994**, *13* (4), 1251.
(88) Vela, J.; Smith, J. M.; Yu, Y.; Ketterer, N. A.; Flaschenriem, C. J.; Lachicotte, R. J.; Holland, P. L. *J. Am. Chem. Soc.* **2005**, *127* (21), 7857.
(89) Ding, K.; Dugan, T. R.; Brennessel, W. W.; Bill, E.; Holland, P. L. *Organometallics* **2009**, *28* (23), 6650.
(90) Hoops, S.; Sahle, S.; Gauges, R.; Lee, C.; Pahle, J.; Simus, N.; Singhal, M.; Xu, L.; Mendes, P.; Kummer, U. *Bioinformatics* **2006**, *22* (24), 3067.
(91) Hill, G. S.; Puddephatt, R. J. *Organometallics* **1997**, *16* (21), 4522.

(92) Hill, G. S.; Yap, G. P. A.; Puddephatt, R. J. *Organometallics* **1999**, *18* (8), 1408.
(93) Schuster, O.; Schmidbaur, H. *Z. Naturforschung B* **2006**, *61* (1), 1.

# Chapter 4

A Catalytic Fluoride-Rebound Mechanism for C($sp^3$)-$CF_3$ Bond Formation

## 4.1 Preface

Chapter 3 focused on a strategy for the acceleration of a challenging reductive elimination from Au(III) (and Pt(IV)) by the implementation of a supramolecular catalyst, wherein the mechanism of acceleration was anticipated based on the binding preferences of the host assembly. In contrast, this chapter concerns itself with a case of catalyzed reductive elimination which was the result of serendipitous discovery, revealing a new mechanism for formal C($sp^3$)-$CF_3$ reductive elimination from Au(III). The mechanistic investigation and synthetic exploration of the new class of gold complexes described ultimately led to the application of this discovery towards the synthesis of previously inaccessible [$^{18}$F] radioisotope tracers.

This work was highly collaborative, with two undergraduates (Tiffany Chen and Megan Neubig) and one visiting student (Cyril Theulier) assisting in much of the synthetic effort. Cynthia Hong was responsible for the crystallography, and Dr. Ilia Kobylianskii for the computational study described below. Finally, Dr. Mustafa Janabi and Dr. Jim P. O'Neil of the Lawrence Berkeley National Lab Biomedical Isotope Facility graciously trained me in the techniques of $^{18}$F-radiochemistry and allowed me access to their facility.

## 4.2 Introduction

The forging of difficult chemical linkages is typically implemented via correspondingly reactive intermediates, with the cost of admission to the prohibitive transition state paid by an energetic ratcheting of the substrate. Emblematic instances of this approach are encountered in the design of organometallic reagents and catalytic intermediates, whose reactivity depends upon weak linkages to the transformed organic fragments they shepherd. Unfortunately, the reliance on these reactive species introduces a strategic roadblock: peripheral chemical modification of the organometallic species, once formed, is functionally impossible. Indeed, even routine functional group tolerance for many organometallic species is lacking, let alone general tolerance to commonly encountered synthetic conditions.

This dichotomy is particularly stark in the arena of short-lived radioisotope chemistry, in which synthetic transformations are called on to achieve demanding chemical transformations under exceptionally strict rate constraints.[1–3] The biomedical applications of positron emission tomography (PET) rely upon the availability of radiolabeled tracers in which a radioactive positron emitting isotope, most commonly [$^{18}$F] ($t_{1/2}$ ~ 110 min), is incorporated into a molecule of biological importance. These compounds can be used for high-resolution real-time imaging of tissue-level phenomena, enabling direct interrogation of disease states and mechanisms of bioactivity.

Unfortunately, their value is undermined by the synthetic difficulty associated with their preparation – desirable targets possess substantial structural complexity, requiring compatible reagents that are reactive enough to enable rapid (i.e. on the radiochemical timescale) assembly of the C-F bond. For these reasons, organometallic reagents have proven valuable in the preparation of radiolabeled tracers. However, their characteristic reactivity simultaneously imposes limitations, necessitating installation of the organometallic functionality in the penultimate step of the synthetic sequence, immediately preceding radiofluorination (Figure 4.1).[4–10]

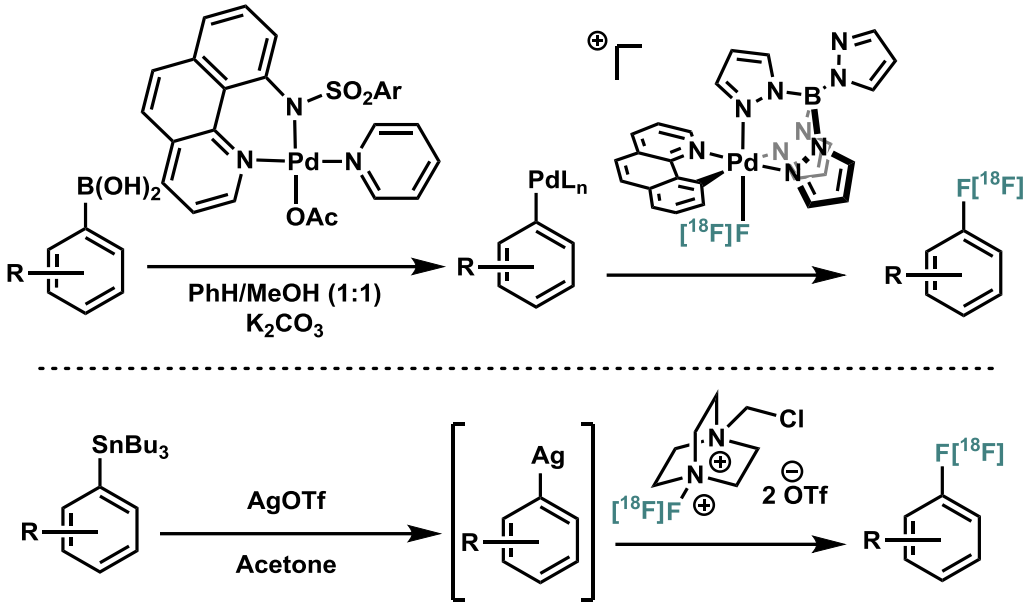


**Figure 4.1** Selected examples of organometallic reagents in [$^{18}$F]-radiosynthesis

A class of organometallic reagents compatible towards multistep synthetic operations while possessing latent and specific reactivity that could be triggered by some orthogonal means to enable late-stage radioisotope incorporation, would allow new classes of PET tracers to be synthesized by an altogether distinct retrosynthetic paradigm.[11,12] This chapter describes the serendipitous discovery of a novel class of Au(III) complexes which match exactly this profile of reactivity, wherein synthetic elaboration of the coordinated organic fragment can be performed prior to activation for radioisotope incorporation. The successful development of this advance has depended crucially on detailed mechanistic investigation of an unexpected C($sp^3$)-$CF_3$ reductive elimination. The medicinally well-represented trifluoromethyl group has remained a particular challenge for radiochemists, and the disclosed technology expands on the state-of-the-art copper-mediated protocols for $CF_3$ radiosynthesis (Figure 4.2).[13–16]

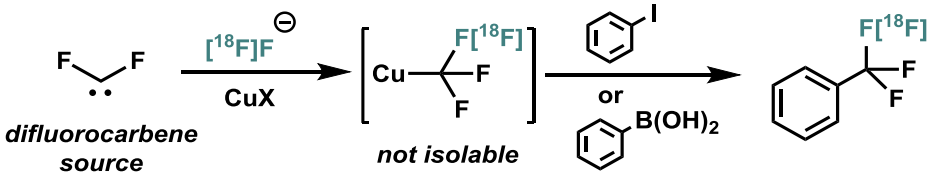


**Figure 4.2** General scheme for copper-mediated $CF_3$ radiosynthesis

## 4.3 Results and Discussion

### 4.3.1 Initial Discovery

In light of the chemistry presented in Chapter 3 we were interested in identifying a complex which would allow us to directly observe the encapsulated, coordinately unsaturated Michaelis complex without resorting to "donor-arrested" analogues. In pursuit of that, known Au(III) complex **2** was prepared, with the expectation that either $F_3C$-$CF_3$ reductive elimination would be sufficiently disfavored to allow characterization of such a species or, more tantalizingly, that the

supramolecular assembly would catalyze the unprecedented bond formation.[17–19] Unfortunately, **2** was found not to be encapsulated under a variety of conditions. We anticipated that the corresponding triethylphosphine analogue **4** might show a higher affinity for the supramolecular assembly; however, the analogous synthetic route *via* photoinitiated $CF_3I$ oxidative addition was not successful, instead affording an Au(I) iodide complex along with fluoroform.[20–24] This limitation extended to all other ligands examined, including $PPh_3$, $PCy_3$, $PtBu_3$ and IPr (Figure 4.3).

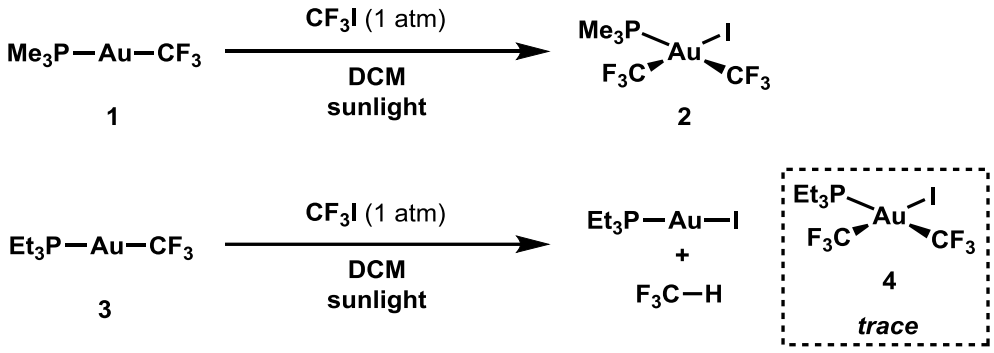


**Figure 4.3** Synthesis of bis(trifluoromethyl) complex **2** and attempted extension to other ligands

We resolved to continue examination of **2** and its related complexes outside of the supramolecular context in search of productive hexafluoroethane reductive elimination. Unfortunately, treatment of **2** with $AgSbF_6$ to generate the presumed cationic product **5** did not result in the desired bond formation, even upon prolonged heating (Figure 4.4).

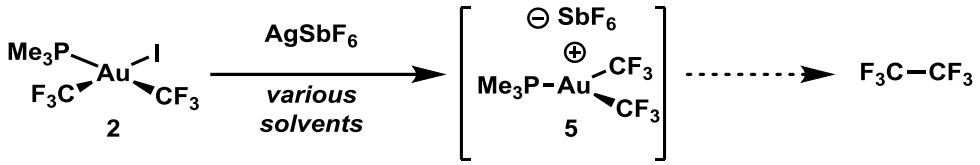


**Figure 4.4** Attempted reductive elimination of hexafluoroethane from *in situ* generated **5**.

Reasoning that a more sterically demanding ligand might promote the desired reaction by virtue of steric compression, we sought an alternative synthetic route. However, attempted ligand exchange starting from complex **2** was not successful. We thus turned our attention to previously reported bis(trifluoromethyl)aurate **6** (available from $Me_3SiCF_3$ and DMSAuCl) as an alternative starting point for synthesis.[25,26]

Based on analogous precedent for dimethylaurate (See Chapter 1), we anticipated that oxidative addition of alkyl halides to **6** might be possible.[27–30] Whereas incubation of **6** with equimolar mixtures of iodomethane under various conditions was unsuccessful, when conducted in *neat* iodomethane, **6** was found to provide the Au(III)-ate complex **7** in good yield after heating at 30°C for 18 hours. Subsequent treatment with free IPr carbene resulted in elimination of $PPh_4I$, affording **8** after purification *via* column chromatography (Figure 4.5). Unusually, **7** and **8** displayed no coupling between the $CF_3$ fluorine resonances and $CH_3$ proton resonances in both their $^{19}F$- or $^{1}H$-NMR spectra, with the latter substituent displaying a single broad resonance at $\delta$ = 1.58 and 0.78 ppm, respectively. As such, both **7** and **8** were characterized crystallographically, confirming their connectivity.

Complex **8** exhibited stability uncharacteristic of Au(III) complexes.[31] In addition to its tolerance of silica gel chromatography, **8** was completely air and moisture tolerant, and was recovered unchanged after heating at 100 °C in toluene solution for 24 hours. Minor light sensitivity was observed, with samples discoloring slightly upon prolonged exposure to sunlight.

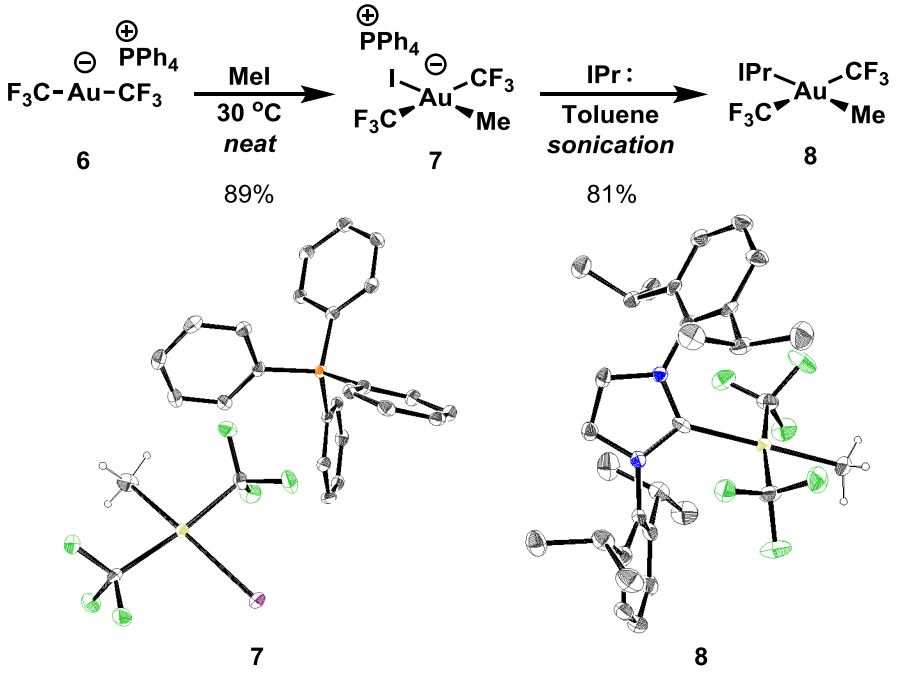


**Figure 4.5** Synthesis of bis(trifluoromethyl) complex **8** *via* oxidative addition of iodomethane and crystallographic structures for **7** and **8**. Hydrogens (except for Au-$CH_3$) omitted for clarity.

In analogy with the activation modes for alkyl metallocene polymerization catalysts studied by Marks, we anticipated that treatment of **8** with tris(pentafluorophenyl)borane (BCF) would lead to formation of ionic complex **9** for ultimate hexafluoroethane reductive elimination.[32–36] Instead, we observed the formation of trifluoroethane, accompanied by the formation of IPrAu$C_6F_5$ (**10**) (Figure 4.6), with the reaction complete in less than 5 minutes at 25 °C. $C_6F_5H$ was also observed, alongside several unidentified $C_6F_5$-containing products.

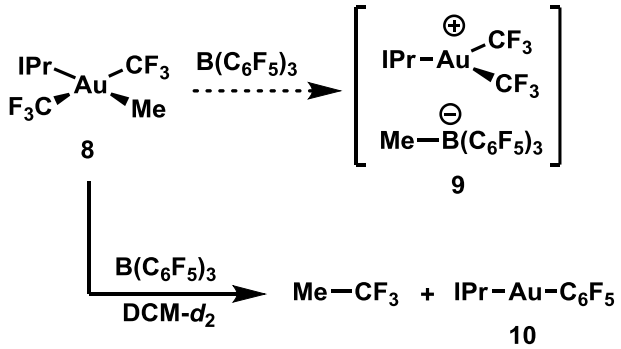


**Figure 4.6.** Unexpected trifluoroethane reductive elimination

This was a highly unexpected result; directly observable C($sp^3$)-$CF_3$ reductive elimination is (to our knowledge) unprecedented at any metal center, with several prominent examples of high-valent metals (Ni, Pd) undergoing a multitude of reductive elimination and disproportionation

chemistry in order to "avoid" such a bond-forming process (Figure 4.7).[37–39] While $CuCF_3$ has been reported to react with iodomethane to directly afford trifluoroethane, no Cu(III) intermediates have been detected, and the mechanism of this process remains unclear.[40] The related C($sp^2$)-$CF_3$ reductive elimination is known for several metals, though it remains among the most challenging bond constructions.[22,41–43]

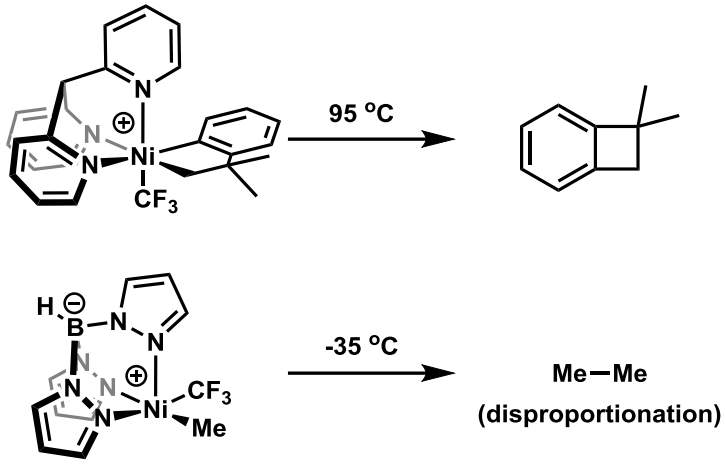


**Figure 4.7** Selected precedent in attempted C($sp^3$)-$CF_3$ reductive elimination from Ni.

### 4.3.2 Mechanistic Investigation

Several features of the reaction depicted in Figure 4.6 were unusual, and we endeavored to understand the underlying mechanism of this unprecedented bond-forming reaction. One particularly obvious and vexing feature was the "missing" additional $CF_3$ group, whose fate was not immediately apparent by $^{19}$F-NMR. The dichotomy between the complete thermal stability of **8** and its rapid reaction with BCF was also surprising, as was the apparent B/Au transmetallation event to afford **10**.

Our initial approach to collect additional information was low temperature monitoring of the reaction by Variable Temperature $^{19}$F-NMR. Slow warming of the probe from - 70°C revealed the onset of reasonably paced, observable reactivity around -20 °C. For convenient analysis, the reaction was monitored at -15 °C, revealing the formation and subsequent decay of a new species, **11**, *en route* to trifluorethane formation. This species featured two $^{19}$F-NMR resonances, a triplet ($\delta$ = -37.5 ppm, $J$ = 11.4 Hz), and a broad multiplet ($\delta$ = -64.9 ppm), with relative integration of 3:2 (Figure 4.8).

A complicating feature of this kinetic behavior was that the rate of the reaction and concentration of the transient species were very sensistive to both the water content and glassware. Whereas routine drying of DCM-$d_2$ with $CaH_2$ and of glassware in the oven provided the reaction profile shown in Figure 4.9 (top left), the use of molecular sieve dried solvent in glassware pretreated with $(Me_3Si)_2NH$ prior to oven drying provided the profile shown in Figure 4.9 (top right).[44,45] The use of degassed but otherwise undried solvent and glassware still ultimately afforded trifluoroethane, but again with a change to the kinetics (Figure 4.9, bottom right).

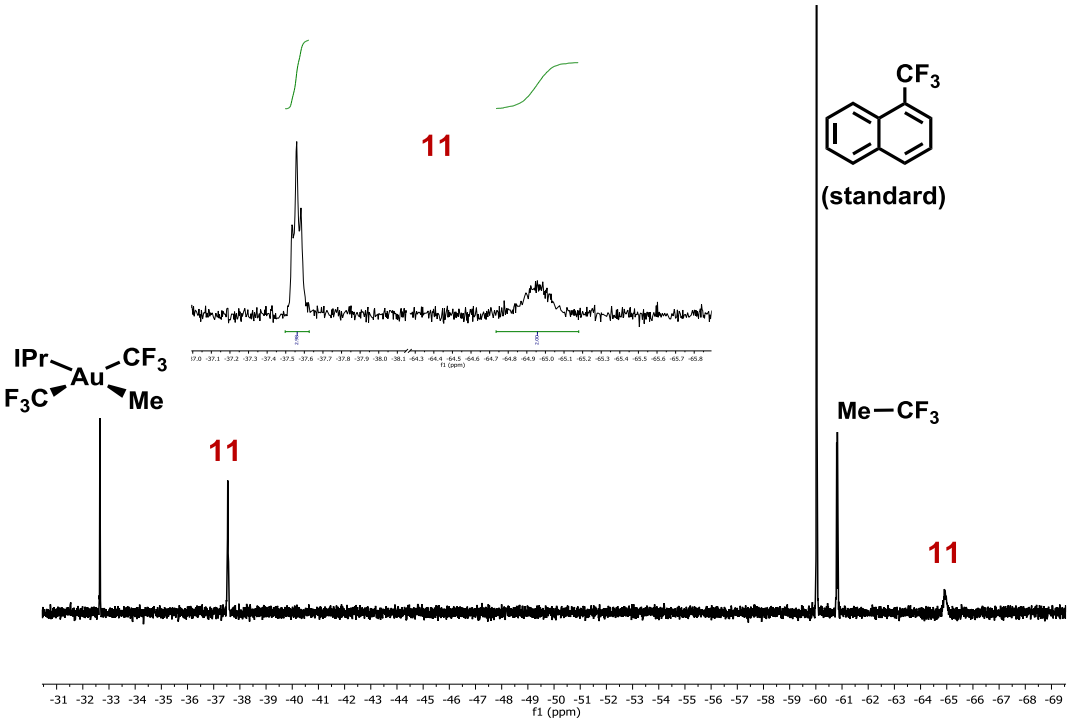


**Figure 4.8** Representative $^{19}$F-NMR spectrum of the reaction between **8** and BCF at -15 ºC.

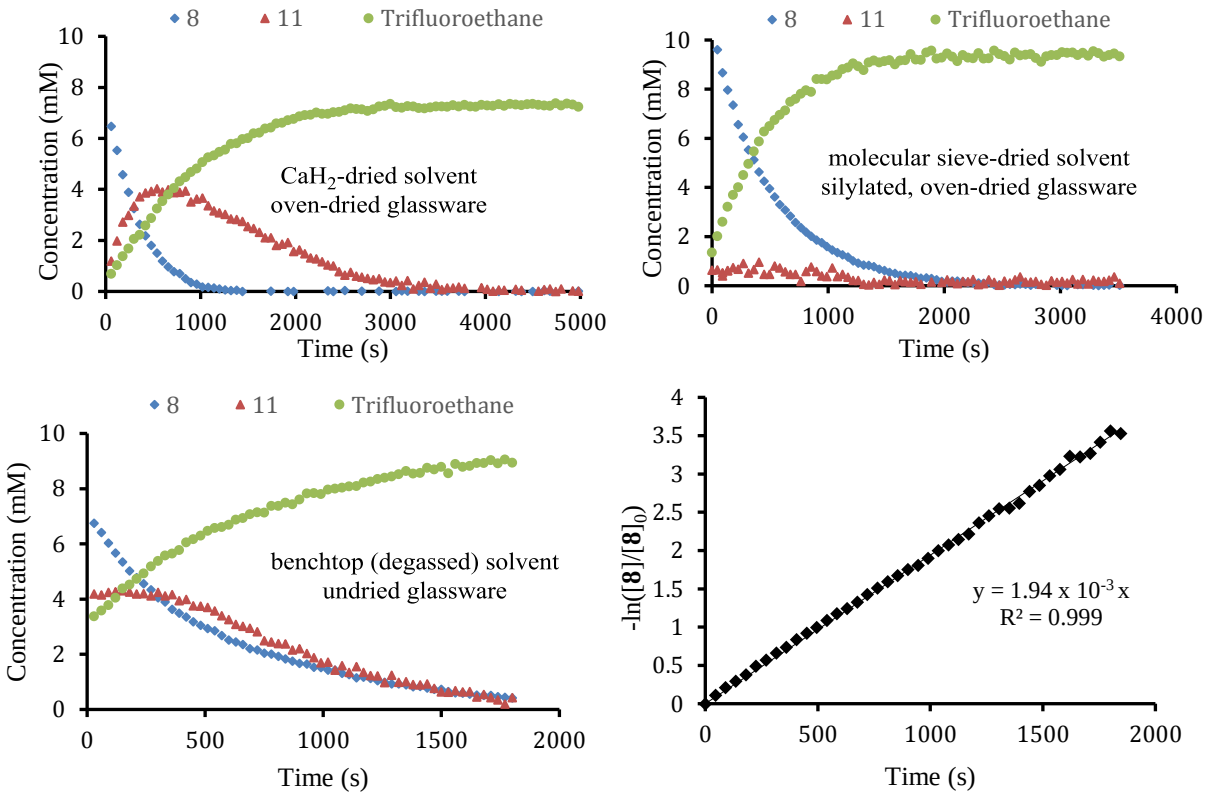


**Figure 4.9** Kinetic profile of the reaction between **8** and BCF in DCM-$d_2$ determined by $^{19}$F-NMR with various levels of water exclusion and log plot of [**8**] showing first order behavior (data from top right).

Based on this, we were comfortable concluding that formation of **11** required the presence of water, and its $^{19}$F-NMR suggested that it was an Au species bearing 1 $CF_3$ and 1 $CF_2$ unit, but a more definitive assignment of its structure required additional information (*vide infra*). Meanwhile, under these same conditions, no new Au-containing products were detected by $^{19}$F-NMR at -15°C, though upon warming to room temperature **10** was formed, suggesting that the formal B/Au transmetallation process occurs in a separate subsequent step from the trifluoroethane formation. A clue to the fate of the gold complex came from examination of the decay of **8**, which proceeded with uninhibited first-order behavior over the entire reaction (Figure 4.9, bottom right). Given the involvement of BCF in the reaction, the absence of bimolecular decay (at a 2:1 loading of BCF/**8**) suggested that the concentration of BCF was unchanging and it was thus acting as a catalyst.

Accordingly, treatment of **8** with a 20 mol% loading of BCF provided complete conversion to $IPrAuCF_3$ (**12**) and trifluoroethane, with minor amounts of **10** formed over extended reaction times (Figure 4.10). *In situ* $^{19}$F-NMR displayed substantial exchange-broadening of the product Au-$CF_3$ resonance, but upon workup and isolation its identity could be verified.[24]

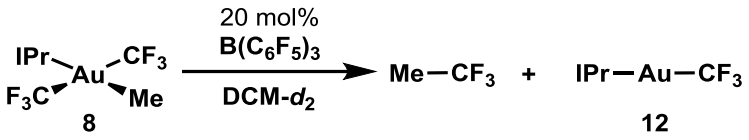


**Figure 4.10** Catalytic action of BCF on **8** to afford $IPrAuCF_3$ and $MeCF_3$

The subsequent transformation of **12** to **10** was further investigated, and was found to occur rapidly at 25 °C with stoichiometric quantities of BCF. A clue to the mechanism of this process was obtained by the addition of tetamethylethylene as a scavenger, which underwent difluorocyclopropanation as detected by $^{19}$F-NMR and GC-MS (Figure 4.11). This was true starting from both **8** and **12**, and was taken (alongside the spectral features of **11**) as a sign that difluorocarbene intermediates were formed in these reactions.[46,47]

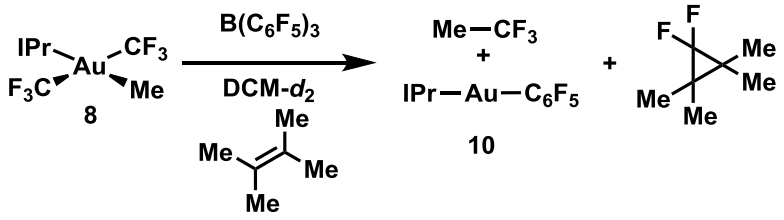


**Figure 4.11** Evidence for difluorocarbene intermediates

Fluoride abstraction from [Au]-$CF_3$ complexes has precedent for Au(I), having been observed in the conversion of **6** to the corresponding gold carbonyl **13** by action of $BF_3$●$Et_2O$ (Figure 4.12).[48]

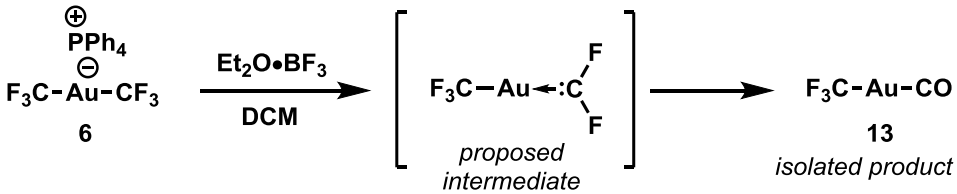


**Figure 4.12** Precedent for fluoride abstraction from [Au]-$CF_3$ complexes

As such, we envisioned two potential mechanisms for C-C bond formation, each arising from the initial formation of difluorocarbenoid intermediate **14**. One possibility is that the fluoride abstraction activates **8** towards migratory insertion of the methyl group into the difluorocarbenoid, which provides cationic difluoroethyl complex **15**. Subsequent, formal C-F reductive elimination upon re-delivery of the fluoride from $B(C_6F_5)_3$ affords **12** and trifluoroethane. Alternatively, **14** could undergo reductive elimination of the remaining fragments, generating trifluoroethane and the Au(I) carbenoid **16**, which upon re-delivery of the fluoride likewise affords **12**. The two mechanisms are summarized in Figure 4.13, and differ most greatly in terms of which of the two $CF_3$ substituents ultimately form the new C-C bond, with C-F abstraction either serving to activate directly or create a spectator ligand from the parent complex.

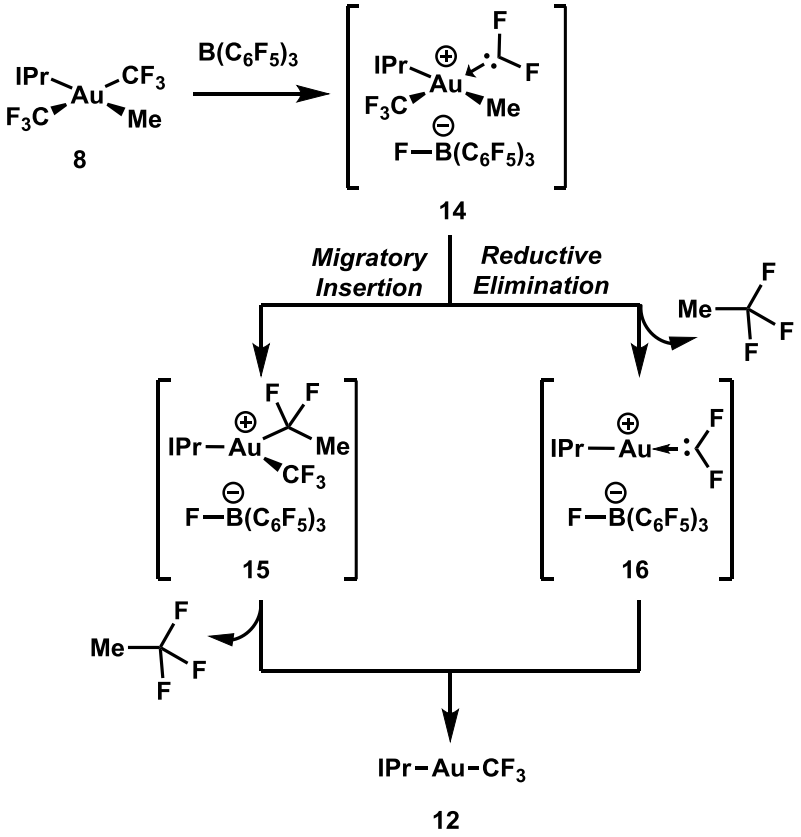


**Figure 4.13** Two potential mechanisms for trifluoroethane elimination *via* C-F abstraction.

Given that water appeared to form a metastable adduct of some fashion in species **11**, we anticipated that interception of any of these cationic intermediates (**14**-**16**) with a halide nucleophile would enable isolation of the resulting neutral analogues ($CF_2X$ substituents from **14** or **16**, Au(III) halides from **15**). Our initial attempts utilizing tetrabutylammonium halides were unsuccessful: chloride and bromide anions were too tightly bound to BCF and completely inhibited reactivity, whereas the iodide afforded only trace amounts of products which were not sufficiently stable to isolate.[49,50] A breakthrough occurred in the implementation of the corresponding trimethylsilyl halides, whose inhibitory effect was diminished compared to their anionic surrogates, but which nonetheless effected efficient trapping. $Me_3SiBr$ was found to react more cleanly than the chloride, allowing isolation of two isomeric trapping products, **17a** and **17b**, as a 2:1 mixture after column chromatography (Figure 4.14). These isomers were typically isolated as a mixture,

but could be separated sufficiently to enable characterization after careful, repeated chromatography affording substantial fractions of each pure isomer. The configuration of **17a** was determined *via* X-Ray crystallography, indicating a *trans* disposition of the halide and N-heterocyclic carbene substituents. Satisfactory crystals of **17b** were not obtained, but its configuration was established by a combination of 1D-NOE experiments (indicating proximity of the $MeCF_2$ and isopropyl groups of the ligand) and $^{13}$C-NMR (with a qt pattern in the resonance for the N-heterocyclic carbene indicating a stronger *trans* coupling to the $CF_3$ ligand). Monitoring of the reaction by $^{19}$F-NMR indicates that **17a** and **17b** are produced simultaneously and their ratio is invariant over the course of the reaction.

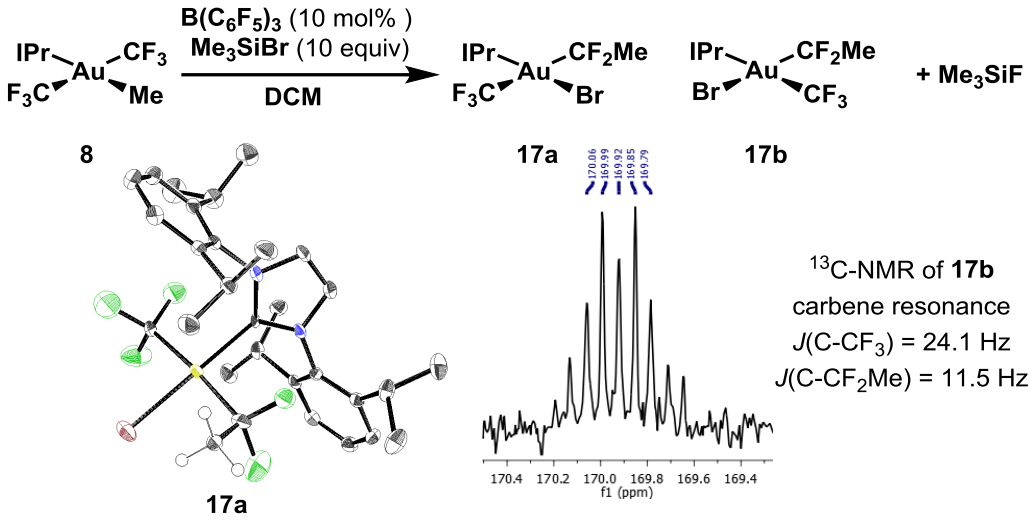


**Figure 4.14** Generation of bromide-trapped products in the reaction with $Me_3SiBr$, crystallographic structure of **17a** (hydrogens omitted except for Au-$CH_3$), and $^{13}$C-NMR of carbene resonance of **17b**.

Though chloro and bromosilanes were unreactive in the absence of catalytic BCF, $Me_3SiOTf$ was found to react spontaneously with **8** at 40 °C, affording $MeCF_2OTf$ and $Me_3SiF$ as the exclusive organic products.[51] Monitoring of the reaction mixture by $^{19}$F-NMR indicated the formation of an Au(III) intermediate **18**, whose stereochemistry was assigned in analogy to **17a** on the basis of its $CF_3/CF_2Me$ coupling constant (Figure 4.15). No **12** was observed, instead IPrAuOTf was formed as the major gold-containing product. The reaction was also found to be accelerated in the presence of BCF, occurring without heating to afford the same organic products on much shorter timescales.

Triphenylboron, triphenylcarbenium salts, and gaseous hydrochloric acid were found to be unreactive with **8**, even upon prolonged heating. Boron trichloride resulted in nonspecific decomposition, whereas the etherates of BCF or $BF_3$ resulted in slow trifluoroethane formation over several hours with observable formation of an intermediate tentatively assigned as the diethyl ether adduct of **15**.

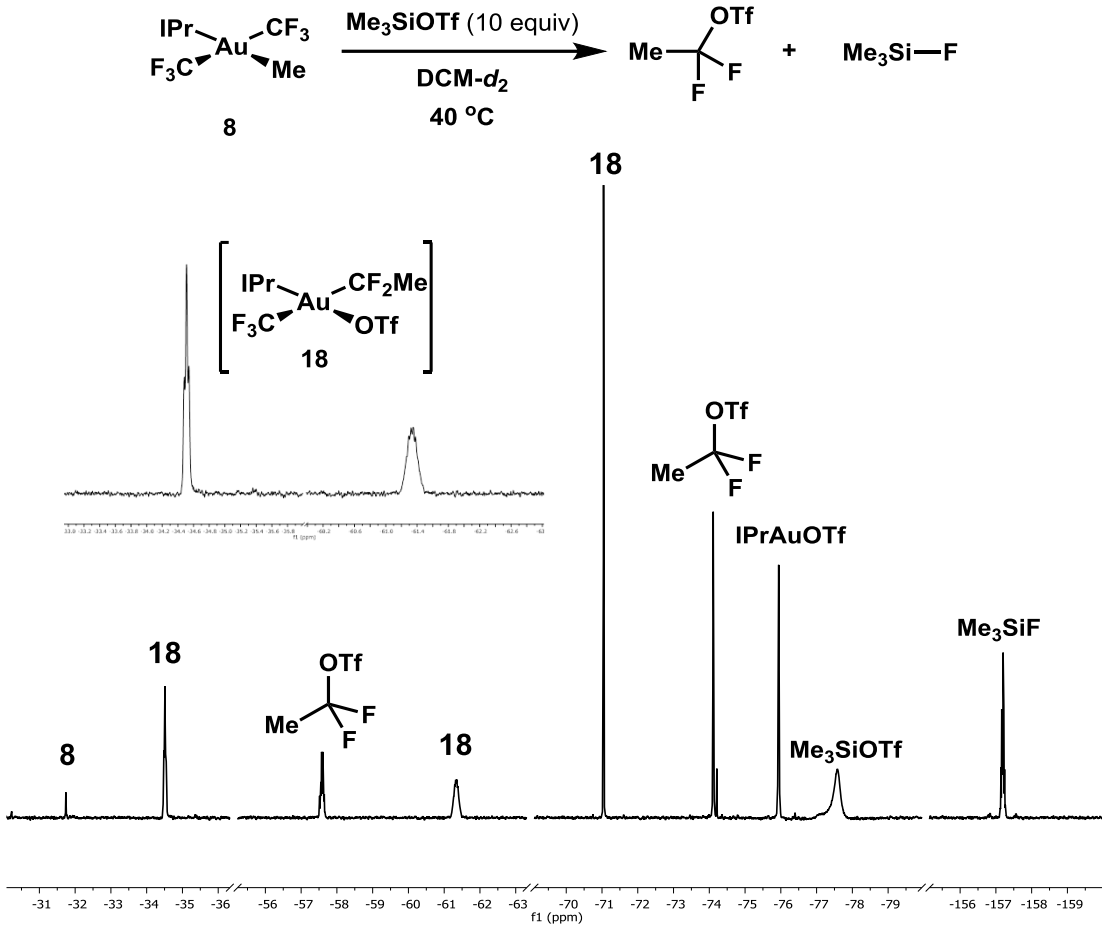


**Figure 4.15** Reaction of **8** with $Me_3SiOTf$ to afford $MeCF_2OTf$, and $^{19}F$-NMR after 4 hours of reaction showing observable intermediate **18**. Baseline has been segmented for ease of interpretation.

Successful trapping of the intermediate was also achieved by the combination of triethylsilane and BCF, affording a mixture of $MeCF_2H$ and $MeCF_3$ (Figure 4.16). No reaction occurred in the absence of BCF. Similar trapping experiments with $Ph_3SiOH$, $Me_3SiOMe$, $(Me_3Si)_2O$, $(Me_3Si)_3N$, $PhSiMe_3$ and vinyl trimethylsilane were unsuccessful, affording only trifluoroethane, whereas $Me_3SiCN$ shut down reactivity altogether.

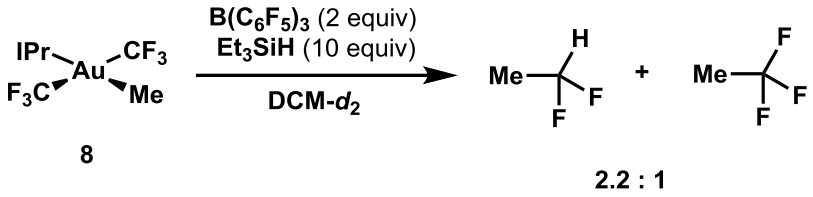


**Figure 4.16** Difluoroethane formation in the reaction of **8** with $Et_3SiH$ and BCF.

In order to close the putative catalytic cycle, we aimed to demonstrate that **17** could undergo productive C-F bond formation to generate trifluoroethane and **12**. Towards this goal, we subjected a mixture of **17a** and **17b** to an excess of silver fluoride, resulting in the formation of

trifluoromethane (Figure 4.17). However, the reaction was much slower than the catalytic process with BCF, requiring 36 hours for complete conversion, and was much less clean, producing difluoroethylene as a side product as well as two isomeric, observable Au(III) fluoride intermediates (See Supporting Information below for more details).[23,52–55]

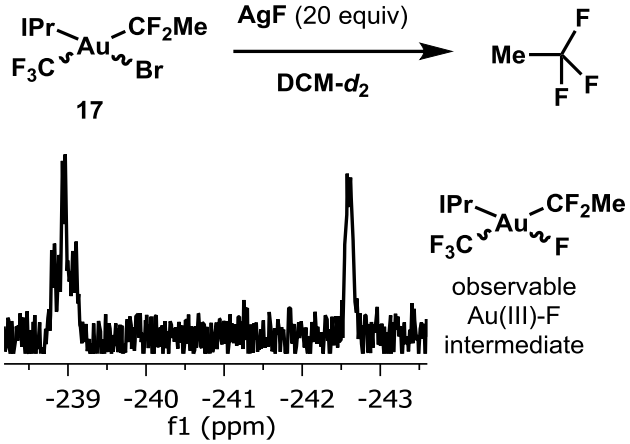


**Figure 4.17** C-F bond formation from **17** by halide metathesis and $^{19}$F-NMR spectrum of Au(III)-F resonances of observable intermediates.

Based on these experiments, we propose an overall mechanism for this process consisting of fluoride abstraction (*i*) from a $CF_3$ moiety of **8** by BCF resulting in difluorocarbenoid intermediate **14**, which undergoes rapid migratory insertion (*ii*) to form difluoroethyl complex **15**.[56] Finally, fluoride re-delivery from BCF to **15** results in the formal reductive elimination (*iii*) of trifluoroethane, with **12** as the Au-containing byproduct. Subsequent fluoride abstraction from **12** (*via* difluorocarbenoid intermediate **16**) ultimately affords **10** by a series of unclear steps involving transmetallation of a $C_6F_5$ unit to gold (Figure 4.18). We have taken to referring to this mechanism as a "fluoride-rebound" to describe the role of BCF in activating **8** towards reductive elimination.

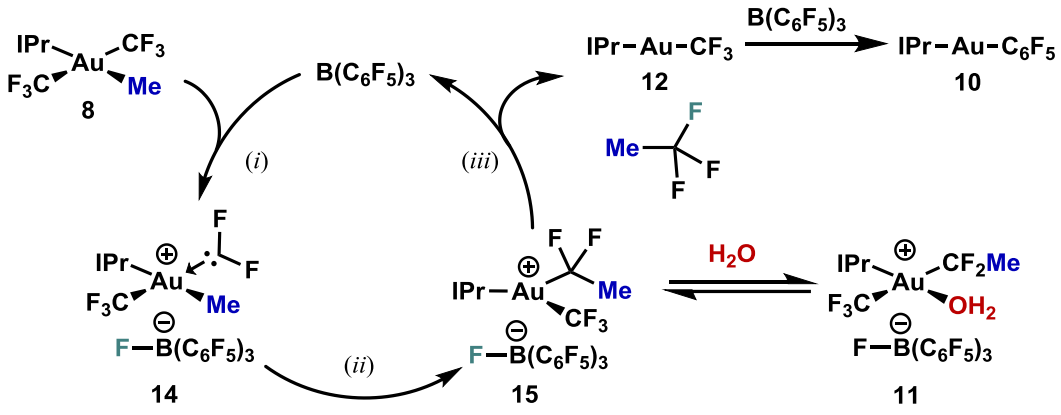


**Figure 4.18** Proposed "fluoride rebound" mechanism for BCF-catalyzed reductive elimination.

This proposal also allows assignment of the identity of species **11** as a reversibly formed *aquo* complex of **15**, with stereochemistry again assigned in analogy to **17a** based on the $CF_3$/$CF_2$Me coupling constant.[57] Several other features of this proposal and their relation to the above experiments merit comment. First, *inner-sphere* migratory insertion at Au(III) is sparsely

precedented, with no reports of $C_1$-insertions, and relatively few reports of $C_2$-insertions at gold for either oxidation state, many of which have been shown to proceed through radical intermediates.[58–63] Second, the evidence points towards an outer sphere mechanism for the formal C-F reductive elimination. No Au(III) fluoride intermediates are observed in the reaction of **8** and BCF, whereas the silver fluoride-mediated reaction from **17** produces long-lived gold fluorides, suggesting that BCF plays a role in assisting the C-F bond forming process. Further evidence is found in the stability of bromide **17** and comparative reactivity of triflate **18**, with reductive elimination occurring only from the more weakly-coordinating anion. Finally, precedent for halogen reductive elimination suggests that such reactions involve dissociative processes, with the best-studied example of C($sp^3$)-F reductive elimination affording Wagner-Meerwein rearrangement of the alkyl substituent reminiscent of $S_N1$ reactivity (Figure 4.19).[23,53,64,65]

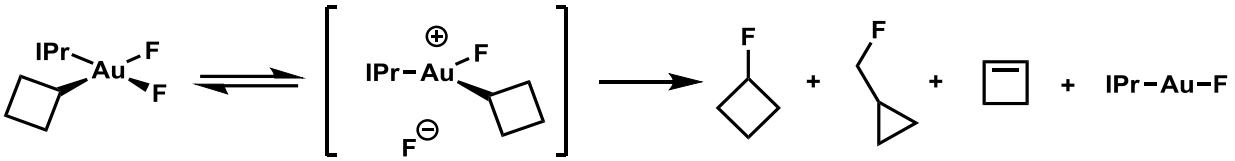


**Figure 4.19** Precedent for $S_N1$-like C($sp^3$)-F reductive elimination from Au(III).

In order to evaluate these aspects of the mechanistic proposal, a DFT computational study on a simplified system bearing a diphenyl NHC ligand and $BF_3$ as the Lewis acid was conducted at the M06-L/cc-PVTZ; Au:SDD(2f,g) level of theory (Figure 4.20).[66,67]

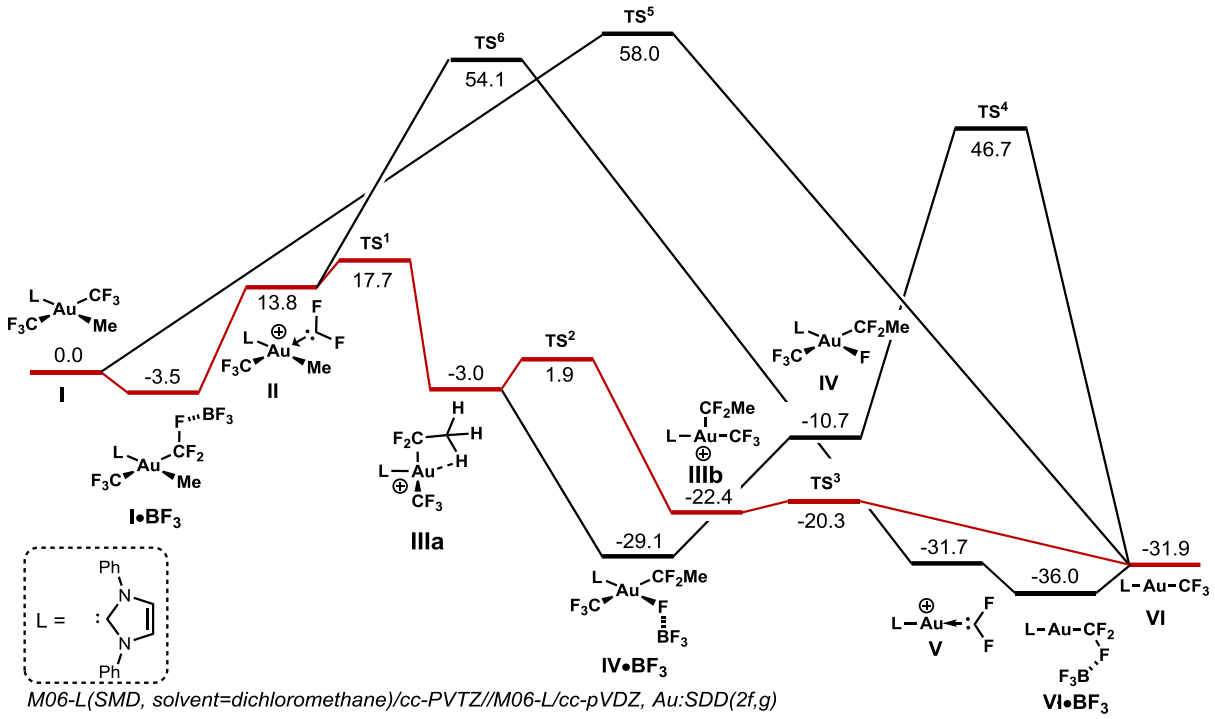


**Figure 4.20** Summary of DFT computational study of the proposed reaction mechanism on a simplified system. Lowest energy path in red.

The lowest energy pathway computed corresponds closely to the proposed mechanism. Borane association to **I** (c.f. **8**) is exothermic, with subsequent C-F cleavage to afford **II** (c.f. **14**) occurring with a barrier indistinguishable from the coulombic penalty for charge separation.

Subsequent migratory insertion occurs with a small barrier ($\Delta H^{\ddagger} < 4$ kcal/mol) to give the T-shaped intermediate **IIIa** (c.f. **15**) which is computed to feature an agostic interaction between the C-H of the $CF_2Me$ group and gold.[68] **IIIa** must undergo an isomerization to its thermodynamically preferred isomer **IIIb** prior to reductive elimination. Such an intrinsic barrier to isomerization of tricoordinate Au(III) complexes has been examined computationally previously as a consequence of Jahn-Teller instability for trigonal planar $d^8$ metals.[69] Notably, these two isomers correspond to the observed trapping products **17a** and **17b**, respectively, suggesting that bromide trapping is not thermodynamically controlled. Rather, either trapping occurs faster than isomerization, or a Curtin-Hammett scenario is established wherein isomer **a** has a lower barrier to bromide association. Finally, the transition state for reductive elimination from **IIIb** (**TS$^3$**) involves outer-sphere attack of the $BF_4$ anion on the $CF_2Me$ group, consistent with the expectations outlined above (Figure 4.21). In the case of $R_3Si$-H trapping (Figure 4.16), it remains unclear whether inner-sphere C-H elimination from a gold hydride or outer-sphere elimination from a borohydride is operative.[70]

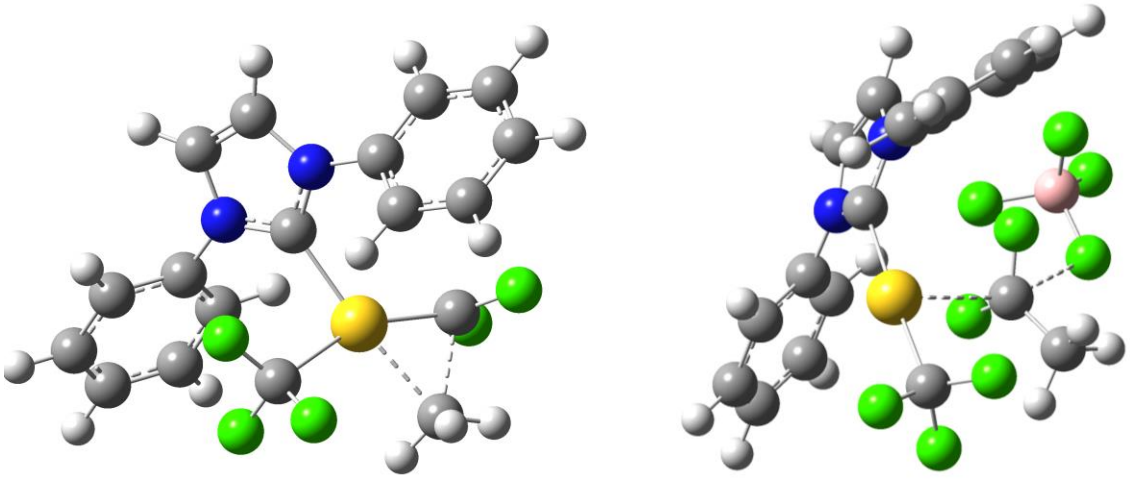

**Figure 4.21** Computed transition states for migratory insertion (**TS$^1$**, left) and reductive elimination (**TS$^3$**, right).

Alternative mechanisms, including direct C-C reductive elimination from **I** (**TS$^5$**), or after activation with $BF_3$ (**TS$^6$**, akin to the alternative in Figure 4.13), as well as inner-sphere C-F reductive elimination (**TS$^4$** from **IV**) were computed to occur with substantially higher barriers. Even accounting for potential systematic errors in the computational results, the predicted magnitude differences are a strong suggestion that such alternatives are unlikely.[71]

In a broad sense, the mechanistic proposal outlined here is remarkable for several reasons. It represents a formal C($sp^3$)-$CF_3$ reductive elimination, itself unprecedented in the literature, by a process involving iterative disassembly and reassembly of a trifluoromethyl group. From a "choreographic" perspective, the report of formal C-F oxidative addition to iridium *via* a sequence of C-H oxidative addition, α-fluoride elimination, and α-hydride insertion is perhaps the closest analogue (Figure 4.22).[72]

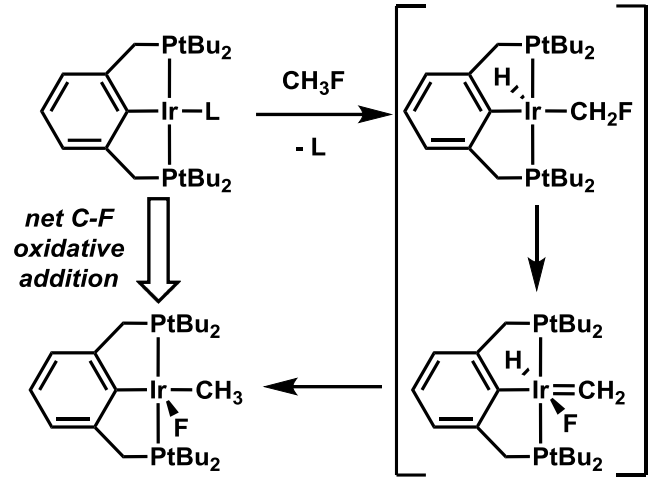


**Figure 4.22** Previously reported mechanism for C-F oxidative addition to Ir.

Furthermore, migratory insertion to an intermediate difluorocarbenoid is rare, especially in the presence of water.[73–78] It seems likely that the rapid migratory insertion serves a protective function in this system, avoiding competitive hydrolysis of **14** to HF and CO.[48] Indeed, a recently reported cobalt difluorocarbene (Figure 4.23) undergoes competitive insertion and hydrolysis even after drying of the solvent over molecular sieves (< 0.1 ppm $H_2O$).[45,77] Such rapid reactivity at gold is likely due to a lack of backbonding to the carbenic center, making it exceptionally electrophilic.[79]

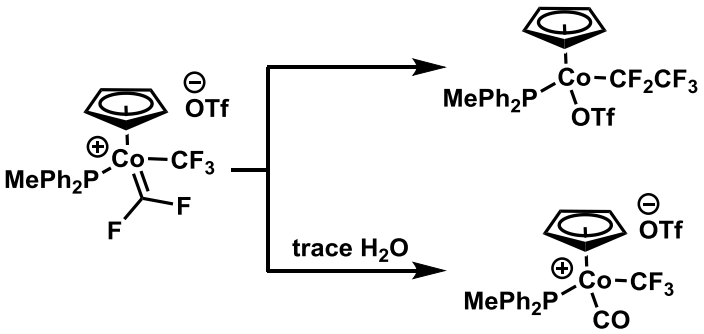


**Figure 4.23** Previously reported Co difluorocarbene complex which undergoes competitive hydrolysis and insertion

Finally, the lack of elimination products (despite the availability of β-hydrogens in intermediate **15**) underscores the low propensity of gold to undergo such eliminations.[80] The observation of difluoroethylene in the silver-mediated elimination (Figure 4.17) but not in the BCF-catalyzed reaction suggests that the borane serves to modulate the tendency for fluoride to entertain basic and nucleophilic reactivity akin to the relationship between hydride and borohydride.

### 4.3.3 Structural and Synthetic Study

Up to this point, only one complex had been examined for its propensity to undergo borane-catalyzed reductive elimination. As such, we endeavored to explore structural analogues of **8**. The analogous synthetic route *via* **7** was not broadly amenable to ligand substitution, requiring a donor strong enough to displace the iodide. However, $PCy_3$ was found to effectively provide this salt

elimination, affording **18** in excellent yield after column chromatography (Figure 4.24). **18** was structurally characterized by X-ray crystallography, exhibited similar levels of air, water, and thermal stability to those of **8**, and similarly underwent reductive elimination of trifluoroethane when treated with BCF. The gold-containing products were likewise controlled by the loading of BCF, primarily forming $Cy_3P$-Au-$CF_3$ (**19**) with catalytic quantities and $Cy_3P$-Au-$C_6F_5$ (**20**) with stoichiometric quantities.

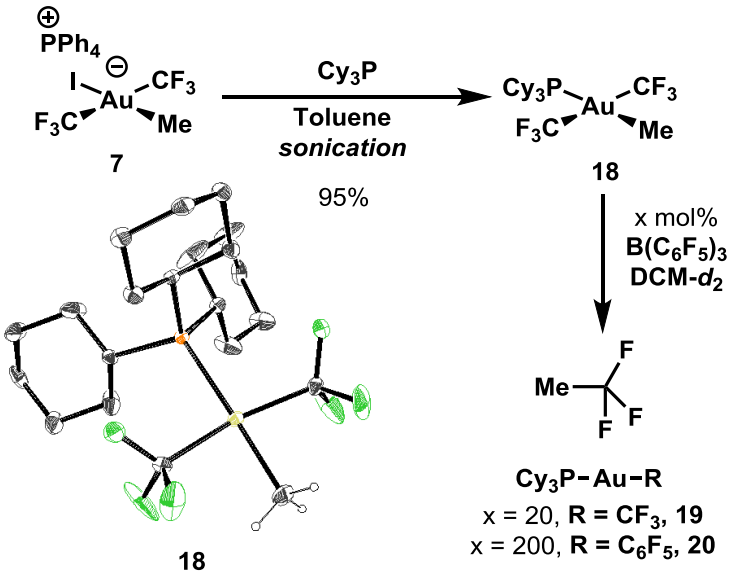


**Figure 4.24** Preparation, crystallographic structure, and reactivity of phosphine supported Au(III) complex **18**. Hydrogens (except Au-$CH_3$) omitted for clarity.

Extension to other alkyl substituents by oxidative addition to **6** proved more challenging. Though iodoethane reacted to afford **21**, the reaction was sluggish and low yielding. Allyl Bromide did not produce an isolable Au(III) complex, instead directly affording 4,4,4-trifluoro-1-butene and mixed aurate **22**.[26] 2-iodopropane provides the tris-trifluoromethyl complex **23** in low yield, with substantial deposition of metallic gold (Figure 4.25).

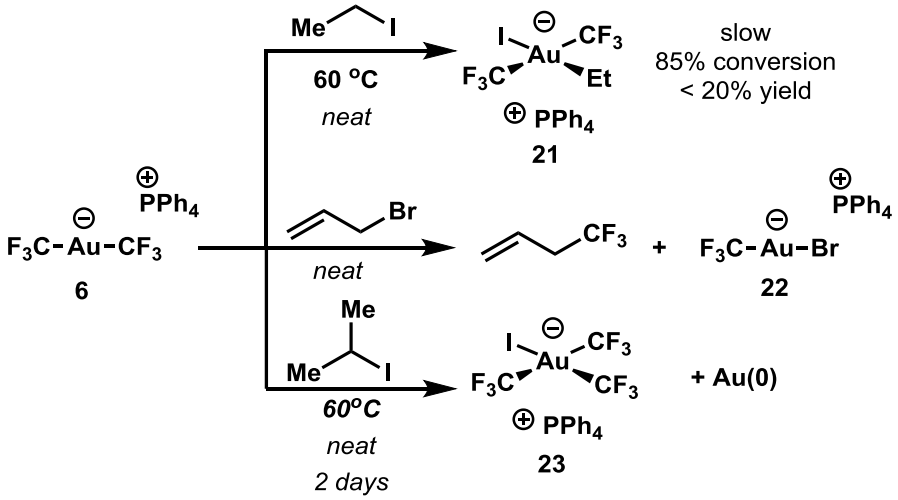


**Figure 4.25** Attempted oxidative addition of other alkyl halides to **6**

As discussed in Chapter 2, the divergent behavior for the allylic halide may arise from direct reductive elimination to an $\eta^3$-allyl species upon halide dissociation. The nature of the disproportionation process occurring in the formation of **23** is unclear, and may involve radical intermediates.[81]

The lack of generality in the preparation of derivatives of **8** by an oxidative addition route led us to consider the polarity-reversed strategy, requiring the synthesis of an Au(III) precursor to which transmetallation could be achieved. To that end, previously reported dichloride **24** was prepared by a modified procedure, and upon reaction with IPr free carbene yielded complex **25** in good yield after column chromatography (Figure 4.26).[82] **25** was characterized crystallographically to confirm its connectivity, and could be prepared in large quantities in a short 4-step sequence from commercially available materials.

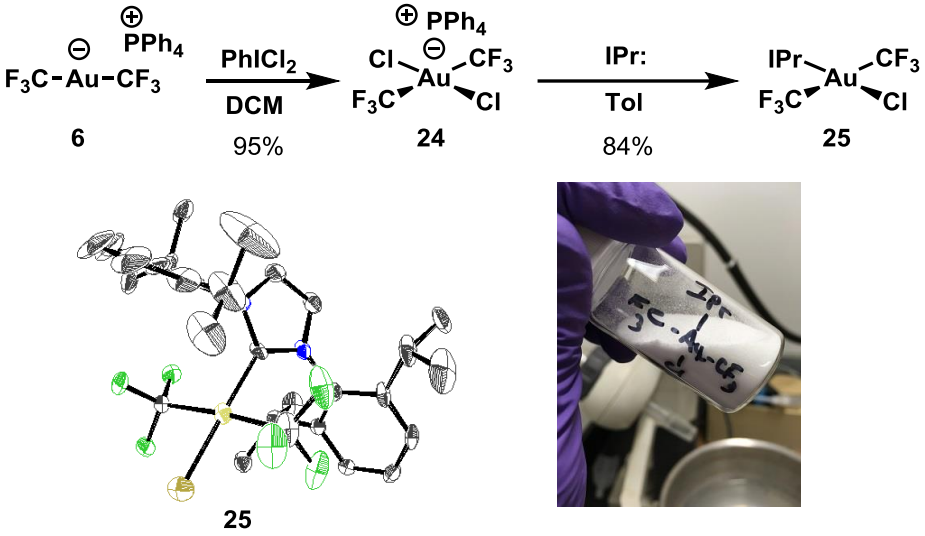


**Figure 4.26** Synthesis and crystallographic structure of Au(III) chloride complex **25** (hydrogens omitted for clarity). Isolated product on seven gram scale pictured.

Transmetallation to **25** proved less straightforward than anticipated, with most classes of nucleophilic alkyl fragment resulting in reduction to **12** and $CF_3H$ or no reaction (Figure 4.27).

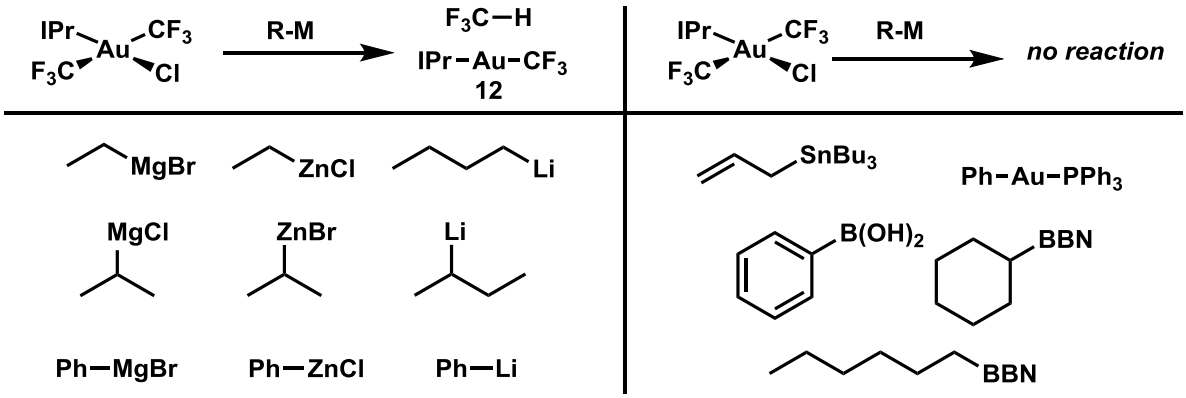


**Figure 4.27** Unsuccessful transmetallations to **25**. Boranes, boronic acids, and stannanes were examined both with and without additional fluoride or alkoxide activators.

Nonetheless, some classes of reagents were found to provide clean transmetallation to give the corresponding organogold(III) complexes. Primary dialkyl zinc, diarylzinc and allylic Grignard reagents were all competent to produce the corresponding Au(III) derivatives **26**, **27**, and **28**. Unfortunately, the corresponding secondary dialkyl zinc formed **12** exclusively. We have been unable, so far, to produce any 2° or 3° alkylgold complexes. $\eta^1$-allyl complex **28** was characterized crystallographically as shown. Whereas **26** and **27** underwent clean BCF-catalyzed reductive elimination to afford the corresponding organic products, **28** gave a complex mixture of products. Trapping with $Et_3SiH$ in the reaction with **27** (akin to Figure 4.16) afforded $PhCF_2H$ as the exclusive product, though subsequent hydrodefluorination catalyzed by BCF occurred to give toluene as the ultimate product.[83–85] This does not occur when starting from aromatic $CF_3$ compounds, suggesting that the initial hydrodefluorination occurs on gold.

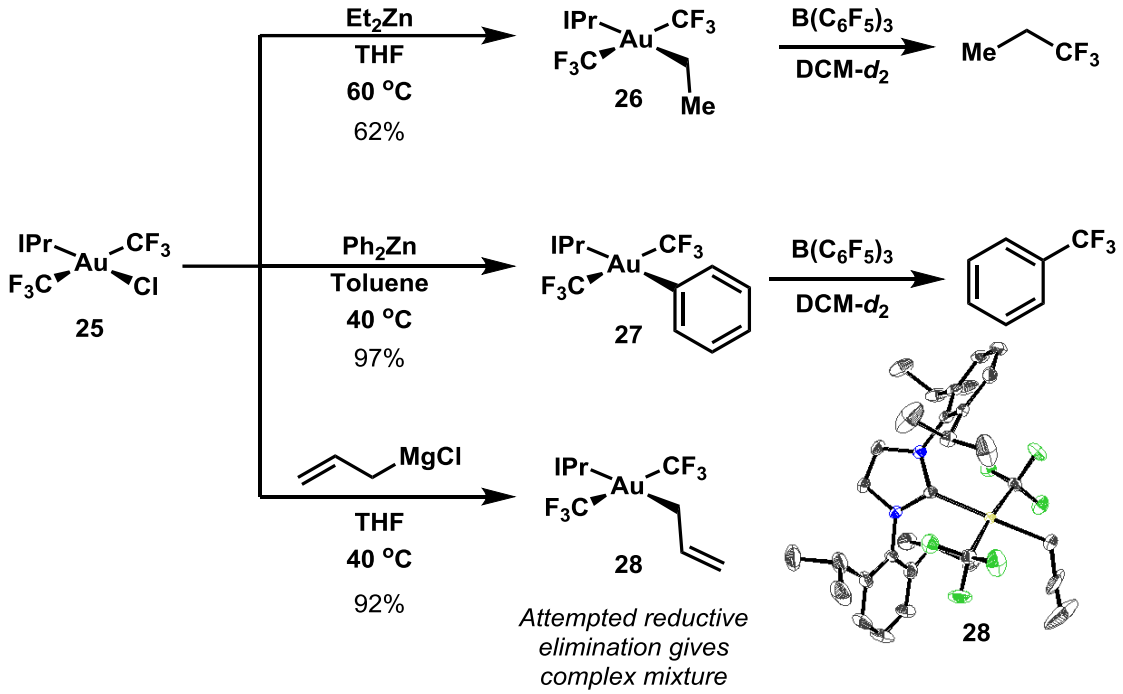


**Figure 4.28** Successful transmetallation to **25** with diorganozinc and allylic Grignard reagents, BCF-catalyzed reductive elimination chemistry of **26** and **27**, and crystallographic structural characterization of **28** (hydrogens omitted for clarity).

A puzzle regarding the comparative efficiency of the diorganozinc transmetallations with their monoorgano counterparts is clearly apparent. Though the latter are typically considered as less reducing, they selectively form the reduction product **12**. Furthermore, the direct product of $R_2Zn$ transmetallation is the corresponding RZnCl complex – and whereas reduction by RZnCl species occurs in minutes at 25°C, the transmetallation reactions from $R_2Zn$ are invariably slower, requiring heating for several hours. A full understanding of these seemingly contradictory features remains elusive.

Along these lines, an unusual reaction occurred when **25** reacted with the substituted allylic Grignard **29**. Though the desired transmetallation product **30** was formed, the major product was **12**. However, rather than forming $CF_3H$, an organic $CF_3$ compound was observed as the major product (Figure 4.29). **30** did not convert to **12** upon further heating.

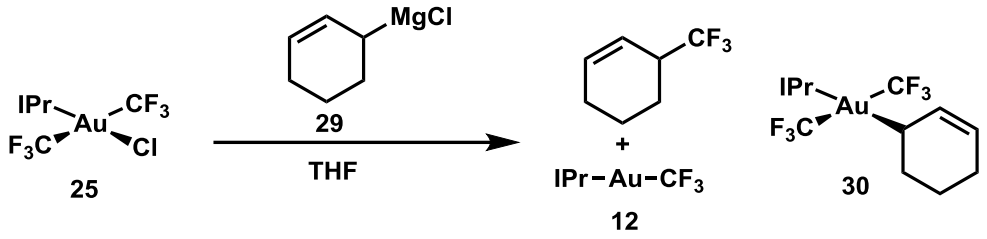


**Figure 4.29** Attempted transmetallation to **25** with a substituted allylic Grignard.

Despite these difficulties, the general tolerance of the organogold complexes (**8**, **18**, **26-28**) to water, air, and silica, led us to consider an alternative means for generating diversity. Direct synthetic elaboration of the pendant olefin of **28** would allow exploration of the scope for the BCF-catalyzed reductive elimination without the need to prepare and purify functionalized diorganozinc reagents. To that end, the chemistry of **28** was explored, uncovering a surprising breadth of synthetic tolerance.

Olefin metathesis between **28** and styrene derivative **31** catalyzed by Grubbs' 2nd generation catalyst affords complex **32**, which can be subsequently hydrogenated with Rh/C and $H_2$ to give the saturated derivative **33** (Figure 4.30). No hydrogenolysis of the Au-C bond, nor any Au(I) byproducts were detected under these conditions.[86] An alternative route involves hydroboration to afford intermediate alkylborane followed by cross-coupling to give **33** (See Supporting Information for details). This latter procedure requires fewer purifications but was ultimately found not to scale reproducibly. Complex **33** was characterized crystallographically, and underwent clean BCF-catalyzed reductive elimination to afford the organic product **34**. In contrast, **32** afforded a complex mixture of products, a feature that seems to be common to the allylic derivatives studied herein.

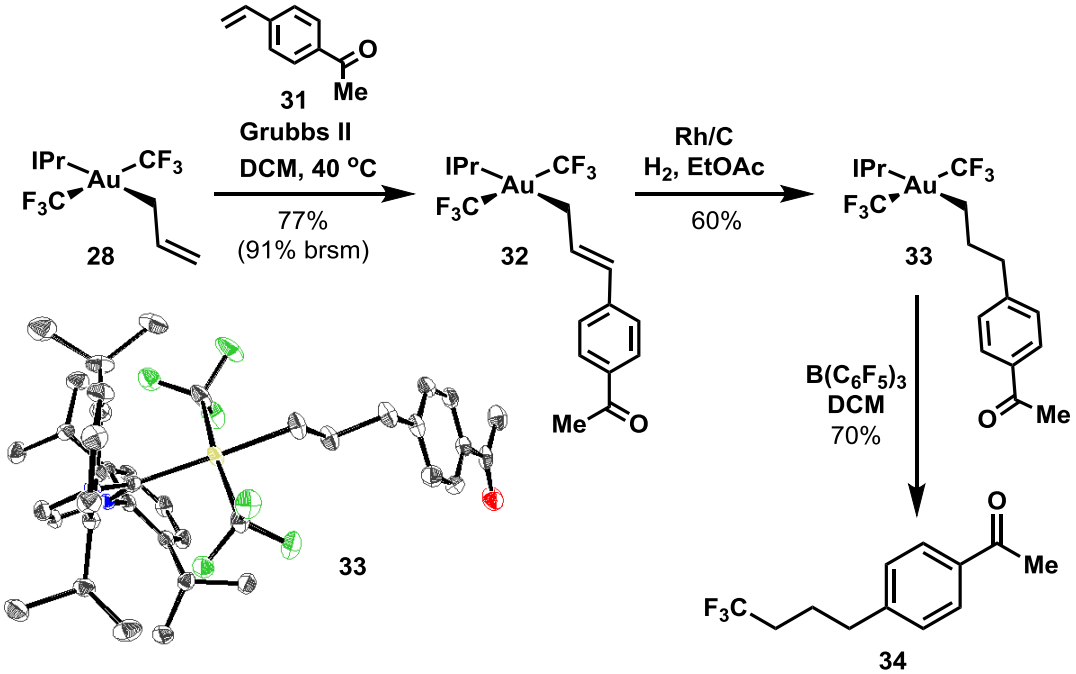


**Figure 4.30** Synthetic elaboration of **28** *via* olefin metathesis and hydrogenation, and crystallographic structure of **33**, hydrogens omitted for clarity.

An alternative sequence commencing with olefin metathesis from dimethyl maleate was also examined. From the acrylate **35**, hydrogenation afforded **36**. Surprisingly, **36** was found to tolerate aluminum hydride reduction to give the alcohol **37**, which could be elaborated under Mitsunobu conditions to give ester **38**. This final compound provides the corresponding product of reductive elimination **39** upon treatment with BCF (Figure 4.31).

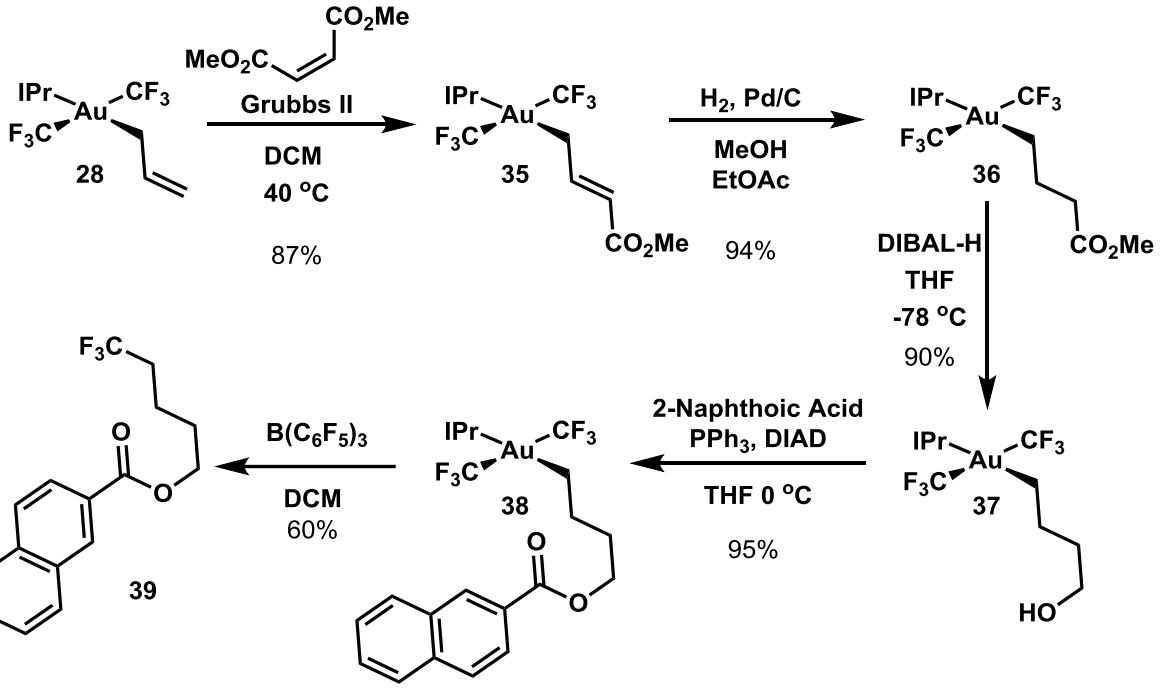


**Figure 4.31** Synthetic elaboration of **28** *via* olefin metathesis, hydrogenation, aluminum hydride reduction, and Mitsunobu esterification.

Acrylate **35** was unreactive towards reductive elimination, instead forming an observable 1:1 complex with BCF. Use of superstoichiometric borane did not induce reductive elimination, presumably by virtue of electronic deactivation towards migratory insertion.[87,88]

Interestingly, both **36** and **37** produced a mixture of desired reductive elimination product and a trapped migratory insertion product which in the case of **36** was persistent in solution over a period of days (Figure 4.32). The proposed structure of this arrested intermediate **40** is shown, and is assigned by analogy to **17a**. Unfortunately, **40** evaded isolation, preventing further characterization; the lack of subsequent reductive elimination is likely due to competitive reaction of the fluoroborate with glass, as evidenced by the formation of $SiF_6$. It seems that generally, coordinating atoms within several carbon atoms of the gold center are not tolerated due to this behavior.

Additional transformations of **28** were found to be tolerated, including Simmons-Smith cyclopropanation, osmium-catalyzed dihydroxylation, and periodate-mediated diol cleavage (Figure 4.33).[89] The corresponding products **41**-**43** did not produce clean reductive elimination products, with cyclopropane **41** and aldehyde **43** giving complex mixtures, and diol **42** undergoing pinacol rearrangement upon treatment with BCF. Complex **41** was characterized by X-ray crystallography as shown.

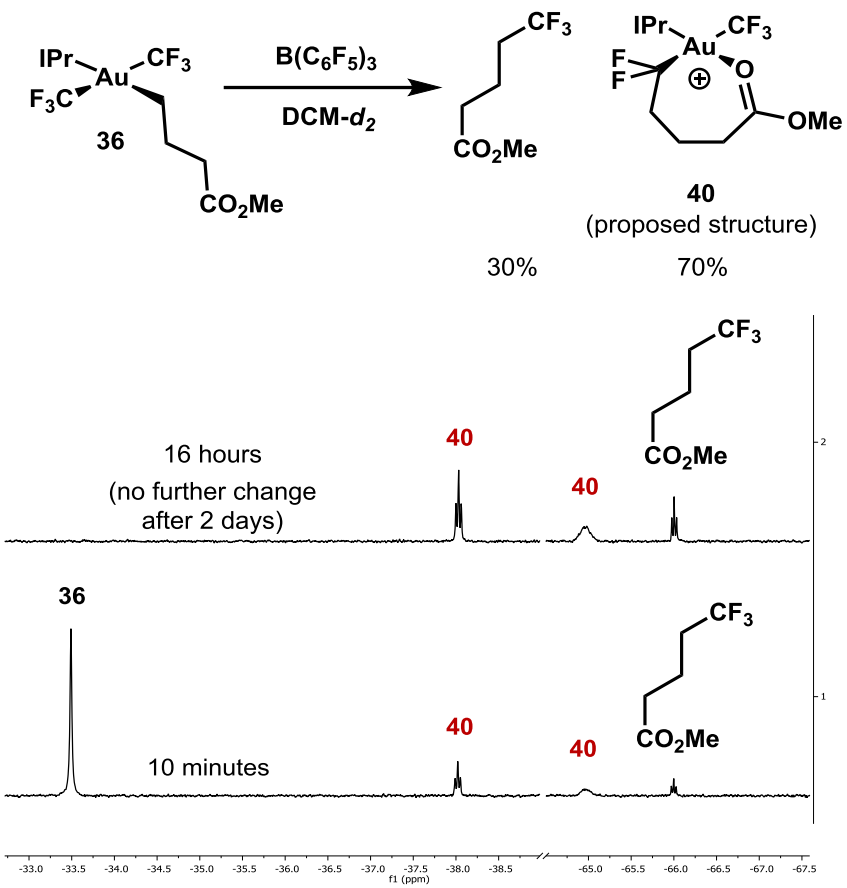


**Figure 4.32** $^{19}$F-NMR spectrum of attempted BCF-catalyzed reductive elimination from **36**, with observation of a trapped migratory insertion product, proposed structure **40**.

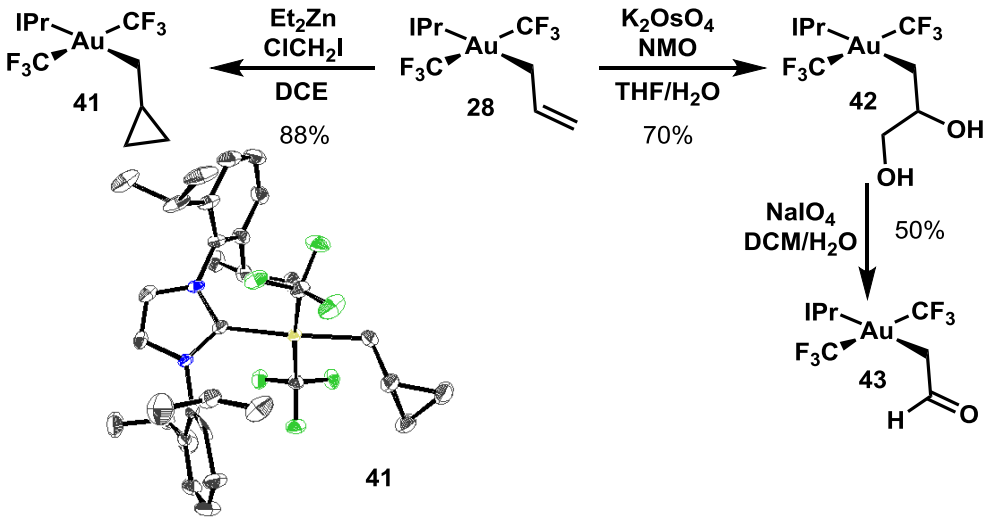


**Figure 4.33** Additional synthetic tolerance of **28** and crystallographic structure of cyclopropane **41**. Hydrogens removed for clarity.

Gold aryl **27** was also found to tolerate an unexpected diversity of synthetic conditions. Aromatic nitration (remarkably without rupture of the Au-C bond) occurred with 1:2 ortho/para selectivity.[90] The resulting mixture of nitroaryl gold complexes could subsequently be reduced with ammonium formate to selectively give aniline **44**.[91] (Reduction of the ortho isomer occurs at a substantially slower rate). Subsequent acylation under standard conditions gave amide **45**, which upon treatment with BCF provided antirheumatic drug Leflunomide (**46**).[92] This latter reductive elimination was slowed by competitive complexation of the borane by Lewis-basic sites on **45**, but after heating at 40 °C for 15 hours, **46** could be isolated in 98% yield, albeit on small scale.[93] In contrast, attempted elimination from **44** resulted in the formation of a bright-red solution and a complex mixture of products, suggesting single-electron oxidation of the aniline by BCF.[94]

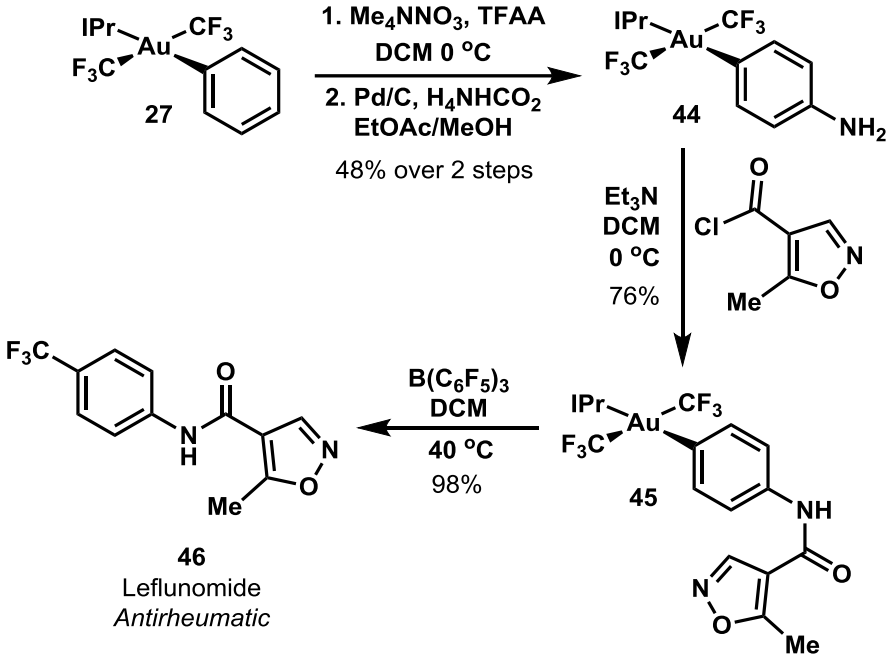


**Figure 4.34** Synthesis of Leflunomide by synthetic elaboration of **27**

A final synthetic endeavor focused on the preparation of Bayer drug candidate BAY 59-3074 (**52**).[95] Aliphatic trifluoromethyl groups are relatively rare in pharmaceuticals, presumably due to a lack of methods for their preparation.[96,97] Most commonly, nucleophilic trifluoromethylation of carbonyl compounds with $Me_3SiCF_3$ is used, with several electrophilic α-functionalizations of enolates also reported.[98–101] Our reactivity seemed uniquely suited to the preparation of the unactivated aliphatic trifluoromethyl group in **52**. To that end, a sequence involving hydroboration/oxidation (**47**), iodination (**48**), thioacetate substitution (**49**) and oxidation afforded sulfonyl chloride **50** without reduction of the gold center or rupture of the Au-C bond, despite the intervention of reducing and oxidizing agents typically competent for such reactivity with high valent metals. Subsequent esterification afforded the sulfonyl ester **51**, which upon treatment with BCF afforded the desired compound **52** in 67% yield. Here the demand of Lewis basic substituents was less intense than for **45**, allowing complete conversion in under 2 hours at room temperature.

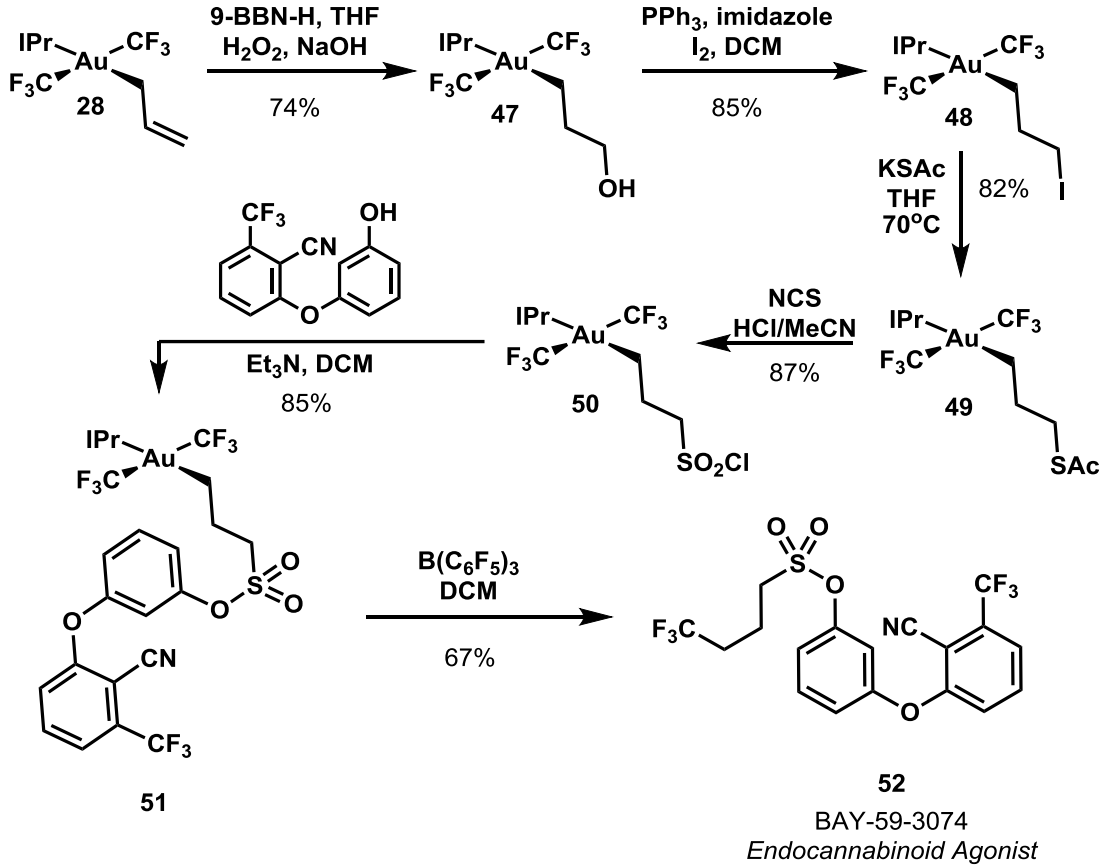


**Figure 4.35** Synthesis of BAY-59-3074 by synthetic elaboration of **28**

All of the intermediate gold complexes were found to exhibit complete air and water tolerance, and were universally amenable to purification by silica gel column chromatography. As such, we have begun to regard the bis($CF_3$)Au moiety as a triggerable but otherwise inert functional group, enabling routine chemical synthesis akin to typical organic substrates.

As a final commentary on the structural aspects of these complexes, we were interested to see if the crystallographic structures collected offered any clues in retrospect to the observed reactivity. Often, the C-F bond distances in metal trifluoromethyl complexes are elongated compared to the average organic $CF_3$ (1.336 Å, compared to for example, 1.370 Å for $CF_3Mn(CO)_5$), which is taken as a sign of backbonding.[102] Though such an interaction is unlikely given that Au(III) carbonyls are nonclassical, we wondered whether such an elongation was still present, given that these complexes seem to activate the $CF_3$ group to some degree.[79] Figure 4.36 contains a summary of the C-F bond distances for all such complexes in the Cambridge Structural Database, alongside those for the 6 complexes described above. Each bond distance has been subtracted from the average organic $CF_3$, and both the average C-F distance in each structure (black diamonds) and the maximum distance (red squares) are shown. In all, it seems that the Au(III) complexes studied herein show more modest elongation than other transition metal trifluoromethyls, though longer than for other previously reported Au(III) $CF_3$ complexes. (The one lower number in the series is gold chloride **25**, which lacks a donating alkyl group.) One possibility is that the mutually *trans* $CF_3$ groups impart some kind of activating influence in these complexes.

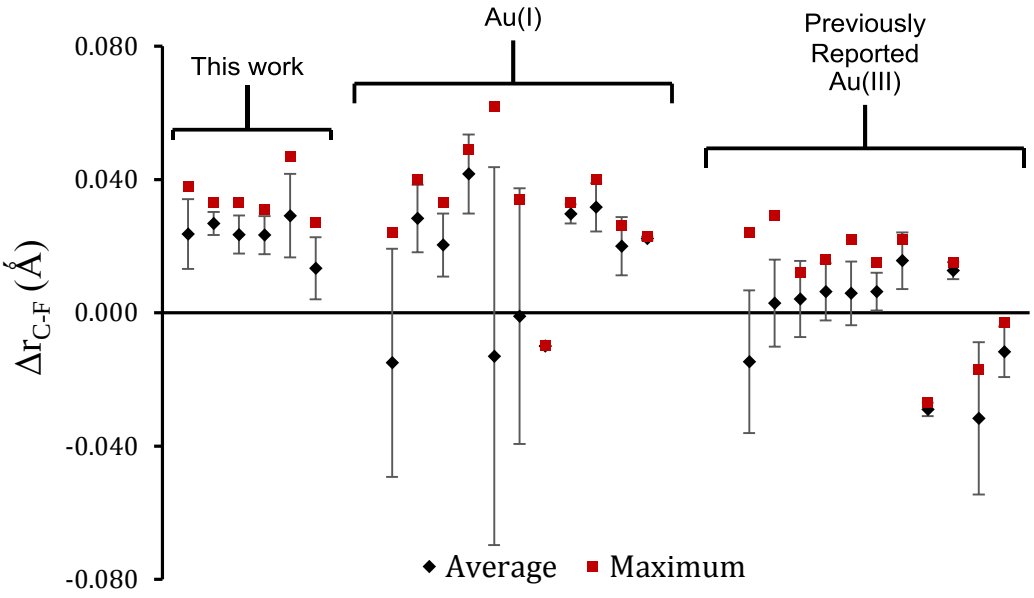


**Figure 4.36** Comparison of the average (black) and maximum (red) C-F bond lengths relative to "the average organic $CF_3$" in crystallographically characterized [Au]-$CF_3$ compounds.

### 4.3.4 Development of a Radiochemical Protocol

It became clear to us that interception of the 'rebounding' fluoride and introduction of a radiolabeled surrogate would hold promise for the synthesis of PET tracers, provided that a protocol equipped for the specific constraints of radiosynthesis could be developed. A brief summary of those constraints is provided.

Fluorine-18 is most commonly produced by the $^{18}O(p,n)^{18}F$ (i.e. proton capture, neutron emission) nuclear reaction by high energy (ca. 10 MeV) proton irradiation in a cyclotron. When $[^{18}O]H_2O$ is employed as the starting material, the resulting solution contains a relatively low concentration of fluoride ions, which are present as a mixture of HF and metal fluorides (leached from the reactor and target window walls, e.g. niobium, silver, tantalum, iron, etc.). This aqueous solution is typically treated with an appropriate base to neutralize any residual acid, and a phase transfer catalyst (typically tetrabutylammonium or Kryptofix[2.2.2], pictured) is added, followed by azeotropic drying with acetonitrile (Figure 4.37).

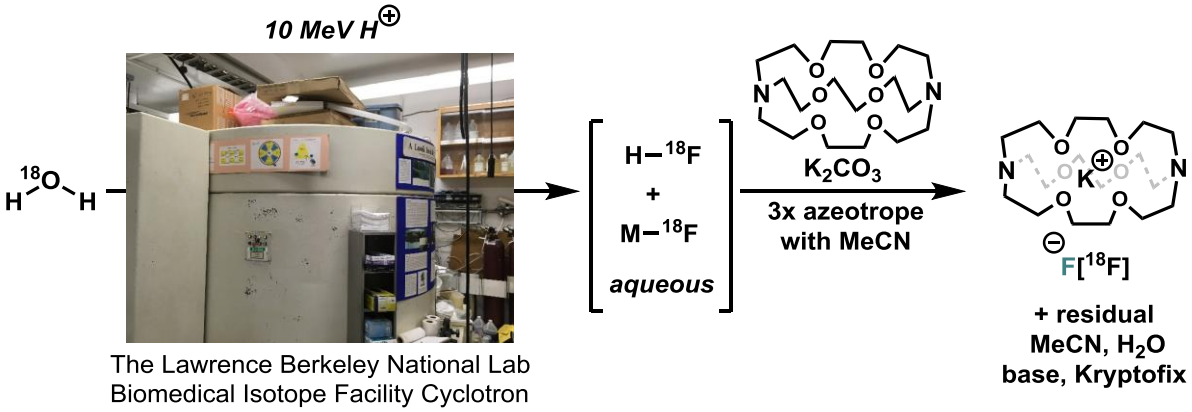


**Figure 4.37** Schematic of typical [$^{18}$F] preparation

The fluoride produced is measured on the basis of its radioactivity, in units of Curies (Ci), with 1 mCi = 3.7 x $10^7$ decays per second. In chemical terms, 1 mCi corresponds to 0.585 nanomoles of $^{18}$F. At these low concentrations, adventitious $^{19}$F is generally unavoidable, such that practically, for every atom of $^{18}$F something like 350 atoms of $^{19}$F is present. Thus in a representative radiochemical experiment, 0.2 μmol of fluoride per mCi is a convenient approximation. In exploratory reactions developing new tracers or methodologies, 0.5-10 mCi per reaction is typical, corresponding to 0.1 to 2 μmol of total fluoride. As such, the other reagents are always present in large excess. (This is by design as well as by necessity, given that $^{18}$F is the most valuable component and therefore must be the limiting reagent.)

The percentage of fluoride converted into the desired tracer product is termed **radiochemical yield** and is the primary metric by which radiosynthesis is judged. If measured without accounting for transfer losses, insoluble fluoride, and/or decay, a **radiochemical conversion** can be reported instead. The percentage of tracer molecules in a given sample containing a radioactive fluoride is termed the **specific activity**, and is also important in the development of tracers as it sets limits on dosing for bioactive compounds.

Given all of this, a number of features of the chemical system employed must be true:

1. The reaction must be fast enough to permit synthesis on the timescale of the isotopic half-life (~ 110 minutes for $^{18}$F). Practically speaking, this requires reaction times less than 30 minutes, though shorter is better.
2. The reaction must tolerate residual water and acetonitrile, because typical radiochemical set-ups are not equipped for rigorous drying. Even with the capability in place, complete desolvation of fluoride often leads to glass etching.
3. Because the base and phase transfer catalyst are used in excess relative to fluoride, the reaction must tolerate their presence as well.

Given the results above, we were not concerned about water tolerance, but the ability to tolerate acetonitrile, base, and phase transfer catalysts were not established. Moreover, we had envisioned introduction of fluoride to complex **17** or some similar analogue, but the silver mediated reaction (Figure 4.17) was far too slow and low yielding for these purposes, even given the availability of procedures for radiosynthesis of silver fluoride.[103] We first examined the reaction of **17** with common radiochemical fluoride reagents such as TBAF and KF/Kryptofix, but observed no reaction on radiochemically-relevant timescales.

We envisioned that exchange of the counterion from bromide to either a more weakly coordinating or more basic substitute would allow exchange with either fluoride or HF, respectively. However, treatment of **17** with AgOTs resulted in the rapid reductive elimination of $MeCF_2OTs$, whereas treatment with KOtBu afforded complete conversion to difluoroethylene, with **12** as the byproduct in each case (Figure 4.38).

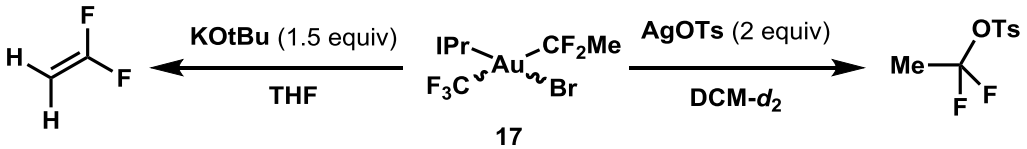


**Figure 4.38** Unsuccessful attempts at salt metathesis from **17**.

Eventually, acetate was identified as a counterion bearing an appropriate level of stability to enable efficient salt metathesis, though unlike **17**, the acetate **53** was found not to be stable toward silica gel chromatography, requiring its use as obtained. Whereas **53** (like **17**) was inert towards TBAF and KF/Kryptofix, treatment with an excess of Pyridine•HF resulted in the rapid reductive elimination of $MeCF_3$. However, as the concentration of HF was decreased, the efficiency of this process severely dropped, with no reductive elimination observed and only trace quantities of the corresponding Au(III)-fluoride detected.

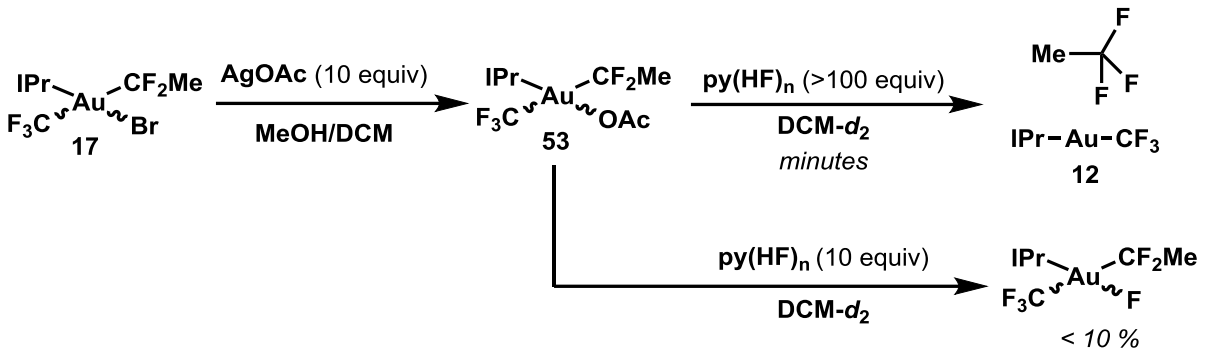


**Figure 4.39** Synthesis of acetate complex **53**, and HF-induced reductive elimination

This substantial requirement of HF loading was not amenable with a radiochemical protocol, despite the availability of methods for preparation of anhydrous [$^{18}$F]HF.[104–106] However, the disparity in reactivity as a function of HF concentration suggested to us that the excess HF might be acting in a manner similar to BCF in catalyzing the reductive elimination (c.f. Figure 4.17) by the formation of $F(HF)_n^-$ as a means to facilitate ionization and induce nucleophilic attack.[107,108]

As such, we re-examined the above reactions in the presence of BCF. Whereas **17** still showed no reactivity, **53** reacted to afford $MeCF_3$ when treated with a combination of fluoride and BCF, though in the case of KF/Kryptofix, an excess of borane was needed to overcome inhibition by coordination of the Lewis basic sites of Kryptofix. Despite this shortcoming, Kryptofix/KF was chosen over TBAF for the ultimate radiochemical protocol for two reasons: (1) residual tetrabutylammonium hydroxide was far less well tolerated than residual $K_2CO_3$ in "cold run" tests, and (2) the increased thermal stability of KF/Kryptofix as compared to TBAF allowed more efficient removal of residual acetonitrile, which was found to have a substantial impact on the rate of the reaction.[109,110]

The corresponding bromides and acetates **54-59** were prepared by analogous methods to those employed for the synthesis of **17** and **53**, though higher temperatures were required for efficient synthesis of the bromides in the presence of coordinating functional groups (see supporting information for details). In all cases, a mixture of two isomers of both complexes was observed, as in **17**. Each was found to undergo efficient reductive elimination of the corresponding trifluoride upon treatment with KF/Kryptofix and BCF, as validated under conditions mimicking the radiochemical protocol, with conversions measured by $^{19}$FNMR (Figure 4.39). Though the isomers of the bromides could not be separated as efficiently as for **17**, **54** was characterized crystallographically by modelling substitutional disorder in a crystal bearing a 60/40 mixture of isomers.

Aromatic analogues remain inaccessible by this method due to accelerated reductive elimination of the benzylic difluoroalkyl moiety; treatment of phenyl complex **27** with $Me_3SiBr$ and BCF results in $PhCF_2Br$ rather than an isolable Au(III) complex.

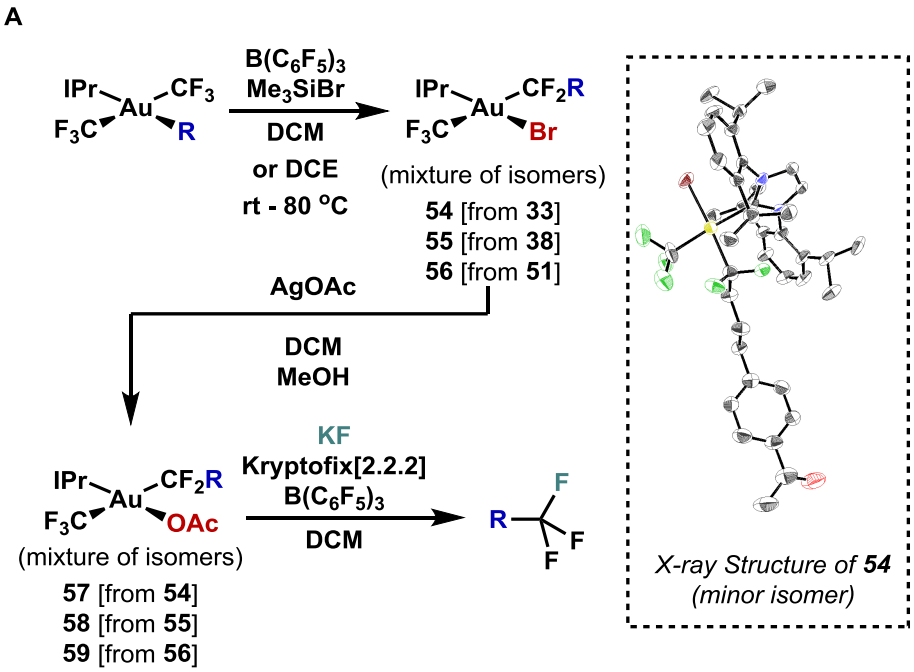


**Figure 4.39** Synthesis of functionalized acetate precursors and validation of reductive elimination reactivity with KF/Kryptofix.

The "cold run" conditions were directly translated to the radiochemical context with one important caveat: addition of the borane prior to the gold complex was necessary to avoid competing residual base-mediated decomposition of the acetate complex. With this modification, the corresponding radiolabeled aliphatic trifluoromethyl complexes were obtained in relatively good radiochemical conversions, as measured by Radio-TLC versus an authentic sample of the product (Figure 4.40, see supporting information for details). No attempts to optimize this protocol beyond the results presented were made, such that if a specific tracer compound is found to be of medicinal interest, further variations in the temperature, solvent, reagent equivalences, and supporting ligand on gold could be explored to improve the efficiency of this transformation.

Future work will focus on these variables, as well as on the determination of the specific activities obtained by this method. Additionally, synthesis of complexes bearing varying spectator X-type ligands (i.e. besides $CF_3$) will be explored as a means to disfavor reductive elimination of $PhCF_2Br$ and thus enable aromatic $CF_3$ radiosynthesis. As the methodology stands, it remains fully complementary to the corresponding Cu-mediated analogue via $CuCF_3$, which is competent for aromatic and benzylic trifluoromethylations but not for the aliphatic substrates accessed herein.

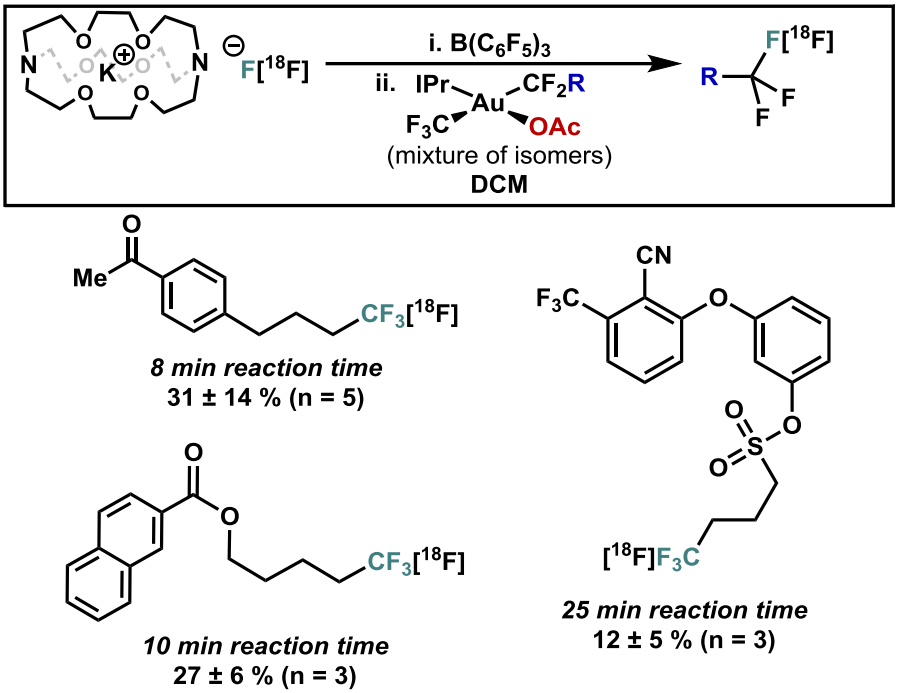


**Figure 4.40** Radiosynthesis of aliphatic trifluoromethyl groups *via* Au(III) acetate precursors. Yields given are radiochemical conversions as measured by Radio-TLC.

We anticipate the disclosed radiochemical technology will enable the preparation and clinical evaluation of previously inaccessible radiochemical tracers once more comprehensive studies on the scope and limitations of this process, as well as optimization with respect to radiochemical yield and specific activity are completed. The costs associated with the syntheses of stoichiometric organogold reagents, though substantial by the metrics of process-scale pharmaceutical preparation, are relatively small in this context given the low concentrations required, the cost of $^{18}$F production, and the costs of the associated medical imaging technology.[111]

## 4.4 Conclusions

The organometallic mechanism uncovered in this chapter is substantially novel, representing an unusual series of elementary reactions which together result in a formal reductive elimination sufficiently challenging that it has otherwise remained unknown. The final step, involving nucleophilic substitution by a fluoroborate on a fluorocarbon, underscores the unique reactivity of cationic Au(III) – in this case acting as an exceptionally good leaving group. Moreover, it has not escaped our attention that this mechanism may in fact be operative in the related copper-mediated protocols currently in broad use as a "cold" synthetic methodology; evaluation of such a mechanistic continuity among the coinage metals is warranted.[112–115] Furthermore, the catalysis demonstrated within this mechanistic manifold represents a new direction for the development and evaluation of organometallic reagents writ large via triggered reductive elimination of synthetically tolerant complexes.

## 4.5 Supporting Information

### 4.5.1 General Considerations

Unless stated otherwise, all reactions were performed in oven-dried or flame-dried glassware. All glassware was cleaned using aqua regia to remove metal impurities. NMR Tubes used for reductive elimination studies with $B(C_6F_5)_3$ were additionally silylated with hexamethyldisilazane at 100°C prior to use. Reactions were sealed with rubber septa under a nitrogen atmosphere and were stirred with Teflon-coated magnetic stir bars. Dry tetrahydrofuran (THF), toluene (Tol), dimethylfomamide (DMF), acetonitrile (MeCN), triethylamine (TEA), diethyl ether ($Et_2O$), benzene (PhH), and dichloromethane (DCM) were obtained by passing these previously degassed solvents through activated alumina columns.

All other reagents were used as received, with the following exceptions: Tris(pentafluorophenyl) borane was purchased from Strem Chemical and purified by hot filtration and recrystallization from hexanes followed by vaccum sublimation at 100 °C. Trimethylbromosilane was purified by distillation. Iodomethane was purified by passing neat over a pad of basic alumina. For all reactions conducted in a glovebox, reagents were thoroughly dried and degassed by standard methods prior to use.

Reactions were monitored by thin layer chromatography (TLC) on Silicycle Siliaplate™ glass backed TLC plates (250 μm thickness, 60 Å porosity, F-254 indicator) and visualized by UV irradiation or by staining as indicated. Volatile solvents were removed under reduced pressure with a rotary evaporator and dried on high vacuum on a Schlenk line. $^1$H NMR, $^{13}$C NMR, $^{19}$F NMR, and $^{31}$P NMR spectra were taken with Bruker spectrometers operating at 300, 400, 500, or 600 MHz for $^1$H. Chemical shifts are reported relative to the residual solvent signal ($^1$H NMR: $\delta = 5.32$; $^{13}$C NMR: $\delta = 53.84$ for DCM-$d_2$). NMR data are reported as follows: chemical shift (multiplicity, coupling constants where applicable, number of hydrogens). Splitting is reported with the following symbols: s = singlet, bs = broad singlet, d = doublet, t = triplet, q = quartet, hept = heptet, m = multiplet. High-resolution mass spectra (HRMS) were performed on a Thermo LTQ-FT-ICR (7T, ESI) by the QB3 mass spectral facility at the University of California, Berkeley. Elemental Analyses were performed by the Microanalytical Facility at the University of California, Berkeley.

Chloro(dimethylsulfide)gold(I) was prepared by reduction of $AuCl_3$ (purchased from Strem) according previously reported procedures. Tetraphenylphosphonium bis(trifluoromethyl)aurate (**6**) was prepared from chloro(dimethylsulfide)gold(I) and $TMSCF_3$ as previously reported and purified by repeated precipitation from DCM with diethyl ether.[25]

Most of the gold complexes reported herein are moderately light sensitive, so reactions, work up procedures, and purifications were conducted with exclusion of light, and all complexes were stored wrapped in aluminum foil.

### 4.5.2 Synthetic Procedures

**Tetraphenylphosphonium *trans*-bis(trifluoromethyl)dichloroaurate, 24**

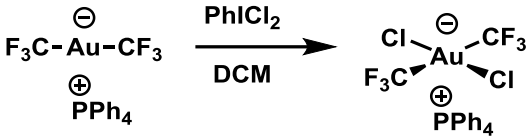


This compound was prepared using a modification of existing literature precedent.[2] Treatment of a solution of tetraphenylphosphonium bis(trifluoromethyl)aurate (5.29 g, 7.84 mmol) in dichloromethane (78 mL, 0.1 M) with freshly prepared iodobenzene dichloride[3] (4.31 g, 15.68 mmol, 2 equiv, added as a solid) resulted in immediate color change from colorless to yellow. The mixture was stirred for 30 minutes and concentrated. The crude solid was washed with copious diethyl ether, extracted with THF, and filtered. Concentration of the THF extract afforded the desired product as a colorless solid (5.8 g, 99% yield).

Spectra were consistent with those previously reported.[25]

$^{1}$H NMR (400 MHz, Methylene Chloride-$d_2$) δ 8.08 – 7.85 (m, 4H), 7.85 – 7.68 (m, 8H), 7.68 – 7.53 (m, 8H).
$^{19}$F NMR (376 MHz, Methylene Chloride-$d_2$) δ -32.82 (s).

**Tetraphenylphosphonium *trans*-bis(trifluoromethyl)methyliodoaurate, 7**

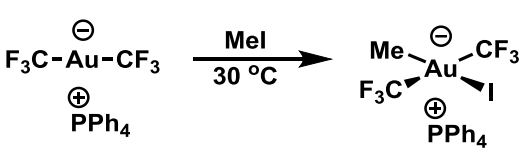


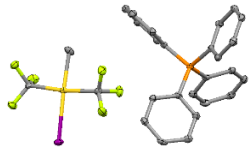

Tetraphenylphosphonium bis(trifluoromethyl)aurate (1.10g, 1.6 mmol) was dissolved in iodomethane (30.1 mL, 410 mmol, 250 equiv), and the mixture was heated with stirring at 30 °C for 18 hrs. The mixture was concentrated, extracted with dichloromethane, and filtered through a glass fiber filter. The filtrate was layered with diethyl ether, and placed in a freezer at -20 °C, resulting in the formation of colorless crystals which were collected by filtration (1.18g, 89% yield). X-ray quality crystals were grown by vapor diffusion of diethyl ether into a dilute dichloromethane solution.

$^{1}$H NMR (600 MHz, Methylene Chloride-$d_2$) δ 7.96 – 7.91 (m, 4H), 7.78 (td, $J$ = 7.8, 3.5 Hz, 8H), 7.64 (ddd, $J$ = 13.1, 8.3, 1.4 Hz, 8H), 1.58 (s, 3H).
$^{13}$C NMR (151 MHz, Methylene Chloride-$d_2$) δ 138.90 (qq, $J$ = 354.7, 31.7 Hz, low intensity $CF_3$ resonance), 135.68 (d, $J$ = 3.1 Hz), 134.38 (d, $J$ = 10.2 Hz), 130.57 (d, $J$ = 12.9 Hz), 117.49 (d, $J$ = 89.7 Hz), 15.24 (hept, $J$ = 5.7 Hz).
$^{19}$F NMR (376 MHz, Methylene Chloride-$d_2$) δ -27.94 (s).
$^{31}$P NMR (162 MHz, Methylene Chloride-$d_2$) δ 23.25 (s).
EA: Calculated: C, 39.73; H, 2.84; Found C, 39.96; H, 2.91.

***trans*-methylbis(trifluoromethyl)-1,3-Bis(2,6-diisopropylphenyl)-1,3-dihydro-2H-imidazol-2-ylidene-gold(III), 8**

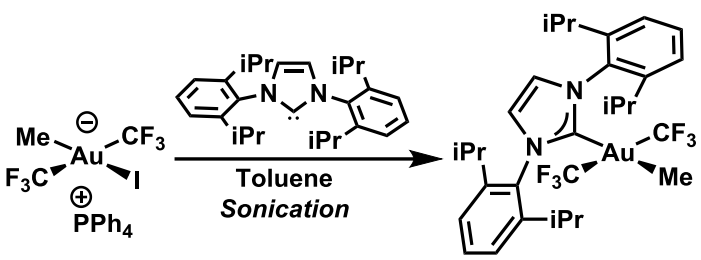


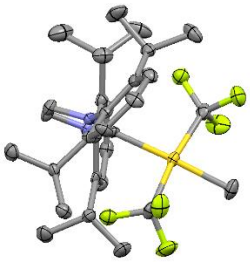

In a nitrogen-filled glovebox, **7** (245 mg, 0.30 mmol, 1.05 equiv) was slurried in Toluene (5 mL) and a solution of IPr free carbene (113 mg, 0.29 mmol, 1.0 equiv) in Toluene (15 mL) was added. The mixture was sealed and brought out of the glovebox, sonicated for 8 minutes, and then stirred for an additional 20 minutes. The mixture was concentrated onto Silica, and chromatographed eluting with 5% diethyl ether in hexanes, affording the desired product as a colorless solid (179 mg, 81% yield). X-ray quality crystals were obtained by layering hexanes onto a solution of **8** in diethyl ether.

$^{1}$H NMR (600 MHz, Methylene Chloride-$d_2$) δ 7.52 (t, $J$ = 7.8 Hz, 2H), 7.37 (d, $J$ = 7.8 Hz, 4H), 7.35 (s, 2H), 2.91 (hept, $J$ = 6.7 Hz, 4H), 1.35 (d, $J$ = 6.7 Hz, 12H), 1.12 (d, $J$ = 6.8 Hz, 12H), 0.78 (s, 3H).
$^{13}$C NMR (151 MHz, Methylene Chloride-$d_2$) δ 186.58, 145.90, 137.60(qq, $J$ = 353.9, 31.0 Hz, low intensity $CF_3$ resonance), 133.72, 130.29, 124.62, 124.27, 28.18, 26.38, 22.01, 4.52 (hept, $J$ = 5.5 Hz).
$^{19}$F NMR (376 MHz, Methylene Chloride-$d_2$) δ -31.74 (s).
EA: Calculated: C, 48.78; H, 5.32; N, 3.79; Found C, 48.66; H, 5.48; N, 3.74.

***trans*-methylbis(trifluoromethyl)-tricyclohexylphosphine-gold(III), 18**

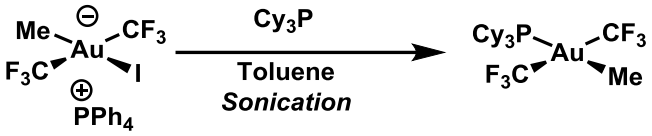


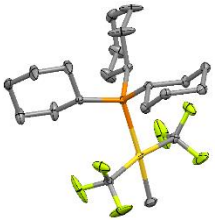

In a nitrogen-filled glovebox, **7** (73 mg, 0.09 mmol, 1.05 equiv) was slurried in Toluene (5 mL) and a solution of tricyclohexylphosphine (24 mg, 0.085 mmol, 1.0 equiv) in Toluene (10 mL) was added. The mixture was sealed and brought out of the glovebox, sonicated for 8 minutes, and then stirred for an additional 20 minutes. The mixture was concentrated onto Silica, and chromatographed eluting with 5% diethyl ether in hexanes, affording the desired product as a colorless solid (52 mg, 99% yield). X-ray quality crystals were obtained by vapor diffusion of hexanes into a solution of **18** in THF.

$^{1}$H NMR (700 MHz, Methylene Chloride-$d_2$) δ 2.60 – 2.52 (m, 3H), 1.93 (dtd, $J$ = 32.7, 8.8, 3.9 Hz, 12H), 1.80 (dd, $J$ = 8.5, 4.4 Hz, 3H), 1.62 – 1.52 (m, 6H), 1.48 (d, $J$ = 7.9 Hz, 3H), 1.39 – 1.29 (m, 9H).
$^{13}$C NMR (176 MHz, Methylene Chloride-$d_2$) δ 138.14 (qqd, $J$ = 356.1, 31.7, 12.3 Hz), 34.15 (d, $J$ = 19.1 Hz), 29.95, 27.66 (d, $J$ = 11.0 Hz), 26.16, 18.09 (dhept, $J$ = 83.4, 7.4 Hz).
$^{19}$F NMR (376 MHz, Methylene Chloride-$d_2$) δ -28.44 (bs).
$^{31}$P NMR (162 MHz, Methylene Chloride-$d_2$) δ 47.84 (bs).

EA: Calculated: C, 40.01; H, 5.76; Found C, 39.83; H, 5.83.

**Bromo-(1,1-difluoroethyl)trifluoromethyl-1,3-Bis(2,6-diisopropylphenyl)-1,3-dihydro-2H-imidazol-2-ylidene-gold(III), 17**

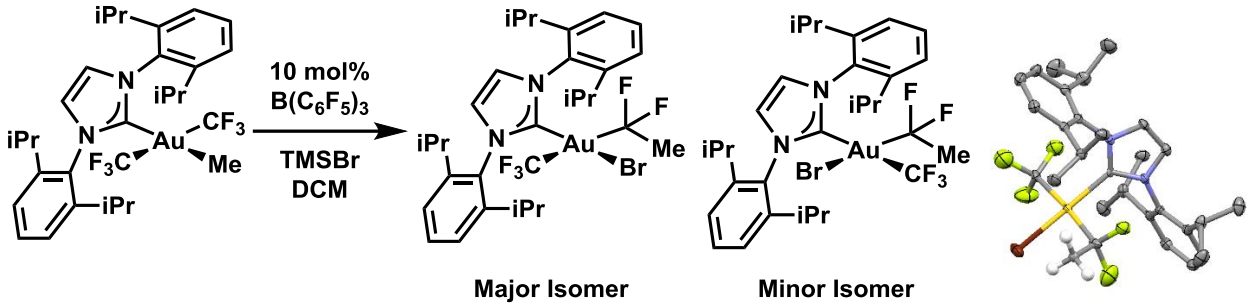


To a solution of **8** (370 mg, 0.5 mmol) in dichloromethane (20 mL) was added bromotrimethylsilane (0.66 mL, 5 mmol, 10 equiv) followed by a solution of tris(pentafluorophenyl)borane (25.6 mg, 0.05 mmol, 0.1 equiv, prepared in a nitrogen filled glovebox) in 5 mL of DCM. The mixture was monitored by TLC for consumption of starting material [Note: the rate varies depending on the purity of the silane and borane reagents].

After 45 minutes of stirring at room temperature, the mixture was quenched by the addition of saturated aqueous sodium bicarbonate. The layers were separated and the aqueous layer was extracted twice with additional dichloromethane. The combined organic fractions were dried over $Na_2SO_4$, filtered, and concentrated. The resulting mixture of isomers was chromatographed on silica gel eluting with a mixture of Hexanes/DCM/$Et_2O$ (85/7.5/7.5) to afford the title compound as a colorless solid containing a mixture of isomers in a ~2:1 ratio (282 mg, 70%).

Figure S1 is a spectrum of a small scale reaction in progress, conducted in an NMR tube. For ease of interpretation, the baseline has been segmented.

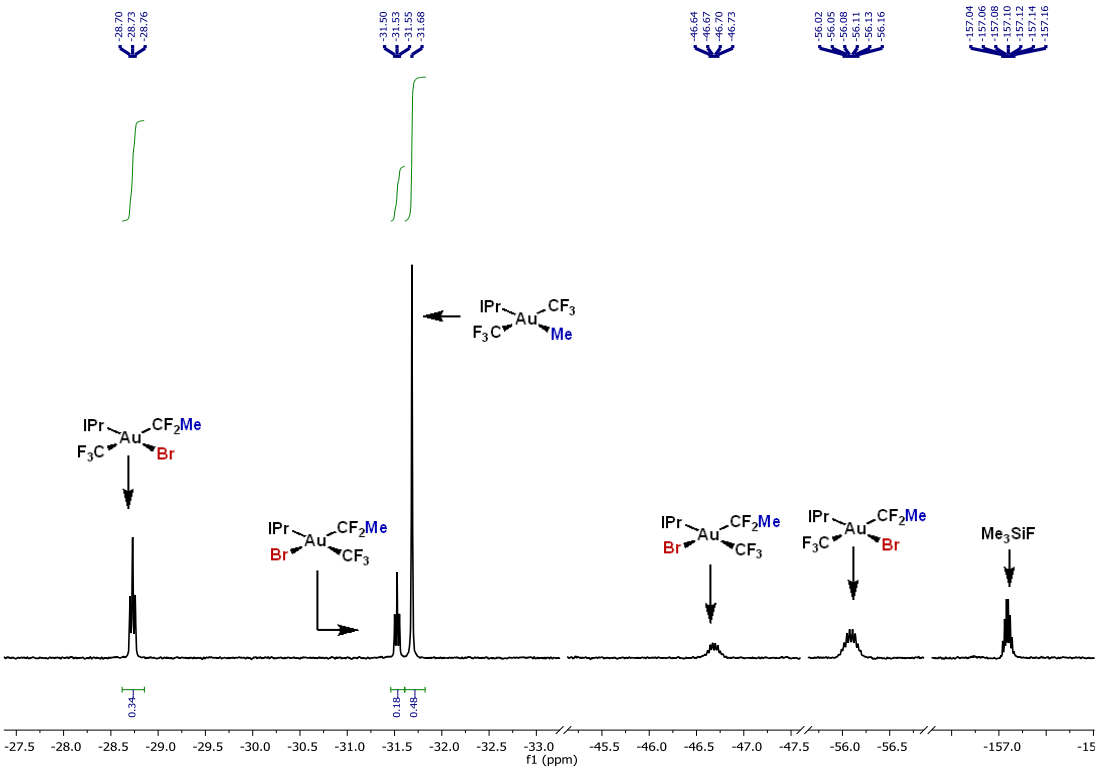


**Figure 4.41**

For the purposes of characterization, the isomers can be carefully separated by repeated chromatography eluting with (90:5:5 Hexanes/DCM/$Et_2O$) to afford fractions of each isomer. Over the course of repeated chromatography additional decomposition byproducts are formed which have not been identified but which can be partially removed by subsequent recrystallization from PhH/Hexanes. The major isomer was assigned structurally by X-ray diffraction and by the $^{13}$C-NMR shift for the carbene carbon which was consistent with a *trans* halide substituent (*cf.* **5** below). The minor isomer was assigned by its $^{13}$C-NMR, which showed a quartet of triplets for the carbene carbon with ca. twice the coupling constant for *C*-C*F*$_3$ as for *C*-C*F*$_2$Me, as well as its 1D-NOE spectrum which showed an interaction between the isopropyl methine and the $CF_2Me$ protons.

Major Isomer (**17a**):

$^1$H NMR (400 MHz, Methylene Chloride-$d_2$) δ 7.56 (t, *J* = 7.7 Hz, 2H), 7.47-7.33 (m, 6H), 2.96 (apparent dhept, *J* = 19.7, 6.7 Hz, 4H), 1.38 (apparent dd, *J* = 9.8, 6.5 Hz, 12H), 1.14 (d, *J* = 6.9 Hz, 6H), 1.09 (d, *J* = 6.8 Hz, 5H), 0.93 (t, *J* = 22.3 Hz, 3H).

$^{13}$C NMR (176 MHz, Methylene Chloride-$d_2$) δ 156.29 (m), 146.17, 146.05, 124.95, 124.77, 124.70, 28.88 (t, *J* = 18.6 Hz), 28.43, 28.38, 26.51, 26.38, 22.27, 21.96.

$^{19}$F NMR (376 MHz, Methylene Chloride-$d_2$) δ -28.76 (t, *J* = 10.3 Hz), -56.13 (qq, *J* = 22.5, 11.5 Hz).

EA Calculated: C, 45.07; H, 4.92; N, 3.50; Found C, 45.36; H, 5.18; N, 3.37.

Minor Isomer (**17b**):

$^1$H NMR (400 MHz, Methylene Chloride-$d_2$) δ 7.59 (t, *J* = 7.8 Hz, 2H), 7.51 – 7.38 (m, 4H), 7.35 (s, 2H), 3.16 (hept, *J* = 6.7 Hz, 2H), 2.92 (hept, *J* = 6.6 Hz, 2H), 1.46 (d, *J* = 6.6 Hz, 6H), 1.40 (d, *J* = 6.7 Hz, 6H), 1.15 (apparent t, *J* = 6.7 Hz, 12H), 0.96 (t, *J* = 20.8 Hz, 3H).

$^{13}$C NMR (151 MHz, Methylene Chloride-$d_2$) δ 169.92 (qt, $J$ = 24.1, 11.7 Hz), 146.55, 145.74, 133.91, 130.82, 124.86, 124.80, 124.3, 28.91, 28.23, 27.13 (t, $J$ = 18.6 Hz), 23.05, 21.99.
$^{19}$F NMR (376 MHz, Methylene Chloride-$d_2$) δ -31.58 (t, $J$ = 9.5 Hz), -46.78 (qq, $J$ = 20.6, 10.8 Hz).
EA Calculated: C, 45.07; H, 4.92; N, 3.50; Found C, 45.09; H, 5.05; N, 3.34.

**Acetato-((4-(4-acetylphenyl)-1,1-difluorobutyl))-trifluoromethyl-1,3-Bis(2,6-diisopropylphenyl)-1,3-dihydro-2H-imidazol-2-ylidene-gold(III) (mixture of coordination isomers)**, **53**

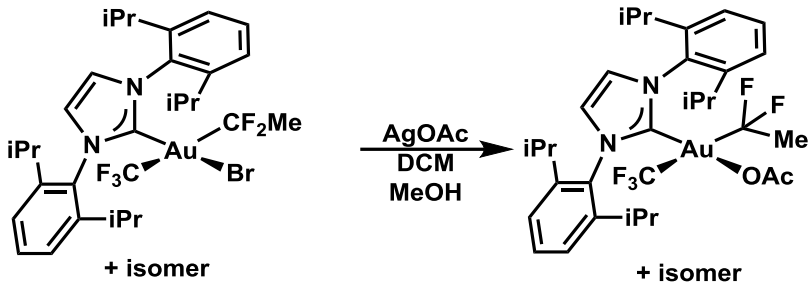


**53** (47 mg, 0.06 mmol) was dissolved in dichloromethane (0.6 mL) and methanol (6 mL) and silver acetate (97 mg, 0.6 mmol, 10 equiv) was added. The mixture was sonicated briefly and stirred for 12 hours at room temperature in the dark. The mixture was filtered, and the filter cake was washed with dichloromethane. The combined filtrates were concentrated, and the residue was again extracted with dichloromethane, filtered and concentrated affording the product as a colorless solid (45 mg). The resulting product was used as soon as possible without further purification. Storage, even at -20°C results in the gradual reductive elimination of R-$CF_2$OAc.

Spectra for $^1$H NMR and $^{13}$C NMR are provided below, but are not indexed due to overlapping signals for the two isomers.
$^{19}$F NMR (376 MHz, Methylene Chloride-$d_2$) δ -35.21 (t, $J$ = 10.0 Hz), -37.96 (t, $J$ = 7.6 Hz), -48.25 (qq, $J$ = 21.1, 7.8 Hz), -64.52 (qq, $J$ = 22.3, 10.9 Hz).
Sample instability prevented a satisfactory elemental analysis.

***trans*-chlorobis(trifluoromethyl)-1,3-Bis(2,6-diisopropylphenyl)-1,3-dihydro-2H-imidazol-2-ylidene-gold(III)**, **25**

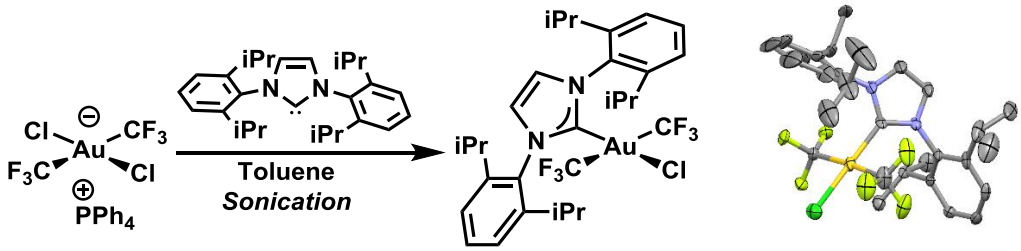


In a nitrogen-filled glovebox, **24** (3.8 g, 5.04 mmol, 1 equiv) was slurried in Toluene (30 mL) and a solution of IPr free carbene (1.96 g, 5.04 mmol, 1 equiv) in Toluene (70 mL) was added. The mixture was sealed and brought out of the glovebox, sonicated for 8 minutes, and then stirred for an additional 1 hour. The mixture was concentrated onto Silica, and chromatographed eluting with 50% dichloromethane in hexanes, affording a pale yellow solid which was washed with hexanes

to remove the co-eluting color impurity. This afforded the desired product as a colorless solid (3.2 g, 84% yield). X-ray quality crystals were obtained by vapor diffusion of hexanes into a saturated THF solution.

$^{1}$H NMR (600 MHz, Methylene Chloride-$d_2$) δ 7.59 (t, $J$ = 7.8 Hz, 2H), 7.49 (s, 2H), 7.43 (d, $J$ = 7.8 Hz, 4H), 2.84 (hept, $J$ = 6.7 Hz, 4H), 1.39 (d, $J$ = 6.7 Hz, 12H), 1.14 (d, $J$ = 6.8 Hz, 12H).
$^{13}$C NMR (151 MHz, Methylene Chloride-$d_2$) δ 153.09, 145.76, 133.11 (qq, $J$ = 360.4, 39.1 Hz, low intensity $CF_3$ resonance) (d, $J$ = 38.6 Hz), 132.43, 125.40, 124.89, 28.48, 26.54, 21.98.
$^{19}$F NMR (376 MHz, Methylene Chloride-$d_2$) δ -30.34 (s).
EA: Calculated: C, 45.89; H, 4.78; N, 3.69; Found C, 45.79; H, 4.72; N, 3.61.

**_trans_-ethylbis(trifluoromethyl)-1,3-Bis(2,6-diisopropylphenyl)-1,3-dihydro-2H-imidazol-2-ylidene-gold(III), 26**

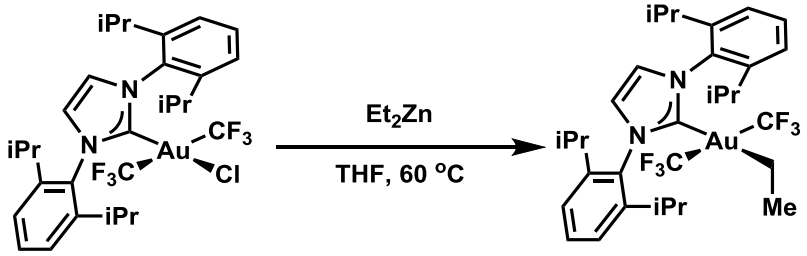


To a solution of **25** (76 mg, 0.1 mL) in THF (10 mL) in a schlenk bomb was added diethyl zinc (1.8 mL of a 1.1M toluene solution, 20 equiv). The flask was sealed with a teflon valve and heated at 60 °C for 12 hours. Upon cooling, the mixture was quenched with $H_2O$ and extracted three times with diethyl ether. The combined organic extracts were dried with sodium sulfate, filtered, and concentrated. The crude material was purified by silica gel chromatography eluting with 6:4 Hexanes/DCM yielding the title compound as a colorless solid (47 mg, 62%).

$^{1}$H NMR (400 MHz, Methylene Chloride-$d_2$) δ 7.50 (t, $J$ = 7.8 Hz, 2H), 7.35 (d, $J$ = 7.8 Hz, 4H), 7.32 (s, 2H), 2.90 (hept, $J$ = 6.7 Hz, 4H), 1.61 – 1.45 (m, 2H), 1.33 (d, $J$ = 6.7 Hz, 12H), 1.11 (d, $J$ = 6.8 Hz, 12H), 0.80 (t, $J$ = 7.6 Hz, 3H).
$^{13}$C NMR (151 MHz, Methylene Chloride-$d_2$) δ 188.12, 145.86, 138.49 (qq, $J$ = 355.1, 31.4 Hz, low intensity $CF_3$ resonance), 133.90, 130.18, 124.51, 124.23, 28.15, 26.33, 22.0 , 20.48 – 20.11 (m), 13.44.
$^{19}$F NMR (376 MHz, Methylene Chloride-$d_2$) δ -33.69 (s).
EA: Calculated: C, 49.47; H, 5.49; N, 3.72; Found C, 49.74; H, 5.68; N, 3.61.

**_trans_-allylbis(trifluoromethyl)-1,3-Bis(2,6-diisopropylphenyl)-1,3-dihydro-2H-imidazol-2-ylidene-gold(III), 28**

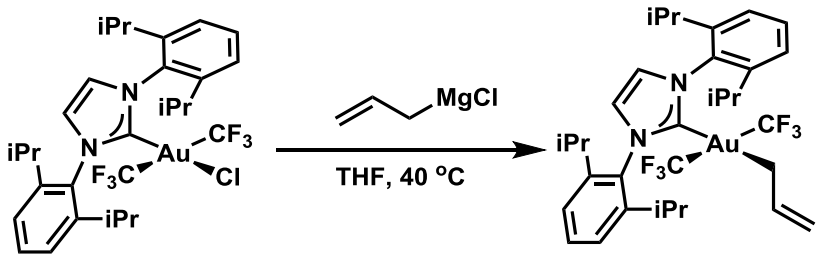


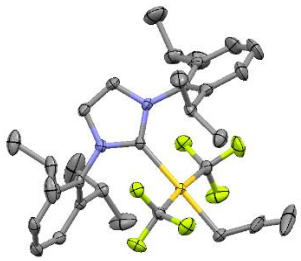

To a solution of **25** (1.0 g, 1.32 mmol) in THF (65 mL, 0.02 M) in a schlenk bomb was added allyl magnesium chloride (6.6 mL of a 2M THF solution, 13.2 mmol, 10 equiv). The flask was sealed with a teflon valve and heated at 40 $^{o}$C for 12 hours. Upon cooling, the mixture was quenched with $H_2O$ and extracted three times with diethyl ether. The combined organic extracts were dried with sodium sulfate, filtered, and concentrated. The crude material was purified by silica gel chromatography eluting with 70:30 Hexanes/DCM yielding the title compound as a colorless solid (930 mg, 92%).

$^{1}$H NMR (600 MHz, Methylene Chloride-$d_2$) δ 7.52 (t, *J* = 7.8 Hz, 2H), 7.36 (d, *J* = 7.8 Hz, 4H), 7.35 (s, 2H), 5.72 (ddt, *J* = 16.7, 10.0, 8.4 Hz, 1H), 4.94 (d, *J* = 16.1 Hz, 1H), 4.72 (dd, *J* = 10.1, 2.5 Hz, 1H), 2.90 (hept, *J* = 6.7 Hz, 4H), 2.40 (d, *J* = 8.3 Hz, 2H), 1.34 (d, *J* = 6.7 Hz, 12H), 1.12 (d, *J* = 6.8 Hz, 12H).
$^{13}$C NMR (151 MHz, Methylene Chloride-$d_2$) δ 184.86, 145.83, 137.36 (qq, *J* = 355.7, 32.4 Hz), 138.19, 133.79, 130.25, 124.58, 124.31, 113.08, 29.14 (m), 28.11, 26.32, 22.09.
$^{19}$F NMR (376 MHz, Methylene Chloride-$d_2$) δ -32.93 (s).
EA: Calculated: C, 50.27; H, 5.40; N, 3.66; Found C, 50.16; H, 5.36; N, 3.55.

***trans*-(E)-(3-(4-acetylphenyl)allyl)-bis(trifluoromethyl)-1,3-Bis(2,6-diisopropylphenyl)-1,3-dihydro-2H-imidazol-2-ylidene-gold(III), 32**

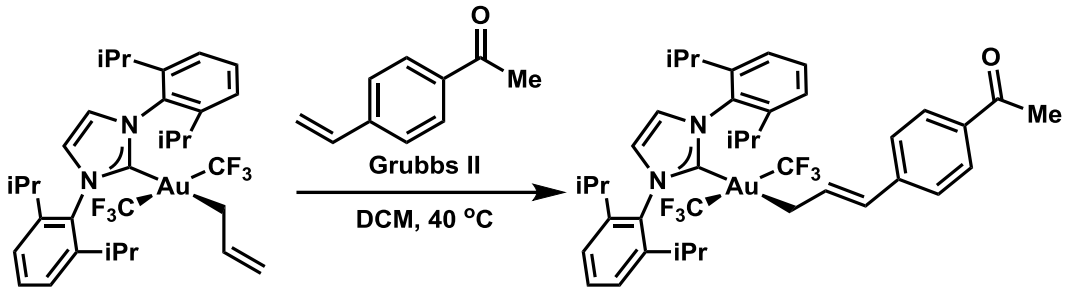


**28** (529 mg, 0.693 mmol), 4-vinylacetophenone (405 mg, 2.77 mmol, 4 equiv), and Grubbs 2$^{nd}$ Generation Catalyst (25 mg, 0.035 mmol, 5 mol%) were weighed into a Schlenk bomb. Dichloromethane (18 mL) was added, the flask was sealed and the mixture was heated at 40$^{o}$C for 12 hours. The mixture was concentrated onto silica gel and chromatographed eluting on a gradient from 90:5:5 Hex/DCM/$Et_2O$ to 80:10:10 Hex/DCM/$Et_2O$ affording 468 mg of the title compound as a colorless solid alongside 88 mg of starting material (76% yield, 91% brsm). Recystallization from $Et_2O$/Hexanes at -20$^{o}$C affords the diethyl ether solvate.

$^{1}$H NMR (400 MHz, Methylene Chloride-$d_2$) δ 7.86 (d, *J* = 8.4 Hz, 2H), 7.49 (t, *J* = 7.8 Hz, 2H), 7.39 (s, 2H), 7.32 (d, *J* = 7.8 Hz, 4H), 7.28 (d, *J* = 8.4 Hz, 2H), 6.47 – 6.26 (m, 2H), 2.90 (hept, *J* = 6.5 Hz, 4H), 2.65 (d, *J* = 7.5 Hz, 2H), 2.60 (s, 3H), 1.33 (d, *J* = 6.7 Hz, 12H), 1.13 (d, *J* = 6.8 Hz, 12H).
$^{13}$C NMR (101 MHz, Methylene Chloride-$d_2$) δ 197.23, 183.72, 145.82, 143.73, 134.78, 134.47, 133.73, 130.33, 128.50, 127.76, 125.40, 124.64, 124.32, 28.86 (m), 28.23, 26.40, 26.31, 22.04. (low intensity $CF_3$ resonance not detected)
$^{19}$F NMR (376 MHz, Methylene Chloride-$d_2$) δ -32.49 (s).
EA: [for **S3●Et$_2$O**] Calculated: C, 55.23; H, 6.00; N, 2.93; Found C, 55.52; H, 5.91; N, 2.93.

***trans*-(3-(4-acetylphenyl)propyl)-bis(trifluoromethyl)-1,3-Bis(2,6-diisopropylphenyl)-1,3-dihydro-2H-imidazol-2-ylidene-gold(III), 33**

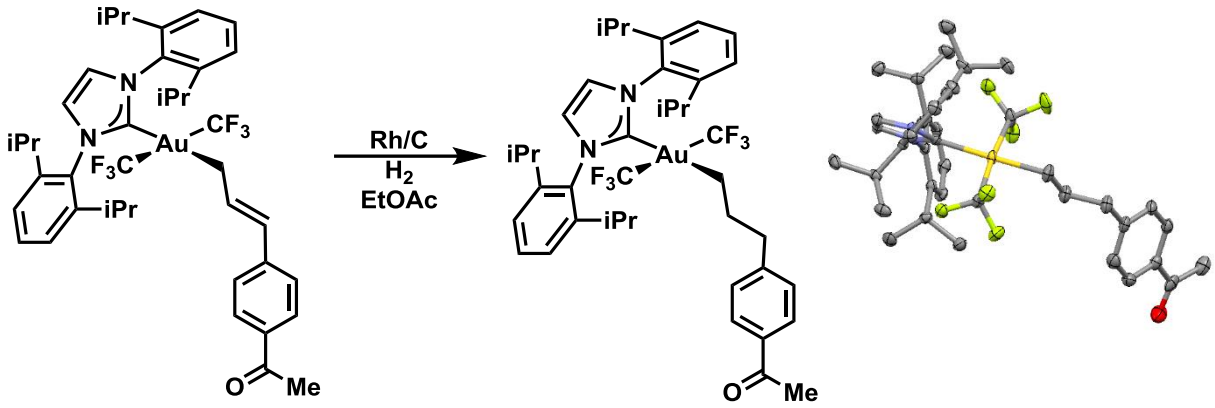


**32** (468 mg, 0.53 mmol) was dissolved in ethyl acetate (50 mL, 0.01M) and rhodium on carbon (109 mg of 5 wt%, 10 mol% Rh) was added. The mixture was sparged with $N_2$ with stirring for 10 minutes, then with $H_2$ (via balloon) for 10 minutes. The mixture was left under a static atmosphere of $H_2$ and monitored by TLC, staining with *p*-Anisaldehyde (the two compounds are copolar but the starting complex stains pink and the product stains orange upon heating). After 6.5 hours, consumption of starting material was observed, and $H_2$ was removed by sparging with $N_2$. The mixture was filtered through a pad of celite eluting with ethyl acetate and concentrated onto silica gel. Chromatography eluting with 85:7.5:7.5 Hexanes/DCM/$Et_2O$ afforded the title compound as a colorless solid (274 mg, 60% yield).

*Alternate procedure:*

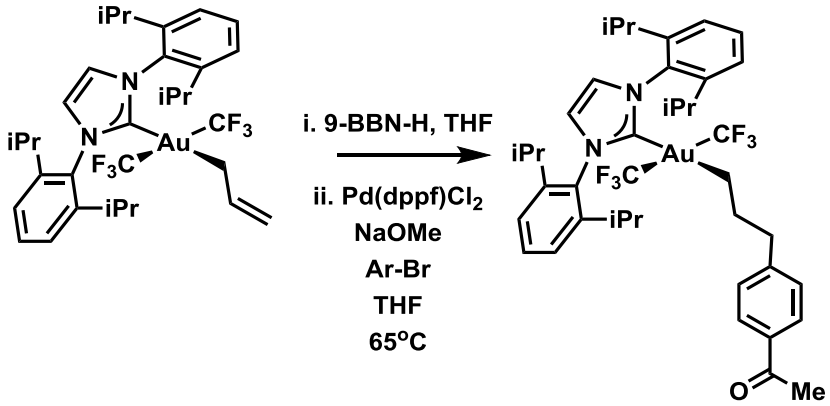


In a nitrogen filled glovebox, to **28** (0.11 mmol, 84 mg) was added 9-BBN-H (0.95 equiv, 12.7 mg) and THF (3 mL). The mixture was stirred overnight, and then Pd(dppf)$Cl_2$ (2.5 mg, 3 mol%), NaOMe (18 mg, 3 equiv), and 4-acetyl-bromobenzene (25 mg, 1.1 equiv) were added. The mixture was heated at 65°C for 1.5 hours and then concentrated. The crude product was purified by column chromatography eluting with 85:7.5:7.5 Hexanes/DCM/$Et_2O$ afforded the title compound as a colorless solid (42 mg, 44% yield). Note: though more rapid than the 2 step

metathesis/hydrogenation procedure, this procedure was found to be less reliable for large scale synthesis of the desired compound.

$^{1}$H NMR (600 MHz, Methylene Chloride-$d_2$) δ 7.86 – 7.75 (m, 2H), 7.51 (t, $J$ = 7.8 Hz, 2H), 7.38 – 7.30 (m, 6H), 7.18 – 7.08 (m, 2H), 2.91 (hept, $J$ = 6.7 Hz, 4H), 2.54 (s, 3H), 2.51 (t, $J$ = 7.3 Hz, 2H), 1.69 – 1.54 (m, 4H), 1.34 (d, $J$ = 6.7 Hz, 12H), 1.12 (d, $J$ = 6.8 Hz, 12H).
$^{13}$C NMR (151 MHz, Methylene Chloride-$d_2$) δ 197.41, 187.43, 148.54, 145.87, 138.11 (qq, $J$ = 355.0, 30.5 Hz, low intensity $CF_3$ resonance) 134.75, 133.83, 130.25, 128.43, 128.05, 38.43, 30.35, 29.63 (m), 28.16, 26.33, 26.25, 22.06.
$^{19}$F NMR (376 MHz, Methylene Chloride-$d_2$) δ -32.93 (s).
EA: Calculated: C, 54.30; H, 5.58; N, 3.17; Found C, 53.97; H, 5.76; N, 2.91.

**Bromo-((4-(4-acetylphenyl)-1,1-difluorobutyl))-trifluoromethyl-1,3-Bis(2,6-diisopropylphenyl)-1,3-dihydro-2H-imidazol-2-ylidene-gold(III) (mixture of coordination isomers)**, **54**

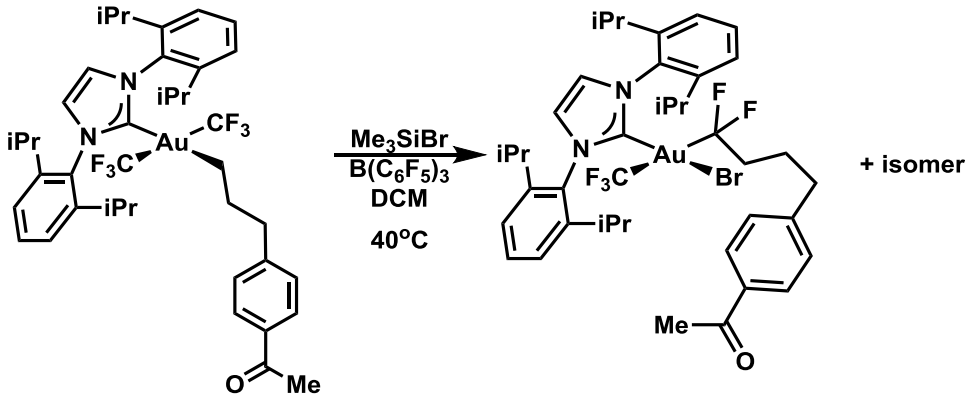


To a solution of **33** (160 mg, 0.18 mmol) in dichloromethane (5 mL) in a schlenk bomb was added bromotrimethylsilane (0.24 mL, 1.81 mmol, 10 equiv) followed by tris(pentafluorophenyl) borane (46 mg, 0.09 mmol, 50 mol%) in dichloromethane (4 mL). The mixture was sealed with a teflon valve and heated at 40°C for 24 hours. Saturated aqueous sodium bicarbonate was added, and the layers were separated. The aqueous layer was extracted 3x with DCM, and the combined organic layers were dried over $Na_2SO_4$, filtered, and concentrated. The crude residue was purified by column chromatography on $SiO_2$, eluting on a gradient from 85:7.5:7.5 to 80:10:10 Hexanes/DCM/$Et_2O$ affording 105 mg of the title compound as a 55:45 mixture of two isomers as well as 36 mg of recovered starting material (61% yield, 78% brsm).

The *trans* isomer crystallizes preferentially from Toluene/Hexanes, but does not afford material of sufficient isomeric purity for characterization purposes. A hexanes extract of a mixture enriched in the *cis* isomer gave a co-crystal of isomers suitable for X-ray diffraction upon slow evaporation. These data were modeled to extract structures for each isomer by accounting for substitutional disorder and refined to an occupancy of approximately 60/40 favoring the *trans* isomer.

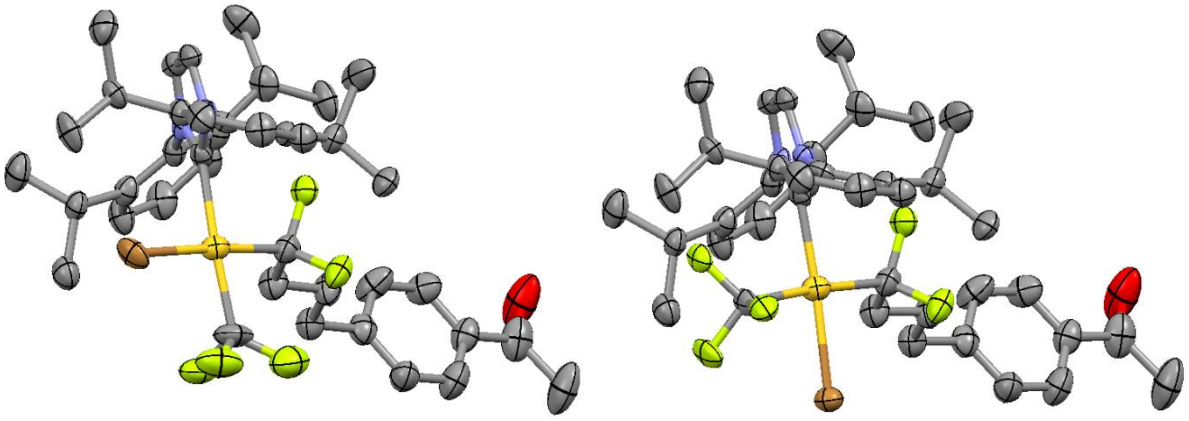

Spectra for $^{1}$H NMR and $^{13}$C NMR are provided below, but are not indexed due to overlapping signals for the two isomers.

$^{19}$F NMR (376 MHz, Methylene Chloride-$d_2$) δ -28.64 (t, $J$ = 10.3 Hz), -31.76 (t, $J$ = 9.7 Hz), -57.51 (m), -67.52 (m).
EA: Calculated: C, 50.80; H, 5.22; N, 2.96; Found C, 50.70; H, 5.37; N, 2.73.

**Acetato-((4-(4-acetylphenyl)-1,1-difluorobutyl))-trifluoromethyl-1,3-Bis(2,6-diisopropylphenyl)-1,3-dihydro-2H-imidazol-2-ylidene-gold(III) (mixture of coordination isomers)**, **57**

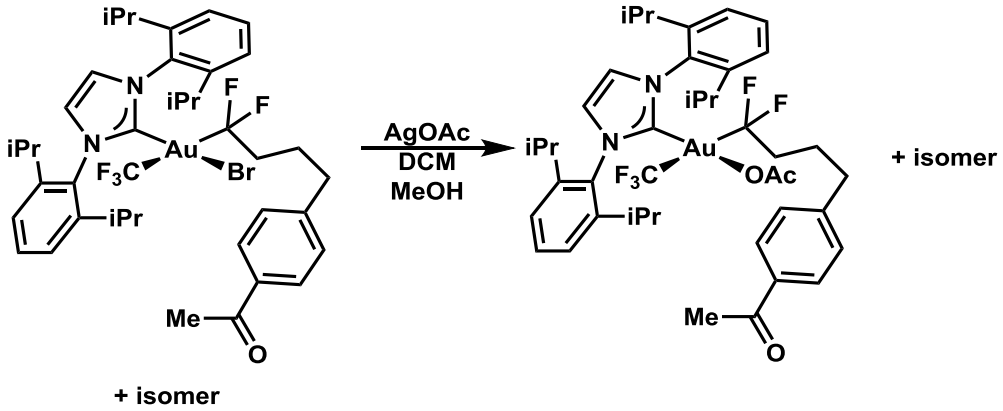


**54** (130 mg, 0.137 mmol) was dissolved in dichloromethane (1.8 mL) and methanol (18 mL) and silver acetate (227 mg, 1.37 mmol, 10 equiv) was added. The mixture was sonicated briefly and stirred for 12 hours at room temperature in the dark. The mixture was filtered, and the filter cake was washed with dichloromethane. The combined filtrates were concentrated, and the residue was again extracted with dichloromethane, filtered and concentrated affording the product as a colorless solid (126 mg). The resulting product was used as soon as possible without further purification. Storage, even at -20°C results in the gradual reductive elimination of R-$CF_2$OAc.

Spectra for $^{1}$H NMR and $^{13}$C NMR are provided below, but are not indexed due to overlapping signals for the two isomers.

$^{19}$F NMR (376 MHz, Methylene Chloride-$d_2$) δ -34.96 (t, $J$ = 10.1 Hz), -37.97 (t, $J$ = 7.0 Hz), -57.87 (m), -75.76 (m).
Sample instability prevented a satisfactory elemental analysis.

***trans*-(*E*)-(4-methoxy-4-oxobut-2-en-1-yl)-bis(trifluoromethyl)-1,3-Bis(2,6-diisopropylphenyl)-1,3-dihydro-2H-imidazol-2-ylidene-gold(III)**, **35**

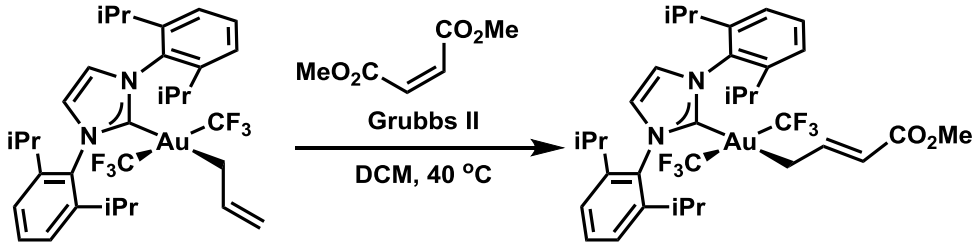


**28** (76 mg, 0.1 mmol), and Grubbs 2nd Generation Catalyst (3 mg, 3 mol%) were weighed into a Schlenk bomb. Dimethyl maleate (0.06 mL, 0.5 mmol) in dichloromethane (6 mL) was added, the flask was sealed and the mixture was heated at 40°C for 1.5 hours. The mixture was concentrated onto silica gel and chromatographed eluting on a gradient from 30% to 50% DCM in Hexanes. The residue was dried *in vacuo* over night to remove residual dimethyl maleate affording 72 mg of the title compound (87% yield).

$^{1}$H NMR (600 MHz, Methylene Chloride-$d_2$) δ 7.52 (t, *J* = 7.8 Hz, 2H), 7.37 (s, 2H), 7.35 (d, *J* = 7.8 Hz, 4H), 6.86 (dt, *J* = 15.2, 9.1 Hz, 1H), 5.65 (d, *J* = 15.4 Hz, 1H), 3.64 (s, 3H), 2.87 (hept, *J* = 6.8 Hz, 4H), 2.51 (d, *J* = 9.1 Hz, 2H), 1.33 (d, *J* = 6.7 Hz, 12H), 1.12 (d, *J* = 6.8 Hz, 12H).
$^{13}$C NMR (151 MHz, Methylene Chloride-$d_2$) δ 181.25, 167.16, 149.81, 145.75, 136.26 (qq, *J* = 355.3, 32.6 Hz, low intensity $CF_3$ resonance), 133.53, 130.41, 124.72, 124.37, 118.55, 50.69, 28.19, 27.07 (m), 26.33, 21.98.
$^{19}$F NMR (376 MHz, Methylene Chloride-$d_2$) δ -32.62 (s).
EA: Calculated: C, 49.64; H, 5.27; N, 3.41; Found C, 49.33; H, 5.14; N, 3.29.

***trans*-(4-methoxy-4-oxobutyl)-bis(trifluoromethyl)-1,3-Bis(2,6-diisopropylphenyl)-1,3-dihydro-2H-imidazol-2-ylidene-gold(III)**, **36**

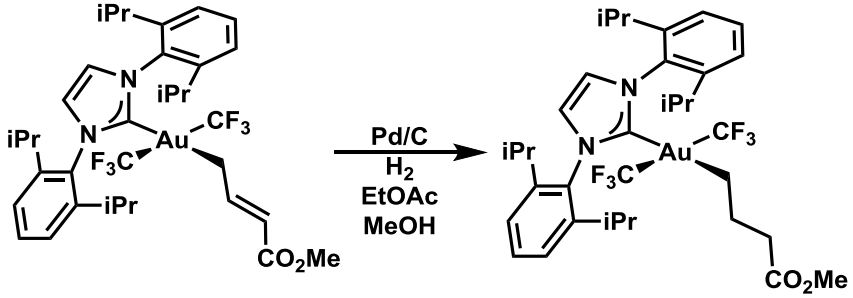


**35** (288 mg, 0.35 mmol) was dissolved in a 1:1 mixture of ethyl acetate and methanol (35 mL). Pd/C (5 wt% palladium, 180 mg, 25 mol% loading) was added, and the mixture was degassed by sparging with $N_2$ for 5 minutes. A hydrogen balloon was then affixed to the flask and the solution was sparged for 5 minutes and then left under a static atmosphere of $H_2$. TLC analysis after 1.5 hours showed complete consumption of the starting material, and the $H_2$ was removed by sparging with $N_2$. The mixture was filtered through a pad of celite, and concentrated. The crude residue was chromatographed on silica gel eluting with 85:7.5:7.5 Hexanes/DCM/$Et_2O$, affording the title compound as a colorless solid (272 mg, 94% yield).

$^{1}$H NMR (600 MHz, Methylene Chloride-$d_2$) δ 7.52 (t, $J$ = 7.8 Hz, 2H), 7.37 (d, $J$ = 7.8 Hz, 4H), 7.35 (s, 2H), 3.56 (s, 3H), 2.90 (hept, $J$ = 6.8 Hz, 4H), 2.10 (d, $J$ = 7.5 Hz, 2H), 1.61 – 1.53 (m, 2H), 1.51 – 1.47 (m, 2H), 1.34 (d, $J$ = 6.7 Hz, 12H), 1.12 (d, $J$ = 6.8 Hz, 12H).
$^{13}$C NMR (151 MHz, Methylene Chloride-$d_2$) δ 186.88, 173.39, 145.84, 137.92 (qq, $J$ = 354.1, 31.1 Hz low intensity $CF_3$ resonance), 133.79, 130.27, 124.59, 124.27, 50.93, 36.18, 28.16, 26.33, 25.28 (m), 24.32, 22.07.
$^{19}$F NMR (376 MHz, Methylene Chloride-$d_2$) δ -33.09 (s).
EA: Calculated: C, 49.52; H, 5.50; N, 3.40; Found C, 49.43; H, 5.70; N, 3.33.

### *trans*-(4-hydroxybutyl)-bis(trifluoromethyl)-1,3-Bis(2,6-diisopropylphenyl)-1,3-dihydro-2H-imidazol-2-ylidene-gold(III), 37

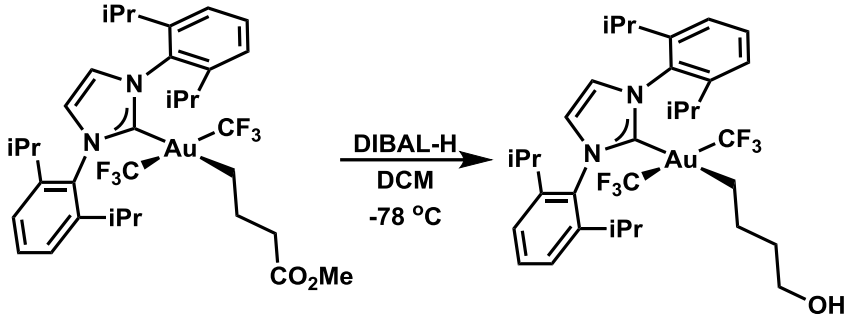


A solution of **36** (220 mg, 0.267 mmol) in DCM (16 mL) was cooled to -78 °C in a dry ice/acetone bath. A solution of DIBAL-H (1M in heptane, 1.35 mL, 5 equiv) was added dropwise, and the solution was stirred for 1 hour at -78 °C. Saturated aqueous ammonium chloride (1 mL) was added in one portion and the mixture was warmed to room temperature, diluted with saturated aqueous Rochelle's salt, and stirred for 1 hour. The layers were separated, and the aqueous layer was extracted 2x with DCM. The combined organic layers were dried over $Na_2SO_4$, filtered and concentrated. [Note: In cases where residual aldehyde remained, the crude mixture was treated with sodium borohydride in methanol to achieve complete conversion.] The crude mixture was purified by column chromatography on $SiO_2$ eluting with on a gradient from 8:1:1 to 6:2:2 Hexanes/DCM/$Et_2O$ affording the title compound as a colorless solid (191 mg, 90% yield).

$^{1}$H NMR (500 MHz, Chloroform-$d$) δ 7.54 (t, $J$ = 7.8 Hz, 2H), 7.38 (d, $J$ = 7.8 Hz, 4H), 7.36 (s, 2H), 3.47 (bs, 2H), 2.92 (hept, $J$ = 6.8 Hz, 4H), 1.59 – 1.51 (m, 2H), 1.44 – 1.32 (m, 16H), 1.14 (d, $J$ = 6.7 Hz, 12H).
$^{13}$C NMR (151 MHz, Methylene Chloride-$d_2$) δ 187.76 , 145.89 , 138.28 (qq, $J$ = 355.2, 31.1 Hz, low intensity $CF_3$ resonance), 133.89 , 130.25 , 124.60 , 124.27 , 62.23 , 35.28 , 28.18 , 26.36 , 26.26 (m), 24.58 , 22.12 .
$^{19}$F NMR (376 MHz, Methylene Chloride-$d_2$) δ -33.13 (s).
EA: Calculated: C, 49.75; H, 5.69; N, 3.52; Found C, 50.07; H, 5.77; N, 3.36.

***trans*-(4-((2-naphthoyl)oxy)butyl)-bis(trifluoromethyl)-1,3-Bis(2,6-diisopropylphenyl)-1,3-dihydro-2H-imidazol-2-ylidene-gold(III)**, **38**

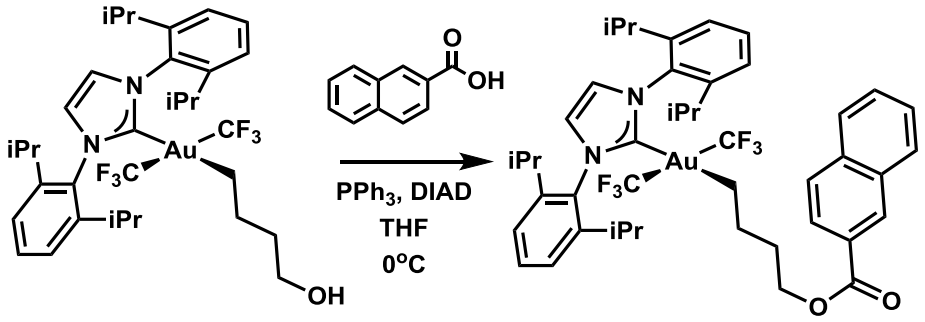


**37** (70 mg, 0.088 mmol), 2-naphthoic acid (15 mg, 1 equiv), and triphenylphosphine (35 mg, 1.5 equiv) were dissolved in dry THF (9 mL), and the mixture was cooled to 0°C. A solution of DIAD (27 mg, 1.5 equiv) in 1 mL of THF was added dropwise. The mixture was allowed to reach room temperature and stirred for 19 hours at which point a solution of brine was added. The layers were separated and the aqueous layer was extracted 3x with DCM. The combined organic layers were dried over $MgSO_4$, filtered, and concentrated. Column chromatography on $SiO_2$ eluiting with 8:1:1 Hexanes/DCM/$Et_2O$ afforded the desired product as a colorless solid (80 mg, 95% yield).

$^1$H NMR (700 MHz, Methylene Chloride-$d_2$) δ 8.59 (s, 1H), 8.05 (dd, *J* = 8.5, 1.7 Hz, 1H), 8.00 (d, *J* = 8.1 Hz, 1H), 7.96 (d, *J* = 8.2 Hz, 1H), 7.94 (d, *J* = 8.6 Hz, 1H), 7.66 (ddd, *J* = 8.1, 6.7, 1.3 Hz, 1H), 7.61 (ddd, *J* = 8.0, 6.7, 1.2 Hz, 1H), 7.49 (t, *J* = 7.8 Hz, 2H), 7.39 – 7.34 (m, 6H), 4.26 (t, *J* = 6.6 Hz, 2H), 2.95 (hept, *J* = 6.7 Hz, 4H), 1.71 – 1.64 (m, 4H), 1.58 – 1.50 (m, 2H), 1.38 (d, *J* = 6.8 Hz, 12H), 1.15 (d, *J* = 6.8 Hz, 12H).
$^{13}$C NMR (176 MHz, Methylene Chloride-$d_2$) δ 187.55, 166.45, 145.88, 138.24 (qq, *J* = 354.7, 31.5 Hz, low intensity $CF_3$ resonance), 135.41, 133.88, 132.54, 130.73, 130.29, 129.35, 128.05, 128.02, 127.92, 127.65, 126.49, 125.23, 124.61, 124.29, 64.72, 31.13, 28.22, 26.41, 26.15 – 25.85 (m), 25.14, 22.14.
$^{19}$F NMR (376 MHz, Methylene Chloride-$d_2$) δ -32.95 (s).
EA: Calculated: C, 55.58; H, 5.41; N, 2.95; Found C, 55.71; H, 5.60; N, 2.87.

**Bromo-(5-((2-naphthoyl)oxy)-1,1-difluoropentyl)-trifluoromethyl-1,3-Bis(2,6-diisopropylphenyl)-1,3-dihydro-2H-imidazol-2-ylidene-gold(III)** (mixture of coordination isomers), **55**

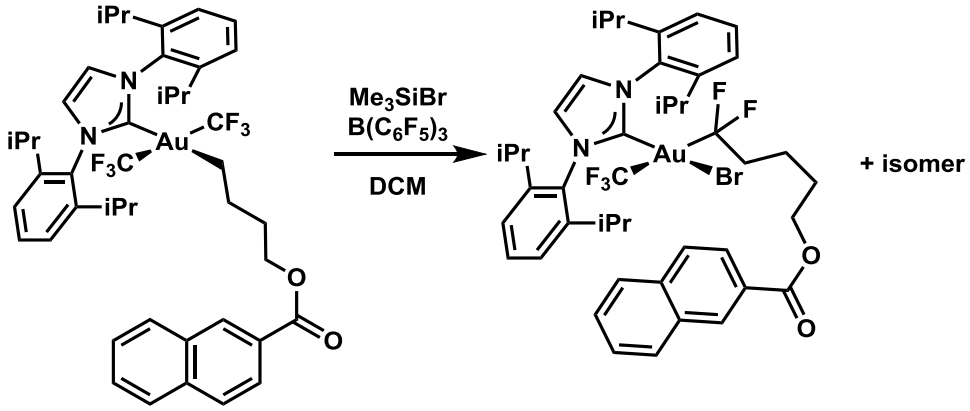

In a schlenk bomb, **38** (135 mg, 0.14 mmol) was dissolved in 6 mL of dichloromethane, and 0.19 mL (10 equiv) of TMSBr was added. A solution of $B(C_6F_5)_3$ (72 mg, 1 equiv) in dichloromethane (3 mL) was added and the mixture was monitored for consumption of the starting material using TLC. After 30 minutes the mixture was quenched with saturated aqueous bicarbonate solution, and the layers were separated. The aqueous layer was washed with DCM 2x, and the combined organics were dried over $Na_2SO_4$, filtered, and concentrated. Chromatography on $SiO_2$ eluting with 8:1:1 Hex/DCM/$Et_2O$ afforded the title compound as a colorless solid (103 mg, 72% yield).

Spectra for $^1$H NMR and $^{13}$C NMR are provided below, but are not indexed due to overlapping signals for the two isomers.

$^{19}$F NMR (376 MHz, Methylene Chloride-$d_2$) δ -28.60 (t, $J$ = 10.2 Hz), -31.72 (t, $J$ = 9.8 Hz), -57.84 (bs), -67.92 (bs).

EA: Calculated: C, 52.23; H, 5.08; N, 2.77; Found C, 52.42; H, 5.20; N, 2.61.

**Acetato-(5-((2-naphthoyl)oxy)-1,1-difluoropentyl)-trifluoromethyl-1,3-Bis(2,6-diisopropylphenyl)-1,3-dihydro-2H-imidazol-2-ylidene-gold(III)** (mixture of coordination isomers), **58**

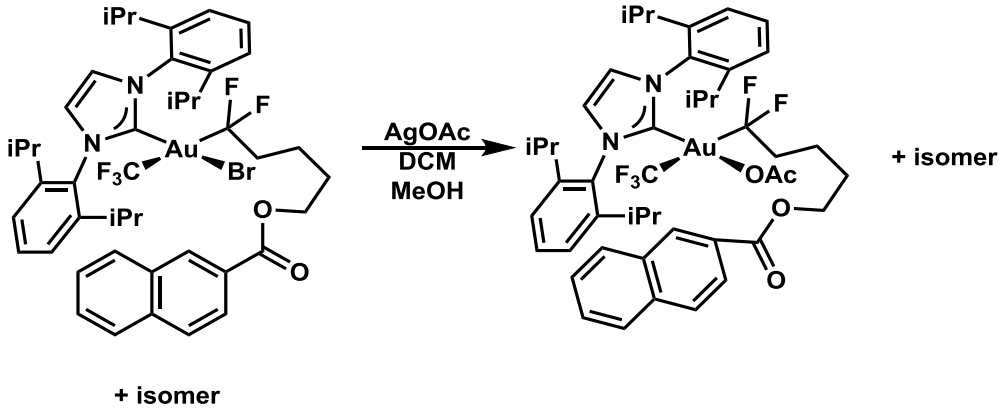


**55** (57 mg, 0.056 mmol) was dissolved in dichloromethane (0.6 mL) and methanol (6 mL) and silver acetate (93 mg, 0.56 mmol, 10 equiv) was added. The mixture was sonicated briefly and stirred for 12 hours at room temperature in the dark. The mixture was filtered, and the filter cake was washed with dichloromethane. The combined filtrates were concentrated, and the residue was again extracted with dichloromethane, filtered and concentrated, affording the product as a colorless solid (50 mg). The resulting product was used as soon as possible without further purification. Storage, even at -20°C, results in the gradual reductive elimination of R-$CF_2$OAc.

Spectra for $^1$H NMR and $^{13}$C NMR are provided below, but are not indexed due to overlapping signals for the two isomers.

$^{119}$F NMR (376 MHz, Methylene Chloride-$d_2$) δ -34.89 (t, $J$ = 10.1 Hz), -38.02 (t, $J$ = 7.2 Hz), -58.30 (bs), -76.33 (bs).

Sample instability prevented a satisfactory elemental analysis.

***trans*-phenylbis(trifluoromethyl)-1,3-Bis(2,6-diisopropylphenyl)-1,3-dihydro-2H-imidazol-2-ylidene-gold(III)**, **27**

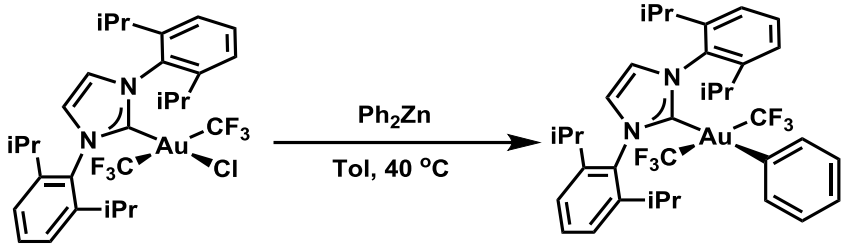


In a nitrogen filled glovebox, **25** (1.52 g, 2 mmol) and diphenyl zinc (1.1 g, 5 mmol, 2.5 equiv) were combined in a schlenk bomb and dissolved in toluene (125 mL). The flask was sealed with a teflon valve, removed from the glovebox and heated at 40 °C for 1.5 hours. Upon cooling, the mixture was quenched with $H_2O$ and extracted three times with diethyl ether. The combined organic extracts were washed with brine, dried with sodium sulfate, filtered, and concentrated. The crude material was purified by silica gel chromatography eluting with 7:3 Hexanes/DCM yielding the title compound as a colorless solid (1.56 g, 97%).

$^1$H NMR (400 MHz, Methylene Chloride-$d_2$) δ 7.57 (t, $J$ = 7.8 Hz, 2H), 7.43 (d, $J$ = 7.8 Hz, 4H), 7.40 (s, 2H), 7.04 – 6.93 (m, 3H), 6.90 (d, $J$ = 6.9 Hz, 2H), 2.94 (hept, $J$ = 6.7 Hz, 4H), 1.38 (d, $J$ = 6.7 Hz, 12H), 1.14 (d, $J$ = 6.7 Hz, 12H).

$^{13}$C NMR (151 MHz, Methylene Chloride-$d_2$) δ 179.93, 145.92 (m), 141.35, 135.89 (qq, $J$ = 355.4, 31.7 Hz, low intensity $CF_3$ resonance), 133.67, 132.31, 130.57, 127.75, 125.01, 124.79, 124.46, 28.31, 26.43, 22.18.

$^{19}$F NMR (376 MHz, Methylene Chloride-$d_2$) δ -31.11 (s).

EA: Calculated: C, 52.50; H, 5.16; N, 3.50; Found C, 52.25; H, 5.38; N, 3.22.

***trans*-(4-aminophenyl)-bis(trifluoromethyl)-1,3-Bis(2,6-diisopropylphenyl)-1,3-dihydro-2H-imidazol-2-ylidene-gold(III)**, **44**

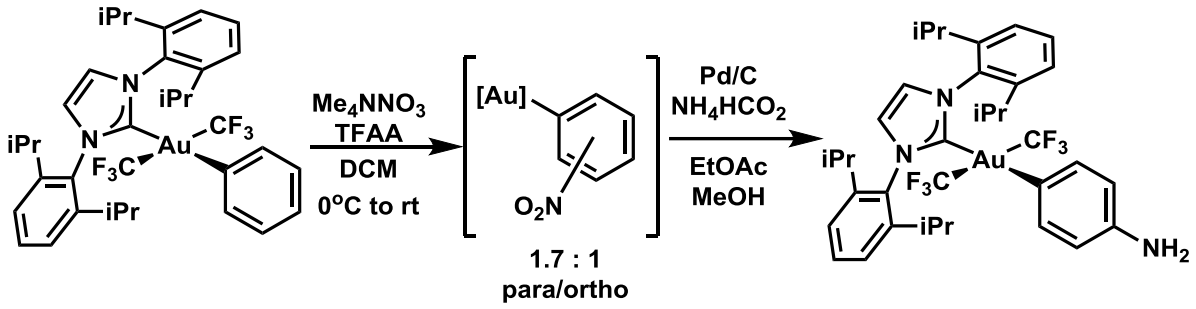


*Stage 1*: **27** (802 mg, 1 mmol) and tetramethylammonium nitrate (408 mg, 3 mmol, 3 equiv) were slurried in DCM (100 mL) and the mixture was cooled to 0°C in an ice bath. Trifluoroacetic anhydride (0.70 mL, 5 mmol, 5 equiv) was added dropwise and the mixture was removed from the ice bath and allowed to warm to room temperature. The reaction was monitored by TLC for consumption of starting material. After 3 hours the mixture was quenched with saturated aqueous sodium bicarbonate and the layers were separated. The aqueous layer was extracted with

dichloromethane and the combined organic layers were dried with $MgSO_4$, filtered and concentrated. The crude mixture was filtered through a short pad of silica with DCM, and the resulting mixture (1.7:1 para/ortho nitroaryl gold complex, 840 mg) was used without further purification.

*Stage 2*: The above crude product, ammonium formate (624 mg, 10 equiv) and 5% Pd/C (525 mg, 25% loading by Pd) were combined in a flask under $N_2$. Ethyl Acetate and Methanol (1:2, 45 mL toal) were degassed by sparging and added to the solids with stirring. The mixture was monitored by TLC for the consumption of the para isomer of the nitroaryl gold complex. After 2 hours, the mixture was filtered through a pad of celite with ethyl acetate and concentrated. The crude mixture was extracted with dichloromethane, the insoluble solids were filtered off, and DCM extract was concentrated onto silica gel. This was dry-loaded onto a column and chromatographed eluting on a gradient from 8:1:1 to 10:5:5 (Hexanes/DCM/$Et_2O$) to afford the title compound as a colorless solid (390 mg, 48% yield over 2 steps), as well as 170 mg of unreacted ortho-nitro complex (20%).

$^1$H NMR (600 MHz, Methylene Chloride-$d_2$) δ 7.59 (t, *J* = 7.8 Hz, 2H), 7.44 (d, *J* = 7.8 Hz, 4H), 7.41 (s, 2H), 6.68 (d, *J* = 8.5 Hz, 2H), 6.44 (d, *J* = 8.5 Hz, 2H), 3.43 (bs, 2H), 2.97 (hept, *J* = 6.7 Hz, 4H), 1.41 (d, *J* = 6.7 Hz, 12H), 1.16 (d, *J* = 6.8 Hz, 12H).

$^{13}$C NMR (151 MHz, Methylene Chloride-$d_2$) δ 180.97, 145.92, 143.96, 136.11 (qq, *J* = 355.3, 31.3 Hz, low intensity $CF_3$ resonance), 133.73, 133.33 (m), 132.24, 130.49, 124.72, 124.42, 114.98, 28.28, 26.40, 22.17.

$^{19}$F NMR (376 MHz, Methylene Chloride-$d_2$) δ -31.19 (s).

EA: Calculated: C, 51.54; H, 5.19; N, 5.15; Found C, 51.45; H, 5.30; N, 4.98.

**_trans_-(4-(5-methylisoxazole-4-carboxamido)phenyl)-bis(trifluoromethyl)-1,3-Bis(2,6-diisopropylphenyl)-1,3-dihydro-2H-imidazol-2-ylidene-gold(III)**, **45**

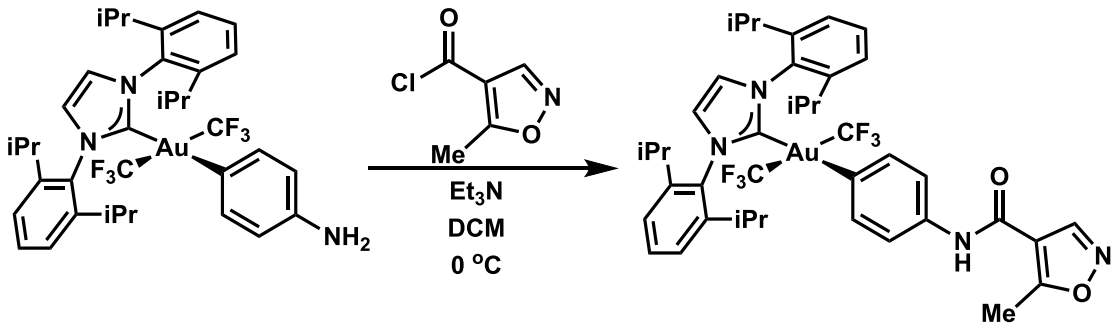


**13** (160 mg, 0.2 mmol) and triethylamine (80 μL, 3 equiv) were dissolved in DCM (2 mL) and the mixture was cooled to 0°C in an ice bath. 5-methylisoxazole-4-carbonyl chloride (prepared from the commercially available acid by treatment with oxalyl chloride and catalytic DMF) in dichloromethane (2 mL) was added dropwise, resulting in a gradual color change from pale yellow to dark purple. The reaction was monitored by TLC for consumption of starting material while maintaining the temperature at 0 °C. After 1 hour the mixture was quenched with saturated aqueous sodium bicarbonate and the layers were separated. The aqueous layer was extracted with dichloromethane and the combined organic layers were dried with $Na_2SO_4$, filtered and concentrated. The crude mixture was purified by silica gel chromatography eluting on a gradient from 30:5:5 to 6:2:2 (Hex/DCM/$Et_2O$) affording the desired product as a pale yellow solid (142 mg, 76% yield).

$^{1}$H NMR (600 MHz, Methylene Chloride-$d_2$) δ 8.40 (bs, 1H), 7.61 (t, $J$ = 7.8 Hz, 2H), 7.47 (apparent d, 6H), 7.43 (s, 1H), 7.25 (d, $J$ = 8.0 Hz, 2H), 6.96 (d, $J$ = 8.4 Hz, 2H), 2.99 (hept, $J$ = 6.7 Hz, 4H), 2.67 (s, 3H), 1.43 (d, $J$ = 6.7 Hz, 12H), 1.18 (d, $J$ = 6.8 Hz, 12H).
$^{13}$C NMR (151 MHz, Methylene Chloride-$d_2$) δ 179.28, 172.56, 158.87, 147.92, 145.93, 141.76, 136.61 (qq, $J$ = 355.3, 31.6 Hz, low intensity $CF_3$ resonance), 134.60, 133.64, 132.50, 130.63, 124.88, 124.50, 120.15, 112.31, 28.34, 26.44, 22.21, 12.17.
$^{19}$F NMR (376 MHz, Methylene Chloride-$d_2$) δ -31.09 (s).
EA: Calculated: C, 51.95; H, 4.90; N, 6.06; Found C, 51.92; H, 5.12; N, 5.99.

### *trans*-(3-hydroxypropyl)-bis(trifluoromethyl)-1,3-Bis(2,6-diisopropylphenyl)-1,3-dihydro-2H-imidazol-2-ylidene-gold(III), 47

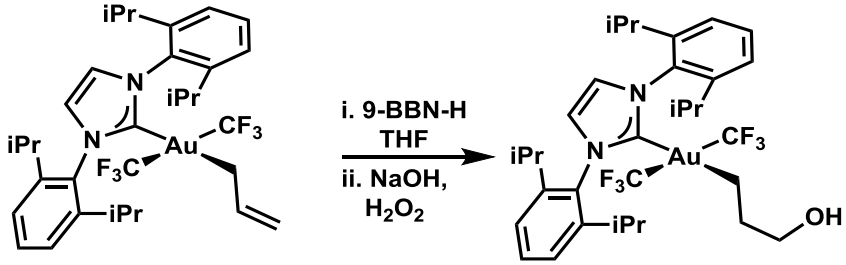


In a nitrogen filled glovebox, **28** (382 mg, 0.5 mmol) and solid 9-borabicyclo[3.3.1]nonane (64 mg, 0.525 mmol, 1.05 equiv) were dissolved in THF (25 mL total) and combined in a roundbottom flask. The flask was sealed with a rubber septum, brought out of the box and stirred for 12 hours under an $N_2$ atmosphere on a Schlenk line. 5 mL of 1M aqueous NaOH followed by 5 mL of 35% aqueous hydrogen peroxide were injected and the mixture was stirred for an additional hour. The mixture was diluted with water and extracted 3x with dichloromethane. The combined organic extracts were dried with sodium sulfate, filtered, and concentrated. The crude residue was purified by column chromatography eluting with 3:1:1 Hexanes/DCM/$Et_2O$ affording the desired product as a colorless solid (290 mg, 74% yield).

$^{1}$H NMR (400 MHz, Methylene Chloride-$d_2$) δ 7.56 (t, $J$ = 7.8 Hz, 2H), 7.47 – 7.36 (m, 6H), 3.38 (bs, 2H), 2.96 (hept, $J$ = 6.7 Hz, 4H), 1.62 – 1.51 (m, 4H), 1.40 (d, $J$ = 6.7 Hz, 12H), 1.17 (d, $J$ = 6.8 Hz, 12H).
$^{13}$C NMR (101 MHz, Methylene Chloride-$d_2$) δ 187.06, 145.91, 138.06 (qq, $J$ = 355.1, 31.2 Hz, low intensity $CF_3$ resonance), 133.87, 130.34, 124.68, 124.33, 64.20, 32.01, 28.24, 26.43, 22.16, 21.91 (m).
$^{19}$F NMR (376 MHz, Methylene Chloride-$d_2$) δ -33.06 (s).
EA: Calculated: C, 49.11; H, 5.54; N, 3.58; Found C, 49.34; H, 5.63; N, 3.42.

***trans*-(3-iodopropyl)-bis(trifluoromethyl)-1,3-Bis(2,6-diisopropylphenyl)-1,3-dihydro-2H-imidazol-2-ylidene-gold(III)**, **48**

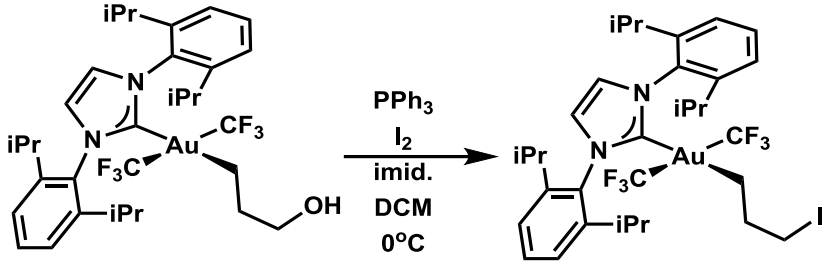


Triphenylphosphine (291 mg, 1.11 mmol, 3 equiv) and imidazole (76 mg, 1.11 mmol, 3 equiv) were dissolved in DCM (12 mL) and cooled to 0°C in an ice bath. Solid iodine (282 mg, 1.11 mmol, 3 equiv) was added and stirred 15 minutes resulting in a yellow-orange solution. **47** (290 mg, 0.37 mmol) in DCM (6 mL) was added slowly and the mixture was removed from the ice bath and allowed to warm to room temperature. After 20 minutes TLC showed complete consumption of the starting material. The mixture was filtered, washing the insoluble material with additional DCM and concentrated directly onto silica which was dry loaded onto a column and chromatographed eluting with 5:1:1 Hex/DCM/$Et_2O$. The resulting product was washed with cold hexanes to remove residual co-eluting $PPh_3$, to afford the title compound as a colorless solid (280 mg, 85% yield).

$^1$H NMR (400 MHz, Methylene Chloride-$d_2$) δ 7.51 (t, *J* = 7.8 Hz, 2H), 7.35 (d, *J* = 7.8 Hz, 4H), 7.34 (s, 2H), 2.93 (t, *J* = 7.5 Hz, 2H), 2.86 (hept, *J* = 6.8 Hz, 4H), 1.76 (apparent p, *J* = 7.9 Hz, 2H), 1.51 – 1.42 (m, 2H), 1.32 (d, *J* = 6.7 Hz, 12H), 1.10 (d, *J* = 6.7 Hz, 12H).

$^{13}$C NMR (151 MHz, Methylene Chloride-$d_2$) δ 185.53, 145.86, 137.59 (qq, *J* = 355.1, 31.6 Hz, low intensity $CF_3$ resonance), 133.74, 130.42, 124.70, 124.35, 33.10, 28.23, 26.46, 26.26 (m), 22.16, 8.04.

$^{19}$F NMR (376 MHz, Methylene Chloride-$d_2$) δ -32.98.

EA: Calculated: C, 43.06; H, 4.74; N, 3.14; Found C, 43.20; H, 4.71; N, 3.06.

***trans*-3-(acetylthio)propyl)(1,3-bis(2,6-diisopropylphenyl)-1,3-dihydro-2H-imidazol-2-ylidene)bis(trifluoromethyl)gold(III), 49**

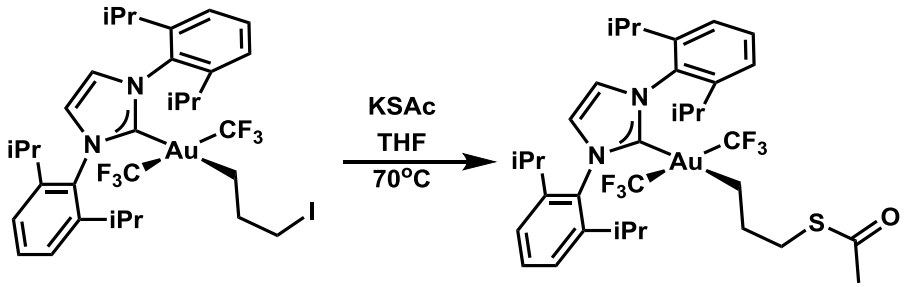


**48** (280 mg, 0.313 mmol) and potassium thioacetate (40 mg, 1.1 equiv) were combined in a Schlenk bomb and dissolved in THF (7 mL). The mixture was degassed by sparging with $N_2$, sealed with a teflon valve and heated at 70°C for 12 hours. Upon cooling, the mixture was filtered, washing the filter cake with diethyl ether, and concentrated directly onto silica which was dry

loaded onto a column and chromatographed eluting on a gradient (18:1:1 to 8:1:1 Hex/DCM/$Et_2O$) to afford the title compound as a yellow solid (217 mg, 82% yield).

$^1$H NMR (400 MHz, Methylene Chloride-$d_2$) δ 7.50 (t, *J* = 7.8 Hz, 2H), 7.35 (d, *J* = 7.8 Hz, 4H), 7.32 (s, 2H), 2.87 (hept, *J* = 6.8 Hz, 4H), 2.65 (s, 2H), 1.49 (d, *J* = 3.5 Hz, 4H), 1.32 (d, *J* = 6.7 Hz, 12H), 1.10 (d, *J* = 6.8 Hz, 12H).

$^{13}$C NMR (151 MHz, Methylene Chloride-$d_2$) δ 195.40, 186.46, 145.8, 137.84 (qq, *J* = 354.9, 32.0 Hz), 133.79, 130.33, 124.65, 124.31, 30.83, 30.29, 28.36, 28.19, 26.38, 24.85 (m), 22.14.

$^{19}$F NMR (376 MHz, Methylene Chloride-$d_2$) δ -33.10 (s).

EA: Calculated: C, 48.57; H, 5.40; N, 3.33; S, 3.81 Found C, 48.80; H, 5.54; N, 3.25; S, 4.10.

**trans-(3-(chlorosulfonyl)propyl)-bis(trifluoromethyl)-1,3-Bis(2,6-diisopropylphenyl)-1,3-dihydro-2H-imidazol-2-ylidene-gold(III)**, **50**

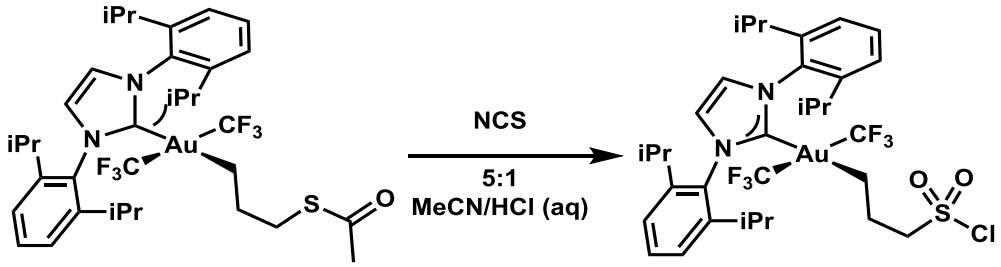


**49** (226 mg, 0.27 mmol) was dissolved in 13.5 mL of acetonitrile, and 2.7 mL of 2M aqueous HCl was added, followed by N-Chlorosuccinimide (144 mg, 4 equiv). The mixture was stirred under air for 1 hour at which time TLC showed consumption of the starting material. The reaction mixture was diluted with diethyl ether and water, and the layers were separated. The aqueous layer was extracted 2x with diethyl ether, and the combined organic fractions were again washed with water before drying with sodium sulfate, filtration, and concentration. Column Chromatography on silica gel eluting with 85:7.5:7.5 Hex/DCM/$Et_2O$ afforded the title compound as a colorless solid (203 mg, 87% yield).

$^1$H NMR (700 MHz, Methylene Chloride-$d_2$) δ 7.58 (t, *J* = 7.8 Hz, 2H), 7.45 – 7.41 (m, 6H), 3.49 – 3.45 (m, 2H), 2.94 (hept, *J* = 6.7 Hz, 4H), 2.11 – 2.02 (m, 2H), 1.62 – 1.59 (m, 2H), 1.40 (d, *J* = 7.1 Hz, 13H), 1.17 (d, *J* = 7.2 Hz, 12H).

$^{13}$C NMR (176 MHz, Methylene Chloride-$d_2$) δ 184.25, 145.88, 137.25 (qq, *J* = 355.5, 31.9 Hz, low intensity $CF_3$ resonance), 133.59, 130.62, 124.84, 124.43, 66.60, 28.30, 26.49, 24.08, 22.08, 21.82 – 21.32 (m).

$^{19}$F NMR (376 MHz, Methylene Chloride-$d_2$) δ -32.73 (s).

EA: Calculated: C, 44.43; H, 4.89; N, 3.24; S, 3.71; Found C, 44.42; H, 5.00; N, 3.19; S, 3.85.

***trans*-(1,3-bis(2,6-diisopropylphenyl)-1,3-dihydro-2H-imidazol-2-ylidene)(3-((3-(2-cyano-3-(trifluoromethyl)phenoxy)phenoxy)sulfonyl)propyl)bis(trifluoromethyl)gold**, **51**

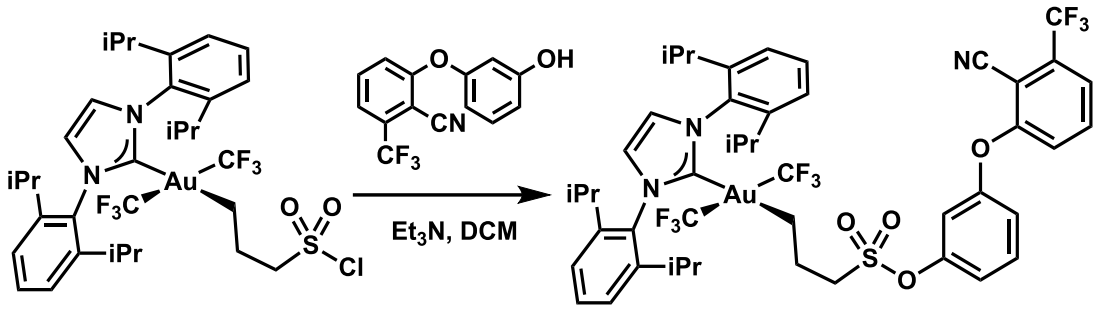


**50** (170 mg, 0.196 mmol), in dichloromethane (10 mL) was added to a solution of 2-(3-hydroxyphenoxy)-6-(trifluoromethyl)benzonitrile (57 mg, 1.05 equiv) and trimethylamine (40 µL, 1.5 equiv) in dichloromethane (10 mL). The solution was stirred for 25 minutes at which point the TLC showed complete consumption of the starting material. Chromatography on silica gel eluting on a gradient from 8:1:1 to 7:1.5:1.5 Hexanes/DCM/$Et_2O$ afforded the title compound as a colorless solid (184 mg, 85% yield).

$^1$H NMR (700 MHz, Methylene Chloride-$d_2$) δ 7.68 (t, *J* = 8.2 Hz, 1H), 7.58 – 7.51 (m, 4H), 7.45 – 7.38 (m, 6H), 7.20 – 7.11 (m, 3H), 7.04 (t, *J* = 2.4 Hz, 1H), 3.17 – 3.04 (m, 2H), 2.93 (hept, *J* = 6.8 Hz, 4H), 2.01 – 1.94 (m, 2H), 1.59 – 1.55 (m, 2H), 1.38 (d, *J* = 7.0 Hz, 12H), 1.17 (d, *J* = 7.1 Hz, 12H).

$^{13}$C NMR (176 MHz, Methylene Chloride-$d_2$) δ 184.58, 160.64, 155.09, 150.30, 145.87, 137.36 (qq, *J* = 355.1, 31.6 Hz), 134.38, 134.12 (q, *J* = 32.6 Hz), 133.63, 131.31, 130.54, 124.82, 124.41, 122.30 (q, *J* = 273.8 Hz), 120.84 (q, *J* = 4.9 Hz), 120.27, 119.31, 118.67, 114.44, 112.11, 101.14, 52.03, 28.27, 26.43, 23.15, 22.68 – 22.37 (m), 22.12.

$^{19}$F NMR (376 MHz, Methylene Chloride-$d_2$) δ -32.87 (s, 6F), -61.61 (s, 3F).

EA: Calculated: C, 49.87; H, 4.46; N, 3.79; S, 2.89; Found C, 49.88; H, 4.78; N, 3.68; S, 3.28.

**Bromo-(4-((3-(2-cyano-3-(trifluoromethyl)phenoxy)phenoxy)sulfonyl)-1,1-difluorobutyl)-trifluoromethyl-1,3-Bis(2,6-diisopropylphenyl)-1,3-dihydro-2H-imidazol-2-ylidene-gold(III)** (mixture of coordination isomers), **56**

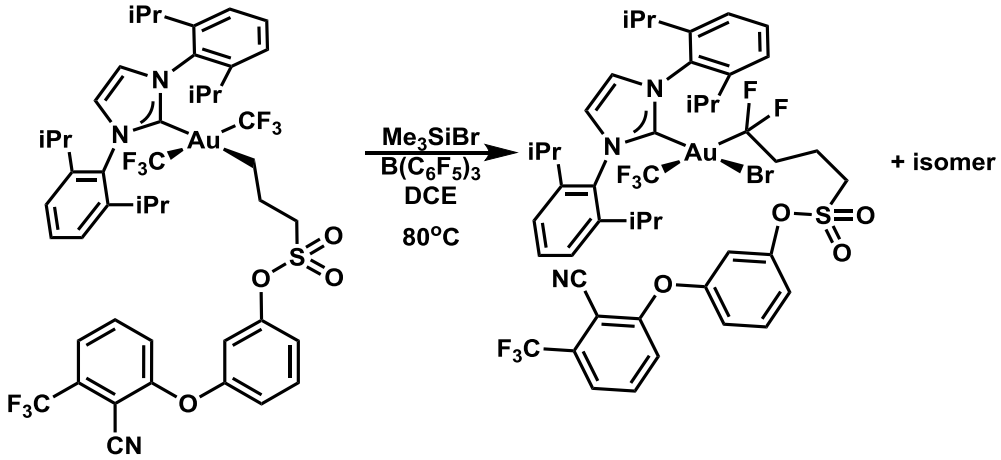

In a schlenk bomb, **51** (116 mg, 0.104 mmol) was dissolved in 3 mL of DCE, and TMSBr (0.14 mL, 10 equiv) followed by a solution of **2** (53 mg, 1 equiv) in 3 mL of DCE. The flask was sealed with a Teflon valve and the solution was heated to 80°C and monitored by TLC for consumption of the starting material. After 1 hour, the solution was cooled to room temperature and quenched with aqueous sodium bicarbonate. The layers were separated, the aqueous layer was extracted with DCM, and the combined organic layers were dried over $Na_2SO_4$, filtered, and concentrated.

Purification by column chromatography on silica (7:1.5:1.5 Hex/DCM/$Et_2O$ eluent) afforded the product as a colorless solid, which was further purified by precipitation from diethyl ether with hexanes (60 mg, 55% yield).

Spectra for $^1$H NMR and $^{13}$C NMR are provided below, but are not indexed due to overlapping signals for the two isomers.

$^{19}$F NMR (376 MHz, Methylene Chloride-$d_2$) δ -28.32 (t, $J$ = 9.9 Hz), -31.71 (t, $J$ = 9.6 Hz), -60.15 (bs), -61.61 (s), -69.89 (bs).

EA: Calculated: C, 47.27; H, 4.23; N, 3.60; S, 2.74; Found C, 46.95; H, 4.36; N, 3.26; S, 2.93.

**Acetato-( 4-((3-(2-cyano-3-(trifluoromethyl)phenoxy)phenoxy)sulfonyl)-1,1-difluorobutyl)-trifluoromethyl-1,3-Bis(2,6-diisopropylphenyl)-1,3-dihydro-2H-imidazol-2-ylidene-gold(III)** (mixture of coordination isomers), **59**

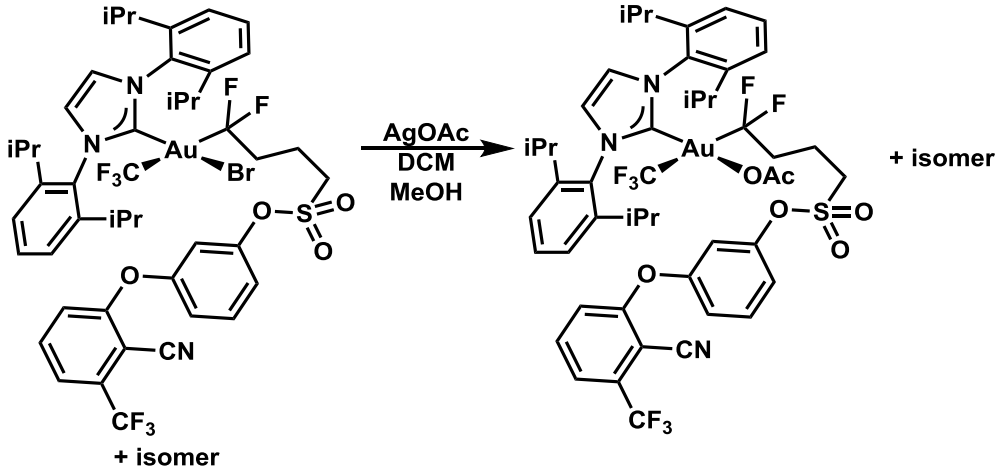


**56** (60 mg, 0.051 mmol) was dissolved in a mixture of 0.6 mL of dichloromethane and 6 mL of methanol, and 85 mg (10 equiv) of silver acetate was added. The mixture was stirred vigorously overnight at room temperature in the dark. The resulting mixture was filtered, concentrated, extracted with DCM, filtered again, and concentrated (56 mg, colorless solid). The resulting product was used as soon as possible without further purification. Storage, even at -20°C, results in the gradual reductive elimination of R-$CF_2$OAc.

Spectra for $^1$H NMR and $^{13}$C NMR are provided below, but are not indexed due to overlapping signals for the two isomers.

$^{19}$F NMR (376 MHz, Methylene Chloride-$d_2$) δ -34.88 (t, $J$ = 9.8 Hz), -38.09 (t, $J$ = 7.1 Hz), -60.39 (bs), -61.58 (s), -77.54 (bs).

Sample instability prevented a satisfactory elemental analysis.

### *trans*-(cyclopropylmethyl)-bis(trifluoromethyl)-1,3-Bis(2,6-diisopropylphenyl)-1,3-dihydro-2H-imidazol-2-ylidene-gold(III), 41

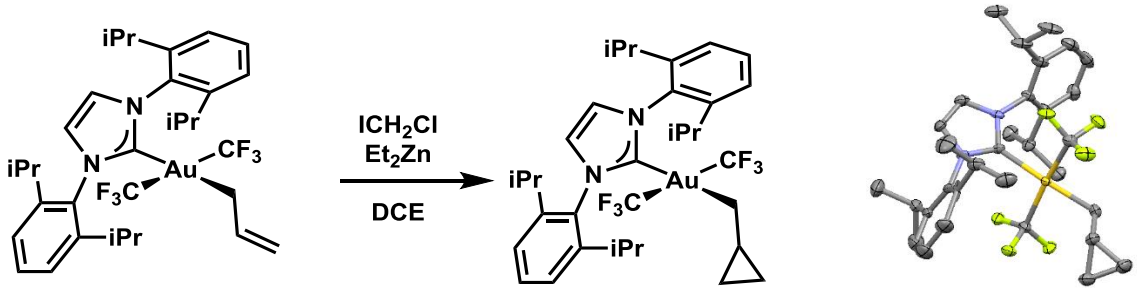


In a nitrogen filled glovebox, **28** (76 mg, 0.1 mmol) and diethyl zinc (0.2 mL of 1M hexanes solution, 2 equiv) were dissolved in DCE (3 mL) in a roundbottom flask. Chloroiodomethane (71 mg, 4 equiv) in 3 mL of DCE was added and the mixture was sealed with a rubber septum, brought out of the box and stirred for 1 hour under an $N_2$ atmosphere on a Schlenk line. 5 mL of $H_2O$ were injected and the mixture was extracted 3x with diethyl ether. The combined organic extracts were dried with sodium sulfate, filtered, and concentrated. The crude residue was purified by column chromatography eluting with 1:1 Hexanes/DCM affording the desired product as a colorless solid (69 mg, 88 % yield).

$^1$H NMR (600 MHz, Methylene Chloride-$d_2$) δ 7.51 (t, $J$ = 7.8 Hz, 2H), 7.36 (d, $J$ = 7.8 Hz, 4H), 7.34 (s, 2H), 2.93 (hept, $J$ = 6.7 Hz, 4H), 1.48 (d, $J$ = 7.3 Hz, 2H), 1.35 (d, $J$ = 6.7 Hz, 12H), 1.13 (d, $J$ = 6.8 Hz, 12H), 0.73 (ddt, $J$ = 9.5, 7.7, 3.8 Hz, 1H), 0.32 – 0.24 (m, 2H), 0.01 – -0.05 (m, 2H).
$^{13}$C NMR (151 MHz, Methylene Chloride-$d_2$) δ 187.89, 145.86, 138.53 (qq, $J$ = 354.9, 30.9 Hz, low intensity $CF_3$ resonance), 133.94, 130.14, 124.51, 124.24, 31.74 (bs), 28.17, 26.30, 22.18, 10.63, 6.85.
$^{19}$F NMR (376 MHz, Methylene Chloride-$d_2$) δ -31.62 (s).
EA: Calculated: C, 50.90; H, 5.57; N, 3.60; Found C, 51.37; H, 5.94; N, 3.37.

### *trans*-(2,3-dihydroxypropyl)-bis(trifluoromethyl)-1,3-Bis(2,6-diisopropylphenyl)-1,3-dihydro-2H-imidazol-2-ylidene-gold(III), 42

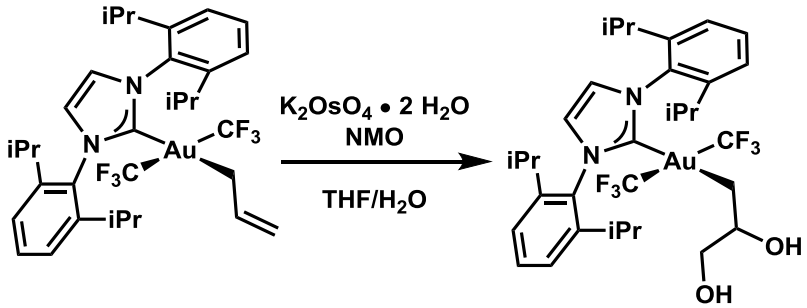


**28** (110 mg, 0.144 mmol) and potassium osmate dihydrate (1 mg, 0.02 equiv) were dissolved in 1:1 THF/$H_2O$ (6 mL) in a roundbottom flask. N-methylmorpholine-N-oxide (34 mg, 2 equiv) was added, and additional THF ~ 1 mL was added to solubilize the gold complex. The mixture was

stirred for 12 hours under air, then 5 mL of 1M aqueous sodium bisulfate was added, and the mixture was extracted 3x with diethyl ether. The combined organic extracts were dried with sodium sulfate, filtered, and concentrated. The crude residue was purified by column chromatography eluting with 3:1:1 Hexanes/DCM/$Et_2O$ affording the desired product as a colorless solid (80 mg, 70% yield).

$^1$H NMR (700 MHz, Methylene Chloride-$d_2$) δ 7.56 (t, *J* = 7.8 Hz, 2H), 7.47 – 7.33 (m, 6H), 3.76 (qd, *J* = 7.8, 3.3 Hz, 1H), 3.26 (dd, *J* = 11.1, 3.4 Hz, 1H), 3.15 (dd, *J* = 11.1, 7.8 Hz, 1H), 2.93 (dhept, *J* = 22.3, 6.7 Hz, 4H), 1.91 (s, 1H), 1.69 (dd, *J* = 10.7, 8.2 Hz, 2H), 1.61 (dd, *J* = 10.5, 7.2 Hz, 1H), 1.42 – 1.35 (m, 12H), 1.15 (dd, *J* = 10.8, 6.8 Hz, 12H).
$^{13}$C NMR (176 MHz, Methylene Chloride-$d_2$) δ 184.44, 145.94, 145.84, 136.99 (qq, *J* = 354.9, 31.7 Hz, low intensity $CF_3$ resonance), 133.65, 130.50, 124.79, 124.41, 124.35, 72.60, 68.01, 28.29, 28.23, 27.72 (bs), 26.50, 26.38, 22.01.
$^{19}$F NMR (376 MHz, Methylene Chloride-$d_2$) δ -31.08 (s).
EA: Calculated: C, 48.12; H, 5.43; N, 3.51; Found C, 47.89; H, 5.61; N, 3.26.

***trans*-(2-oxoethyl)-bis(trifluoromethyl)-1,3-Bis(2,6-diisopropylphenyl)-1,3-dihydro-2H-imidazol-2-ylidene-gold(III)**, **43**

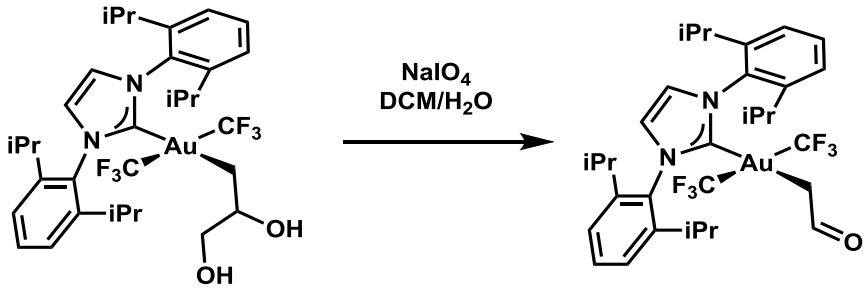


**42** (75 mg, 0.095 mmol) and sodium periodate (100 mg, 5 equiv) were dissolved in 4:1 DCM/$H_2O$ (2.5 mL). The mixture was vigorously stirred for 18 hours under air, diluted with DCM and washed 3x with brine. The organic layer was dried with sodium sulfate, filtered, and concentrated. The crude residue was purified by column chromatography eluting with 85:7.5:7.5 Hexanes/DCM/$Et_2O$ affording the desired product as a colorless solid (36 mg, 50% yield).

$^1$H NMR (700 MHz, Methylene Chloride-$d_2$) δ 9.40 (t, *J* = 4.5 Hz, 1H), 7.57 (t, *J* = 7.8 Hz, 2H), 7.43 (s, 2H), 7.41 (d, *J* = 7.8 Hz, 4H), 2.89 (hept, *J* = 6.7 Hz, 4H), 2.62 (d, *J* = 4.5 Hz, 2H), 1.36 (d, *J* = 6.8 Hz, 13H), 1.16 (d, *J* = 6.8 Hz, 13H).
$^{13}$C NMR (176 MHz, Methylene Chloride-$d_2$) δ 200.70, 177.29, 145.78, 135.24 (qq, *J* = 356.5, 32.8 Hz, low intensity $CF_3$ resonance), 133.22, 130.71, 124.98, 124.58, 36.79 (bs), 28.32, 26.46, 22.15.
$^{19}$F NMR (376 MHz, Methylene Chloride-$d_2$) δ -30.27 (s).
EA: Calculated: C, 48.57; H, 5.13; N, 3.65; Found C, 48.18; H, 5.01; N, 3.21.

**Reductive Elimination of 1-(4-(4,4,4-trifluorobutyl)phenyl)ethan-1-one (Stoichiometric Borane)**

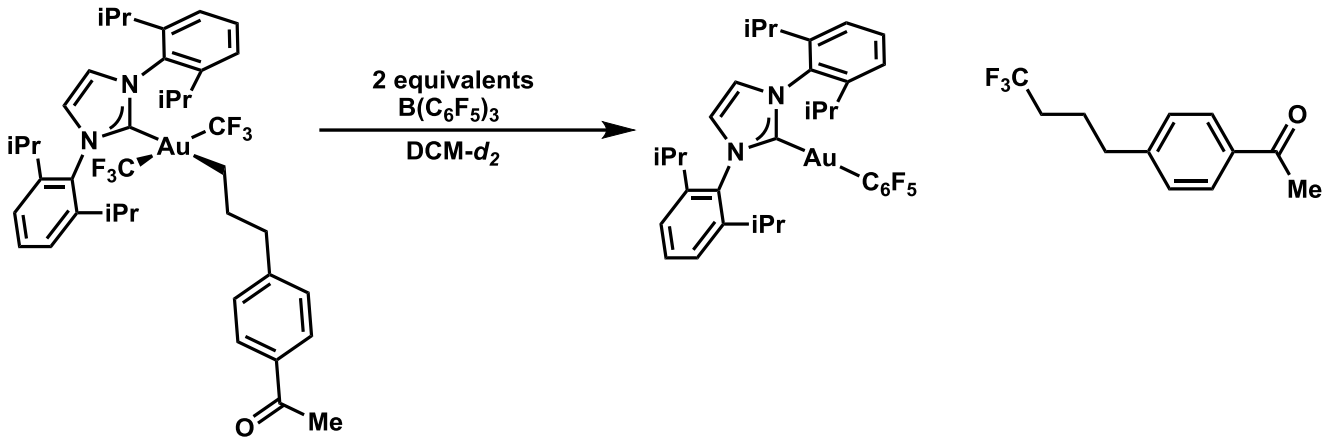


In a nitrogen filled glovebox, to a solution of **33** (66 mg, 0.075 mmol) in 2 mL of DCM was added a solution of $B(C_6F_5)_3$ (77 mg, 0.15 mmol) in 2 mL of DCM. An immediate color change to pale yellow occurred, and the mixture was capped with a septum cap, and brought out of the glovebox. After 10 minutes, TLC analysis indicated complete consumption of the starting material, and a solution of saturated aqueous sodium bicarbonate was injected through the septum, and the mixture was vigorously stirred for 10 minutes. The solution was diluted with water and dichloromethane. The organic layer was separated and the aqueous layer was washed 2x with DCM. The combined organic layers were dried over $Na_2SO_4$, filtered, and concentrated. The crude residue was purified by column chromatography eluting with (18:1:1 Hexanes/DCM/$Et_2O$) to afford the title compound (12 mg, 70% yield).

When conducted in an NMR tube on 0.005 mmol scale, 97% yield by $^{19}$FNMR was observed.

$^1$H NMR (600 MHz, Methylene Chloride-$d_2$) δ 7.90 (d, $J$ = 8.2 Hz, 2H), 7.31 (d, $J$ = 8.2 Hz, 2H), 2.77 (t, $J$ = 7.7 Hz, 2H), 2.57 (s, 3H), 2.20 – 2.07 (m, 2H), 1.92 (tt, $J$ = 10.6, 7.0 Hz, 2H).
$^{13}$C NMR (151 MHz, Methylene Chloride-$d_2$) δ 197.34 , 146.42 , 135.45 , 128.51 , 128.46 , 127.20 (q, $J$ = 276.2 Hz, low intensity $CF_3$ resonance), 34.43 , 32.89 (q, $J$ = 28.5 Hz), 26.34 , 23.14 (q, $J$ = 3.0 Hz).
$^{19}$F NMR (376 MHz, Methylene Chloride-$d_2$) δ -65.82 (t, $J$ = 11.1 Hz).
HRMS (EI) m/z: calculated for $[C_{12}H_{13}O_1F_3]^+$ 230.0918, found 230.0919.

**Reductive Elimination of 5,5,5-trifluoropentyl 2-naphthoate (Stoichiometric Borane)**

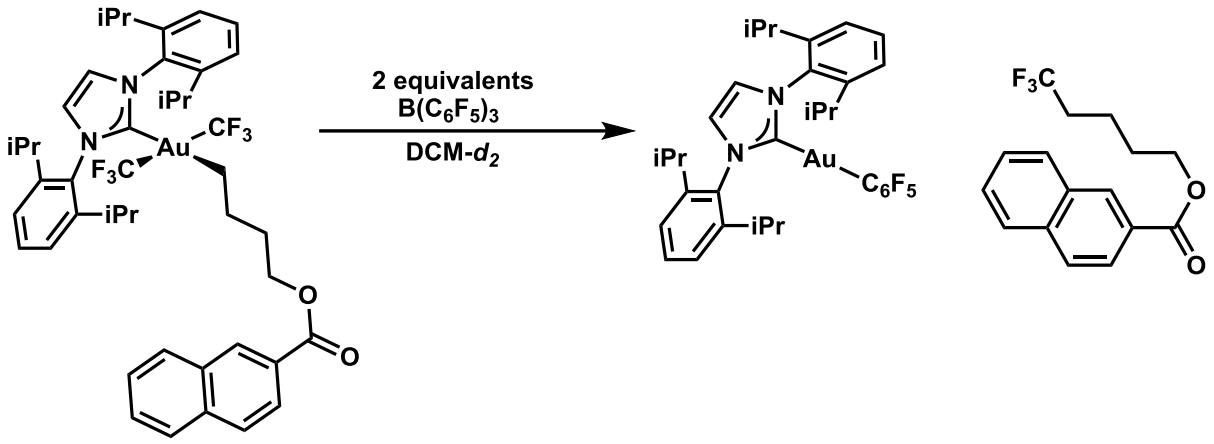


In a nitrogen filled glovebox, to a solution of **38** (54 mg, 0.058 mmol) in 2 mL of DCM was added a solution of $B(C_6F_5)_3$ (59 mg, 0.116 mmol) in 2 mL of DCM. An immediate color change to orange occurred, and the mixture was capped with a septum cap and brought out of the glovebox. TLC analysis after 45 minutes indicated complete consumption of the starting material.

A solution of saturated aqueous sodium bicarbonate was injected through the septum, and the mixture was vigorously shaken. The septum was removed and the solution was diluted with water and dichloromethane. The organic layer was separated and the aqueous layer was washed 2x with DCM. The combined organic layers were dried over $MgSO_4$, filtered, and concentrated. The crude residue was purified by silica gel chromatography (97:3 Hexanes/$Et_2O$). The resulting residue was extracted with cold hexanes to remove the desired product from co-eluting $IPrAuC_6F_5$ (12 mg, 60%).

When conducted in an NMR tube on 0.005 mmol scale, 80% yield by $^{19}$FNMR was observed.

$^1$H NMR (400 MHz, Methylene Chloride-$d_2$) δ 8.62 (s, 1H), 8.06 (dd, *J* = 8.7, 1.7 Hz, 1H), 8.00 (d, *J* = 8.0 Hz, 1H), 7.92 (d, *J* = 8.6 Hz, 2H), 7.68 – 7.56 (m, 2H), 4.40 (t, *J* = 6.3 Hz, 2H), 2.36 – 2.12 (m, 2H), 1.92 (p, *J* = 6.5 Hz, 2H), 1.80 (qd, *J* = 7.6, 7.1, 4.1 Hz, 2H).

$^{13}$C NMR (176 MHz, Methylene Chloride-$d_2$) δ 166.44, 135.49, 132.49, 130.80, 129.25, 128.27, 128.13, 127.71, 127.59, 127.29 (q, *J* = 276.4 Hz), 126.70, 125.06, 64.29, 33.29 (q, *J* = 28.2 Hz), 27.84, 18.82 (q, *J* = 2.7 Hz).

$^{19}$F NMR (376 MHz, Methylene Chloride-$d_2$) δ -65.94 (t, *J* = 11.0 Hz).

HRMS (EI) m/z: calculated for $[C_{16}H_{15}O_2F_3]^+$ 296.1024, found 296.1022.

**Reductive Elimination of Leflunomide (Stoichiometric Borane)**

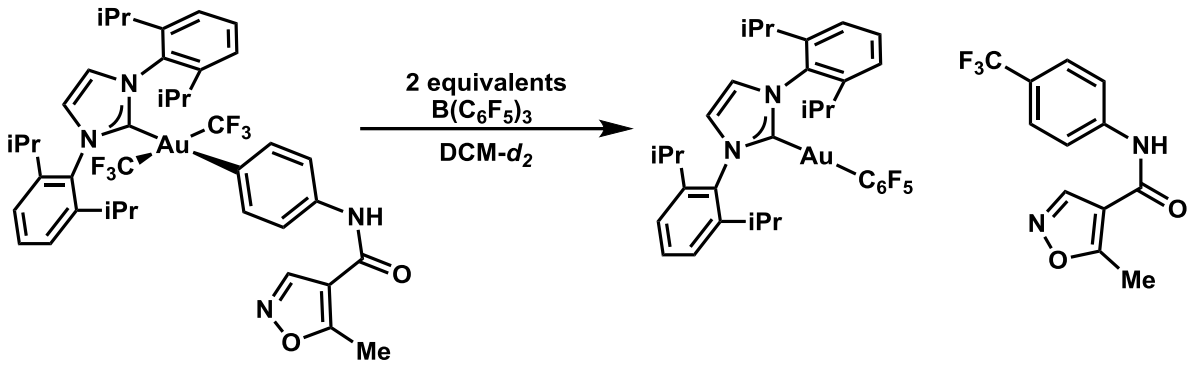


In a nitrogen filled glovebox, to a solution of **45** (5.2 mg, 0.0056 mmol) in 0.3 mL of DCM-$d_2$ in a silylated NMR tube was added a solution of $B(C_6F_5)_3$ (5.6 mg, 0.011 mmol) in 0.3 mL of DCM-$d_2$. An immediate color change to pale yellow occurred, and the mixture was capped with an NMR tube septum and sealed with electrical tape. The mixture was heated at 40°C in an oil bath for 15 hours, at which point $^1$HNMR and $^{19}$FNMR spectra were recorded, indicating complete conversion to the desired product relative to [Au].

A solution of saturated aqueous sodium bicarbonate was injected through the septum, and the mixture was vigorously shaken. The septum was removed and the solution was diluted with water and dichloromethane. The organic layer was separated and the aqueous layer was washed 2x with DCM. The combined organic layers were dried over $MgSO_4$, filtered, and concentrated. The crude residue was purified by prep TLC (70:15:15 Hexanes/DCM/$Et_2O$) to afford the title compound (1.5 mg, 98% yield).

$^1$H NMR (400 MHz, Methylene Chloride-$d_2$) δ 8.51 (s, 1H), 7.76 (d, $J$ = 8.6 Hz, 2H), 7.64 (d, $J$ = 8.2 Hz, 2H), 2.75 (s, 3H).
$^{19}$F NMR (376 MHz, Methylene Chloride-$d_2$) δ -61.70 (s).

Spectra were in accordance with those previously reported.[92]

**Reductive Elimination of BAY 59-3074 (Stoichiometric Borane)**

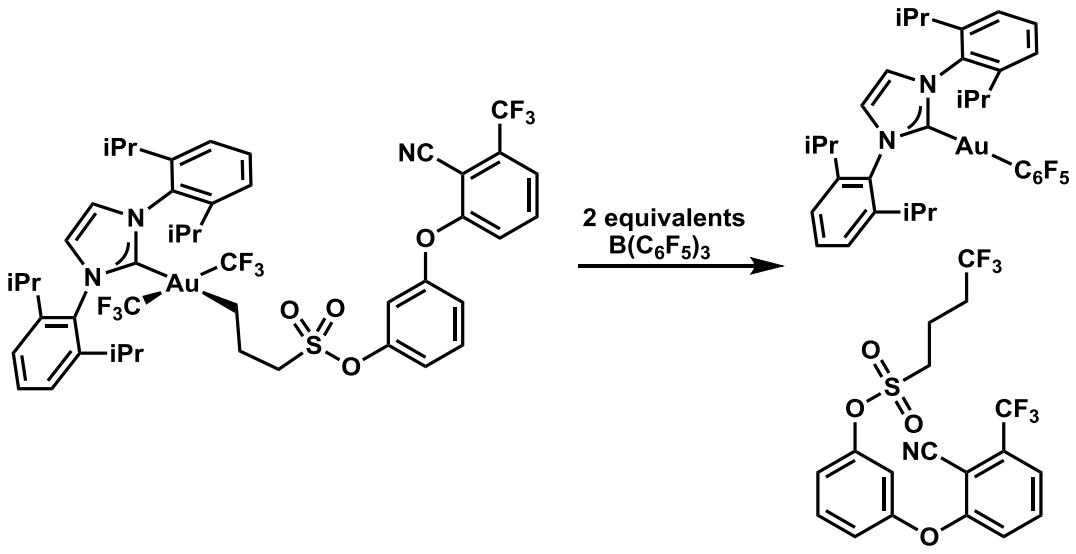


In a nitrogen filled glovebox, to a solution of **51** (22 mg, 0.02 mmol) in 0.5 mL of DCM-$d_2$ in a silylated NMR tube was added a solution of $B(C_6F_5)_3$ (20 mg, 0.04 mmol) in 0.5 mL of DCM-$d_2$. An immediate color change to pale yellow occurred, and the mixture was capped with an NMR tube septum and sealed with electrical tape. After 2 hours, $^1$HNMR and $^{19}$FNMR spectra were recorded, indicating complete conversion to the desired product relative to [Au].

A solution of saturated aqueous sodium bicarbonate was injected through the septum, and the mixture was vigorously shaken. The septum was removed and the solution was diluted with water and dichloromethane. The organic layer was separated and the aqueous layer was washed 2x with DCM. The combined organic layers were dried over $MgSO_4$, filtered, and concentrated. The crude residue was purified by prep TLC (6:2:2 Hexanes/DCM/$Et_2O$) to afford the title compound (6 mg, 67% yield).

$^1$H NMR (400 MHz, Methylene Chloride-$d_2$) δ 7.67 (t, $J$ = 8.3 Hz, 1H), 7.57 – 7.49 (m, 2H), 7.23 – 7.19 (m, 1H), 7.17 (d, $J$ = 8.5 Hz, 1H), 7.14 – 7.06 (m, 2H), 3.39 (t, $J$ = 7.3 Hz, 2H), 2.45 – 2.20 (m, 4H).
$^{19}$F NMR (376 MHz, Methylene Chloride-$d_2$) δ -61.62 (s, 3F), -65.86 (t, $J$ = 10.5 Hz, 3F).

Spectra were in accordance with those previously reported.[95]

### 4.5.3 Non-preparative Reactions

**Attempted Oxidative Addition of Iodoethane**

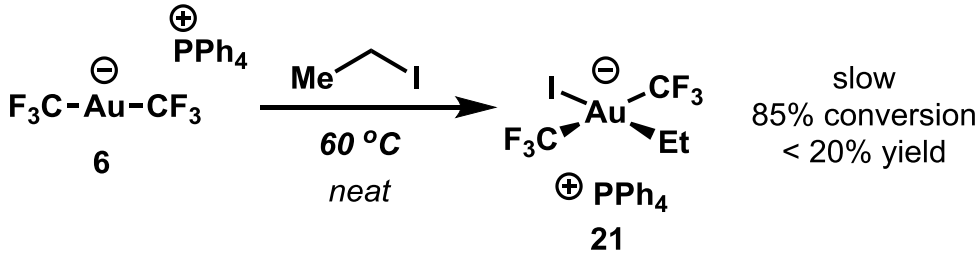


**6** (33 mg, 0.05 mmol) was dissolved in iodoethane (1.5 mL) and the mixture was heated at 65°C in an NMR tube. $^{19}$F-NMR spectra were recorded periodically. The spectrum below was taken after 2 days of heating, at which point no further conversion was observed (spectrum unlocked on deuterated solvent, so absolute shifts are not meaningful). Concentration of the solution, an extraction of the distilland with dichloromethane, filtration, and concentration afforded approximately 20% mass recovery, indicating substantial decomposition.

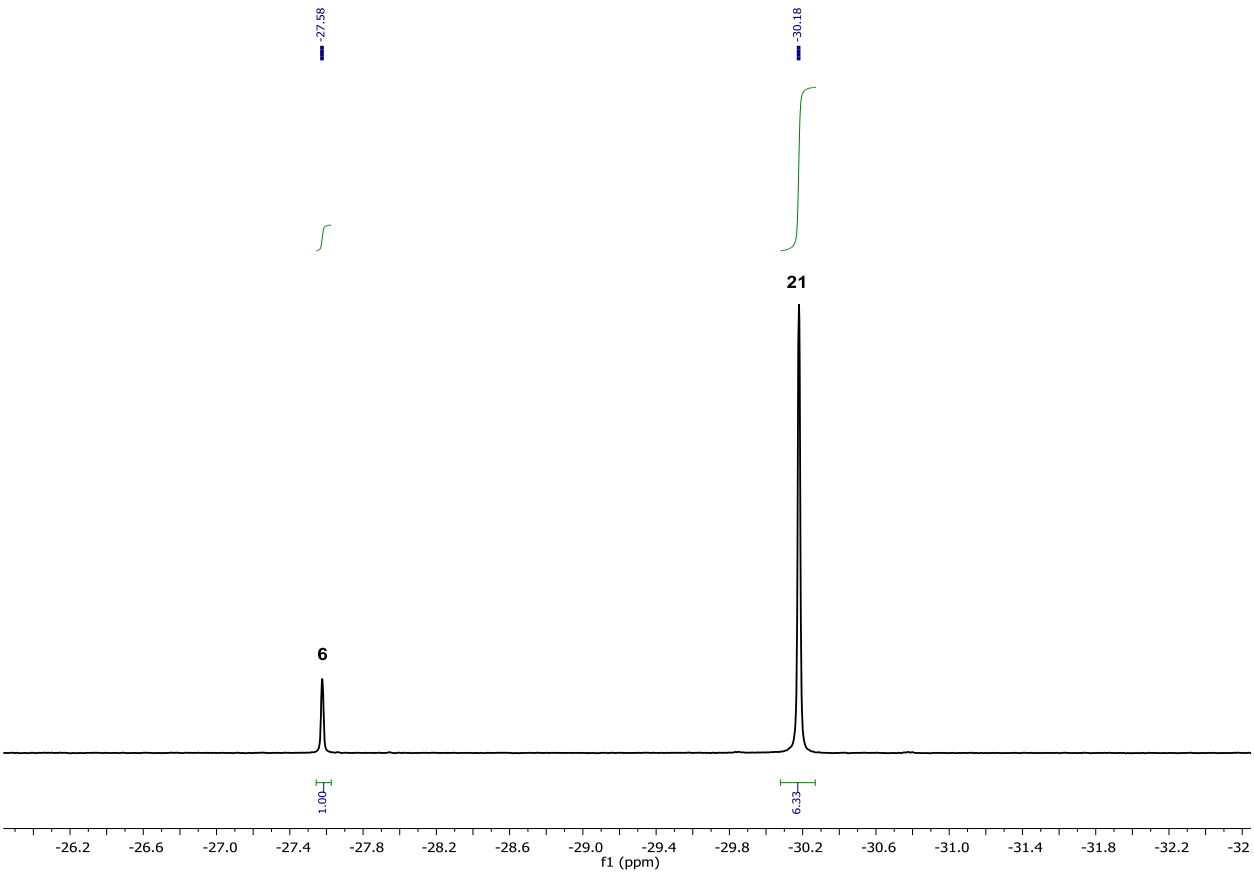


**Figure 4.42**

**Attempted oxidative addition of allyl bromide**

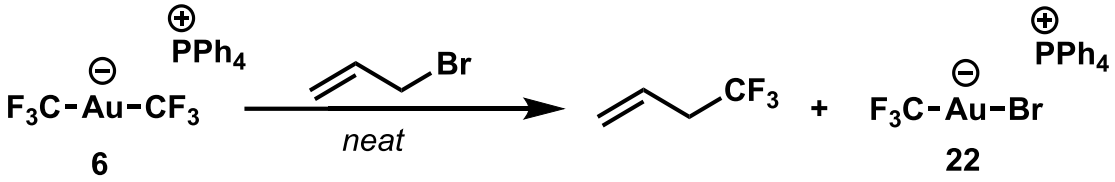


**6** (33 mg, 0.05 mmol) was dissolved in allyl bromide (1.5 mL) and the mixture was heated in an NMR tube at 40°C until the complex dissolved and then allowed to react at room temperature, with $^{19}$F-NMR spectra recorded periodically. The spectrum below was recorded after 14 hours, showing the presence of a species tentatively identified as the oxidative addition product, as well as allyl-$CF_3$ and a new Au(I) species identified as **22** (spectrum unlocked on deuterated solvent, so absolute shifts are not meaningful). Continued heating resulted in consumption of the oxidative addition product prior to complete conversion of **6**, affording a mixture of **22** and dibromoaurate, as determined by negative mode direct-inject mass spec.

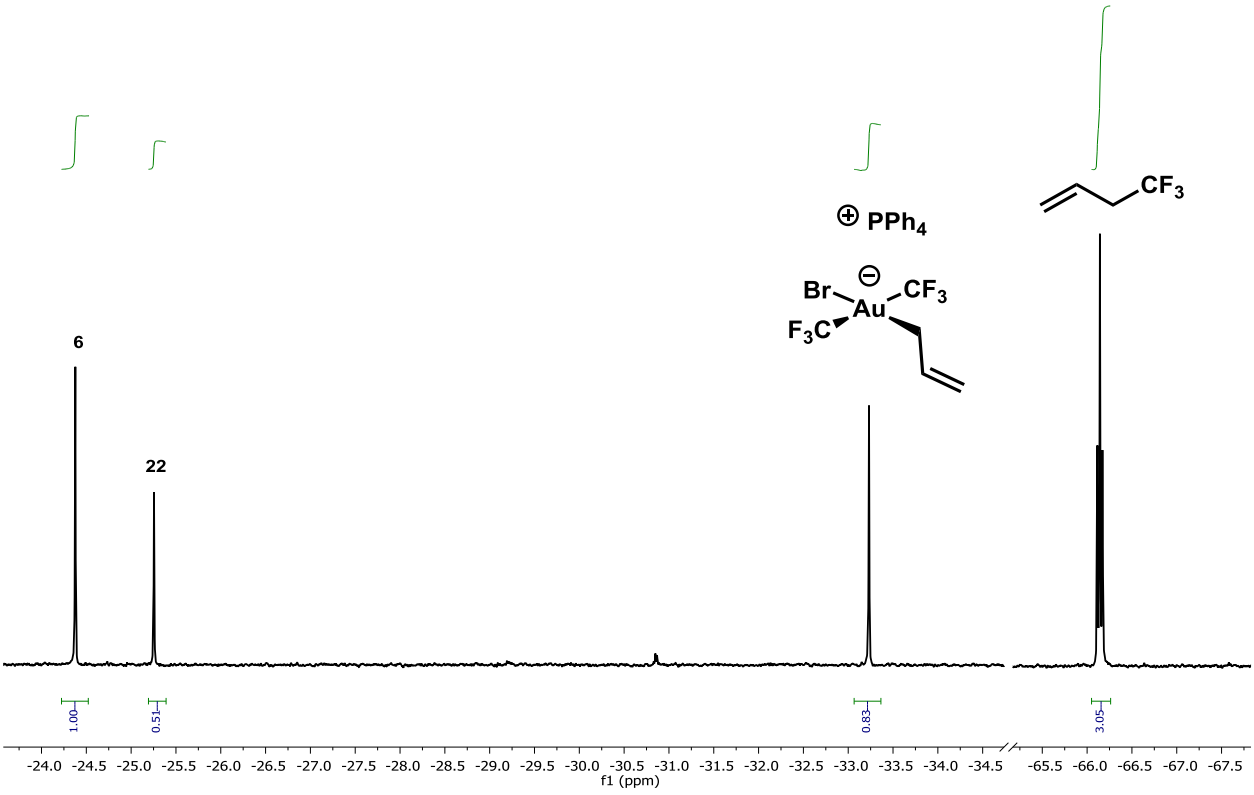


**Figure 4.43**

**Attempted Oxidative Addition of 2-iodopropane**

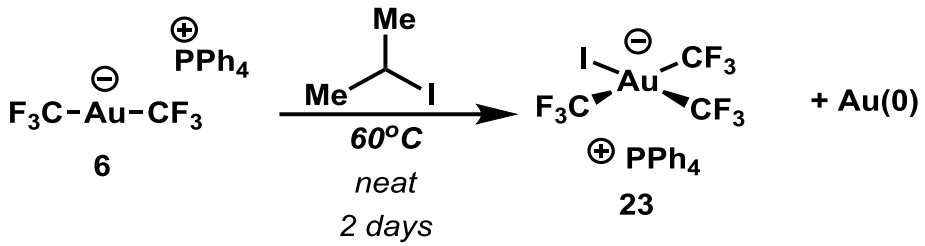


**6** (12 mg, 0.018 mmol) was dissolved in 2-iodopropane (0.6 mL) and the mixture was heated in an NMR tube at 60°C. After 24 hours, the $^{19}$F-NMR spectrum shown below was recorded, showing a small amount of conversion to **23** as noted, with substantial Au(0) plating of the NMR tube observed (spectrum unlocked on deuterated solvent, so absolute shifts are not meaningful). Continued heating did not drive the reaction to completion, with progressively more Au(0) formed.

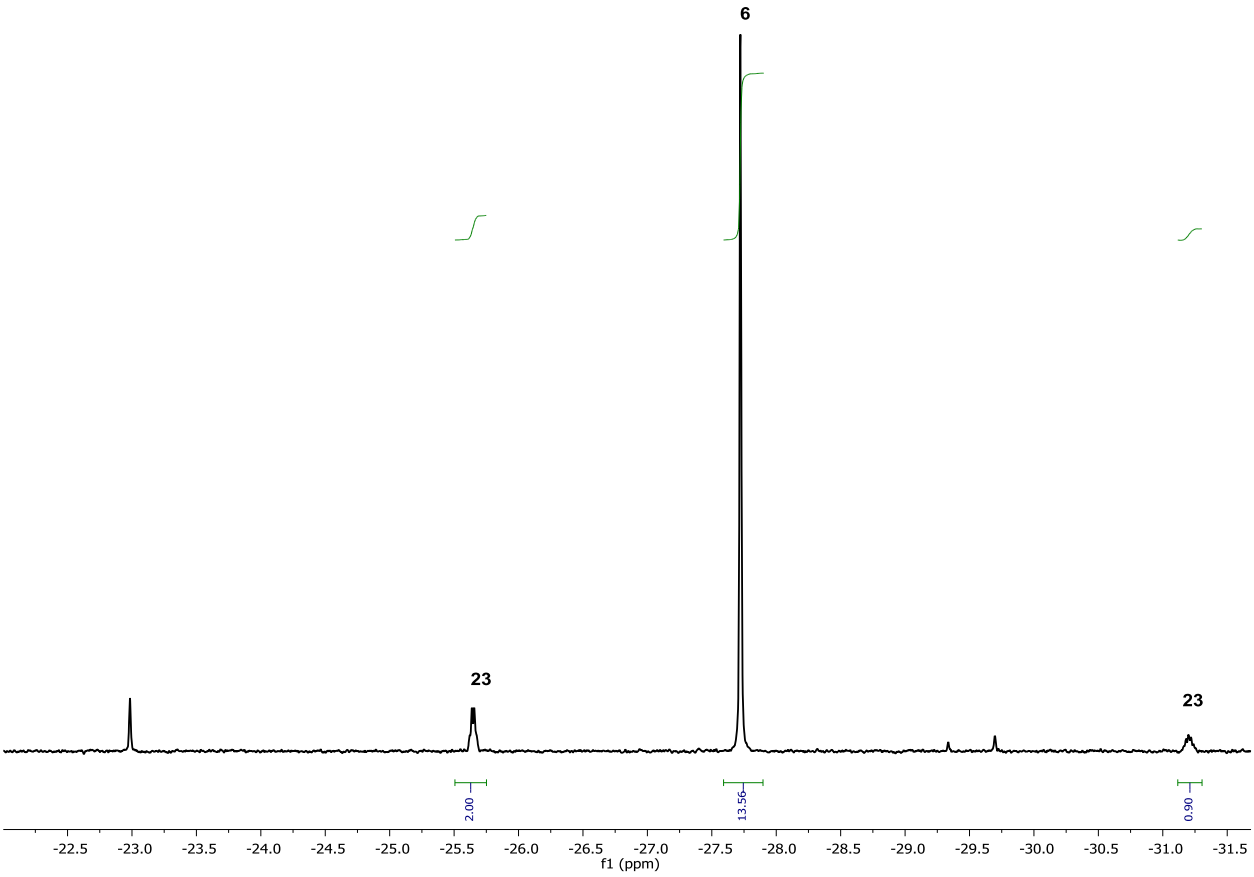


**Figure 4.44**

**Attempted Transmetallation with cyclohex-2-en-1-ylmagnesium chloride**

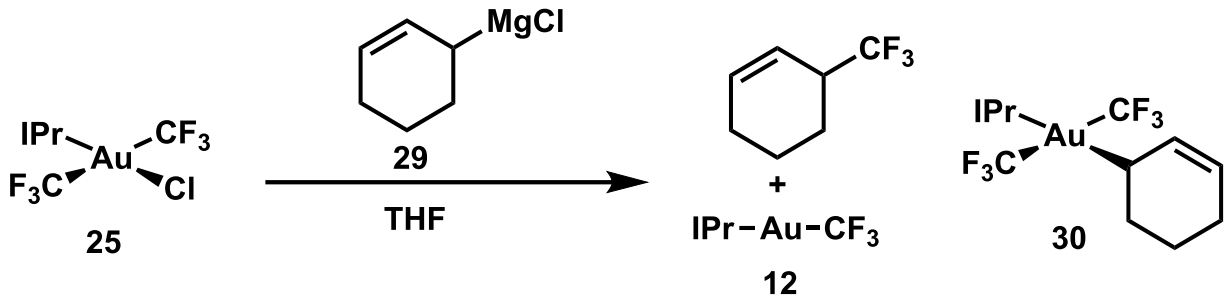


**25** (7.6 mg, 0.01 mmol) was dissolved in THF (0.1 mL) in a nitrogen filled glovebox. Cyclohex-2-en-1-ylmagnesium chloride (prepared from the corresponding allylic chloride and magnesium, filtered in the glovebox and titrated by No-D NMR, 0.6 mL, 0.15M, 10 equiv) was added and the solution was transferred to an NMR tube, capped with a rubber septum and sealed with electrical tape. A $^{19}$F-NMR spectrum was recorded, shown below, after 10 minutes, indicating the presence of **12**, **30**, and the cyclohex-2-en-3-yl-trifluoromethane as shown.

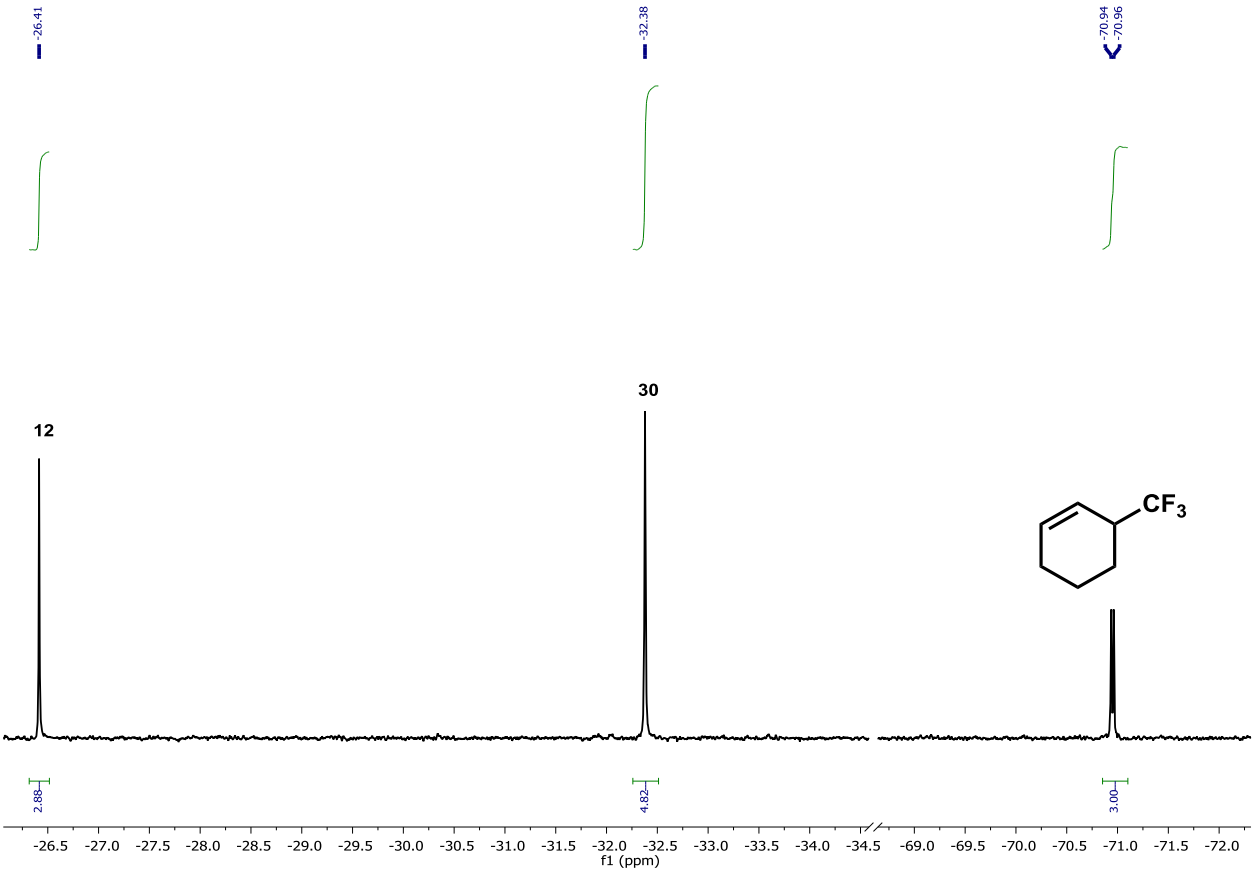


**Figure 4.45**

**Reductive Elimination of Trifluoroethane (Catalytic Borane)**

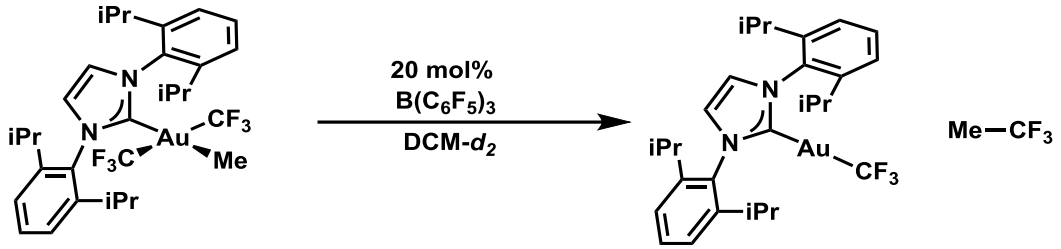


In a nitrogen-filled glovebox, to a solution of **8** (7.4 mg, 0.01 mmol) in DCM-$d_2$ (0.3 mL) in a silylated NMR tube was added a solution of tris(pentafluorophenylborane) in DCM-$d_2$ (1 mg, 0.002 mmol, in 0.3 mL, prepared a stock solution). The mixture was capped with an NMR-tube septum and sealed with electrical tape. Analysis by $^{19}$FNMR after 5 minutes showed the complete consumption of **8**, formation of Me-$CF_3$ as the major product, along with $C_6F_5H$, and IPr-Au-$CF_3$ as the major Au-containing product.

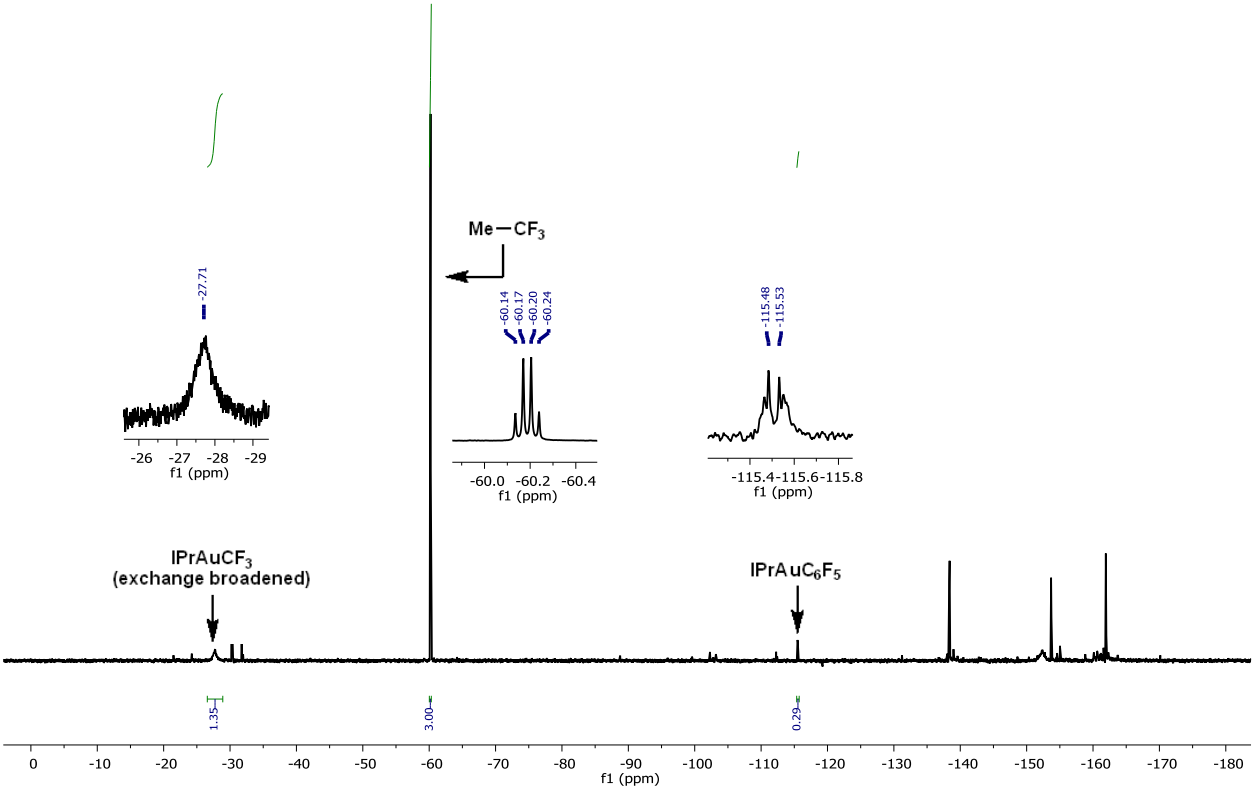


**Figure 4.46**

**Reductive Elimination of Trifluoroethane (Stoichiometric Borane)**

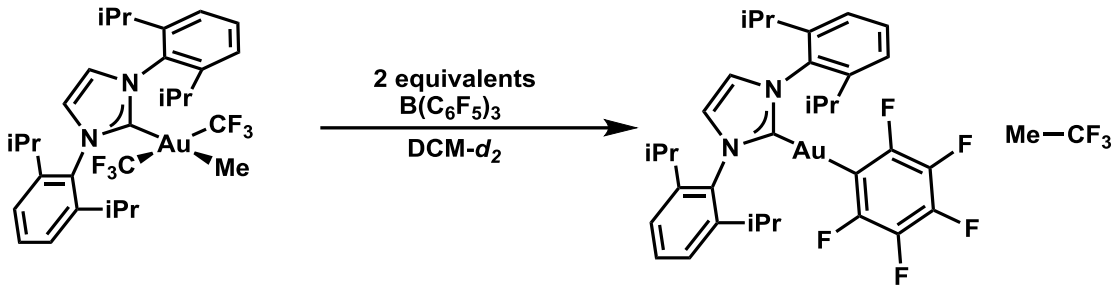


In a nitrogen-filled glovebox, to a solution of **8** (7.4 mg, 0.01 mmol) in DCM-$d_2$ (0.3 mL) in a silylated NMR tube was added a solution of tris(pentafluorophenylborane) in DCM-$d_2$ (10.2 mg, 0.02 mmol, in 0.3 mL). The mixture was capped with an NMR-tube septum and sealed with electrical tape. Analysis by $^{19}$FNMR after 5 minutes showed the complete consumption of **8**, formation of Me-$CF_3$ as the major product, along with $C_6F_5H$, and IPr-Au-$C_6F_5$ as the excluisive Au-containing product.

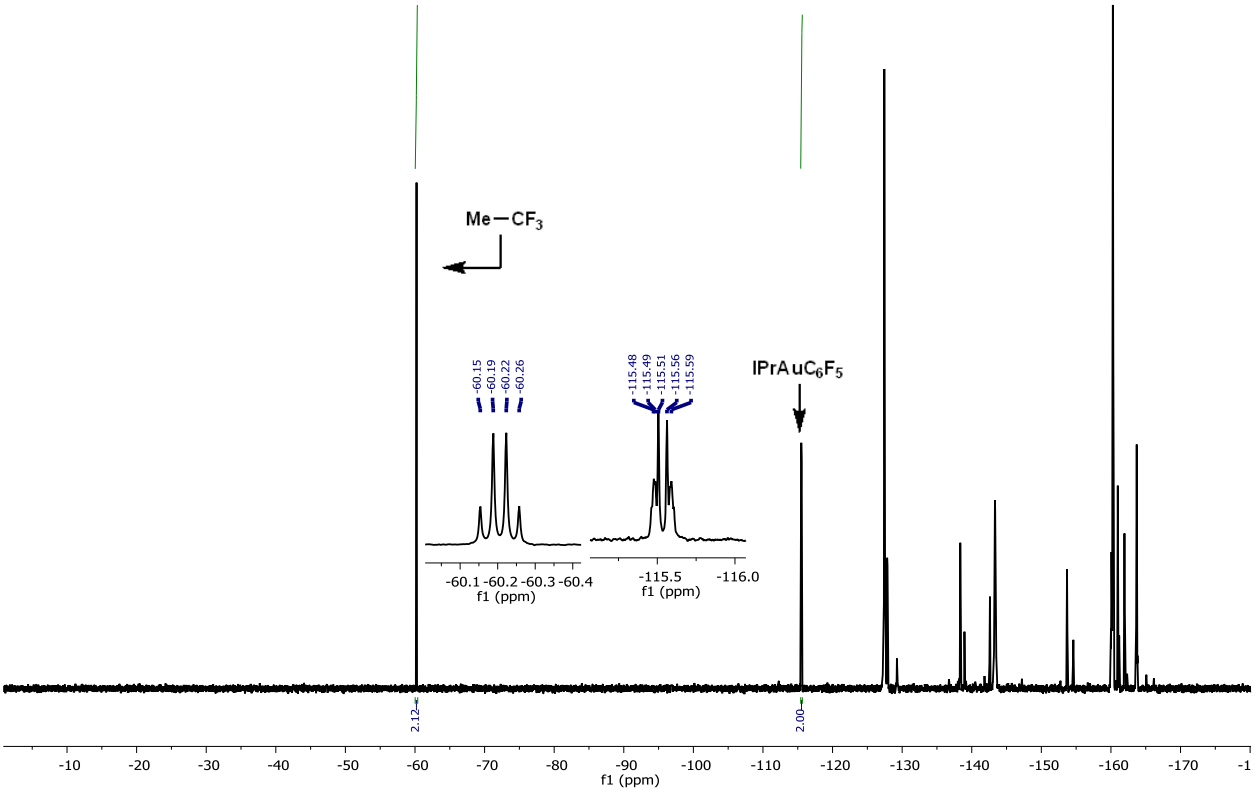


**Figure 4.47**

**Reductive Elimination of Trifluoropropane (Stoichiometric Borane)**

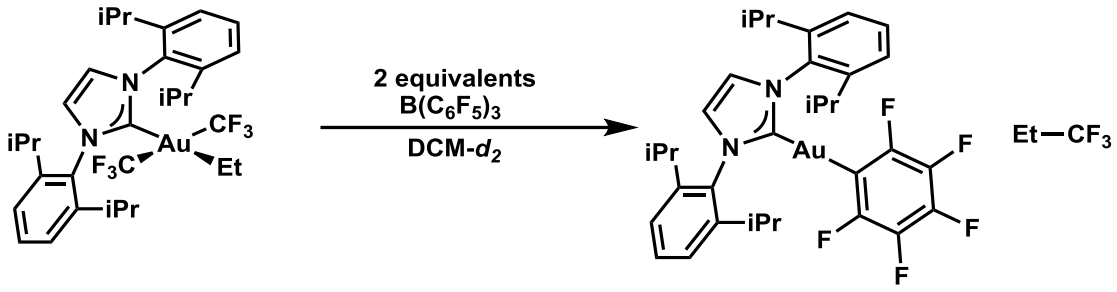


In a nitrogen-filled glovebox, to a solution of **26** (7.3 mg, 0.01 mmol) in DCM-$d_2$ (0.3 mL) in a silylated NMR tube was added a solution of tris(pentafluorophenylborane) in DCM-$d_2$ (10.2 mg, 0.02 mmol, in 0.3 mL). The mixture was capped with an NMR-tube septum and sealed with electrical tape. Analysis by $^{19}$FNMR after 5 minutes showed the complete consumption of **26**, formation of Me-$CF_3$ as the major product, along with $C_6F_5H$, and IPr-Au-$C_6F_5$ as the excluisive Au-containing product.

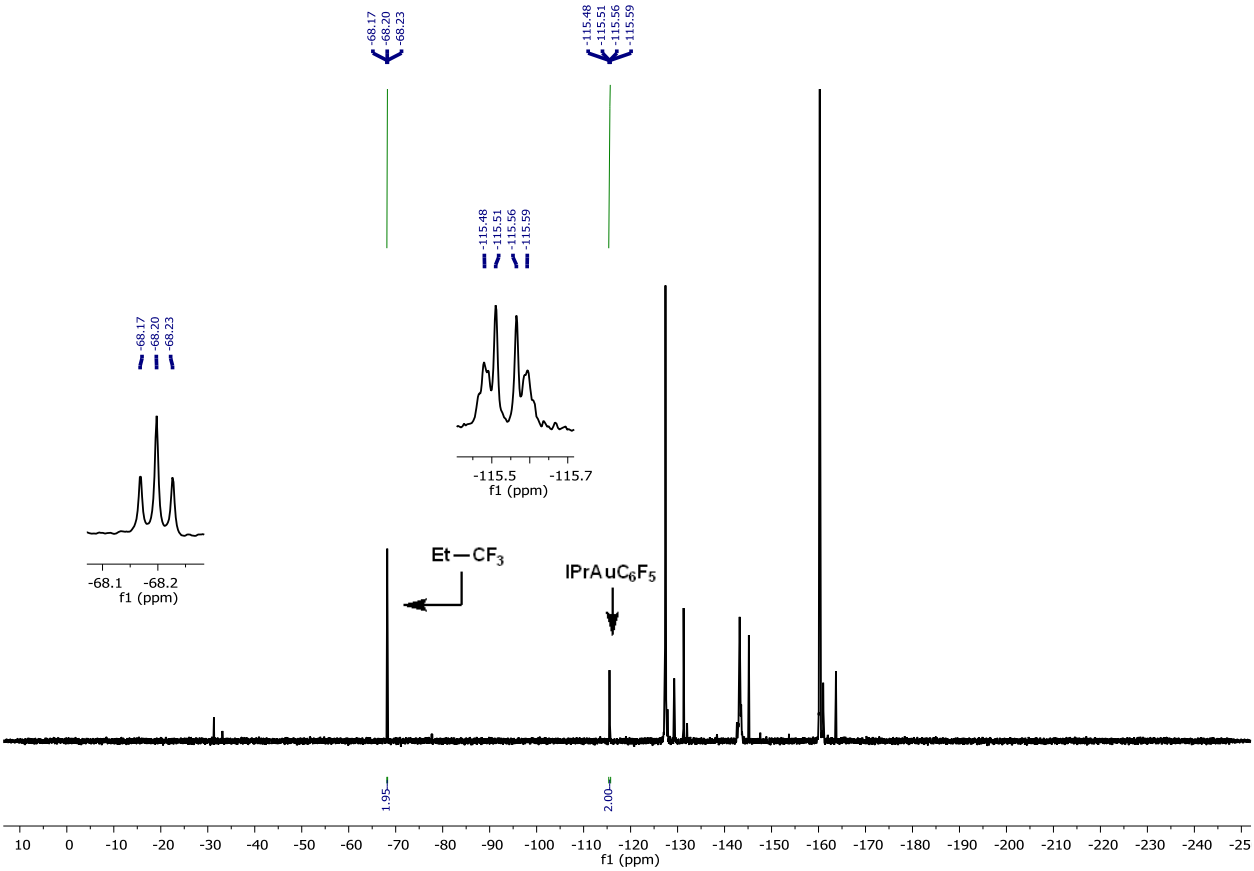


**Figure 4.48**

**Reductive Elimination of Trifluoroethane (Stoichiometric Borane with Alkene Trap)**

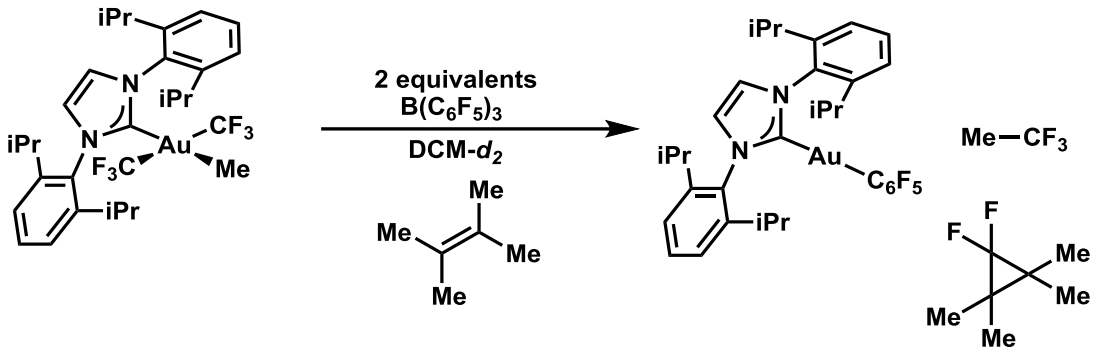


In a nitrogen-filled glovebox, to a solution of **8** (7.4 mg, 0.01 mmol) and tetramethylethylene (1.6 mg, 0.02 mmol, prepared as a stock solution) in DCM-$d_2$ (0.3 mL) in a silylated NMR tube was added a solution of tris(pentafluorophenylborane) in DCM-$d_2$ (10.2 mg, 0.02 mmol, in 0.3 mL). The mixture was capped with an NMR-tube septum and sealed with electrical tape. Analysis by $^{19}$FNMR after 5 minutes showed the complete consumption of **8**, formation of Me-$CF_3$ as the major product, along with $C_6F_5H$, 1,1,2,2-dimethyl-3,3-difluorocyclopropane, and IPr-Au-$C_6F_5$ as the excluisive Au-containing product. GC-MS analysis of the mixture also indicated the presence of the difluorocyclopropane product (m/z = 41, 119, and 134, consistent with literature spectrum).[116]

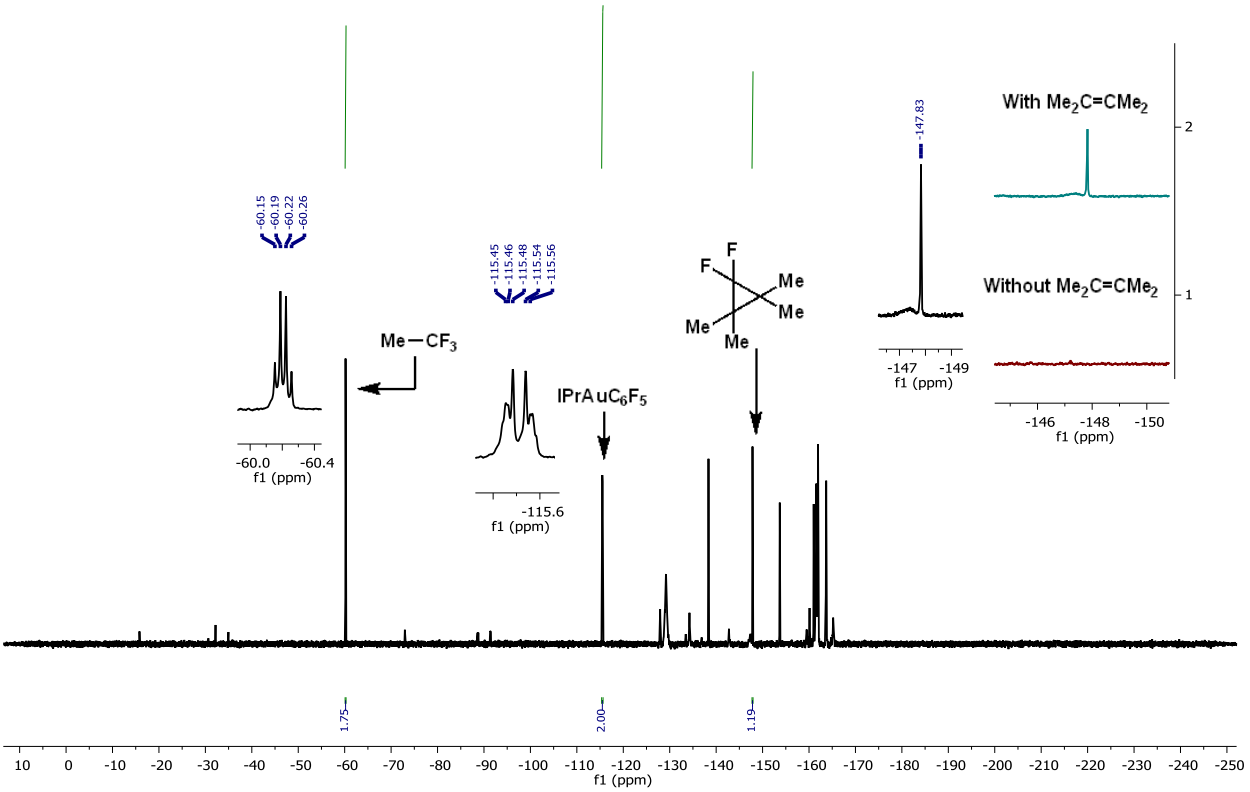


**Figure 4.49**

**Reductive Elimination of Difluoroethyltriflate (Stoichiometric TMSOTf)**

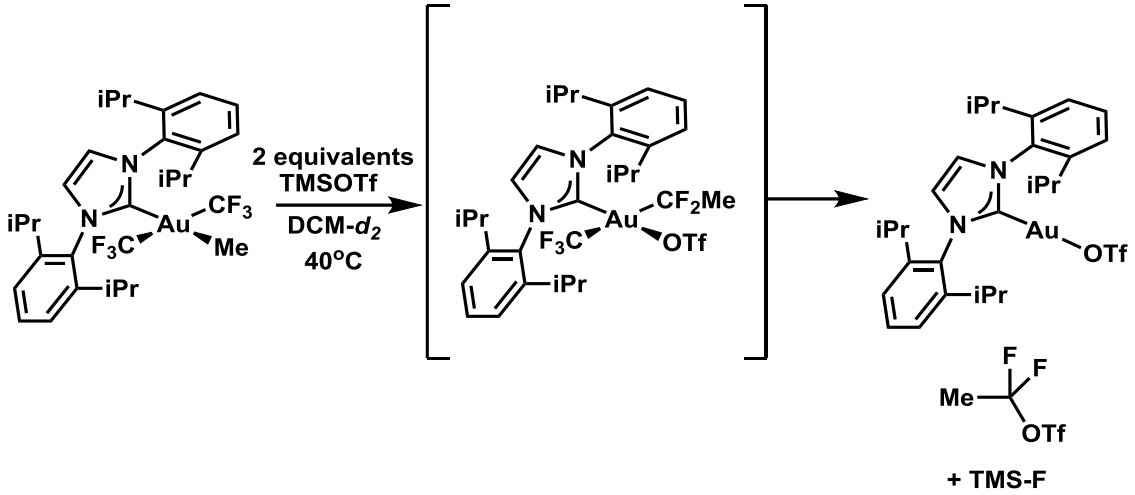


In a nitrogen filled glovebox, **8** (7.4 mg, 0.01 mmol) was dissolved in DCM-$d_2$ (0.3 mL) in a silylated NMR tube and a solution of TMSOTf (4.4 mg, 2 equiv) in DCM-$d_2$ (0.3 mL) was added. The solution was capped with a rubber septum and heated at 40°C. Conversion was monitored by $^{19}$FNMR, indicating the formation of $MeCF_2OTf$ {$^{19}$F NMR (376 MHz, Methylene Chloride-$d_2$) δ -57.59 (qq, $J$ = 14.7, 5.6 Hz, 2F), -74.11 (d, $J$ = 5.6 Hz, 3F)}[31], along with IPrAuOTf and TMSF. An intermediate was also detected and assigned as the difluoroethyl Au(III) triflate shown above by analogy to **17** {$^{19}$F NMR (376 MHz, Methylene Chloride-$d_2$) δ -34.51 (t, $J$ = 11.9 Hz, 3F), -61.14 – -61.50 (m, 2F), -71.04 (s, 3F)}.[51] The NMR spectrum shown in Figure 4.15 above was acquired after 4 hours of heating. For ease of interpretation, the X-axis has been segmented to show relevant peaks.

**Reductive Elimination of Difluoroethane (Stoichiometric Borane with Triethylsilane)**

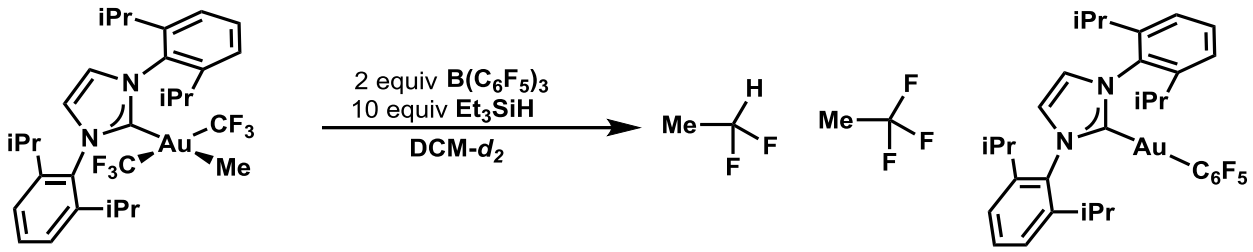


In a nitrogen-filled glovebox, to a solution of **8** (7.4 mg, 0.01 mmol) and triethylsilane (12 mg, 0.1 mmol, prepared as a stock solution) in DCM-$d_2$ (0.3 mL) in a silylated NMR tube was added a solution of tris(pentafluorophenylborane) in DCM-$d_2$ (10.2 mg, 0.02 mmol, in 0.3 mL). The mixture was capped with an NMR-tube septum and sealed with electrical tape. Analysis by $^{19}$FNMR after 5 minutes showed the complete consumption of **8**, formation of Me-$CF_3$ and $MeCF_2H$ as the major products, along with IPr-Au-$C_6F_5$ as the excluisive Au-containing product.

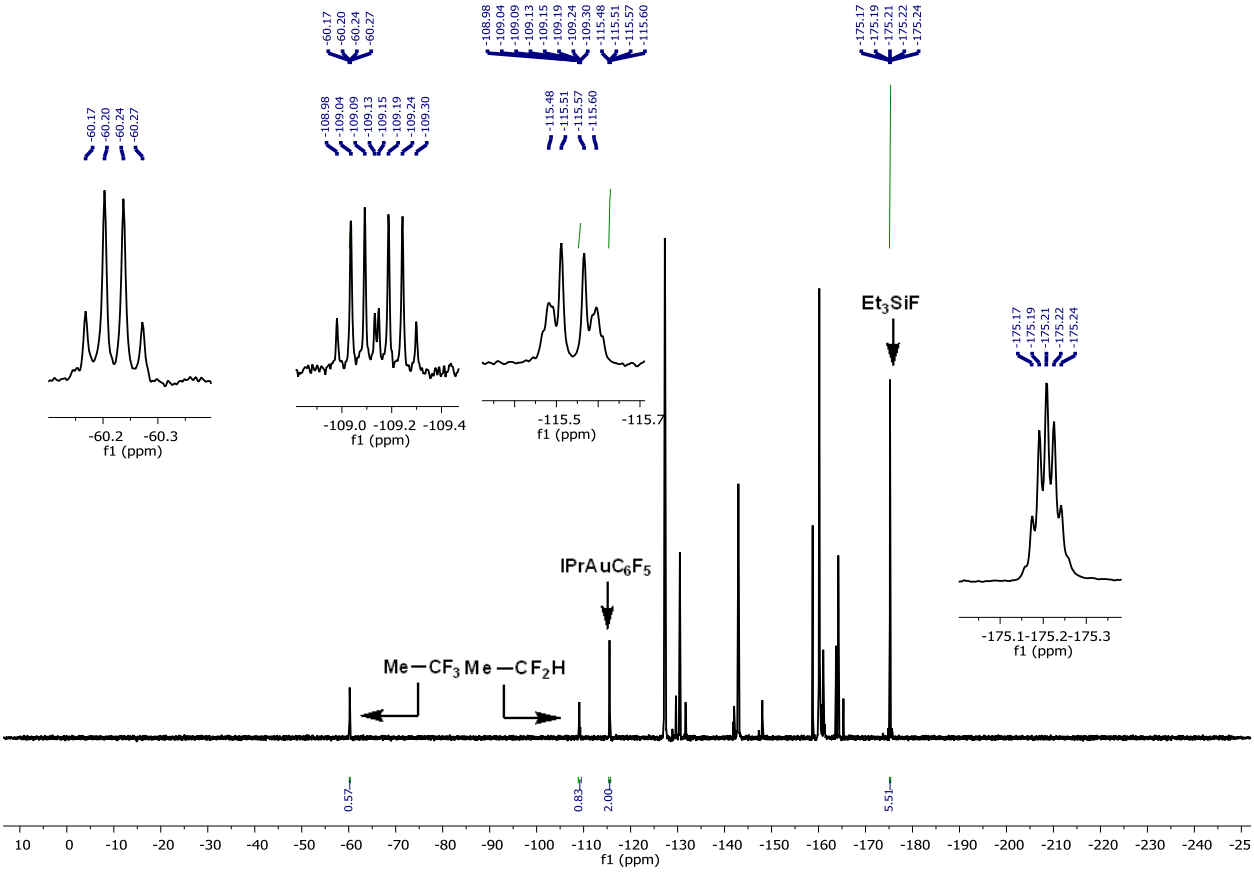


**Figure 4.50**

**Reductive Elimination of Trifluoroethane (Silver Mediated from 17)**

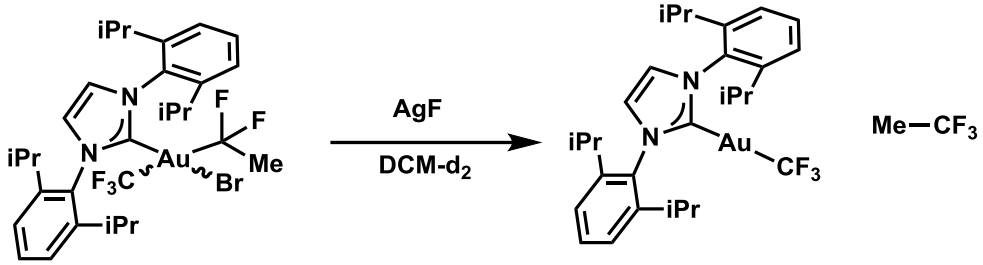


**17** (39 mg, 0.05 mmol, mixture of isomers) was dissolved in DCM-$d_2$ (1 mL), and silver fluoride was added (64 mg, 10 equiv). The mixture was sonicated briefly and stirred vigorously for 12 hours in the dark. The mixture was filtered directly into an NMR tube, and an additional 64 mg (10 equiv) of AgF was added. The tube was sealed with a rubber septum and sonicated for an additional 20 minutes. The mixture was allowed to stand with occasional agitation for an additional 24 hours, with NMR spectra recorded periodically. These indicated the formation of two isomers of an intermediate Au(III)-fluoride which is observable, as well as another unidentified Au(III) product. The majority of the material is observed to convert to $IPrAuCF_3$ and $MeCF_3$, with a small amount of 1,1-difluoroethylene formed as a byproduct. The spectrum below was recorded after a total of 18 hours of reaction. After 36 hours, the starting complex was consumed, with 32% conversion to $IPrAuCF_3$ observed, the remainder of the mass balance taken up by the Au(III)-F and unidentified Au(III) species. For ease of interpretation, the X-axis has been segmented to show relevant peaks.

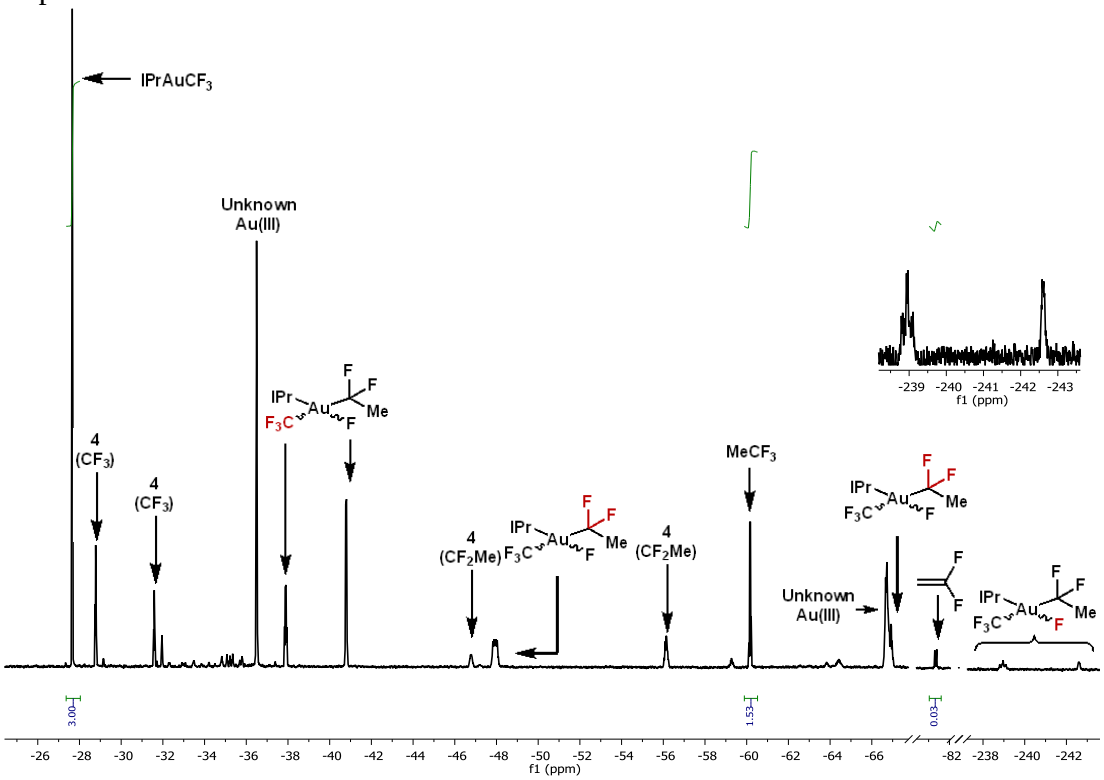


**Figure 4.51**

**Reductive Elimination of 1,1-difluoroethyltosylate (Silver Mediated from 17)**

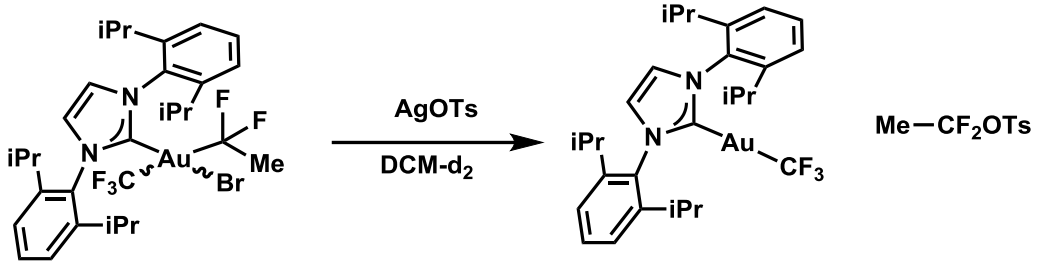


**17** (6 mg, 0.0075 mmol, mixture of isomers) was dissolved in DCM-$d_2$ (0.6 mL), and silver tosylate was added (4.2 mg, 2 equiv). The mixture was sonicated briefly and then filtered directly into an NMR tube, capped with a rubber septum, and a $^{19}$F-NMR spectrum was recorded after 5 minutes, shown below, indicating formation of $MeCF_2OTs$ and $IPrAuCF_3$ (**12**), with substantial amounts of **17** remaining.

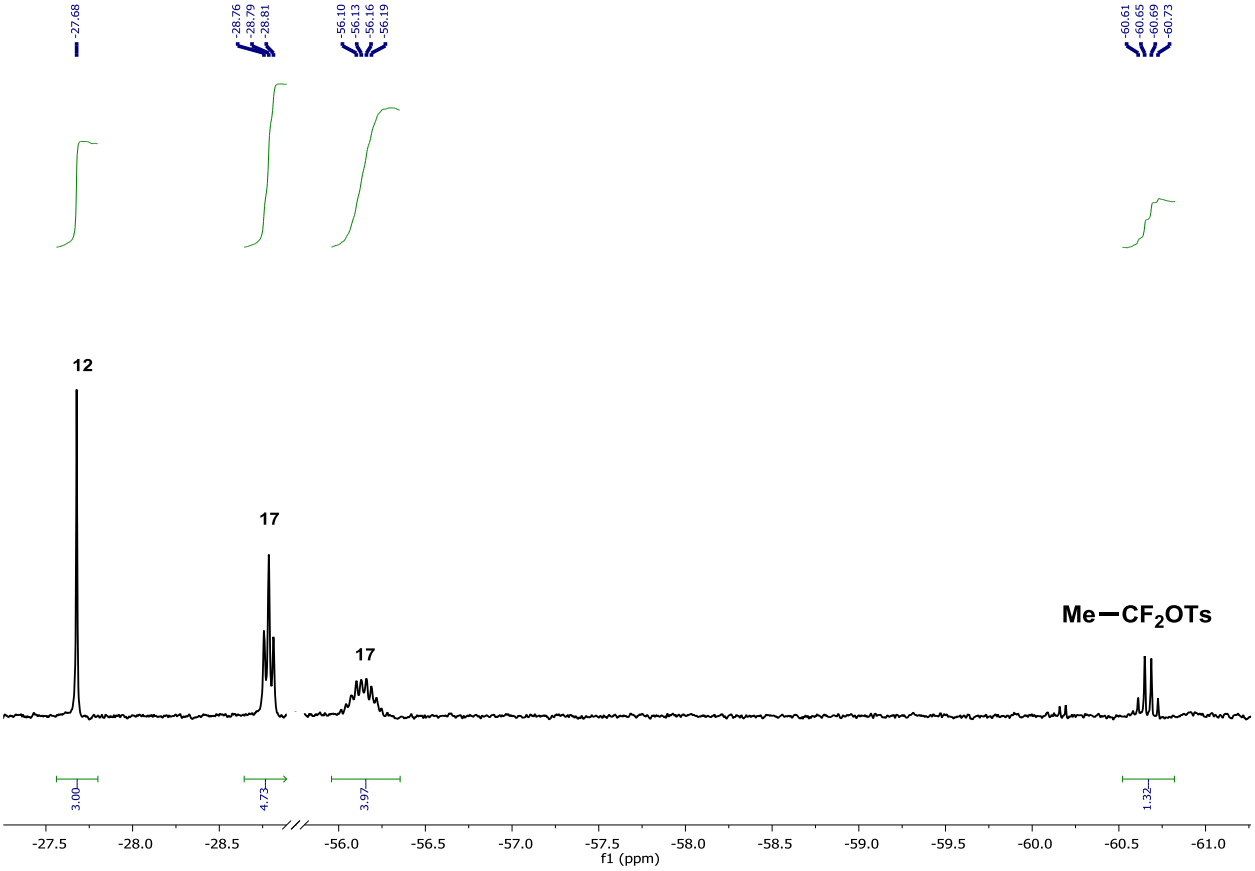


**Figure 4.52**

**Elimination of 17 with KOtBu**

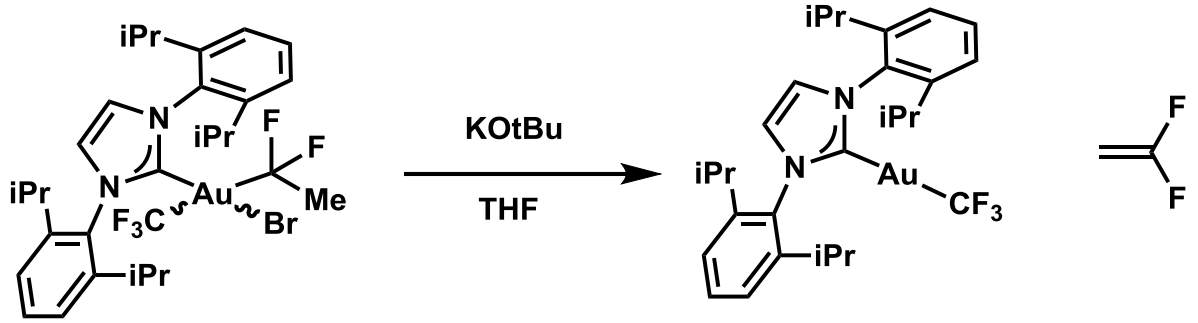


In a nitrogen filled glovebox, **17** (4 mg, 0.005 mmol) was dissolved in THF (0.3 mL) and a solution of KOtBu (0.8 mg, 1.5 equiv) in 0.3 mL of THF. The mixture was transferred to an NMR tube and after 5 minutes a $^{19}$F-NMR spectrum was recorded, showing complete consumption of **17**, and the presence of IPrAuCF$_3$ (**12**) and 1,1-difluoroethylene, as shown.

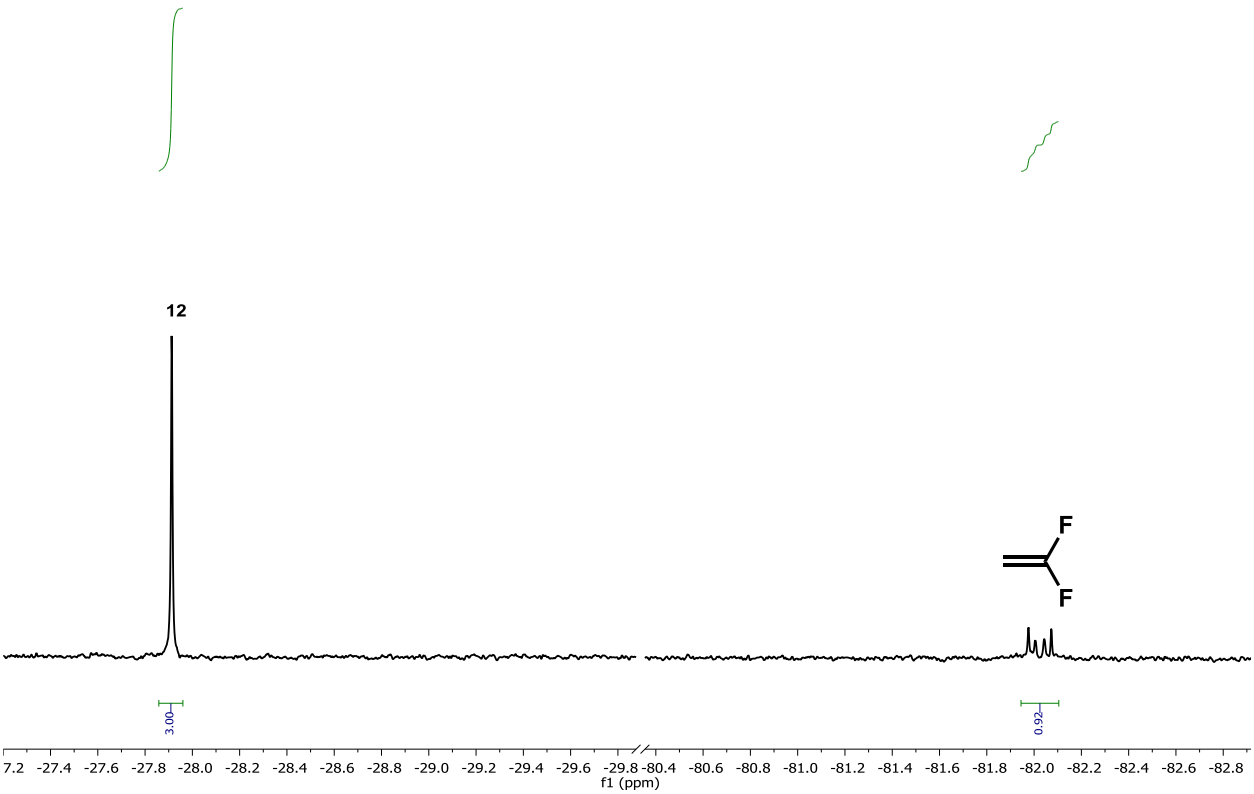


**Figure 4.53**

**Reductive Elimination of Trifluoromethane from 53 with py(HF)**

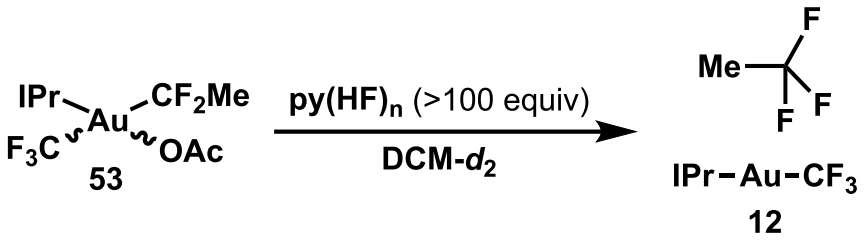


**53** (8 mg, 0.01 mmol) was dissolved in DCM-$d_2$, and 1 drop of neat pyridine(HF) was added and the solution was transferred to an NMR tube. A $^{19}$F-NMR spectrum was recorded, showing complete conversion of **52** to equimolar **12** and $MeCF_3$, as well as substantial glass etching ($BF_4$) and remaining py(HF)$_n$.

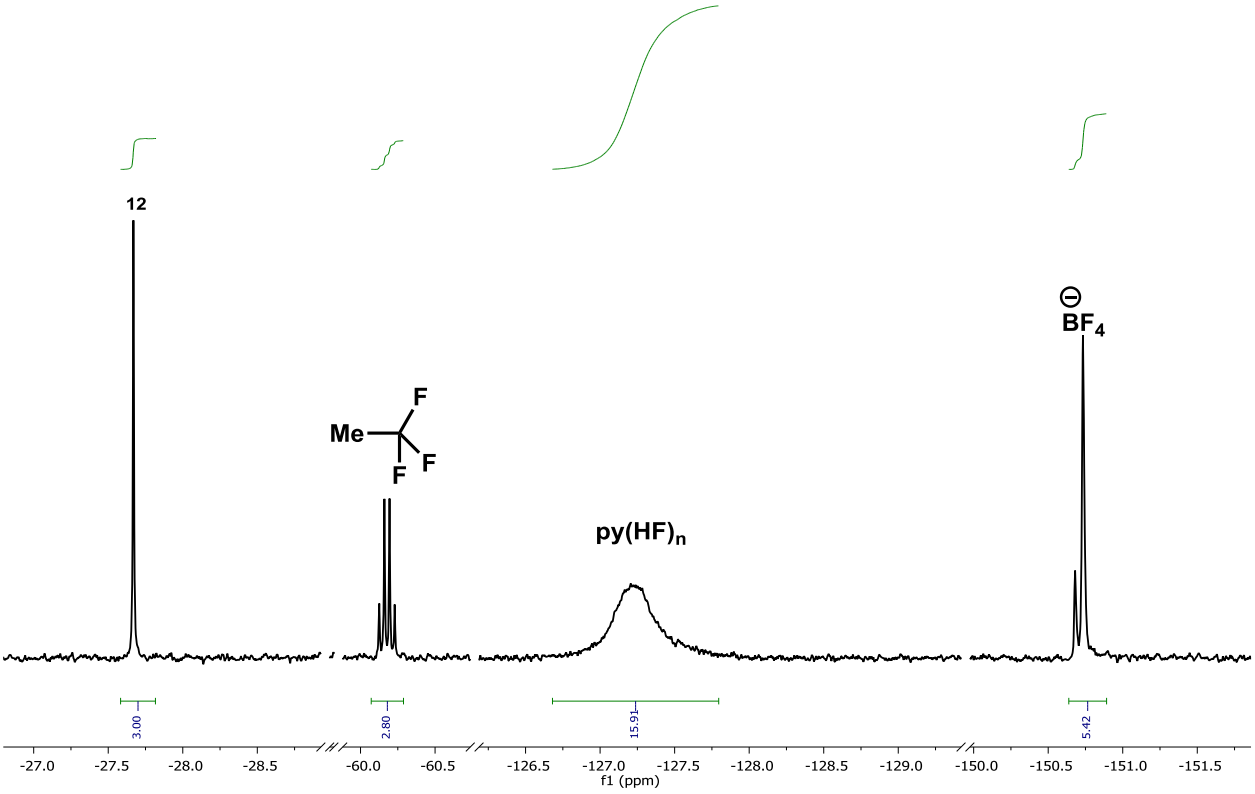


**Figure 4.54**

**Reductive Elimination of Trifluoroethane ($PCy_3$; Catalytic Borane)**

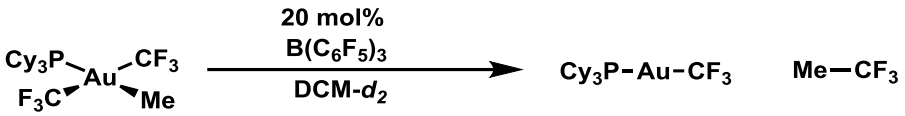


In a nitrogen-filled glovebox, to a solution of **18** (6.1 mg, 0.01 mmol) in DCM-$d_2$ (0.3 mL) in a silylated NMR tube was added a solution of tris(pentafluorophenylborane) in DCM-$d_2$ (1 mg, 0.002 mmol, in 0.3 mL, prepared a stock solution). The mixture was capped with an NMR-tube septum and sealed with electrical tape. Analysis by $^{19}$FNMR after 5 minutes showed the complete consumption of **1**, formation of Me-$CF_3$ as the major product, along with $Cy_3$P-Au-$CF_3$ as the major Au-containing product.

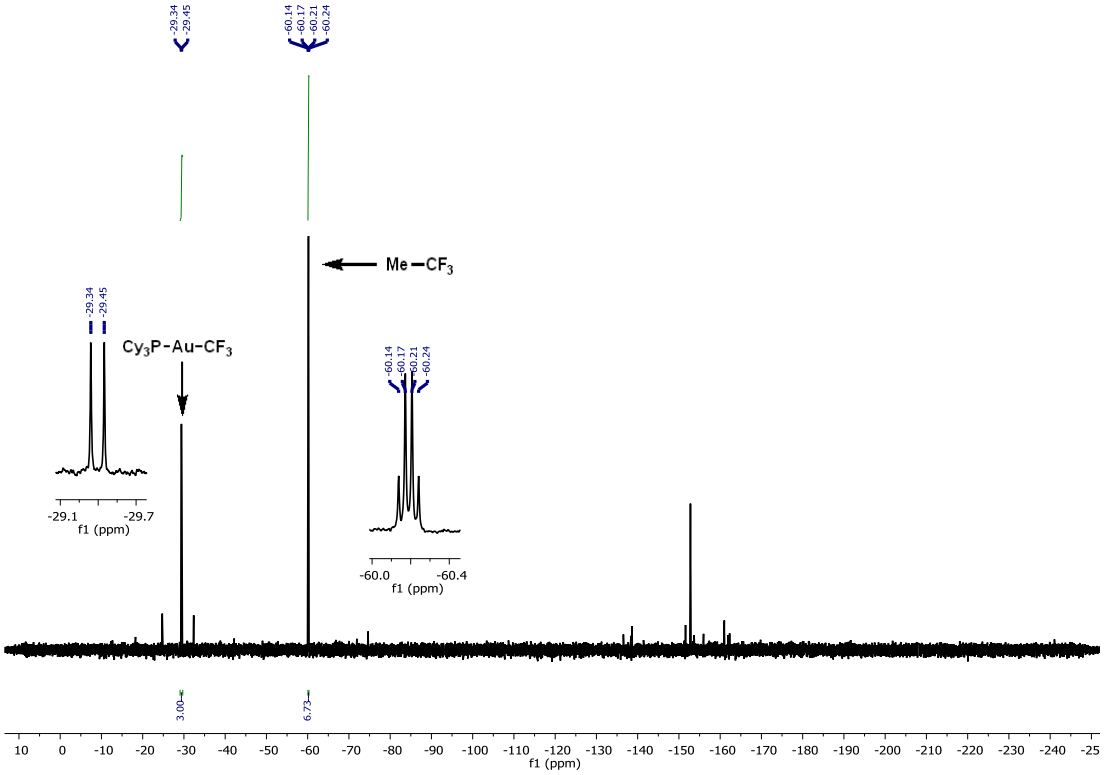


**Figure 4.55**

**Reductive Elimination of Trifluoroethane ($PCy_3$; Stoichiometric Borane)**

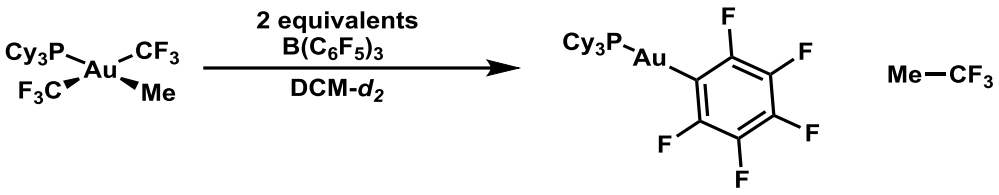


In a nitrogen-filled glovebox, to a solution of **18** (6.1 mg, 0.01 mmol) in DCM-$d_2$ (0.3 mL) in a silylated NMR tube was added a solution of tris(pentafluorophenylborane) in DCM-$d_2$ (10.2 mg, 0.02 mmol, in 0.3 mL). The mixture was capped with an NMR-tube septum and sealed with electrical tape. Analysis by $^{19}$FNMR after 5 minutes showed the complete consumption of **1**, formation of Me-$CF_3$ as the major product, along with $C_6F_5H$, and $Cy_3P$-Au-$C_6F_5$ as the excluisive Au-containing product.

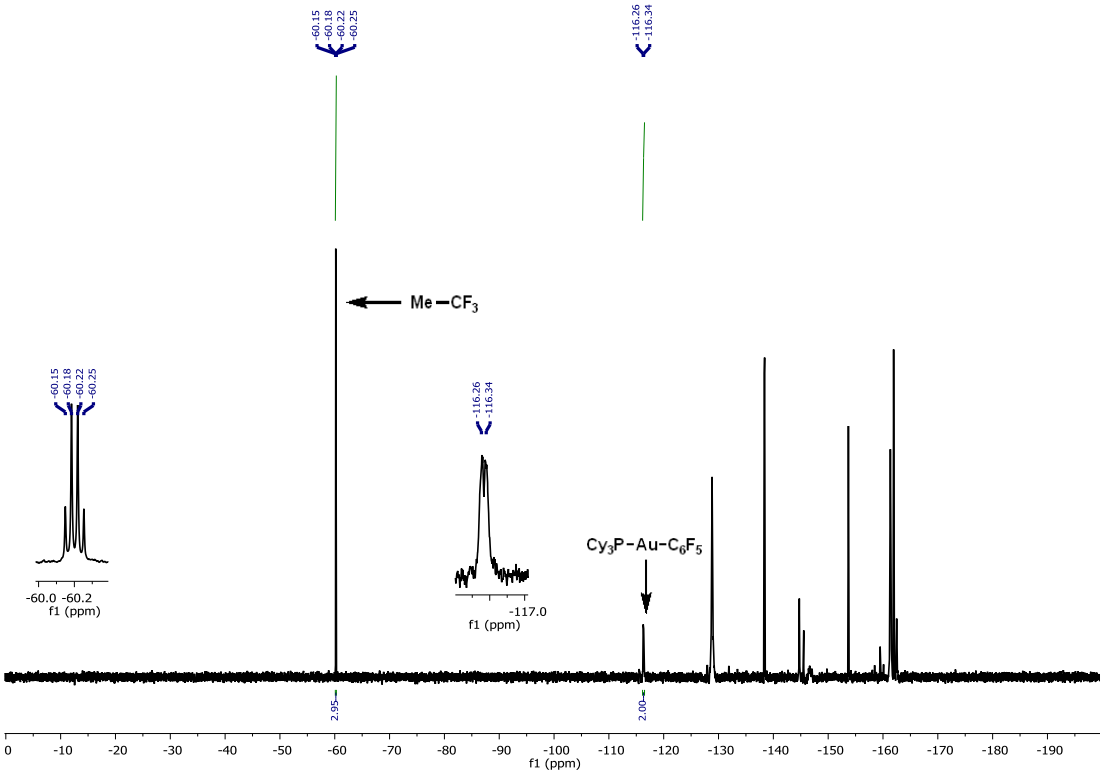


**Figure 4.56**

**Reductive Elimination of Trifluorotoluene (Stoichiometric Borane)**

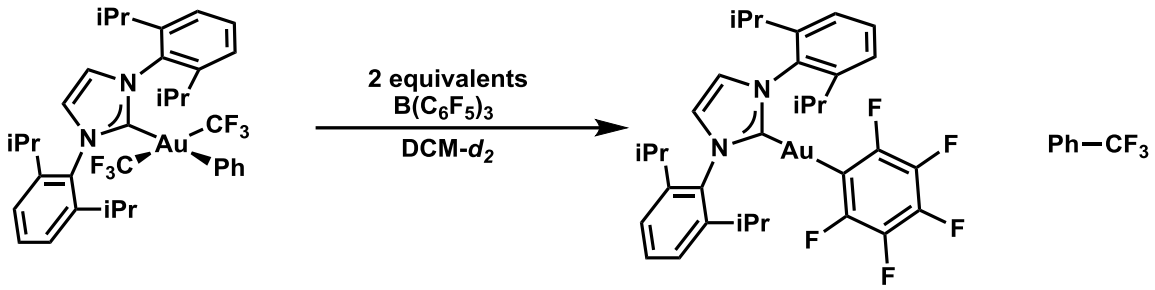


In a nitrogen-filled glovebox, to a solution of **27** (8 mg, 0.01 mmol) in DCM-$d_2$ (0.3 mL) in a silylated NMR tube was added a solution of tris(pentafluorophenylborane) in DCM-$d_2$ (10.2 mg, 0.02 mmol, in 0.3 mL). The mixture was capped with an NMR-tube septum and sealed with electrical tape. Analysis by $^{19}$FNMR after 5 minutes showed the almost complete consumption of **27**, formation of Ph-$CF_3$ as the major product, along with $C_6F_5H$, and IPr-Au-$C_6F_5$ as the major Au-containing product.

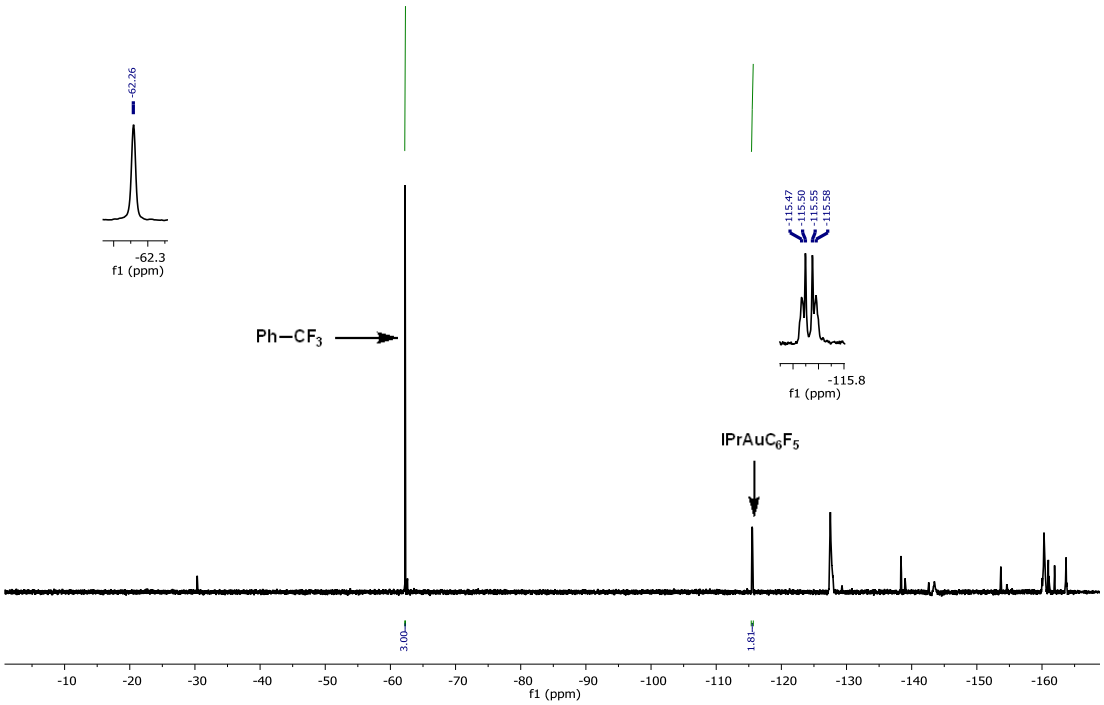


**Figure 4.57**

**Reductive Elimination of Bromodifluorotoluene (Catalytic Borane)**

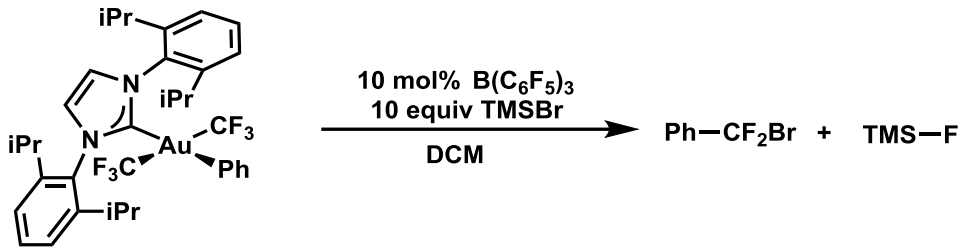


In a nitrogen-filled glovebox, to a solution of **27** (8 mg, 0.01 mmol) in DCM (0.3 mL) in a silylated NMR tube was added TMS-Br (0.01 mL, 10 equiv) followed by a solution of tris(pentafluorophenylborane) in DCM (0.5 mg, 0.001 mmol, in 0.3 mL). The mixture was capped with an NMR-tube septum and sealed with electrical tape. Analysis by $^{19}$FNMR after 1 hour showed ~15% conversion to afford a mixture of $PhCF_2Br$ and TMS-F. Peaks for **2** are too small to be seen at this scale.

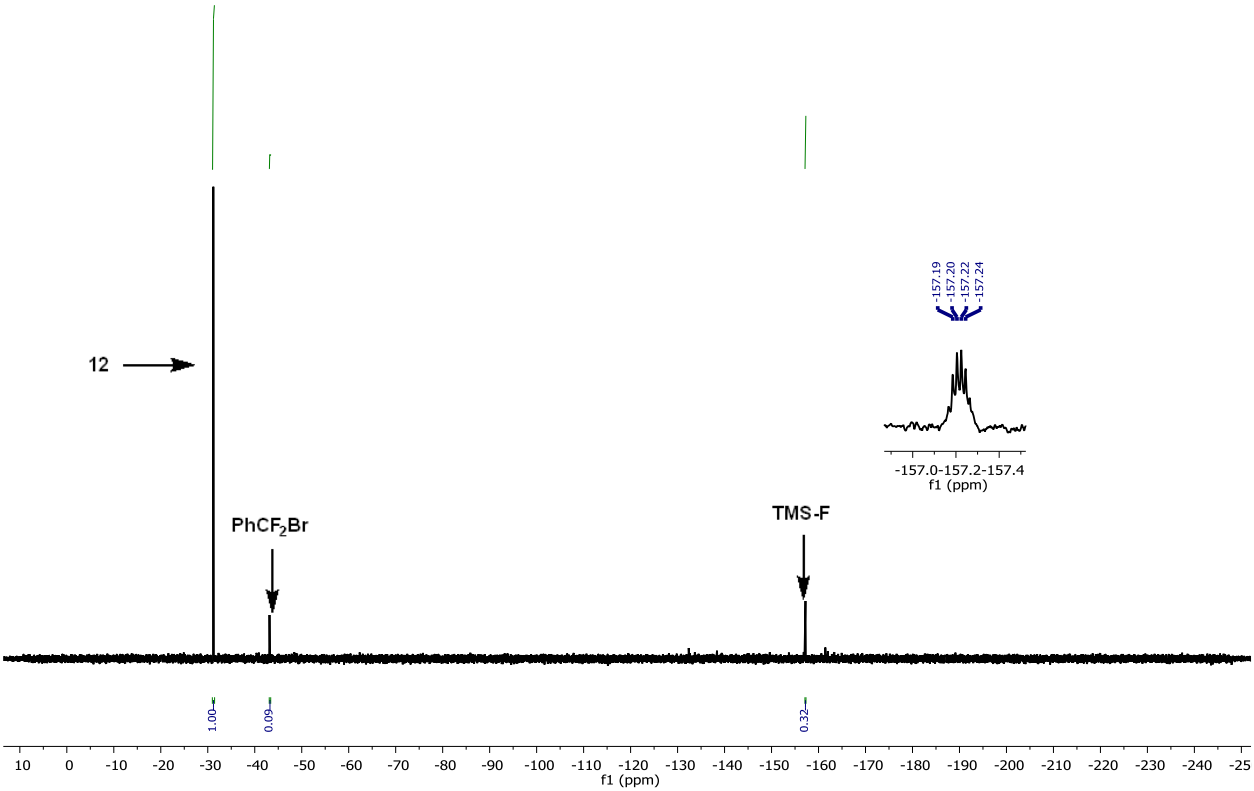


**Figure 4.58**

**Reductive Elimination of Difluorotoluene (Stoichiometric Borane with Triethylsilane)**

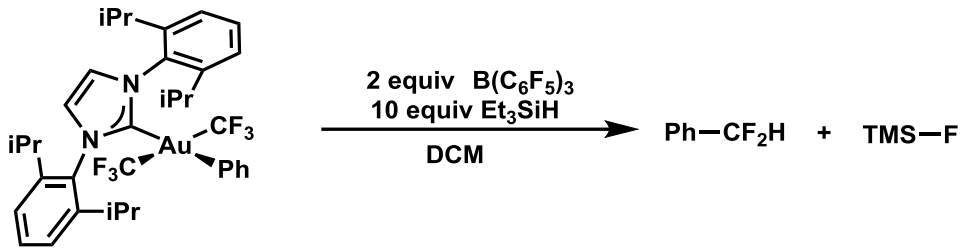


In a nitrogen filled glovebox, **27** (8 mg, 0.01 mmol) was dissolved in 0.3 mL of DCM-$d_2$ and 12 mg of $Et_3SiH$ was added, followed by a solution of $B(C_6F_5)_3$ in DCM-$d_2$ (10 mg, 2 equiv, in 0.3 mL). The mixture was transferred into an NMR tube and capped with a rubber septum. A $^{19}F$-NMR spectrum recorded after 5 minutes indicated partial conversion to afford $PhCF_2H$ and $IPrAuC_6F_5$ (**10**), shown below. Monitoring over the course of 2 hours showed eventual consumption of **27** and conversion of $PhCF_2H$ to toluene.

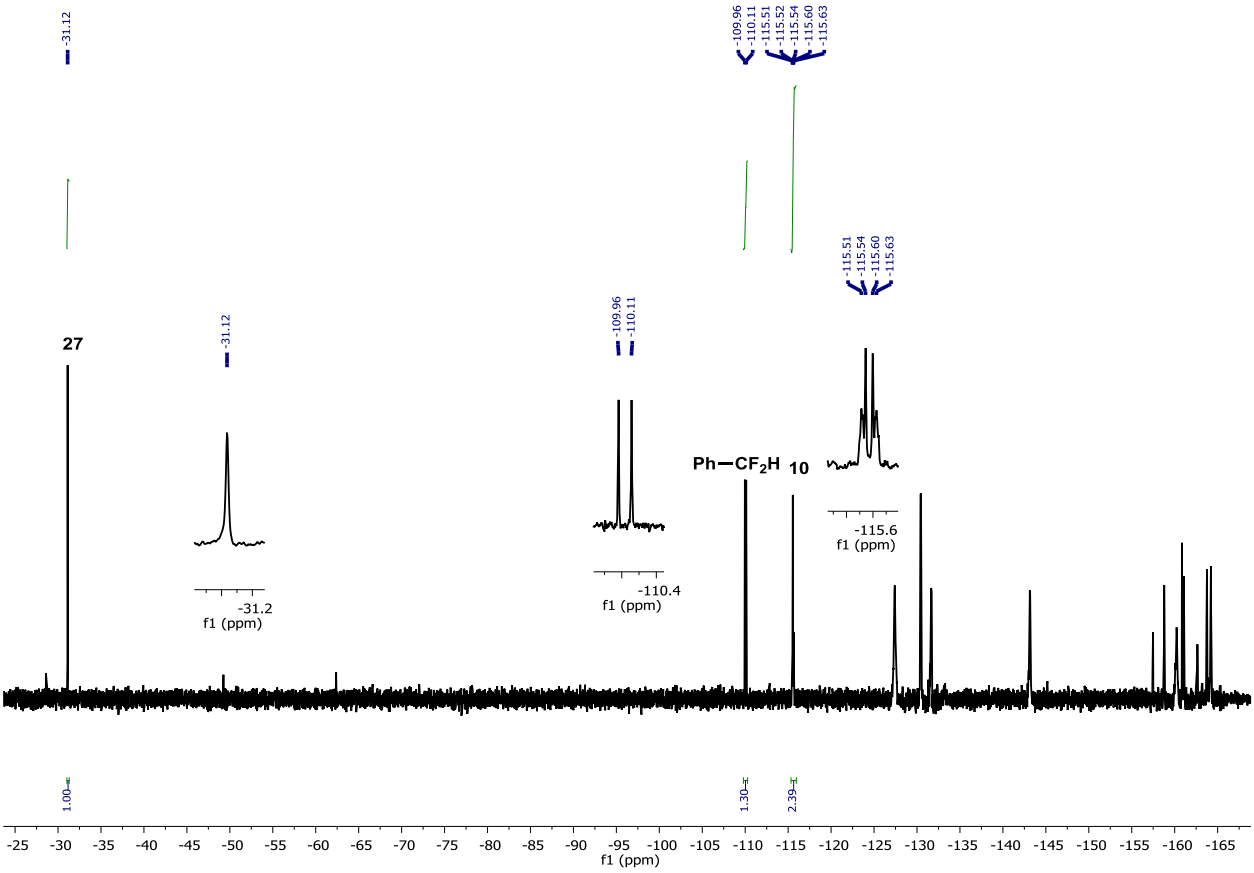


**Figure 4.59**

**Low Temperature NMR Reaction Monitoring**

*General procedure for kinetics*

In a nitrogen filled glovebox, a solution of **1** (7.40 mg, 0.01 mmol in 400 μL DCM-$d_2$, prepared as a stock solution) was combined with 1-trifluoromethyl napthalene (internal standard, 1.96 mg, 0.01 mmol in 100 μL DCM-$d_2$, prepared as a stock solution) in a silylated NMR tube and fitted with a septum cap and sealed with electrical tape. In a separate septum-capped 2 dram vial was prepared a solution of $B(C_6F_5)_3$ in DCM-$d_2$ (102 mg in 1000 μL).

The two solutions were brought out of the glovebox and connected to $N_2$ atmosphere on a Schlenk line. The NMR tube solution was cooled to -78ºC, and a portion of the $B(C_6F_5)_3$ solution (100 μL, 0.02 mmol) was added dropwise via syringe.

The mixture was agitated briefly, and then injected into a pre-cooled, tuned, and shimmed NMR probe at -15 ºC. $^{19}$F-NMR scans were collected at 60 second intervals, utilizing one scan per time point.

**Radiochemistry Cold Run**

To a solution of 0.05M aqueous hydrofluoric acid (0.1 mL, 0.005 mmol) was added potassium carbonate (1.4 mg, 2 equiv) and Kryptofix [2.2.2] (3.8 mg, 2 equiv), and acetonitrile (0.4 mL). The mixture was concentrated at 30ºC, and the process was repeated 2x with 0.4 mL of additional acetonitrile.

The resulting residue was extracted 2x with 0.1 mL of dichloromethane, and placed into a septum capped vial. After purging the headspace with nitrogen, a solution of **2** (12.7 mg, 5 equiv) in 0.3 mL of dichloromethane was added, followed by the corresponding [Au]-OAc complex (0.006 mmol) in 0.3 mL of DCM. The entire mixture was then transferred into a septum capped NMR tube.

The $^{19}$FNMR spectra for each substrate is shown below. Note that the spectra are not locked to deuterated solvent. Due to the longer reaction time for **23**, $IPrAuC_6F_5$ is formed from $IPrAuCF_3$. Additionally, difluoroalkene resulting from elimination is seen in the reaction from **23**.

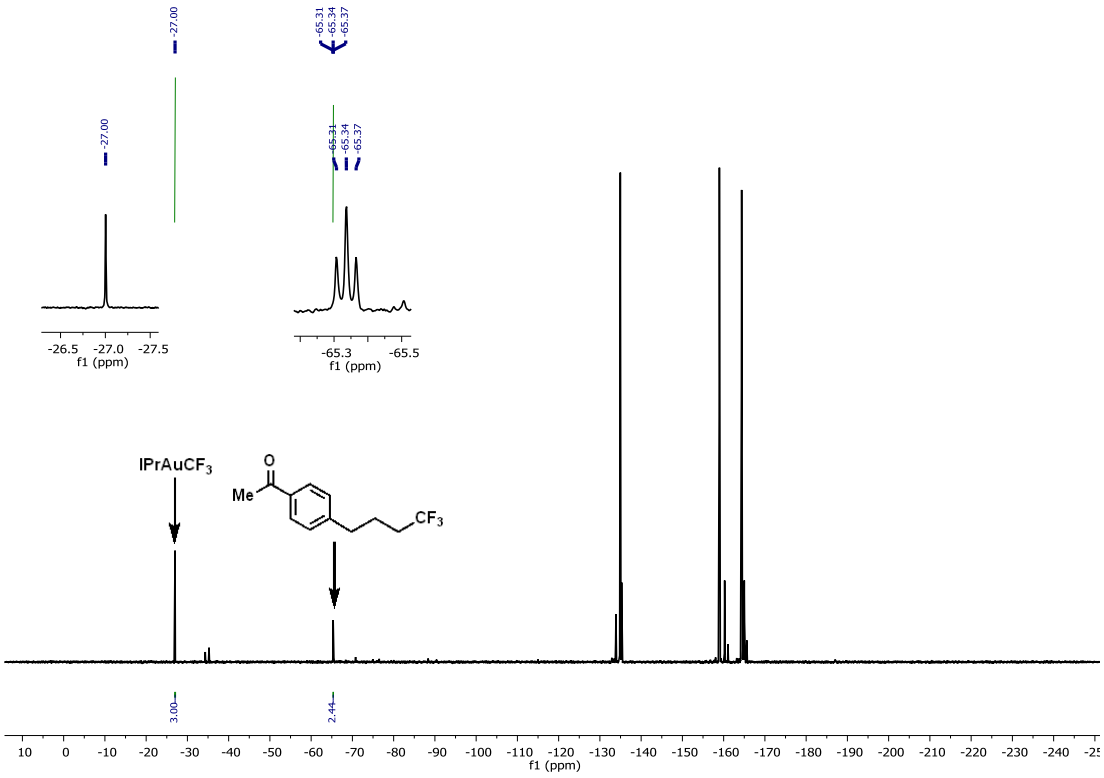


**Figure 4.60**. After 10 minutes of reaction

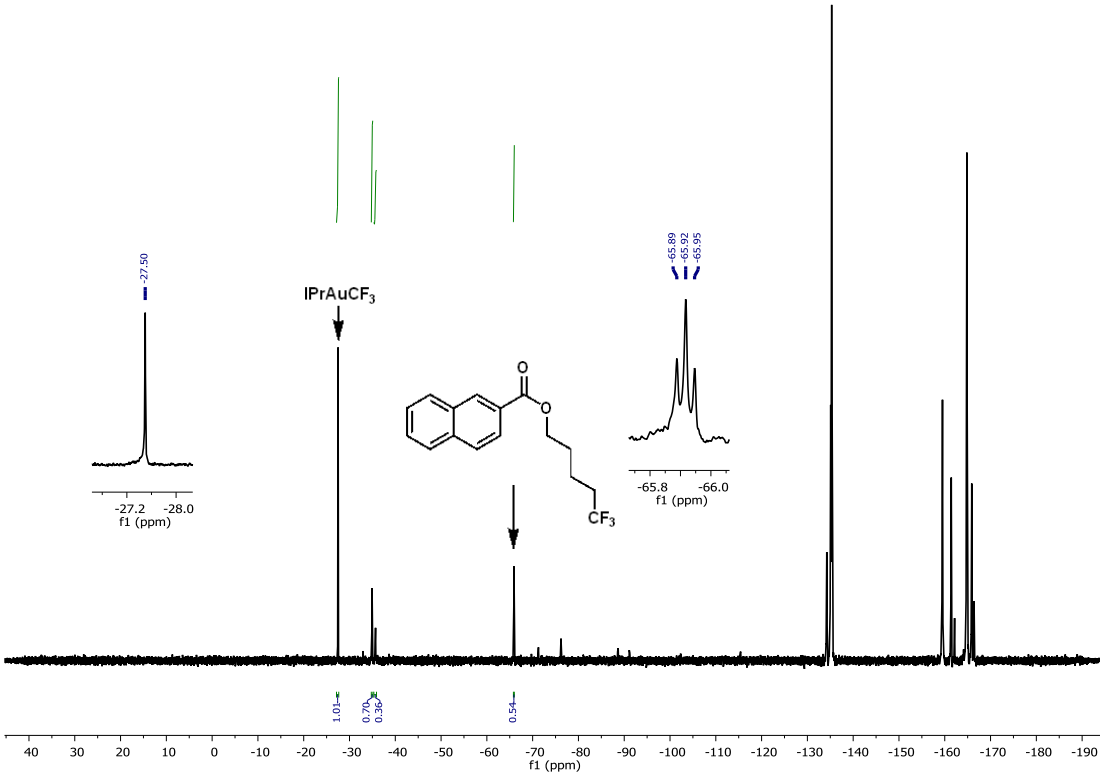


**Figure 4.61**. After 10 minutes of reaction

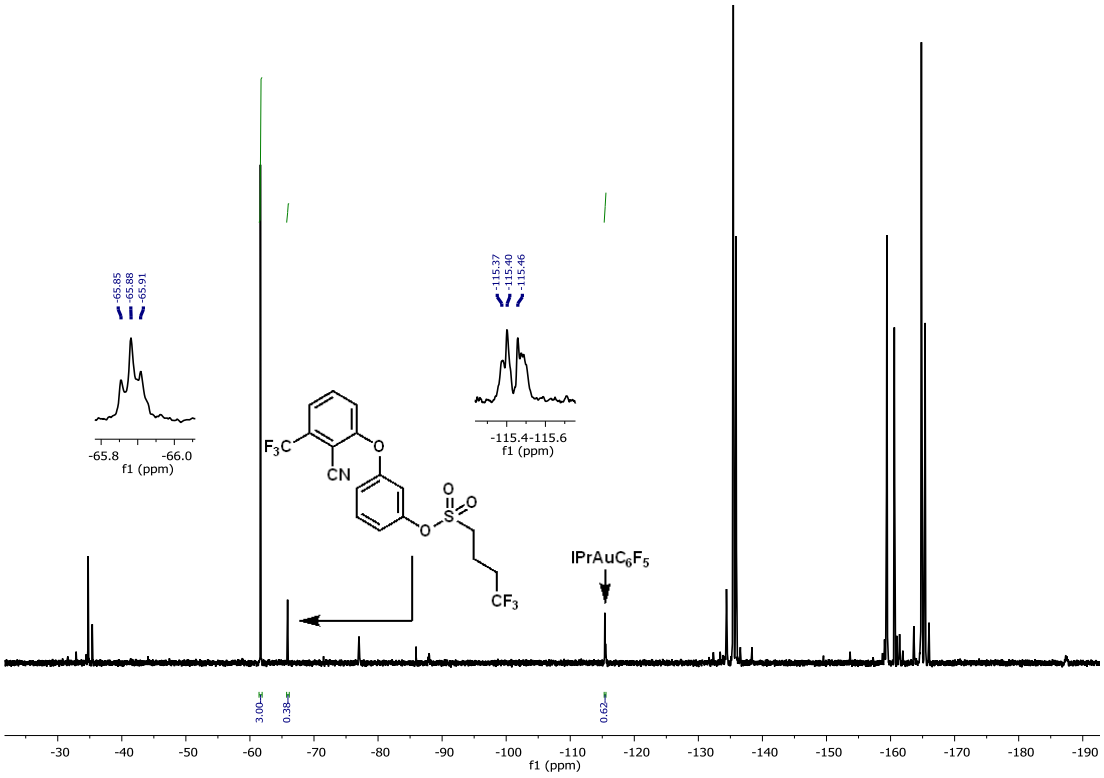


**Figure 4.62**. After 30 minutes of reaction

### 4.5.4 Radiochemistry

No-carrier-added $^{18}$F-fluoride was produced by ~10 MeV proton irradiation of 97+% enriched [$^{18}$O]$H_2O$ at low pressure in a Niobium target by the $^{18}O(p,n)^{18}F$ nuclear reaction on the Biomedical Isotope Facility CTI RDS 111-DV001 cyclotron. The [$^{18}$O]$H_2O$/$^{18}F^-$ (25 µl) was transferred into a conical glass vial containing Kryptofix® 222 (3.5 mg, 9.3 µmol), and $K_2CO_3$ (0.375 mg, 2.7 µmol) in 400 µL of $CH_3CN/H_2O$. The water was removed by azeotropic distillation with anhydrous $CH_3CN$ (0.4 mL) at 100°C in vacuo, under a stream of nitrogen. The azeotropic drying process was repeated two additional times. Residual acetonitrile was found to substantially slow the reaction, so care was taken to thoroughly dry the remaining fluoride.

The residue was extracted with dichloromethane (2x 0.1 mL) to a glass vial and capped with a septum cap. This transferred on average 88 ± 1% of the radioactivity (n =11). Initial activities listed below are for the reaction vial post transfer, and total times include azeotropic drying. The headspace was purged with $N_2$ for 2 minutes, and a solution of tris(pentafluorophenyl)borane in dichloromethane (0.25 mL of 0.1 M solution, 25 µmol) was injected through the septum followed by a solution of the relevant Au(III) acetate complex (5 µmol) in dichrolomethane (0.25 mL). After the indicated reaction time, the solution was spotted onto a TLC plate, eluted with the indicated solvent mixture, and the radiochemical conversion was measured using a radio-TLC scanner (AR-2000 Imaging Scanner, Bioscan) as counts with identical retention as an authentic sample of the product as a fraction of total counts.

**[$^{18}$F]-1-(4-(4,4,4-trifluorobutyl)phenyl)ethan-1-one**

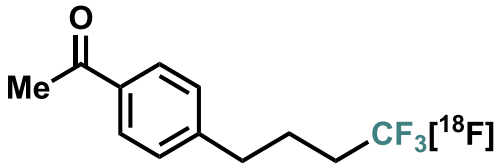


Reaction Time: 8 minutes
TLC solvent: 7:3 Hexanes/Diethyl Ether
The radiochemical conversions obtained were as follows for 5 trials:

| Run | Initial Activity | Total Time | Radiochemical Conversion (TLC) | |
|---|---|---|---|---|
| 1 | 6.55 mCi | 24 min | 38.4% | 31.2 ± 13.8% |
| 2 | 1.30 mCi | 23 min | 52.0% | |
| 3 | 0.73 mCi | 22 min | 24.3% | |
| 4 | 0.72 mCi | 28 min | 18.4% | |
| 5 | 0.57 mCi | 32 min | 22.7% | |

Run 1 (*TLC eluted twice to increase baseline separation):

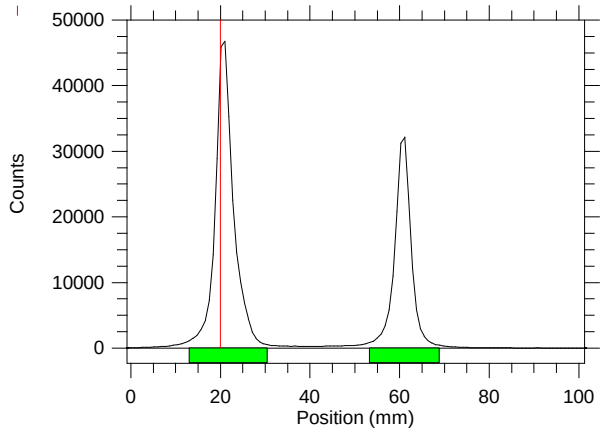


| | (mm) | (mm) | (mm) | | Region | Region | Pct of | Pct of |
|---|---|---|---|---|---|---|---|---|
| **Reg** | **Start** | **Stop** | **Centroid** | **$R_F$** | **Counts** | **CPM** | **Total** | **ROI** |
| **Rgn 1** | 13.1 | 30.6 | 21 | 0.016 | 254391 | 254391 | 59.29 | 61.63 |
| **Rgn 2** | 53.3 | 69 | 60.7 | 0.625 | 158351 | 158351 | 36.91 | 38.37 |
| **2 Peaks** | | | | | 412742 | 412742 | 96.2 | 100 |

Run 2:

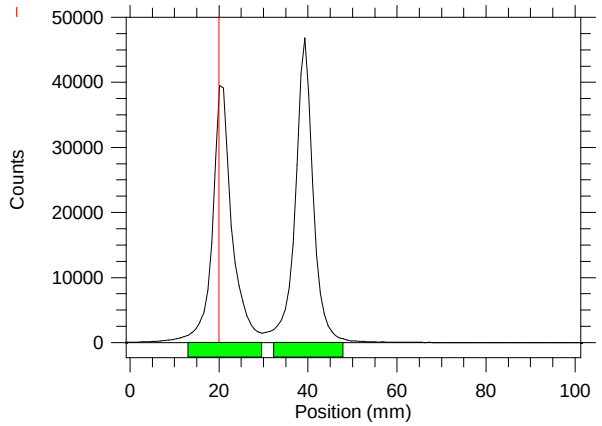


| | (mm) | (mm) | (mm) | | Region | Region | Pct of | Pct of |
|---|---|---|---|---|---|---|---|---|
| **Reg** | **Start** | **Stop** | **Centroid** | **$R_F$** | **Counts** | **CPM** | **Total** | **ROI** |
| **Rgn 1** | 13.1 | 29.7 | 20.9 | 0.015 | 227803 | 227803 | 46.66 | 47.97 |
| **Rgn 2** | 32.3 | 48 | 39.2 | 0.32 | 247034 | 247034 | 50.6 | 52.03 |
| **2 Peaks** | | | | | 474837 | 474837 | 97.26 | 100 |

Run 3:

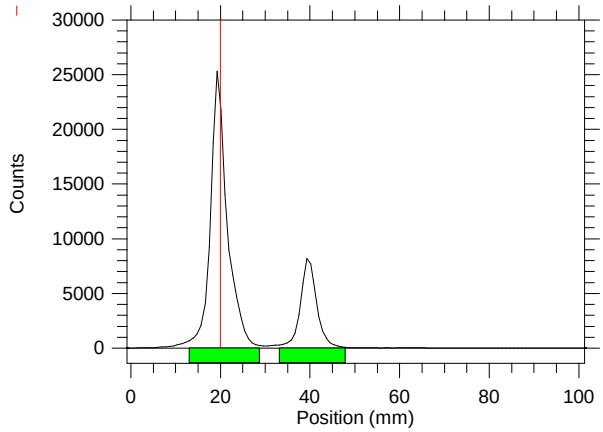


| | (mm) | (mm) | (mm) | | Region | Region | Pct of | Pct of |
|---|---|---|---|---|---|---|---|---|
| **Reg** | **Start** | **Stop** | **Centroid** | **$R_F$** | **Counts** | **CPM** | **Total** | **ROI** |
| **Rgn 1** | 13.1 | 28.8 | 19.9 | -0.002 | 124953 | 124953 | 73.79 | 75.66 |
| **Rgn 2** | 33.2 | 48 | 39.7 | 0.329 | 40200 | 40200 | 23.74 | 24.34 |
| **2 Peaks** | | | | | 165153 | 165153 | 97.52 | 100 |

Run 4:

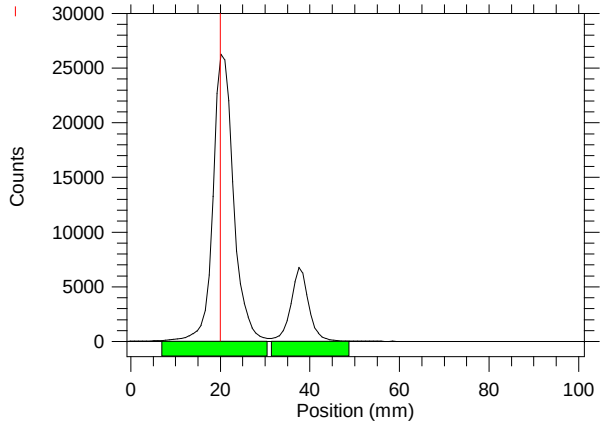


| | (mm) | (mm) | (mm) | | Region | Region | Pct of | Pct of |
|---|---|---|---|---|---|---|---|---|
| **Reg** | **Start** | **Stop** | **Centroid** | **$R_F$** | **Counts** | **CPM** | **Total** | **ROI** |
| **Rgn 1** | 7 | 30.6 | 20.7 | 0.015 | 160860 | 160860 | 81.09 | 81.6 |
| **Rgn 2** | 31.4 | 48.9 | 37.8 | 0.356 | 36279 | 36279 | 18.29 | 18.4 |
| **2 Peaks** | | | | | 197139 | 197139 | 99.38 | 100 |

Run 5:

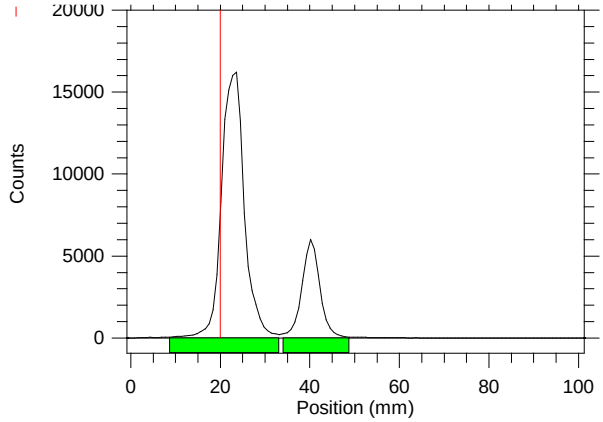


| | (mm) | (mm) | (mm) | | Region | Region | Pct of | Pct of |
|---|---|---|---|---|---|---|---|---|
| **Reg** | **Start** | **Stop** | **Centroid** | **$R_F$** | **Counts** | **CPM** | **Total** | **ROI** |
| **Rgn 1** | 8.7 | 33.2 | 22.8 | 0.052 | 110549 | 110549 | 76.69 | 77.3 |
| **Rgn 2** | 34.1 | 48.9 | 40.3 | 0.369 | 32467 | 32467 | 22.52 | 22.7 |
| **2 Peaks** | | | | | 143016 | 143016 | 99.21 | 100 |

**[$^{18}$F]- 5,5,5-trifluoropentyl 2-naphthoate**

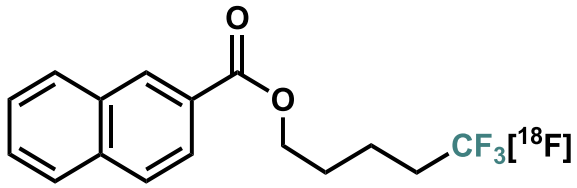


Reaction Time: 10 minutes
TLC solvent: 7:3 Hexanes/Diethyl Ether
The radiochemical conversions obtained were as follows for 3 trials:

| Run | Initial Activity | Total Time | Radiochemical Conversion (TLC) | |
|---|---|---|---|---|
| 1 | 3.92 mCi | 40 min | 23.8% | |
| 2 | 1.79 mCi | 36 min | 23.3% | 26.8 ± 5.6% |
| 3 | 0.95 mCi | 44 min | 33.3% | |

Run 1:

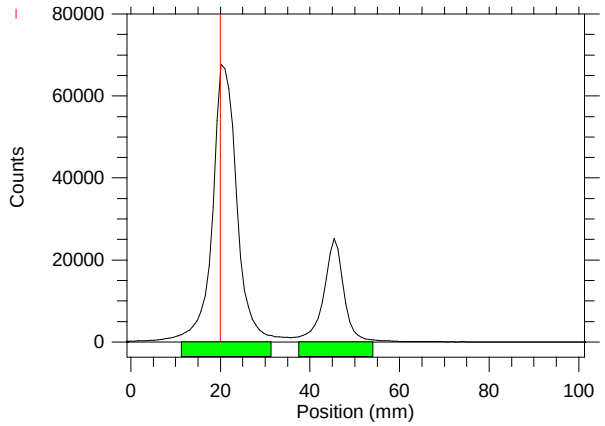


| | (mm) | (mm) | (mm) | | Region | Region | Pct of | Pct of |
|---|---|---|---|---|---|---|---|---|
| **Reg** | **Start** | **Stop** | **Centroid** | **$R_F$** | **Counts** | **CPM** | **Total** | **ROI** |
| **Rgn 1** | 3.5 | 35.8 | 21 | 0.018 | 496437 | 496437 | 75.94 | 76.2 |
| **Rgn 2** | 34.9 | 61.1 | 45.2 | 0.458 | 155040 | 155040 | 23.72 | 23.8 |
| **2 Peaks** | | | | | 651477 | 651477 | 99.66 | 100 |

Run 2:

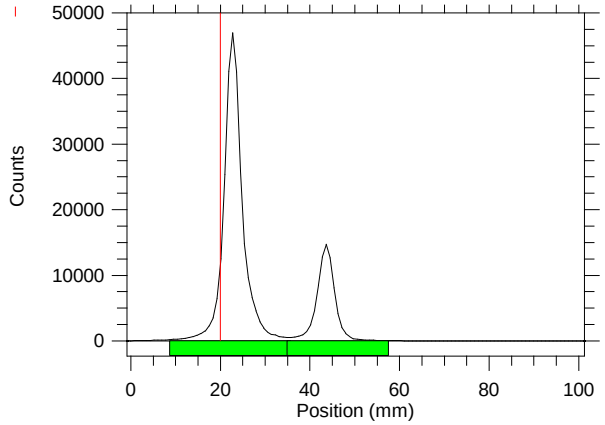


| | (mm) | (mm) | (mm) | | Region | Region | Pct of | Pct of |
|---|---|---|---|---|---|---|---|---|
| **Reg** | **Start** | **Stop** | **Centroid** | **$R_F$** | **Counts** | **CPM** | **Total** | **ROI** |
| **Rgn 1** | 8.7 | 35.8 | 23 | 0.06 | 256667 | 256667 | 76.44 | 76.68 |
| **Rgn 2** | 34.9 | 57.6 | 43.5 | 0.47 | 78048 | 78048 | 23.24 | 23.32 |
| **2 Peaks** | | | | | 334715 | 334715 | 99.68 | 100 |

Run 3:

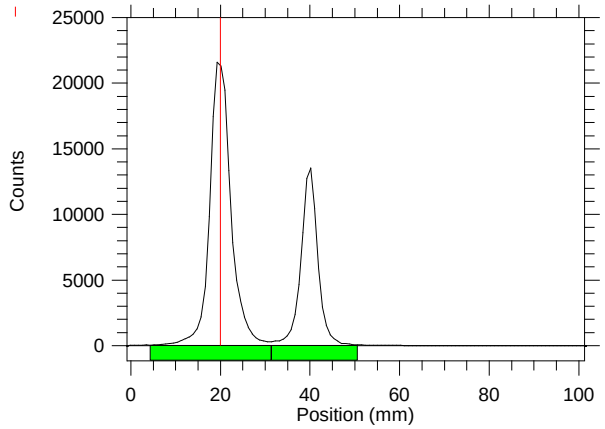


| | (mm) | (mm) | (mm) | | Region | Region | Pct of | Pct of |
|---|---|---|---|---|---|---|---|---|
| **Reg** | **Start** | **Stop** | **Centroid** | **$R_F$** | **Counts** | **CPM** | **Total** | **ROI** |
| **Rgn 1** | 4.4 | 31.4 | 20.1 | 0.001 | 136959 | 136959 | 66.35 | 66.64 |
| **Rgn 2** | 31.4 | 50.6 | 39.8 | 0.397 | 68559 | 68559 | 33.22 | 33.36 |
| **2 Peaks** | | | | | 205518 | 205518 | 99.57 | 100 |

**[$^{18}$F]-3-(2-cyano-3-(trifluoromethyl)phenoxy)phenyl-4,4,4-trifluorobutane-1-sulfonate**

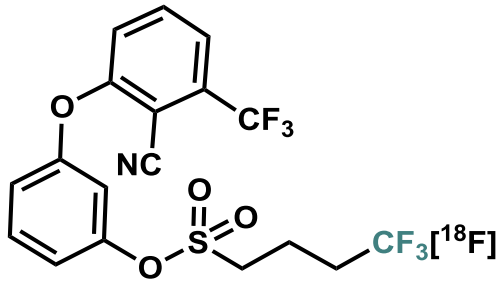


Reaction Time: 25 minutes

TLC solvent: 1:9 Hexanes/Diethyl Ether (Note: F-B($C_6F_5$)$_3$ is mobile at this solvent polarity)

The radiochemical conversions obtained were as follows for 3 trials:

| Run | Initial Activity | Total Time | Radiochemical Conversion (TLC) | |
|---|---|---|---|---|
| 1 | 5.06 mCi | 52 min | 6.3% | |
| 2 | 1.60 mCi | 56 min | 12.0% | 11.7 ± 5.3% |
| 3 | 1.11 mCi | 63 min | 16.9% | |

Run 1 (* Eluted twice with 30:70 $Et_2O$/Hex instead of once with 10:90):

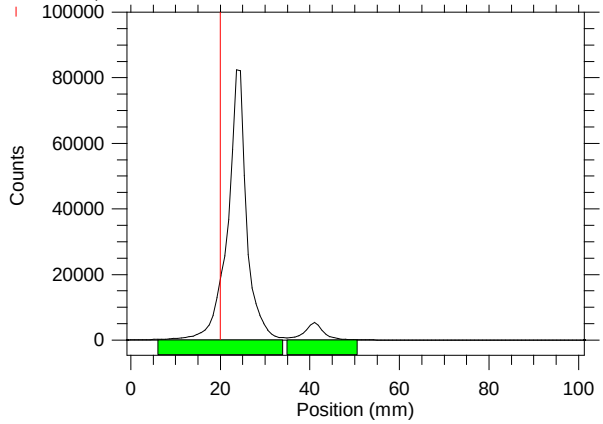


| | (mm) | (mm) | (mm) | | Region | Region | Pct of | Pct of |
|---|---|---|---|---|---|---|---|---|
| Reg | Start | Stop | Centroid | RF | Counts | CPM | Total | ROI |
| Rgn 1 | 6.1 | 34.1 | 23.5 | 0.063 | 466356 | 466356 | 93.01 | 93.7 |
| Rgn 2 | 34.9 | 50.6 | 41 | 0.381 | 31368 | 31368 | 6.26 | 6.3 |
| 2 Peaks | | | | | 497724 | 497724 | 99.27 | 100 |

Run 2:

**Figure S29**

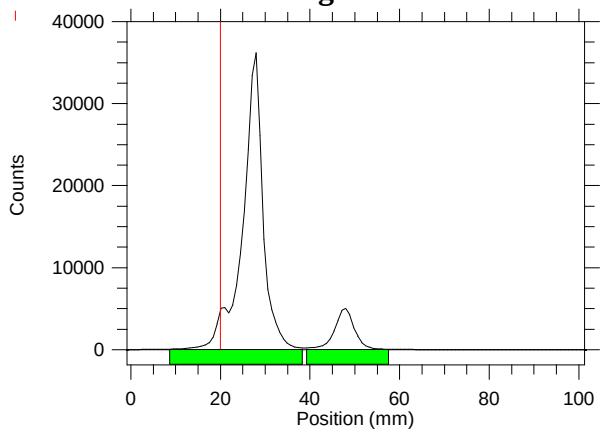


| | (mm) | (mm) | (mm) | | Region | Region | Pct of | Pct of |
|---|---|---|---|---|---|---|---|---|
| Reg | Start | Stop | Centroid | RF | Counts | CPM | Total | ROI |
| Rgn 1 | 8.7 | 38.4 | 26.7 | 0.134 | 219400 | 219400 | 87.51 | 87.95 |
| Rgn 2 | 39.3 | 57.6 | 47.6 | 0.553 | 30059 | 30059 | 11.99 | 12.05 |
| 2 Peaks | | | | | 249459 | 249459 | 99.5 | 100 |

Run 3:

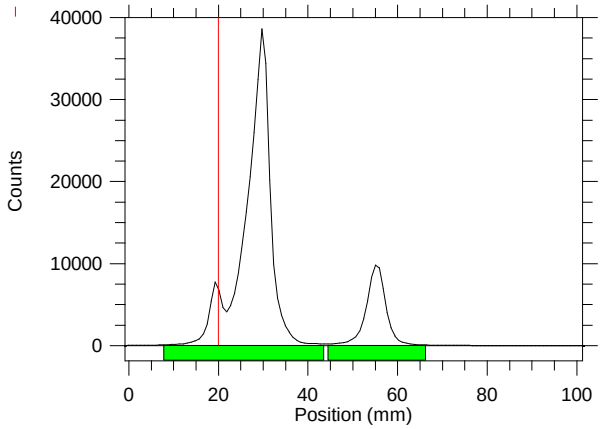


| | (mm) | (mm) | (mm) | | Region | Region | Pct of | Pct of |
|---|---|---|---|---|---|---|---|---|
| Reg | Start | Stop | Centroid | RF | Counts | CPM | Total | ROI |
| Rgn 1 | 7.9 | 43.7 | 27.7 | 0.119 | 284631 | 284631 | 82.63 | 83.03 |
| Rgn 2 | 44.5 | 66.4 | 55 | 0.539 | 58192 | 58192 | 16.89 | 16.97 |
| 2 Peaks | | | | | 342823 | 342823 | 99.52 | 100 |

### 4.5.5 X-Ray Crystallography

Crystal data and structure refinement for **8**.

| | | |
|---|---|---|
| Identification code | shelx | |
| Empirical formula | C30 H39 Au1 F6 N2 | |
| Formula weight | 738.60 | |
| Temperature | 100(2) K | |
| Wavelength | 0.71073 Å | |
| Crystal system | Orthorhombic | |
| Space group | P b c a | |
| Unit cell dimensions | a = 19.3702(6) Å | alpha= 90°. |
| | b = 16.5858(5) Å | beta= 90°. |
| | c = 37.4869(12) Å | gamma = 90°. |
| Volume | 12043.4(6) $Å^3$ | |
| Z | 17 | |
| Density (calculated) | 1.629 $Mg/m^3$ | |
| Absorption coefficient | 4.944 $mm^{-1}$ | |
| F(000) | 5856 | |
| Crystal size | 0.200 x 0.200 x 0.040 $mm^3$ | |
| Theta range for data collection | 1.512 to 25.365°. | |
| Index ranges | -21<=h<=23, -19<=k<=18, -45<=l<=45 | |
| Reflections collected | 111842 | |
| Independent reflections | 11032 [R(int) = 0.0468] | |
| Completeness to theta = 25.000° | 100.0 % | |
| Absorption correction | Semi-empirical from equivalents | |
| Max. and min. transmission | 0.646 and 0.457 | |
| Refinement method | Full-matrix least-squares on $F^2$ | |
| Data / restraints / parameters | 11032 / 0 / 721 | |
| Goodness-of-fit on $F^2$ | 1.112 | |
| Final R indices [I>2sigma(I)] | R1 = 0.0325, wR2 = 0.0746 | |
| R indices (all data) | R1 = 0.0401, wR2 = 0.0779 | |
| Extinction coefficient | n/a | |
| Largest diff. peak and hole | 3.291 and -0.739 $e.Å^{-3}$ | |

Crystal data and structure refinement for **18**.

| | | |
|---|---|---|
| Identification code | shelx | |
| Empirical formula | C21 H36 Au F6 P | |
| Formula weight | 630.43 | |
| Temperature | 100(2) K | |
| Wavelength | 0.71073 Å | |
| Crystal system | Orthorhombic | |
| Space group | P n m a | |
| Unit cell dimensions | a = 14.6624(5) Å | a= 90°. |
| | b = 16.5973(5) Å | b= 90°. |
| | c = 9.1732(3) Å | g = 90°. |
| Volume | 2232.36(13) $Å^3$ | |
| Z | 4 | |
| Density (calculated) | 1.876 $Mg/m^3$ | |
| Absorption coefficient | 6.716 $mm^{-1}$ | |
| F(000) | 1240 | |
| Crystal size | 0.300 x 0.240 x 0.200 $mm^3$ | |
| Theta range for data collection | 2.454 to 25.347°. | |
| Index ranges | -17<=h<=17, -19<=k<=19, -11<=l<=11 | |
| Reflections collected | 40240 | |
| Independent reflections | 2118 [R(int) = 0.0392] | |
| Completeness to theta = 25.000° | 100.0 % | |
| Absorption correction | Semi-empirical from equivalents | |
| Max. and min. transmission | 0.646 and 0.557 | |
| Refinement method | Full-matrix least-squares on $F^2$ | |
| Data / restraints / parameters | 2118 / 0 / 139 | |
| Goodness-of-fit on $F^2$ | 1.143 | |
| Final R indices [I>2sigma(I)] | R1 = 0.0248, wR2 = 0.0586 | |
| R indices (all data) | R1 = 0.0280, wR2 = 0.0602 | |
| Extinction coefficient | n/a | |
| Largest diff. peak and hole | 2.447 and -0.662 $e.Å^{-3}$ | |

Crystal data and structure refinement for **4**.

| | |
|---|---|
| Identification code | shelx |
| Empirical formula | C30 H39 Au Br F5 N2 |
| Formula weight | 799.51 |
| Temperature | 100(2) K |
| Wavelength | 0.71073 A |
| Crystal system, space group | Monoclinic, P 21/c |
| Unit cell dimensions | a = 20.6333(15) A alpha = 90 deg.<br>b = 9.9414(7) A beta = 107.3480(10) deg.<br>c = 16.0121(12) A gamma = 90 deg. |
| Volume | 3135.1(4) A^3 |
| Z, Calculated density | 4, 1.694 Mg/m^3 |
| Absorption coefficient | 6.018 mm^-1 |
| F(000) | 1568 |
| Crystal size | 0.300 x 0.300 x 0.200 mm |
| Theta range for data collection | 2.068 to 25.359 deg. |
| Limiting indices | -24<=h<=24, -11<=k<=11, -19<=l<=1 |
| Reflections collected / unique | 97533 / 5736 [R(int) = 0.0269] |
| Completeness to theta = 25.000 | 100.0 % |
| Refinement method | Full-matrix least-squares on F^2 |
| Data / restraints / parameters | 5736 / 0 / 348 |
| Goodness-of-fit on F^2 | 1.058 |
| Final R indices [I>2sigma(I)] | R1 = 0.0300, wR2 = 0.0785 |
| R indices (all data) | R1 = 0.0313, wR2 = 0.0795 |
| Extinction coefficient | n/a |
| Largest diff. peak and hole | 2.261 and -1.658 e.A^-3 |

Crystal data and structure refinement for **5**.

| | | |
|---|---|---|
| Identification code | shelx | |
| Empirical formula | C29 H36 Au Cl F6 N2 | |
| Formula weight | 759.01 | |
| Temperature | 100(2) K | |
| Wavelength | 0.71073 Å | |
| Crystal system | Monoclinic | |
| Space group | P 21/n | |
| Unit cell dimensions | a = 11.6081(6) Å | alpha= 90°. |
| | b = 17.2245(9) Å | beta= 105.8830(10)°. |
| | c = 15.6653(8) Å | gamma = 90°. |
| Volume | 3012.6(3) $Å^3$ | |
| Z | 4 | |
| Density (calculated) | 1.673 $Mg/m^3$ | |
| Absorption coefficient | 5.030 $mm^{-1}$ | |
| F(000) | 1496 | |
| Crystal size | 0.100 x 0.080 x 0.040 $mm^3$ | |
| Theta range for data collection | 1.796 to 25.409°. | |
| Index ranges | -13<=h<=14, -20<=k<=20, -18<=l<=18 | |
| Reflections collected | 82795 | |
| Independent reflections | 5531 [R(int) = 0.0823] | |
| Completeness to theta = 25.000° | 100.0 % | |
| Absorption correction | Semi-empirical from equivalents | |
| Refinement method | Full-matrix least-squares on $F^2$ | |
| Data / restraints / parameters | 5531 / 0 / 369 | |
| Goodness-of-fit on $F^2$ | 1.056 | |
| Final R indices [I>2sigma(I)] | R1 = 0.0428, wR2 = 0.0956 | |
| R indices (all data) | R1 = 0.0564, wR2 = 0.1031 | |
| Extinction coefficient | n/a | |
| Largest diff. peak and hole | 3.188 and -1.027 $e.Å^{-3}$ | |

Crystal data and structure refinement for **6**.

| | |
|---|---|
| Identification code | shelx |
| Empirical formula | C32 H41 Au F6 N2 |
| Formula weight | 764.63 |
| Temperature | 100(2) K |
| Wavelength | 0.71073 A |
| Crystal system, space group | Orthorhombic, P b c a |
| Unit cell dimensions | a = 16.3403(11) A alpha = 90 deg.<br>b = 17.0007(11) A beta = 90 deg.<br>c = 23.2921(15) A gamma = 90 deg. |
| Volume | 6470.5(7) A^3 |
| Z, Calculated density | 8, 1.570 Mg/m^3 |
| Absorption coefficient | 4.605 mm^-1 |
| F(000) | 3040 |
| Crystal size | 0.200 x 0.100 x 0.100 mm |
| Theta range for data collection | 1.749 to 25.390 deg. |
| Limiting indices | -19<=h<=19, -20<=k<=20, -28<=l<=28 |
| Reflections collected / unique | 144595 / 5953 [R(int) = 0.0352] |
| Completeness to theta = 25.000 | 100.0 % |
| Refinement method | Full-matrix least-squares on F^2 |
| Data / restraints / parameters | 5953 / 0 / 370 |
| Goodness-of-fit on F^2 | 1.155 |
| Final R indices [I>2sigma(I)] | R1 = 0.0309, wR2 = 0.0753 |
| R indices (all data) | R1 = 0.0341, wR2 = 0.0774 |
| Extinction coefficient | n/a |
| Largest diff. peak and hole | 3.800 and -1.210 e.A^-3 |

Crystal data and structure refinement for **7**.

| | | |
|---|---|---|
| Identification code | shelx | |
| Empirical formula | C40 H49 Au F6 N2 O | |
| Formula weight | 884.78 | |
| Temperature | 100(2) K | |
| Wavelength | 0.71073 A | |
| Crystal system, space group | Monoclinic, P 21/n | |
| Unit cell dimensions | a = 12.1671(6) A | alpha = 90 deg. |
| | b = 22.4672(11) A | beta = 105.4170(10) deg. |
| | c = 14.5163(7) A | gamma = 90 deg. |
| Volume | 3825.4(3) A^3 | |
| Z, Calculated density | 4, 1.536 Mg/m^3 | |
| Absorption coefficient | 3.908 mm^-1 | |
| F(000) | 1776 | |
| Crystal size | 0.200 x 0.120 x 0.100 mm | |
| Theta range for data collection | 1.714 to 25.373 deg. | |
| Limiting indices | -14<=h<=14, -26<=k<=27, -17<=l<=17 | |
| Reflections collected / unique | 114481 / 7027 [R(int) = 0.0374] | |
| Completeness to theta = 25.000 | 100.0 % | |
| Refinement method | Full-matrix least-squares on F^2 | |
| Data / restraints / parameters | 7027 / 0 / 451 | |
| Goodness-of-fit on F^2 | 1.138 | |
| Final R indices [I>2sigma(I)] | R1 = 0.0341, wR2 = 0.0788 | |
| R indices (all data) | R1 = 0.0386, wR2 = 0.0823 | |
| Extinction coefficient | n/a | |
| Largest diff. peak and hole | 3.633 and -1.245 e.A^-3 | |

Crystal data and structure refinement for **18**.

| | |
|---|---|
| Identification code | shelx |
| Empirical formula | C40 H49 Au Br F5 N2 O |
| Formula weight | 945.69 |
| Temperature | 100(2) K |
| Wavelength | 0.71073 A |
| Crystal system, space group | Monoclinic, P 21/c |
| Unit cell dimensions | a = 9.2424(3) A alpha = 90 deg.<br>b = 20.6341(6) A beta = 101.456(2) deg.<br>c = 23.2072(6) A gamma = 90 deg. |
| Volume | 4337.6(2) A^3 |
| Z, Calculated density | 4, 1.448 Mg/m^3 |
| Absorption coefficient | 4.364 mm^-1 |
| F(000) | 1880 |
| Crystal size | 0.300 x 0.100 x 0.100 mm |
| Theta range for data collection | 1.332 to 25.386 deg. |
| Limiting indices | -11<=h<=11, -24<=k<=24, -27<=l<=27 |
| Reflections collected / unique | 99742 / 7958 [R(int) = 0.0791] |
| Completeness to theta = 25.000 | 100.0 % |
| Absorption correction | None |
| Refinement method | Full-matrix least-squares on F^2 |
| Data / restraints / parameters | 7958 / 48 / 497 |
| Goodness-of-fit on F^2 | 1.148 |
| Final R indices [I>2sigma(I)] | R1 = 0.0585, wR2 = 0.1599 |
| R indices (all data) | R1 = 0.0768, wR2 = 0.1675 |
| Extinction coefficient | n/a |
| Largest diff. peak and hole | 1.928 and -0.625 e.A^-3 |

Crystal data and structure refinement for **7**.

| | | |
|---|---|---|
| Identification code | shelx | |
| Empirical formula | C27 H23 Au F6 I P | |
| Formula weight | 816.29 | |
| Temperature | 100(2) K | |
| Wavelength | 0.71073 Å | |
| Crystal system | Monoclinic | |
| Space group | P 21/n | |
| Unit cell dimensions | a = 7.5619(3) Å | a= 90°. |
| | b = 14.3616(5) Å | b= 95.4860(10)°. |
| | c = 24.1182(9) Å | g = 90°. |
| Volume | 2607.26(17) $Å^3$ | |
| Z | 4 | |
| Density (calculated) | 2.080 $Mg/m^3$ | |
| Absorption coefficient | 6.946 $mm^{-1}$ | |
| F(000) | 1544 | |
| Crystal size | 0.500 x 0.500 x 0.500 $mm^3$ | |
| Theta range for data collection | 1.652 to 25.361°. | |
| Index ranges | -9<=h<=9, -17<=k<=17, -29<=l<=29 | |
| Reflections collected | 73049 | |
| Independent reflections | 4778 [R(int) = 0.0341] | |
| Completeness to theta = 25.000° | 100.0 % | |
| Absorption correction | Semi-empirical from equivalents | |
| Max. and min. transmission | 0.745 and 0.588 | |
| Refinement method | Full-matrix least-squares on $F^2$ | |
| Data / restraints / parameters | 4778 / 0 / 325 | |
| Goodness-of-fit on $F^2$ | 1.130 | |
| Final R indices [I>2sigma(I)] | R1 = 0.0204, wR2 = 0.0481 | |
| R indices (all data) | R1 = 0.0211, wR2 = 0.0484 | |
| Extinction coefficient | n/a | |
| Largest diff. peak and hole | 1.471 and -0.799 $e.Å^{-3}$ | |

Crystal data and structure refinement for **S8**.

| | |
|---|---|
| Identification code | shelx |
| Empirical formula | C33 H43 Au F6 N2 |
| Formula weight | 778.66 |
| Temperature | 100(2) K |
| Wavelength | 0.71073 A |
| Crystal system, space group | Orthorhombic, P b c a |
| Unit cell dimensions | a = 15.9214(14) A alpha = 90 deg.<br>b = 17.6740(15) A beta = 90 deg.<br>c = 23.278(2) A gamma = 90 deg. |
| Volume | 6550.2(10) A^3 |
| Z, Calculated density | 8, 1.579 Mg/m^3 |
| Absorption coefficient | 4.550 mm^-1 |
| F(000) | 3104 |
| Crystal size | 0.140 x 0.060 x 0.060 mm |
| Theta range for data collection | 1.750 to 25.384 deg. |
| Limiting indices | -19<=h<=19, -21<=k<=21, -28<=l<=28 |
| Reflections collected / unique | 214909 / 6017 [R(int) = 0.0352] |
| Completeness to theta = 25.000 | 100.0 % |
| Absorption correction | None |
| Refinement method | Full-matrix least-squares on F^2 |
| Data / restraints / parameters | 6017 / 6 / 379 |
| Goodness-of-fit on F^2 | 1.157 |
| Final R indices [I>2sigma(I)] | R1 = 0.0345, wR2 = 0.0741 |
| R indices (all data) | R1 = 0.0393, wR2 = 0.0780 |
| Extinction coefficient | n/a |
| Largest diff. peak and hole | 3.893 and -1.409 e.A^-3 |

### 4.5.6 Computational Methodology

Gaussian 09 suite was employed for all Density Functional Theory (DFT) calculations as described below. Initially, full geometry optimizations were performed with the M06-L density functional and the cc-pVDZ basis set. A Stuttgart/Dresden effective core potential (ECP) MWB28 was used for gold atoms, which was augmented with a set of diffuse functions (2f and g). The redundant internal coordinates were modified to remove angles and dihedrals through nearly collinear bonds, which considerably improved the performance of the full optimizations. The final geometries were obtained with tight SCF and geometry convergence criteria in combination with the ultrafine integration grid. Subsequent frequency calculations were performed to confirm the nature of each stationary point (one imaginary frequency along the reaction coordinate for transition states and zero imaginary frequencies for ground states) and to obtain enthalpy corrections. Afterwards, more accurate single-point electronic energies were obtained with M06-L functional and adequate cc-pVTZ basis set on the aforementioned geometries. Finally, the Polarizable Continuum Model (PCM) was implemented for dichloromethane (25°C) using SMD radii of Truhlar and coworkers to account for solution-phase effects. All calculated energies and corrections and xyz geometries are listed below.

Following the lowest energy pathway to **VI**: Initial coordination between fluorine, in gold complex **I,** and the Lewis-acidic $BF_3$ is followed by cleavage of the C−F bond to provide access to gold carbene **II**. Migratory insertion of the $CF_2$ group into the Au−$CH_3$ bond proceeds with a small barrier ($TS^1$) to afford a T-shaped gold complex **IIIa**, which can rearrange into the thermodynamically more stable T-shaped isomer **IIIb** via $TS^2$. Outer-sphere attack of $BF_4^-$ on the $CF_2CH_3$ group in **IIIb** is easily accessible ($TS^3$) due to the favorable linear arrangement of the NHC−Au−$CF_3$ bonds and yields the linear complex **VI**. We consider migratory insertion to be the rate limiting step in this case, because charge separation accounts for a large fraction of the required energy during C−F bond breaking (**I·BF₃ ⟶ II**).

Complex **IIIa** can be trapped by $BF_4^-$ to form the adduct **IV·BF₃** which, upon dissociation of $BF_3$, results in complex **IV**. Calculation of inner-sphere C−F bond formation from complex **IV,** of the type that would be required to form complex **VI,** resulted in a prohibitively high barrier ($TS^4$) - similar in energy to those for the direct C−C bond forming reactions **I ⟶ VI** ($TS^5$) and **II ⟶ V** ($TS^6$).

**Optimized Energies and Thermochemistry**

Electronic energies[a] and enthalpy (H) corrections[b] with M06-L functional and given basis sets.

| Structure | cc-pVDZ | cc-pVTZ | cc-pVTZ+SMD | H correction[b] |
|---|---|---|---|---|
| **1** | -1539.255606 | -1539.582215 | -1539.614146 | 0.324062 |
| **1·BF3** | -1863.801535 | -1864.221654 | -1864.253308 | 0.342693 |
| **2** | -1439.139035 | -1439.443154 | -1439.526706 | 0.320813 |
| **TS1** | -1439.130478 | -1439.433553 | -1439.519145 | 0.319451 |
| **3a** | -1439.154077 | -1439.465517 | -1439.553341 | 0.320719 |
| **TS2** | -1439.149097 | -1439.449460 | -1439.545567 | 0.320659 |
| **3b** | -1439.193853 | -1439.494445 | -1439.586078 | 0.322479 |
| **TS3** | -1863.809537 | -1864.230778 | -1864.279746 | 0.342433 |
| **6** | -1161.756861 | -1161.986303 | -1162.020425 | 0.266615 |
| **4·BF3** | -1863.836303 | -1864.250644 | -1864.294457 | 0.343181 |
| **4** | -1539.266994 | -1539.590002 | -1539.632410 | 0.325236 |
| **TS4** | -1539.172170 | -1539.498091 | -1539.538419 | 0.322782 |
| **TS5** | -1539.160807 | -1539.489710 | -1539.519732 | 0.322051 |
| **TS6** | -1439.076412 | -1439.382683 | -1439.460805 | 0.319207 |
| **5** | -1061.669520 | -1061.875643 | -1061.954767 | 0.263598 |
| **$CH_3CF_3$** | -377.538001 | -377.640825 | -377.645216 | 0.058055 |
| **$BF_3$** | -324.631677 | -324.628614 | -324.631677 | 0.016792 |
| **$BF_4^-$** | -424.482887 | -424.610518 | -424.696552 | 0.019458 |

[a] All energies are in units of Hartree; [b] Calculated H corrections at M06-L/cc-pVTZ//cc-pVDZ, Au: SDD(2f,g) level of theor

## M06-L/cc-pVTZ//cc-pVDZ, Au: SDD(2f,g) Optimized Geometries

**1** *($C_1$, $N_{imag}$ = 0)*

| | | | |
|---|---|---|---|
| Au | -0.016979567 | -0.941733241 | 0.020847306 |
| C | -0.077759717 | -3.017458914 | 0.039730280 |
| C | 0.026047576 | 1.180610471 | -0.022125017 |
| C | 0.713703790 | 3.333073656 | 0.048809308 |
| C | -0.627988675 | 3.340232768 | -0.160728404 |
| H | 1.426049854 | 4.141629150 | 0.162938762 |
| H | -1.327858475 | 4.155965599 | -0.298659233 |
| C | 2.420774529 | 1.520519841 | 0.349030540 |
| C | 3.451279688 | 1.969961800 | -0.474012073 |
| C | 2.652608325 | 0.580542442 | 1.353584888 |
| C | 4.735462244 | 1.463464389 | -0.289226385 |
| C | 3.938277404 | 0.070751656 | 1.517500896 |
| C | 4.978548878 | 0.510656509 | 0.699613043 |
| H | 5.545697029 | 1.801990204 | -0.936575324 |
| H | 4.125226709 | -0.670623153 | 2.295407554 |
| H | 5.983661689 | 0.107270040 | 0.831783115 |
| C | -2.361563897 | 1.543014880 | -0.407214135 |
| C | -3.383853976 | 2.010793767 | 0.415372987 |
| C | -2.605352712 | 0.592028075 | -1.398549920 |
| C | -4.673116745 | 1.513330640 | 0.241861025 |
| C | -3.896150762 | 0.091609361 | -1.551464899 |
| C | -4.928891218 | 0.551299287 | -0.734921469 |
| H | -5.477433111 | 1.865442679 | 0.889312117 |
| H | -4.092896413 | -0.658174205 | -2.318872612 |
| H | -5.938121965 | 0.155275735 | -0.857772201 |
| N | 1.092103465 | 2.000684566 | 0.138139629 |
| N | -1.026621977 | 2.012201199 | -0.209295632 |
| C | 0.938944657 | -1.035827391 | -1.849626386 |
| C | -0.979690146 | -0.909445835 | 1.890367144 |
| F | 0.975236829 | 0.178625565 | -2.508865401 |
| F | 0.350907634 | -1.887578729 | -2.738048755 |
| F | 2.242923157 | -1.427040167 | -1.764583019 |
| F | -0.332185987 | -1.617978341 | 2.863038336 |
| F | -2.247922548 | -1.407140949 | 1.847228588 |
| F | -1.114095193 | 0.357698186 | 2.423537935 |
| H | 0.854633031 | -3.417914200 | -0.379135408 |
| H | -0.223752196 | -3.395876253 | 1.058097133 |
| H | -0.916175213 | -3.335280870 | -0.596328392 |
| H | -3.158267747 | 2.728355651 | 1.206129123 |
| H | -1.788458221 | 0.259045321 | -2.042431889 |
| H | 1.832417070 | 0.262580642 | 2.000700034 |
| H | 3.236842969 | 2.682824606 | -1.272215615 |

**1·$BF_3$** *($C_1$, $N_{imag}$ = 0)*

| | | | |
|---|---|---|---|
| Au | 0.105893104 | 0.309559200 | -0.744811490 |
| C | -0.225312073 | 1.688583006 | -2.262669215 |
| C | 0.498601862 | -1.162995330 | 0.749893815 |
| C | 0.274083004 | -2.857027528 | 2.231261757 |
| C | 1.596591441 | -2.561396975 | 2.149420024 |
| H | -0.262918046 | -3.582855060 | 2.830451162 |
| H | 2.461162644 | -2.995783994 | 2.637322596 |
| N | -0.379656827 | -1.985315904 | 1.373122191 |
| N | 1.712541612 | -1.526870698 | 1.232077711 |
| C | -0.370108517 | -1.197093051 | -2.126646146 |
| C | 0.623177057 | 1.853231776 | 0.595185321 |
| F | -0.017002523 | -2.460794807 | -1.697033236 |
| F | 0.252379750 | -1.061685251 | -3.331829217 |
| F | -1.701677518 | -1.274704282 | -2.398763470 |
| F | 1.894251490 | 2.297090290 | 0.412084541 |
| F | -0.151136840 | 3.012648402 | 0.529942598 |
| H | -0.280040335 | 2.708507901 | -1.867116784 |
| H | 0.601126040 | 1.605734841 | -2.981954598 |
| H | -1.165341300 | 1.436093532 | -2.770625467 |
| F | -2.398861093 | 2.559432155 | 1.993090899 |
| B | -2.437191523 | 3.042409336 | 0.755848117 |
| F | -2.639938224 | 2.198578040 | -0.250672570 |
| F | 0.547584230 | 1.490356055 | 1.915850241 |
| F | -2.465075703 | 4.346326277 | 0.547916336 |
| C | -1.788010019 | -1.953686827 | 1.136565752 |
| C | -2.456104164 | -3.130254156 | 0.803290889 |
| C | -2.457055382 | -0.733565320 | 1.212176577 |
| H | -1.900492734 | -4.065719499 | 0.716310020 |
| H | -1.911579330 | 0.166322173 | 1.500084709 |
| C | -3.822737759 | -3.078358162 | 0.540736824 |
| C | -3.820773098 | -0.693365455 | 0.933073282 |
| H | -4.353405933 | -3.991801947 | 0.268334253 |
| H | -4.348812706 | 0.259657791 | 0.982856896 |
| C | -4.503812384 | -1.862341811 | 0.600359659 |
| H | -5.572266913 | -1.826142076 | 0.382204431 |
| C | 2.936786541 | -0.915330180 | 0.820057315 |
| C | 3.230442936 | -0.835061702 | -0.541415007 |
| C | 3.796279330 | -0.384962894 | 1.779681906 |
| H | 2.551924882 | -1.284766143 | -1.269554017 |
| H | 3.529839310 | -0.439033974 | 2.836801257 |
| C | 4.396231787 | -0.187927558 | -0.943726112 |
| C | 4.965725278 | 0.247518520 | 1.364603009 |
| H | 4.628539753 | -0.113157609 | -2.006874474 |
| H | 5.638731469 | 0.676632955 | 2.108262734 |
| C | 5.262015382 | 0.353605561 | 0.005971154 |
| H | 6.172902670 | 0.861740501 | -0.314234798 |

**2** *($C_1$, $N_{imag}$ = 0)*

| | | | |
|---|---|---|---|
| Au | 0.070646707 | -0.933472906 | -0.052291701 |
| C | 0.017831057 | -3.040102832 | 0.182435536 |
| C | 0.012145585 | 1.188373443 | -0.158033606 |
| C | -0.717960862 | 3.312305365 | -0.232329924 |
| C | 0.626567908 | 3.349236190 | -0.033778850 |
| H | -1.446772080 | 4.106837376 | -0.343625627 |
| H | 1.310235492 | 4.180547046 | 0.093763982 |
| C | -2.404621886 | 1.470865155 | -0.489130845 |
| C | -3.420633366 | 1.920221705 | 0.351376622 |
| C | -2.645912291 | 0.515364636 | -1.476979254 |
| C | -4.700458598 | 1.391748299 | 0.201916800 |
| C | -3.928293888 | -0.013404656 | -1.608148493 |
| C | -4.953160001 | 0.422795566 | -0.769242498 |
| H | -5.501232540 | 1.730251936 | 0.860036513 |
| H | -4.128923202 | -0.757574092 | -2.379654419 |
| H | -5.956464306 | 0.009112786 | -0.876411607 |
| C | 2.401815854 | 1.584831768 | 0.221443163 |
| C | 3.413315290 | 2.023032298 | -0.631976777 |
| C | 2.662136178 | 0.688618650 | 1.260473235 |
| C | 4.707443536 | 1.538615491 | -0.447490817 |
| C | 3.958333481 | 0.203825897 | 1.425772544 |
| C | 4.977946156 | 0.624794397 | 0.571493516 |
| H | 5.506348731 | 1.873859666 | -1.109864839 |
| H | 4.173522880 | -0.490943799 | 2.238496642 |
| H | 5.992280928 | 0.248097068 | 0.708423162 |
| N | -1.075206476 | 1.976077464 | -0.313879426 |
| N | 1.056676017 | 2.032195828 | 0.012337976 |

| | | | |
|---|---|---|---|
| C | -1.063662320 | -0.870827855 | 1.705648845 |
| C | 1.226188714 | -1.314714146 | -1.697292718 |
| F | -1.133631994 | 0.374376794 | 2.238353965 |
| F | -0.530720108 | -1.658706383 | 2.657932632 |
| F | -2.326738192 | -1.279449986 | 1.490270318 |
| F | 2.496514907 | -1.505365284 | -1.673911508 |
| F | 0.781278254 | -1.598046785 | -2.871333369 |
| H | -0.992613295 | -3.296862454 | 0.518920278 |
| H | 0.240626367 | -3.583476494 | -0.743324359 |
| H | 0.753083065 | -3.295172225 | 0.955493416 |
| H | 3.185813211 | 2.723677243 | -1.437731706 |
| H | 1.862997874 | 0.405434964 | 1.950176138 |
| H | -1.843141842 | 0.214858921 | -2.155187114 |
| H | -3.201587159 | 2.649047079 | 1.133576885 |

**TS[1]** *($C_1$, $N_{imag}$ = 1)*

| | | | |
|---|---|---|---|
| Au | 0.120726707 | -0.835160743 | -0.000114927 |
| C | 0.499667089 | -3.010247345 | 0.132687663 |
| C | -0.068430715 | 1.179689639 | -0.280589153 |
| C | -0.880351226 | 3.242924592 | -0.584490755 |
| C | 0.464372193 | 3.351790142 | -0.415473061 |
| H | -1.641225786 | 3.990567662 | -0.776153235 |
| H | 1.117742997 | 4.216235379 | -0.397027386 |
| C | -2.503050277 | 1.323325247 | -0.594662082 |
| C | -3.514799056 | 1.810945598 | 0.229366237 |
| C | -2.726754139 | 0.272663587 | -1.484657912 |
| C | -4.775488369 | 1.223007184 | 0.163301298 |
| C | -3.990284161 | -0.312785148 | -1.532195116 |
| C | -5.011571332 | 0.160266336 | -0.708944333 |
| H | -5.573476400 | 1.590018134 | 0.809374967 |
| H | -4.179590945 | -1.131218617 | -2.227630236 |
| H | -5.999945637 | -0.298668014 | -0.751064693 |
| C | 2.312834420 | 1.698250820 | 0.023978895 |
| C | 3.299879431 | 2.057940328 | -0.891133080 |
| C | 2.612012435 | 0.958459031 | 1.170230887 |
| C | 4.613503853 | 1.656397551 | -0.654640783 |
| C | 3.928033077 | 0.553856573 | 1.386698985 |
| C | 4.925728813 | 0.900330016 | 0.475386145 |
| H | 5.394726728 | 1.929837062 | -1.364626092 |
| H | 4.175111237 | -0.017213335 | 2.282398584 |
| H | 5.955525493 | 0.587594962 | 0.651897454 |
| N | -1.191034173 | 1.894860452 | -0.502221595 |
| N | 0.949219930 | 2.067421459 | -0.225078023 |
| C | -1.004074666 | -0.644205010 | 1.775067661 |
| C | 1.209120763 | -1.816331648 | -1.349134459 |
| F | -1.166287538 | 0.612203715 | 2.254754211 |
| F | -0.379046601 | -1.349299372 | 2.752678373 |
| F | -2.235795362 | -1.176717245 | 1.627432564 |
| F | 2.507988274 | -1.965816379 | -1.282626362 |
| F | 0.769132794 | -2.354828915 | -2.458926362 |
| H | -0.551793168 | -3.320349907 | 0.200785843 |
| H | 0.995770716 | -3.729411816 | -0.528200799 |
| H | 1.022879799 | -3.027951303 | 1.096344471 |
| H | 3.039339510 | 2.630757861 | -1.782922382 |
| H | 1.827959604 | 0.737337036 | 1.899322718 |
| H | -1.928234586 | -0.059176972 | -2.152858750 |
| H | -3.305512608 | 2.615825950 | 0.935942110 |

**3a** *($C_1$, $N_{imag}$ = 0)*

| | | | |
|---|---|---|---|
| Au | 0.017676771 | -0.884517295 | 0.118144703 |
| C | 0.845132723 | -3.007362038 | -0.736793032 |
| C | 0.018492586 | 1.076225041 | -0.329573840 |
| C | -0.697365204 | 3.151019220 | -0.714701162 |
| C | 0.647751435 | 3.206250809 | -0.521883617 |
| H | -1.420405946 | 3.923457583 | -0.949520518 |
| H | 1.339488437 | 4.040527662 | -0.521407469 |
| C | -2.406456485 | 1.300733506 | -0.664329843 |
| C | -3.395326571 | 1.860445547 | 0.140786691 |
| C | -2.667062183 | 0.218807006 | -1.506198336 |
| C | -4.675397430 | 1.313283749 | 0.104977913 |
| C | -3.950063869 | -0.325006263 | -1.520807655 |
| C | -4.950550676 | 0.219954661 | -0.716451093 |
| H | -5.457240659 | 1.735429168 | 0.736807002 |
| H | -4.171027825 | -1.166760225 | -2.177986197 |
| H | -5.953682316 | -0.207432435 | -0.733485870 |
| C | 2.416963781 | 1.501681004 | 0.033410644 |
| C | 3.447159466 | 1.813026995 | -0.850142147 |
| C | 2.646886157 | 0.782568202 | 1.207864285 |
| C | 4.736628434 | 1.375320848 | -0.556018389 |
| C | 3.940526333 | 0.341685067 | 1.481665478 |
| C | 4.981338108 | 0.634189495 | 0.600333380 |
| H | 5.551889990 | 1.606573021 | -1.242150473 |
| H | 4.136058591 | -0.213511233 | 2.399808817 |
| H | 5.992925095 | 0.291977373 | 0.821763493 |
| N | -1.071880046 | 1.822948285 | -0.592188998 |
| N | 1.076611827 | 1.910565861 | -0.277230508 |
| C | -1.032472396 | -0.559505048 | 1.948170657 |
| C | 1.051885814 | -1.725810260 | -1.496934713 |
| F | -1.128168117 | 0.753846245 | 2.306522399 |
| F | -0.391357810 | -1.181515042 | 2.977209709 |
| F | -2.297252584 | -1.042701625 | 1.923244794 |
| F | 0.425193709 | -1.683223208 | -2.689462811 |
| F | 2.337387318 | -1.378102643 | -1.669188088 |
| H | 0.225851161 | -2.883278196 | 0.225939244 |
| H | 0.245927432 | -3.733828990 | -1.297366695 |
| H | 1.786904139 | -3.424944346 | -0.365291499 |
| H | -1.883207011 | -0.167697840 | -2.162443489 |
| H | -3.154072038 | 2.686025149 | 0.812175521 |
| H | 3.237358213 | 2.368180391 | -1.765975676 |
| H | 1.833002626 | 0.607771390 | 1.916453540 |

**TS[2]** *($C_1$, $N_{imag}$ = 1)*

| | | | |
|---|---|---|---|
| Au | -0.094591464 | 0.818818786 | 0.141304956 |
| C | 1.981405655 | 0.865409821 | 2.145698045 |
| C | 0.034771014 | -1.133817841 | -0.330599697 |
| C | -0.562647086 | -3.173806926 | -1.010534279 |
| C | 0.785511809 | -3.073037110 | -1.146199027 |
| H | -1.244898506 | -3.991331857 | -1.213004951 |
| H | 1.523739662 | -3.771829891 | -1.522194878 |
| C | -2.390717981 | -1.634715736 | -0.248445119 |
| C | -3.339058661 | -1.896461477 | -1.235409575 |
| C | -2.742667964 | -1.053284419 | 0.968979027 |
| C | -4.668552787 | -1.559056846 | -0.993782242 |
| C | -4.074130846 | -0.708217714 | 1.189821722 |
| C | -5.034918738 | -0.961171858 | 0.211905158 |
| H | -5.418507901 | -1.753289943 | -1.761023762 |
| H | -4.360852547 | -0.253875529 | 2.138663094 |
| H | -6.076644005 | -0.693808937 | 0.390941353 |
| C | 2.471661536 | -1.263349271 | -0.703094416 |
| C | 3.456638306 | -1.927531045 | 0.026630927 |
| C | 2.743885897 | -0.083177521 | -1.397579128 |
| C | 4.740936101 | -1.387931576 | 0.067405814 |
| C | 4.029832889 | 0.451053094 | -1.336387781 |
| C | 5.025233519 | -0.198333130 | -0.605203531 |
| H | 5.520529782 | -1.897513318 | 0.634913420 |
| H | 4.254954892 | 1.370011772 | -1.878866609 |
| H | 6.032145543 | 0.219649277 | -0.567593427 |
| N | -1.016362463 | -1.965623298 | -0.501055023 |

| | | | |
|---|---|---|---|
| N | 1.141323352 | -1.800525468 | -0.726602528 |
| C | -0.739039632 | 2.578033662 | -0.851799441 |
| C | 0.808671765 | -0.040827757 | 1.998022286 |
| F | 0.104238555 | 2.977042293 | -1.838737484 |
| F | -0.764007141 | 3.600614920 | 0.061953738 |
| F | -1.972850071 | 2.519373729 | -1.395277472 |
| F | -0.206490577 | 0.247100465 | 2.825347919 |
| F | 1.086985241 | -1.337294314 | 2.119608596 |
| H | 1.704266311 | 1.912932961 | 1.972066872 |
| H | 2.331107730 | 0.783539158 | 3.187595300 |
| H | 2.789102913 | 0.571830380 | 1.466536983 |
| H | -1.991764945 | -0.902441635 | 1.745596822 |
| H | -3.037785353 | -2.333889890 | -2.188897547 |
| H | 3.212627247 | -2.842033354 | 0.570593862 |
| H | 1.968205773 | 0.398215984 | -1.997445314 |

**3b** *($C_1$, $N_{imag}$ = 0)*

| | | | |
|---|---|---|---|
| Au | 0.064718564 | -0.698200876 | -0.284642004 |
| C | -2.252496561 | -1.445175415 | 1.486676622 |
| C | 0.158797114 | 1.405675244 | -0.180657439 |
| C | 0.930352824 | 3.511145611 | 0.053999897 |
| C | -0.425952353 | 3.580346897 | -0.034384210 |
| H | 1.677868818 | 4.285812027 | 0.181104549 |
| H | -1.100277153 | 4.429062923 | -0.029076136 |
| C | 2.603246820 | 1.652251109 | 0.043456472 |
| C | 3.592950746 | 2.195858831 | -0.773385178 |
| C | 2.883006866 | 0.609376516 | 0.928656732 |
| C | 4.883841153 | 1.675614131 | -0.706520346 |
| C | 4.175068559 | 0.089198403 | 0.974307006 |
| C | 5.173576634 | 0.620644991 | 0.158555901 |
| H | 5.663902526 | 2.092179276 | -1.344499438 |
| H | 4.403149859 | -0.722722166 | 1.665581708 |
| H | 6.184791536 | 0.214826638 | 0.202207787 |
| C | -2.250665475 | 1.887161558 | -0.290588684 |
| C | -3.167234613 | 2.333315923 | 0.661256673 |
| C | -2.640413049 | 1.044087133 | -1.333556693 |
| C | -4.494953729 | 1.918672062 | 0.567260786 |
| C | -3.968399205 | 0.627147654 | -1.408816424 |
| C | -4.894353158 | 1.062746288 | -0.460123237 |
| H | -5.218468894 | 2.262358784 | 1.307466059 |
| H | -4.282081735 | -0.025273099 | -2.224637548 |
| H | -5.934661357 | 0.742171912 | -0.527868950 |
| N | 1.268232159 | 2.172971608 | -0.029421785 |
| N | -0.879061933 | 2.282519935 | -0.182479871 |
| C | 0.158767918 | -2.723303559 | -0.700469019 |
| C | -0.804660718 | -1.139268345 | 1.637752224 |
| F | 0.467495340 | -2.750791205 | -2.025646069 |
| F | -0.970555753 | -3.441844590 | -0.539016665 |
| F | 1.140367097 | -3.360513677 | -0.044468476 |
| F | -0.080156751 | -2.115268607 | 2.173360204 |
| F | -0.564665235 | -0.014920750 | 2.331095750 |
| H | -2.398370085 | -2.346954938 | 0.887558292 |
| H | -2.650886261 | -1.617195730 | 2.498547127 |
| H | -2.781438940 | -0.598351611 | 1.036747466 |
| H | 2.107854294 | 0.239636505 | 1.603729953 |
| H | 3.350471665 | 3.002937492 | -1.467095948 |
| H | -2.839259423 | 2.982960384 | 1.475016038 |
| H | -1.914793923 | 0.745059325 | -2.093200249 |

**TS$^3$** *($C_1$, $N_{imag}$ = 1)*

| | | | |
|---|---|---|---|
| Au | 0.202340414 | -1.481236156 | -0.122799903 |
| C | -0.111357926 | -0.164752129 | 3.015446337 |
| C | -0.042428995 | 0.145175912 | -1.422407003 |
| C | 0.339067541 | 2.204687158 | -2.287457068 |
| C | -1.001923518 | 2.010826825 | -2.280346069 |
| H | 0.935463385 | 3.052432366 | -2.599256093 |
| H | -1.818323731 | 2.648078679 | -2.596825090 |
| C | 2.302739004 | 0.899908532 | -1.500453011 |
| C | 2.933742338 | -0.306963410 | -1.802526033 |
| C | 2.995671803 | 1.954168775 | -0.904417963 |
| C | 4.283809483 | -0.461075098 | -1.495335010 |
| C | 4.348467947 | 1.788980090 | -0.616905941 |
| C | 4.992760282 | 0.586020151 | -0.907649961 |
| H | 4.783460742 | -1.402892052 | -1.726868027 |
| H | 4.896217793 | 2.603311284 | -0.140078905 |
| H | 6.051072414 | 0.462290396 | -0.671847944 |
| C | -2.507180199 | 0.212973326 | -1.463413006 |
| C | -3.447014466 | 1.038018163 | -0.843834958 |
| C | -2.795689905 | -1.116961847 | -1.769874029 |
| C | -4.702406441 | 0.514919823 | -0.542407934 |
| C | -4.051251878 | -1.628514186 | -1.449145006 |
| C | -5.006120145 | -0.813371351 | -0.841835959 |
| H | -5.440380649 | 1.149502697 | -0.049517898 |
| H | -4.285307647 | -2.667517318 | -1.685889023 |
| H | -5.990220100 | -1.216719616 | -0.597551940 |
| N | 0.909936859 | 1.056689209 | -1.770026030 |
| N | -1.217186229 | 0.746257674 | -1.760229028 |
| C | 0.450420793 | -2.987702209 | 1.256686204 |
| C | 0.007416926 | 0.489416950 | 1.725536236 |
| F | 0.640004100 | -4.212305259 | 0.691927157 |
| F | -0.611041250 | -3.143594477 | 2.115897270 |
| F | 1.535150830 | -2.799349933 | 2.086242267 |
| F | 1.127436900 | 0.952177253 | 1.325707206 |
| F | -1.022174247 | 0.895712733 | 1.095741188 |
| H | 0.764906287 | -0.785342965 | 3.219339352 |
| H | -0.155178130 | 0.671587922 | 3.736348393 |
| H | -1.036014857 | -0.743013394 | 3.072188341 |
| H | 2.455241547 | 2.857655714 | -0.614415940 |
| H | 2.371079488 | -1.107790607 | -2.285923068 |
| H | -3.169767689 | 2.054051309 | -0.552775935 |
| H | -2.044867697 | -1.733522712 | -2.267534069 |
| B | -0.526065868 | 3.634002062 | 1.436066216 |
| F | 0.425239285 | 3.298880265 | 0.423565138 |
| F | -1.816745894 | 3.331426730 | 0.945796179 |
| F | -0.405439172 | 4.945204192 | 1.830480245 |
| F | -0.256156636 | 2.753001060 | 2.570787304 |

**6** *($C_1$, $N_{imag}$ = 0)*

| | | | |
|---|---|---|---|
| Au | -0.002955584 | 0.888883896 | 0.000583462 |
| C | 0.008526240 | -1.178902155 | 0.000472365 |
| C | -0.661116822 | -3.355193413 | -0.013161564 |
| C | 0.694470843 | -3.350162732 | 0.006302664 |
| H | -1.371696482 | -4.172651018 | -0.045529884 |
| H | 1.411176100 | -4.162368210 | 0.035880468 |
| N | -1.063007257 | -2.027833195 | -0.022179965 |
| N | 1.086339296 | -2.019878370 | 0.020103562 |
| C | -0.022150475 | 2.946955963 | -0.001106356 |
| F | -0.917712722 | 3.501072314 | -0.887919201 |
| F | -0.350371746 | 3.507505025 | 1.211051430 |
| C | 2.452126260 | -1.599982018 | 0.038613267 |
| C | 3.367060033 | -2.239804641 | -0.798166268 |
| C | 2.858983717 | -0.572833758 | 0.890680776 |
| H | 3.028126170 | -3.027149150 | -1.474359181 |
| H | 2.133014275 | -0.094678622 | 1.549476791 |
| C | 4.702088548 | -1.842180295 | -0.784068510 |
| C | 4.193242506 | -0.174244389 | 0.884727913 |
| H | 5.417235971 | -2.336662911 | -1.443174384 |
| H | 4.510767620 | 0.634822264 | 1.543764317 |

| | | | |
|---|---|---|---|
| C | 5.116209005 | -0.806416290 | 0.052156373 |
| H | 6.160453299 | -0.490273981 | 0.054293983 |
| C | -2.432196164 | -1.618646247 | -0.038862938 |
| C | -2.848132027 | -0.591547911 | -0.886728489 |
| C | -3.341465248 | -2.269595336 | 0.795547359 |
| H | -2.127261404 | -0.103384633 | -1.543814038 |
| H | -2.995553860 | -3.056583719 | 1.468617861 |
| C | -4.185888953 | -0.204707767 | -0.878920224 |
| C | -4.679911830 | -1.883582303 | 0.783339701 |
| H | -4.510248333 | 0.604177048 | -1.534857295 |
| H | -5.390534216 | -2.386898681 | 1.440653580 |
| C | -5.103216328 | -0.848231897 | -0.048793555 |
| H | -6.150231976 | -0.541349844 | -0.049664021 |
| F | 1.183989342 | 3.522489964 | -0.328136888 |

**4·BF$_3$** *($C_1$, $N_{imag}$ = 0)*

| | | | |
|---|---|---|---|
| Au | -0.027804727 | -0.510107443 | 0.146558483 |
| C | 0.999962927 | -1.401301806 | 2.922675898 |
| C | -0.480492222 | 1.409776907 | 0.006110813 |
| C | -0.385840500 | 3.617424516 | -0.352489563 |
| C | -1.687937071 | 3.289660140 | -0.154035988 |
| H | 0.090896576 | 4.565158220 | -0.570710255 |
| H | -2.586135815 | 3.894749151 | -0.132149800 |
| N | 0.347973259 | 2.443892277 | -0.257834927 |
| N | -1.729188697 | 1.923517188 | 0.071344074 |
| C | -0.830561997 | -0.854083317 | -1.805955081 |
| C | 0.757049042 | -0.177032430 | 2.100228062 |
| F | 0.072533012 | -1.428410159 | -2.633611995 |
| F | -1.251804962 | 0.288219267 | -2.459054407 |
| F | -1.912937638 | -1.672081714 | -1.770246464 |
| F | 1.924949703 | 0.547433626 | 1.978922147 |
| F | -0.112561409 | 0.675852884 | 2.799025701 |
| H | 0.065843218 | -1.960102080 | 3.056259582 |
| H | 1.723271940 | -2.060210064 | 2.430853382 |
| H | 1.384299293 | -1.101781275 | 3.908722045 |
| F | 0.340319826 | -2.582586989 | 0.283855247 |
| B | 1.823015432 | -2.972798477 | -0.204355786 |
| F | 1.647941124 | -3.739447736 | -1.306526277 |
| F | 2.360801972 | -1.702189010 | -0.457757845 |
| F | 2.380024219 | -3.588637226 | 0.881125343 |
| C | -2.919893907 | 1.142009314 | 0.228819382 |
| C | -3.918868664 | 1.245141679 | -0.736858120 |
| C | -3.036207834 | 0.272458536 | 1.312481161 |
| H | -3.779022347 | 1.903945621 | -1.595429765 |
| H | -2.242893920 | 0.229203855 | 2.060527861 |
| C | -5.060109761 | 0.457516830 | -0.612352662 |
| C | -4.178272346 | -0.519151162 | 1.415257326 |
| H | -5.842665956 | 0.520888452 | -1.369445716 |
| H | -4.277859186 | -1.208739576 | 2.254422755 |
| C | -5.187991084 | -0.427089629 | 0.458147251 |
| H | -6.077863388 | -1.052327508 | 0.543903453 |
| C | 1.765397576 | 2.346047108 | -0.447423543 |
| C | 2.282987939 | 1.344423554 | -1.265031441 |
| C | 2.594753710 | 3.247849819 | 0.216672680 |
| H | 1.623354623 | 0.662197159 | -1.803545361 |
| H | 2.164267182 | 4.004853670 | 0.874572192 |
| C | 3.665033350 | 1.222644883 | -1.384343093 |
| C | 3.973123260 | 3.130232682 | 0.067200838 |
| H | 4.073817705 | 0.418800308 | -1.996747736 |
| H | 4.631892911 | 3.823813719 | 0.591544905 |
| C | 4.508666770 | 2.112721428 | -0.723328249 |
| H | 5.590613805 | 2.011293612 | -0.819919951 |

**4** *($C_1$, $N_{imag}$ = 0)*

| | | | |
|---|---|---|---|
| Au | -0.018429380 | -0.892583195 | 0.045543471 |
| C | -2.010181017 | -1.974362158 | -2.007236664 |
| C | 0.014546930 | 1.093739760 | -0.095908749 |
| C | -0.641566824 | 3.244514203 | -0.146484980 |
| C | 0.701542942 | 3.220564186 | -0.341462499 |
| H | -1.344044293 | 4.066908227 | -0.085790909 |
| H | 1.416089341 | 4.015763278 | -0.516206592 |
| N | -1.045706760 | 1.927338975 | 0.011281515 |
| N | 1.086842247 | 1.888347587 | -0.314055845 |
| C | 0.820334762 | -0.793602035 | 2.001401136 |
| C | -0.831447543 | -1.060304945 | -1.904841348 |
| F | 0.164507765 | -1.564307322 | 2.905256774 |
| F | 0.796903217 | 0.485465079 | 2.543057707 |
| F | 2.124535083 | -1.170655679 | 2.044239664 |
| F | -1.168555634 | 0.188482893 | -2.443124748 |
| F | 0.186585337 | -1.519300633 | -2.733206037 |
| H | -1.740177417 | -2.954516191 | -1.598504973 |
| H | -2.844388468 | -1.568147445 | -1.419658165 |
| H | -2.324183102 | -2.076173177 | -3.056619756 |
| F | -0.085285983 | -2.871738661 | 0.155605762 |
| C | 2.427419529 | 1.403581803 | -0.437436271 |
| C | 3.417692279 | 1.942285010 | 0.381562945 |
| C | 2.703686800 | 0.377227727 | -1.340332612 |
| H | 3.163456187 | 2.720396301 | 1.103511087 |
| H | 1.913922310 | -0.022427522 | -1.980240915 |
| C | 4.712808176 | 1.438201092 | 0.294825963 |
| C | 4.000642721 | -0.127186906 | -1.403730417 |
| H | 5.492909587 | 1.844517343 | 0.940038683 |
| H | 4.223775562 | -0.938517992 | -2.097497613 |
| C | 5.003157017 | 0.401119449 | -0.591210676 |
| H | 6.015897897 | -0.001236794 | -0.644728547 |
| C | -2.385708583 | 1.487253701 | 0.245891854 |
| C | -2.648816416 | 0.664382343 | 1.341320824 |
| C | -3.394372221 | 1.870711151 | -0.635351764 |
| H | -1.842607278 | 0.396437610 | 2.027016913 |
| H | -3.150924979 | 2.485952767 | -1.503090801 |
| C | -3.949595833 | 0.207977043 | 1.543361068 |
| C | -4.693296205 | 1.419805594 | -0.412366379 |
| H | -4.162679758 | -0.441222471 | 2.393474248 |
| H | -5.488724377 | 1.708165654 | -1.101094811 |
| C | -4.970333391 | 0.585742773 | 0.671160998 |
| H | -5.987635492 | 0.226956925 | 0.835441598 |

**TS$^4$** *($C_1$, $N_{imag}$ = 1)*

| | | | |
|---|---|---|---|
| Au | -0.060681857 | 0.749829467 | 0.145372304 |
| C | 2.209605073 | 1.236227138 | -1.993733336 |
| C | -0.078884236 | -1.251736910 | -0.090360361 |
| C | 0.499470644 | -3.450075164 | 0.093790973 |
| C | -0.844514591 | -3.398088537 | -0.065373524 |
| H | 1.170896529 | -4.289951262 | 0.228998827 |
| H | -1.583419045 | -4.187330972 | -0.136929059 |
| N | 0.955158997 | -2.137877472 | 0.091946584 |
| N | -1.187994552 | -2.057129337 | -0.177974120 |
| C | -0.448412482 | 1.568401391 | 2.125957675 |
| C | 0.793867311 | 1.483086594 | -2.348011837 |
| F | -0.613613438 | 2.920134206 | 2.179779346 |
| F | 0.598483128 | 1.306795284 | 3.001365835 |
| F | -1.553069793 | 1.043944890 | 2.750409489 |
| F | 0.115284843 | 0.469345704 | -2.905115632 |
| F | 0.574567983 | 2.531808785 | -3.107458957 |
| H | 2.511711676 | 1.928989246 | -1.201910242 |
| H | 2.347312932 | 0.204893735 | -1.655660587 |
| H | 2.834324940 | 1.427938784 | -2.883208837 |

| | | | |
|---|---|---|---|
| F | 0.192359066 | 2.700139195 | -0.836744242 |
| C | -2.524599433 | -1.581152579 | -0.304900755 |
| C | -3.536272026 | -2.192466752 | 0.437318576 |
| C | -2.812390596 | -0.512485450 | -1.155847865 |
| H | -3.292414603 | -3.005906134 | 1.123094090 |
| H | -2.015844828 | -0.060679470 | -1.747372407 |
| C | -4.844850426 | -1.729449089 | 0.324676298 |
| C | -4.122018815 | -0.049060840 | -1.247898512 |
| H | -5.633555004 | -2.201773355 | 0.912276251 |
| H | -4.345072391 | 0.790544047 | -1.907678463 |
| C | -5.140355305 | -0.654811744 | -0.512624758 |
| H | -6.164424509 | -0.286521237 | -0.589335420 |
| C | 2.319691350 | -1.759016344 | 0.250129272 |
| C | 2.665682755 | -0.777341191 | 1.182209280 |
| C | 3.292808702 | -2.369914378 | -0.543481677 |
| H | 1.900933316 | -0.327425752 | 1.818278693 |
| H | 2.999852409 | -3.128225793 | -1.272745194 |
| C | 3.999264515 | -0.388278959 | 1.290103668 |
| C | 4.624877740 | -1.980809669 | -0.414624516 |
| H | 4.270715690 | 0.381534642 | 2.014203558 |
| H | 5.386493154 | -2.452075310 | -1.038137959 |
| C | 4.978543734 | -0.983195173 | 0.493917411 |
| H | 6.021015729 | -0.673998213 | 0.586308886 |

**TS[5]** *($C_1$, $N_{imag}$ = 1)*

| | | | |
|---|---|---|---|
| Au | 0.068088112 | -0.845342240 | -0.038888414 |
| C | -0.252482645 | -2.725602633 | 1.323105919 |
| C | 0.039982785 | 1.294871000 | -0.064046256 |
| C | 0.732690596 | 3.454809993 | -0.268318465 |
| C | -0.610756828 | 3.442369507 | -0.450443032 |
| H | 1.443018886 | 4.273147461 | -0.256785669 |
| H | -1.309764921 | 4.240891943 | -0.670716256 |
| C | 2.463428025 | 1.717258010 | 0.146857707 |
| C | 3.464433743 | 2.282861577 | -0.643725518 |
| C | 2.769140167 | 0.740217353 | 1.095313243 |
| C | 4.782945863 | 1.864212061 | -0.483111709 |
| C | 4.089676290 | 0.320482479 | 1.236043788 |
| C | 5.098119748 | 0.879633344 | 0.452185620 |
| H | 5.564462712 | 2.299934380 | -1.107427036 |
| H | 4.330054129 | -0.445488885 | 1.974882741 |
| H | 6.130591297 | 0.546931770 | 0.568965578 |
| C | -2.359350830 | 1.673567623 | -0.508392810 |
| C | -3.385309171 | 2.320856477 | 0.178518103 |
| C | -2.626834695 | 0.594543250 | -1.351493066 |
| C | -4.695334511 | 1.871185612 | 0.030856035 |
| C | -3.939235315 | 0.145969920 | -1.480026230 |
| C | -4.973190096 | 0.779171747 | -0.790626974 |
| H | -5.499821330 | 2.368416340 | 0.575045296 |
| H | -4.151179598 | -0.701154711 | -2.134072011 |
| H | -5.999164254 | 0.422784515 | -0.896019624 |
| N | 1.113827689 | 2.140566915 | -0.033428337 |
| N | -1.014252009 | 2.119401487 | -0.335358176 |
| C | 0.668978904 | -1.950389947 | -1.756510775 |
| C | -0.906942970 | -0.998774130 | 2.221814769 |
| F | -0.297046029 | -1.959148936 | -2.741541431 |
| F | 0.957672266 | -3.284171048 | -1.553219810 |
| F | 1.787602256 | -1.450720140 | -2.371979095 |
| F | -1.397631961 | -1.735761131 | 3.246665044 |
| F | -1.972145958 | -0.254305804 | 1.818454253 |
| F | 0.000744409 | -0.170052082 | 2.809985544 |
| H | 0.289945115 | -2.892570602 | 2.257602772 |
| H | -1.262997807 | -3.138700365 | 1.375194560 |
| H | 0.300033994 | -3.191313194 | 0.498349323 |
| H | -3.150974811 | 3.150717822 | 0.848115515 |
| H | -1.816942494 | 0.116466042 | -1.905763842 |
| H | 1.978432213 | 0.331693828 | 1.724819540 |
| H | 3.205807062 | 3.024474614 | -1.401783278 |

**TS[6]** *($C_1$, $N_{imag}$ = 1)*

| | | | |
|---|---|---|---|
| Au | -0.152950979 | -0.930759608 | 0.195580513 |
| C | 1.493424738 | -2.504384640 | -0.165380657 |
| C | 0.032082448 | 1.206025860 | 0.047719704 |
| C | 0.759170371 | 3.343205638 | 0.163055585 |
| C | -0.581710585 | 3.379624712 | -0.047508676 |
| H | 1.484668358 | 4.137730622 | 0.293905558 |
| H | -1.264501285 | 4.212158460 | -0.172184814 |
| C | 2.441915922 | 1.533809683 | 0.486698623 |
| C | 3.509689193 | 2.068724203 | -0.231607758 |
| C | 2.641772760 | 0.535805062 | 1.440480369 |
| C | 4.792553627 | 1.576851135 | -0.005507330 |
| C | 3.928979273 | 0.043244746 | 1.649941562 |
| C | 5.002928830 | 0.558460680 | 0.924916401 |
| H | 5.631410990 | 1.984732418 | -0.570474548 |
| H | 4.095274139 | -0.731157908 | 2.400639732 |
| H | 6.009645667 | 0.174954379 | 1.094719675 |
| C | -2.377222977 | 1.658252995 | -0.258798157 |
| C | -3.324697749 | 2.149730365 | 0.638976390 |
| C | -2.733434853 | 0.771074070 | -1.274658239 |
| C | -4.650211477 | 1.736993442 | 0.517444395 |
| C | -4.061635389 | 0.361108000 | -1.380367337 |
| C | -5.018288719 | 0.840608887 | -0.486159460 |
| H | -5.396704740 | 2.114711664 | 1.217135417 |
| H | -4.350050975 | -0.325823620 | -2.177052559 |
| H | -6.057283209 | 0.521381765 | -0.576309119 |
| N | 1.116712419 | 2.005354074 | 0.228790847 |
| N | -1.009769015 | 2.064099268 | -0.115175377 |
| C | 1.141676906 | -1.140433646 | -1.833705723 |
| C | -1.494006410 | -1.785463401 | 1.405039766 |
| F | 0.089039278 | -0.574478319 | -2.472881528 |
| F | 1.508639717 | -2.160189395 | -2.605308457 |
| F | 2.138195672 | -0.261427881 | -1.787713780 |
| F | -2.751780058 | -1.961864896 | 1.133286547 |
| F | -1.318502505 | -2.055951542 | 2.666999687 |
| H | 2.502602837 | -2.277553738 | -0.511618726 |
| H | 1.481149985 | -2.533415114 | 0.932275224 |
| H | 1.062859029 | -3.393117139 | -0.628335905 |
| H | -3.022411130 | 2.835840351 | 1.432496725 |
| H | -1.982206729 | 0.431965264 | -1.988167582 |
| H | 1.800207644 | 0.179276164 | 2.039113916 |
| H | 3.331618604 | 2.837933416 | -0.985230775 |

**5** *($C_1$, $N_{imag}$ = 0)*

| | | | |
|---|---|---|---|
| Au | 0.000916787 | 0.995852659 | -0.003597611 |
| C | -0.001813784 | -1.052250952 | -0.008399779 |
| C | 0.679049665 | -3.203035094 | -0.013710625 |
| C | -0.683004022 | -3.202740194 | -0.023285373 |
| H | 1.392536561 | -4.018850778 | 0.005368811 |
| H | -1.396955530 | -4.017992829 | -0.048872360 |
| N | 1.078081115 | -1.883056158 | -0.000568377 |
| N | -1.081685801 | -1.882570151 | -0.023611842 |
| C | 0.004813369 | 2.970265760 | -0.002251337 |
| F | 1.044846312 | 3.721642001 | -0.118647687 |
| F | -1.031983876 | 3.726140733 | 0.114052294 |
| C | -2.449152178 | -1.450995063 | -0.036028243 |
| C | -3.332256030 | -1.982118737 | 0.903001562 |
| C | -2.873306968 | -0.523934574 | -0.988903847 |
| H | -2.976491684 | -2.697286480 | 1.646911451 |
| H | -2.175075421 | -0.160311938 | -1.745600140 |

| | | | |
|---|---|---|---|
| C | -4.662018014 | -1.567430648 | 0.890425543 |
| C | -4.204122030 | -0.110819767 | -0.983664156 |
| H | -5.358476394 | -1.973961211 | 1.624427710 |
| H | -4.547328720 | 0.606459120 | -1.730122716 |
| C | -5.097012127 | -0.630457938 | -0.046701291 |
| H | -6.139167938 | -0.309153911 | -0.051833900 |
| C | 2.445264519 | -1.452299226 | 0.031165541 |
| C | 2.855204311 | -0.531377293 | 0.996186966 |
| C | 3.342815836 | -1.979074777 | -0.896433885 |
| H | 2.145022006 | -0.171928192 | 1.743719222 |
| H | 2.998628057 | -2.690001853 | -1.649815846 |
| C | 4.186051622 | -0.119349742 | 1.015008780 |
| C | 4.672689455 | -1.565936039 | -0.859580839 |
| H | 4.517942168 | 0.593081868 | 1.771146854 |
| H | 5.380560918 | -1.969603002 | -1.584171561 |
| C | 5.093459897 | -0.634818337 | 0.089819965 |
| H | 6.135869470 | -0.315235457 | 0.113779946 |

**$CH_3CF_3$** *($C_{3v}$, $N_{imag}$ = 0)*

| | | | |
|---|---|---|---|
| C | 0.000000000 | 0.000000000 | 1.469027196 |
| H | -0.892687411 | 0.515393317 | 1.837422558 |
| H | 0.000000000 | -1.030786633 | 1.837422558 |
| H | 0.892687411 | 0.515393317 | 1.837422558 |
| C | 0.000000000 | 0.000000000 | -0.023087215 |
| F | 0.000000000 | 1.252975365 | -0.525478058 |
| F | 1.085108493 | -0.626487680 | -0.525478058 |
| F | -1.085108493 | -0.626487680 | -0.525478058 |

**$BF_3$** *($D_{3h}$, $N_{imag}$ = 0)*

| | | | |
|---|---|---|---|
| B | 0.000000000 | 0.000000000 | 0.000000000 |
| F | 0.000000000 | 1.320701856 | 0.000000000 |
| F | -1.143761356 | -0.660350928 | 0.000000000 |
| F | 1.143761356 | -0.660350928 | 0.000000000 |

**$BF_4^-$** *($T_d$, $N_{imag}$ = 0)*

| | | | |
|---|---|---|---|
| B | 0.000000000 | 0.000000000 | 0.000000000 |
| F | 0.818207544 | 0.818207544 | 0.818207544 |
| F | -0.818207544 | -0.818207544 | 0.818207544 |
| F | 0.818207544 | -0.818207544 | -0.818207544 |
| F | -0.818207544 | 0.818207544 | -0.818207544 |

## 4.5.7 NMR Spectra of New Compounds

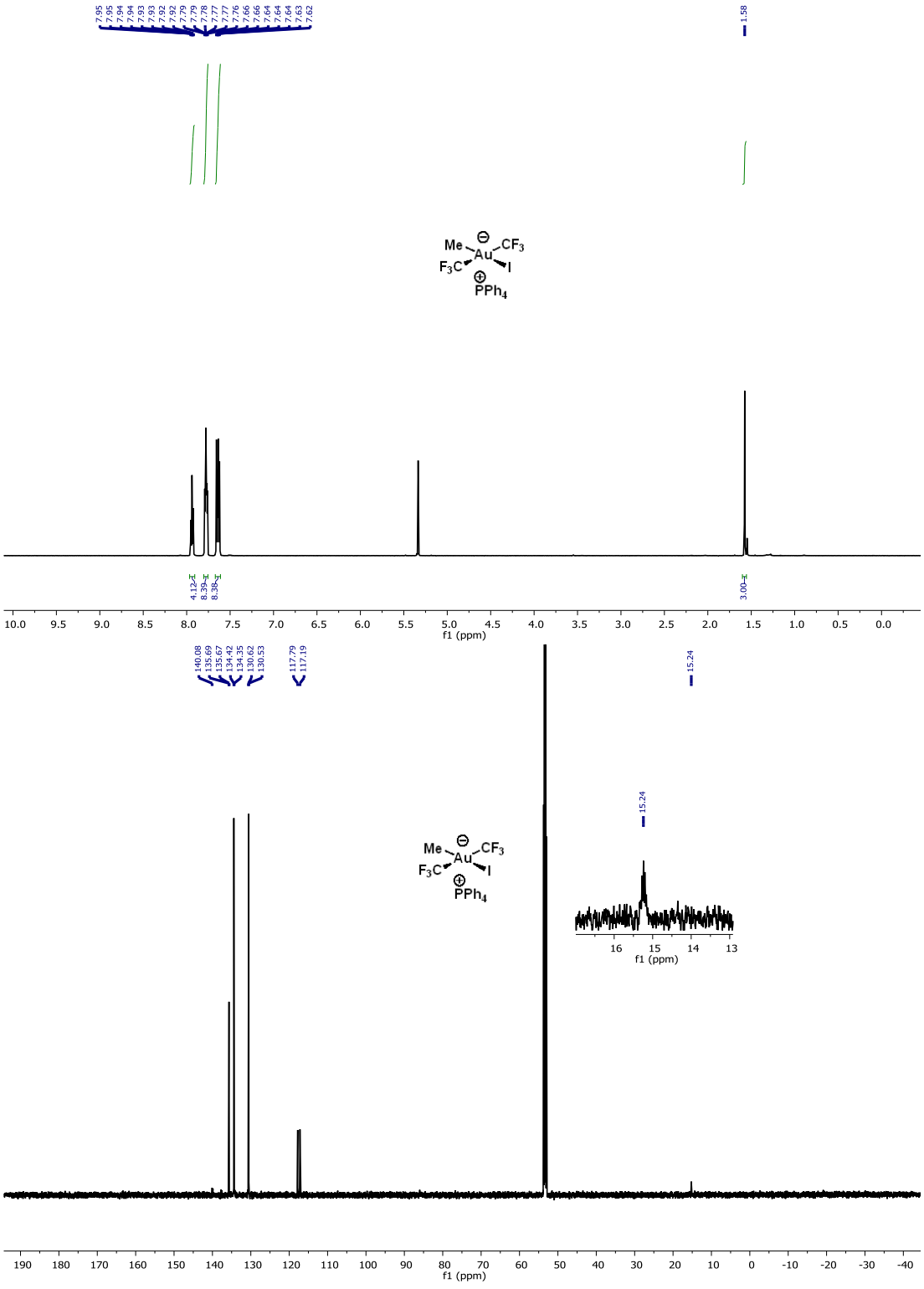

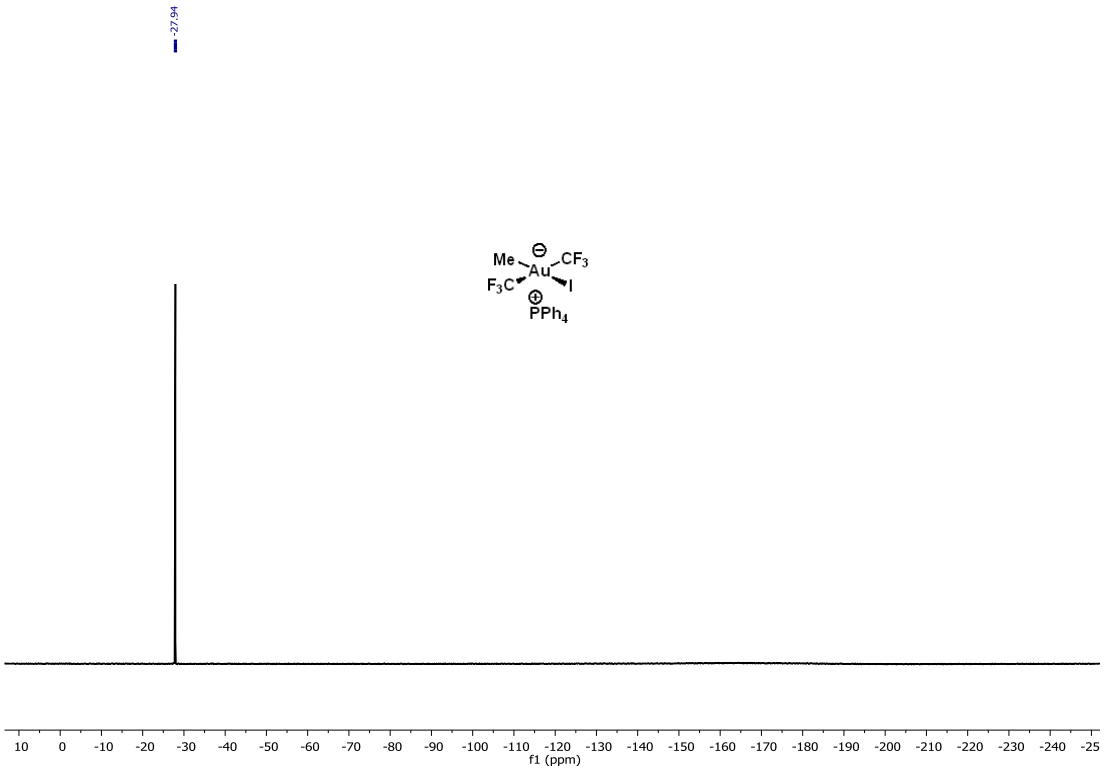
-27.94
Me
Au
CF3
F3C
I
PPh4
10 0 -10 -20 -30 -40 -50 -60 -70 -80 -90 -100 -110 -120 -130 -140 -150 -160 -170 -180 -190 -200 -210 -220 -230 -240 -25
f1 (ppm)

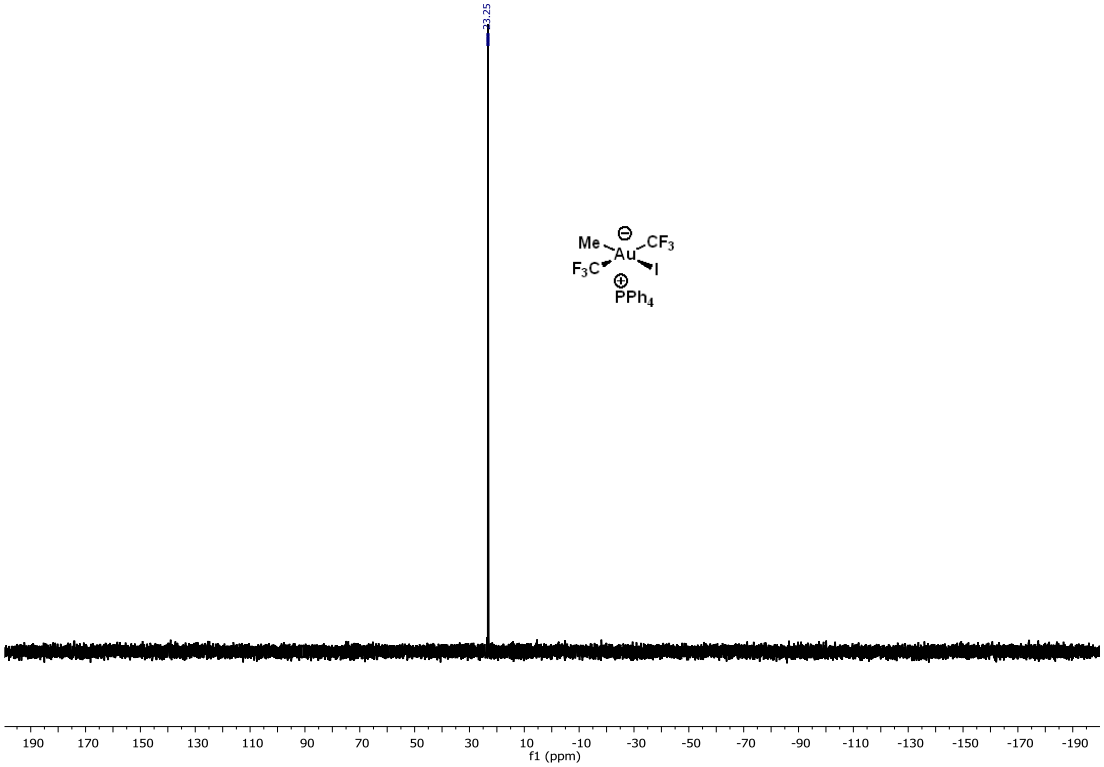
33.25
Me
Au
CF3
F3C
I
PPh4
190 170 150 130 110 90 70 50 30 10 -10 -30 -50 -70 -90 -110 -130 -150 -170 -190
f1 (ppm)

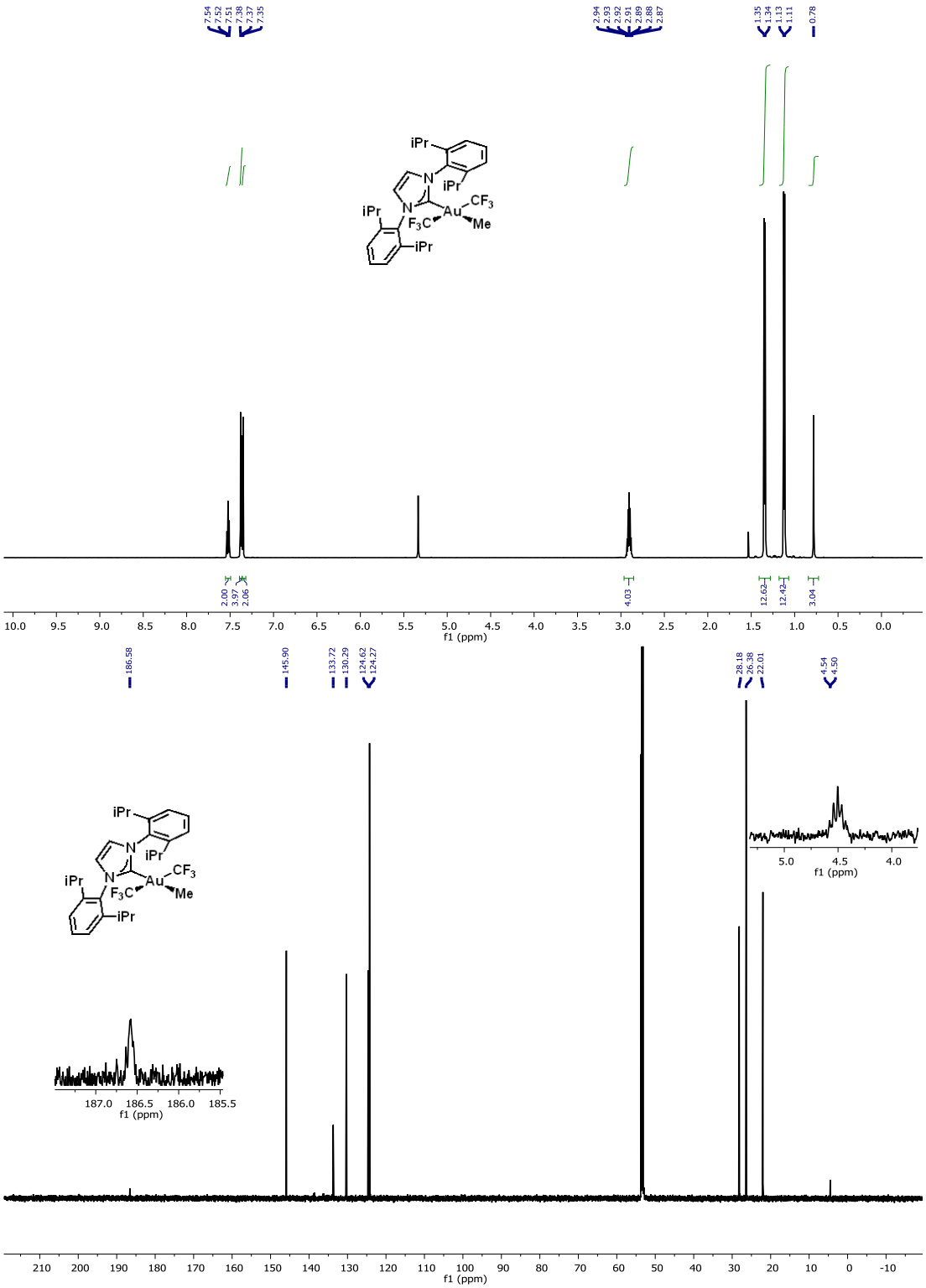
7.54
7.52
7.51
7.38
7.37
7.36
7.35
2.94
2.93
2.92
2.91
2.89
2.88
2.87
1.35
1.34
1.13
1.11
0.78
iPr
iPr
iPr
iPr
N
N
Au
CF3
F3C
Me
2.00
3.97
2.06
4.03
12.62
12.42
3.04
f1 (ppm)
186.58
145.90
133.72
130.29
124.62
124.27
28.18
26.38
22.01
4.54
4.50
187.0
186.5
186.0
185.5
5.0
4.5
4.0
210
200
190
180
170
160
150
140
130
120
110
100
90
80
70
60
50
40
30
20
10
0
-10

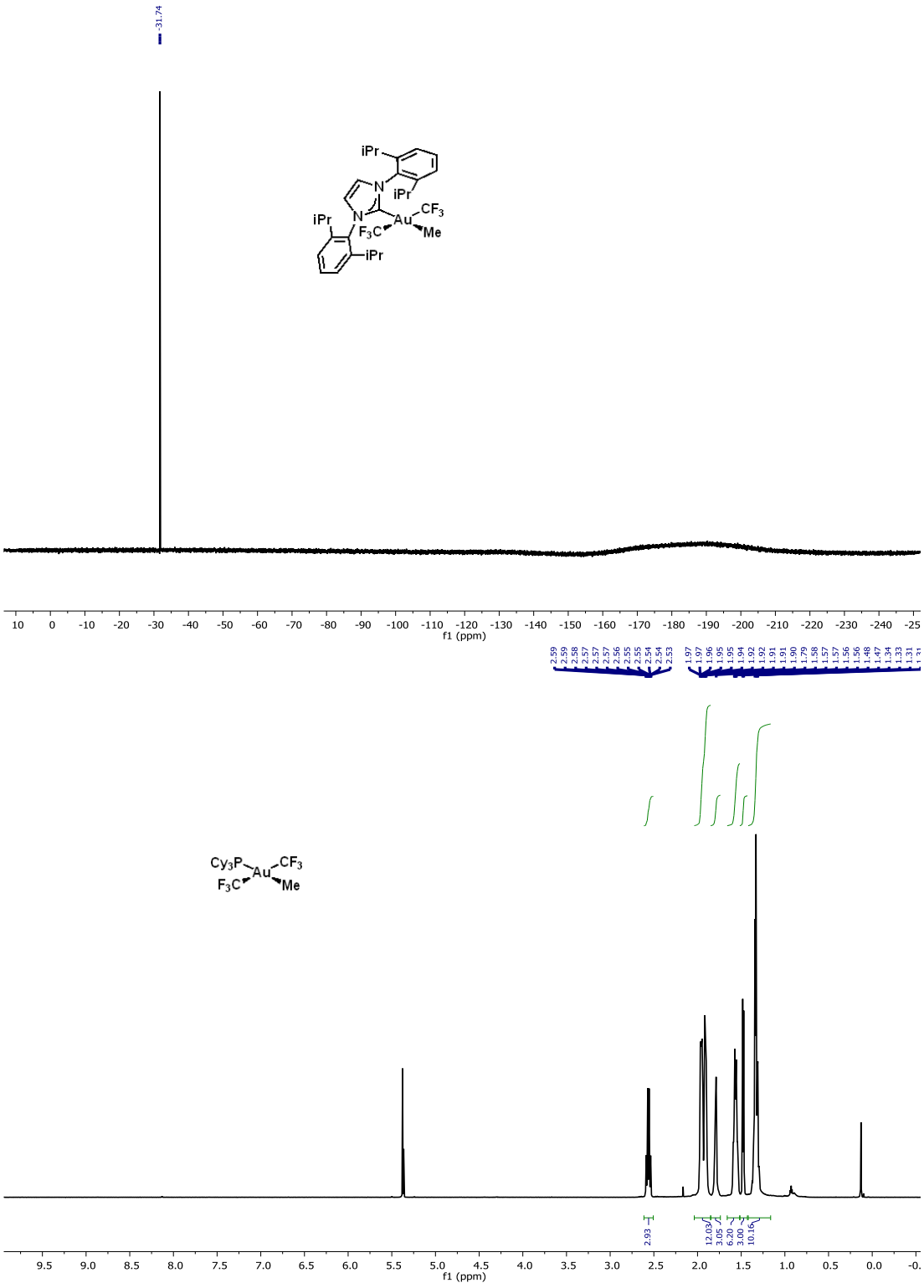
-31.74
iPr
iPr
iPr
iPr
N
N
Au
CF3
F3C
Me
f1 (ppm)
Cy3P
Au
CF3
F3C
Me
2.93
12.03
3.05
6.20
3.00
10.16
f1 (ppm)

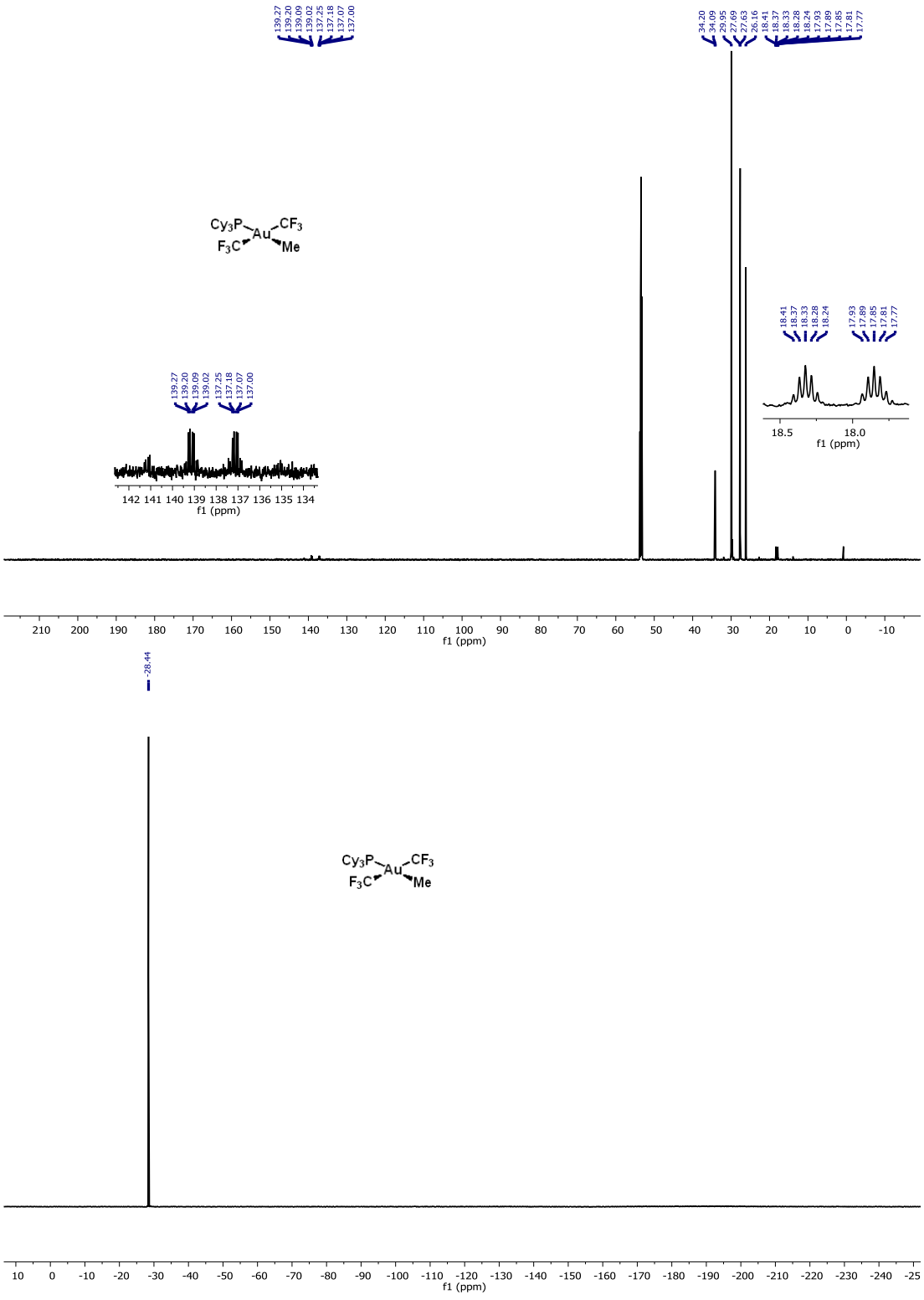
139.27
139.20
139.09
139.02
137.25
137.18
137.07
137.00
34.20
34.09
29.95
27.69
27.63
26.16
18.41
18.37
18.33
18.28
18.24
17.93
17.89
17.85
17.81
17.77
Cy3P
Au
CF3
F3C
Me
142 141 140 139 138 137 136 135 134
f1 (ppm)
18.5
18.0
f1 (ppm)
210 200 190 180 170 160 150 140 130 120 110 100 90 80 70 60 50 40 30 20 10 0 -10
f1 (ppm)
-28.44
10 0 -10 -20 -30 -40 -50 -60 -70 -80 -90 -100 -110 -120 -130 -140 -150 -160 -170 -180 -190 -200 -210 -220 -230 -240 -25
f1 (ppm)

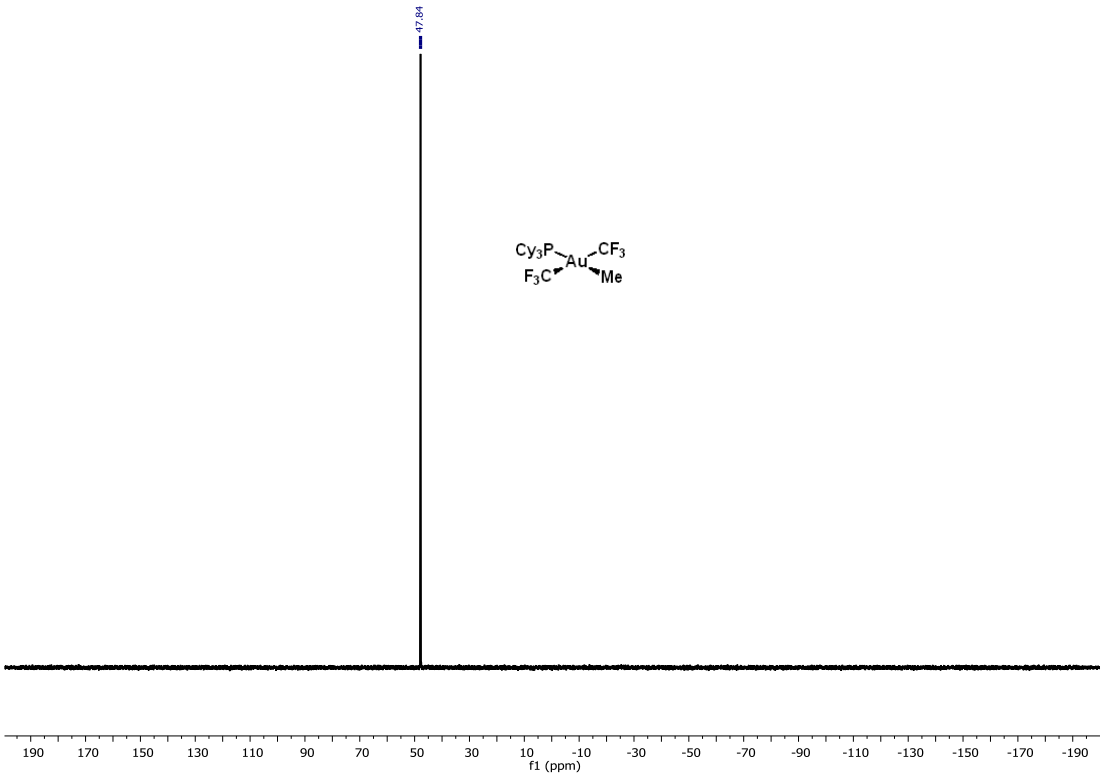
47.84
Cy3P
Au
CF3
F3C
Me
190 170 150 130 110 90 70 50 30 10 -10 -30 -50 -70 -90 -110 -130 -150 -170 -190
f1 (ppm)

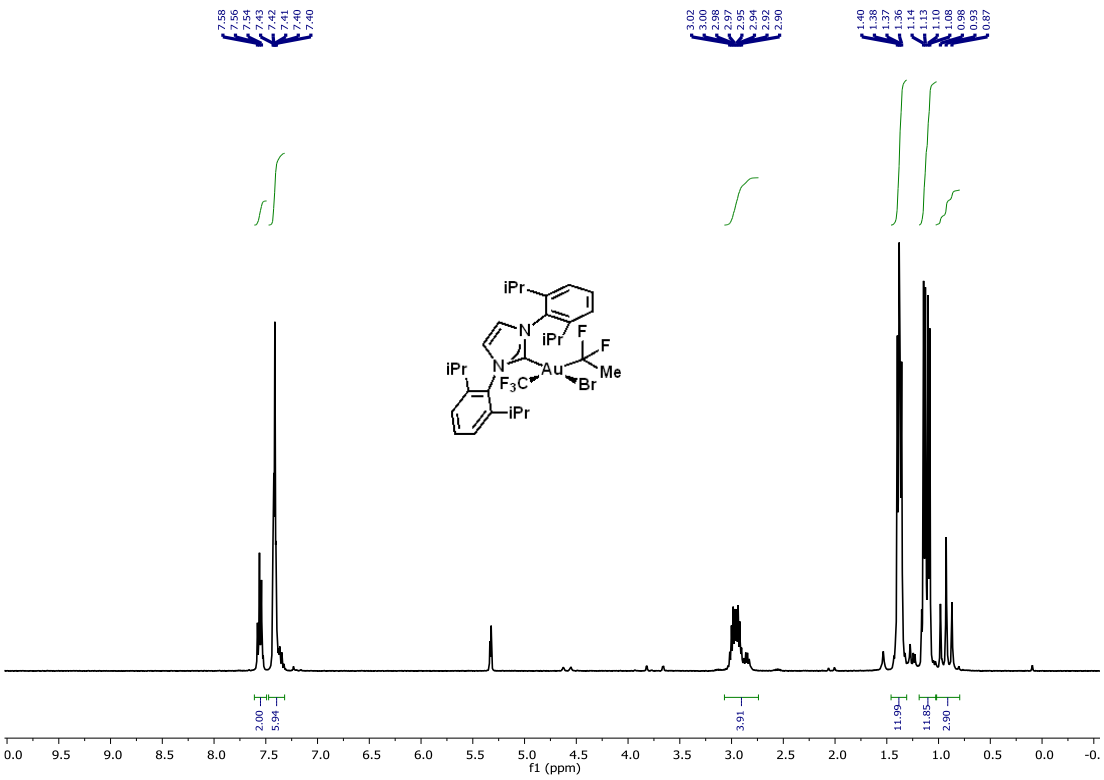
7.58 7.56 7.54 7.43 7.42 7.41 7.40 7.40
3.02 3.00 2.98 2.97 2.95 2.94 2.92 2.90
1.40 1.38 1.37 1.36 1.14 1.13 1.10 1.08 0.98 0.93 0.87
iPr
N
iPr
F
F
Me
Au
Br
F3C
iPr
iPr
2.00
5.94
3.91
11.99
11.85
2.90
0.0 9.5 9.0 8.5 8.0 7.5 7.0 6.5 6.0 5.5 5.0 4.5 4.0 3.5 3.0 2.5 2.0 1.5 1.0 0.5 0.0
f1 (ppm)

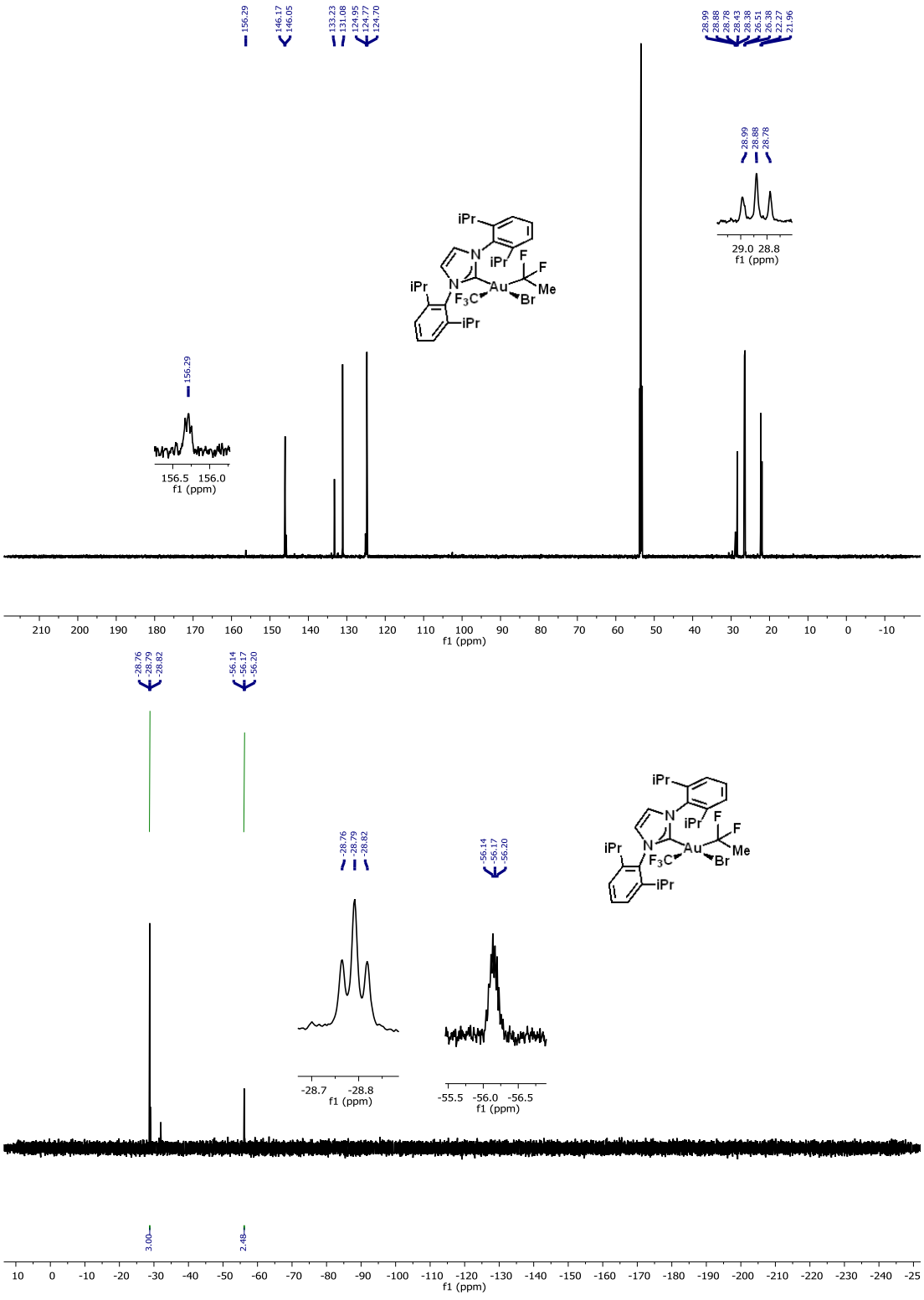
156.29
146.17
146.05
133.23
131.08
124.95
124.77
124.70
28.99
28.88
28.78
28.43
28.38
26.51
26.38
22.27
21.96
iPr
iPr
F
F
N
N
Au
Me
Br
F3C
iPr
iPr
29.0 28.8
f1 (ppm)
156.29
156.5 156.0
f1 (ppm)
210 200 190 180 170 160 150 140 130 120 110 100 90 80 70 60 50 40 30 20 10 0 -10
f1 (ppm)
-28.76
-28.79
-28.82
-56.14
-56.17
-56.20
-28.7 -28.8
f1 (ppm)
-55.5 -56.0 -56.5
f1 (ppm)
3.00
2.48
10 0 -10 -20 -30 -40 -50 -60 -70 -80 -90 -100 -110 -120 -130 -140 -150 -160 -170 -180 -190 -200 -210 -220 -230 -240 -25
f1 (ppm)

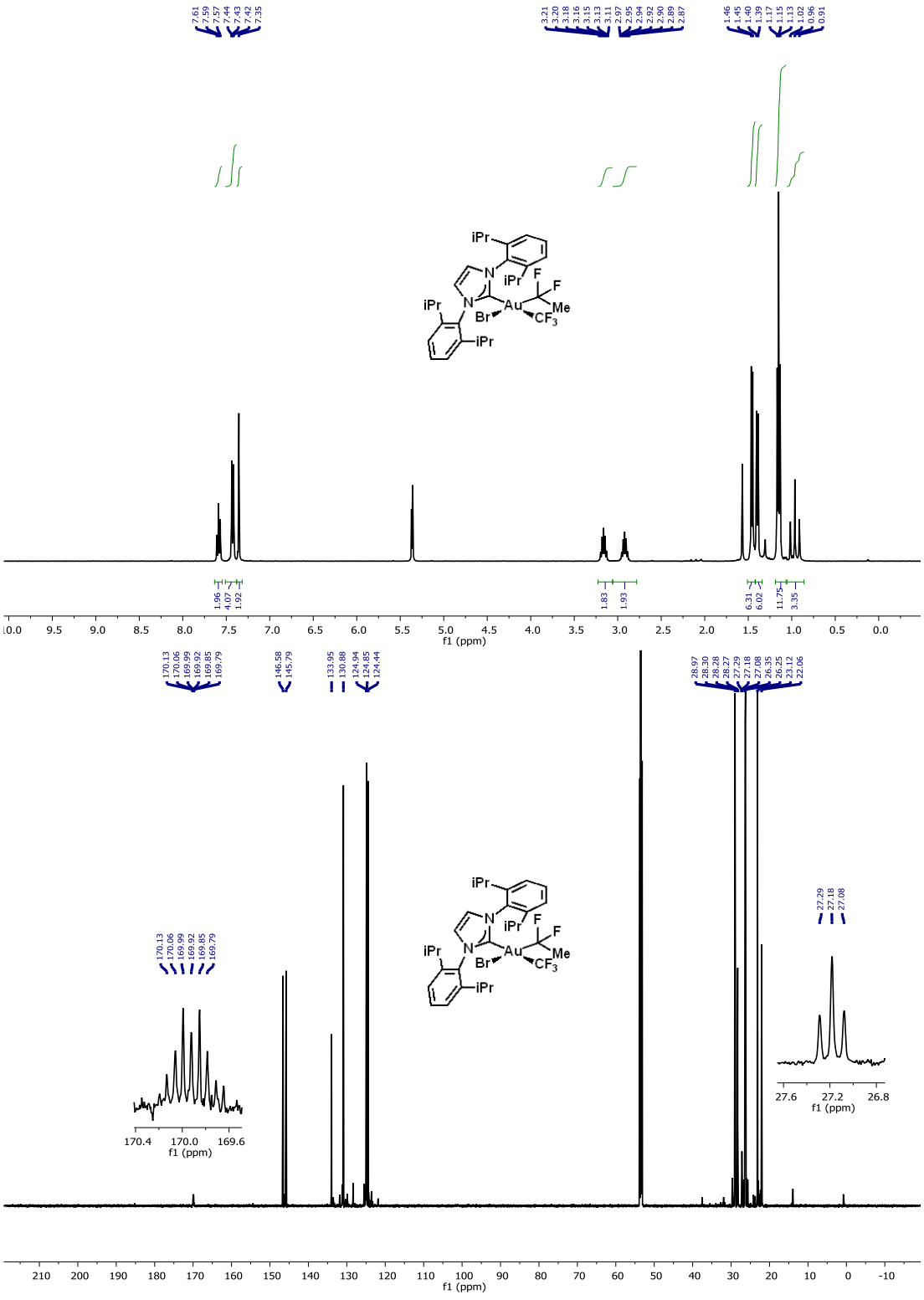
7.61
7.59
7.57
7.44
7.43
7.42
7.35
3.21
3.20
3.18
3.16
3.15
3.13
3.11
2.97
2.95
2.94
2.92
2.90
2.89
2.87
1.46
1.45
1.40
1.39
1.17
1.15
1.13
1.02
0.96
0.91
iPr
iPr
F
F
iPr
N
N
Au
Me
Br
CF3
iPr
iPr
1.96
4.07
1.92
1.83
1.93
6.31
6.02
11.75
3.35
f1 (ppm)
170.13
170.06
169.99
169.92
169.85
169.79
146.58
145.79
133.95
130.88
124.94
124.85
124.44
28.97
28.30
28.28
28.27
27.29
27.18
27.08
26.35
26.25
23.12
22.06
27.29
27.18
27.08
27.6
27.2
26.8
f1 (ppm)
170.4
170.0
169.6
f1 (ppm)
f1 (ppm)

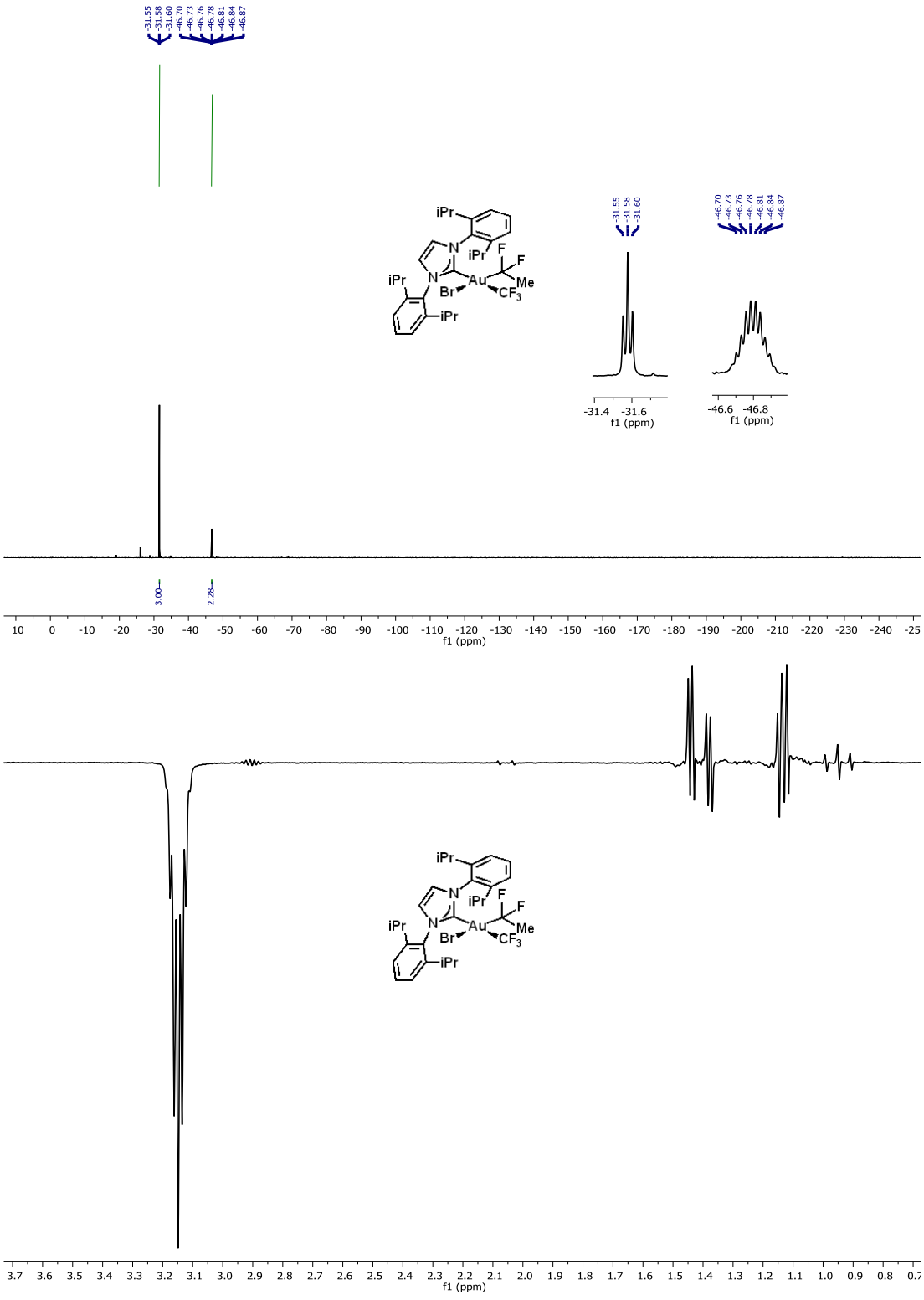
-31.55
-31.58
-31.60
-46.70
-46.73
-46.76
-46.78
-46.81
-46.84
-46.87
iPr
N
iPr
F
F
iPr
N
Au
Me
Br
CF3
iPr
iPr
-31.4
-31.6
f1 (ppm)
-46.6
-46.8
f1 (ppm)
3.00
2.28
f1 (ppm)
f1 (ppm)

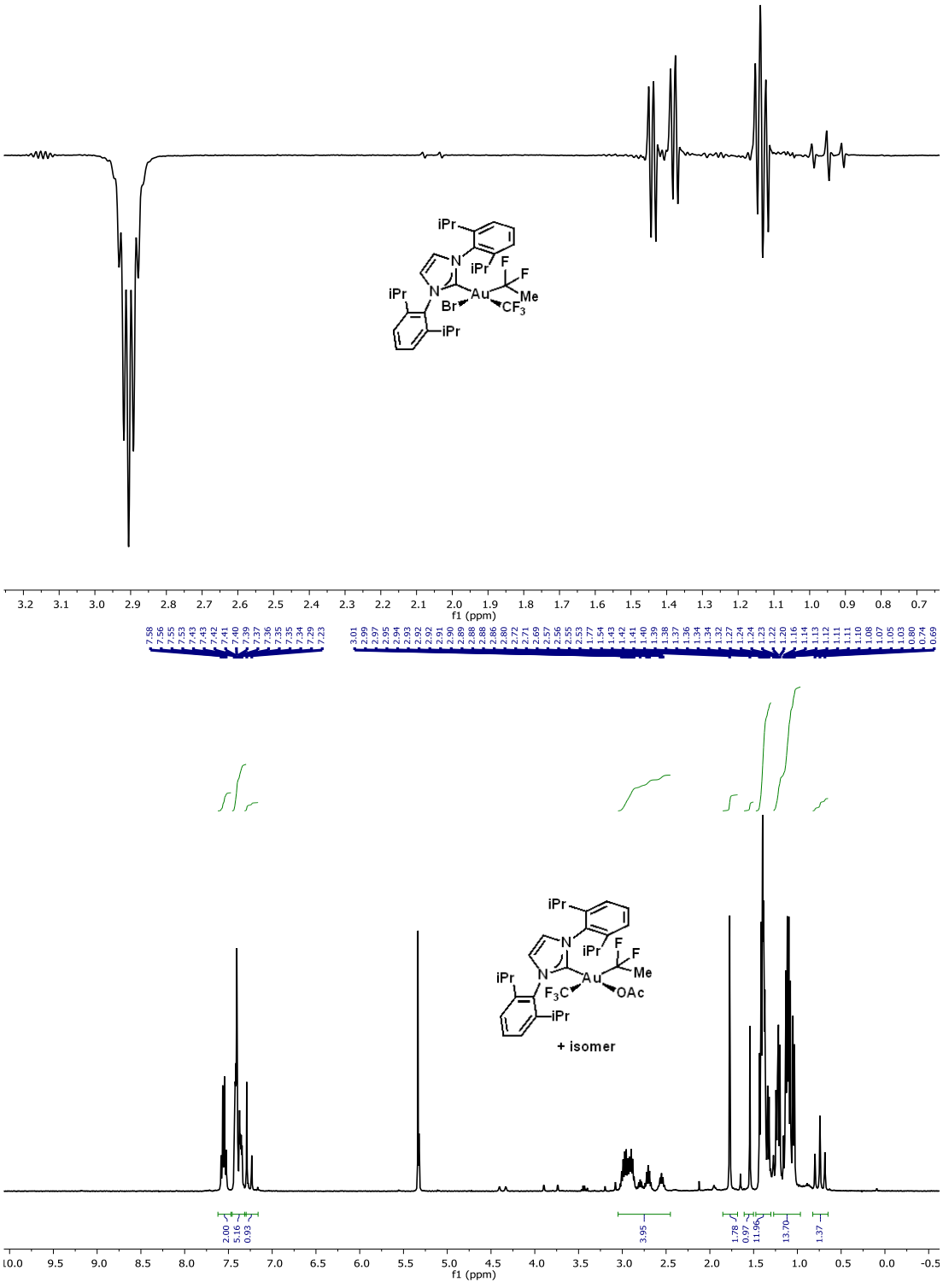
iPr
iPr
F
F
Me
iPr
Br
Au
CF3
iPr
f1 (ppm)
iPr
iPr
F
F
Me
iPr
F3C
Au
OAc
iPr
+ isomer
f1 (ppm)

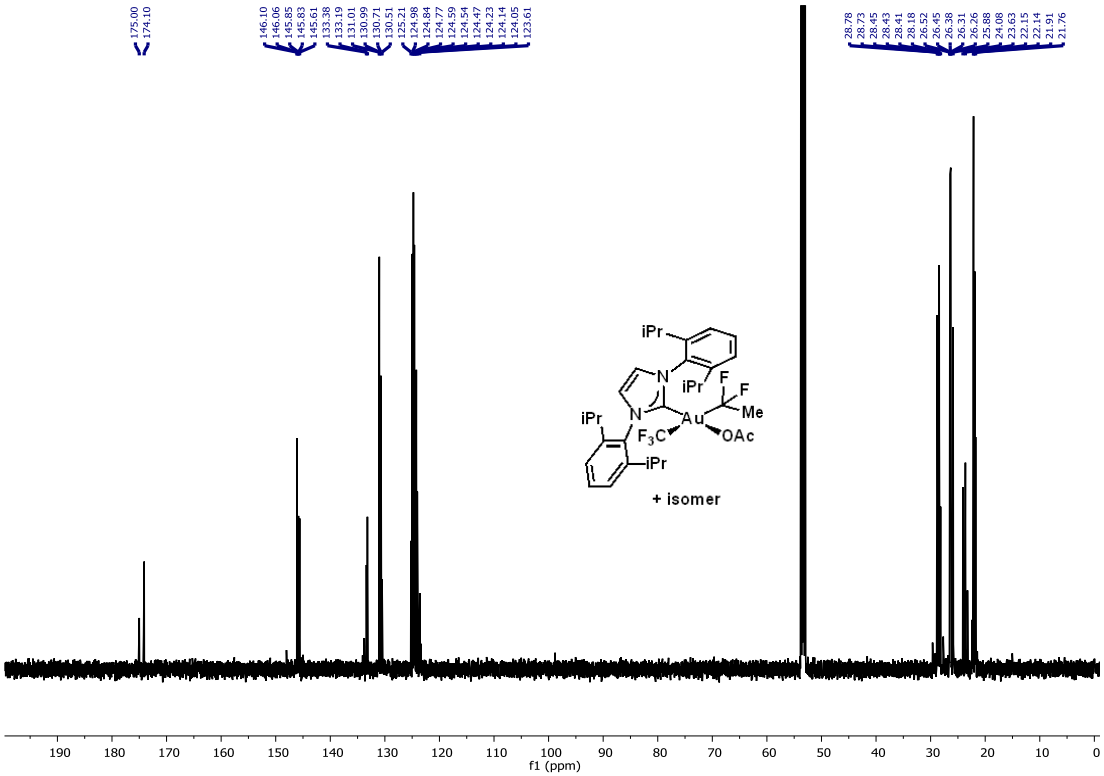
175.00
174.10
146.10
146.06
145.85
145.83
145.61
133.38
133.19
131.01
130.99
130.71
130.51
125.21
124.98
124.84
124.77
124.59
124.54
124.47
124.23
124.14
124.05
123.61
28.78
28.73
28.45
28.43
28.41
28.18
26.52
26.45
26.38
26.31
26.26
25.88
24.08
23.63
22.15
22.14
21.91
21.76
iPr
iPr
F
F
Me
iPr
N
N
Au
F3C
OAc
iPr
+ isomer
190 180 170 160 150 140 130 120 110 100 90 80 70 60 50 40 30 20 10 0
f1 (ppm)

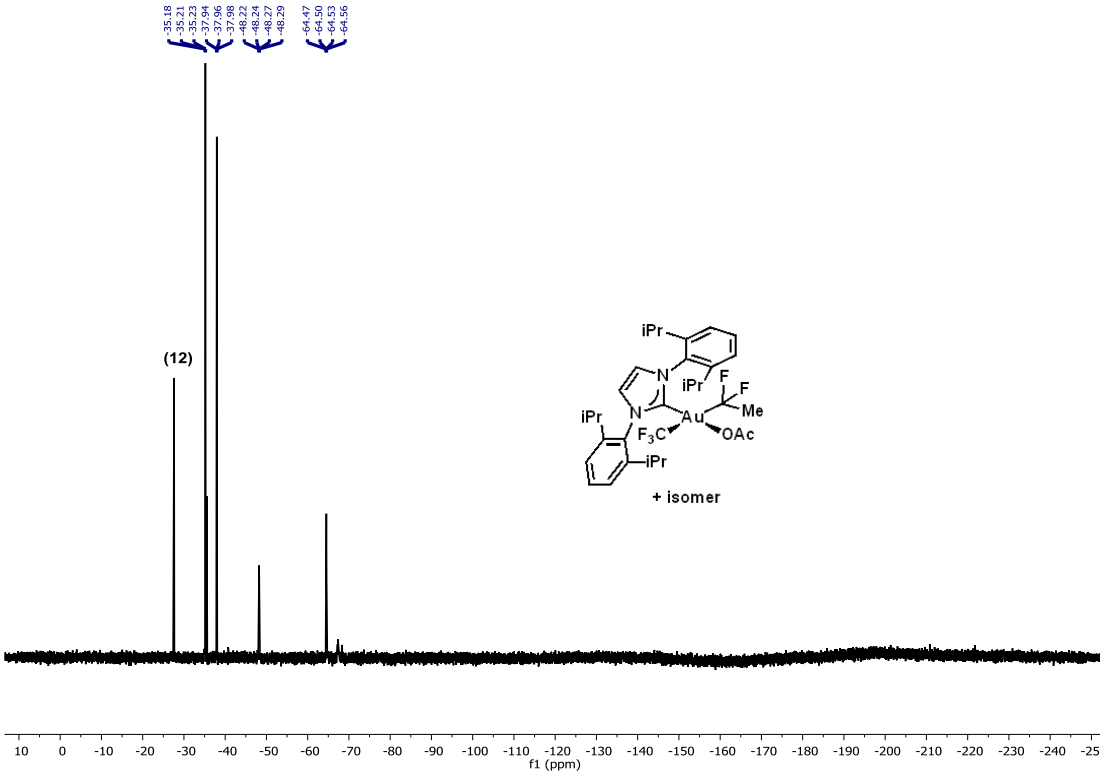
35.18
35.21
35.23
37.94
37.96
37.98
48.22
48.24
48.27
48.29
64.47
64.50
64.53
64.56
(12)
iPr
iPr
F
F
Me
iPr
N
N
Au
F3C
OAc
iPr
+ isomer
10 0 -10 -20 -30 -40 -50 -60 -70 -80 -90 -100 -110 -120 -130 -140 -150 -160 -170 -180 -190 -200 -210 -220 -230 -240 -25
f1 (ppm)

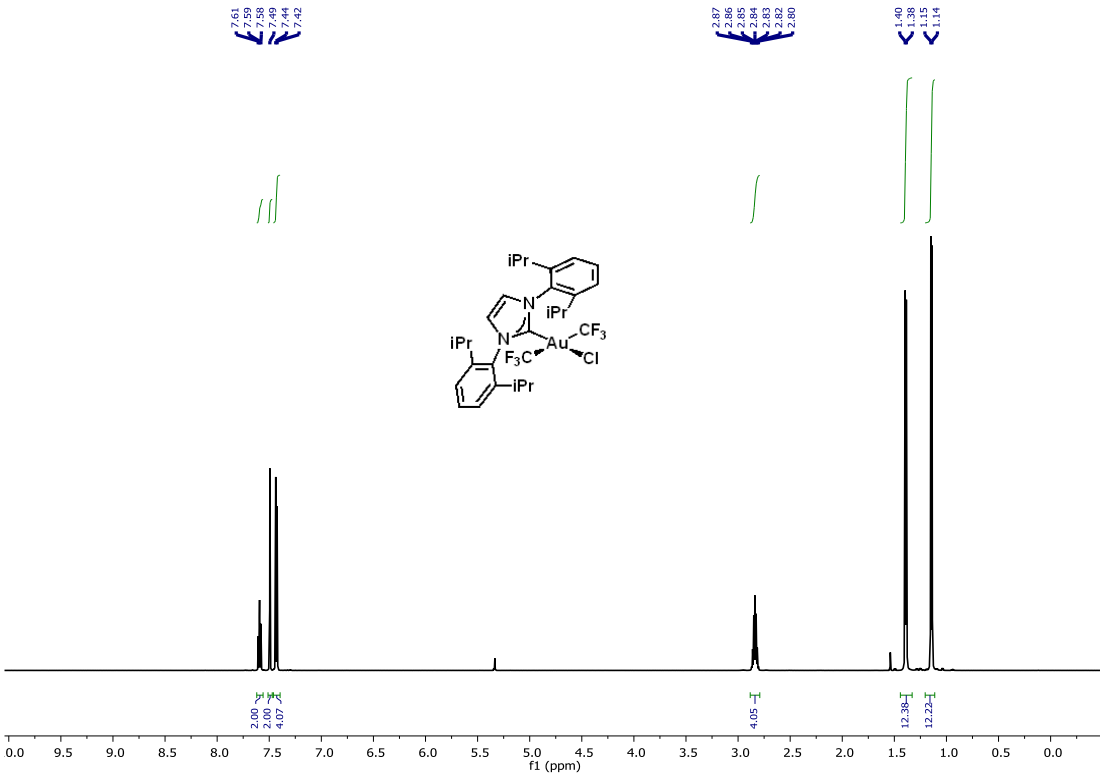
7.61
7.59
7.58
7.49
7.44
7.42
2.87
2.86
2.85
2.84
2.83
2.82
2.80
1.40
1.38
1.15
1.14
iPr
iPr
iPr
iPr
N
N
Au
CF3
F3C
Cl
2.00
2.00
4.07
4.05
12.38
12.22
f1 (ppm)

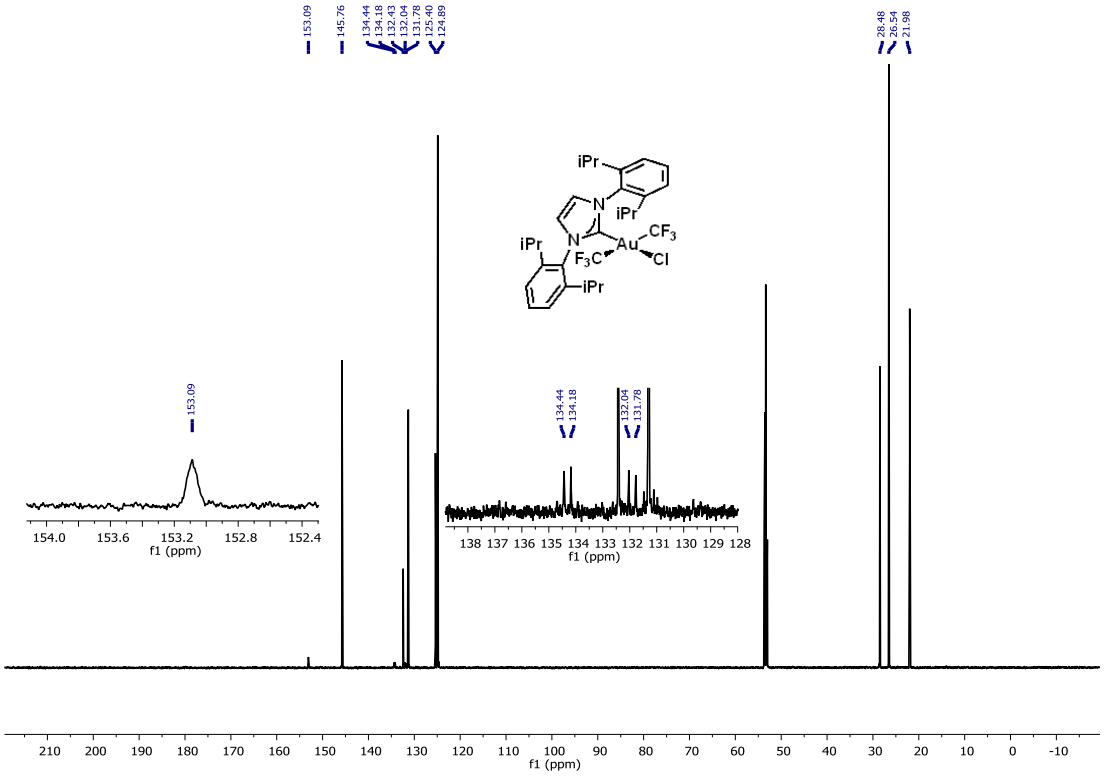
153.09
145.76
134.44
134.18
132.43
132.04
131.78
125.40
124.89
28.48
26.54
21.98
iPr
iPr
iPr
iPr
N
N
Au
CF3
F3C
Cl
153.09
154.0
153.6
153.2
152.8
152.4
f1 (ppm)
134.44
134.18
132.04
131.78
138 137 136 135 134 133 132 131 130 129 128
f1 (ppm)
f1 (ppm)

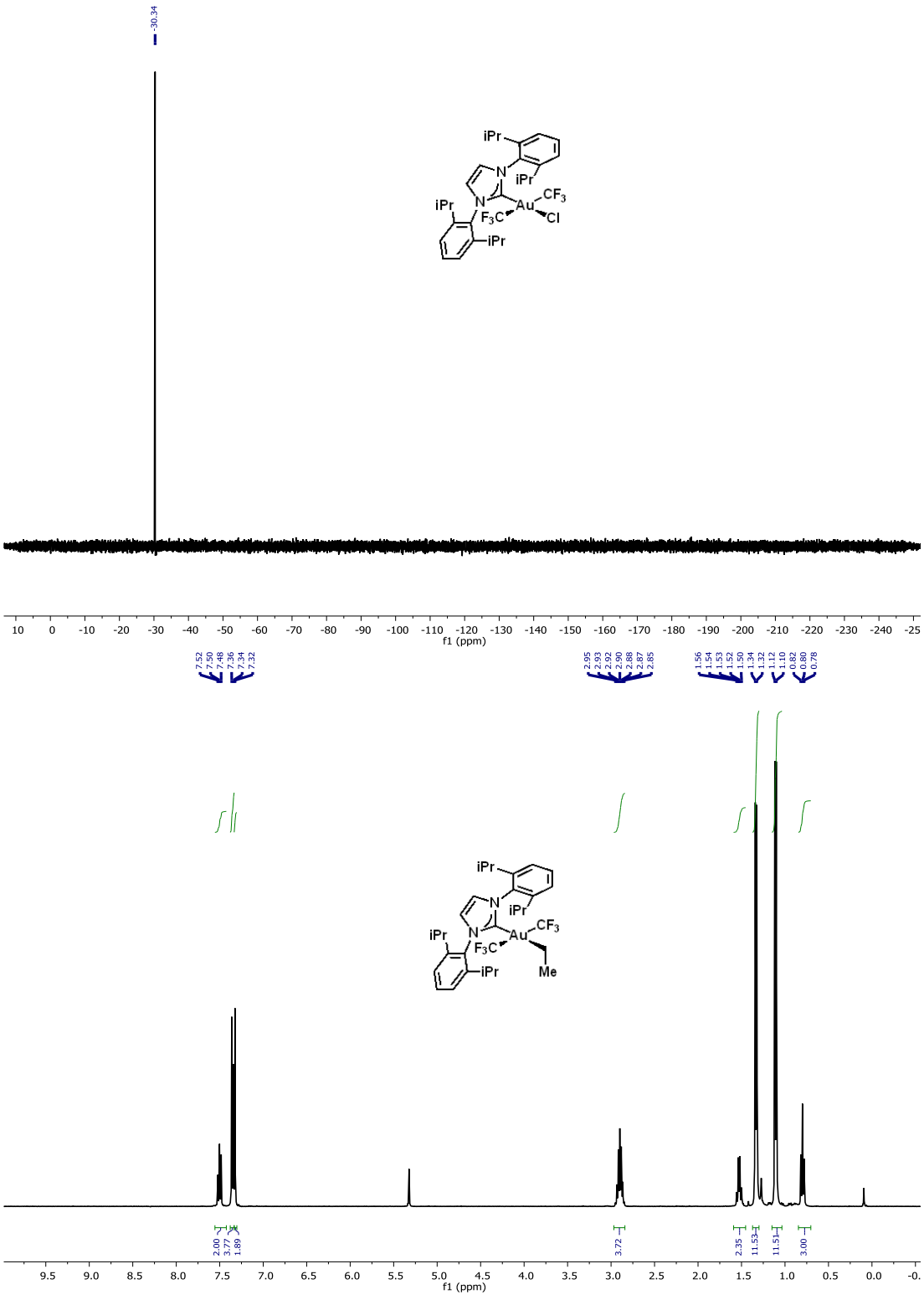
-30.34
iPr
iPr
iPr
iPr
N
N
Au
CF3
F3C
Cl
f1 (ppm)
7.52
7.50
7.48
7.36
7.34
7.32
2.95
2.93
2.92
2.90
2.88
2.87
2.85
1.56
1.54
1.53
1.52
1.50
1.34
1.32
1.12
1.10
0.82
0.80
0.78
iPr
iPr
iPr
iPr
N
N
Au
CF3
F3C
Me
2.00
3.77
1.89
3.72
2.35
11.53
11.51
3.00
f1 (ppm)

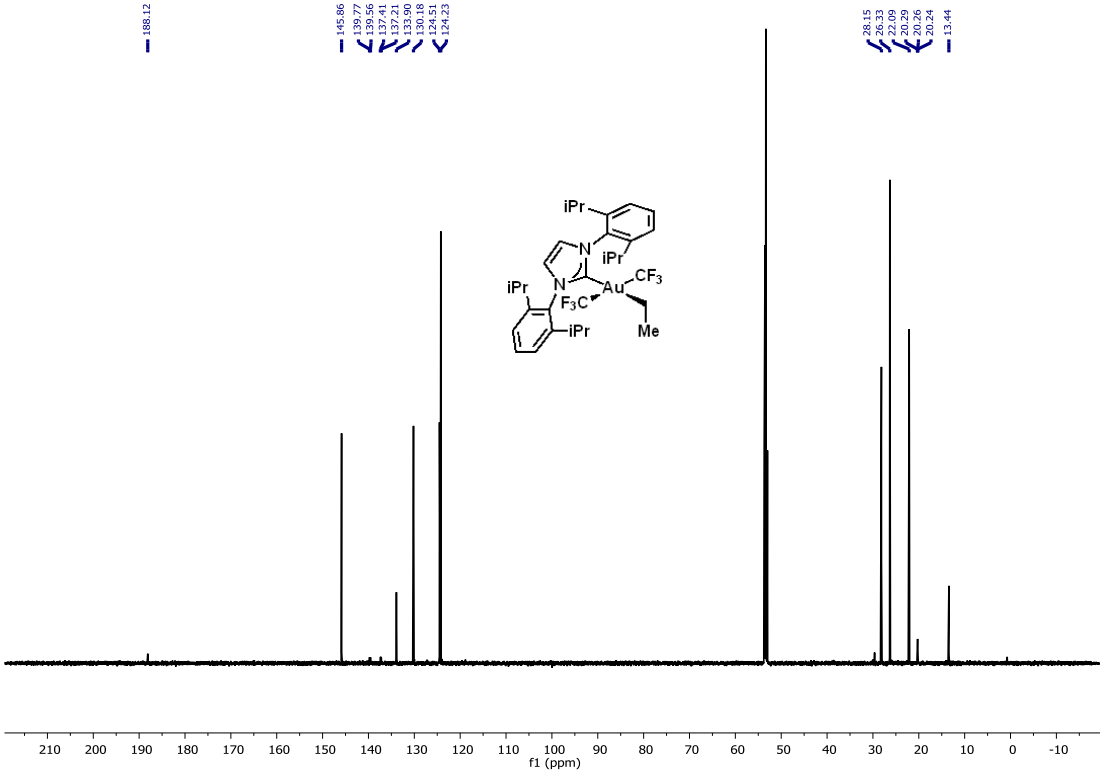
188.12
145.86
139.77
139.56
137.41
137.21
133.98
130.18
124.51
124.23
28.15
26.33
22.09
20.29
20.26
20.24
13.44
iPr
iPr
iPr
iPr
N
N
Au
CF3
F3C
Me
210 200 190 180 170 160 150 140 130 120 110 100 90 80 70 60 50 40 30 20 10 0 -10
f1 (ppm)

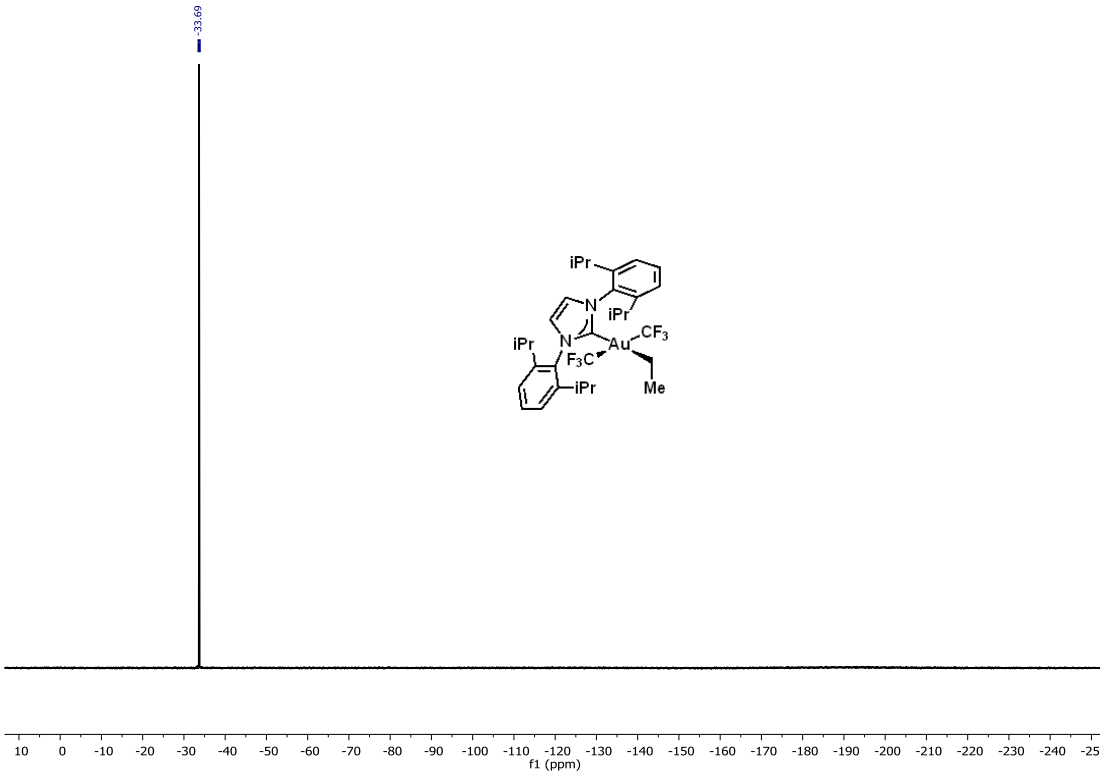
33.69
iPr
iPr
iPr
iPr
N
N
Au
CF3
F3C
Me
10 0 -10 -20 -30 -40 -50 -60 -70 -80 -90 -100 -110 -120 -130 -140 -150 -160 -170 -180 -190 -200 -210 -220 -230 -240 -25
f1 (ppm)

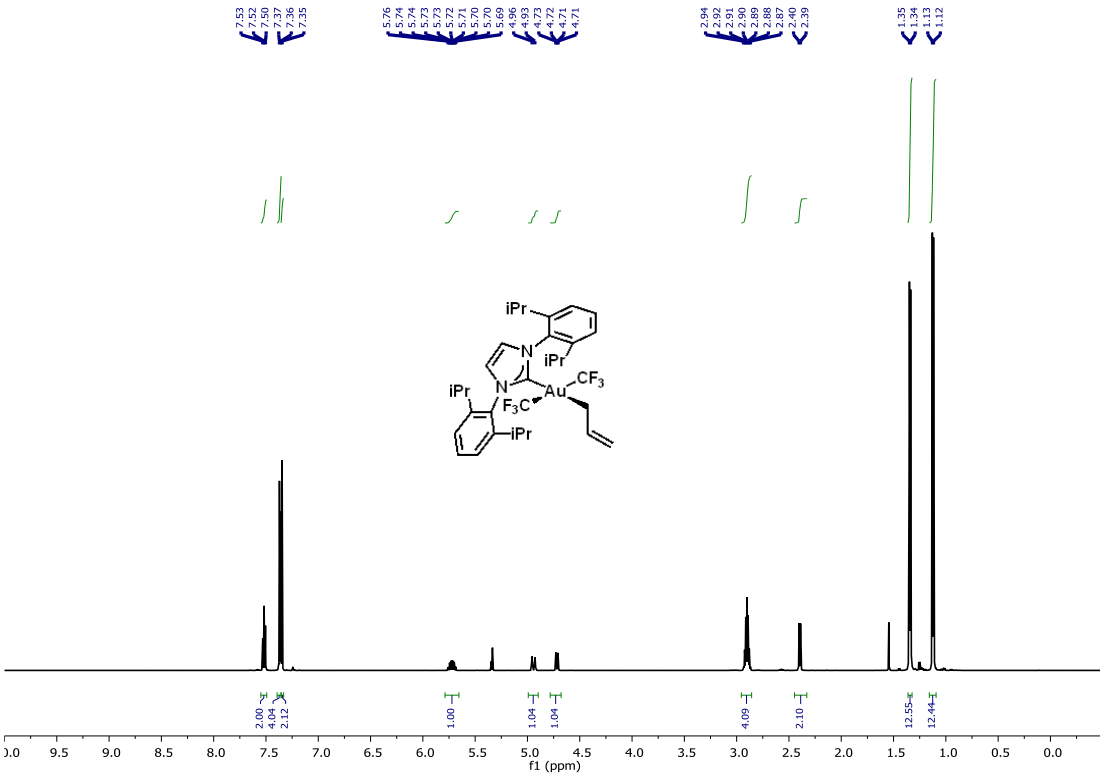
7.53
7.52
7.50
7.37
7.36
7.35
5.76
5.74
5.73
5.72
5.71
5.70
5.69
4.96
4.93
4.73
4.72
4.71
4.71
2.94
2.92
2.91
2.90
2.89
2.88
2.87
2.40
2.39
1.35
1.34
1.13
1.12
iPr
iPr
iPr
iPr
N
N
Au
CF3
F3C
2.00
4.04
2.12
1.00
1.04
1.04
4.09
2.10
12.55
12.44
f1 (ppm)

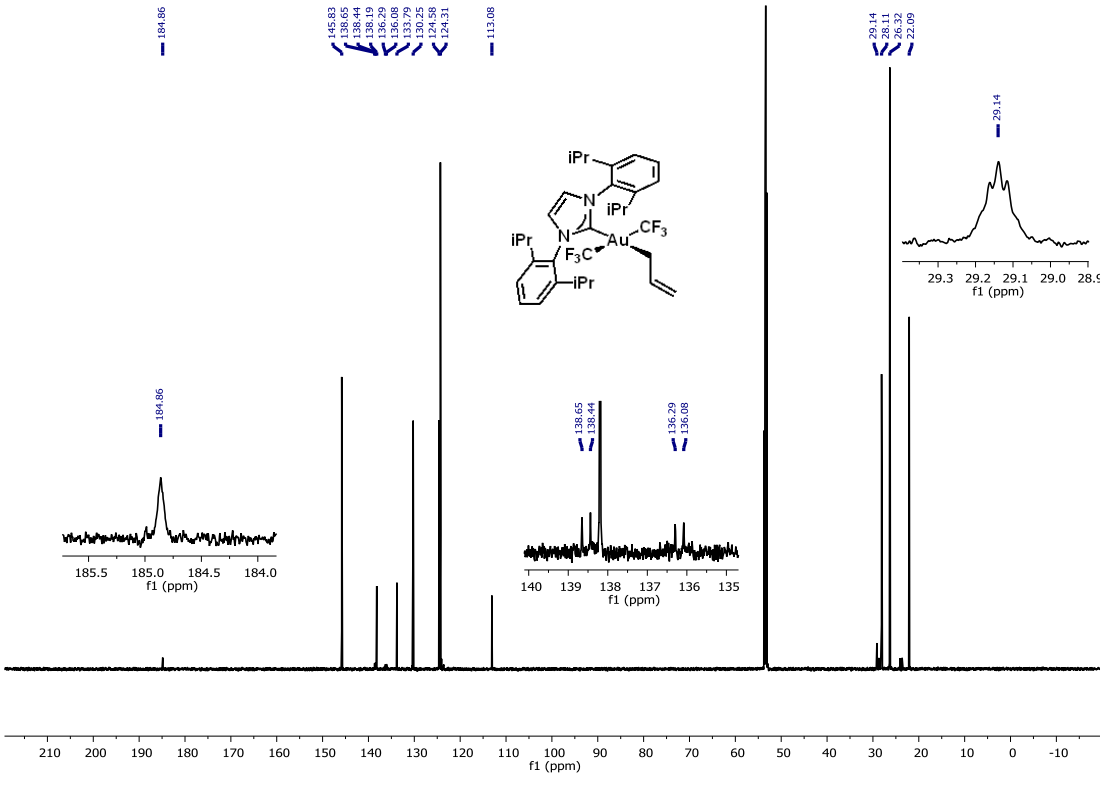
184.86
145.83
138.65
138.44
138.19
136.29
136.08
133.29
130.25
124.58
124.31
113.08
29.14
28.11
26.32
22.09
iPr
iPr
iPr
iPr
N
N
Au
CF3
F3C
f1 (ppm)

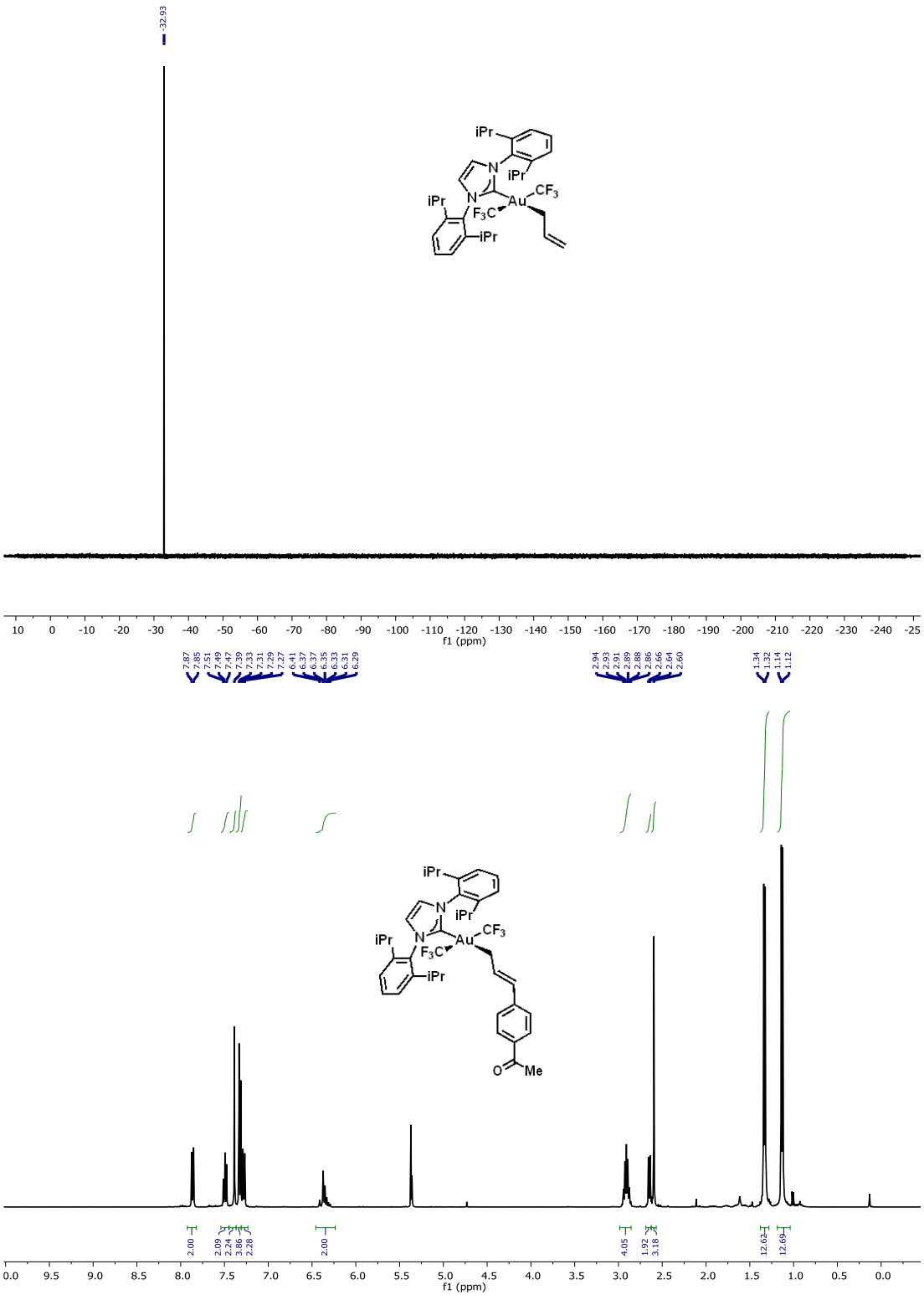
-32.93
iPr
N
iPr
N
Au
CF3
F3C
iPr
iPr
f1 (ppm)
7.87
7.85
7.51
7.49
7.47
7.39
7.33
7.31
7.29
7.27
6.41
6.37
6.35
6.33
6.31
6.29
2.94
2.93
2.91
2.89
2.88
2.86
2.66
2.64
2.60
1.34
1.32
1.14
1.12
2.00
2.09
2.24
3.86
2.28
2.00
4.05
1.92
3.18
12.62
12.69
O
Me

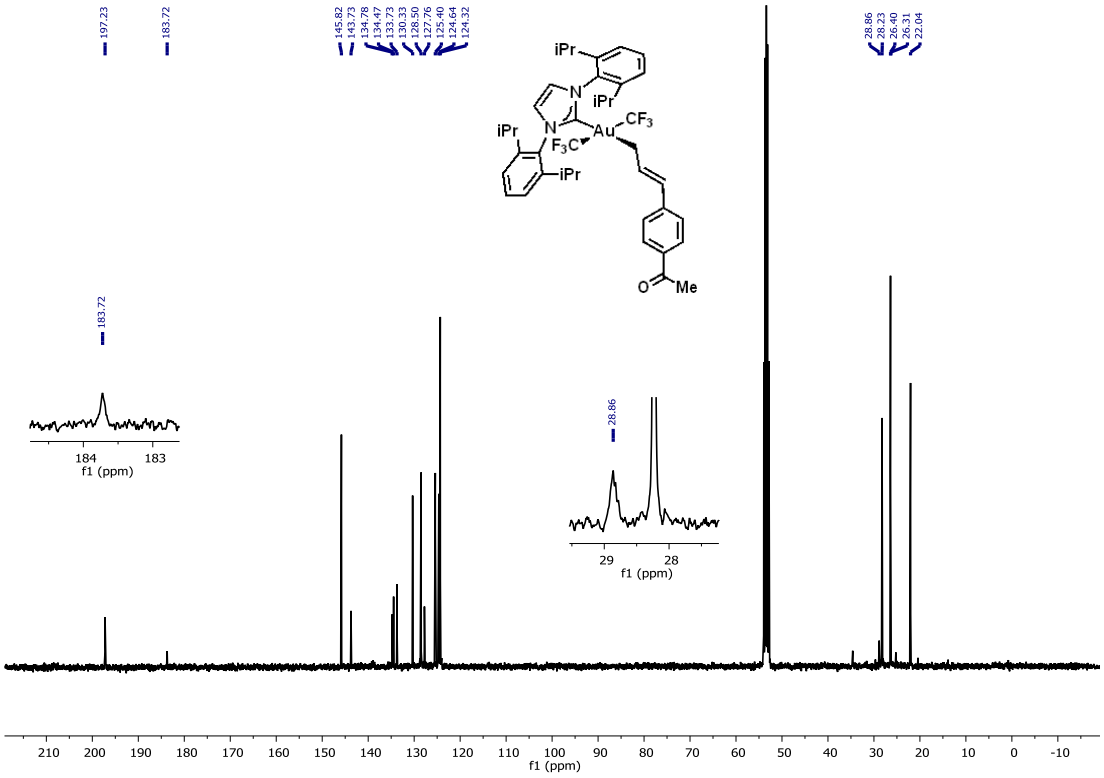
197.23
183.72
145.82
145.73
134.78
134.47
133.73
130.33
128.50
127.76
125.40
124.64
124.32
28.86
28.23
26.40
26.31
22.04
iPr
iPr
iPr
iPr
N
N
Au
CF3
F3C
O
Me
183.72
184
183
f1 (ppm)
28.86
29
28
f1 (ppm)
210 200 190 180 170 160 150 140 130 120 110 100 90 80 70 60 50 40 30 20 10 0 -10
f1 (ppm)

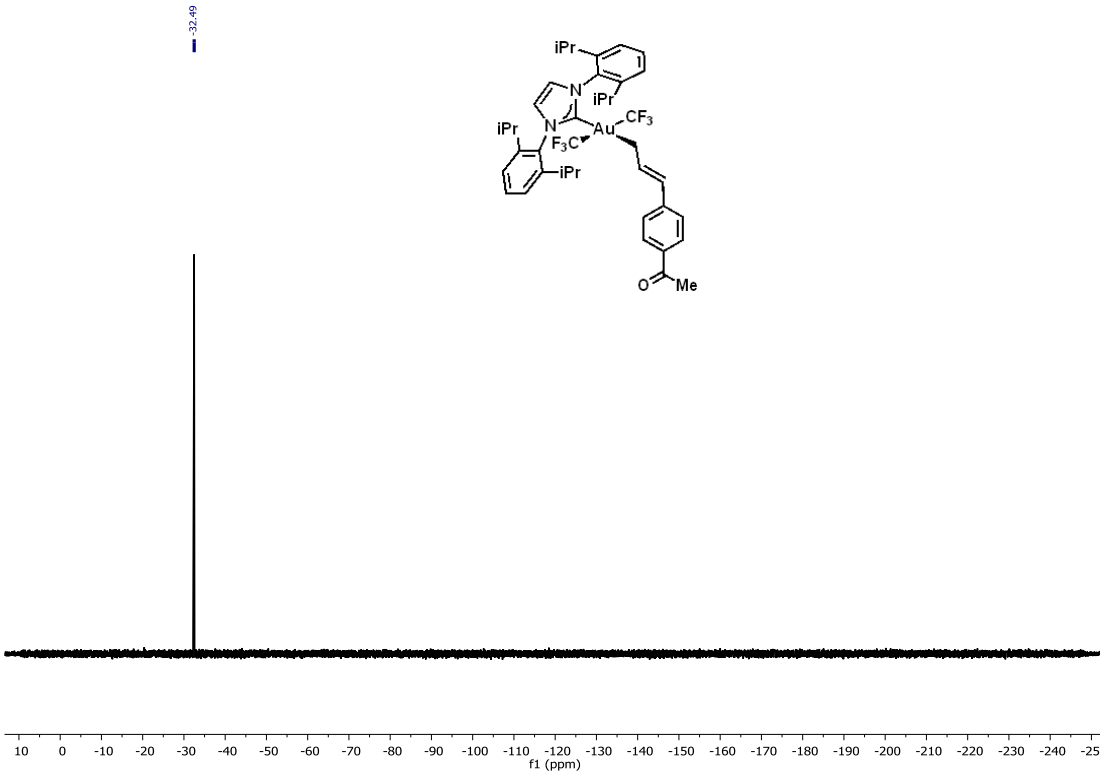
-32.49
iPr
iPr
iPr
iPr
N
N
Au
CF3
F3C
O
Me
10 0 -10 -20 -30 -40 -50 -60 -70 -80 -90 -100 -110 -120 -130 -140 -150 -160 -170 -180 -190 -200 -210 -220 -230 -240 -25
f1 (ppm)

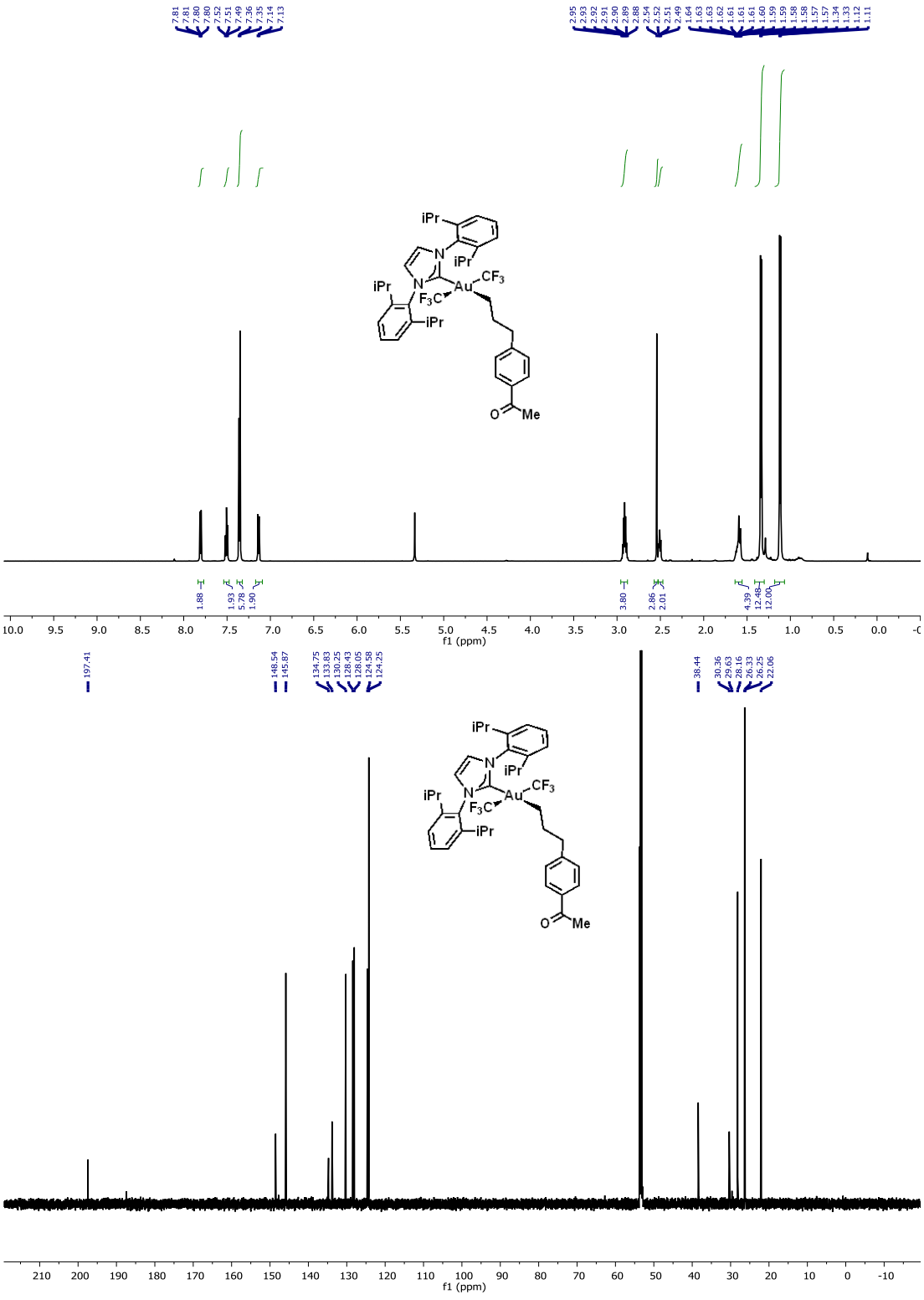
iPr
iPr
iPr
iPr
N
N
Au
CF3
F3C
O
Me
f1 (ppm)

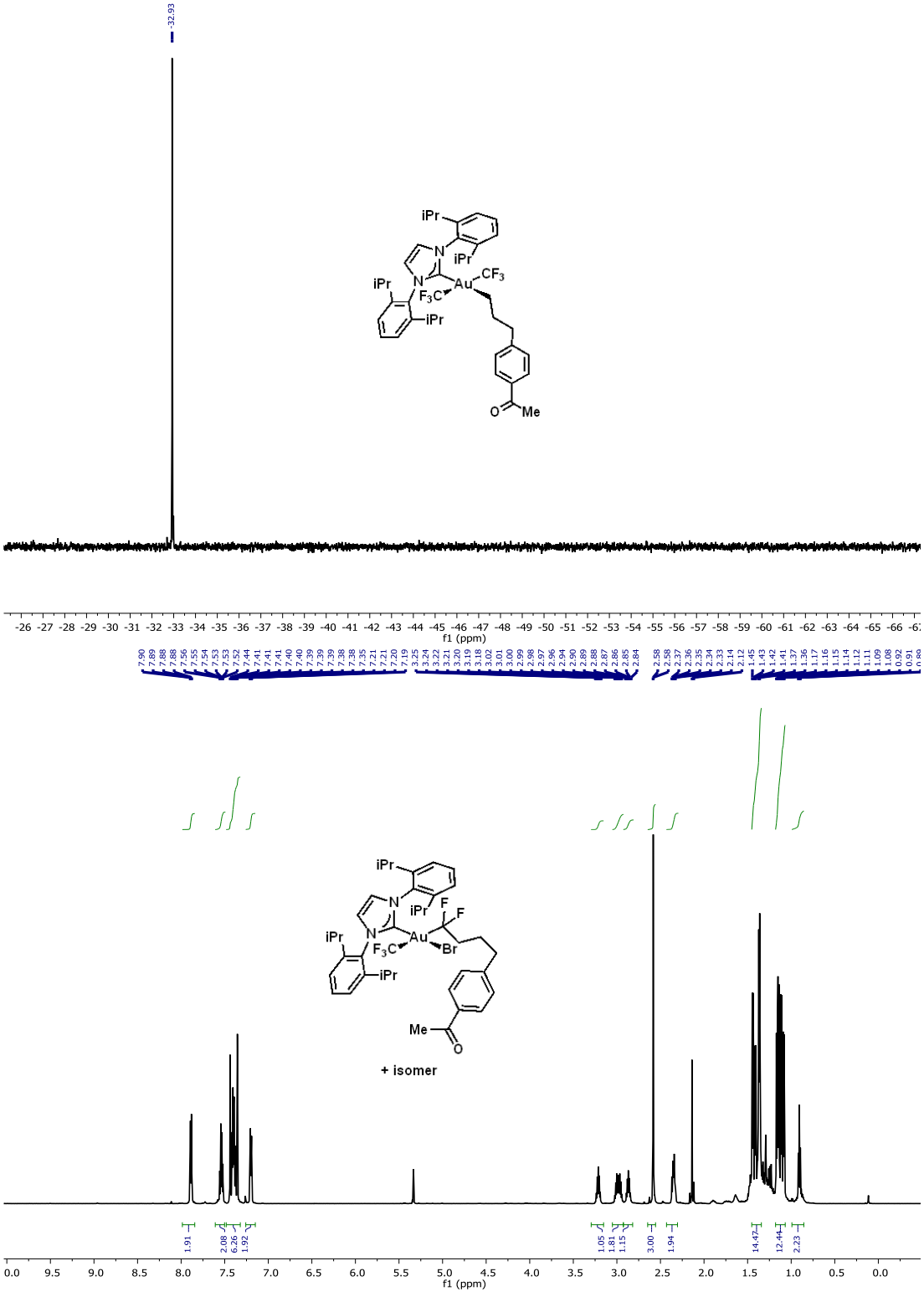
-32.93
iPr
iPr
iPr
iPr
N
N
Au
CF3
F3C
O
Me
f1 (ppm)
iPr
iPr
iPr
iPr
N
N
Au
F
F
Br
F3C
Me
O
+ isomer
1.91
2.08
6.26
1.92
1.05
1.81
1.15
3.00
1.94
14.47
12.44
2.23
f1 (ppm)

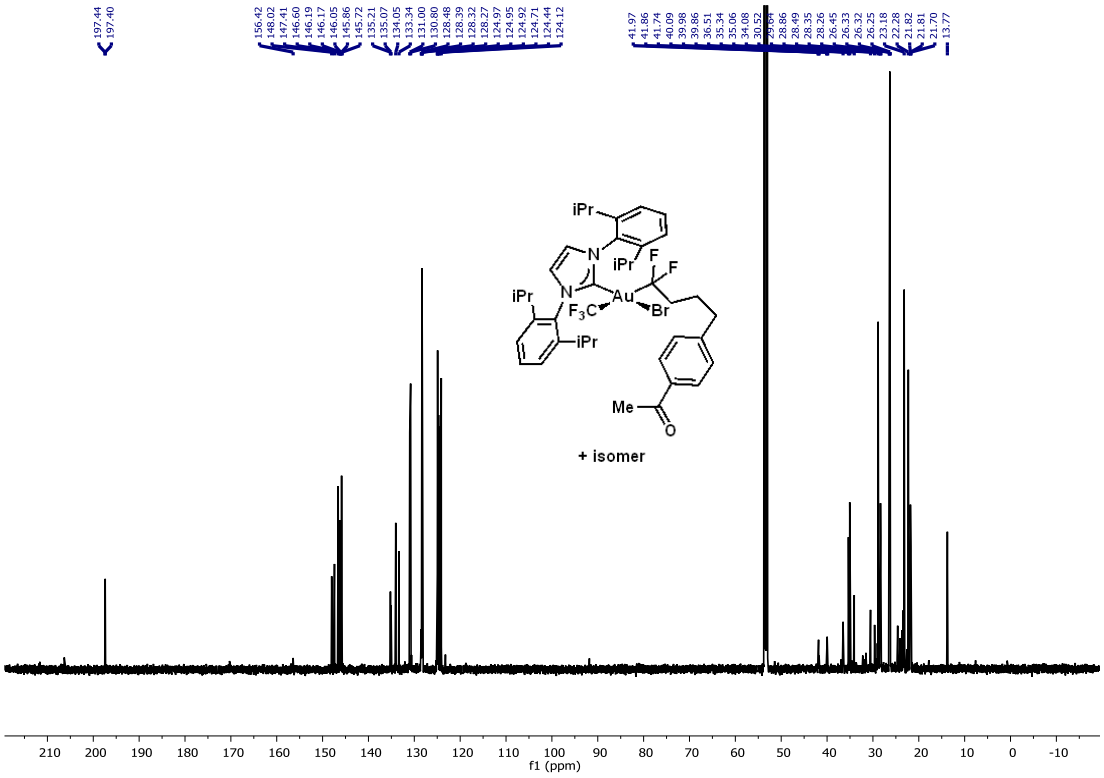
197.44
197.40
156.42
148.02
147.41
146.60
146.19
146.17
146.05
145.86
145.72
135.21
135.07
134.05
133.34
131.00
130.80
128.48
128.39
128.32
128.27
124.97
124.95
124.92
124.71
124.44
124.12
41.97
41.86
41.74
40.09
39.98
39.86
36.51
35.34
35.06
34.68
30.37
29.65
28.86
28.49
28.35
28.26
26.45
26.33
26.32
26.25
23.18
22.28
21.82
21.81
21.70
13.77
iPr
N
iPr
F
F
N
iPr
F3C
Au
Br
iPr
iPr
Me
O
+ isomer
210
200
190
180
170
160
150
140
130
120
110
100
90
80
70
60
50
40
30
20
10
0
-10
f1 (ppm)

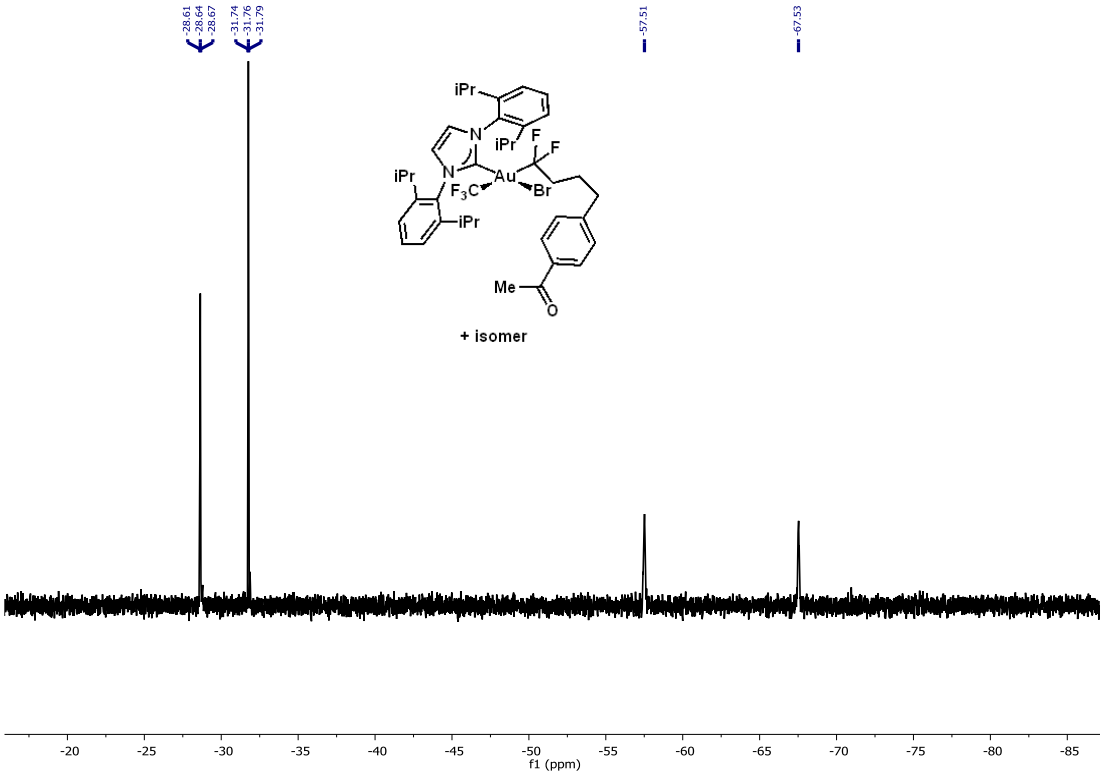
28.61
28.64
28.67
31.74
31.76
31.79
-57.51
-67.53
iPr
N
iPr
F
F
iPr
N
F3C
Au
Br
iPr
Me
O
+ isomer
-20
-25
-30
-35
-40
-45
-50
-55
-60
-65
-70
-75
-80
-85
f1 (ppm)

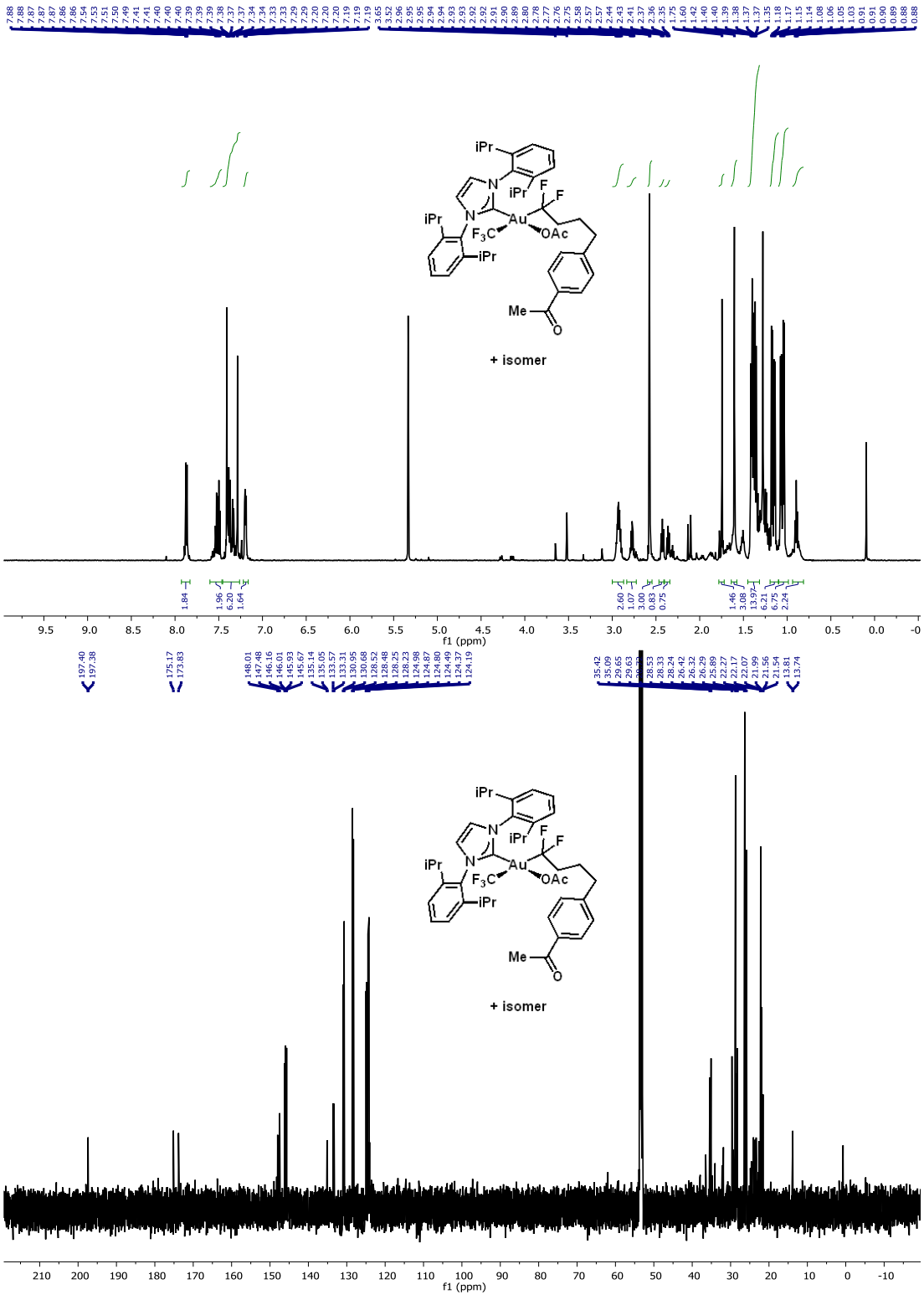
iPr
iPr
F
F
iPr
N
N
Au
F3C
OAc
iPr
Me
O
+ isomer
f1 (ppm)

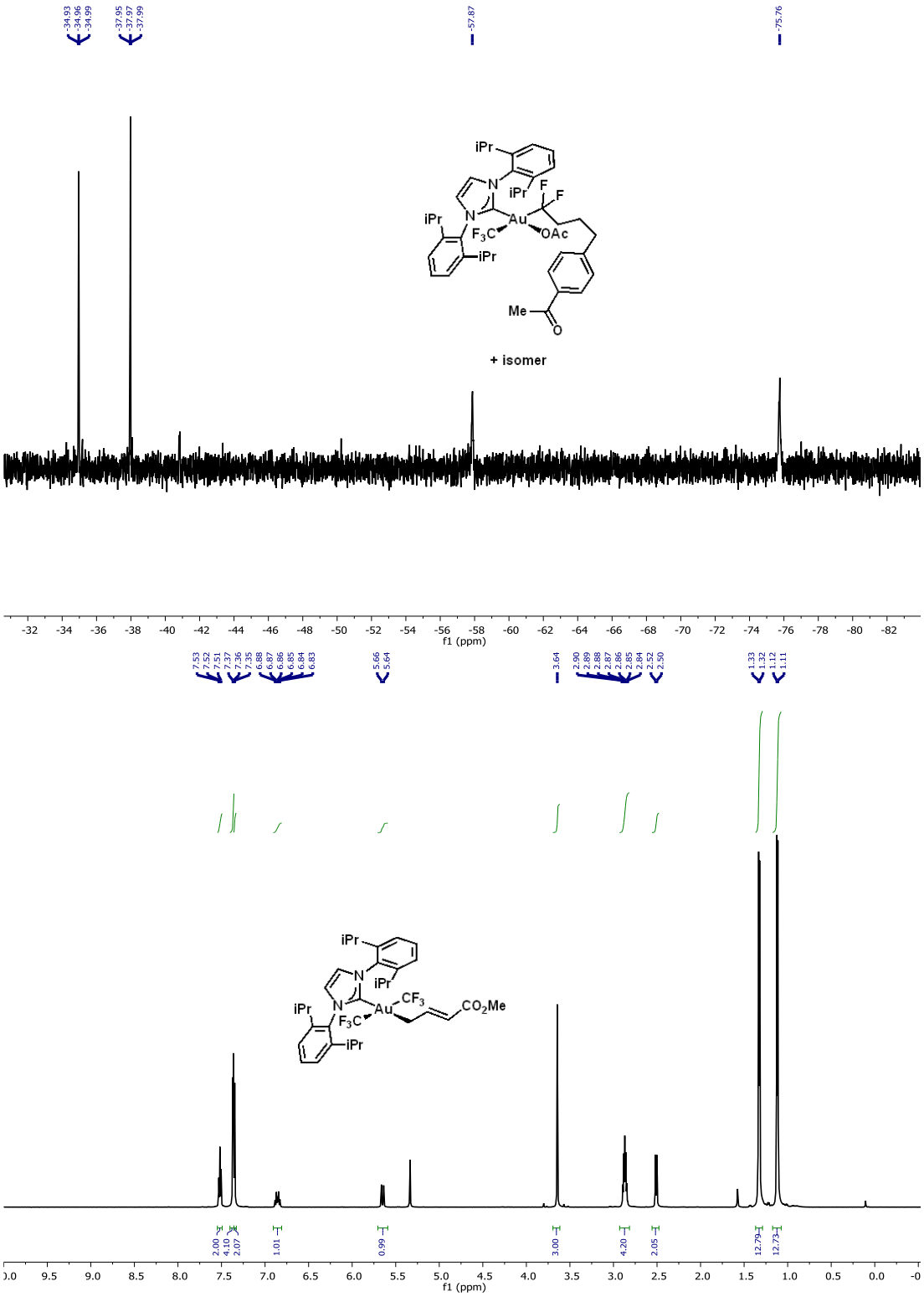
-34.93
-34.96
-34.99
-37.95
-37.97
-37.99
-57.87
-75.76
iPr
iPr
F
F
iPr
N
N
Au
F3C
OAc
iPr
Me
O
+ isomer
f1 (ppm)
7.53
7.52
7.51
7.37
7.36
7.35
6.88
6.87
6.86
6.85
6.84
6.83
5.66
5.64
3.64
2.90
2.89
2.88
2.87
2.86
2.85
2.84
2.52
2.50
1.33
1.32
1.12
1.11
iPr
iPr
N
N
Au
CF3
CO2Me
F3C
iPr
iPr
2.00
4.10
2.07
1.01
0.99
3.00
4.20
2.05
12.79
12.73
f1 (ppm)

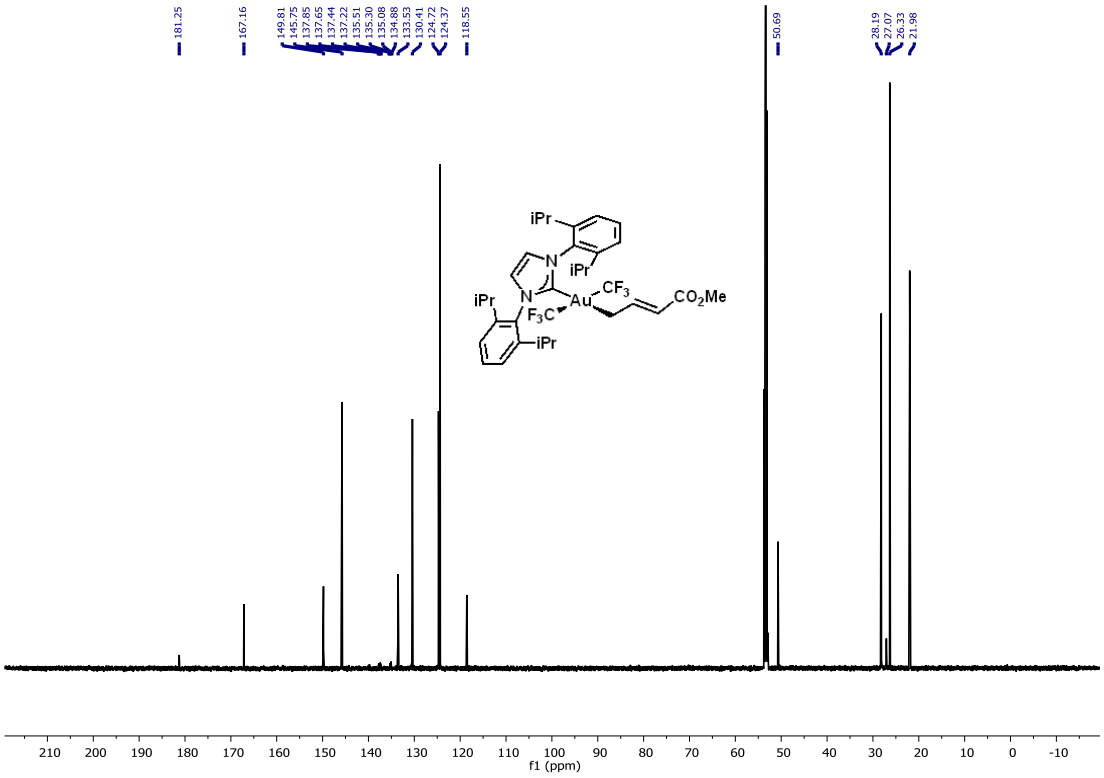
181.25
167.16
149.81
145.75
137.85
137.65
137.44
137.22
135.51
135.30
135.08
134.88
133.53
130.41
124.72
124.37
118.55
50.69
28.19
27.07
26.33
21.98
iPr
iPr
iPr
iPr
N
N
Au
CF3
F3C
CO2Me
210 200 190 180 170 160 150 140 130 120 110 100 90 80 70 60 50 40 30 20 10 0 -10
f1 (ppm)

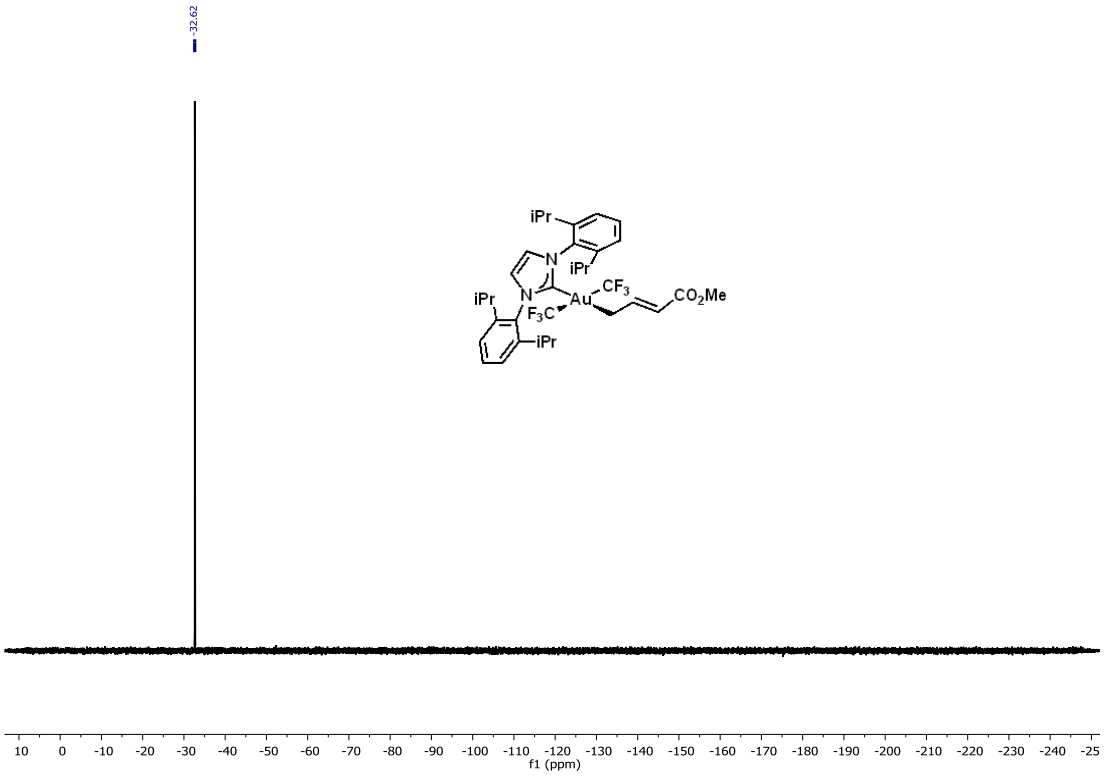
32.62
iPr
iPr
iPr
iPr
N
N
Au
CF3
F3C
CO2Me
10 0 -10 -20 -30 -40 -50 -60 -70 -80 -90 -100 -110 -120 -130 -140 -150 -160 -170 -180 -190 -200 -210 -220 -230 -240 -25
f1 (ppm)

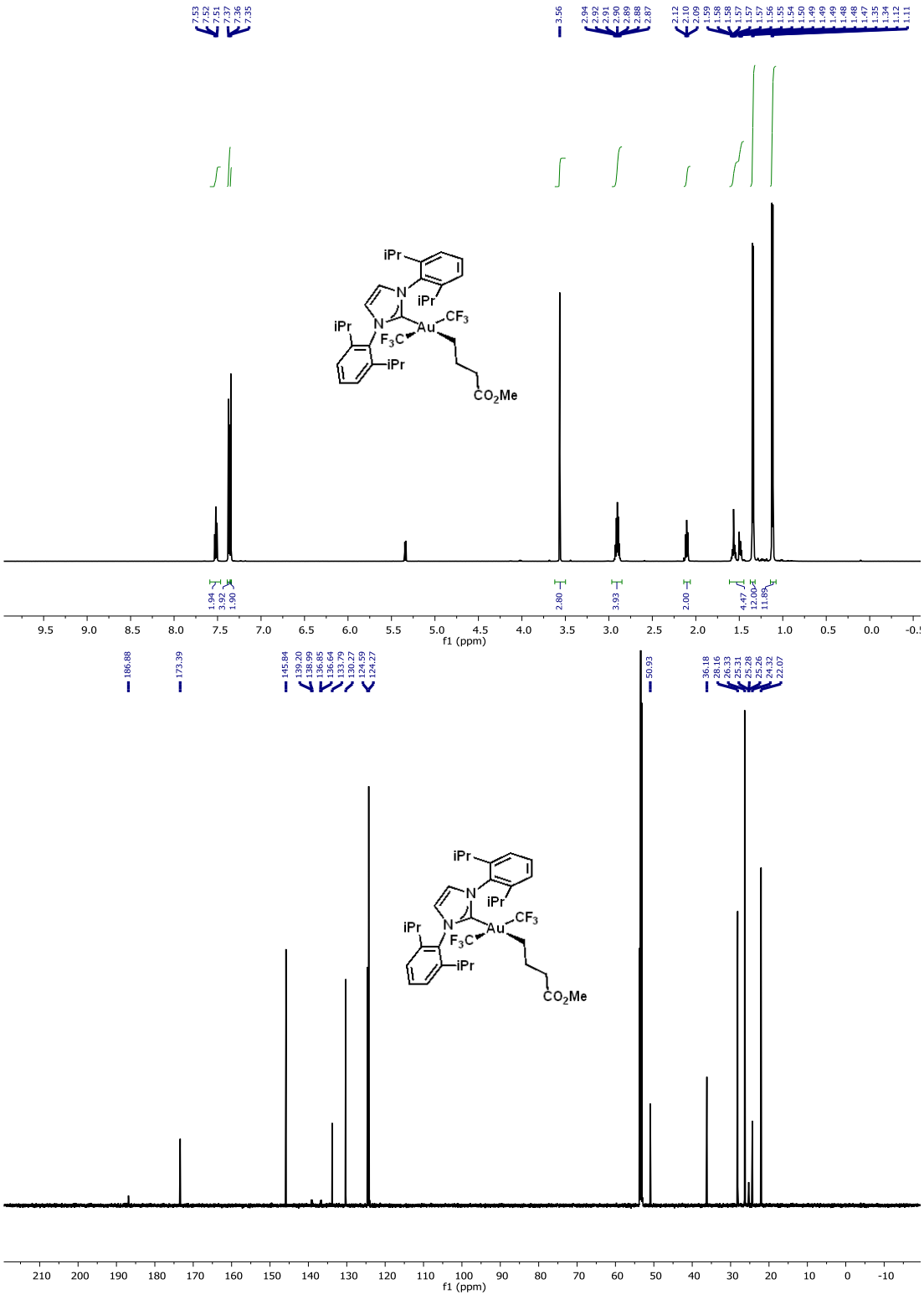
iPr
iPr
iPr
N
N
Au
CF3
F3C
iPr
CO2Me
f1 (ppm)

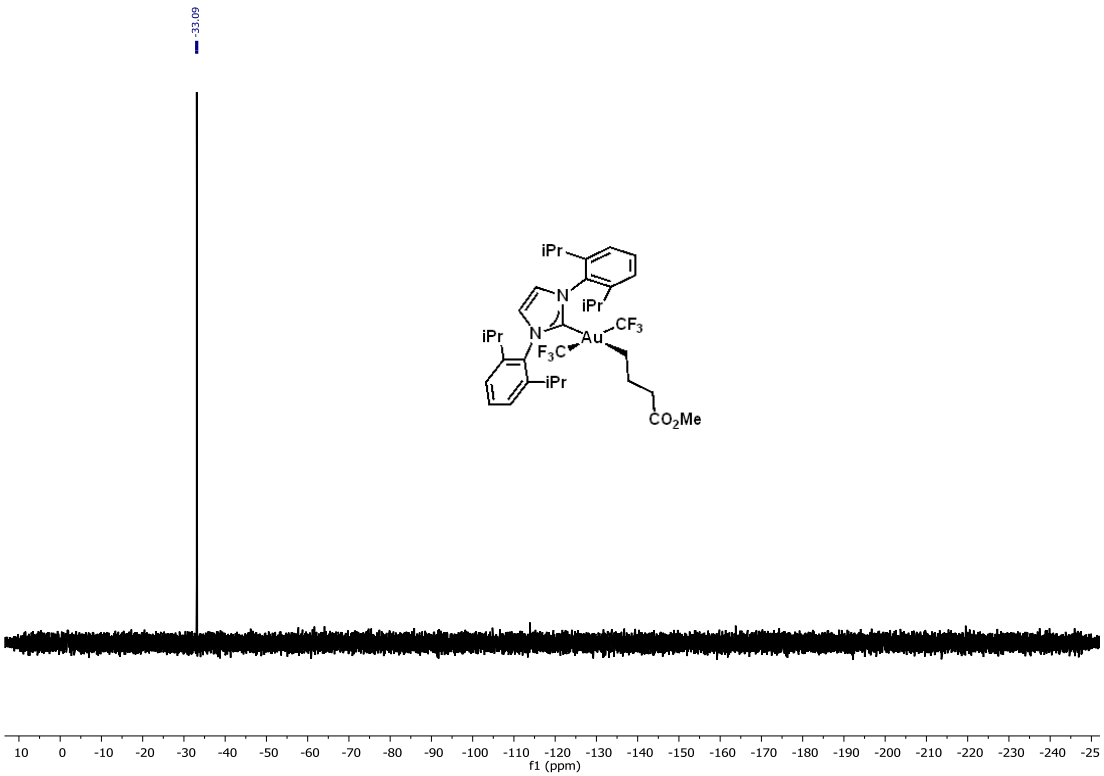
-33.09
iPr
iPr
iPr
iPr
N
N
Au
CF3
F3C
CO2Me
10 0 -10 -20 -30 -40 -50 -60 -70 -80 -90 -100 -110 -120 -130 -140 -150 -160 -170 -180 -190 -200 -210 -220 -230 -240 -25
f1 (ppm)

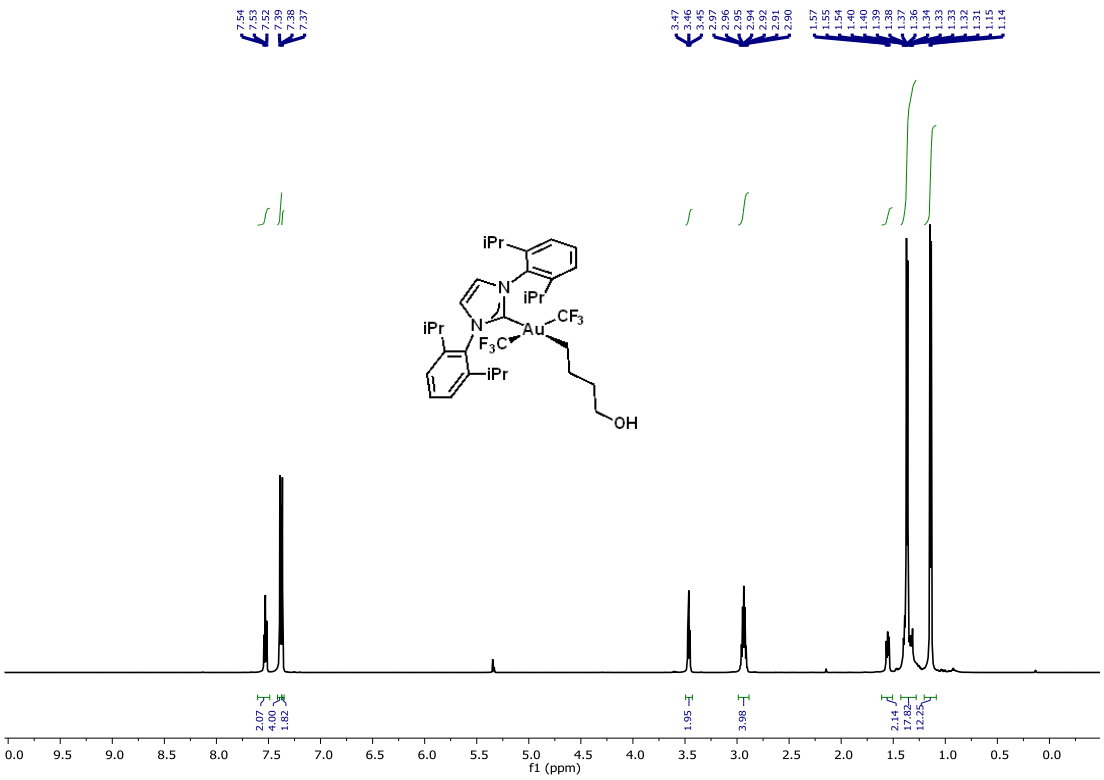
7.54
7.53
7.52
7.39
7.38
7.37
3.47
3.46
3.45
2.97
2.96
2.95
2.94
2.92
2.91
2.90
1.57
1.55
1.54
1.40
1.39
1.38
1.37
1.36
1.34
1.33
1.32
1.31
1.15
1.14
iPr
iPr
iPr
iPr
N
N
Au
CF3
F3C
OH
2.07
4.00
1.82
1.95
3.98
2.14
17.82
12.25
0.0 9.5 9.0 8.5 8.0 7.5 7.0 6.5 6.0 5.5 5.0 4.5 4.0 3.5 3.0 2.5 2.0 1.5 1.0 0.5 0.0
f1 (ppm)

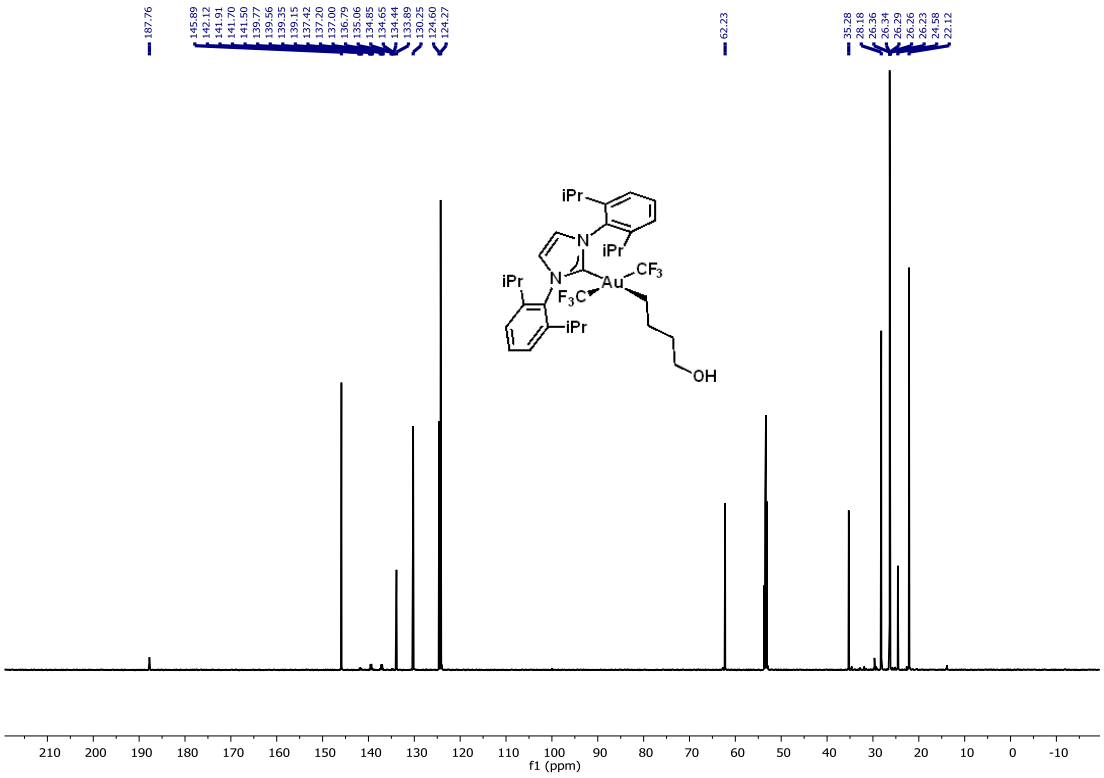
187.76
145.89
142.12
141.91
141.70
141.50
139.77
139.56
139.35
139.15
137.42
137.20
137.00
136.79
135.06
134.85
134.65
134.44
133.98
130.25
124.60
124.27
62.23
35.28
28.18
26.36
26.34
26.30
26.26
26.23
24.58
22.12
iPr
iPr
iPr
iPr
N
N
Au
CF3
F3C
OH
210 200 190 180 170 160 150 140 130 120 110 100 90 80 70 60 50 40 30 20 10 0 -10
f1 (ppm)

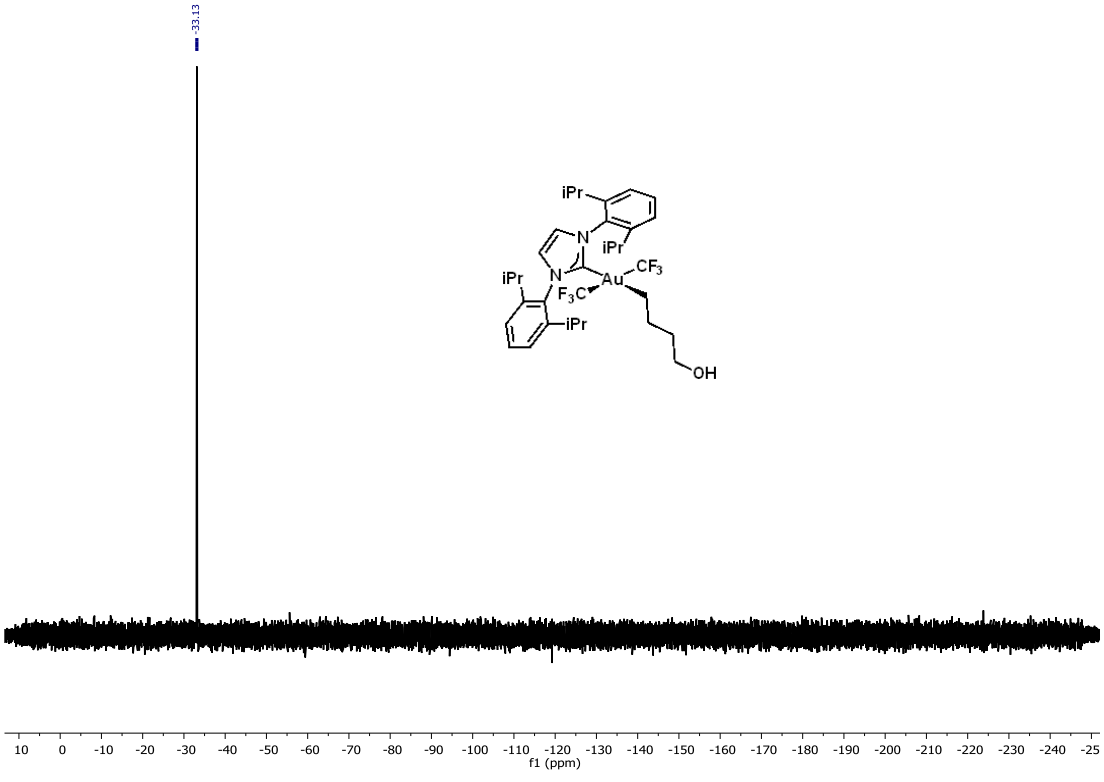
-33.13
iPr
iPr
iPr
iPr
N
N
Au
CF3
F3C
OH
10 0 -10 -20 -30 -40 -50 -60 -70 -80 -90 -100 -110 -120 -130 -140 -150 -160 -170 -180 -190 -200 -210 -220 -230 -240 -25
f1 (ppm)

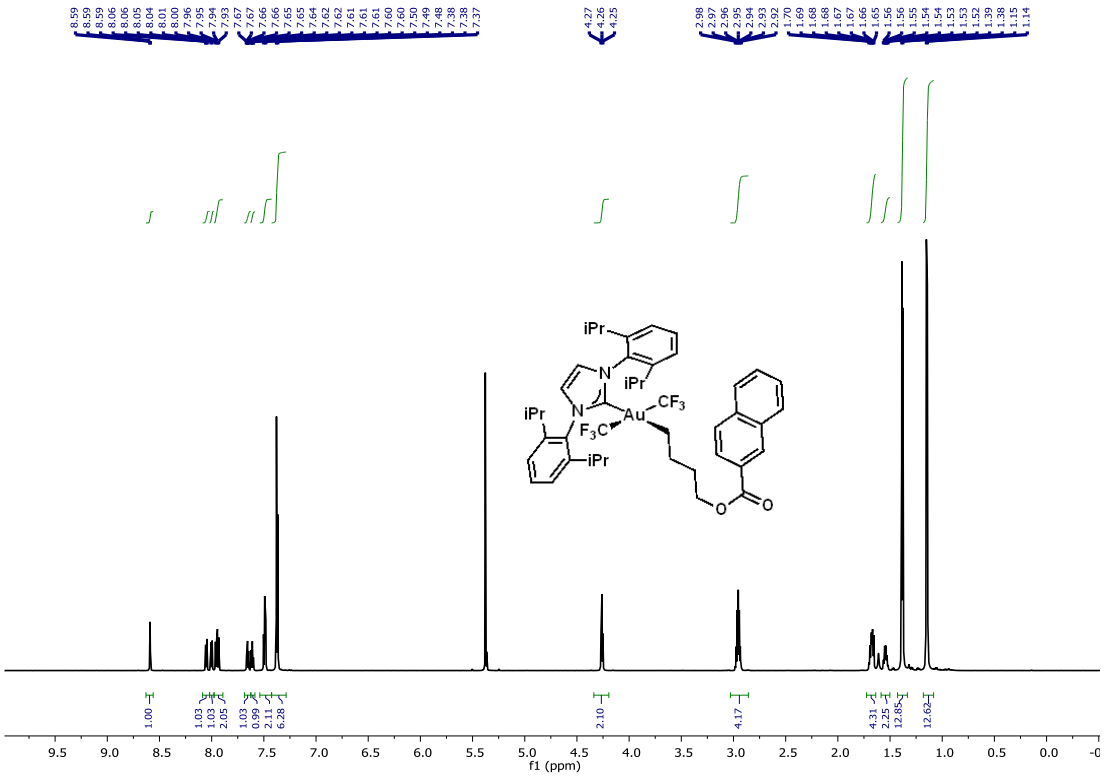
iPr
iPr
iPr
iPr
N
N
Au
CF3
F3C
O
O
f1 (ppm)

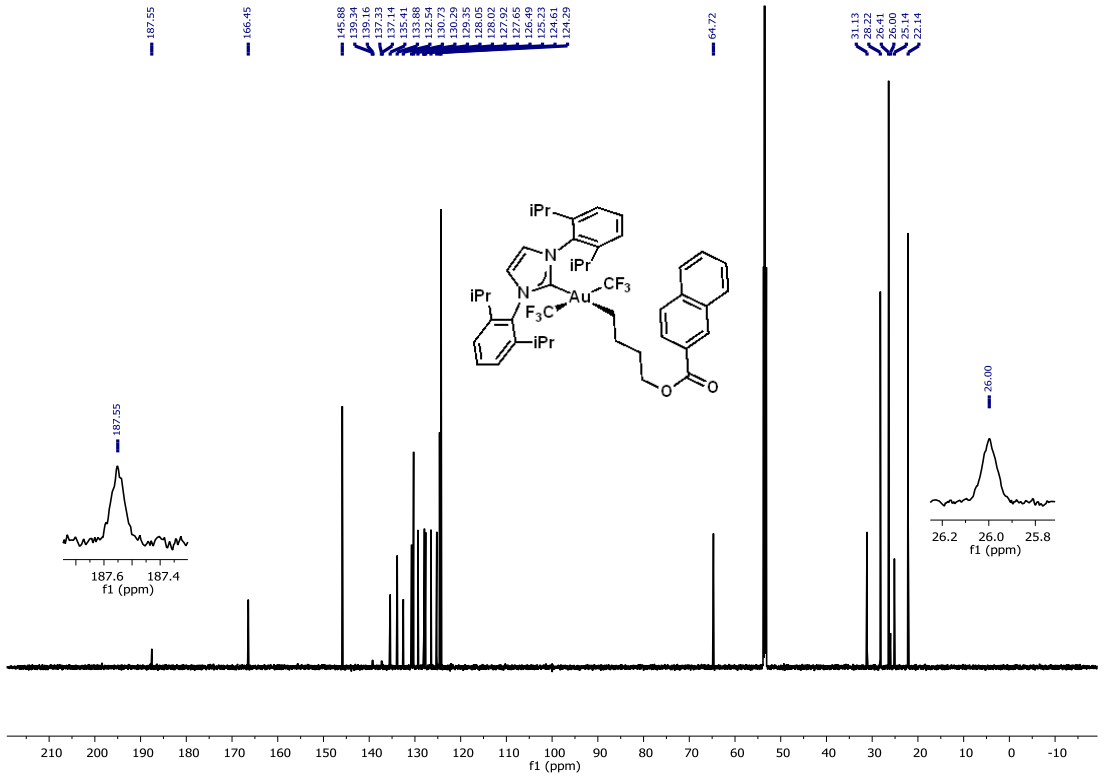
iPr
iPr
iPr
iPr
N
N
Au
CF3
F3C
O
O
187.55
26.00
f1 (ppm)

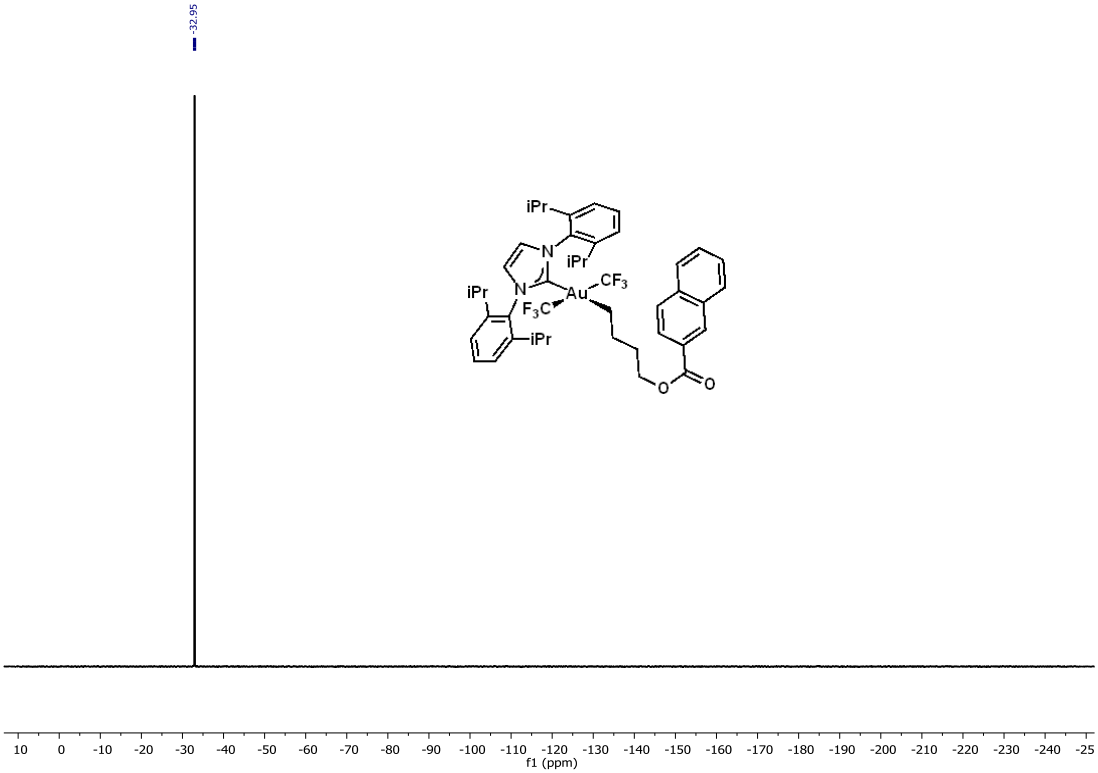
-32.95
iPr
iPr
iPr
iPr
N
N
Au
CF3
F3C
O
O
10 0 -10 -20 -30 -40 -50 -60 -70 -80 -90 -100 -110 -120 -130 -140 -150 -160 -170 -180 -190 -200 -210 -220 -230 -240 -25
f1 (ppm)

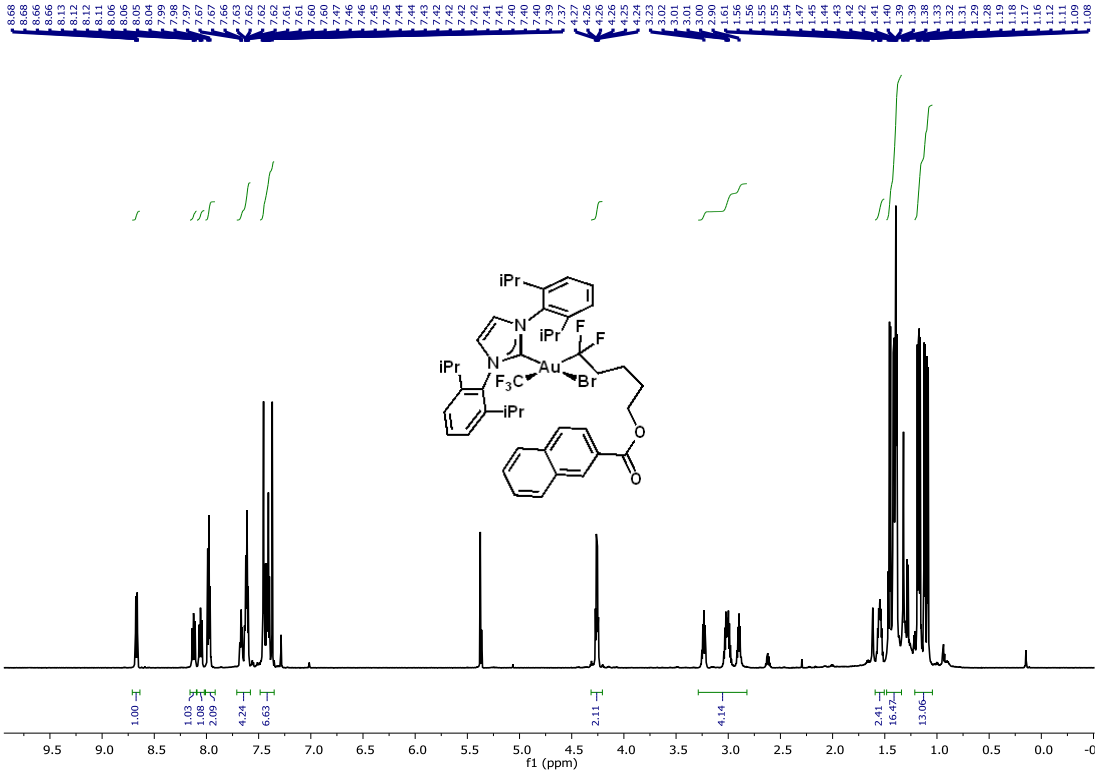
iPr
iPr
iPr
iPr
N
N
Au
F
F
F3C
Br
O
O
1.00
1.03
1.08
2.09
4.24
6.63
2.11
4.14
2.41
16.47
13.06
9.5 9.0 8.5 8.0 7.5 7.0 6.5 6.0 5.5 5.0 4.5 4.0 3.5 3.0 2.5 2.0 1.5 1.0 0.5 0.0
f1 (ppm)

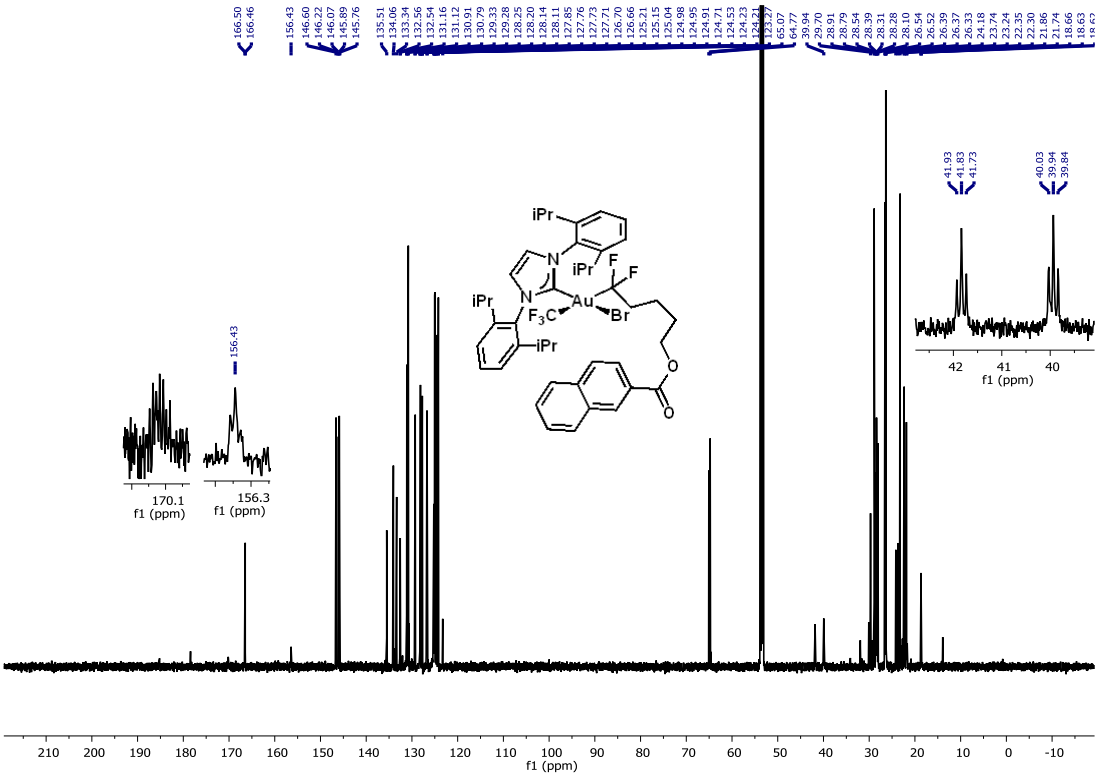
iPr
iPr
F
F
N
N
Au
Br
F3C
iPr
iPr
O
O
156.43
170.1
f1 (ppm)
156.3
f1 (ppm)
41.93
41.83
41.73
40.03
39.94
39.84
42
41
40
f1 (ppm)
210 200 190 180 170 160 150 140 130 120 110 100 90 80 70 60 50 40 30 20 10 0 -10
f1 (ppm)

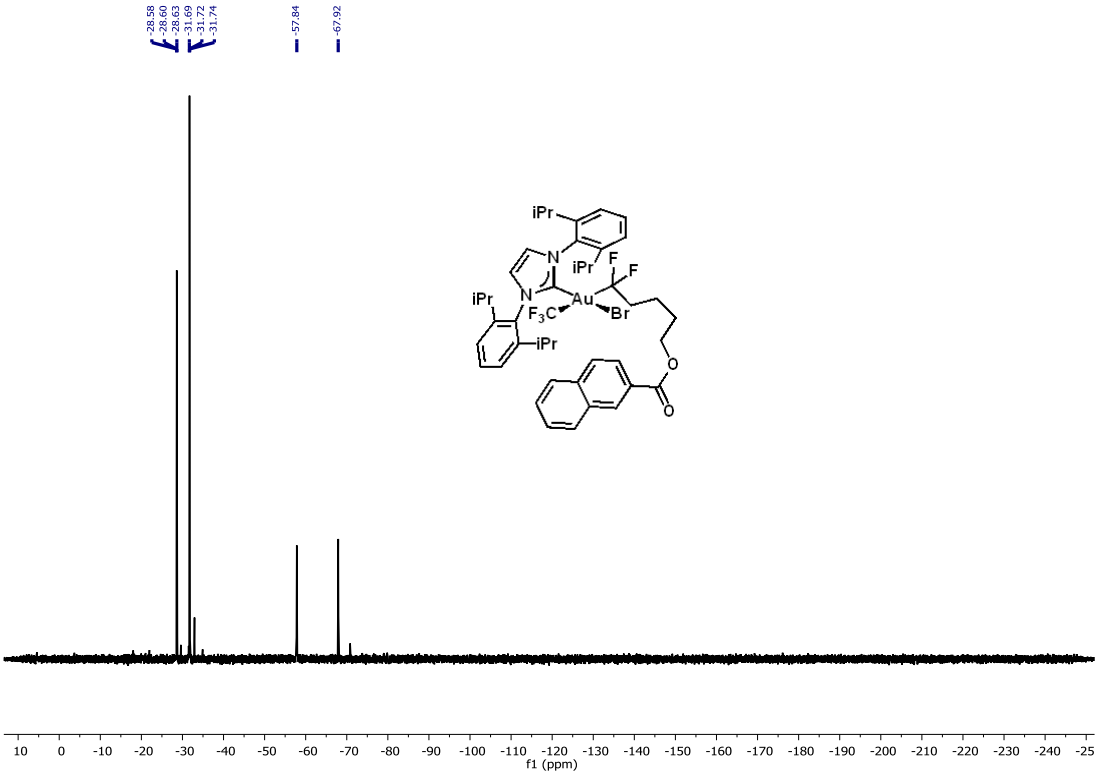
28.58
28.60
28.63
31.69
31.72
31.74
-57.84
-67.92
iPr
iPr
F
F
N
N
Au
Br
F3C
iPr
iPr
O
O
10 0 -10 -20 -30 -40 -50 -60 -70 -80 -90 -100 -110 -120 -130 -140 -150 -160 -170 -180 -190 -200 -210 -220 -230 -240 -25
f1 (ppm)

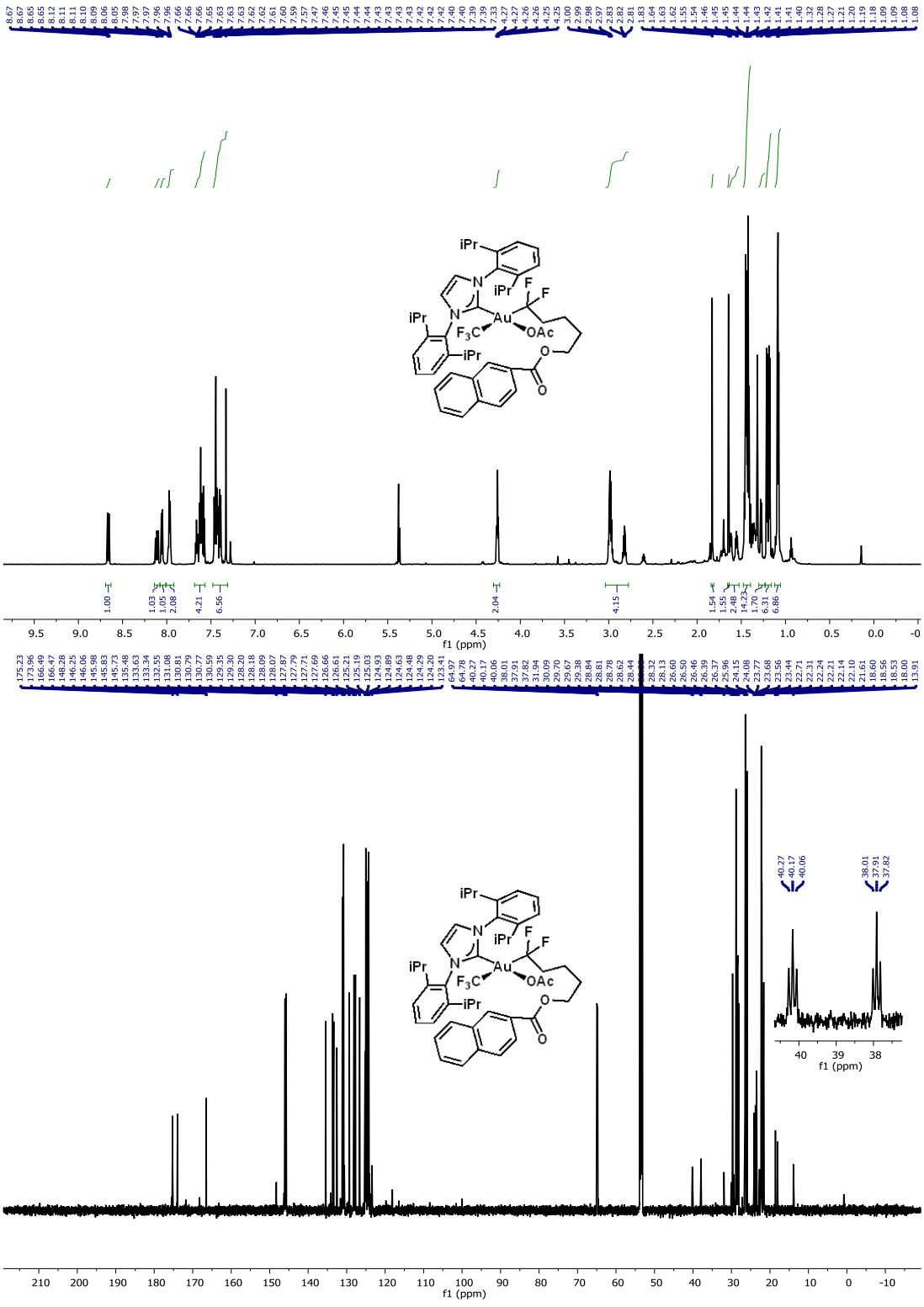
iPr
iPr
F
F
N
N
iPr
Au
F3C
OAc
iPr
O
O
f1 (ppm)
f1 (ppm)

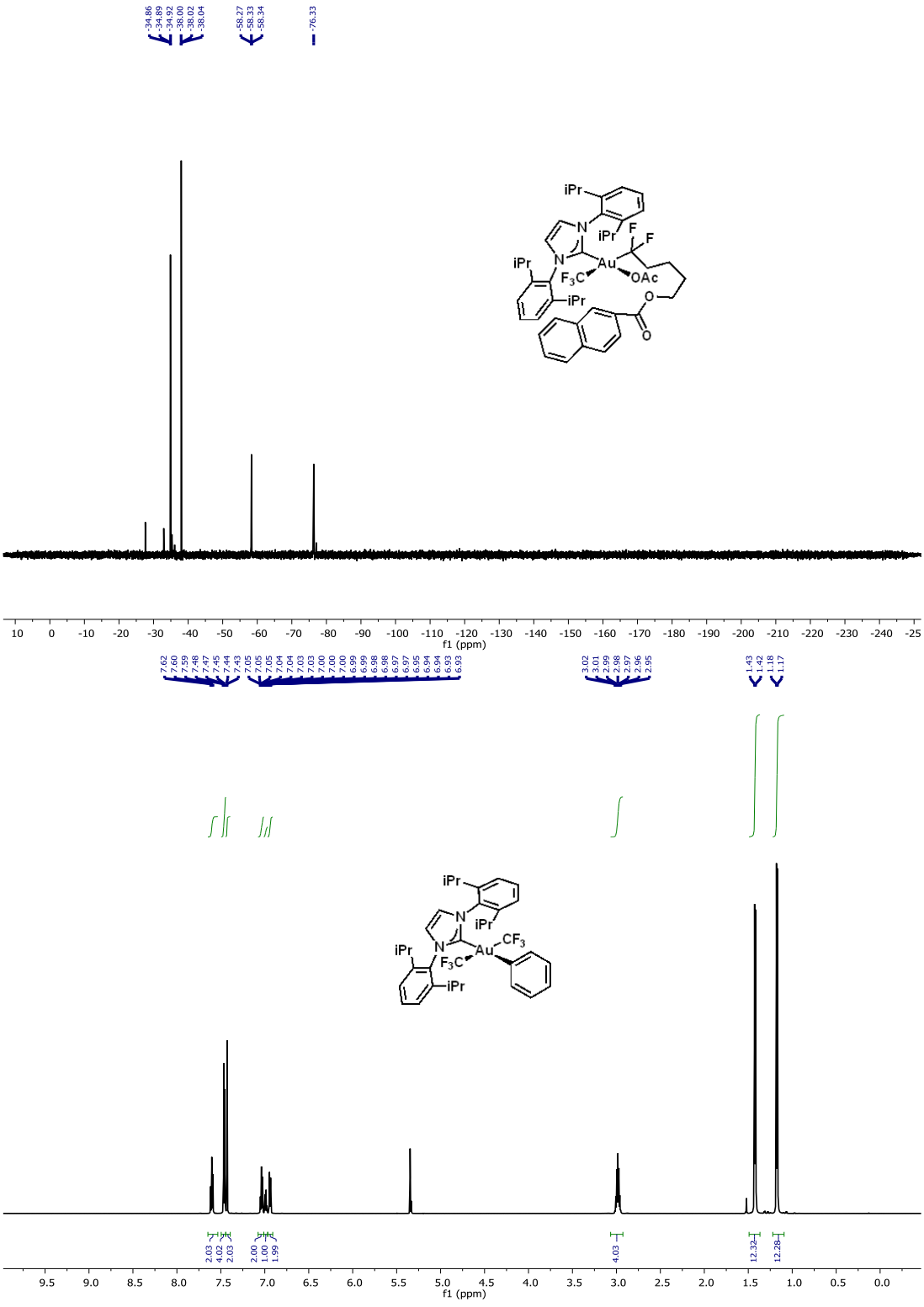
-34.86
-34.89
-34.92
-38.00
-38.02
-38.04
-58.27
-58.33
-58.34
-76.33
iPr
iPr
F
F
iPr
N
N
Au
F3C
OAc
iPr
O
O
f1 (ppm)
7.62
7.60
7.59
7.48
7.47
7.45
7.44
7.43
7.05
7.05
7.05
7.04
7.04
7.03
7.03
7.00
7.00
7.00
6.99
6.99
6.98
6.98
6.97
6.97
6.95
6.94
6.94
6.93
6.93
3.02
3.01
2.99
2.98
2.97
2.96
2.95
1.43
1.42
1.18
1.17
iPr
iPr
N
N
iPr
CF3
Au
F3C
iPr
2.03
4.02
2.03
2.00
1.00
1.99
4.03
12.32
12.28
f1 (ppm)

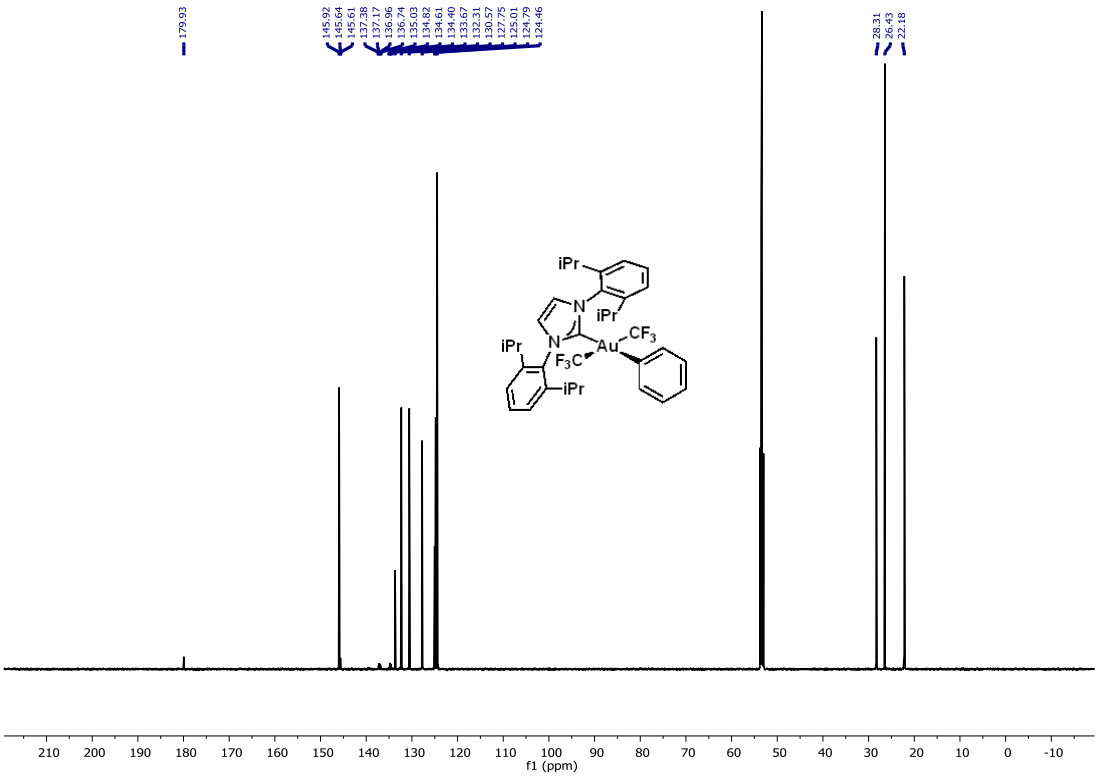
179.93
145.92
145.64
145.61
137.38
137.17
136.96
136.74
135.03
134.82
134.61
134.40
133.67
132.31
130.57
127.75
125.01
124.79
124.46
28.31
26.43
22.18
iPr
iPr
iPr
iPr
N
N
Au
CF3
F3C
210 200 190 180 170 160 150 140 130 120 110 100 90 80 70 60 50 40 30 20 10 0 -10
f1 (ppm)

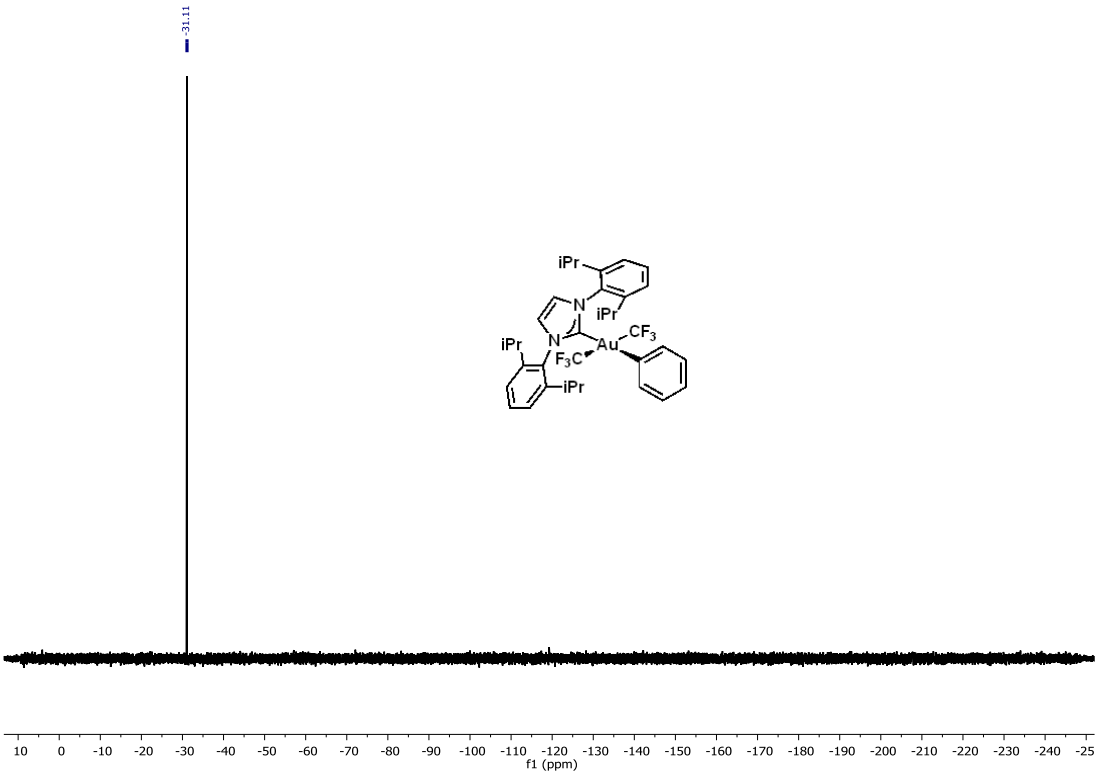
31.11
iPr
iPr
iPr
iPr
N
N
Au
CF3
F3C
10 0 -10 -20 -30 -40 -50 -60 -70 -80 -90 -100 -110 -120 -130 -140 -150 -160 -170 -180 -190 -200 -210 -220 -230 -240 -25
f1 (ppm)

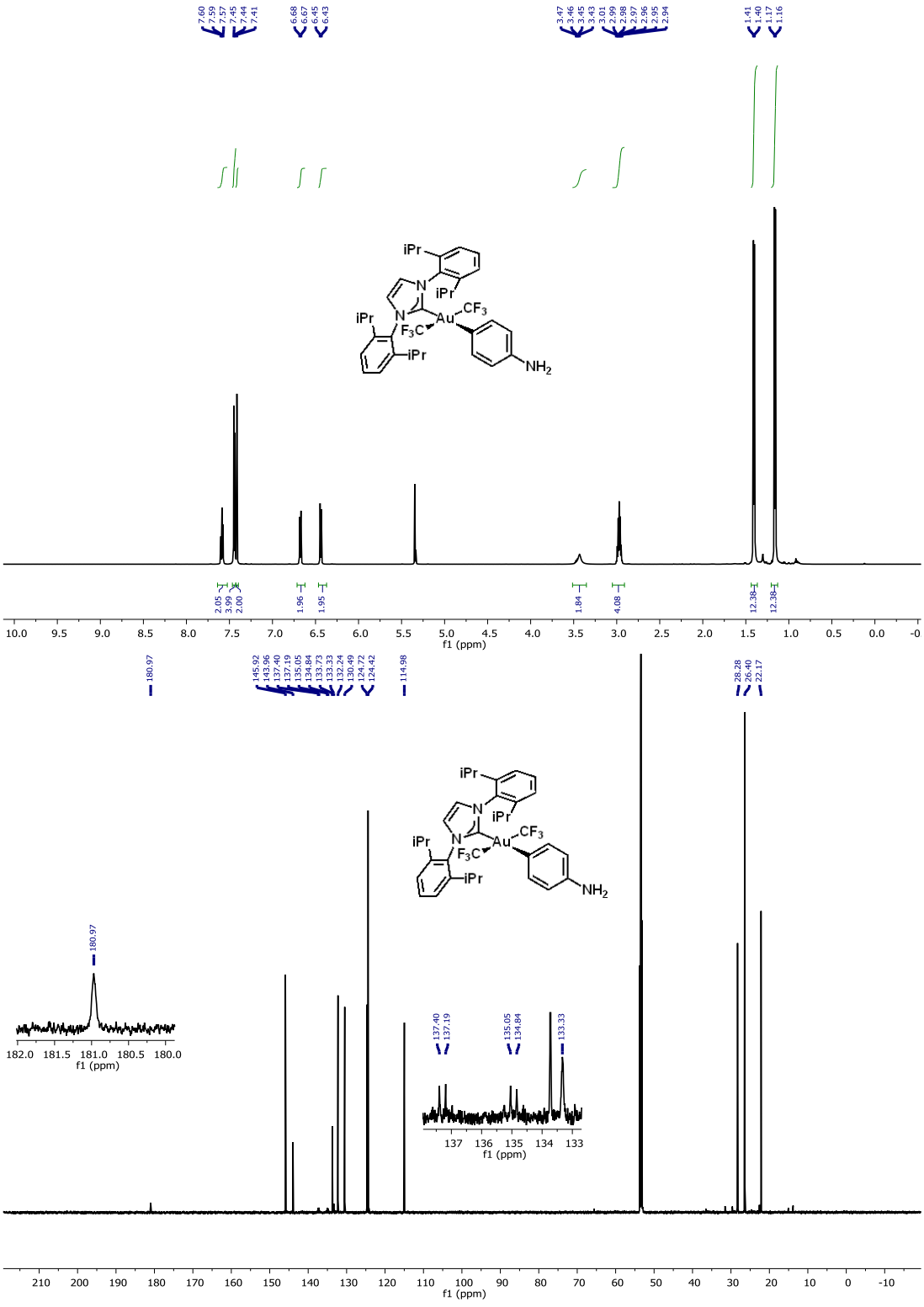
7.60
7.59
7.57
7.45
7.44
7.41
6.68
6.67
6.45
6.43
3.47
3.46
3.45
3.43
3.01
2.99
2.98
2.97
2.96
2.95
2.94
1.41
1.40
1.17
1.16
iPr
iPr
iPr
iPr
N
N
Au
CF3
F3C
NH2
2.05
3.99
2.00
1.96
1.95
1.84
4.08
12.38
12.38
f1 (ppm)
180.97
145.92
143.96
137.40
137.19
135.05
134.84
133.73
133.33
132.24
130.49
124.72
124.42
114.98
28.28
26.40
22.17
182.0 181.5 181.0 180.5 180.0
f1 (ppm)
137 136 135 134 133
f1 (ppm)
210 200 190 180 170 160 150 140 130 120 110 100 90 80 70 60 50 40 30 20 10 0 -10
f1 (ppm)

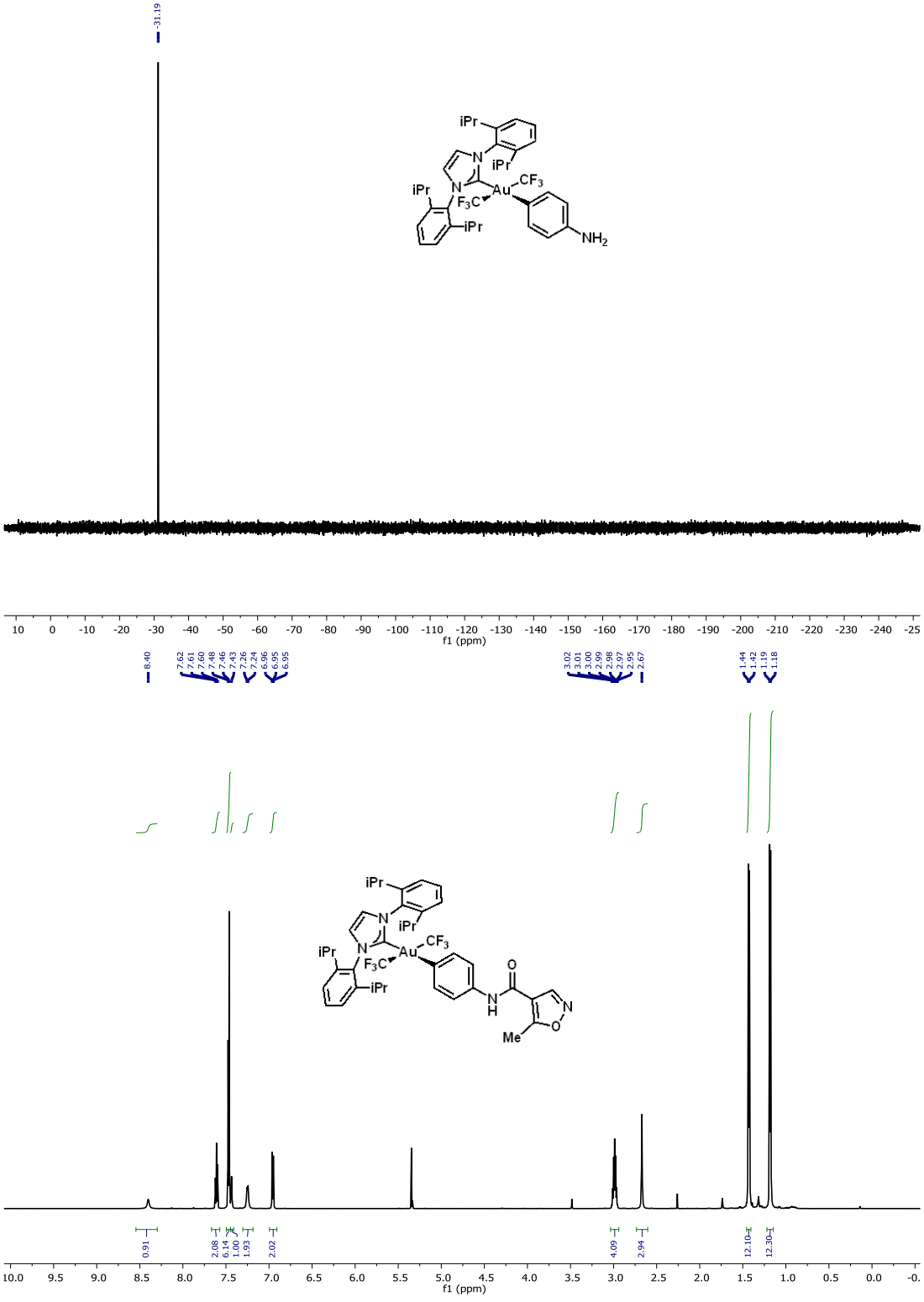
-31.19
iPr
iPr
iPr
iPr
N
N
Au
CF3
F3C
NH2
f1 (ppm)
8.40
7.62
7.61
7.60
7.48
7.46
7.43
7.26
7.24
6.96
6.95
6.95
3.02
3.01
3.00
2.99
2.98
2.97
2.95
2.67
1.44
1.42
1.19
1.18
O
N
H
O
N
Me
0.91
2.08
6.14
1.00
1.93
2.02
4.09
2.94
12.10
12.36

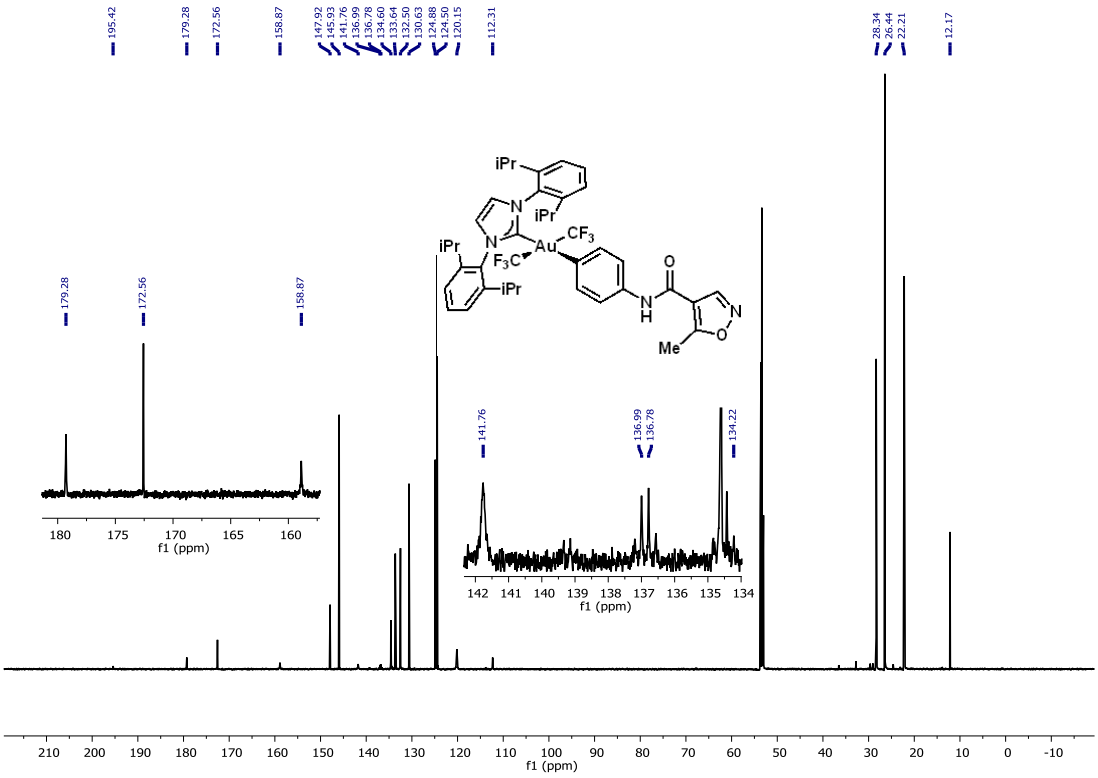
195.42
179.28
172.56
158.87
147.92
145.93
141.76
136.99
136.78
134.60
133.64
132.50
130.63
124.88
124.50
120.15
112.31
28.34
26.44
22.21
12.17
iPr
iPr
iPr
iPr
N
N
Au
CF3
F3C
O
N
H
N
O
Me
179.28
172.56
158.87
180 175 170 165 160
f1 (ppm)
141.76
136.99
136.78
134.22
142 141 140 139 138 137 136 135 134
f1 (ppm)
210 200 190 180 170 160 150 140 130 120 110 100 90 80 70 60 50 40 30 20 10 0 -10
f1 (ppm)

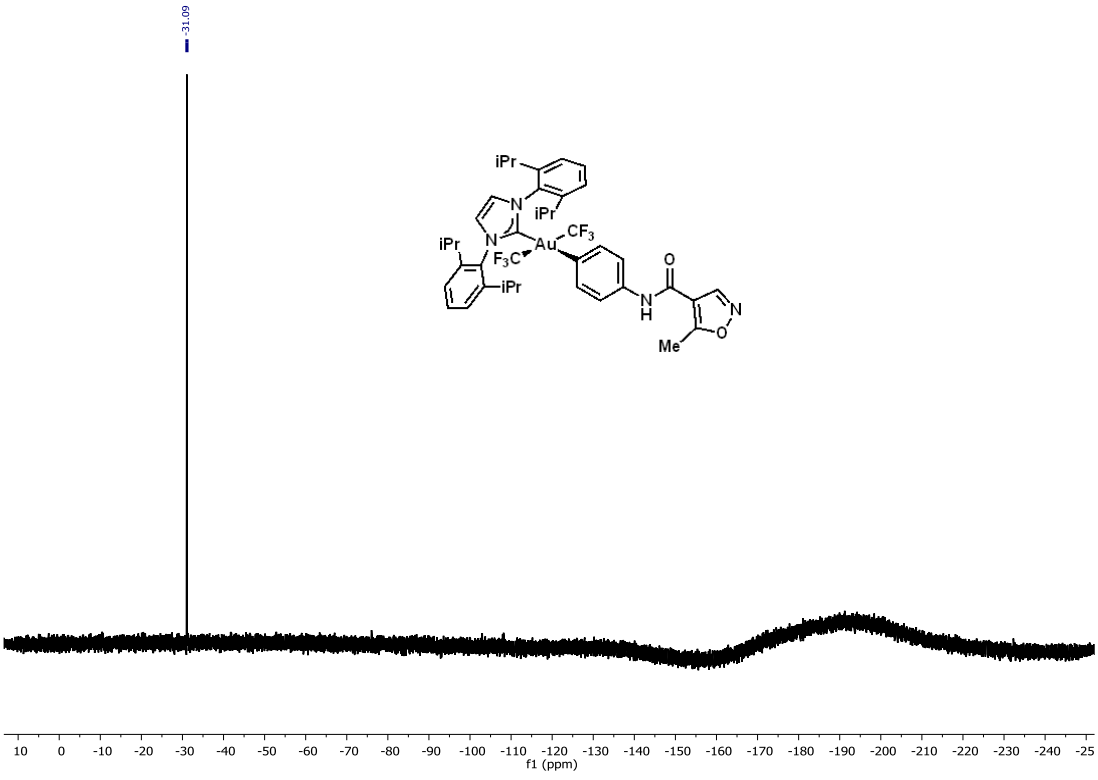
31.09
iPr
iPr
iPr
iPr
N
N
Au
CF3
F3C
O
N
H
N
O
Me
10 0 -10 -20 -30 -40 -50 -60 -70 -80 -90 -100 -110 -120 -130 -140 -150 -160 -170 -180 -190 -200 -210 -220 -230 -240 -25
f1 (ppm)

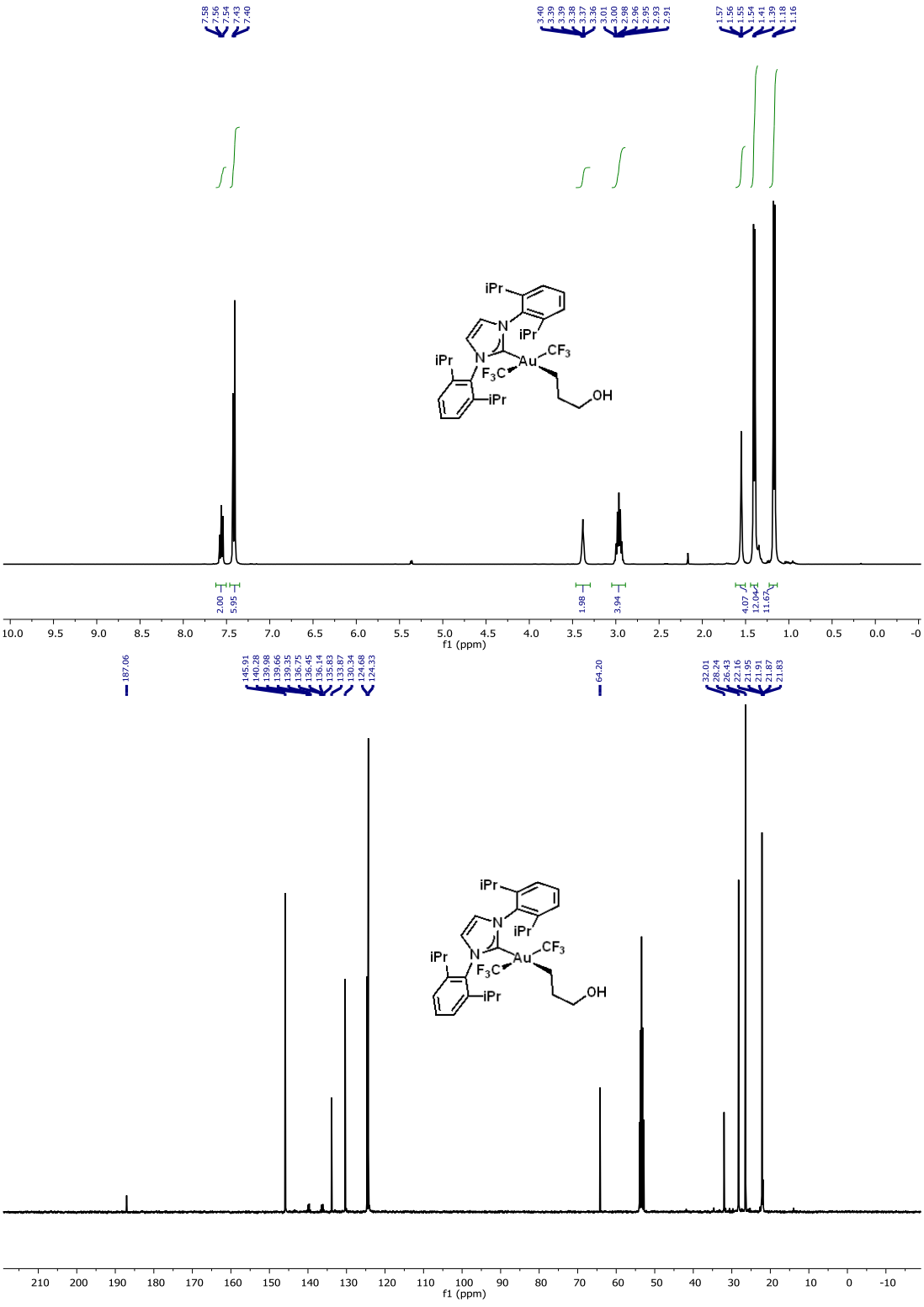
7.58
7.56
7.54
7.43
7.40
3.40
3.39
3.38
3.37
3.36
3.01
3.00
2.98
2.96
2.95
2.93
2.91
1.57
1.56
1.55
1.54
1.41
1.39
1.18
1.16
iPr
N
iPr
N
Au
CF3
F3C
iPr
OH
2.00
5.95
1.98
3.94
4.07
12.04
11.65
f1 (ppm)
187.06
145.91
140.28
139.98
139.66
139.35
136.75
136.45
136.14
135.83
133.97
130.34
124.68
124.33
64.20
32.01
28.24
26.43
22.16
21.95
21.91
21.87
21.83
f1 (ppm)

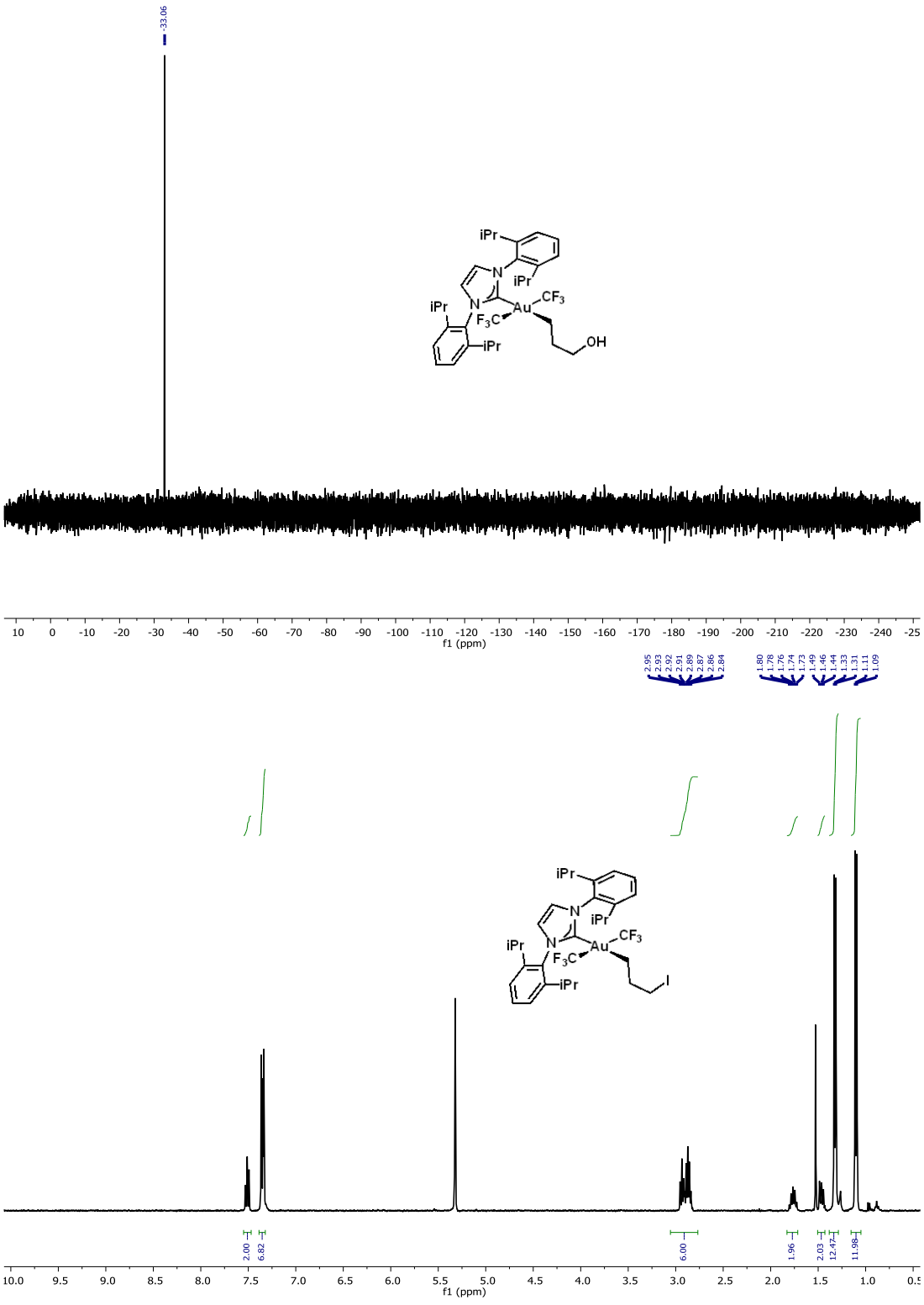
-33.06
iPr
iPr
iPr
iPr
N
N
Au
CF3
F3C
OH
f1 (ppm)
2.95
2.93
2.92
2.91
2.89
2.87
2.86
2.84
1.80
1.78
1.76
1.74
1.73
1.49
1.46
1.44
1.33
1.31
1.11
1.09
I
2.00
6.82
6.00
1.96
2.03
12.47
11.98

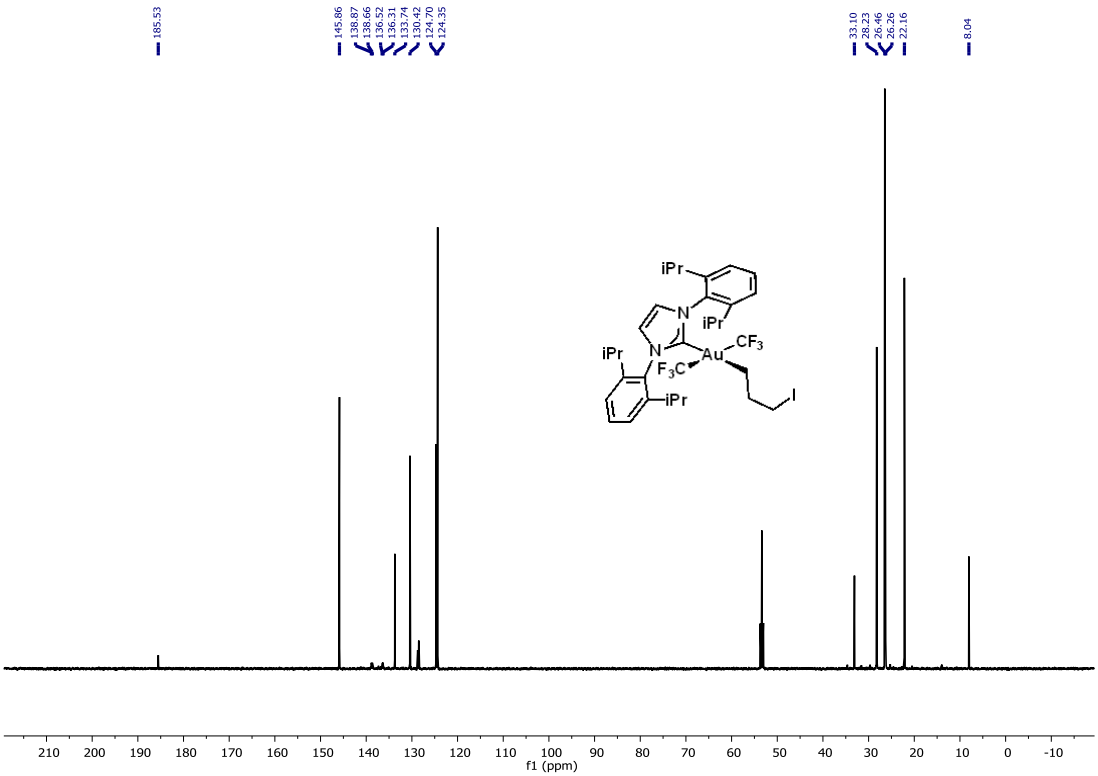
185.53
145.86
138.87
138.66
136.52
136.31
133.74
130.42
124.70
124.35
33.10
28.23
26.46
26.26
22.16
8.04
iPr
iPr
iPr
iPr
N
N
Au
CF3
F3C
I
210 200 190 180 170 160 150 140 130 120 110 100 90 80 70 60 50 40 30 20 10 0 -10
f1 (ppm)

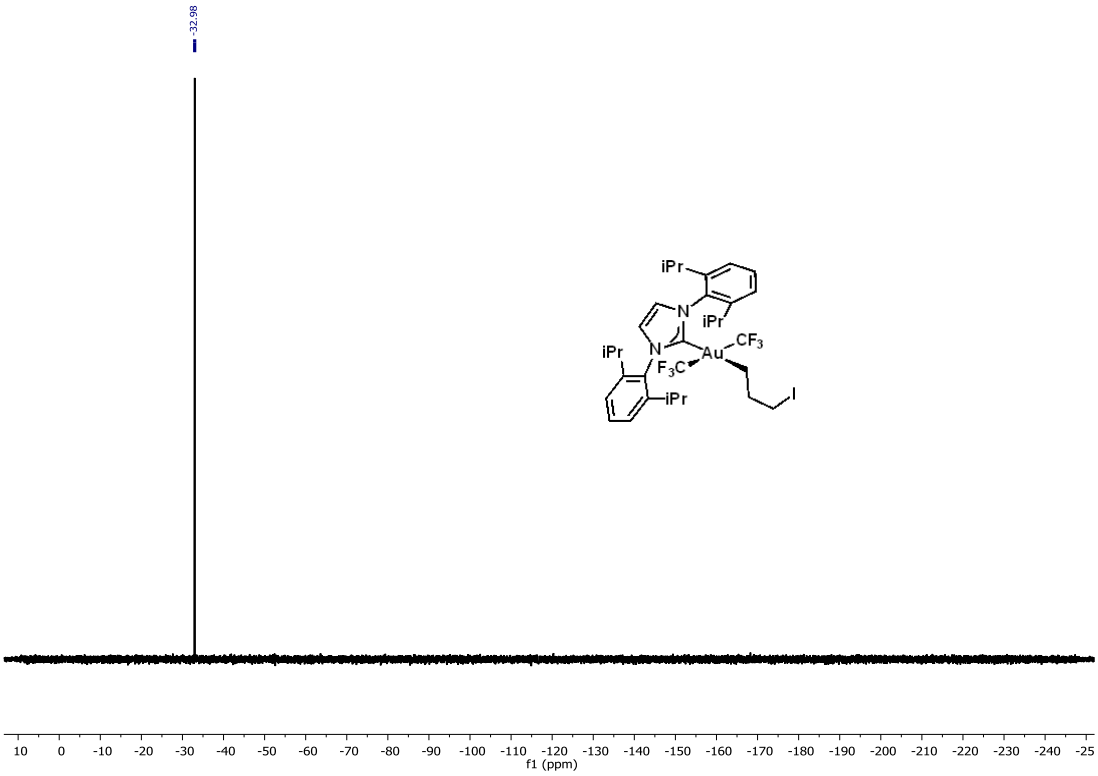
-32.98
iPr
iPr
iPr
iPr
N
N
Au
CF3
F3C
I
10 0 -10 -20 -30 -40 -50 -60 -70 -80 -90 -100 -110 -120 -130 -140 -150 -160 -170 -180 -190 -200 -210 -220 -230 -240 -25
f1 (ppm)

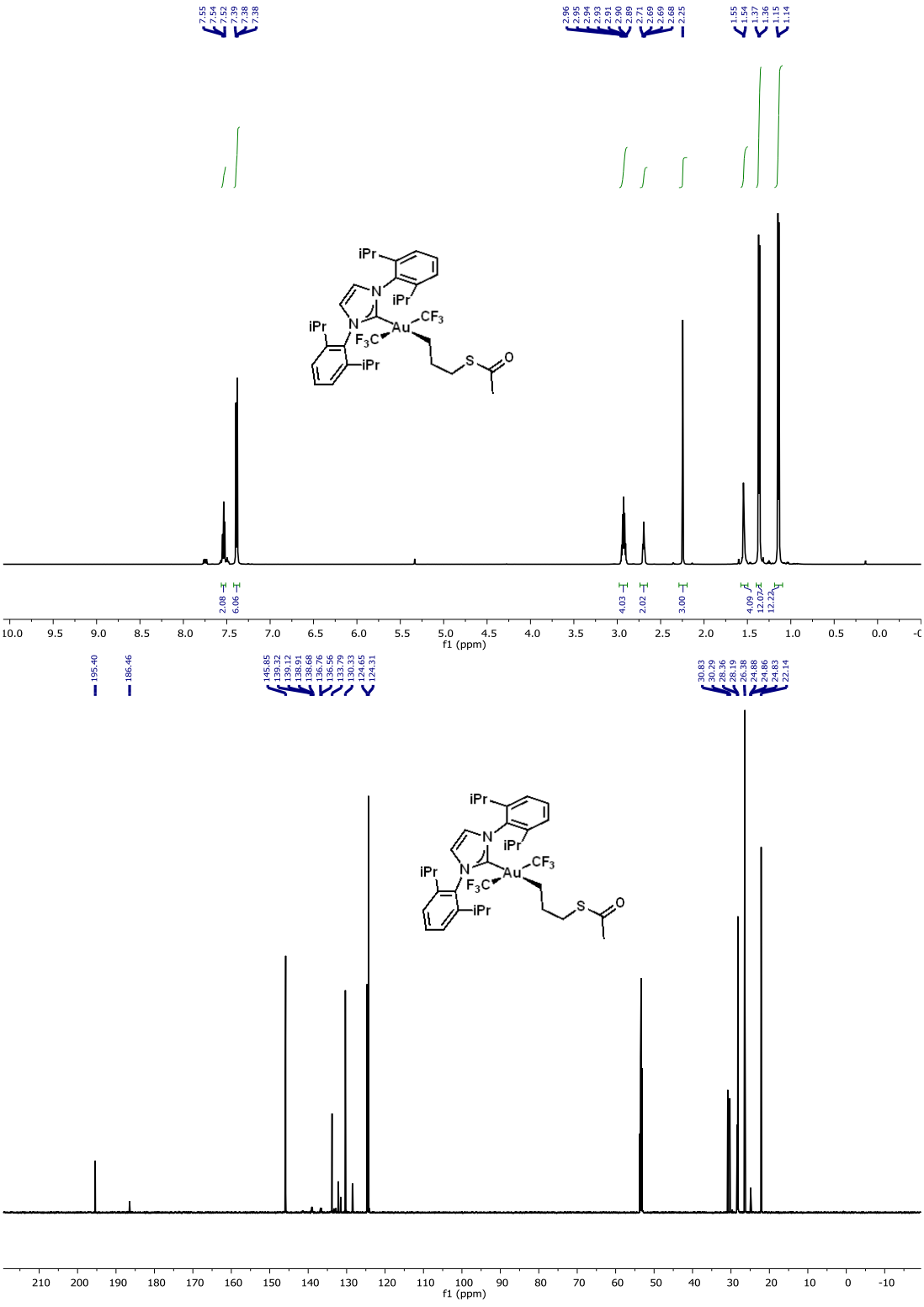
7.55
7.54
7.52
7.39
7.38
7.38
2.96
2.95
2.94
2.93
2.91
2.90
2.89
2.71
2.69
2.69
2.68
2.25
1.55
1.54
1.37
1.36
1.15
1.14
iPr
iPr
iPr
iPr
N
N
Au
CF3
F3C
S
O
2.08
6.06
4.03
2.02
3.00
4.09
12.07
12.22
f1 (ppm)
195.40
186.46
145.85
139.32
139.12
138.91
138.68
136.76
136.56
133.79
130.33
124.65
124.31
30.83
30.29
28.36
28.19
26.38
24.88
24.86
24.83
22.14
f1 (ppm)

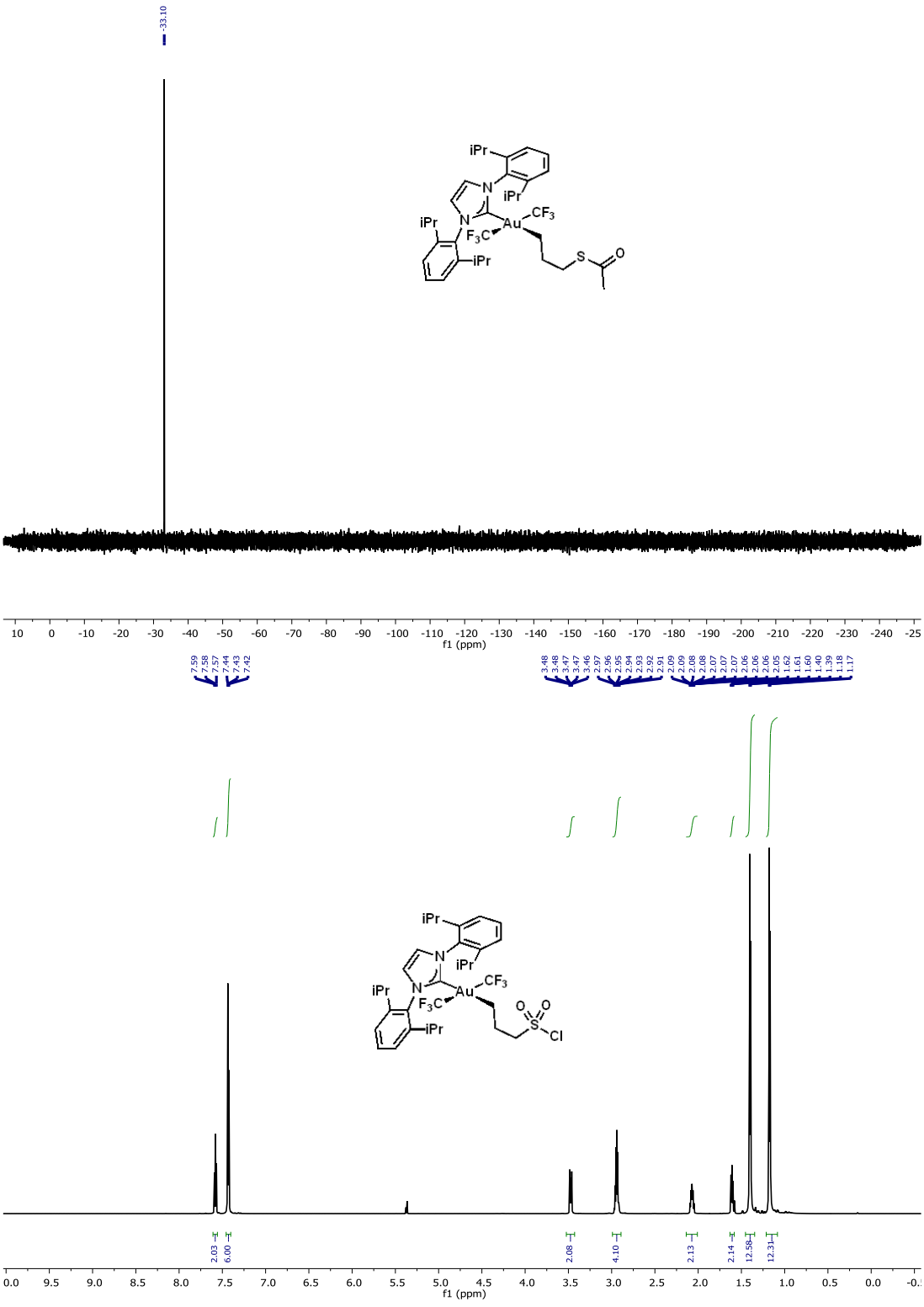
-33.10
iPr
iPr
iPr
iPr
N
N
Au
CF3
F3C
S
O
f1 (ppm)
7.59
7.58
7.57
7.44
7.43
7.42
3.48
3.47
3.46
2.97
2.96
2.95
2.94
2.93
2.92
2.91
2.09
2.08
2.07
2.06
2.05
1.62
1.61
1.60
1.40
1.39
1.18
1.17
2.03
6.00
2.08
4.10
2.13
2.14
12.58
12.31
O
S
Cl

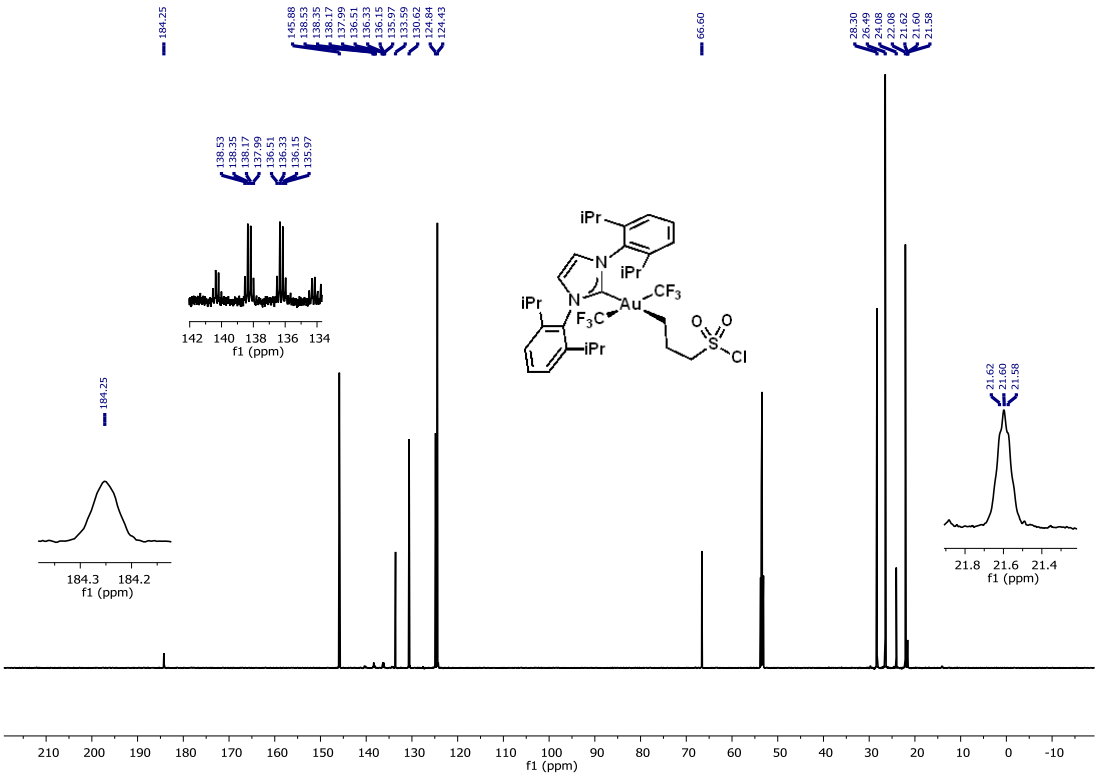
184.25
145.88
138.53
138.35
138.17
137.99
136.51
136.33
136.15
135.97
133.59
130.62
124.84
124.43
66.60
28.30
26.49
24.08
22.08
21.62
21.60
21.58
iPr
iPr
iPr
iPr
N
N
Au
CF3
F3C
O
O
S
Cl
142 140 138 136 134
f1 (ppm)
184.3 184.2
f1 (ppm)
21.8 21.6 21.4
f1 (ppm)
210 200 190 180 170 160 150 140 130 120 110 100 90 80 70 60 50 40 30 20 10 0 -10
f1 (ppm)

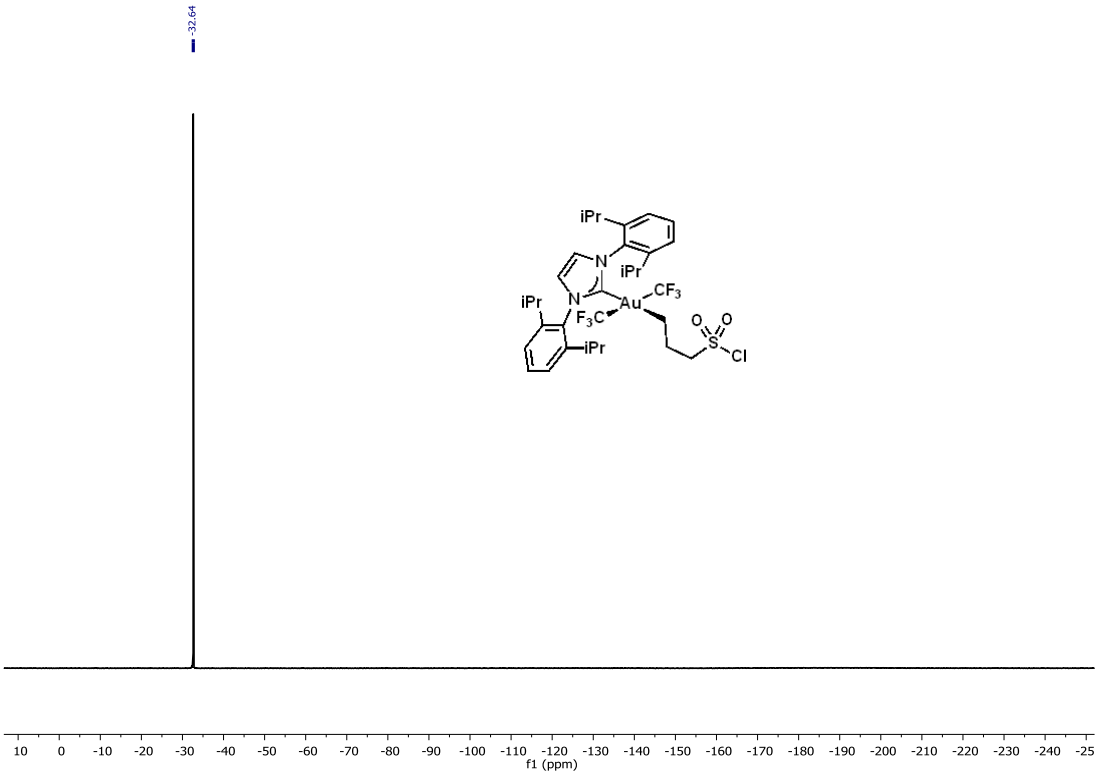
-32.64
iPr
iPr
iPr
iPr
N
N
Au
CF3
F3C
O
O
S
Cl
10 0 -10 -20 -30 -40 -50 -60 -70 -80 -90 -100 -110 -120 -130 -140 -150 -160 -170 -180 -190 -200 -210 -220 -230 -240 -25
f1 (ppm)

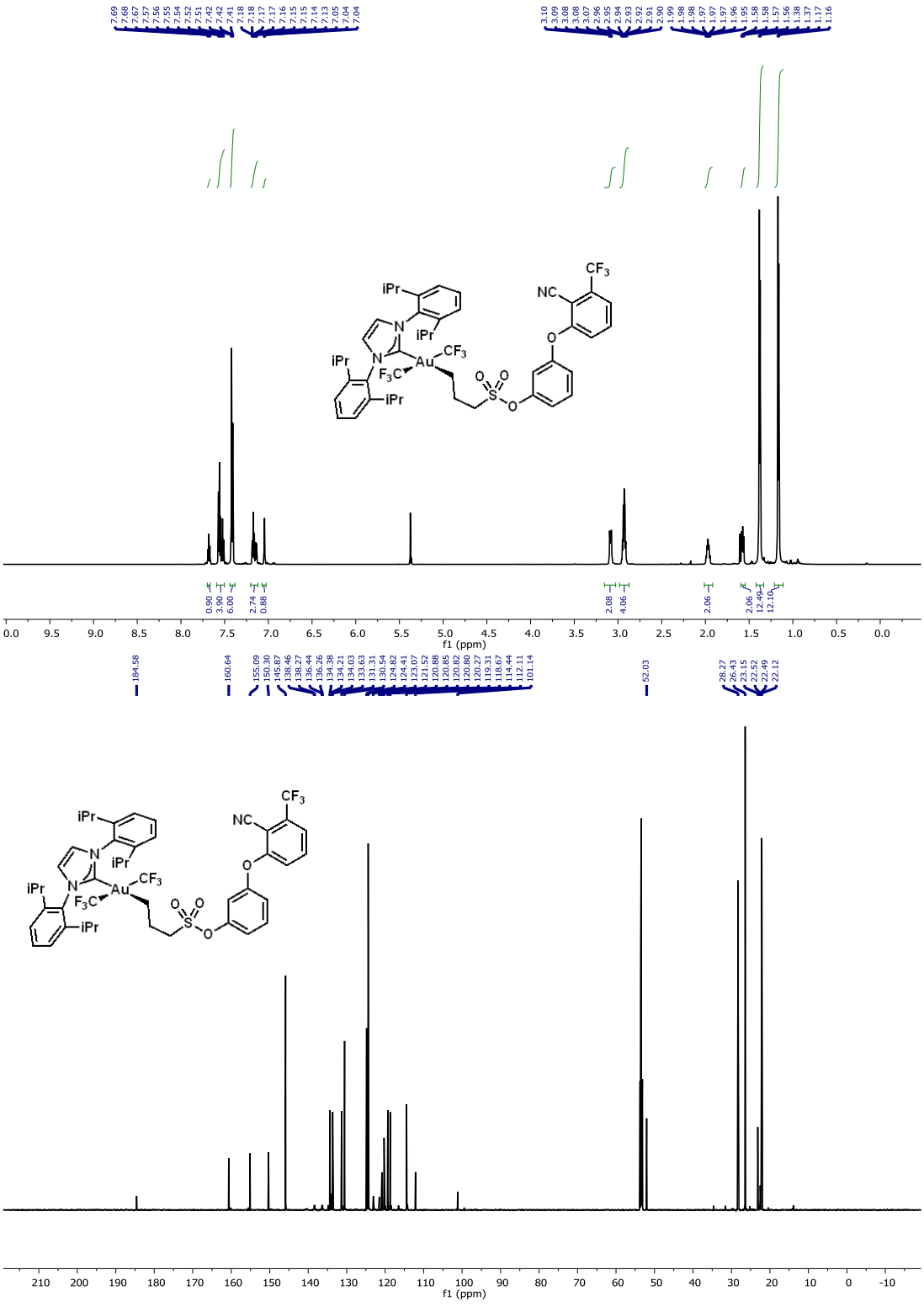
iPr
iPr
iPr
iPr
N
N
Au
CF3
F3C
O
S
O
O
NC
CF3
O
f1 (ppm)

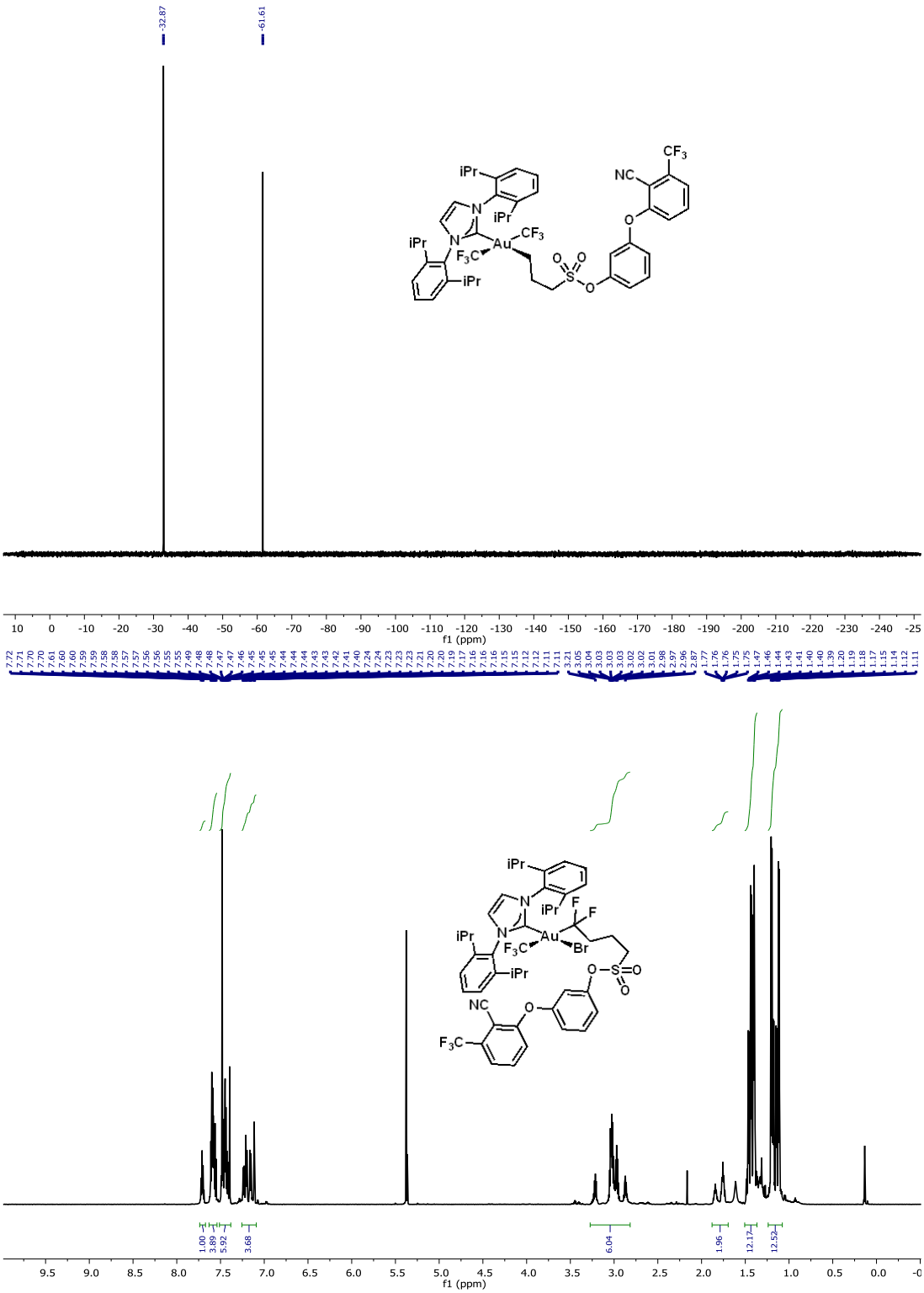
-32.87
-61.61
iPr
iPr
iPr
iPr
N
N
Au
CF3
F3C
O
S
O
O
NC
CF3
f1 (ppm)
1.00
3.89
5.92
3.68
6.04
1.96
12.17
12.52

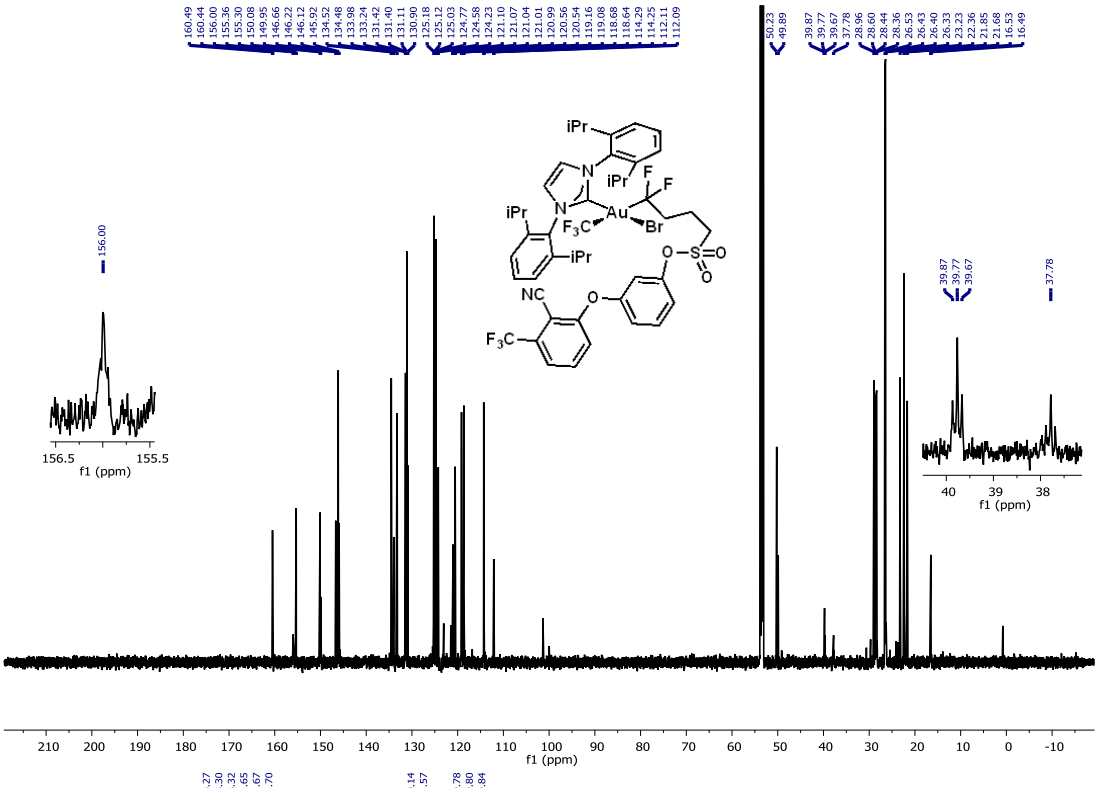
160.49
160.44
156.00
155.36
155.30
150.08
149.95
146.66
146.22
146.12
145.92
134.52
134.48
133.98
133.24
131.42
131.40
131.11
130.90
125.18
125.12
125.03
124.77
124.58
124.23
121.10
121.07
121.04
121.01
120.99
120.56
120.54
119.16
119.08
118.68
118.64
114.29
114.25
112.11
112.09
50.23
49.89
39.87
39.77
39.67
37.78
28.96
28.60
28.44
28.36
26.53
26.43
26.40
26.33
23.23
22.36
21.85
21.68
16.53
16.49
156.00
156.5
155.5
f1 (ppm)
39.87
39.77
39.67
37.78
40
39
38
f1 (ppm)
iPr
N
iPr
F
F
N
Au
Br
iPr
F3C
iPr
O
S
O
O
NC
O
F3C
210
200
190
180
170
160
150
140
130
120
110
100
90
80
70
60
50
40
30
20
10
0
-10
f1 (ppm)

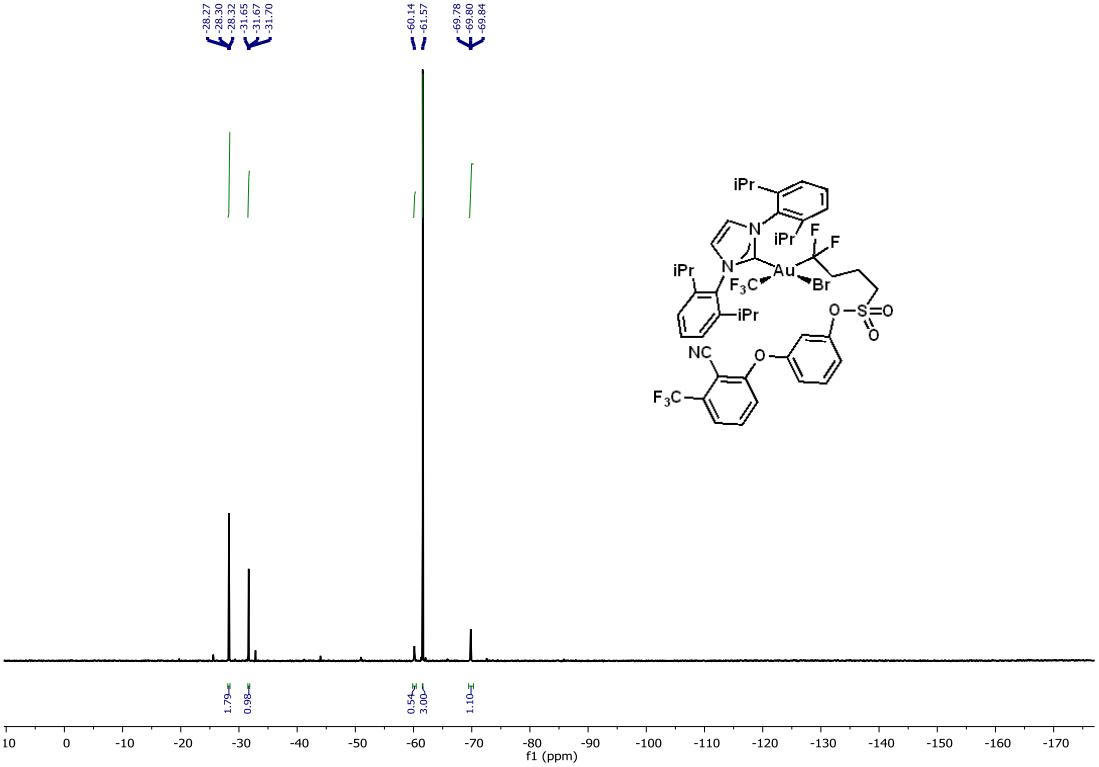
-28.27
-28.30
-28.32
-31.65
-31.67
-31.70
-60.14
-61.57
-69.78
-69.80
-69.84
1.79
0.98
0.54
3.00
1.10
iPr
N
iPr
F
F
N
Au
Br
iPr
F3C
iPr
O
S
O
O
NC
O
F3C
10
0
-10
-20
-30
-40
-50
-60
-70
-80
-90
-100
-110
-120
-130
-140
-150
-160
-170
f1 (ppm)

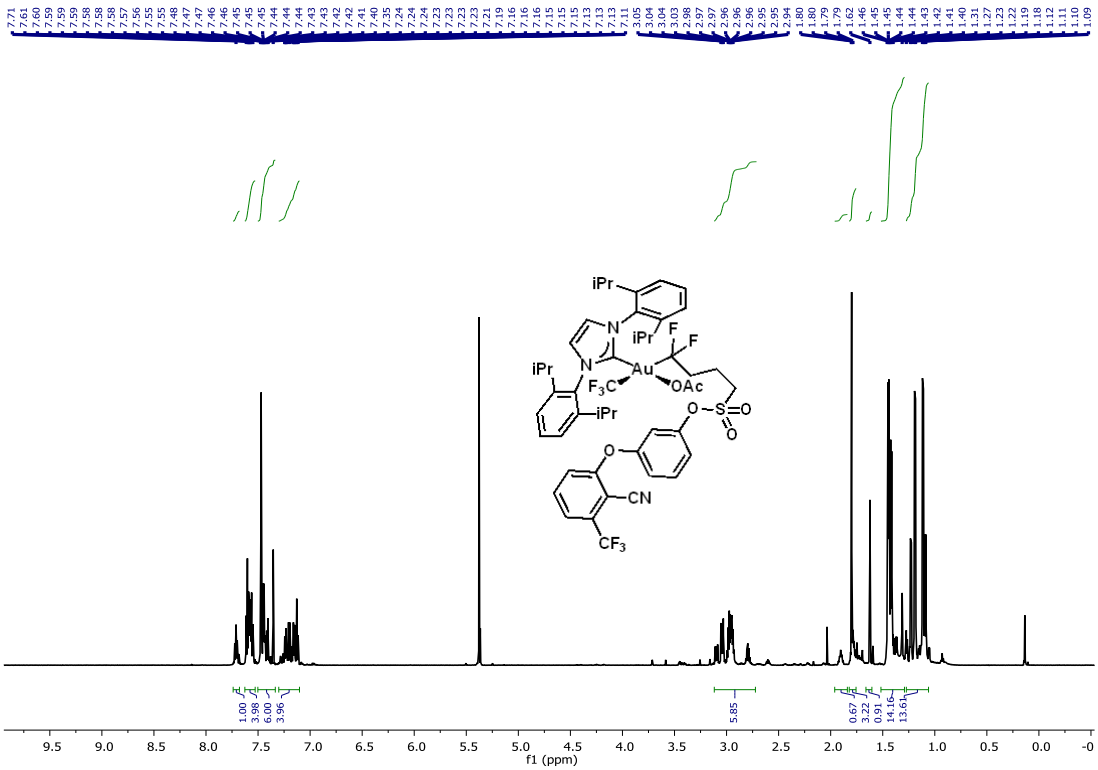
iPr
iPr
F
F
iPr
N
N
Au
F3C
OAc
iPr
O
S
O
O
O
CN
CF3
1.00
3.98
6.00
3.96
5.85
0.67
3.22
0.91
14.16
13.61
f1 (ppm)

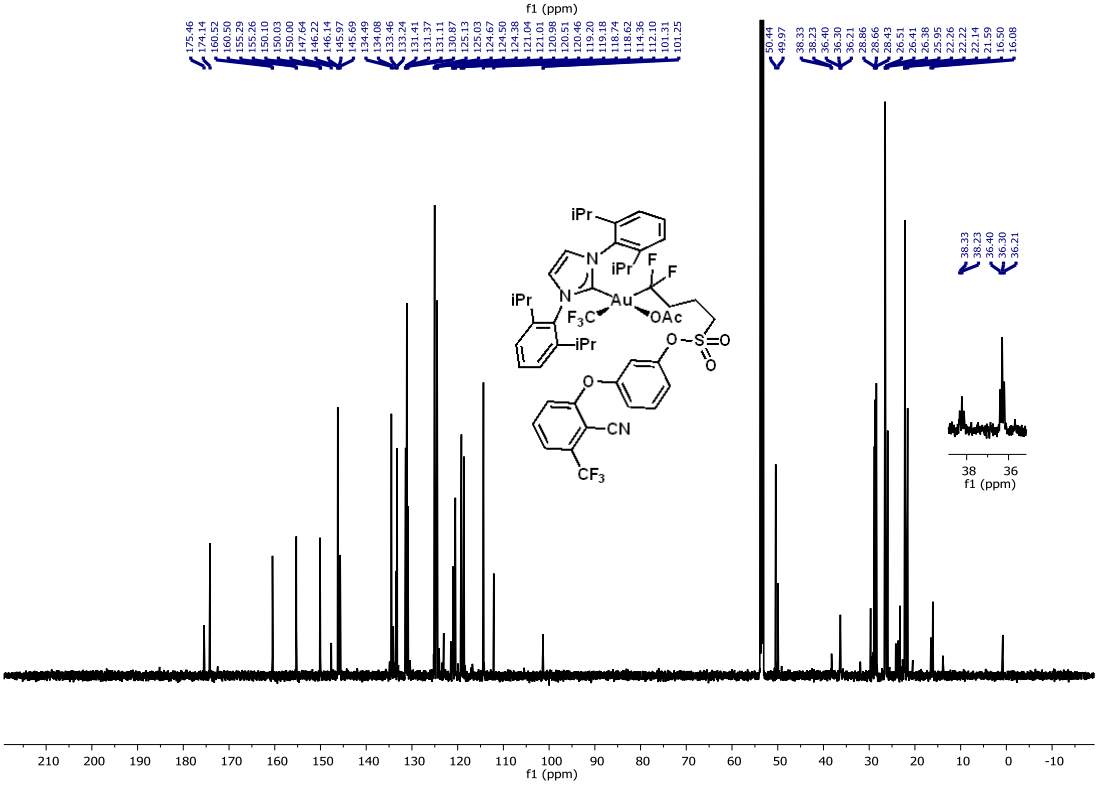
iPr
iPr
F
F
iPr
N
N
Au
F3C
OAc
iPr
O
S
O
O
O
CN
CF3
38.33
38.23
36.40
36.30
36.21
38
36
f1 (ppm)
f1 (ppm)

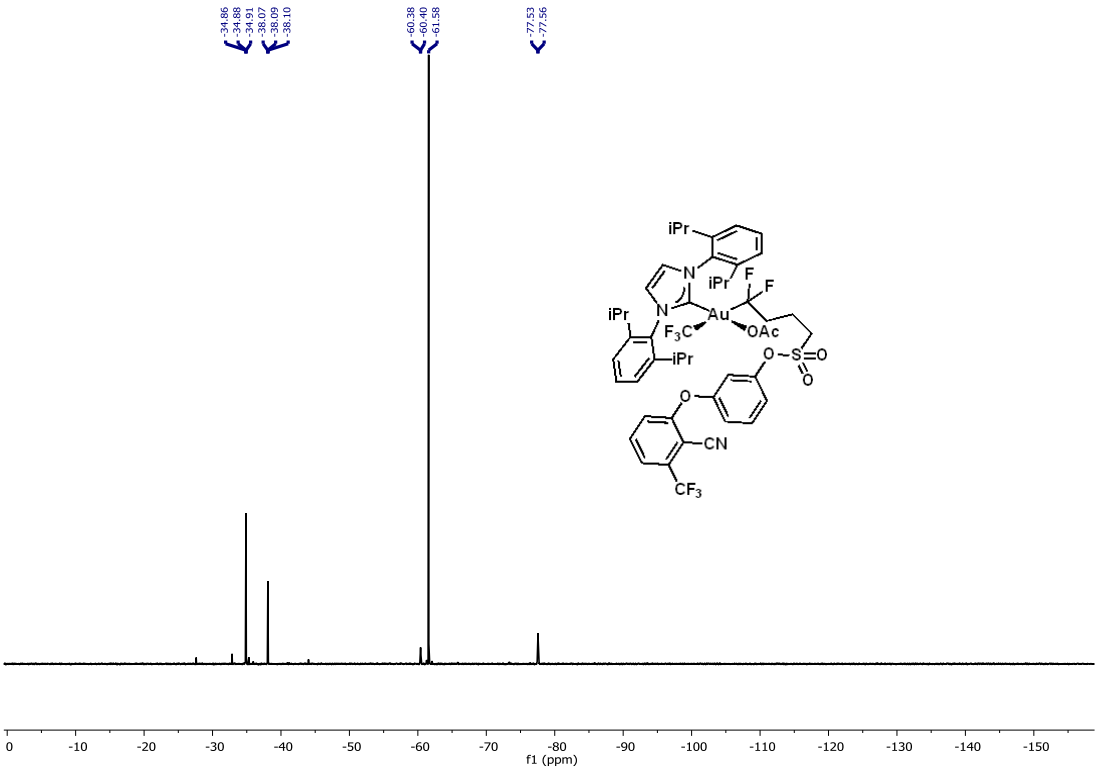
-34.86
-34.88
-34.91
-38.07
-38.09
-38.10
-60.38
-60.40
-61.58
-77.53
-77.56
iPr
iPr
F
F
iPr
N
N
Au
F3C
OAc
iPr
O
S
O
O
O
CN
CF3
0
-10
-20
-30
-40
-50
-60
-70
-80
-90
-100
-110
-120
-130
-140
-150
f1 (ppm)

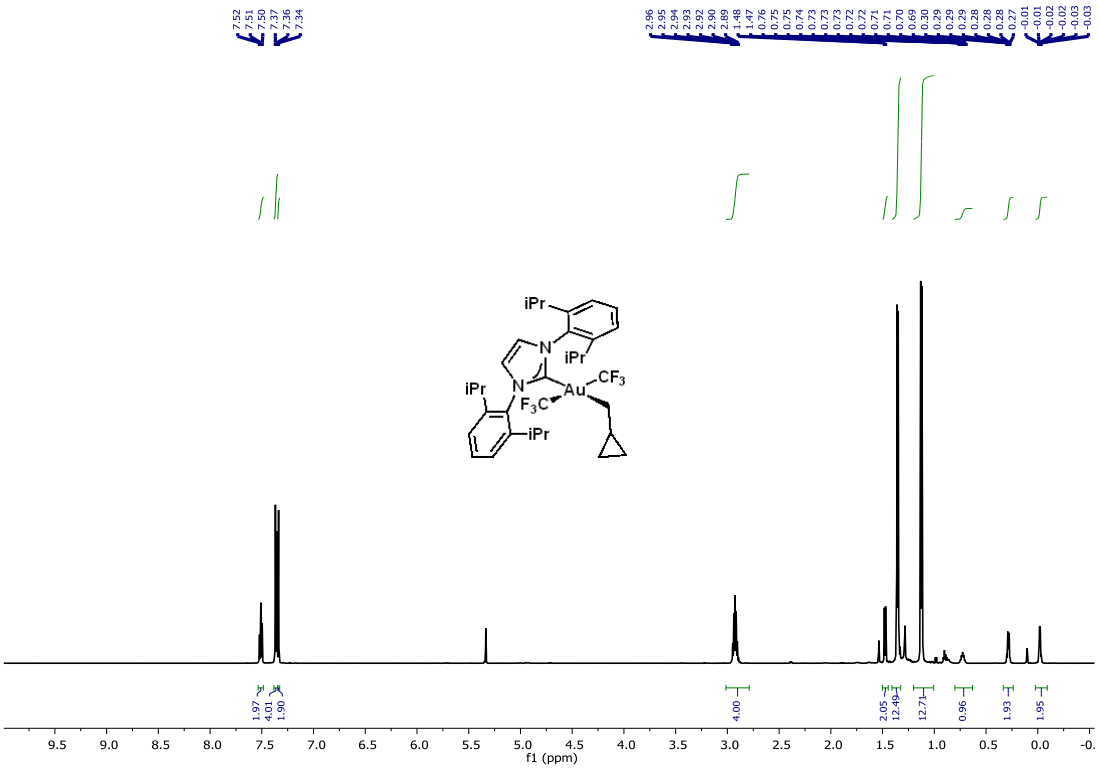
7.52
7.51
7.50
7.37
7.36
7.34
2.96
2.95
2.94
2.93
2.92
2.90
2.89
1.48
1.47
0.76
0.75
0.75
0.74
0.73
0.73
0.73
0.72
0.72
0.71
0.71
0.70
0.69
0.30
0.29
0.29
0.29
0.28
0.28
0.28
0.27
-0.01
-0.01
-0.02
-0.02
-0.03
-0.03
iPr
iPr
iPr
N
N
Au
CF3
F3C
iPr
1.97
4.01
1.90
4.00
2.05
12.49
12.71
0.96
1.93
1.95
9.5
9.0
8.5
8.0
7.5
7.0
6.5
6.0
5.5
5.0
4.5
4.0
3.5
3.0
2.5
2.0
1.5
1.0
0.5
0.0
f1 (ppm)

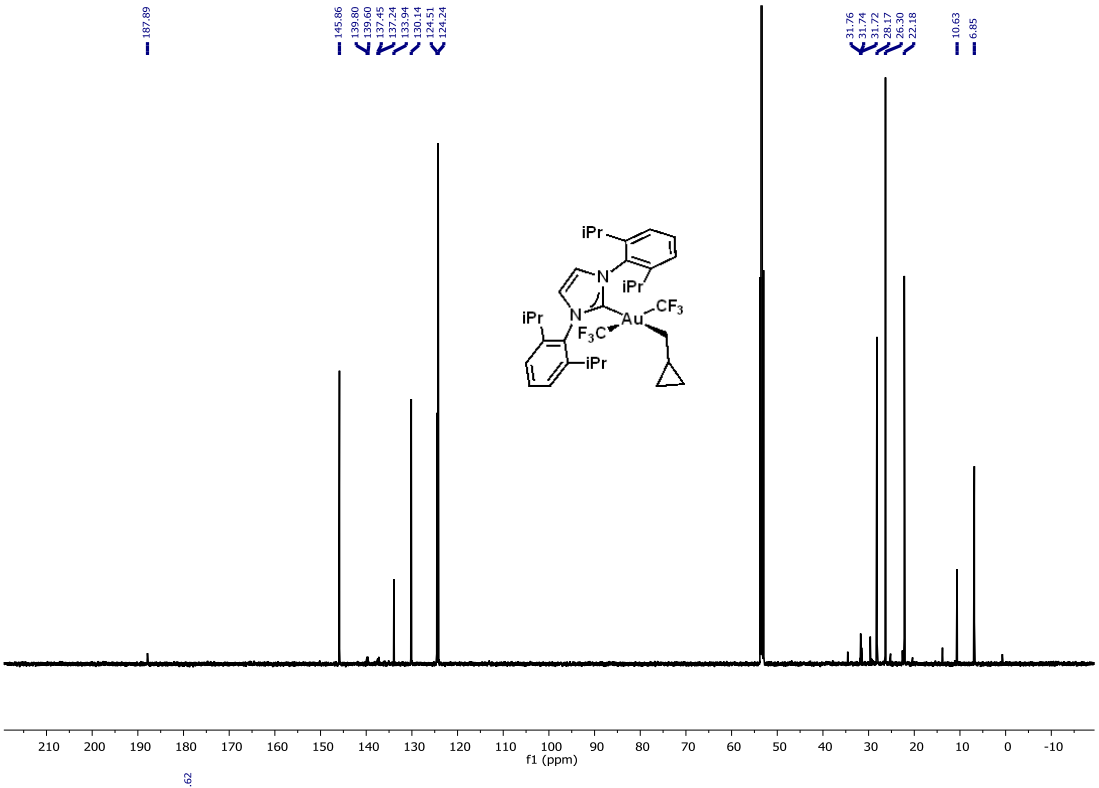
187.89
145.86
139.80
139.60
137.45
137.24
133.94
130.14
124.51
124.24
31.76
31.74
31.72
28.17
26.30
22.18
10.63
6.85
iPr
iPr
iPr
iPr
N
N
Au
CF3
F3C
210 200 190 180 170 160 150 140 130 120 110 100 90 80 70 60 50 40 30 20 10 0 -10
f1 (ppm)

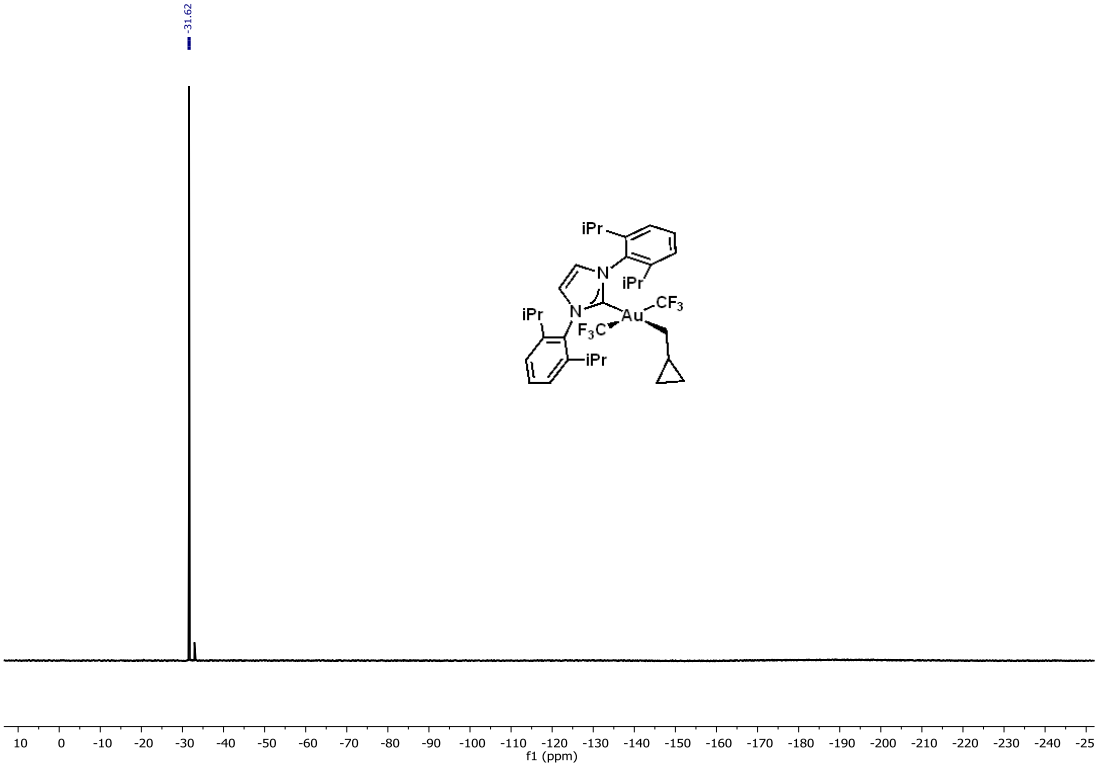
-31.62
iPr
iPr
iPr
iPr
N
N
Au
CF3
F3C
10 0 -10 -20 -30 -40 -50 -60 -70 -80 -90 -100 -110 -120 -130 -140 -150 -160 -170 -180 -190 -200 -210 -220 -230 -240 -25
f1 (ppm)

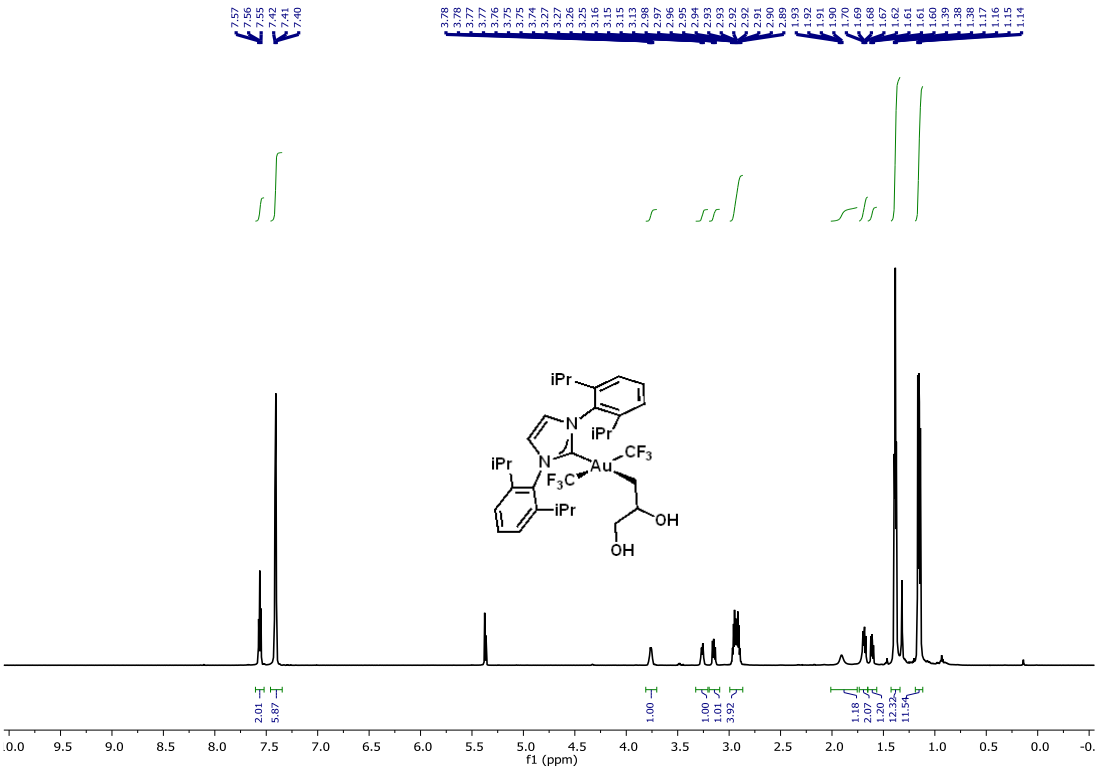
iPr
iPr
iPr
iPr
N
N
Au
CF3
F3C
OH
OH
f1 (ppm)

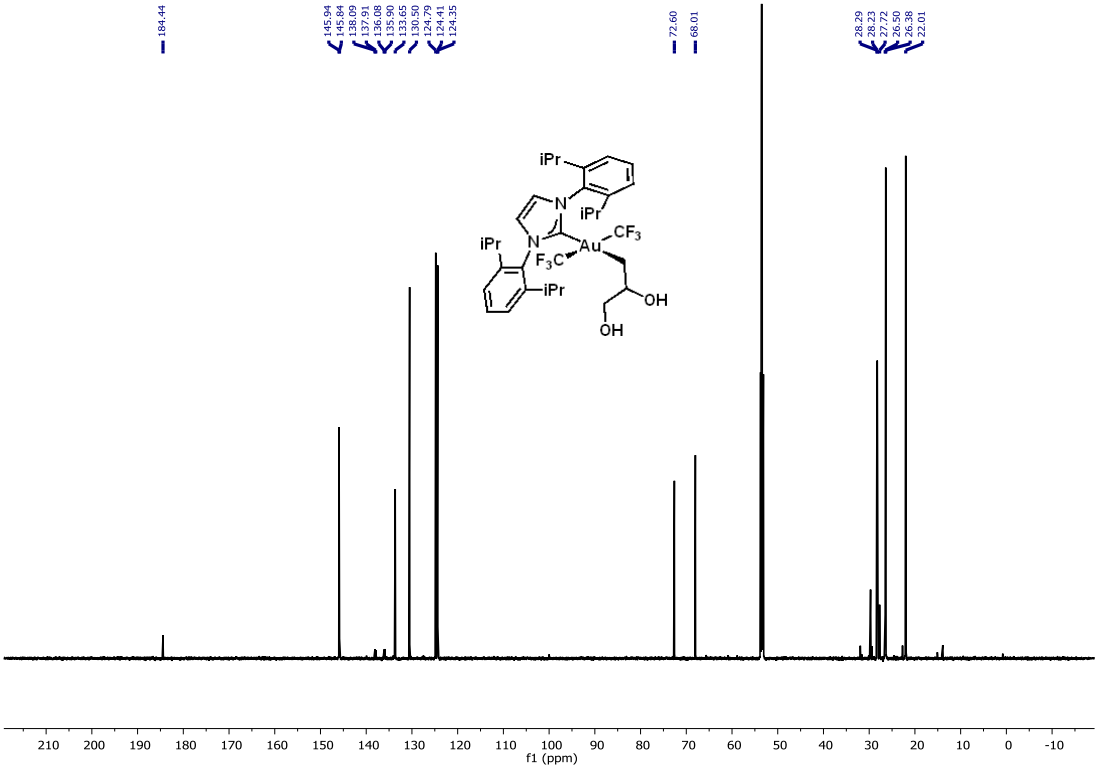
iPr
iPr
iPr
iPr
N
N
Au
CF3
F3C
OH
OH
f1 (ppm)

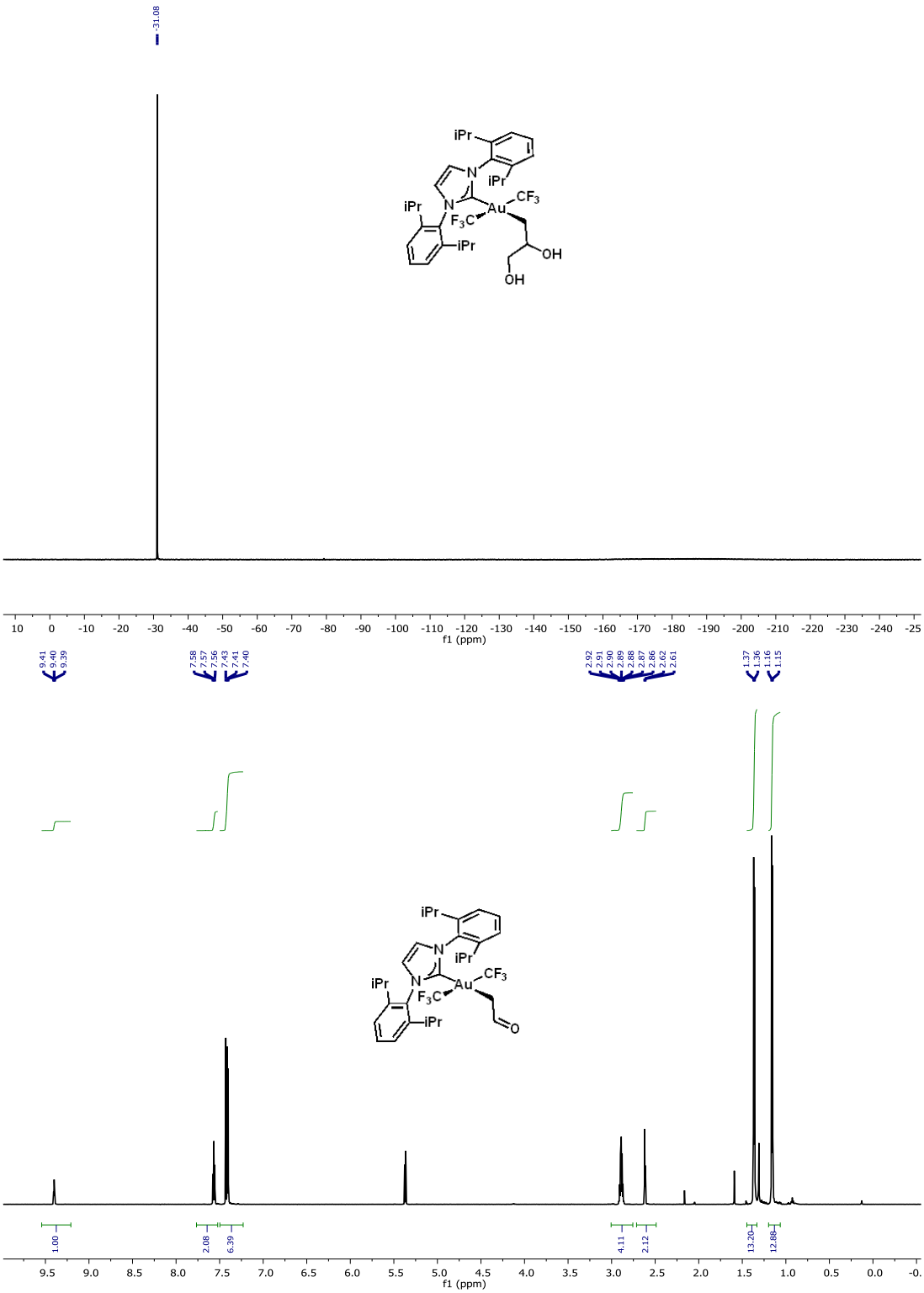
-31.08
iPr
N
iPr
N
Au
CF3
F3C
iPr
iPr
OH
OH
f1 (ppm)
9.41
9.40
9.39
7.58
7.57
7.56
7.43
7.41
7.40
2.92
2.91
2.90
2.89
2.88
2.87
2.86
2.62
2.61
1.37
1.36
1.16
1.15
1.00
2.08
6.39
4.11
2.12
13.20
12.88
f1 (ppm)

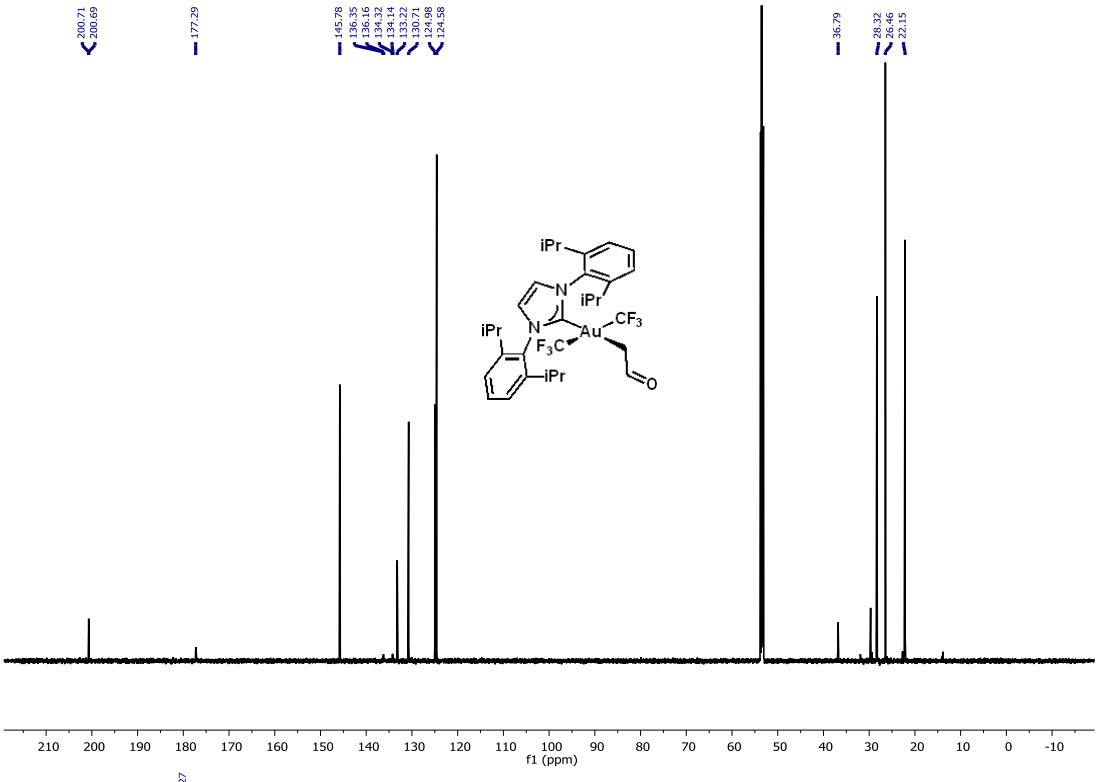
200.71
200.69
177.29
145.78
136.35
136.16
134.32
134.14
133.22
130.71
124.98
124.58
36.79
28.32
26.46
22.15
iPr
iPr
iPr
iPr
N
N
Au
CF3
F3C
O
210 200 190 180 170 160 150 140 130 120 110 100 90 80 70 60 50 40 30 20 10 0 -10
f1 (ppm)

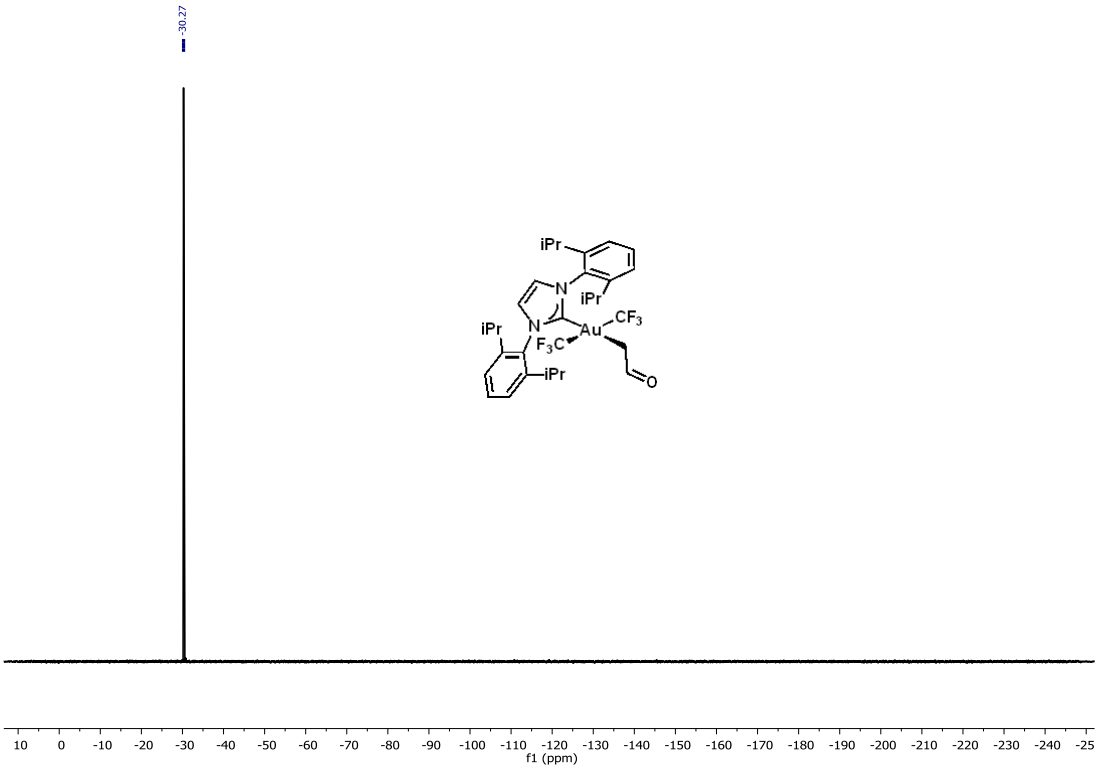
-30.27
iPr
iPr
iPr
iPr
N
N
Au
CF3
F3C
O
10 0 -10 -20 -30 -40 -50 -60 -70 -80 -90 -100 -110 -120 -130 -140 -150 -160 -170 -180 -190 -200 -210 -220 -230 -240 -25
f1 (ppm)

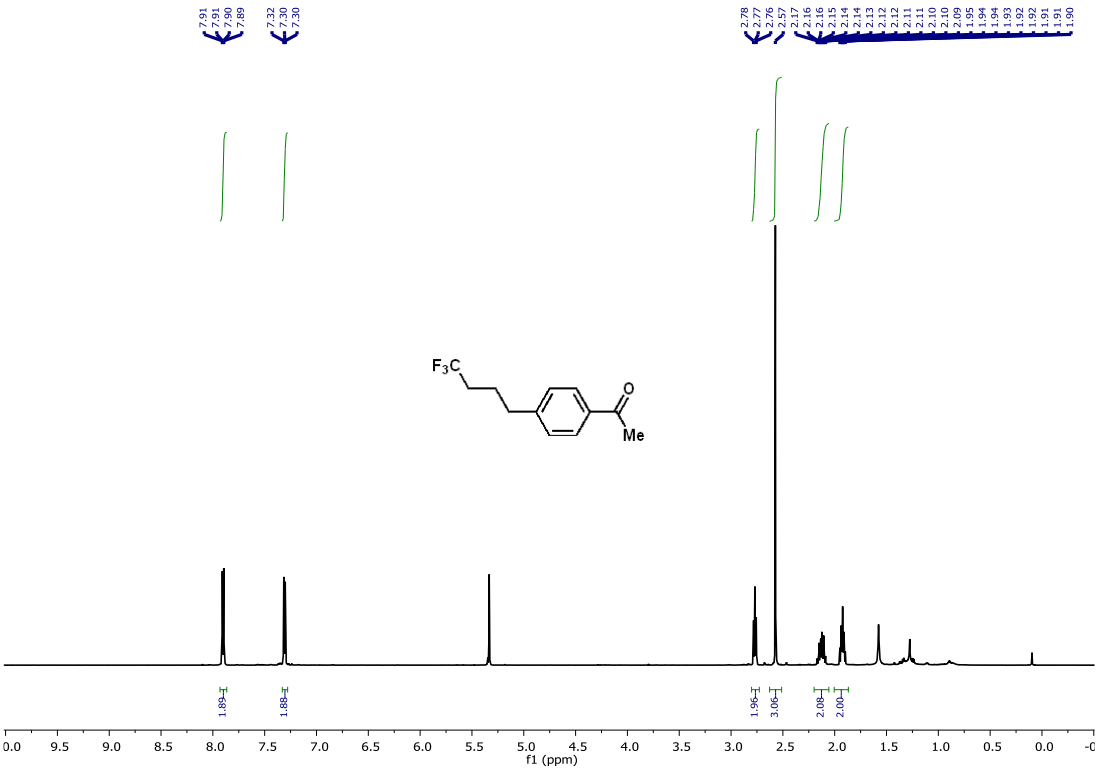
7.91
7.91
7.90
7.89
7.32
7.30
7.30
2.78
2.77
2.76
2.57
2.17
2.16
2.16
2.15
2.14
2.14
2.13
2.12
2.12
2.11
2.11
2.10
2.10
2.09
1.95
1.94
1.94
1.93
1.92
1.92
1.91
1.91
1.90
F3C
O
Me
1.89
1.88
1.96
3.06
2.08
2.00
f1 (ppm)

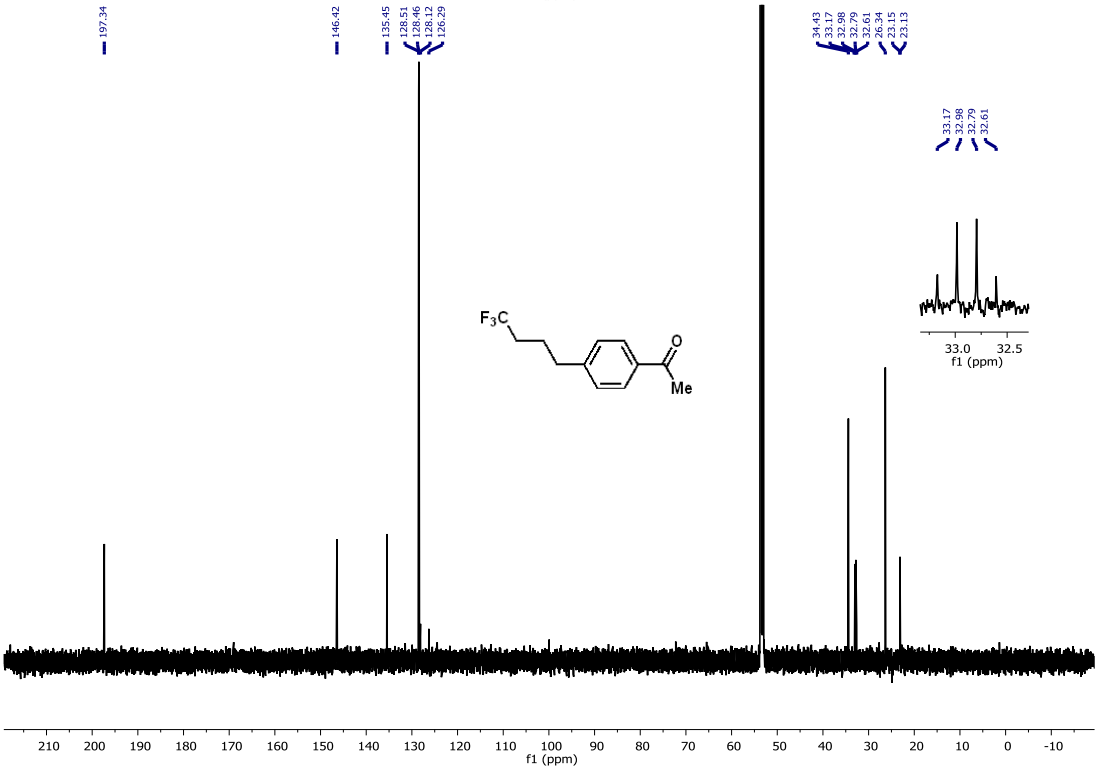
197.34
146.42
135.45
128.51
128.46
128.12
126.29
34.43
33.17
32.98
32.79
32.61
26.34
23.15
23.13
33.17
32.98
32.79
32.61
33.0
32.5
f1 (ppm)
F3C
O
Me
f1 (ppm)

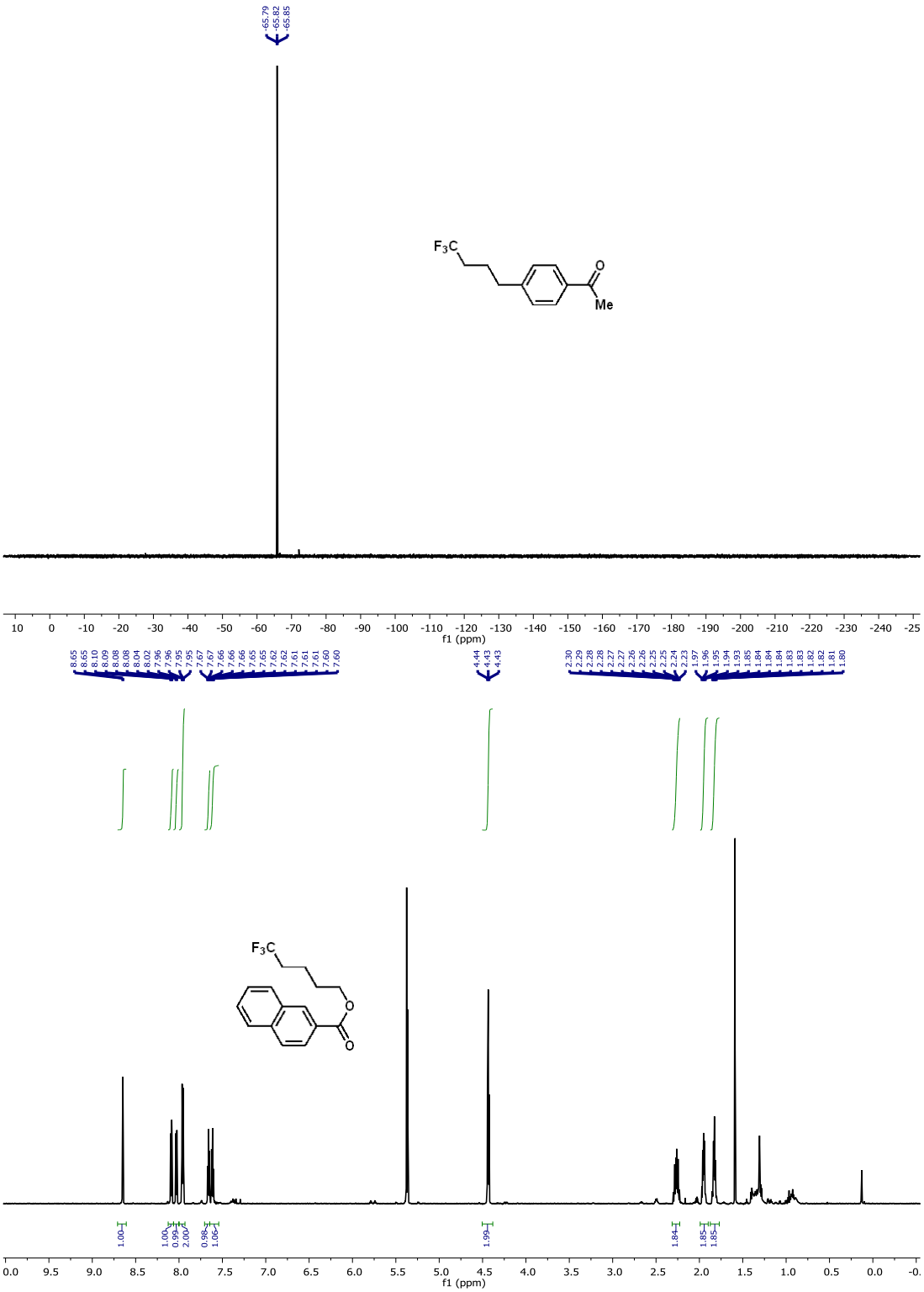
-65.79
-65.82
-65.85
F3C
O
Me
f1 (ppm)
F3C
O
O
f1 (ppm)

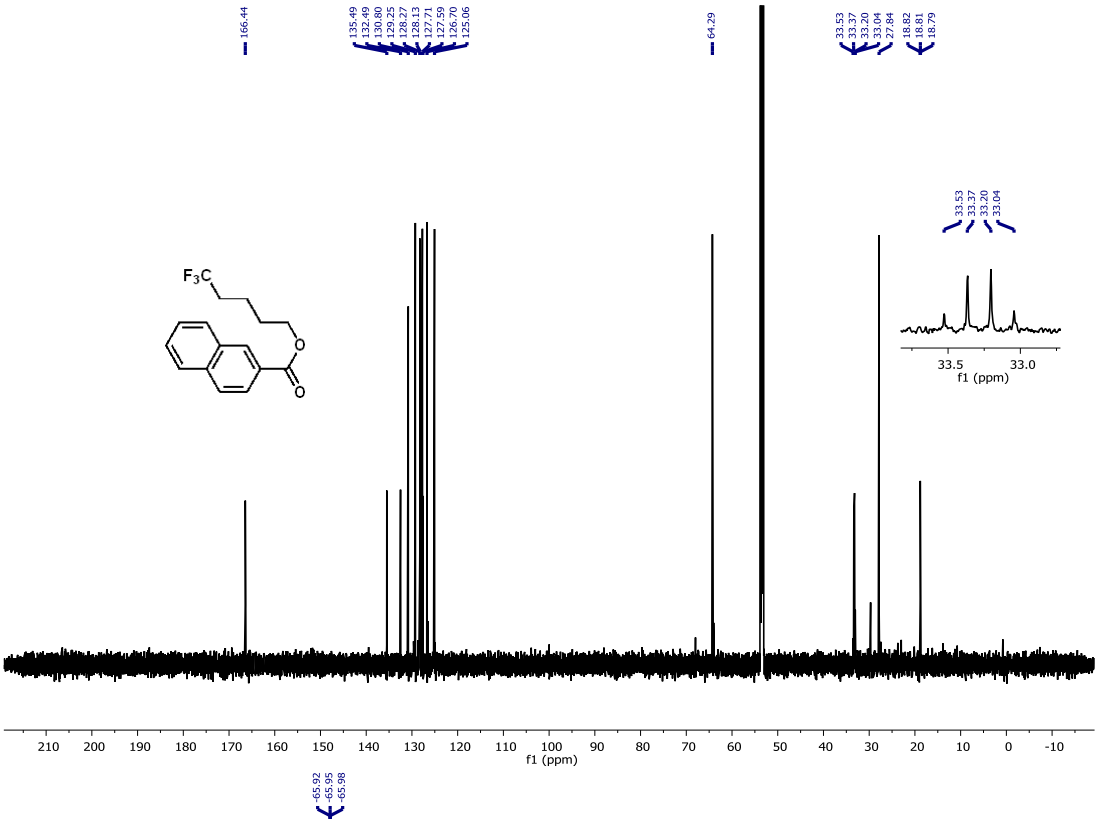
166.44
135.49
132.49
130.80
130.25
128.27
128.13
127.71
127.59
126.70
125.06
64.29
33.53
33.37
33.20
33.04
27.84
18.82
18.81
18.79
F3C
O
O
33.5
33.0
f1 (ppm)
210 200 190 180 170 160 150 140 130 120 110 100 90 80 70 60 50 40 30 20 10 0 -10
f1 (ppm)

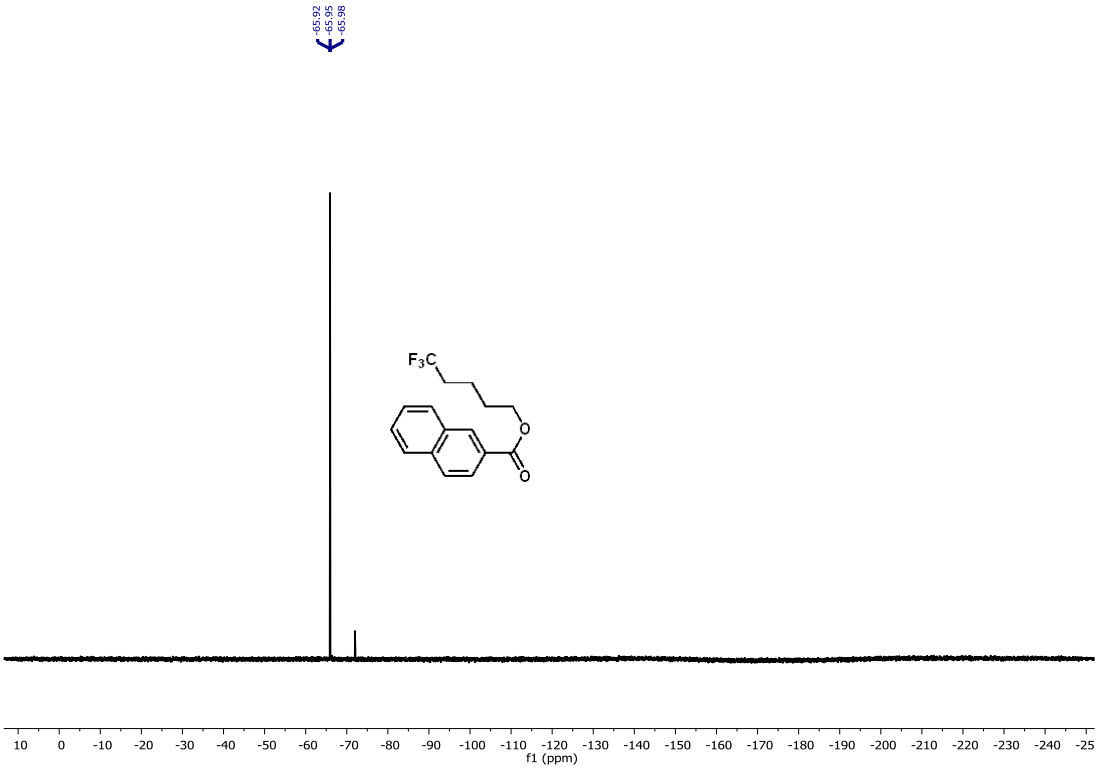
-65.92
-65.95
-65.98
F3C
O
O
10 0 -10 -20 -30 -40 -50 -60 -70 -80 -90 -100 -110 -120 -130 -140 -150 -160 -170 -180 -190 -200 -210 -220 -230 -240 -25
f1 (ppm)

## 4.6 References


(1) Preshlock, S.; Tredwell, M.; Gouverneur, V. *Chem. Rev.* **2016**, *116* (2), 719.
(2) Brooks, A. F.; Topczewski, J. J.; Ichiishi, N.; Sanford, M. S.; Scott, P. J. H. *Chem Sci* **2014**, *5* (12), 4545.
(3) Campbell, M. G.; Mercier, J.; Genicot, C.; Gouverneur, V.; Hooker, J. M.; Ritter, T. *Nat Chem* **2017**, *9* (1), 1.
(4) Lee, E.; Kamlet, A. S.; Powers, D. C.; Neumann, C. N.; Boursalian, G. B.; Furuya, T.; Choi, D. C.; Hooker, J. M.; Ritter, T. *Science* **2011**, *334* (6056), 639.
(5) Lee, E.; Hooker, J. M.; Ritter, T. *J. Am. Chem. Soc.* **2012**, *134* (42), 17456.
(6) Teare, H.; Robins, E. G.; Kirjavainen, A.; Forsback, S.; Sandford, G.; Solin, O.; Luthra, S. K.; Gouverneur, V. *Angew. Chem. Int. Ed.* **2010**, *49* (38), 6821.
(7) Stenhagen, I. S. R.; Kirjavainen, A. K.; Forsback, S. J.; Jorgensen, C. G.; Robins, E. G.; Luthra, S. K.; Solin, O.; Gouverneur, V. *Chem Commun* **2013**, *49* (14), 1386.
(8) Graham, T. J. A.; Lambert, R. F.; Ploessl, K.; Kung, H. F.; Doyle, A. G. *J. Am. Chem. Soc.* **2014**, *136* (14), 5291.
(9) Gray, E. E.; Nielsen, M. K.; Choquette, K. A.; Kalow, J. A.; Graham, T. J. A.; Doyle, A. G. *J. Am. Chem. Soc.* **2016**, *138* (34), 10802.
(10) Huang, X.; Liu, W.; Ren, H.; Neelamegam, R.; Hooker, J. M.; Groves, J. T. *J. Am. Chem. Soc.* **2014**, *136* (19), 6842.
(11) Liang, S. H.; Vasdev, N. *Aust. J. Chem.* **2015**, *68* (9), 1319.
(12) Van de Bittner, G. C.; Ricq, E. L.; Hooker, J. M. *Acc. Chem. Res.* **2014**, *47* (10), 3127.
(13) Lien, V. T.; Riss, P. J. *BioMed Res. Int.* **2014**, *2014*, 10.
(14) Huiban, M.; Tredwell, M.; Mizuta, S.; Wan, Z.; Zhang, X.; Collier, T. L.; Gouverneur, V.; Passchier, J. *Nat Chem* **2013**, *5* (11), 941.
(15) van der Born, D.; Sewing, C.; Herscheid, J. (Koos) D. M.; Windhorst, A. D.; Orru, R. V. A.; Vugts, D. J. *Angew. Chem. Int. Ed.* **2014**, *53* (41), 11046.
(16) Riss, P. J.; Aigbirhio, F. I. *Chem Commun* **2011**, *47* (43), 11873.
(17) Gil-Rubio, J.; Vicente, J. *Dalton Trans* **2015**, *44* (45), 19432.
(18) Sanner, R. D.; Satcher, J. H.; Droege, M. W. *Organometallics* **1989**, *8* (6), 1498.
(19) Nair, H. K.; Morrison, J. A. *J. Organomet. Chem.* **1989**, *376* (1), 149.
(20) Johnson, A.; Puddephatt, R. J. *J Chem Soc Dalton Trans* **1976**, No. 14, 1360.
(21) Margrave, J. L.; Whitmire, K. H.; Hauge, R. H.; Norem, N. T. *Inorg. Chem.* **1990**, *29* (17), 3252.
(22) Winston, M. S.; Wolf, W. J.; Toste, F. D. *J. Am. Chem. Soc.* **2014**, *136* (21), 7777.
(23) Winston, M. S.; Wolf, W. J.; Toste, F. D. *J. Am. Chem. Soc.* **2015**, *137* (24), 7921.
(24) Blaya, M.; Bautista, D.; Gil-Rubio, J.; Vicente, J. *Organometallics* **2014**, *33* (22), 6358.
(25) Martínez-Salvador, S.; Falvello, L. R.; Martín, A.; Menjón, B. *Chem. – Eur. J.* **2013**, *19* (43), 14540.
(26) Menjón, B.; Baya, M.; Pérez-Bitrián, A.; Martínez-Salvador, S.; Casas, J. M.; Orduna, J. *Chem. – Eur. J.* **2016**, n/a.
(27) Rice, G. W.; Tobias, R. S. *Inorg. Chem.* **1976**, *15* (2), 489.
(28) Tamaki, A.; Kochi, J. K. *J Chem Soc Dalton Trans* **1973**, No. 23, 2620.
(29) Tamaki, A.; Kochi, J. K. *J. Organomet. Chem.* **1973**, *51*, C39.
(30) Schuster, O.; Schmidbaur, H. *Inorganica Chim. Acta* **2006**, *359* (11), 3769.

(31) Johnson, M. W.; DiPasquale, A. G.; Bergman, R. G.; Toste, F. D. *Organometallics* **2014**, *33* (16), 4169.
(32) Yang, X.; Stern, C. L.; Marks, T. J. *J. Am. Chem. Soc.* **1991**, *113* (9), 3623.
(33) Yang, X.; Stern, C. L.; Marks, T. J. *J. Am. Chem. Soc.* **1994**, *116* (22), 10015.
(34) Chen, E. Y.-X.; Marks, T. J. *Chem. Rev.* **2000**, *100* (4), 1391.
(35) Massey, A. G.; Park, A. J. *J. Organomet. Chem.* **1964**, *2* (3), 245.
(36) Massey, A. G.; Park, A. J. *J. Organomet. Chem.* **1966**, *5* (3), 218.
(37) Lotz, M. D.; Remy, M. S.; Lao, D. B.; Ariafard, A.; Yates, B. F.; Canty, A. J.; Mayer, J. M.; Sanford, M. S. *J. Am. Chem. Soc.* **2014**, *136* (23), 8237.
(38) Camasso, N. M.; Sanford, M. S. *Science* **2015**, *347* (6227), 1218.
(39) Bour, J. R.; Camasso, N. M.; Meucci, E. A.; Kampf, J. W.; Canty, A. J.; Sanford, M. S. *J. Am. Chem. Soc.* **2016**, *138* (49), 16105.
(40) Zanardi, A.; Novikov, M. A.; Martin, E.; Benet-Buchholz, J.; Grushin, V. V. *J. Am. Chem. Soc.* **2011**, *133* (51), 20901.
(41) Ball, N. D.; Kampf, J. W.; Sanford, M. S. *J. Am. Chem. Soc.* **2010**, *132* (9), 2878.
(42) Grushin, V. V.; Marshall, W. J. *J. Am. Chem. Soc.* **2006**, *128* (39), 12644.
(43) Cho, E. J.; Senecal, T. D.; Kinzel, T.; Zhang, Y.; Watson, D. A.; Buchwald, S. L. *Science* **2010**, *328* (5986), 1679.
(44) Deyhimi, F.; Coles, J. A. *Helv. Chim. Acta* **1982**, *65* (6), 1752.
(45) Williams, D. B. G.; Lawton, M. *J. Org. Chem.* **2010**, *75* (24), 8351.
(46) Dolbier, W. R.; Wojtowicz, H.; Burkholder, C. R. *J. Org. Chem.* **1990**, *55* (19), 5420.
(47) Eujen, R.; Hoge, B. *J. Organomet. Chem.* **1995**, *503* (Copyright (C) 2017 American Chemical Society (ACS). All Rights Reserved.), C51.
(48) Martínez-Salvador, S.; Forniés, J.; Martín, A.; Menjón, B. *Angew. Chem. Int. Ed.* **2011**, *50* (29), 6571.
(49) The trend of inhibitory tendencies of the halides tracks with the B-X bond strengths, as would be expected for the formation of X-B($C_6F_5$)$_3$ anionic adducts, which are observed by $^{19}$F-NMR in each case. See Ref. 47.
(50) Haynes, W. M. (ed. *CRC Handbook of Chemistry and Physics*, 97th ed.; CRC Press/Taylor & Francis: Boca Raton, FL.
(51) Marival-Hodebar, L.; Tordeux, M.; Wakselman, C. *J Chem Res S* **1998**, No. 4, 192.
(52) Laitar, D. S.; Müller, P.; Gray, T. G.; Sadighi, J. P. *Organometallics* **2005**, *24* (19), 4503.
(53) Mankad, N. P.; Toste, F. D. *Chem Sci* **2012**, *3* (1), 72.
(54) Mankad, N. P.; Toste, F. D. *J. Am. Chem. Soc.* **2010**, *132* (37), 12859.
(55) Wolf, W. J.; Dean Toste, F. In *PATAI'S Chemistry of Functional Groups*; John Wiley & Sons, Ltd, 2009.
(56) Ung, G.; Bertrand, G. *Angew. Chem. Int. Ed.* **2013**, *52* (43), 11388.
(57) In line with the relationship between **17** and **11**, a second isomer of **11** can be observed at late reaction times (c.f. **17b**), which does not undergo trifluoroethane elimination until warming past 0 $^{o}$C.
(58) Rekhroukh, F.; Brousses, R.; Amgoune, A.; Bourissou, D. *Angew. Chem. Int. Ed.* **2015**, *54* (4), 1266.
(59) Johnson, A.; Puddephatt, R. J. *J Chem Soc Dalton Trans* **1977**, No. 14, 1384.
(60) Joost, M.; Gualco, P.; Mallet-Ladeira, S.; Amgoune, A.; Bourissou, D. *Angew. Chem. Int. Ed.* **2013**, *52* (28), 7160.

(61) Joost, M.; Estevez, L.; Mallet-Ladeira, S.; Miqueu, K.; Amgoune, A.; Bourissou, D. *J. Am. Chem. Soc.* **2014**, *136* (29), 10373.
(62) Tsui, E. Y.; Müller, P.; Sadighi, J. P. *Angew. Chem. Int. Ed.* **2008**, *47* (46), 8937.
(63) Pintus, A.; Rocchigiani, L.; Fernandez-Cestau, J.; Budzelaar, P. H. M.; Bochmann, M. *Angew. Chem. Int. Ed.* **2016**, *55* (40), 12321.
(64) Scott, V. J.; Labinger, J. A.; Bercaw, J. E. *Organometallics* **2010**, *29* (18), 4090.
(65) Ghidiu, M. J.; Pistner, A. J.; Yap, G. P. A.; Lutterman, D. A.; Rosenthal, J. *Organometallics* **2013**, *32* (18), 5026.
(66) *Gaussian 09*; Gaussian, Inc.: Wallingford, CT, 2009.
(67) Marenich, A. V.; Cramer, C. J.; Truhlar, D. G. *J. Phys. Chem. B* **2009**, *113* (18), 6378.
(68) Rekhroukh, F.; Estévez, L.; Bijani, C.; Miqueu, K.; Amgoune, A.; Bourissou, D. *Angew. Chem. Int. Ed.* **2016**, *55* (10), 3414.
(69) Komiya, S.; Albright, T. A.; Hoffmann, R.; Kochi, J. K. *J. Am. Chem. Soc.* **1976**, *98* (23), 7255.
(70) Wolf, W. J. Studies on the Organometallic Reactivity of Gold(III). Doctoral Dissertation, University of California, Berkeley: Berkeley, California, 2016.
(71) Dissociation of the difluorocarbene from **II** was also examined, occuring by a TS for which $\Delta H^{\ddagger} > 40$ kcal/mol. No transition states for reductive elimination directly from **IIIa** were located.
(72) Choi, J.; Wang, D. Y.; Kundu, S.; Choliy, Y.; Emge, T. J.; Krogh-Jespersen, K.; Goldman, A. S. *Science* **2011**, *332* (6037), 1545.
(73) Brothers, P. J.; Roper, W. R. *Chem. Rev.* **1988**, *88* (7), 1293.
(74) Martinez-Salvador, S.; Menjon, B.; Fornies, J.; Martin, A.; Uson, I. *Angew. Chem. Int. Ed.* **2010**, *49* (Copyright (C) 2017 American Chemical Society (ACS). All Rights Reserved.), 4286.
(75) Harrison, D. J.; Daniels, A. L.; Korobkov, I.; Baker, R. T. *Organometallics* **2015**, *34* (Copyright (C) 2017 American Chemical Society (ACS). All Rights Reserved.), 5683.
(76) Harrison, D. J.; Lee, G. M.; Leclerc, M. C.; Korobkov, I.; Baker, R. T. *J. Am. Chem. Soc.* **2013**, *135* (Copyright (C) 2017 American Chemical Society (ACS). All Rights Reserved.), 18296.
(77) Leclerc, M. C.; Bayne, J. M.; Lee, G. M.; Gorelsky, S. I.; Vasiliu, M.; Korobkov, I.; Harrison, D. J.; Dixon, D. A.; Baker, R. T. *J. Am. Chem. Soc.* **2015**, *137* (51), 16064.
(78) Lee, G. M.; Harrison, D. J.; Korobkov, I.; Baker, R. T. *Chem. Commun. Camb. U. K.* **2014**, *50* (Copyright (C) 2017 American Chemical Society (ACS). All Rights Reserved.), 1128.
(79) Roşca, D.-A.; Fernandez-Cestau, J.; Morris, J.; Wright, J. A.; Bochmann, M. *Sci. Adv.* **2015**, *1* (9).
(80) Rekhroukh, F.; Estevez, L.; Mallet-Ladeira, S.; Miqueu, K.; Amgoune, A.; Bourissou, D. *J. Am. Chem. Soc.* **2016**, *138* (36), 11920.
(81) Hill, R. H.; Puddephatt, R. J. *J. Am. Chem. Soc.* **1985**, *107* (5), 1218.
(82) The corresponding displacement with $PCy_3$ was far less clean, giving P(V) byproducts in addition to the desired product.
(83) Gevorgyan, V.; Rubin, M.; Benson, S.; Liu, J.-X.; Yamamoto, Y. *J. Org. Chem.* **2000**, *65* (19), 6179.
(84) Scott, V. J.; Çelenligil-Çetin, R.; Ozerov, O. V. *J. Am. Chem. Soc.* **2005**, *127* (9), 2852.

(85) Douvris, C.; Ozerov, O. V. *Science* **2008**, *321* (5893), 1188.
(86) Other heterogeneous catalysts were found to be too active, reducing the ketone to the corresponding alcohol or alkane. In none of these cases, however, was hydrogenolysis of the Au-C bond observed.
(87) Hartwig, J. F. *Organotransition Metal Chemistry: From Bonding to Catalysis*; University Science Books, 2010.
(88) This interpretation relies on the assumption that C-F abstraction is readily reversible, a feature borne out in the computational study presented above, given that formation of the carbenoid is uphill and essentially barrierless beyond coulombic penalties, starting from the C-F-B adduct.
(89) Denmark, S. E.; Edwards, J. P. *J. Org. Chem.* **1991**, *56* (25), 6974.
(90) Crivello, J. V. *J. Org. Chem.* **1981**, *46* (15), 3056.
(91) Ram, S.; Ehrenkaufer, R. E. *Synthesis* **1988**, No. 2, 91.
(92) Bartlett, R. R.; Dimitrijevic, M.; Mattar, T.; Zielinski, T.; Germann, T.; Rüde, E.; Thoenes, G. H.; Küchle, C. C. A.; Schorlemmer, H.-U.; Bremer, E.; Finnegan, A.; Schleyerbach, R. *Agents Actions* **1991**, *32* (1), 10.
(93) Jacobsen, H.; Berke, H.; Döring, S.; Kehr, G.; Erker, G.; Fröhlich, R.; Meyer, O. *Organometallics* **1999**, *18* (9), 1724.
(94) Lawrence, E. J.; Oganesyan, V. S.; Wildgoose, G. G.; Ashley, A. E. *Dalton Trans* **2013**, *42* (3), 782.
(95) De Vry, J.; Denzer, D.; Reissmueller, E.; Eijckenboom, M.; Heil, M.; Meier, H.; Mauler, F. *J. Pharmacol. Exp. Ther.* **2004**, *310* (2), 620.
(96) Xu, J.; Xiao, B.; Xie, C.-Q.; Luo, D.-F.; Liu, L.; Fu, Y. *Angew. Chem. Int. Ed.* **2012**, *51* (50), 12551.
(97) Zhu, W.; Wang, J.; Wang, S.; Gu, Z.; Aceña, J. L.; Izawa, K.; Liu, H.; Soloshonok, V. A. *J. Fluor. Chem.* **2014**, *167*, 37.
(98) Prakash, G. K. S.; Yudin, A. K. *Chem. Rev.* **1997**, *97* (3), 757.
(99) Teruo, U.; Sumi, I. *Tetrahedron Lett.* **1990**, *31* (25), 3579.
(100) Kieltsch, I.; Eisenberger, P.; Togni, A. *Angew. Chem. Int. Ed.* **2007**, *46* (5), 754.
(101) Nagib, D. A.; Scott, M. E.; MacMillan, D. W. C. *J. Am. Chem. Soc.* **2009**, *131* (31), 10875.
(102) García-Monforte, M. A.; Martínez-Salvador, S.; Menjón, B. *Eur. J. Inorg. Chem.* **2012**, *2012* (31), 4945.
(103) Lee, S. J.; Brooks, A.; Ichiishi, N.; Makaravage, K.; Mossine, A.; Sanford, M.; Scott, P. *J. Nucl. Med.* **2016**, *57* (supplement 2), 324.
(104) Mathiessen, B.; Jensen, M.; Zhuravlev, F. *J. Label. Compd. Radiopharm.* **2011**, *54* (13), 816.
(105) Revunov, E.; Zhuravlev, F. *J. Fluor. Chem.* **2013**, *156*, 130.
(106) Tewson, T. J.; Welch, M. J. *J Chem Soc Chem Commun* **1979**, No. 24, 1149.
(107) Tramšek, M.; Goreshnik, E.; Lozinšek, M.; Žemva, B. *Contrib. Int. Conf. Fluor. Chem. 09 KyotoThe Int. Conf. Fluor. Chem. 09 Organised Jpn. Soc. Promot. Sci. 155th Comm. Fluor. Chem.* **2009**, *130* (12), 1093.
(108) Landini, D.; Maia, A.; Rampoldi, A. *J. Org. Chem.* **1989**, *54* (2), 328.
(109) Sharma, R. K.; Fry, J. L. *J. Org. Chem.* **1983**, *48* (12), 2112.
(110) Sun, H.; DiMagno, S. G. *J. Am. Chem. Soc.* **2005**, *127* (7), 2050.

(111) Buck, A. K.; Herrmann, K.; Stargardt, T.; Dechow, T.; Krause, B. J.; Schreyögg, J. *J. Nucl. Med.* **2010**, *51* (3), 401.
(112) Wiemers, D. M.; Burton, D. J. *J. Am. Chem. Soc.* **1986**, *108* (4), 832.
(113) Yang, Z.-Y.; Burton, D. J. *J. Fluor. Chem.* **2000**, *102* (Copyright (C) 2017 American Chemical Society (ACS). All Rights Reserved.), 89.
(114) Yang, Z. Y.; Wiemers, D. M.; Burton, D. J. *J. Am. Chem. Soc.* **1992**, *114* (11), 4402.
(115) Burton, D. J.; Wiemers, D. M.; Easdon, J. C. Compounds containing perfluoroalkyl groups., April 15, 1986.
(116) Hu, C.-M.; Qing, F.-L.; Shen, C.-X. *J Chem Soc Perkin Trans 1* **1993**, No. 3, 335.